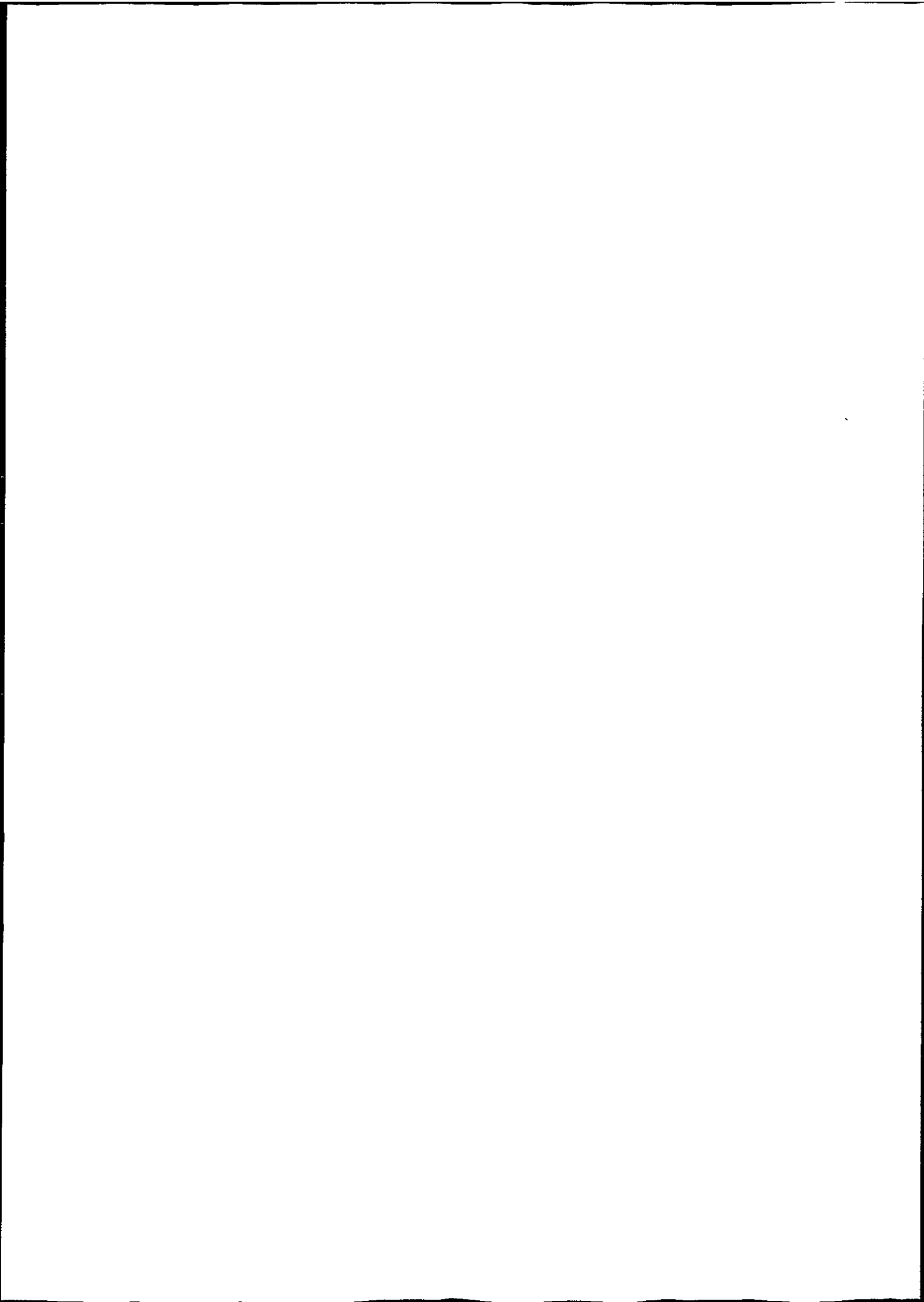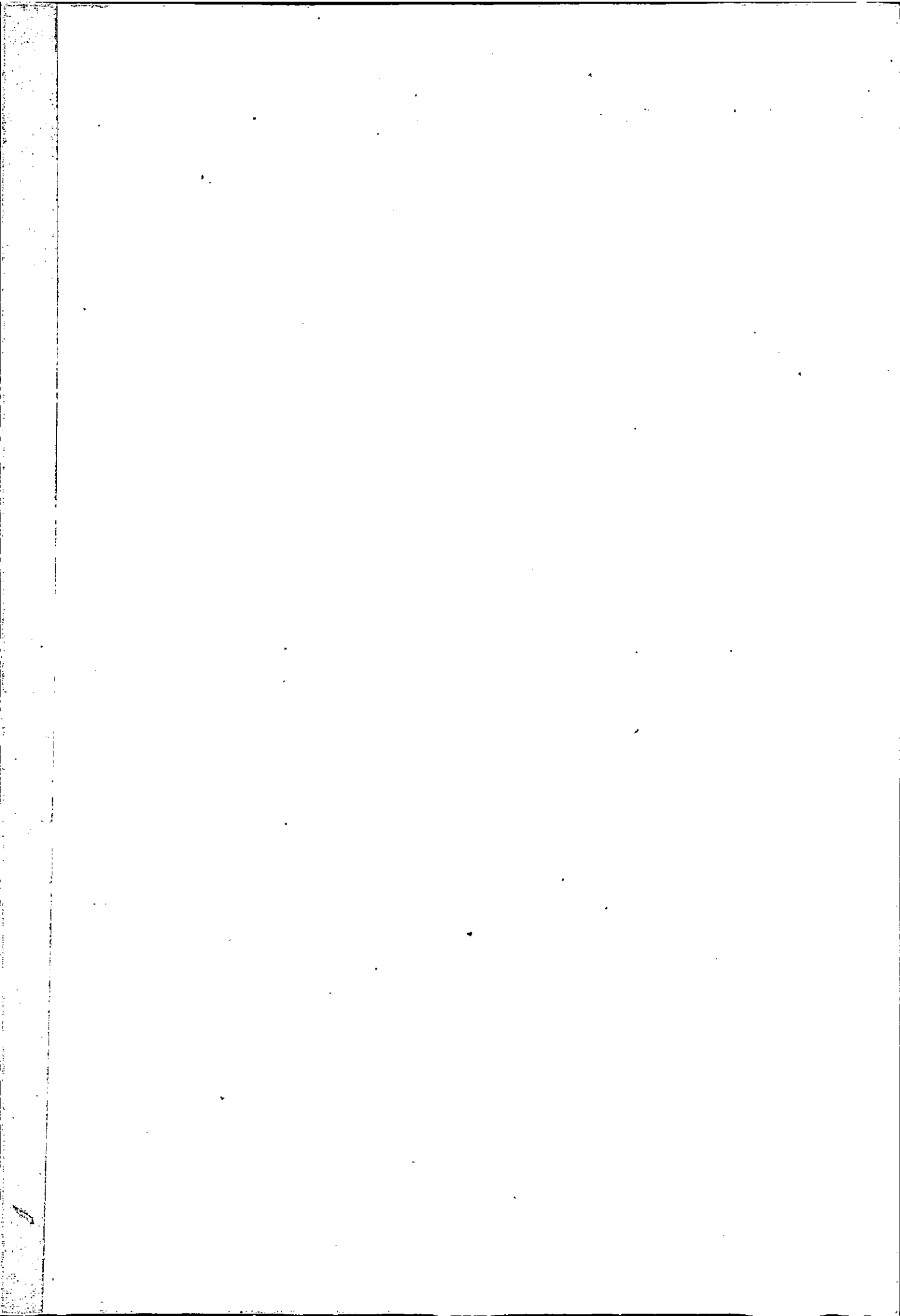# CARBON AND COKE
REACTIVITY IN ZINC-LEAD
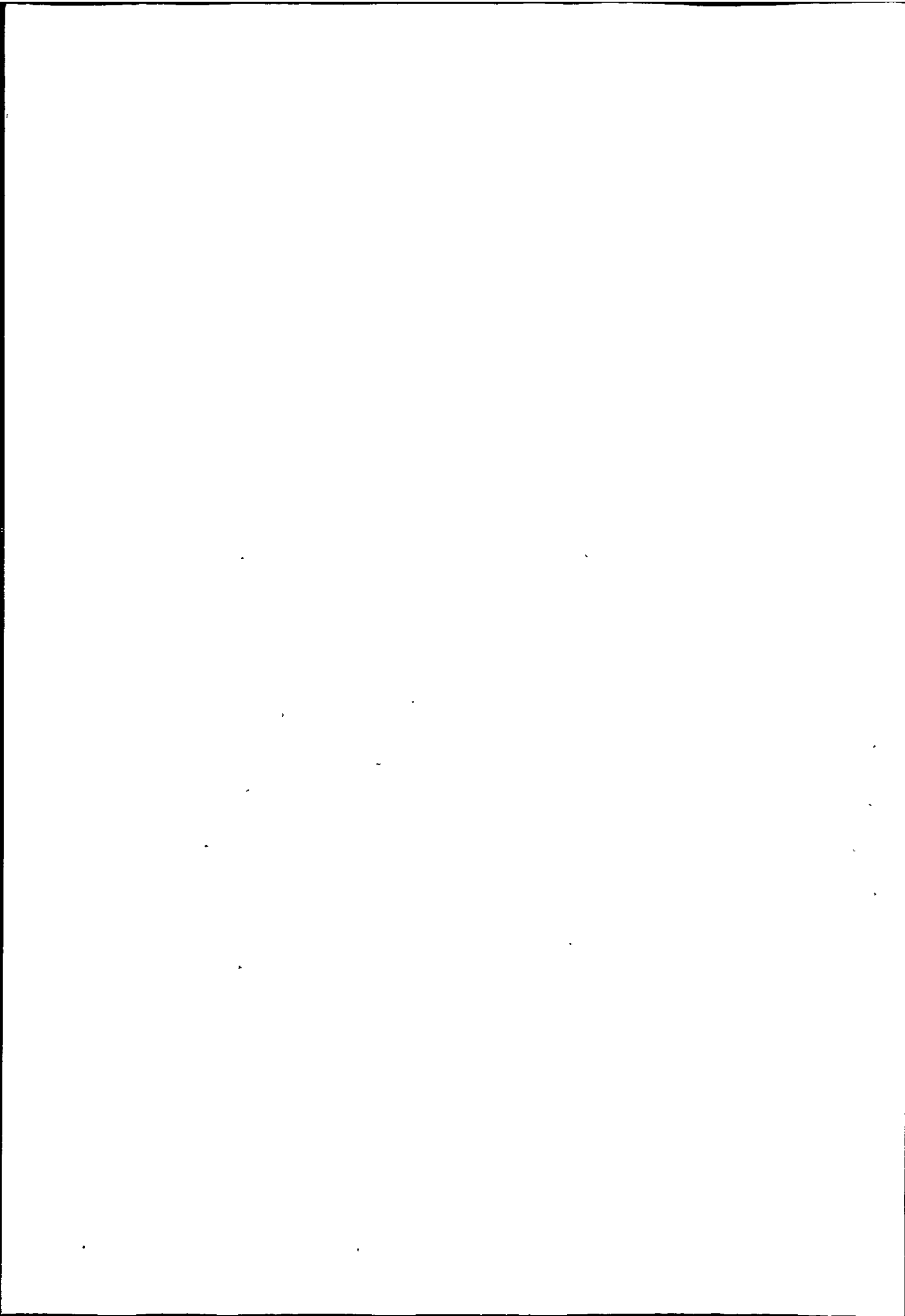# BLAST FURNACE PRACTICE

M. A. CARTER

Ph. D.   1983

This thesis is dedicated to Miss B.J.Noble

CARBON AND COKE REACTIVITY IN

ZINC-LEAD BLAST FURNACE PRACTICE

Margaret Ann CARTER B.Sc. C.Chem. MRSC

A thesis submitted in partial fulfilment

of the requirements for the degree of

DOCTOR OF PHILOSOPHY

of the

COUNCIL FOR. NATIONAL ACADEMIC. AWARDS

LONDON

John Graymore Chemistry Laboratories

Department of Environmental Sciences

Plymouth Polytechnic

Plymouth PL4 8AA

In collaboration with

Imperial Smelting Processes Ltd.,

Avonmouth

Bristol BS11 9HP

December 1983.

CARBON AND COKE REACTIVITY IN

ZINC-LEAD BLAST FURNACE PRACTICE

Margaret Ann CARTER

ABSTRACT

Previous research on the oxidation of coke in air, O_2 and CO_2 has been reviewed, especially with regard to kinetic studies and Zn/Pb blast furnace practice.

Coke "reactivity" has been discussed and correlated with surface area changes on carbon burn-off (in air and CO_2 at various temperatures) for Nantgarw and two other metallurgical cokes.

Other carbons (charcoals and graphite) and a brown coal char have been examined by gas sorption, X ray diffraction and thermal analysis in an attempt to relate reactivity, as determined by rate of reaction in CO_2 at 1000 ^{o}C, with other solid state properties. Reactivity studies on coal chars have been reviewed also.

The inhibition of the Boudouard reaction, by modification of the carbon surface, has been reviewed, especially by the action of B_2O_3. Cokes and coal char have been subject to B_2O_3 solution treatment and the mode of action of the inhibitor investigated by isothermal and dynamic thermal analysis and estimation of surface area by gravimetric gas sorption. The action of B_2O_3 at both low and high degree of carbon burn off has been studied.

The mineral matter of coke (which forms about 10% by weight of the material) and the coal char (which forms about 2%) has been examined by X ray diffraction, optical and electron microscopy and thermal and chemical analysis. Its affect upon the kinetics of oxidation has been investigated.

Results have been discussed in relation to the industrial usage of coke in the Zn/Pb blast furnace.

CARBON AND COKE REACTIVITY IN

ZINC-LEAD BLAST FURNACE PRACTICE

Margaret Ann CARTER

ABSTRACT

Previous research on the oxidation of coke in air, O_2 and CO_2 has been reviewed, especially with regard to kinetic studies and Zn/Pb blast furnace practice.

Coke "reactivity" has been discussed and correlated with surface area changes on carbon burn-off (in air and CO_2 at various temperatures) for Nantgarw and two other metallurgical cokes.

Other carbons (charcoals and graphite) and a brown coal char have been examined by gas sorption, X ray diffraction and thermal analysis in an attempt to relate reactivity, as determined by rate of reaction in CO_2 at 1000 °C, with other solid state properties. Reactivity studies on coal chars have been reviewed also.

The inhibition of the Boudouard reaction, by modification of the carbon surface, has been reviewed, especially by the action of B_2O_3. Cokes and coal char have been subject to B_2O_3 solution treatment and the mode of action of the inhibitor investigated by isothermal and dynamic thermal analysis and estimation of surface area by gravimetric gas sorption. The action of B_2O_3 at both low and high degree of carbon burn off has been studied.

The mineral matter of coke (which forms about 10% by weight of the material) and the coal char (which forms about 2%) has been examined by X ray diffraction, optical and electron microscopy and thermal and chemical analysis. Its effect upon the kinetics of oxidation has been investigated.

Results have been discussed in relation to the industrial usage of coke in the Zn/Pb blast furnace.

CONTENTS

CHAPTER ONE. INTRODUCTION.

1.1.1 Forms of Carbon

1.1.2 Coal

1.1.3 The Coking Process and Coke Formation

1.1.4 Coke Testing and Analysis

1.1.5 Coke for the Zn/Pb Blast Furnace

1.2.1 The Oxides of Carbon in Pyrometallurgy

1.2.2 The Blast Furnace

1.2.3 The Zinc/Lead Blast Furnace

1.3.1 Gas-Solid Reactions

1.3.2 Non-porous solids

1.3.3 Porous Solids

1.3.4 Sintering of Solids

1.4.1 Fundamental Nature of the C/O_2 and C/CO_2 Reactions

1.4.2 Other Factors in Gas-Carbon Reactions.

1

CHAPTER 1

INTRODUCTION.

1.1.1 Forms of Carbon

The element carbon crystallises in two allotropic forms – diamond and graphite. In diamond the C–C bonds are formed by the overlapping of sp^3 hybrid orbitals, resulting in a tetrahedral distribution of bonds around each carbon atom. The structure of diamond belongs to the cubic system with space group Fd3m. (Hexagonal diamond also exists with space group $P6_3/mmc$)[1].

In graphite sp^2 hybrid orbitals form the intra layer C–C bonds . Hexagonal graphite (space group $P6_3/mmc$) has an ABAB layer stack sequence and is the thermodynamically stable form of carbon below 2600 K at any pressure. A thermodynamically unstable form, rhombohedral graphite, with ABCABC layer stack sequence also exists. General chemistry is described by Heslop and Robinson[2].

The various forms of carbon – soots, chars, cokes, carbon blacks etc. have a structure based upon the graphite modification in which the layers may be associated in stacks with a high degree of layer disorder. The crystal structure of graphite can tolerate a high concentration of defects. Carbons, such as cokes, charcoals, etc. prepared from natural materials also contain hydrogen and other heteroatoms. Such materials fall into two groups, the hard (non-graphitising) and the

2

soft (graphitising) carbons. The former group on heating to about 3000°K will develop the 3-dimensional symmetry of crystalline graphite, but the latter group will not.

Non-graphitising carbons are generally formed from non melting parent substances (e.g. wood husks etc.) and are microporous. Terminology is clarified as reported at the 5th London International Carbon and Graphite Conference[3].

The macrostructure of a carbon can be described in terms of different orders of magnitude.

1) Deviations from a perfect graphite lattice with layer planes 0.3354 nm apart.

2) Arrangement of graphite crystallites. These form areas of homogeneous optical anisotropy in cokes.

3) Preferred orientation of crystallite areas. This influences the macrostructure of coke (texture).

4) Orientation of particles within a bulk structure. This is influenced by industrial processes such as extrusion.

Thus in considering the characterisation of a carbon by the various methods available, the structural unit being investigated should be borne   in mind. The many variables of polygranular materials result in differences in physical and mechanical bulk properties. e.g. Lattice imperfections etc. may be completely overshadowed by heterogeneity of pore structure.

A large number of industrial carbon and graphite products are obtained by the thermal degradation of natural carbonaceous raw materials.

1.1.2 Coal

Coke is the major commercial product of the carbonisation of coal. Coal reserves represent the largest global source of carbon that can react with oxygen, most carbon being present in the earth's crust in the form of carbonates etc.

The coalification of plant debris that grew some 300 million years ago has led to a heterogeneous material. Differences in coal composition are expressed as the "rank" of the coal, and determined by the presence of various petrographic types known as "macerals", by analogy with the minerals of rocks, but unlike minerals they do not have a fixed chemical composition.

"Rank" expresses the degree of coalification and increases in going from peat, brown coal, bituminous coal to anthracite. With increasing rank carbon content increases and oxygen and hydrogen content decrease. Typical elemental analysis of coals of different ranks are expressed on a dry, mineral-matter-free basis (d.m.m.f.). Compared with the carbon, hydrogen, nitrogen and oxygen content of wood it appears that coalification involves plant material being dehydrated, decarboxylated and finally demethanated. The economics, science, technology and constitution of coal are described in

4

the authoritative work of Van Krevelen[4].

Rank provides a useful series for British coals. Of lowest rank are the high volatile, non coking coals suitable for combustion and used in electricity generation. Of higher rank are coals used in blends for carbonisation and of highest rank are anthracites used for smokeless combustion and as a starting material for active carbons. A single coalfield will produce a range of coals. In the South Wales coalfield there is a steady progression from east to west of low to high rank coals.

The structure of coal has been investigated by many physical and chemical methods, as detailed in the series edited by Karr[5].

X-ray diffraction provides information on the carbon skeleton suggesting layer planes of the graphite type with a higher degree of orientation the higher the rank, as described by Ergun[6].

N.M.R. and measurements of molar refraction and heats of combustion confirm the highly aromatic nature of coal. Spectroscopic methods applied to side group analysis and heteroatoms suggest a molecular structure of several benzene rings linked by methylene bridges to give folded rings with extensive cross linking and dimerisation. This structure is described by Pitt and Millward[7], and given in detail by Bouska[8]. The carbonisation of model organic precursors is described by Walker[9] and by Kipling and Shooter[10].

For coking, a coal must become fluid during the carbonisation process and swell up, due to evolved gases, forming a uniform coke. This ability to swell or cake together is the basis of the Gray-King coke type used by the N.C.B.

The coke type is based on the appearance of coke specimens prepared under standard conditions, prime coking coal being class "301" and Gray King coke type G4 and over. Prime coking coals yield a strong coke and become plastic before decomposition occurs. Outside the 20 to 32% volatile matter range the coal mass may foam on heating giving a coke of large pores with thin walls and low resistance to abrasion. Details and illustrations are given in reference 7.

Prime coking coals are now in short supply, but good blast furnace coke may be produced by blending coals which by themselves do not make the required product.

Properties relating to fluidity and swelling are not necessarily additive. The effects of coal blends are detailed by Hyslop[11]. The further removed the additive from prime coking coal, e.g. coke, breeze or char, the more critical are the blend characteristics.

Although passing through a plastic stage the coal does not actually melt during carbonisation. A coke does not retain the structure of the parent coal but its properties are dependent upon it.

Chars are also primary products prepared from the carbonisation of coal, or from synthetic polymeric

6

materials. Thermal degradation does not produce a plastic phase so chars retain the macrostructure of the precursor. Lower rank coals are generally used for char preparation.

1.1.3 The Coking Process and Coke Formation

Although coke was produced in British coalfields as a fuel for blacksmith's fires it was not until the beginning of the industrial revolution that there was a need for coke as a metallurgical fuel.

Coke had been used by Abraham Darby of Coalbrookdale for iron smelting early in the eighteenth century, although the hearth process and beehive oven were primitive processes of production. Indirectly heated slot ovens were used in the nineteenth century leading to the development of the modern coke oven. Coking takes from 12 to 80 hours. A ram pushes the coke into a quenching car and the oven is recharged making a fairly continuous process.

Considerable thermal and mechanical stress is imposed upon the coke which is eventually relieved by fissuring. The lumps of coke have a rounded "cauliflower" end, which was nearer the oven wall and a more reactive "chemical" end, nearer the centre of the oven. Low temperature carbonisation (450-700 ^{o}C) produces a reactive coke of the "Coalite" and "Rexco" type. Medium temperature carbonisation (750 - 900 ^{o}C) produces "Phurnacite" etc. and high temperature carbonisation

(900 - 1100 $^{\circ}$C) yields a hard unreactive coke for metallurgical use. Details are given in reference 7 and the manufacture of hard coke is reviewed by Barker and Lee[12].

As coal is heated in the absence of air it loses gases and vapours and leaves a solid porous residue of carbon containing some mineral matter.

Depending on rank, coking coals soften, become plastic and coalesce in the temperature range 350° to 500 $^{\circ}$C. The plastic mass resolidifies and as the temperature further increases it contracts at a rate that is non-uniform and dependent on coal type. This "semi-coke" has visco elastic properties up to about 700 $^{\circ}$C, but at higher temperatures becomes a brittle solid.

The behaviour of the parent coal in the plastic zone determines the inherent strength of the coke and resistance to abrasion whereas the primary and secondary fissure network, which is associated with impact strength depends upon the contraction stage.

These physical changes on passing from coal to coke are accompanied by chemical changes. During the plastic stage cross linkages between neighbouring aromatic groups are broken. Low molecular weight fractions can be lost as gas or tar while the higher molecular weight fractions form semi coke. As the temperature rises to 1000 $^{\circ}$C aromatic layers link and the coke becomes further cross linked and involatile. Layer growth of graphite type crystallites occurs although the structure is far from

8

"ordered" in the crystalline sense. Stacks of aromatic layers are present but are not mutually well orientated for further growth. Thus cokes may be graphitising or non graphitising forms of carbon. These transformations are described in more detail of Chapter 14 of reference 4.

Structural studies of the plastic stage were elucidated by the work of Brooks and Taylor[13]. Using reflected polarised light microscopy they showed that the ultimate crystallite alignment in cokes and graphites depended on the formation of spheres of optical anistropy growing, with increasing temperature and time, from a molten isotropic precursor. These spheres they named "mesophase". The mesophase spheres grow and coalesce into mosaic regions prior to the formation of a coke. Mesophase spheres were observed by these authors in a coal seam part of which had been transformed into coke by an igneous intrusion.

Coke formation in relation to the properties of liquid crystals has been described by Marsh et al[14].

Because high-volatile, weakly coking coals are cheaper and more widely available, the production of coke by non-classical methods has become important in many European countries. This involves the production of "formed coke" i.e. a uniform product made by a process involving briquetting at some stage.

Production, properties and potential advantages of formed coke are described by Metcalf[15]. Classification

of formed coke production and consideration of this

material in blast furnace trials are given by Barker[16].

The type of coke produced ;thus ; depends upon

(1) nature of the coal blends, (2) temperature and

duration of the coking process.

1.1.4 Coke Testing and Analysis

The chemical, physical and mechanical properties of

coke are evaluated by many methods, some standard and

widely employed. Data obtained from them may not be

particularly meaningful under operational conditions, as

pointed out by Wilkinson[17].

Industrial analysis of coke is often limited to

"proximate analysis", involving the determination of

moisture, ash, volatile matter and sulphur. Details with

lists of standard methods are given by Patrick and

Wilkinson[18]. Montgomery[19] also describes the standard

methods for "ultimate analysis". Trace elements are

determined by spectroscopic methods, principally atomic

absorption spectroscopy. Physical tests include density,

porosity (from density, mercury porosimetry and optical

microscopy) and apparent crystallite size from X-ray

line broadening.

Mechanical properties of coke are important in

assessing resistance to fracture and abrasion. In the

"shatter test" breakage is by impact alone and in the "drum

test" breakage is by impact and abrasion. This latter

method, by ASTM and Micum test, is more widely used.

Tensile strength, compressive strength and Young's Modulus are also determined. Details are given in the above references. Coke strength is related to bulk porosity and associated with structure within the cell walls of the coke.

1.1.5 Coke for the Zinc/Lead Blast Furnace

Coke acts as fuel, reducing agent and as support for the burden, being the only solid component in the hearth region. A coke of high mechanical strength but low reactivity is required.

The demands of the iron and steel industry dominate supplies of coke because the consumption of coke for zinc/lead production is a very small part of the total produced for metallurgical use. Changes in oven blends that have little effect in ferrous use often have damaging effect in the zinc/lead blast furnace.

Desirable properties of coke for the Imperial Smelting Furnace are given below. (From reference 15 of Chapter 2.)

Table 1.1   Target Coke Specification for the Zn/Pb Blast Furnace.

Size	90%	-80 + 60 mm
Strength	Half Micum	M40 + 75
		M10 - 10
Moisture	< 5%	
Ash (dry basis)	< 10%	

Volatile matter

(dry basis)   < 1%

reactivity   Nantgarw ratio 1.0

                    ECE k_m 0.10 cm^3 g^{-1} s^{-1}

general   very consistent

delivery   about 250 tonnes/day

cost   low.

These properties are described in detail by Bryson[20].

Imperial Smelting Processes Ltd.   use   a South Wales coke – Nantgarw coke. In reactivity testing the rate of weight loss of a coke is compared with that of Nantgarw and results expressed as the "Nantgarw ratio". South Wales cokes in general have low reactivity, making them ideal for zinc/lead production.

The effect of a too reactive coke is to allow the Boudouard reaction to proceed in the upper part of the shaft with consequent reduction in temperature. Less carbon reaches the hearth zone, ZnO is reformed from zinc vapour and more zinc is lost into the slag. Shaft operation becomes erratic and eventually "pipes" are formed in the shaft burden.

Small increases in reactivity can be tolerated (up to approximately a Nantgarw ratio of 2) the result being a higher carbon/zinc ratio, but at higher reactivities the furnace becomes difficult to operate.

Low reactivity coke is desirable in the iron blast furnace, but crucial in the zinc/lead blast furnace.

12

1.2.1 The Oxides of Carbon in Pyrometallurgy

Blast furnace processes rely on the existence of the lower oxide of carbon, CO.

Carbon is able to reduce the oxide of any other element, provided the temperature is high enough, although at the limit of the blast furnace, (about 1600 $^{\circ}$C) the reduction of Al_2O_3, MgO and CaO cannot occur.

The thermodynamic tendency for a process to occur is measured by the loss of Gibbs free energy $-\Delta G$. The graphical method of representing free energy changes, due to Ellingham[21] is of great use in collating data for metallurgical processes. The free energy of formation of oxides at a potential of one mole of oxygen at one atmosphere pressure is plotted against temperature. These plots are almost linear (enthalpy change ΔH and entropy change ΔS often vary oppositely with temperature), and since $(\frac{\partial \Delta G^{\circ}}{\partial T})_p = -\Delta S^{\circ}$ the slope of the plot gives the accompanying standard entropy change ΔS°.

Values for some metal oxides are given in Figure 1.1. ΔG° values for reactions which involve one mole of a common reactant (O_2) are plotted. As free energy is a thermodynamic function ΔG° for a reduction may be found by subtracting the values for one oxidation reaction from another at the appropriate temperature. Any metal oxide represented in Figure 1.1 will be reduced by a metal for which the ΔG° versus T line for the formation of oxide lies lower. (Provided there is no kinetic barrier to reaction.)

13
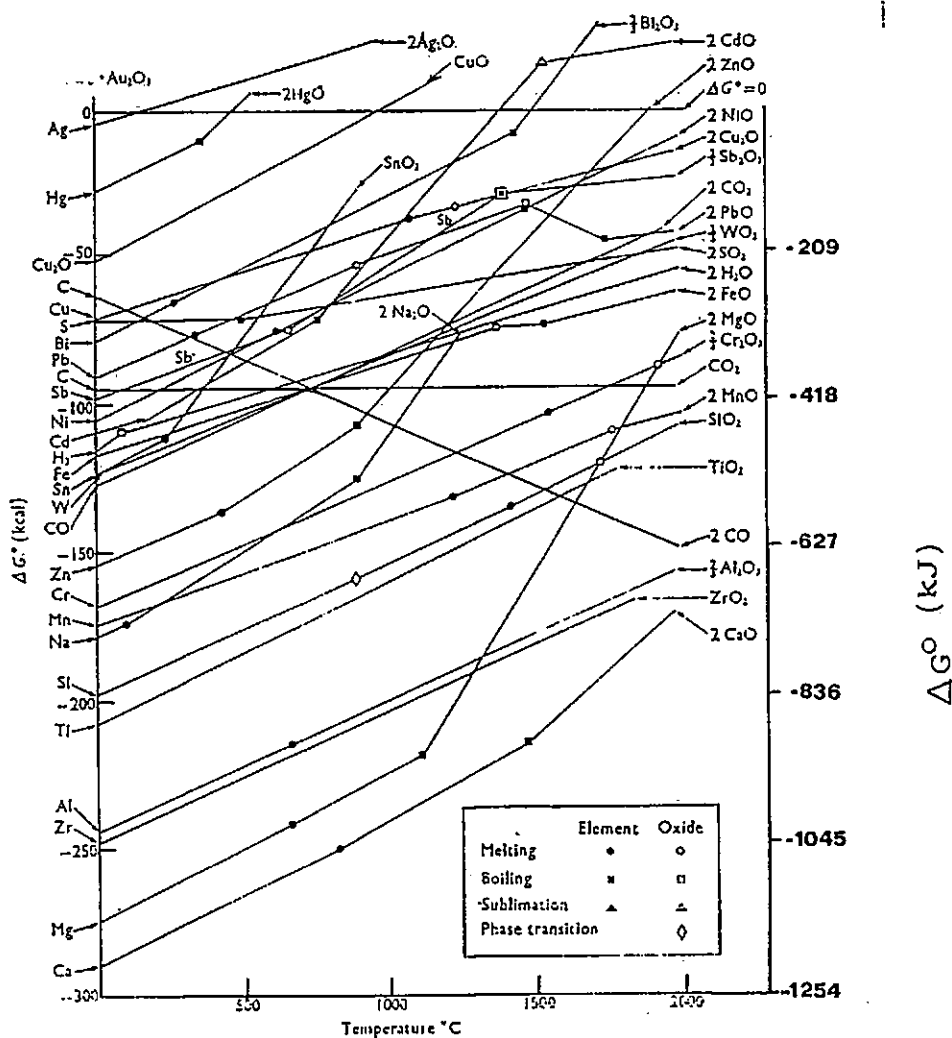
Figure 1.1 ΔG^O,T diagram for oxide formation
(after reference 23.)

diffusion from boundary layer
rate controlling

in-pore diffusion
rate controlling

LOG REACTION RATE

chemical rate
control

III   II   I

RECIPROCAL TEMPERATURE $\frac{1}{T}$
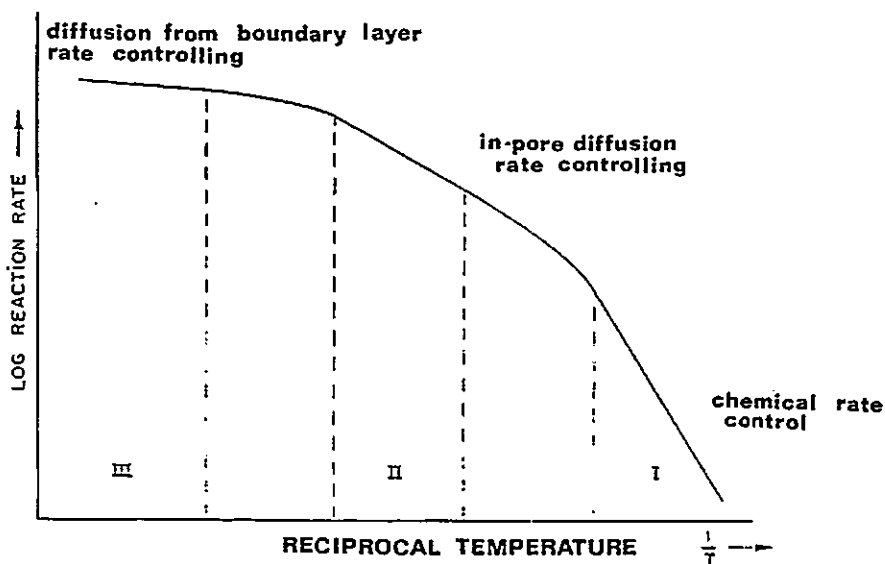
Figure 1.2. Idealised three zones representing the
change of reaction rate of a porous carbon with
temperature (after reference 40).

14

As shown in Figure 1.1 the two lines for the oxidation of carbon have negative slopes. From tabulated values of standard entropies the standard entropy changes ΔS^O for the oxidation of carbon may be calculated.

For $C(s) + O_2(g, 1\ atm) = CO_2(g, 1\ atm)$, ΔS^O is small ($0.8\ J\ K^{-1}$). This reaction will have little change in $-\Delta G^O$ over a wide temperature range.

For $2C(s) + O_2(g, 1\ atm) = 2CO(g, 1\ atm)$, ΔS^O is considerably higher ($170\ J\ K^{-1}$) making this reaction the more thermodynamically favoured the higher the temperature. The two lines intersect at about $710\ ^OC$. This is the lowest temperature at which CO_2 will gasify carbon, for the conditions considered, by the Boudouard reaction $C + CO_2 \rightleftharpoons 2CO$.

Although carbon is formally the reducing agent for metal oxides, reactions between solids can only occur where the surfaces meet. Reduction by CO is thus kinetically more favourable as it is a gas-solid reaction. CO acts as the reducing intermediary, the overall thermo-dynamics corresponding to reduction by carbon. As the temperature increases CO is able to reduce more metal oxides.

The application of Ellingham diagrams to the iron blast furnace are described by Mott[22], and to other pyrometallurgical processes by Ives[23].

The ΔG^O versus T lines change slope steeply at the boiling points of the metals due to greater entropy loss

accompanying oxidation. The reduction of ZnO proceeds above the boiling point of zinc (907 $^{\circ}$C). The rate of reaction of

$$ZnO + CO \rightleftharpoons Zn + CO_2$$
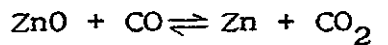
is faster than the Boudouard reaction, therefore the latter controls the rate of zinc production.

The older "zinc distillation" processes resulted in a film of oxide forming on the zinc droplets, by reversion of the former reaction, giving the product "blue powder". Liquid zinc cannot be obtained in a shaft furnace unless the pressure of the system is increased until the boiling point of zinc is shifted to the right of the intersection with the carbon line. This is not commercially practicable.

Although of great use, the free energy diagrams are not universally applicable. Blast furnace conditions may be far removed from equilibrium and processes may depend on kinetic rather than thermodynamic considerations.

1.2.2 The Blast Furnace

The blast furnace is a tall, vertical shaft furnace which employs carbon (in the form of coke) to extract metals such as iron, zinc and lead from their oxide ores at elevated temperatures. Theory and practice of the iron blast furnace is described by Peacey and Davenport[24].

Preheated air is introduced via the tuyeres and coke burns in this zone with release of heat.

$$C + O_2 = CO_2 \qquad \Delta H = -393 \text{ kJ mol}^{-1} \quad \ldots\ldots \text{ 1}$$

and $$2C + O_2 = 2CO \qquad \Delta H = -226 \text{ kJ mol}^{-1} \quad \ldots\ldots \text{ 2}$$
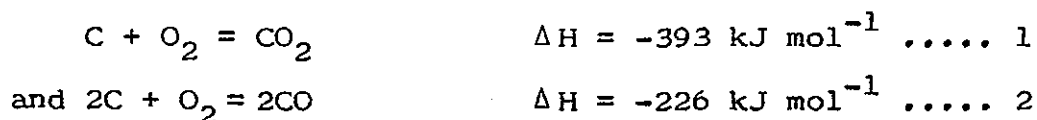
The CO_2 produced in reaction 1 will react with more coke by the Boudouard reaction.

$$CO_2 + C = 2CO \qquad \Delta H = +167 \text{ kJ mol}^{-1} \quad \ldots\ldots 3$$
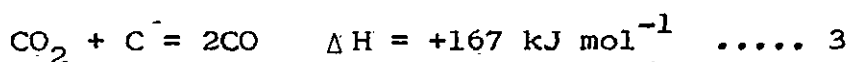
The overall reaction 2 is the sum of 1 and 3 by Hess's Law. The equilibrium constant of reaction 3 is large at high temperatures, so CO will predominate over CO_2 when carbon is present in excess. The exothermic nature of reactions 1 and 2 keeps the blast furnace processes going.

The extraction and refining of metals is described by Parker[25], from which reference the enthalpy values were taken.

The actual reduction of the metal oxide MO_n takes place via

$$MO_n(s) + nCO(g) = M(g \text{ or } l) + nCO_2(g) \quad \ldots\ldots 4$$

and the Boudouard reaction 3.

Reaction 4 is known as "indirect" reduction. Combining 4 and 3 gives $MO_h(s) + nC(s) = M + nCO(g)$ which is known as "direct" reduction. The historical background and controversy over these terms are reviewed by Mott.[22]

1.2.3 The Zinc/Lead Blast Furnace

Primary zinc has been produced by five main processes, four of them pyrometallurgical, as given in Table 1.2, of which the electrolytic and the Imperial Smelting Furnace have become the most important.

Table 1.2 Zinc Production[20]

Process	First Commercially Operated.
Horizontal distillation	1800
Electrolytic	1915
Vertical retort	1930
Electrothermic	1936
Imperial Smelting Furnace (I.S.F.)	1950

The I.S.F. is well established in eleven countries, producing about 12% of the world's zinc. The history of zinc smelting at Avonmouth, shaft reactions and zinc collecting and refining are given by Richards[26].

Lump coke and oxide sinter from the air roasting of sulphide ore concentrates are fed into the top of the shaft blown with preheated air. Temperature increases and conditions become more reducing as the hearth region is approached. The overall reduction reactions are

$$ZnO(s) + CO(g) = Zn(g) + CO_2(g) \quad \Delta H_{1200} = 185 \text{ kJ mol}^{-1}$$

..... 1

$$PbO(s) + CO(g) = Pb(l) + CO_2(g) \quad \Delta H_{1200} = -66 \text{ kJ mol}^{-1}$$

..... 2
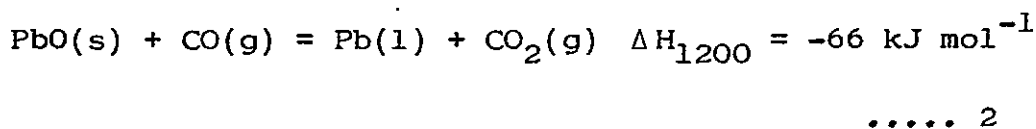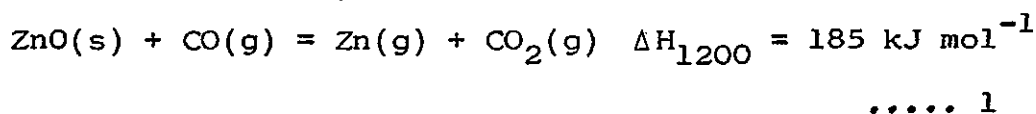
As reaction 1 is highly endothermic shaft temperature must be maintained above 1000 $^\circ$C or ZnO will be reformed. Some of the remaining CO is combusted with air above the charge level to ensure this

$$CO + 1/2O_2 = CO_2 \quad \Delta H = -280 \text{ kJ mol}^{-1}$$

18
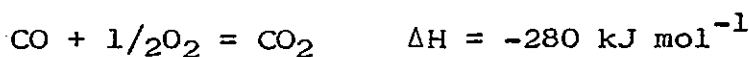
The reduction of lead oxide proceeds at moderate temperatures and is slightly exothermic so imposes no additional thermal load on the furnace. Enthalpy data are given by Hopkin and Richards[27], from which the ΔH values were taken. The reaction becomes more endothermic the higher the temperature due to the contribution of the latent heat of evaporation of zinc. The physical chemistry of zinc distillation is considered by Hopkins[28] and of the Imperial Smelting Process by Morgan[29], Lumsden[30] and Woods and Temple[31].

Gas leaves the furnace top at about 1000 to 1020 $^\circ$C with a composition[20]

Zn	6 to 7%
CO_2	9 to 12%
CO	21 to 24%
H_2	1 to 2 %
N_2	remainder.

The collection of zinc in the presence of oxides of carbon was a difficulty in blast furnace practice until the introduction of the I.S.F. The furnace gases are passed into a lead splash condenser where the zinc is absorbed in a shower of molten lead droplets. The liquid lead is cooled to 450 $^\circ$C, when the maximum solubility of zinc is 2.15%. Because of this limited mutual solubility the lead and zinc separate. Lead is recycled to the condenser and the zinc is cast.

19

Lead from the furnace reduction of PbO, and slag are tapped at the hearth, into a fore hearth which allows separation of the molten phases. Amounts of Cu, Sb, Bi, Sn, Ag and Au are present in the lead.

Reducing conditions in the hearth zone must not become so strong as to reduce iron oxides in the slag or blockage by irony accretions occurs. Some of the ZnO enters the molten slag where some direct reduction may occur by

$$ZnO(l) + C(s) = Zn(g) + CO(g).$$
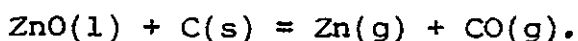
This reaction, the thermodynamics of the zinc blast furnace and the recovery of copper are considered by Yazawa and Azakami[32]. Heat balance for the zinc/lead furnace is given by Richardson[33].

Hopkin[34] compares the energy requirements of zinc production processes. Increase in the cost of coke is unlikely to exceed increases in cost of electrical power needed in the electrolytic process.

Just under one tonne of coke liberates one tonne of zinc and half a tonne of lead and continued economies are made by improvements in flow patterns throughout the system as reviewed by Davey and Willis[35]. Past and future progress is considered by Harris and Richards[36].

1.3.1 Gas-solid Reactions

"Gasification" reactions are of the type

solid + gas $\rightarrow$ gas

Gas-solid reactions are important in the extraction of metals, the combustion of fuels, coal gasification, refuse incineration etc.

For reactions involving porous solids (which includes most industrial forms of carbon) the overall process may involve

(1) Gaseous diffusion (mass transfer) from the bulk of the gas to the external surface of the reacting solid

(2) Diffusion through pores of the partially reacted solid or of a solid reaction product

(3) Adsorption

(4) Chemical reaction

(5) Desorption of products

(6) Escape of products by the reverse of (2) and (1).

The kinetics of a reaction may thus depend upon external mass transfer, pore diffusion, adsorption/desorption and chemical reaction. Heat transfer and structural changes such as sintering and cracking may also be involved. Numerous mathematical models involving surface structure have been applied, as detailed with many industrial applications by Szekely et al[37].

The factors affecting the rate of reaction may assume different relative importance if temperature, particle size etc. are changed. Where transfer of gas to reaction sites in a solid is easy (e.g. small particle size, large

pore size) the reaction is likely to be controlled by a chemical step. Where a chemical reaction is favoured (e.g. at high temperatures) the rate may be limited by the arrival of gas molecules i.e. diffusion controlled. At temperatures between these limits a process may be under "mixed control".

1.3.2 Non Porous Solids

If the solid reactant is non porous reaction occurs at a sharp interface and systems may be described in terms of simple geometrical models. This approach also may be a useful first approximation in the study of porous solids.

Progress of a reaction is controlled by shrinkage of the interface in the chemical rate regime and the surface is one of the boundary conditions in the diffusion controlled regime. A shape factor F, which may be observed visually if the particles are large enough, can be considered.

Where diffusion effects are absent a conversion function for a reaction $f_F(\alpha)$ may then be defined such that $f_F(\alpha) = 1 - (1 - \alpha)^{\frac{1}{F}}$.

Where α represents the fraction of solid reacted and F = 1, 2 and 3 for infinite slabs, long cylinders and spheres respectively.

F can be obtained as the value that gives a straight line between the experimental values of $f_F(\alpha)$ and reaction time t.

The conversion function $f_F(\alpha)$ is given by the dimensionless quantity:-

$$\frac{\text{time } (t)}{\text{time of complete reaction } (t_{\alpha = 1})}$$

thus $\dfrac{t}{t_{\alpha = 1}}$ = 1 - (fraction remaining)$^{\frac{1}{F}}$

A straight line for a plot of experimental data using this equation does not necessarily mean that the rate is controlled by chemical reaction. The effect of particle size on time to reach a given extent of reaction yields additional evidence. This is proportional to d^2 for diffusion control, d for chemical control of non-porous material and independent of d for chemical control of porous material, where d is the particle diameter.

Where rate of reaction is controlled by diffusion through reactant or product layer the conversion factor $g_F(\alpha)$ is given by

$$g_F(\alpha) = \begin{cases} \alpha^2 & \text{for F = 1 \quad (infinite slabs)} \\ \alpha + (1-\alpha)\ln(1-\alpha) & \text{for F = 2 \quad (long cylinders)} \\ 1-3(1-\alpha)^{2/3}+2(1-\alpha) & \text{for F = 3 \quad (spheres)} \end{cases}$$

Plotting the conversion data according to an assumed mechanism and finding a reasonable straight line fit does not always give an unambiguous result. Both chemical and diffusional factors may operate. These equations are derived and discussed in detail by Szekely et al[37].

Other equations have been used in representing diffusion controlled gas-solid reactions.

23

(i) The Jander equation for a spherical solid reacting under diffusion control

$$\frac{kt}{r^2} = \left[1 - (1-\alpha)^{\frac{1}{3}} \right]^2$$

where k is a constant, α and t as above and r the radius of the sphere. Applications of the Jander equation are given by Budnikov and Ginstling[38].

(ii) Where product and reactant differ in volume Carter[39] proposed

$$\frac{Z - \left[1+(Z-1)\,\alpha \right]^{2/3} - (Z-1)-(1-\alpha)^{2/3}}{2(Z-1)} = \frac{k't}{r^2}$$

where r is the initial radius of the particle k' a constant, α the fraction of solid reacted and Z the ratio of final volume of product to initial volume of reactant. This reduces to the Jander equation for $Z = 1$. The Jander equation assumes that the product layer round the spherical particle is flat, which holds at low conversion rates. Szekely et al[37] compare the Jander equation with exact solutions for slab and sphere models.

In the derivation of these equations it is assumed that the shrinking unreacted core is non-porous. It is useful to apply this to coke and char gasifications, where the ash forms a more or less porous layer round a shrinking core, depending on temperature.

Metallurgical cokes contain about 10% mineral matter which remains as ash; chars generally contain less. Temperature will affect the ash layer in that above

24

$\frac{Tm}{3}$, surface diffusion (in which coalescence of particles by movement of species along the surface) will occur and above $\frac{Tm}{2}$, sintering (bulk diffusion) will occur, where T_m is the melting point in Kelvin.

1.3.3 Porous Solids

Here diffusion and chemical reaction occur throughout the solid and analysis of experimental data is difficult in exact parameters.

Reaction occurs in a diffuse zone rather that at a sharp boundary, as described for the gas reactions of carbon by Walker et al[40]. Three kinetic zones may be distinguished as shown in Figure 1.2.

In Zone I the chemical reactivity of the solid controls the rate of reaction. The concentration of gas is the same within the pores as in the bulk gas stream. The energy of activation E_A and other kinetic parameters have their intrinsic values and rate does not depend on sample size. Pores are enlarged during reaction but the solid particle remains of the same overall size until almost completely consumed. Total surface area may be linked to extent of reaction in this zone only.

At higher temperatures, Zone II, a gas molecule reacts before penetrating deeply. Gaseous diffusion influences rate and is proportional to $\sqrt{D_e}$, where D_e is the effective diffusion coefficient. E_A falls to approximately half its intrinsic value and apparent order of reaction, n, changes to $\frac{(n+1)}{2}$. Reaction occurs

close to the outer surface of the solid and the core remains unaffected.

At still higher temperatures, Zone III, gas molecules react with the surface at the boundary and rate depends on mass transfer of the gas, which increases only little with temperature. The solid particle shrinks during reaction. Porosity is relatively unimportant and rate expressions derived for non porous solids may be applied.

Parameters describing these kinetic zones are detailed for the carbon-oxygen reaction by Mulcahy[41] with regard to coals and coal chars.

There is a gradual change from one zone to the next on increasing temperature, the ranges depending on pore diffusivity etc. The effective gas diffusivity is made up of several factors. Where pores are small the mean free path of molecules becomes comparable with pore dimensions. "Knudsen diffusion" rather than molecular diffusion is important. The laws of molecular (bulk) diffusion are independent of the material considered but diffusion in "real" systems is more complex and specific to the nature of the substance investigated.

The porosity of coals and coal products is reviewed by Mahajan and Walker[42]. Origins and characterization of microporosity in carbons are reviewed by Marsh and Rand[43].

1.3.4 Sintering

Sintering is the process by which small particles of a solid form larger aggregates when the solid is held at elevated temperatures below its melting point. It is of great importance in ceramics and powder metallurgy. The volume of the solid is much reduced, although the density is less than that of a single crystal as some voids and pores still remain.

Sintering is a complex phenomenon usually considered to occur in three stages, as shown schematically below.
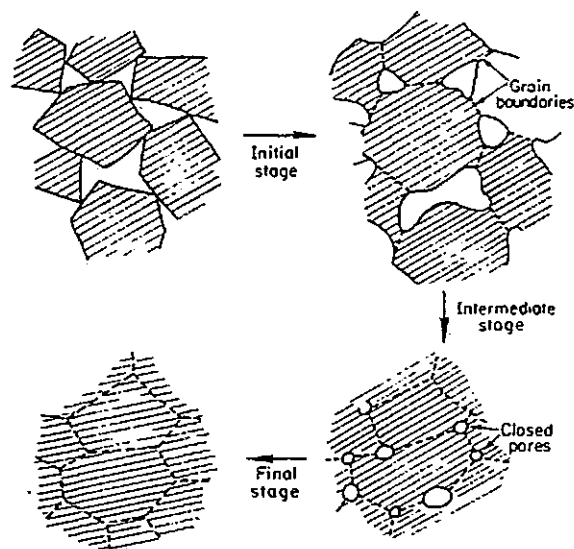
The initial stage is accompanied by an increase in mechanical strength and grain size and a decrease in electrical resistivity.

The activation energy for sintering is high. It takes place at an appreciable rate above 0.4 to 0.5 of the thermodynamic temperature of the melting point of the

solid (the Tammann temperature).

Solids are thought to sinter via grain boundary or volume diffusion (surface diffusion is possible at lower temperature). Vacancies at the particle surfaces diffuse through the bulk to disappear at grain boundaries, i.e. there is a net flow of atoms from grain boundaries to pores. The grain boundary is a sink for vacancies and alteration of vacancy concentration, e.g. by impurities, affects the rate of sintering. This effect in metal oxides is described by Hannay[44].

The kinetics of sintering by migration of vacancies to grain boundaries is given by Kingery[45]. As sintering rate depends inversely on the third power of particle size large effects can be introduced by grinding.

The driving force for sintering is the decrease in surface free energy. A compact of powder particles has an excess surface energy and sintering brings about reduction in the total interfacial energy by a reduction in surface area. Thus sintered material has a smoothed, rounded surface.

The surface energy of solids is more complex than that of liquids, making modelling of sintering processes difficult. Sintering theory is reviewed by Coble[46] and various models are discussed by Waldron and Daniell[47].

The temperature at which sintering will become appreciable can thus be determined from the melting point of a solid. Unlike ceramic materials, carbon will not sinter at the temperature of industrial processes.

28

1.4.1 Fundamental Nature of the C/O₂ and C/CO₂ Reactions

Under fixed experimental conditions the rate of removal of carbon atoms from a surface by a reacting gas depends upon the nature of the gas and the nature of the carbon. This poses many difficulties in an understanding of gas-carbon reactions at a fundamental level. Although simple stoichiometric equations may be written for the reaction of carbon with O_2, CO_2, H_2O and H_2 their kinetic complexity, particularly of the C/O₂ reaction has long been known.

The thermodynamics and kinetics of these gasifications are definitively reviewed by Walker, Rusinko and Austin[40]. At elevated temperatures and for all forms of carbon, rate of reaction is greatest in oxygen and least in hydrogen as given below (from ref.40).

Approximate Relative Rates at 800 $^{\circ}$C and 0.1 atm. pressure

C/O_2	1×10^5
C/H_2O	3
C/CO_2	1
C/H_2	3×10^{-3}

Rates are generally given as weight burnt-off per initial weight in unit time. Absolute rates depend on the nature of the carbon, traces of impurities etc. Much work has been done using single crystal graphite and synthetic (polycrystalline) graphite where it is possible to

distinguish reaction on defined crystallographic planes. Physical effects such as diffusion (which may be absent only at very low pressures) also significantly affect reactivity studies.

In gas-carbon reactions it is generally accepted that one of the steps is chemisorption of the gas to form a surface complex. The nature and role of these surface complexes is discussed by Puri[48] for graphites, chars and carbon blacks. The stability of surface oxygen complexes even at low pressures and high temperatures is emphasised. It is thought that there are separate CO and CO_2 forming sites.

The Carbon-Molecular Oxygen Reaction

It is accepted that CO, CO_2 and surface oxide complexes are primary products of the reaction, the ratio CO/CO_2 depending on several factors. This ratio was investigated using mass spectrometry by Marsh and Foord[49] who found it dependent upon the structural parameters and purity of the carbon. They postulate the formation of a stable surface oxide complex $C(O_2)^*$, which then becomes mobile and reacts by the following scheme,

$$C+O_2 \rightarrow C(O_2)^*$$
$$C(O_2)^* + C \rightarrow C(O) + C(O) \rightarrow C+CO_2$$
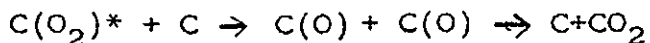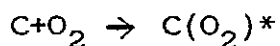
$$\text{mobile oxide}$$
$$\text{complexes}$$

i.e. lowering the surface oxide mobility raises the CO/CO_2 ratio. The more perfect the structure of the surface (achieved e.g. by high temperature treatment), the more mobile the complex and the more CO_2 is produced. These authors point out that microporosity is associated with high CO/CO_2 ratios, under comparable conditions of oxidation.

Studies using $^{16}O_2$ and $^{18}O_2$ show the mobility of the surface complexes.

The idea of "active surface area" in the C/O_2 reaction in relation to total surface area is discussed by Laine, et al[50] and Walker[9] proposes a rate equation in terms of active surface area, which for a graphitic carbon may be a few percent of the B.E.T. surface area. Active sites are thought to be located at edges of basal planes of carbon crystallites and defects within basal planes. Nascent active sites are produced during gasification.

The significance of kinetic results for the oxidation of graphite at low oxygen pressures and high temperatures is discussed by Strickland-Constable[51] in terms of defects and surface sites. The temperature coefficient of reaction passes through a minimum, considered to be due to annealing of reactive sites at higher temperatures by surface diffusion of carbon atoms.

Mechanisms for the reaction including many stages involving chemisorbed mobile or localised oxygen atoms have been postulated and are reviewed by Marsh[52].

Rate expressions are derived with the aim of relating mechanism to measurable kinetic parameters, but the porosity and impurity content of many of the carbons studied has led to a wide variation in values reported. "True" activation energies have been suggested as given below.

Table 1. Activation Energy for the Reaction $C + \frac{1}{2}O_2 \rightarrow CO$
   (with pure graphite).

Value	Reference
209 to 243 kJ mol^{-1} (50 to 58 kcal mol^{-1})	40
255 $\pm$ 13 kJ mol^{-1} (61 $\pm$ 3 kcal mol^{-1})	59
239 kJ mol^{-1} at 1.3 kPa pressure	9

The value for "impure carbons" is given as 130 to 170 kJ mol^{-1} (30 to 40 kcal mol^{-1}). [41]

The rate of oxidation of carbon atoms at prismatic edges is 10^2 to 10^3 faster than at basal planes. The difference in activation energies, using gold decoration in transmission electron microscopy, was studied by Evans and Thomas[53]. Hennig [54] developed this technique in the 1960s to enlarge vacancies in graphite basal planes during exposure to oxygen. Oxidation at point defects of graphite by Thomas[55] showed that not all crystallographic planes oxidize at the same rate, explaining some of the topographical features on oxidation large enough to be seen under the optical microscope.

Phase contrast, high resolution transmission electron microscopy has also been used in the study of carbons on oxidation, giving detailed information on the degree of ordering of constituent molecules. The technique and some problems of interpretation are described for some graphitizing carbons by Marsh and Crawford[56] and by Fryer[57]. The latter study describes surface structure and pore sizes. Theoretically it should be possible to image periodicities in carbon above $3\mathring{A}$ (0.3 nm). Lattice resolution is reviewed by Millward and Jefferson[58].

The study of the carbon/oxygen reaction has been extensive. Reviews are given by Marsh[52], Thomas[55] and Lang and Magnier[59].

Work using industrial carbons such as cokes and chars has been done on materials, and under conditions far removed from those of fundamental studies.

The Carbon-Carbon Dioxide Reaction (Boudouard Reaction).

Kinetic considerations in gas-solid adsorption yield the Langmuir isotherm, which relates surface coverage to pressure of adsorbate gas (assuming ideal gas laws) at a constant temperature.

Reactions of carbon with O_2, CO_2 etc. can only occur at the gas-solid interface and may involve the six consecutive steps outlined in 1.3.1. In heterogeneous reactions Langmuir assumed that surface reaction of the chemisorbed species is rate determining, that adsorption and desorption processes reach equilibrium and that the

concentrations of adsorbed reactants may be estimated using the Langmuir isotherm. Many of the rate laws found experimentally are predictable using mechanisms based on this treatment and are known as Langmuir-Hinshlewood mechanisms.

Consideration of the order and molecularity of heterogeneous reactions leads to rate laws which may reduce to a simpler form when reactant and product are strongly and weakly adsorbed respectively or vice versa. These rate laws and activation energy ranges are treated by Wilkinson[60].

When CO_2 is chemisorbed on carbon CO is an immediate product and CO_2 is not reversibly desorbed. Adsorbed CO_2 and CO are likely to be shortlived species.

In the late 1940s Long and Sykes[61] postulated a mechanism in which CO_2 reacts with the carbon surface to give an adsorbed oxygen atom and CO which passes into the gas phase

$$CO_2 + C \rightarrow C(O) + CO \quad \ldots\ldots\ldots \quad 1$$
gas surface surface gas
     oxide
     complex
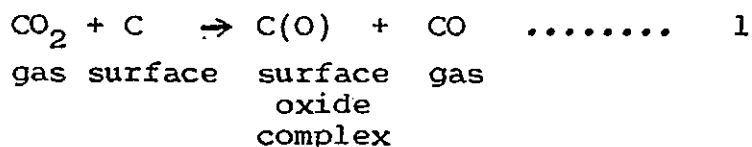
This oxide complex then decomposes to CO

$$C(O) \rightarrow CO \quad \ldots\ldots\ldots\ldots\ldots \quad 2$$

Some CO may also be adsorbed on the carbon surface

$$C + CO \rightleftharpoons C(CO) \quad \ldots\ldots\ldots\ldots \quad 3$$

The formulae in brackets denote species adsorbed on the carbon surface, which may be only a small fraction of the total surface. CO is known to have a pronounced

34

retarding effect in the oxidation of carbon by CO_2.

Such a reaction sequence yields a rate expression of the form

$$\text{rate} = \frac{K_1 P_{CO_2}}{1 + K_2 P_{CO} + K_3 P_{CO_2}}$$

Where p_x denotes partial pressure of gas X and K_1, K_2 and K_3 are functions of one or more rate constants. Several possible mechanisms give this rate law. Derivation and discussion are given by Walker et al[40], with possible inhibiting pathways for CO.

Adsorbed CO may compete for active sites that would otherwise be occupied by C(O) (reaction 3) or the adsorbed surface oxide C(O) may react with gaseous CO to give again CO_2 (i.e. the reverse of reaction 1.)

$$\underset{\text{surface}}{C(O)} + CO \rightarrow C + \underset{\text{surface}}{CO_2} \quad \dots\dots\dots\dots\dots \quad 4$$
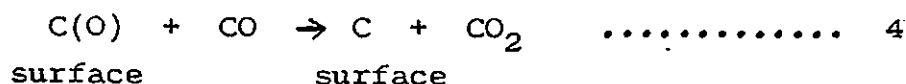
Reif[62] has shown that the experimentally verified rate expression can only be produced by considering steps 1, 2 and 4 or 1, 2 and 3 and concludes that retardation occurs by the reverse of step 1, i.e. the former sequence. The reaction mechanism is discussed by Ergun and Mentser[63]. Detailed investigation of the kinetics of the reaction by the same authors[64] shows that decomposition of the surface oxide is the rate controlling step.

Thus for the mechanism of carbon gasification by CO_2 the sequence may be represented by

$$C + CO_2 \xrightleftharpoons[k_3]{k_1} C(O) + CO$$

$$C(O) \xrightarrow{k_2} CO$$
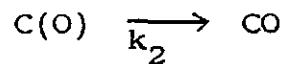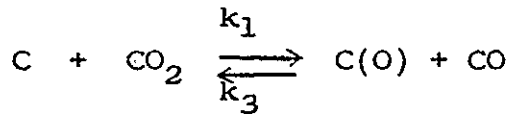
where k represents an intrinsic rate constant.

If Θ is the fraction of carbon surface occupied by chemisorbed oxygen atoms, then a steady state will be reached at which the rate of formation of C(O) on unit effective surface equals its rate of removal

ie $\quad k_1 P_{CO_2}(1-\Theta) = k_3 P_{CO}\Theta + k_2\Theta$

$$k_1 P_{CO_2} - k_1 P_{CO_2}\Theta = k_3 P_{CO}\Theta + k_2\Theta$$

and $\quad \Theta = \dfrac{k_1 P_{CO_2}}{k_1 P_{CO_2} + k_3 P_{CO} + k_2}$

The overall rate of gasification is $k_2\Theta$

so rate $= \dfrac{k_1 P_{CO_2}}{1 + \dfrac{k_1}{k_2}P_{CO_2} + \dfrac{k_3}{k_2}P_{CO}}$

If $K_1 = k_1$

$\quad K_2 = \dfrac{k_3}{k_2}$

and $K_3 = \dfrac{k_1}{k_2}$

then rate $= \dfrac{K_1 P_{CO_2}}{1 + K_2 P_{CO} + K_3 P_{CO_2}}$

Which is the well known Langmuir-Hinshlewood rate
expression. Thus K_2 refers to the competition between
reformation of CO_2 and bonding of the surface oxide to
carbon and forming one molecule of CO. K_3 refers to the
competition between adsorption of CO_2 and chemical bonding
of the sorbed complex to give the second molecule of CO.

As CO_2 is a linear molecule the influence of the
carbon surface is to break one C to O bond. How this may
come about in terms of charge transfer mechanisms within
the carbon lattice is considered by Franke and Meraikib[65].

The C/CO_2 reaction is reviewed by Lang and Magnier[59].
A "true" activation energy of 360 kJ mol^{-1} (86 kcal mol^{-1})
has been suggested[40], a higher value than for C/O_2
gasification. The overall gasification rate is controlled
not by the rate of formation of the surface complex but
by its rate of removal or rearrangement to a desorbable
product. It is pointed out[40] that the formation of a
surface oxygen complex is exothermic, more so for C/O_2
than for C/CO_2. This excess energy could determine the
lifetime of the surface complex and the extent of cover.
If the overall energy of activation is determined by the
desorption step this would lead to a higher value for the
C/CO_2 reaction than the C/O_2 reaction.

1.4.2 Other factors Influencing Gas-Carbon Reactions

Orientation of crystallites and their size, heat
treatment surface area, presence of impurities etc. may
influence a rate of reaction. Impurities can either
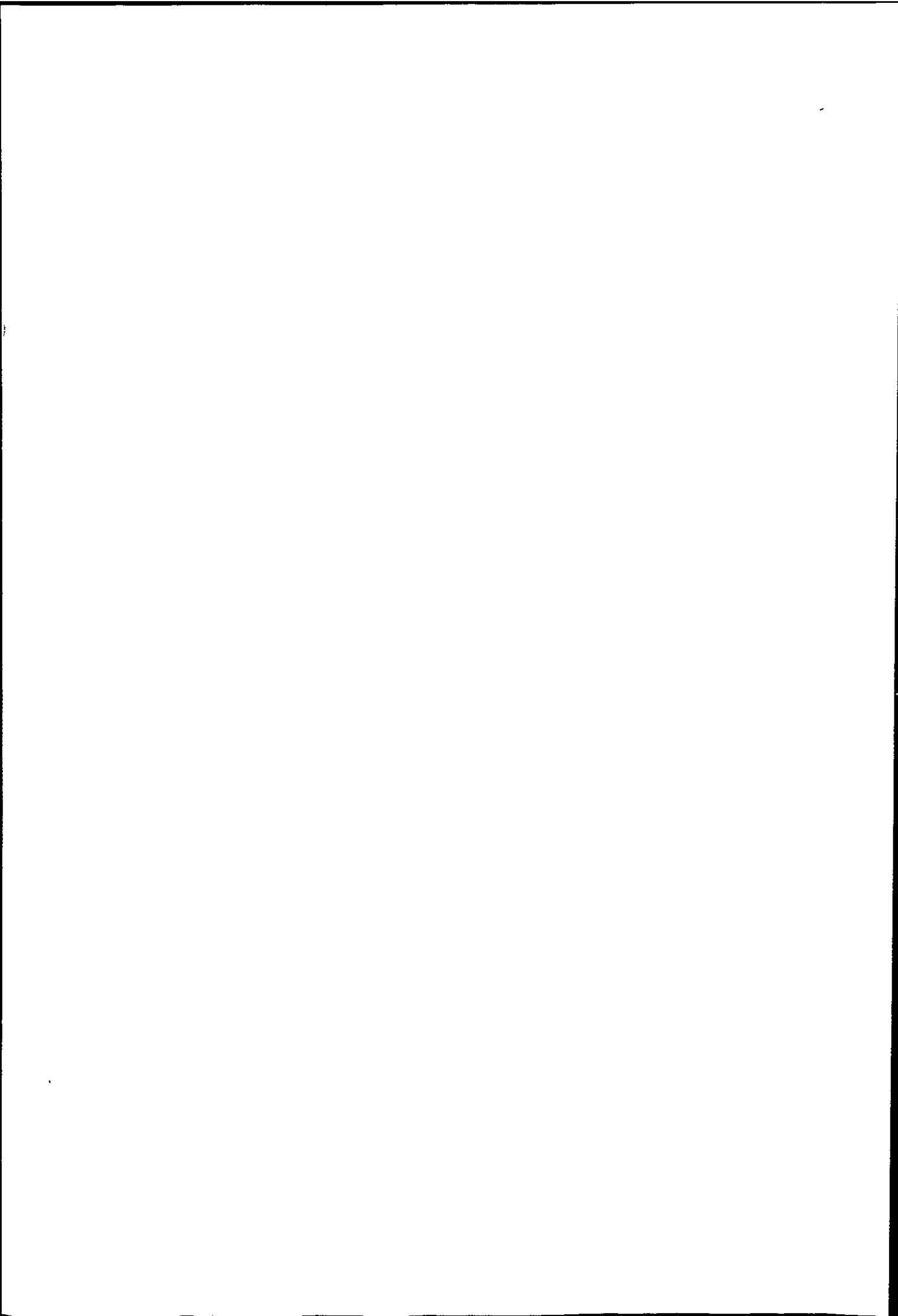
accelerate or retard carbon reactivity, depending upon amount and location in the carbon lattice.

Walker and Rusinko[66] investigated the gasification of carbon rods with CO_2 between 900 and 1300 ^{O}C. No correlation between rate of reaction and any physical property investigated was found. Transient phenomena in the gasification of very pure well out-gassed graphite with CO_2 were investigated by Shelef and Walker[67]. Kinetics were explained in terms of two types of surface oxide differing in reactivity. The development of steps and etch pits during the initial gasification was suggested giving a surface with vacancies and defects and therefore of higher chemical reactivity. The high initial (transient) rates were susceptible to traces of CO and H_2.

Thus even with "pure carbons" the mechanism of reaction and rate determining steps in gasifications can seldom be assigned unambiguously.

REFERENCES

1. International Tables for X ray Crystallography,
    Volume I, 1965, The Kynoch Press.

2. R.B. Heslop and P.L. Robinson. "Inorganic Chemistry"
    3rd Ed. 1967, Elsevier.

3. Proceedings of the 5th London International Carbon
    and Graphite Conference, Volume III, SCI London,
    99-184.

4. D.W. Van Krevelen. "Coal. Typology, Chemistry,
    Physics and Constitution."Volume 3 of Coal Science and
    Technology, 1981. Elsevier.

5. C. Karr, Jr. (Ed.), "Analytical Methods for Coal and Coal
    Products". Vol. I and II, 1978. Vol. III 1980, Academic
    Press.

6. S. Ergun, "Chemistry and Physics of Carbon", 3, 1967,
    P.L. Walker, Jr. (Ed.), Marcel Dekker N.Y. 211-86.

7. G.J. Pitt & G.R. Millward "Coal and Modern Coal
    Processing: An Introduction", 1979, Academic Press.

8. V. Bouska, "Geochemistry of Coal". Volume I of Coal
    Science and Technology, 1981. Elsevier.

9. P.L. Walker, Jr. Chemistry and Industry, 1982, No.18,
    683-91.

10. J.J. Kipling & P.V. Shooter, Proc. 2nd Industrial
    Carbon and Graphite Conference, 1965, SCI London, 15-19.

11. W. Hyslop, Coke Oven Managers Yearbook, 1974, 285-98.

12. J.E. Barker & G.W. Lee, The Mining Electrical and
    Mechanical Engineer, 1967, 1-11.

13. D.J. Brooks & G.H. Taylor, "Chemistry and Physics of
    Carbon", 4, 1968. P.L. Walker Jr. (Ed.), Marcel Dekker
    N.Y.

14. H. Marsh, F. Dachille, J. Melvin & P.L. Walker, Jr.
    Carbon, 1971, 9, 159-77 and C. Cornford & H. Marsh.
    Extended abstracts, 4th London International Carbon
    and Graphite Conference 1974, SCI. 6-7.

15. A.J.H. Metcalf, The Coke Oven Managers Yearbook, 1973,
    163-82.

16. J.E. Barker, J. Iron and Steel Institute, 1971, 100-8.

17. H.C. Wilkinson, Coke Oven Managers Yearbook, 1974,
    145-62.

18. J.W. Patrick and H.C. Wilkinson, Chapter 29 of
    "Analytical Methods for Coal and Coal Products",
    Volume II, 1978, Karr (Ed.), Academic Press, 339-70.

19. W.J. Montgomery, Chapter 6, "Analytical Methods for
    Coal and Coal Products", Volume I, 1978, Karr (Ed.),
    Academic Press. 191-229.

20. J.L. Bryson, Coke Oven Manager's Yearbook, 1972,
    267-87.

21. H.J.T. Ellingham, J.Soc. Chem. Ind. 1944, 63,125-33.

22. R.A. Mott, Steel Times Annual Review, 1977, 843-74.

23. D.J.G. Ives, "Principles of the Extraction of Metals",
    RIC Monographs, No.3, 1969, The Royal Institute of
    Chemistry.

24. J.G. Peacey & W.G. Davenport, "The Iron Blast Furnace.
    Theory and Practice", 1979, Pergamon Press.

25. R.H. Parker, "An Introduction to Chemical Metallurgy",
    2nd edition, 1978. Pergamon Press.

26. A.W. Richards, Mining Magazine, 1975, 133, 79-87.

27. W. Hopkin and A.W. Richards, J. Metals, 1978, 30 Part II. 12-17.

28. D.W. Hopkins, Chapter 9, "Physical Chemistry and Metal Extraction", 1954, reprinted 1961, J. Garnet Miller Ltd.

29. S.W.K. Morgan, Trans. Inst. Min. Met. 1956-7, 66, 553.

30. J. Lumsden, "The Physical Chemistry of the Zinc Blast Furnace", 1972, H.M.S.O. London.

31. S.E. Woods & D.A. Temple, Trans. Inst. Min. Met. 1964-5, 74, 297.

32. A. Yazawa & T. Azakami, Canadian Metallurgical Quarterly 1969, 8, No.4, 313-8.

33. F.D. Richardson, Trans. Inst. Min. Met. 1967, 76, 51-67.

34. W. Hopkin, "Energy Considerations in Electrolytic Processes", 1980. SCI London, 43-52.

35. T.R.A. Davey & G.M. Willis, J. Metals, April 1981, 52-66.

36. C.F. Harris & A.W. Richards, 104th A.I.M.E. Meeting 1975, New York.

37. J. Szekely, J.W. Evans & H.Y. Sohn, "Gas Solid Reactions", 1976, Academic Press.

38. P.P. Budnikov and A.M. Ginstling, "Principles of Solid State Chemistry Reactions in Solids". 1968, Maclaren and Sons Ltd., London.

39. R.E. Carter, J. Chem. Phys. 1961, 35, 1137.

40. P.L. Walker, Jr., F. Rusinko, Jr., & L.G. Austin, Advances in Catalysis, 1959, 11, 133-218. Academic Press.

41. M.F.R. Mulcahy, "Oxygen in the Metal and Gaseous Fuel Industries". Plenary Lectures of the First BOC Priestly Conference 1977, The Chemical Society, 1978, 175-208.

42. O.P. Mahajan & P.L. Walker, Jr., "Analytical Methods for Coal and Coal Products", Volume 1, Chapter 4, Karr (Ed.). 1978. Academic Press.

43. H. Marsh & B. Rand, Proc. 3rd Conference Industrial Carbons and Graphite 1970, SCI London, 172-83.

44. N.B. Hannay, "Solid State Chemistry", 1967, Prentice-Hall Inc.

45. W.D. Kingery, "Introduction to Ceramics", 1960, John Wiley.

46. R.L. Coble, "Sintering and Related Phenomena", Materials Science Research Vol. 6, 1973, G.C. Kuczynski (Ed.) Plenum Press, 177-190.

47. M.B. Waldron & B.L. Daniell, "Sintering" 1978, Heyden.

48. B.R. Puri, "Chemistry and Physics of Carbon", Volume 6, 1970. P.L. Walker, Jr., (Ed.) Marcel Dekker N.Y.

49. H. Marsh & A.D. Foord, Carbon, 1973, 11, 421-4.

50. N.R. Laine, F.J. Vastola & P.L. Walker, Jr. J. Phys. Chem. 1963, 67, 2030.

51. R.F. Strickland-Constable, Proc. 2nd Conf. Industrial Carbon and Graphite, 1965, SCI London, 235-42.
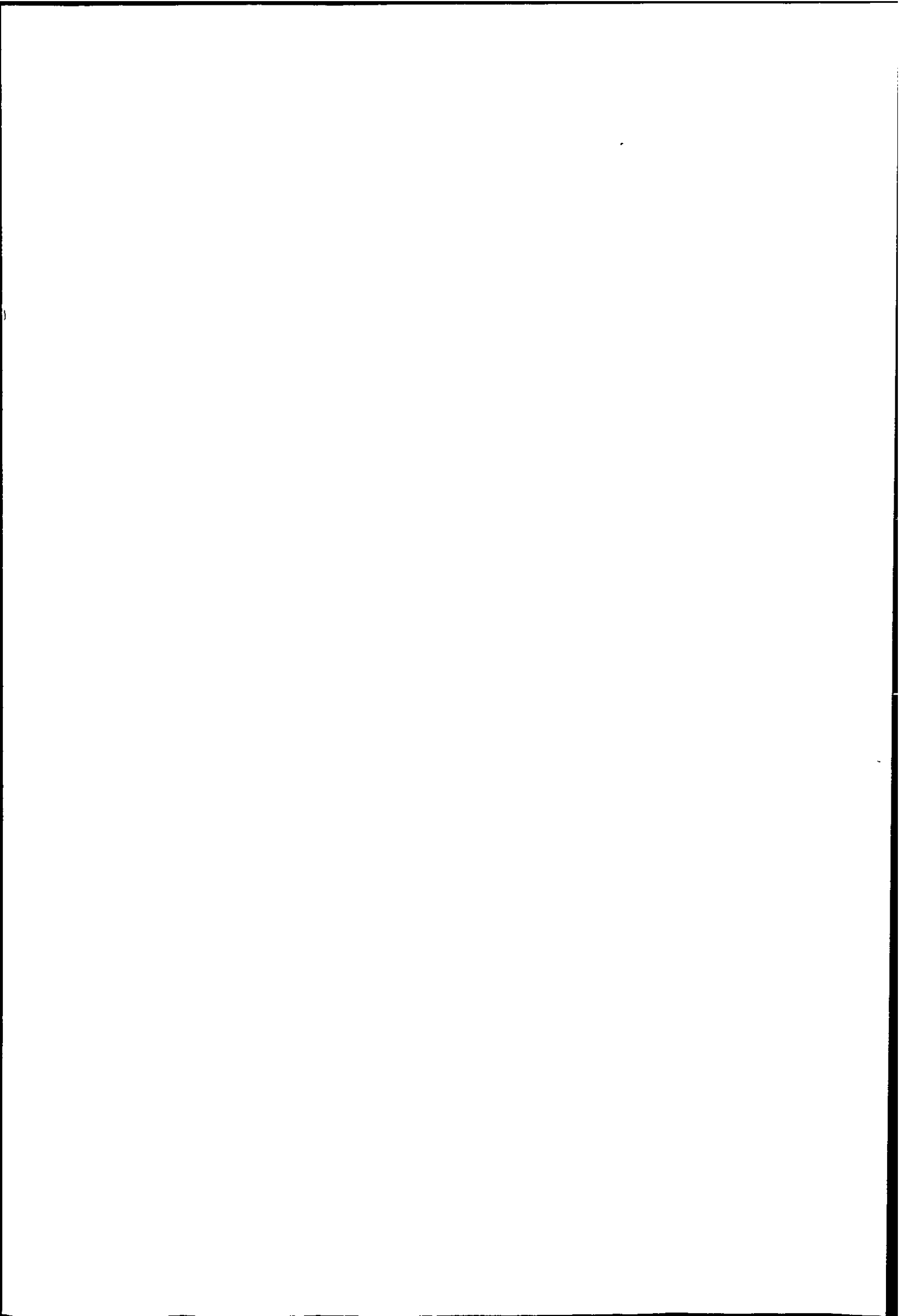
52. H. Marsh, "Oxygen in the Metal and Gaseous Fuel Industries", Plenary Lectures of the First BOC Priestly Conference 1977. The Chemical Society 1978. 133-74.

53. E.L. Evans & J.M. Thomas, Proc. 3rd Conf. Industrial Carbon and Graphite 1970, SCI London 3-9.

54. G.R. Hennig "Chemistry and Physics of Carbon", 2, 1966, P.L. Walker Jr. (Ed.), Marcel Dekker N.Y. 1-49.

55. J.M. Thomas, Carbon, 1970, 8, 413-21.

56. H. Marsh & D. Crawford, Carbon Prog. and extended abs. 13th Biennial Conf. Am. Carbon Soc. 1977, 13, 205-6.

57. J.R. Fryer, "Characterisation of Porous Solids", 1979, Gregg, Sing & Stoeckli (Eds.), SCI, 41-52.

58. R. Millward & D.A. Jefferson. "Chemistry and Physics of Carbon". 14, 1978, P.L. Walker Jr. & P.A. Thrower (Eds.) Marcel Dekker N.Y. 1-82.

59. F.M. Lang & P. Magnier, ibid. 3, 1967, P.L. Walker, Jr. (Ed.) Marcel Dekker N.Y. 121.

60. F. Wilkinson, "Chemical Kinetics and Reaction Mechanisms", 1980, Van Nostrand Reinhold.

61. F.J. Long & K.W. Sykes. J. Chem. Phys. 1950, 47, No. 3-4, 361-78.

62. A.E. Reif, J. Phys. Chem. 1952, 56, 778 and 785.

63. S. Ergun & M. Mentser, "Chemistry and Physics of Carbon", 1, 1965, P.L. Walker, Jr. (Ed.) Marcel Dekker N.Y.

64. M. Menser & S. Ergun, Carbon, 1967, 5, 331-7.

65. F.H. Franke and M. Meraikib, Carbon, 1970, 8, 423-33.

66. P.L. Walker, Jr., F. Rusinko, Jr. J. Phys. Chem.
     1955, 59, 241-4.

67. M. Shelef & P.L. Walker, Jr. Carbon, 1967, 5, 93-105.

CHAPTER TWO.

REVIEW OF WORK ON COKES AND COAL CHARS.

CHAPTER 2.

REVIEW OF WORK ON COKES AND COAL CHARS

2.1.1 Coke Reactivity

This is a loosely defined term commonly understood to refer to the rate at which coke reacts with oxidising gases. As coke lumps fall through the blast furnace their temperature, porosity, topography, mineral matter etc. are constantly changing. Thus "reactivity" is a constantly changing multidependent parameter, being not so much an intrinsic property of a fuel as an implied behaviour.

There has long been interest in coke reactivity. In a study of American blast furnaces Howland[1] stated in 1916 "the most desirable thing about a coke is that quality in the carbon which will allow of its being instantaneously burnt to carbon monoxide". The application of reactivity testing up to 1945 is reviewed by Mayers[2] who reserves the term "reactivity" for tests in which the oxidising gas is CO_2, and "combustibility" for tests using air or oxygen in which extent of reaction was determined by weighing or gas analysis and "ignition point" for tests using air or oxygen in which extent of reaction was determined by temperature measurement. This latter test is related to the "critical air blast test" developed by the Northern Coke Research Committee. Coke reactivity is also reviewed by Blayden.[3]

Although great disparity exists between laboratory test and blast furnace conditions, importance is placed industrially on the measurement of reactivity to assess coke quality and to predict blast furnace performance. The test indicates to what extent the Boudouard reaction will proceed in the upper part of the furnace shaft, i.e. to what extent carbon will be lost before it takes part in the reduction of metal oxides.

Many tests have been developed to measure reactivity. These vary in detail but in principle measure the rate of conversion of CO_2 to CO by granular coke in the temperature range $950°$ to $1100°$C. Extent of reaction may be determined by weight loss of the coke or CO/CO_2 ratio of the effluent gas. Although Mayers states "... all the methods mentioned (i.e. reactivity, combustibility, ignition point) are simply different devices for measuring the same property", when a series of similar cokes are compared by different reactivity tests they are not necessarily placed in the same order by all of them. Physical factors which are not evaluated must play some part in effective reaction rate.

Indirect methods such as measurement of electrical conductivity, and measurement of strength after reaction have also been investigated.[4]

The E.C.E. test[5] for measurement of reactivity of metallurgical coke was published in 1965 to standardise tests for the chemical reactivity of cokes. Dry coke

47

(7-10g) of 1 to 3 mm particle size is reacted with CO_2 at 1000 $^{\circ}$C, under standard flow conditions, and the effluent gas sampled after a set time. The CO content of the reaction gas is determined by I.R., thermal conductivity or absorbing the CO_2 in KOH solution. A coefficient of reaction speed k_m is calculated from the conversion of CO_2 per second and the sample mass.

Many laboratories use their own standard test. Two methods[6] are currently in use at the I.S.P. Research Laboratory, Avonmouth, namely the 1000 $^{\circ}$C and 1300 $^{\circ}$C reactivity tests. The former approximates to temperatures in the upper shaft and the latter to that in the tuyere zone. In both cases rate of weight loss of a sample exposed to a stream of moist CO_2 is determined. A coke block is used for the 1300 $^{\circ}$C test and 10g of coke ground to -0.70 mm +0.42 mm for the 1000 $^{\circ}$C test. Weight is recorded every 5 minutes for 40 minutes and reactivity expressed as percentage weight loss per minute. The major criticism of laboratory tests is that they are carried out in a pure gas and on finely ground material.

I.S.P. use a standard low reactivity coke from Nantgarw, South Wales, expressing their coke reactivity values in terms of a "Nantgarw ratio". The variation of Nantgarw coke reactivity itself is small. Thus a good coke has a Nantgarw ratio near 1 and k_m value near 0.11 cm^3 g^{-1} s^{-1}.

(Nantgarw ratio = 0.21 + 7.3 k_m value).[*]

---

[*]This expression is a correlation between data on samples from the same stock but individual cokes may not fit the equation very well because of differences between the techniques.

The method used to measure reactivity is obviously chosen with the intended use of the coke in mind and the limitations of it being a routine comparative test.

A review of work on metallurgical cokes and coal chars is presented from the point of view of "reactivity studies" and kinetic (oxidation) studies although this is a somewhat artificial distinction.

2.1.2 <u>Review of Reactivity Measurement Studies on Cokes</u>

The methods used to measure reactivity are summarised in Table 2.1. All except that of Banerjee and Sarjant use CO_2 as the oxidising gas. Iron is often present as Fe_2O_3 in considerable amounts in coke ash and is an effective catalyst for the Boudouard reaction when in a lower oxidation state. Combustibility and ignition point tests will thus not assess this effect, and these authors note that their cokes were placed in a different order of reactivity by testing in CO_2.

Percentage weight loss has been used widely and was the criterion adopted in the present work. The test must be conducted at a temperature in the zone of chemical control, or pore diffusion will have an effect.

King and Jones found the "reactivity value" of a coke not to be constant but to alter as the passage of CO_2 continued. They singled out three values - RI. the initial value, RIII the "constant" value after continued passage of CO_2 and RII a value after heat
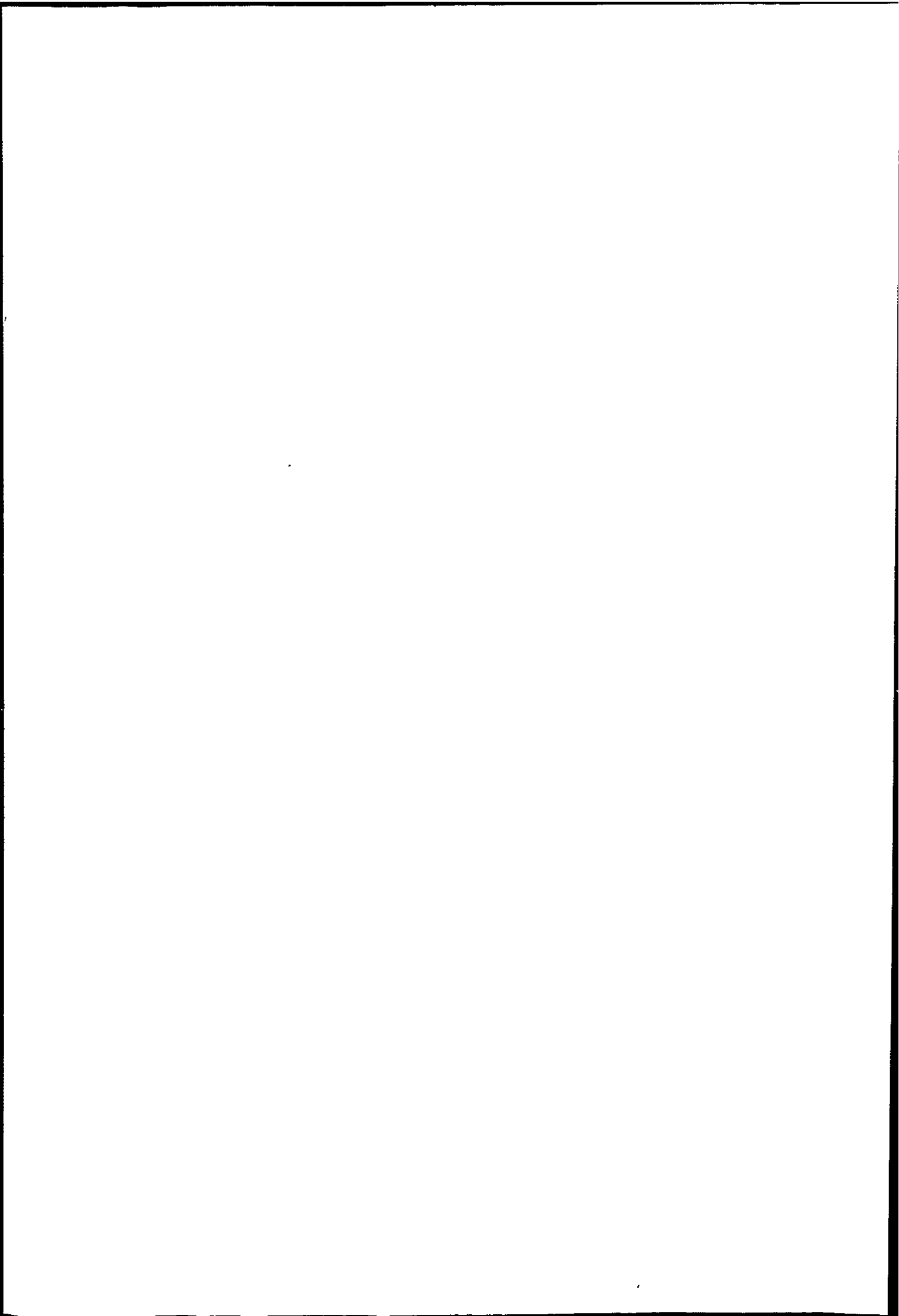
49

Table 2.1 <u>Methods of Measurement of Coke Reactivity.</u>

Author	Ref.	Test Method	Temperature ($^{\circ}$C)	Sample Size	Criterion of Reactivity
King & Jones 1931	7	Sample preheated in N_2, 100 cm^3 CO_2 passed over hot coke. Exit gas passed through KOH solution	950	10-20 mesh	Vol. of CO formed from 100 cm^3 of CO_2
Banerjee and Sarjant 1951	8	Coke heated in air at fixed flow rate. Air and furnace temp. maintained constant or coke temp. held at 1300 $^{\circ}$C by adjusting air and furnace temp.	-	200 g of "graded coke"	ratio of CO/CO_2 in exit gas to that of all the carbon were converted to CO.
Okstad and Hoy 1965	9	Coke heated in CO_2 stream to desired temp. Flow regulated to give 18.2% CO in exit gas (corresponding to 10% conversion of CO_2)	750 to 1000 Results recalculated to 950 using a value of 356 kJ mol^{-1} (85 kcal mol^{-1}) for E_A	fixed weight of -20 +40 mesh preheated coke	Vol. CO_2 converted s^{-1} g^{-1} of fixed carbon.
Barbu and Reinhorn 1966	10	Sample held in CO_2 flow	950	50 g of 25 to 30 mm lumps	Vol. CO to 100 vol of CO_2

Table 2.1 continued.

Author	Ref.		Test Method	Temperature (°C)	Sample Size	Criterion of Reactivity
Patrick & Wilkinson	29		Continuous weight change on an electrobalance in CO_2, CO_2/N_2 or CO_2/CO mixtures	970	Cylinders 1.5 cm x 1 cm, cut from coke pieces	% burn-off with time.
Reeve et al. 1972	11	(i)	CO_2 oxidation for 2 h.	1000	5 g of 25 to 30 mesh coke. Pre-heated in N_2	loss in weight as % sample weight, correcting for ash.
		(ii)	90 min. reaction time in CO_2. Product gas analysis by G.C.	"		$\dfrac{CO_2}{CO+CO_2}$ ratio
		(iii)	CO_2 flow adjusted to give rate resulting in 20% vol. CO in product gases after 90 min.	"	fixed vol. of 25-30 mesh coke.	the ratio $\dfrac{V}{G-a}$ where V is CO_2 flow G is sample wt. a is ash content
Goldshtein al 1975	12		reaction in CO_2/N_2 and H_2O/N_2 mixtures.	1050	2 cm^3 of 2 to 3 mm coke.	
Lu, Samaan & Uribe 1981	13		Powdered specimens burnt off in Ar/CO/ CO_2 50/5/45.	850-950		% weight loss.
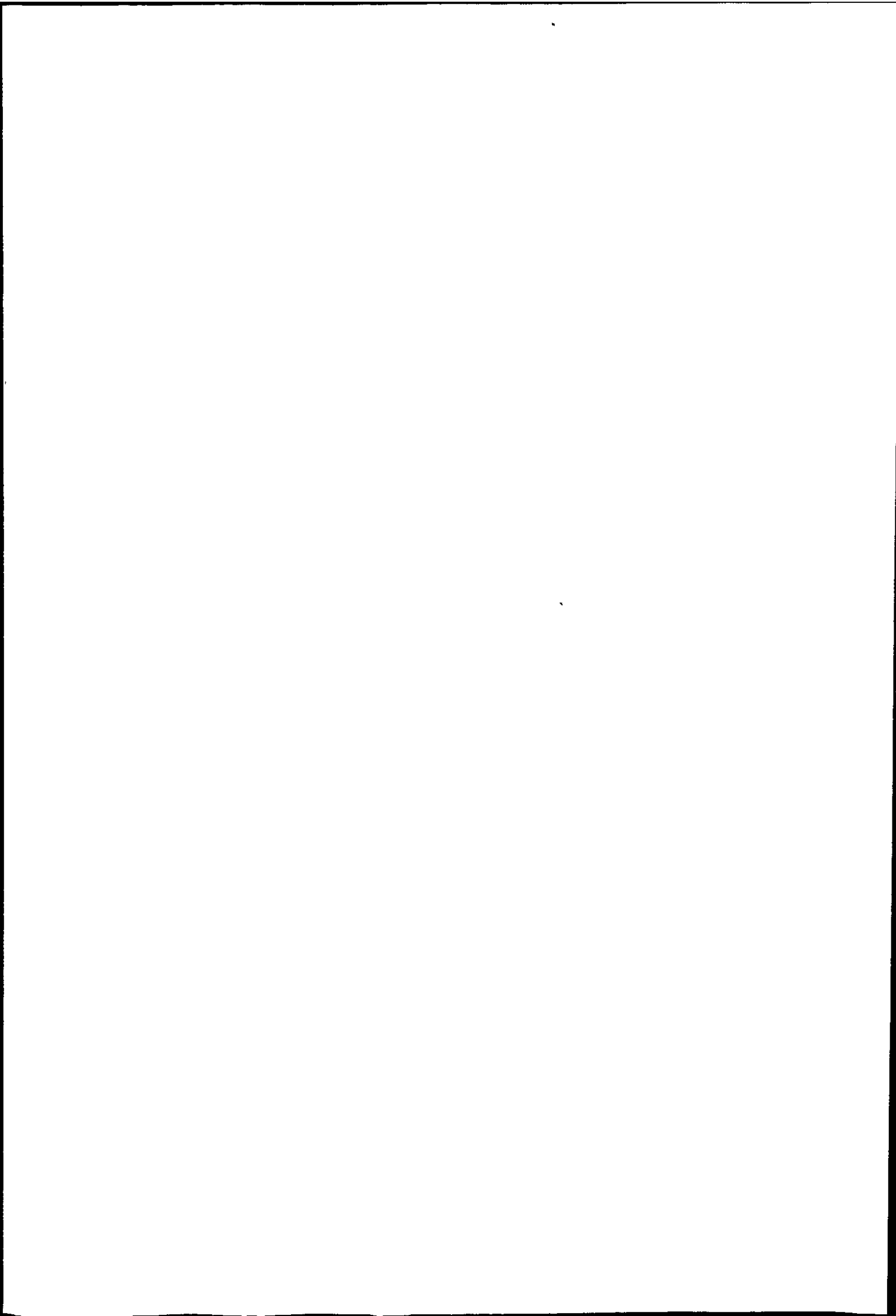
treating coke in N_2. (Treatment of coke with CO_2 then led to RIII). RII was only significant where RIII was considerably greater than RI.

Barbu and Reinhorn determined reactivities of cokes and charcoal in small lumps and 0.5 to 1.0 mm granules and found consistent comparisons only with the larger sized material.

The method of Okstad and Hoy was developed as an industrial standard. The fixed degree of conversion of CO_2 to CO eliminates the possible inhibiting effect of CO and a small sample size and low measurement temperature reduce thermal gradients in the sample. In calculating reactivity it is assumed that the rate of gasification is a function of the carbon weight and a formula is derived for a rate constant in terms of flow rate of CO_2, initial weight of carbon and degree of conversion of CO_2 (i.e. CO_2 reacted: CO_2 introduced). Combining with the Arrhenius equation for the temperature dependence of reaction rate constant, allows reactivity to be calculated as a rate constant in terms of gas flow, sample weight and a logarithmic function which is a constant at a given temperature when a standard temperature (here 950 $^{\circ}$C) and a value for the energy of activation E_A for the reaction are taken.

These authors take a value of 356 kJ mol^{-1} (85 kcal mol^{-1}) for E_A although a range of 393 to 318 kJ mol^{-1} (94 to 76 kcal mol^{-1}) was found for different

52

types of coal, coke and charcoal sample. Actual

reactivity measurements are carried out at a temperature

giving best test conditions and the reactivity values

recalculated to the standard temperature of 950 ^{o}C.

This method however does not take into account the effect

of degree of coke burnt off on reactivity.

The three test methods of Reeve et al on a series

of eight cokes of widely different reactivities showed

that each method gave acceptable selective reactivity

values. The authors consider that at the test temperature

there will be some effect of chemical reactions in pore

walls and counter diffusion of CO and CO_2 within pores

and therefore express some preference for method (iii).

Lu et al studied the reactivities of the carbon of

various optical texture and defined a "relative micro

reactivity" index.

Donelly et al[14] used both weight loss and outlet

gas analysis to determine the reactivities of cokes and

chars between 800 and 1100 ^{o}C . Results were consistent

but the authors preferred the weight loss method,

considering that volatile material affects the gas analysis.

The more significant industrial reactivity tests

are summarised in Table 2.2, as described by Cross[15].

The ECE test has become widespread in use, with

some modifications as in the Norwegian CORMA and

Australian tests. The Polish and Russian methods are

basically similar, depending on the measurement of CO_2

53

Table 2.2   Industrial Test Methods for Coke Reactivity

Test	Temperature	Measurement
Nantgarw Ratio	1000 $^{\circ}$C	Weight Change
United Nations ECE 1965	1000	% CO_2
Japanese JIS K2151-1960	950	CO flow rate
Polish Chemical Coal Treatment Inst.	1000	% CO_2
Russian GOST 10089-73	1000	% CO_2
Koppers Yugoslav JUS IL S_3-03	950	% CO_2
Norwegian CORMA	750-1000	% CO_2
Australian ACIRL - CRA	1000	% CO_2
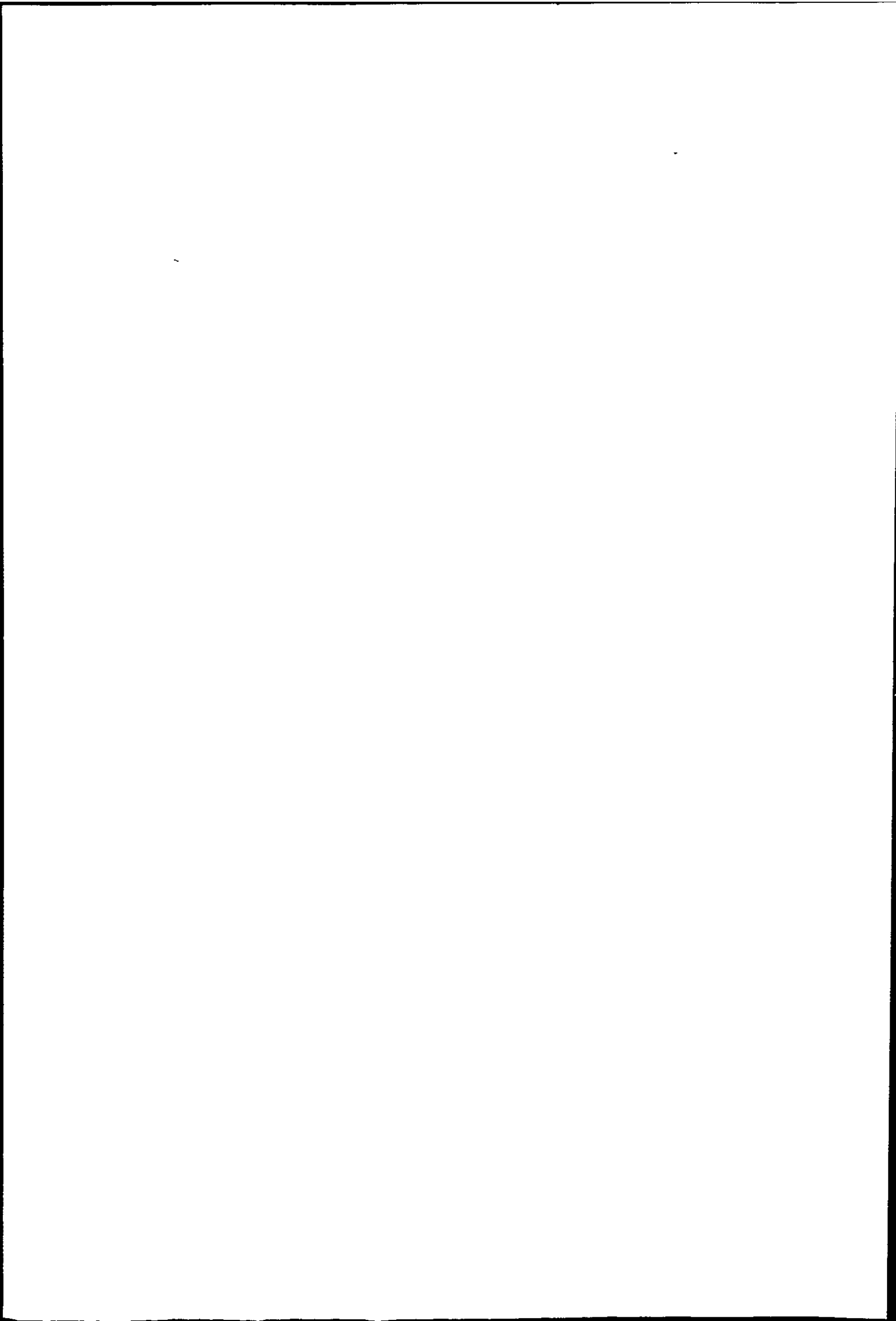
content of reacted gas, flow rate and coke sample weight. The relative merits of the tests are discussed in the above reference, in relation to zinc-lead production.

2.1.3   Review of Coal Char Reactivity Studies.

Methods used to measure coal char reactivity are given in Table 2.3. No standard test exists and there is considerable variation in the methods that have been employed. Data given refers to initial rates of reaction, as in coke testing. The methods fall into direct weighing and product gas analysis and are carried out at a lower temperature than coke reactivity tests. Gray and Misra point out that pore diffusion is likely to affect rate in CO_2 even at 800 $^{\circ}C$.

These authors preferred the method of Okstad and Hoy because there is a fixed extent of conversion of CO_2 to CO. However, they made their measurements "well below 950 $^{\circ}C$", calculating reactivity values at 950 and 900 $^{\circ}C$ using a value of E_A of 104.7 kJ mol^{-1} based on their data for browncoal chars. The reactivities of the chars thus examined were related to the nature of the parent coal, although other factors, including pretreat-ment had an effect. Where chars were prepared from coals of the same lithotype, reactivity differences were primarily a function of porosity. (Lithotype refers to the banded appearance of coal.)

Watson and Gray in a study of chars from highly reactive subbituminous coals discuss the likely nature of active centres, and used the method of Okstad and Hoy

55

Table 2.3. Measurement of Coal Char Reactivity

Authors	Ref	Test Method	Temperature (^{o}C)	Sample Size	Criterion of Reactivity
Donnelly et al 1970	14	Crushed coal charred under N_2 CO_2 admitted. Exit gas sampled at fixed intervals.	850 and 950		Volume of CO produced from 100 volumes of CO_2
Hippo and Walker 1975	16	Coal carbonised in situ at 1000 ^{o}C. Char held at 900 ^{o}C under N_2. CO_2 admitted weight loss monitored on microbalance.	900	5-10 mg	Rate of weight loss per initial weight (on ash free basis).
Walker, Mahajan & Komatsu 1979	17	Treated lignite carbonised in N_2 at 800 ^{o}C. Weight loss measured in various gases.	390 air 760 CO_2 650 steam 790 H_2 790 mixtures with N_2		"
Watson & Gray 1980	18	Coal carbonised in fluidised bed. 1 hr soak time at 920 ^{o}C under N_2. Reacted with N_2/CO_2.		25g	Method of Okstad and Hoy using 226 kJ mol^{-1} for E_A.
Gray & Misra 1980	19	-	-	-	As above using 104.7 kJ mol^{-1} for E_A.
Knight & Sergeant 1980	20	Coal charred in situ. Samples reground 3 size fractions taken on thermal balance. CO_2/N_2 mixture.	800 to 970		Rate of weight loss per initial sample weight.
Jenkins et al 1973	21	Sample heated in N_2 to 500 ^{o}. Air admitted. Weight loss monitored.	500	5-10 mg	Max. rectilinear weight loss/ initial (ash free) weight.

56
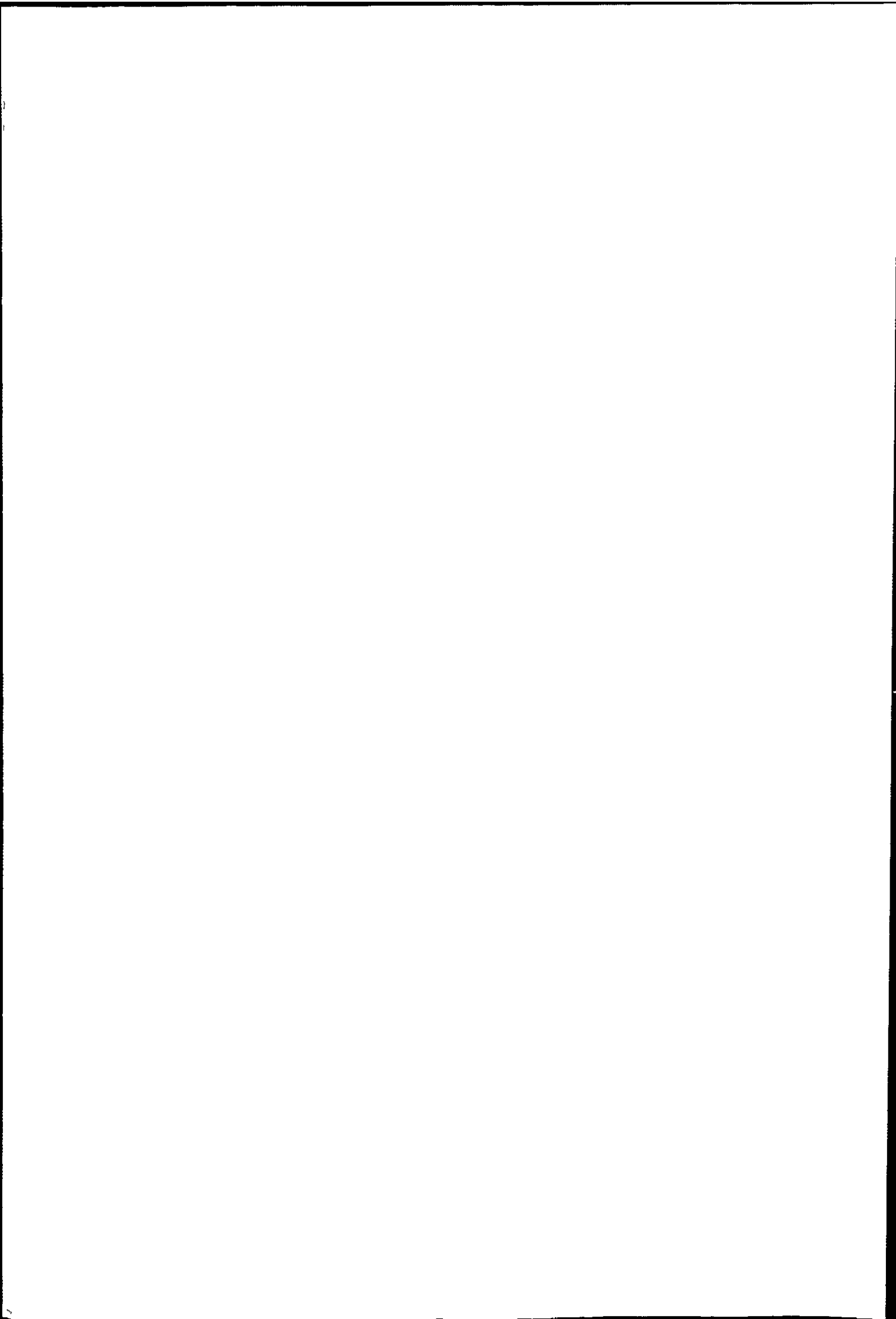
to determine reactivity using a value of 226 kJ mol^{-1} for the activation energy, the mean of their experimentally determined values. The reactivity values, related to 1173 K fall within a similar range to those of Gray and Misra although a widely different value of E_A was taken.

Where the criterion for reactivity is weight loss, extent of weight loss versus time plots are often presented. These generally show three regions - a slow initial rate, a rectilinear burn off portion and a decreasing burn off. The rectilinear portion usually lasts to about 40% burn off in which the char is increasing its specific surface area due to activation.

Knight and Sergeant[20] found char reactivity greater, the lower the rank of the parent coal.

No general correlation of reactivity with mineral (ash) content has been found, although several workers[16,21] note high calcium content is associated with high reactivity.

Jenkins used air as the oxidizing gas and found lower rank coals gave more reactive chars. Hippo and Walker, using the same chars found the same general order of reactivity to CO_2. Chars of high calcium and magnesium content were most reactive, although the amount and type of porosity had a marked influence on reactivity. The effect of decreasing particle size is generally to increase reactivity. Demineralisation by acid washing decreased reactivity, although in some cases additional porosity is

57

created which increases reactivity. This showed the important role and opposing balance of catalysis and mass transport resistance in the reactivity of these materials.

Knight and Sergeant[22] in a reactivity study of chars from Australian coals conclude that no strong correlation exists between any one mineral matter component and char reactivity.

## 2.1.4 Studies Relating Reactivity to Other Coke Properties.

Many studies have been made in an attempt to relate reactivity to other physical properties. The reactivity of cokes from all coals decreases markedly with increasing temperature of carbonisation. It may be expected that reactivity could be correlated with other temperature dependent properties, such as "true" density, which is a measure of degree of graphitization.

Optical and scanning electron microscopy have been widely used to study coke structural changes on gasification, as described by Marsh and Smith[23].

The crystal structure of carbon causes directional variations in the transmission or reflection of polarized light and a polished coke section viewed between crossed polarisers presents an appearance described as "mosaic texture". Coke structure has thus been studied by quantitative reflectance measurements. Intensity of reflectance is dependent on rank of parent coal and temperature of coking process. Patrick et al[24] categorise the optically identifiable types from "isotropic" through "mosaic" type of various grain sizes to a "flow type anisotropy".

Schapiro and Gray[25] correlated reactivity with

pore volume for various cokes made from coal of the same

rank. The former quantity was determined by automated

reflectance microscopy and the latter by weight loss

in CO_2 at 2000 $^{\circ}$F (1093 $^{\circ}$C). Both are related to coal

rank in the same way.

Thompson et al[26] studied coke reactivity with the

aim of finding a test for the chemical quality of coke.

After a daily monitoring of iron plant cokes for about 2

years they concluded that the weight loss in CO_2 test

was a sensitive test of plant operation and coke

uniformity. In a study of reactivity, strength, porosity

and coal composition Benedict and Thompson[27] found low

reactivity associated with thick pore walls, a low

percentage of pores and small pores. The same tests on

actual blast furnace samples showed similar trends

although the structural changes were more severe than

laboratory tested cokes. As weight loss occurred coke

lost strength progressively. Carbon of the lowest

crystallographic order e.g. that from low rank high

volatile coal, was preferentially attacked by CO_2. This

confirms previous work by the same authors[28] in a study

of the influence of coal composition on coke making.

High reactivity cokes were low in reflectance and described

as "amorphous in appearance" and produced from certain

coals of low rank. These reactive carbon forms produced
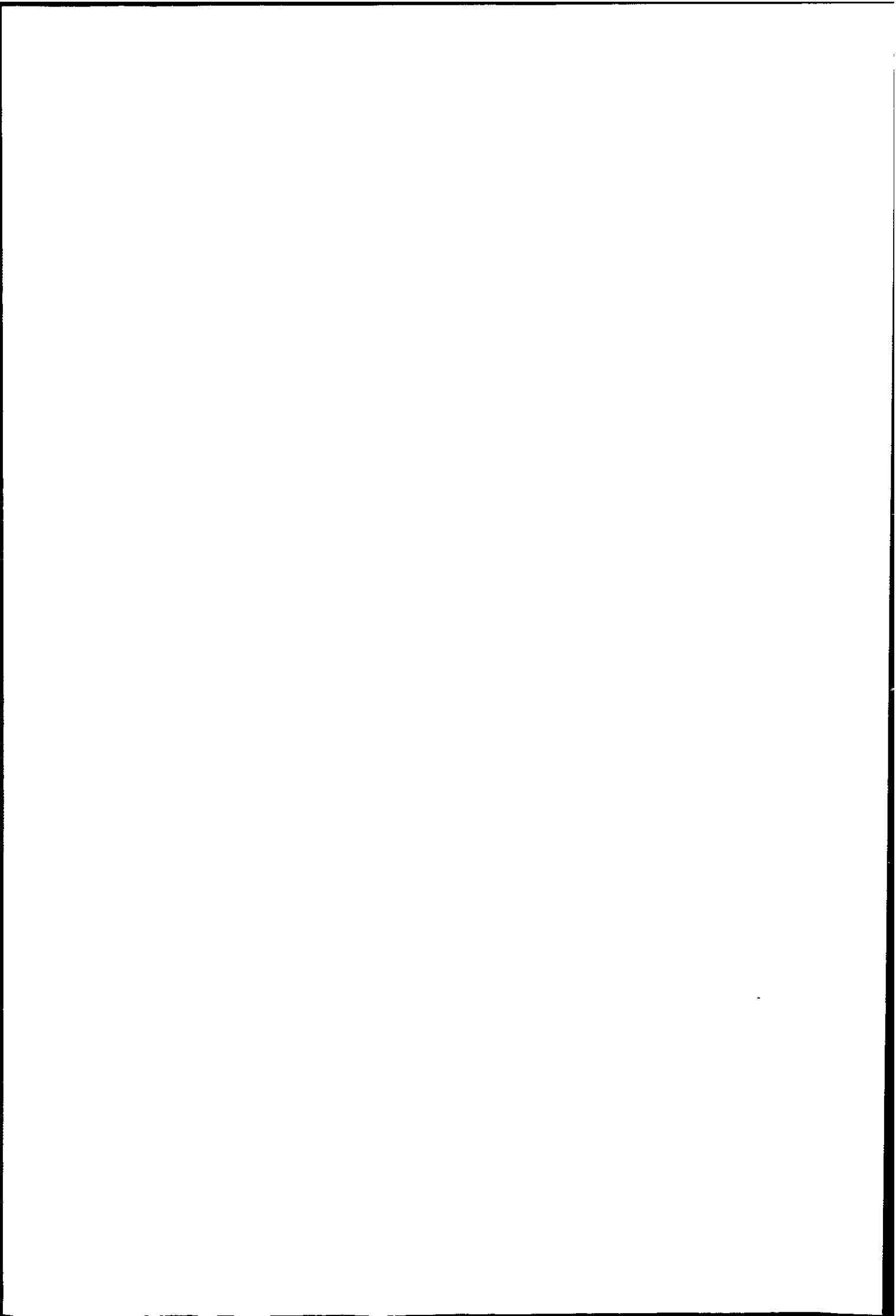
from the inert and semi-inert macerals can, however, if thoroughly incorporated into the coke walls, tend to thicken them and reduce reactivity. Thus the effect of coke structure, coke texture and carbon form influence reactivity in an interrelated way.

Work by Patrick and Wilkinson[29] on reactivity, coke strength and coal rank used weight loss in CO_2 at 1000 $^{\circ}$C as the criterion of reactivity. Relationship between reactivity and coal rank is discussed and between reactivity and optical texture under polarized light. Isotropic material was found to be the most reactive component, completely overriding the effect of anisotropic composition, but the authors conclude that the differences in crystallographic structure of the carbon cause only small differences in reaction rates. No simple relationship was found between reactivity and total pore volume (from mercury pressure porosimetry) or total porosity (from density measurements), although a broad relationship existed between burn-off rate and the ratio of pore-wall thickness to pore diameter. On gasification pore enlargement and reduction in pore wall thickness occurs and is responsible for the decrease in coke strength.

Nishida et al[30] measured the L_c (002) value i.e. mean stack height of layer planes, for a series of metallurgical cokes, and their "reactivity index" by weight loss in CO_2 at 1100 $^{\circ}$C. Although L_c could be related to the rank of parent coal, the authors found no correlation between coke crystallinity and reactivity and suggest this is due to
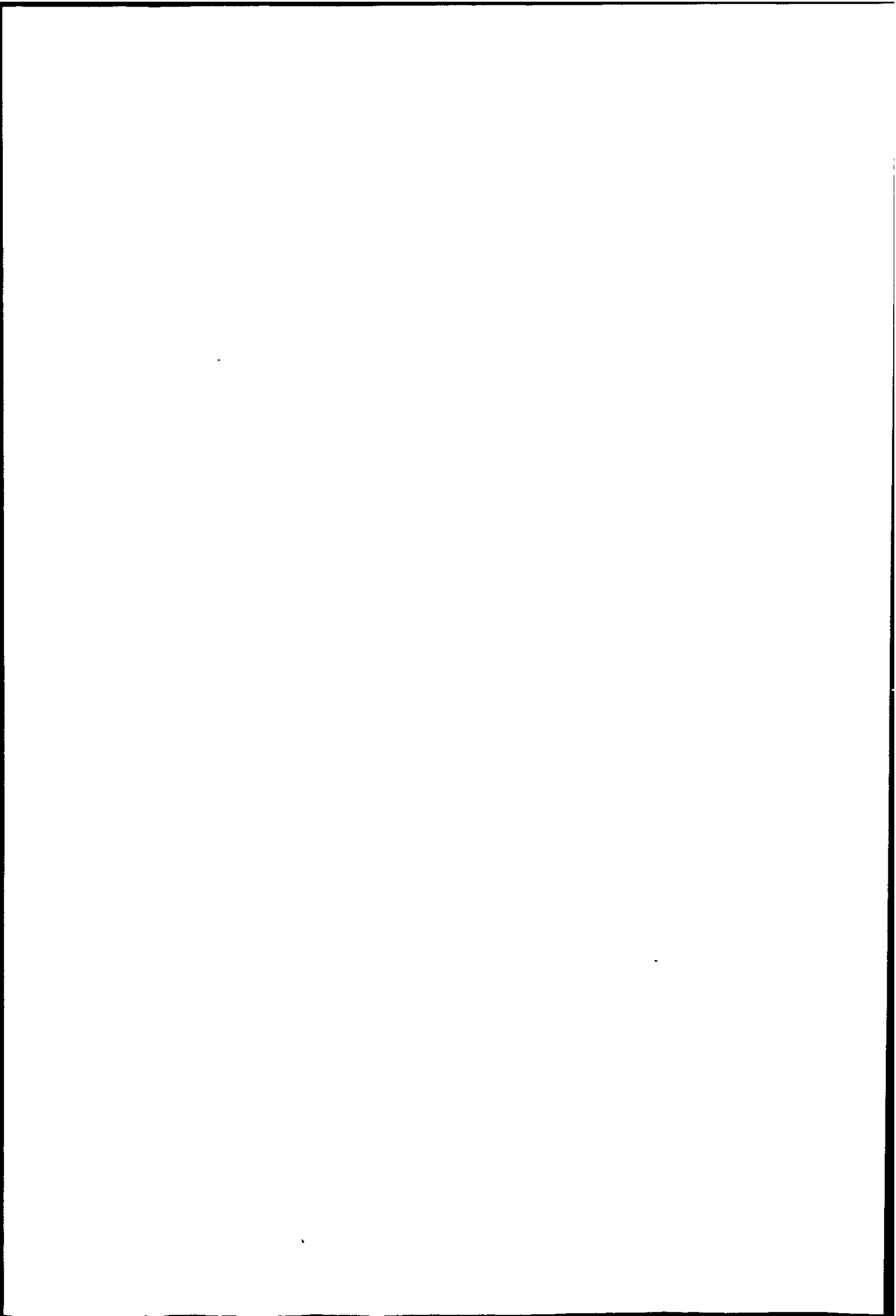
the effect of pore structure, coke ash, etc.

In a study of blast furnace samples, Gill and Coin[21] investigated the relative sensitivity of coke structural components to CO_2 attack by etching polished coke surfaces at elevated temperatures. The most reactive components were derived from inert materials (corresponding to Patrick's[24] isotropic structure) and it is suggested that the reactivity depends on crystalline structure and specific surface of these. Breakdown of coke strength is also discussed.

A detailed study of the reactivity and structure of seven cokes produced from single coking coals of various ranks by Fujita et al[32] showed high reactivity associated with a low mean maximum reflectance of parent coal. Pore diffusion resistance tended to decrease with increasing average macropore radius. Where specific surface area was high due to microporosity, CO_2 reactivity was high, in spite of high content of flow type (optical) texture.

The ash from the seven single cokes was added to coal tar pitch by Fujita et al[33] to evaluate its effect on CO_2 reactivity as distinct from the optical texture and pore structure. Fe_2O_3 and K_2O in the ash correlated with increased reactivity of the carbonised pitch. Thus although their previous study indicated reactivity depended upon pore structure, ash constituent must also play a significant role.

2.2.1 Kinetic Studies on Metallurgical Coke in the Boudouard Reaction.

Kinetic studies have centred on the determination of the temperature dependent rate constants in the Langmuir-Hinshlewood rate equation

$$\text{rate } R = \frac{K_1 P_{CO_2}}{1 + K_2 P_{CO} + K_3 P_{CO_2}}$$

Where the symbols have the meanings described in 1.4.1. Interpretation of the constants depends on the mechanism assumed for the reaction. In principle K_2 and K_3 should be independent of the type of carbon since they are functions of ratios of intrinsic rate constants. However, in practice, they are not universal constants, their values depending on the nature of the carbon used. This aspect of the possible relationship of kinetic parameters to actual coke reactivity has been dealt with by Marsh[34].

When $K_2 P_{CO} \ll 1$ and $K_3 P_{CO_2} \gg 1$, rate $= \dfrac{K_1}{K_3}$ i.e. the reaction will be of zero order. This will be the case at low temperatures and high CO_2 pressures.

But if $K_2 P_{CO} \gg 1$ and $K_3 P_{CO_2} \ll 1$ the reaction will be first order with respect to CO_2 at fixed CO pressures. Thus the order of reaction may vary from zero to one depending on experimental conditions and type of carbon.

In order to evaluate the rate constants the L-H equation is rearranged as

$$\frac{1}{R} = \frac{1}{K_1}\left(\frac{1}{P_{CO_2}}\right) + \frac{K_2}{K_1}\left(\frac{P_{CO}}{P_{CO_2}}\right) + \frac{K_3}{K_1}$$

Thus by keeping the ratio $\frac{P_{CO}}{P_{CO_2}}$ constant, while varying p_{CO_2} the constants K_1, K_2 and K_3 can be evaluated from the slope and intercept of the plots of $\frac{1}{rate}$ vs $\frac{1}{P_{CO2}}$ at two different ratios of $\frac{P_{CO}}{P_{CO_2}}$.

Aderibigbe and Szekely[35] reacted coke discs (cut from the same sample) in $CO/CO_2/Ar$ mixtures on a thermal balance in the temperature range 840 to 1000 $^\circ C$. Coke structure was also characterised by porosity, surface area measurements and scanning electron microscopy.

Partial pressure ratios of 0.25 and 0.5 were used and the coke was reacted to about 40% weight loss. As found by other investigators, with increasing temperature K_1 increases and K_2 and K_3 decrease. On plotting $\ln K$ against $\frac{1}{T}$ the activation energies of the elemental steps can be evaluated.

In an earlier study, Heuchamps[36] investigated the gasification of 0.5 to 1 mm metallurgical coke granules in $CO/CO_2/N_2$ mixtures between 900 $^\circ C$ and 1100 $^\circ C$ using the E.C.E. reactivity test method. The ratio $\frac{K_2}{K_1}$ decreased with increasing temperature and the value of K_3 in comparison was very small. The negative energy of activation associated with K_2 shows the inhibiting power of CO, which decreases with increasing temperature.
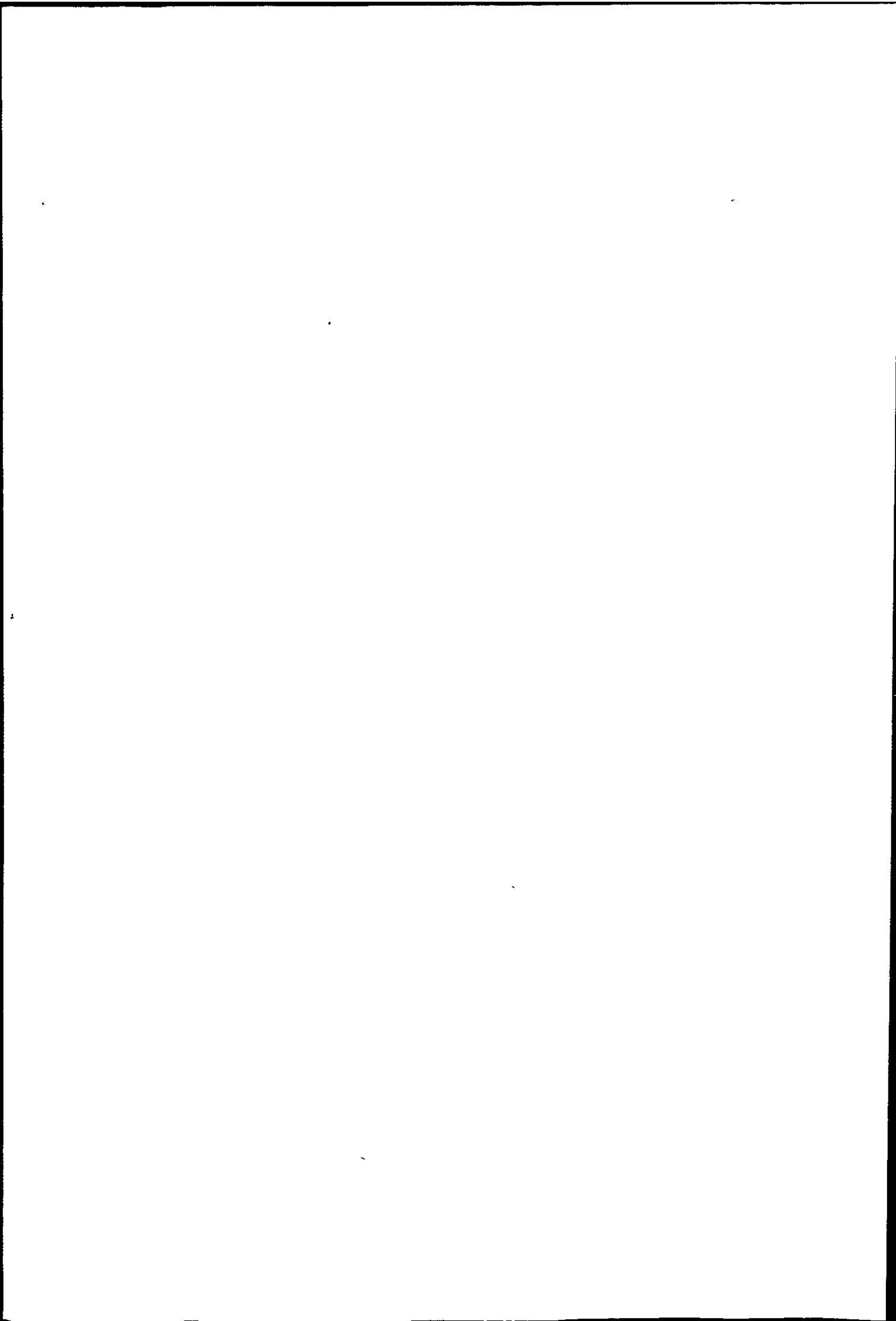
Turkdogan and Vinters[37] studied the rate of
oxidation of several carbons, including metallurgical
coke granules in CO_2/CO and $CO_2/CO/He$ mixtures in the
temperature range 700 °C to 1400 °C, up to approximately
15% weight loss. The greater retardation by CO on graphite
and coke (which was partially graphitized) than on
charcoal was attributed to stronger chemisorption of
CO. Detailed discussion of reaction mechanisms in terms
of the thermodynamics of chemisorbed layers is given.
Pore diffusion did not lower the reaction rate with coke
granules at temperatures above 900 °C unless p_{CO_2} was
greater than 1 atmosphere. (101 kPa).

Kinetics of the C/CO_2 reaction on Nantgarw coke
between 1000 °C and 1200 °C was studied by Richards and
Tandy[38] following rate of reaction by exit gas
composition. Above 1000 °C for any given size of coke
there was a minimum gas velocity to be maintained in order
that a true conversion rate of CO_2 to CO be measured.
The reaction was found to be first order with respect to
CO_2, when p_{CO} was fixed and p_{CO_2} varied from 5 to 30%,
the balance being N_2. When p_{CO_2} was held and p_{CO} varied,
CO was found to inhibit, the effect becoming less marked
with increasing temperature.

The constants K_1 and K_2 were evaluated from plots
of $\frac{1}{rate}$ versus p_{CO}, the constant K_3 being neglected.
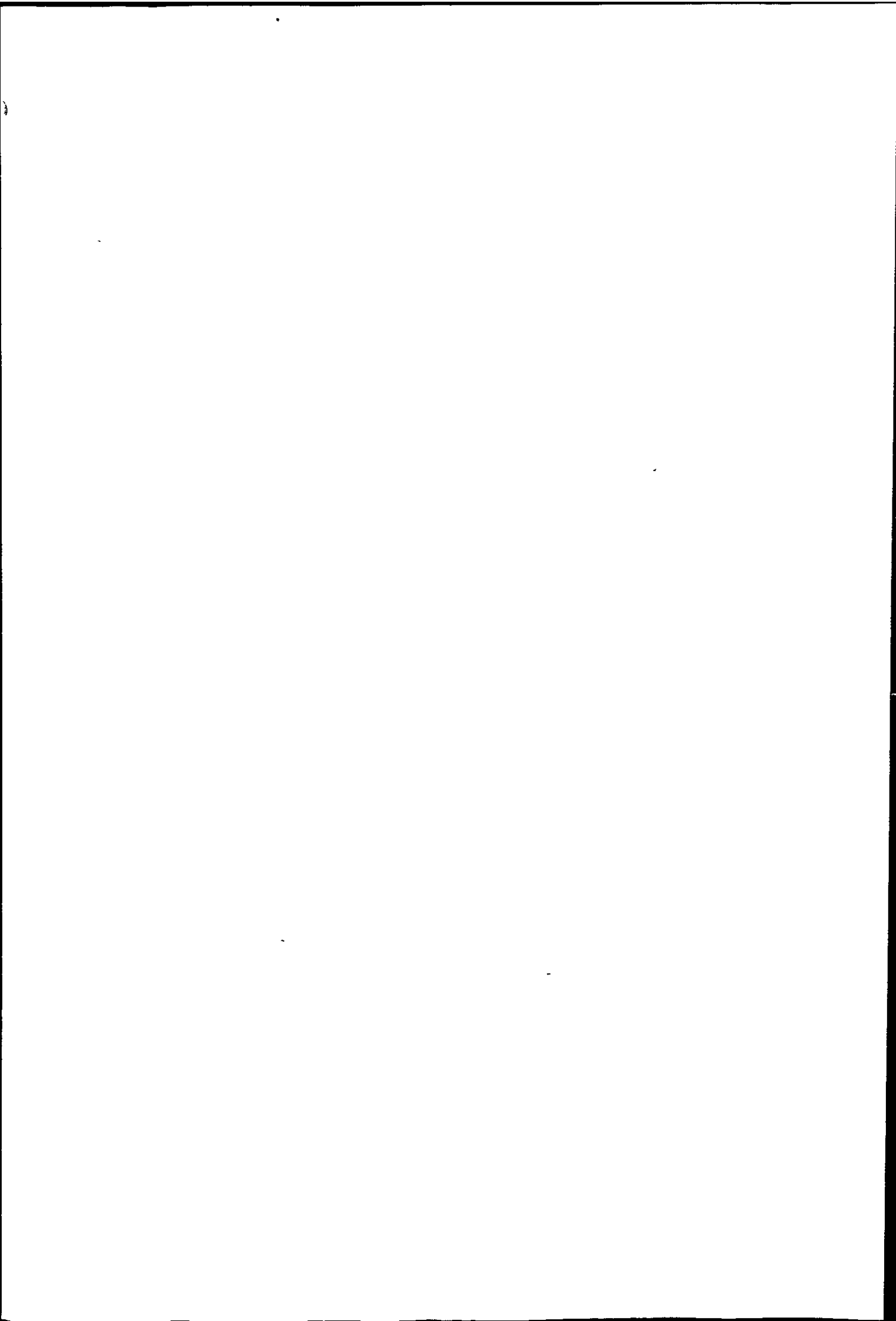Results, in a general form of the rate expression are
reproduced in Table 2.4.

Table 2.4. Rate of Gasification of Nantgarw coke from Reference 38. (in mol min^{-1} atm $^{-1}$ g^{-1}).

at 1000 °C   rate = $\dfrac{2.03 \times 10^{-4} P_{CO_2}}{1 + 4.5 \ P_{CO}}$

at 1100 °C   rate = $\dfrac{8.94 \times 10^{-4} P_{CO_2}}{1 + 2.2 P_{CO}}$

at 1200 °C   rate = $\dfrac{2.05 \times 10^{-3} P_{CO_2}}{1 + 0.36 P_{CO}}$

The effect of temperature is implicit in the three expressions. Plots of log K_1 and log K_2 versus $\frac{1}{T}$ yield activation energies. Thus the results were expressed as

$$Rate = \frac{K_1 P_{CO_2}}{1 + K_2 P_{CO}}$$

where $K_1 = 10^{3.9} e^{\frac{-43.5}{RT}}$

and $K_2 = 10^{-7.2} e^{\frac{46.0}{RT}}$ where the activation energies were given in kcal.

These results were then applied to the conversion of CO_2 in the hearth and shaft of the Imperial Smelting Furnace, it being estimated that about 90% of the C/CO_2 reaction takes place in the hearth and the CO_2/CO ratio being 0.32. If this drops to 85% the CO_2/CO ratio becomes 0.37. This gas ratio determines the temperature below which the gas would be reducing to FeO.
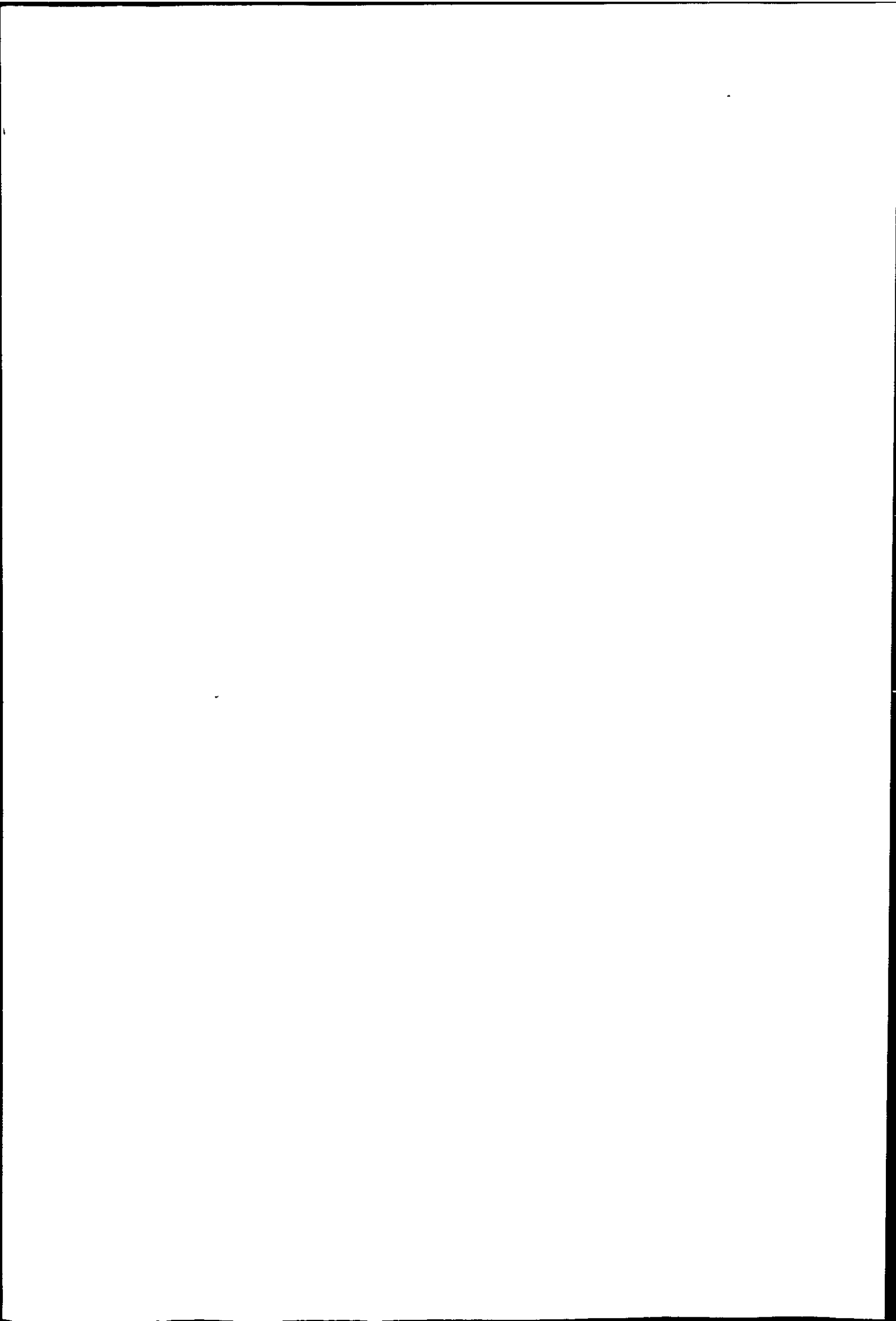
Thus a detailed kinetic study of Nantgarw coke
had already been undertaken. Comparison of the values of
the rate constants K_1 and K_2 given by various workers
shows that they are specific to the coke studied, although
the temperature dependence is the same.

2.2.2 <u>Review of Mechanistic and Structural Studies on</u>

<u>Coal Chars</u>

Char reactivity depends on the source and thermal
history of the char, and kineticists are far from able to
make a priori predictions of reaction rates. A
fundamental approach is given by Isaacs[39] who has
correlated the free energy of formation of chars with
reactivity. The equilibrium constant K at a given
temperature for a char may be calculated from
experimental data and compared with that for graphite
under the same conditions. Then,

$$\ln\left(\frac{K^{char}}{K^{graphite}}\right) = \frac{1}{RT}\left(\Delta G^{gr.} - \Delta G^{char}\right)$$

The term $(\Delta G^{gr.} - \Delta G^{char})$ is equated to
$G_f^{char} - G_f^{graphite}$ where G_f is the free energy of
formation at the given temperature. Thus a test of this
hypothesis depends upon the estimation of G_f at the
reaction temperature, calculating the ratio of the
equilibrium constants and comparison with the
experimentally determined ratio. Heats of formation,
absolute entropy of formation and specific heat data are
correlated by this author, in order to calculate G_f.

67

Since chars are not fully ordered solids there is a residual entropy of formation making G_f^{char} positive relative to graphite. Prolonged heat treatment may be expected to reduce this term, hence reduce chemical reactivity. Calculation for values at 1200 K are given, which agree reasonably well with experimental data. Thus the intrinsically high reactivity of chars may be related to thermodynamic functions.

Similar treatment is given by Sinteza[40] with data for anthracite, coke, diamond and graphite.

Much work has been reported on the kinetics of the O_2, CO_2 and steam gasification of chars produced by carbonisation of organic polymers. (e.g. the CO_2 oxidation of cellulose and cellulose triacetate chars by Dovaston et al[41] and McEnaney and Willis[42] of polyfurfuryl alcohol (PFA) chars by Marsh and Taylor[43] and the oxygen oxidation of pitch resins by Dollimore and Turner[44], PVA (poly-vinyl acetate) char by Marsh and Taylor[45] and cellulose char by McEnaney and Weedon[46]). These are chars prepared under controlled conditions and containing no mineral matter, although heteroatoms would be present. Coal chars must represent a more heterogeneous group of materials.

Recent work has focussed on coal chars as a large number of existing and proposed coal conversion technologies depend upon their gasification.

In a study of the reaction rates of <100 μm sized particles of coal char with CO_2, O_2 and H_2O at very high
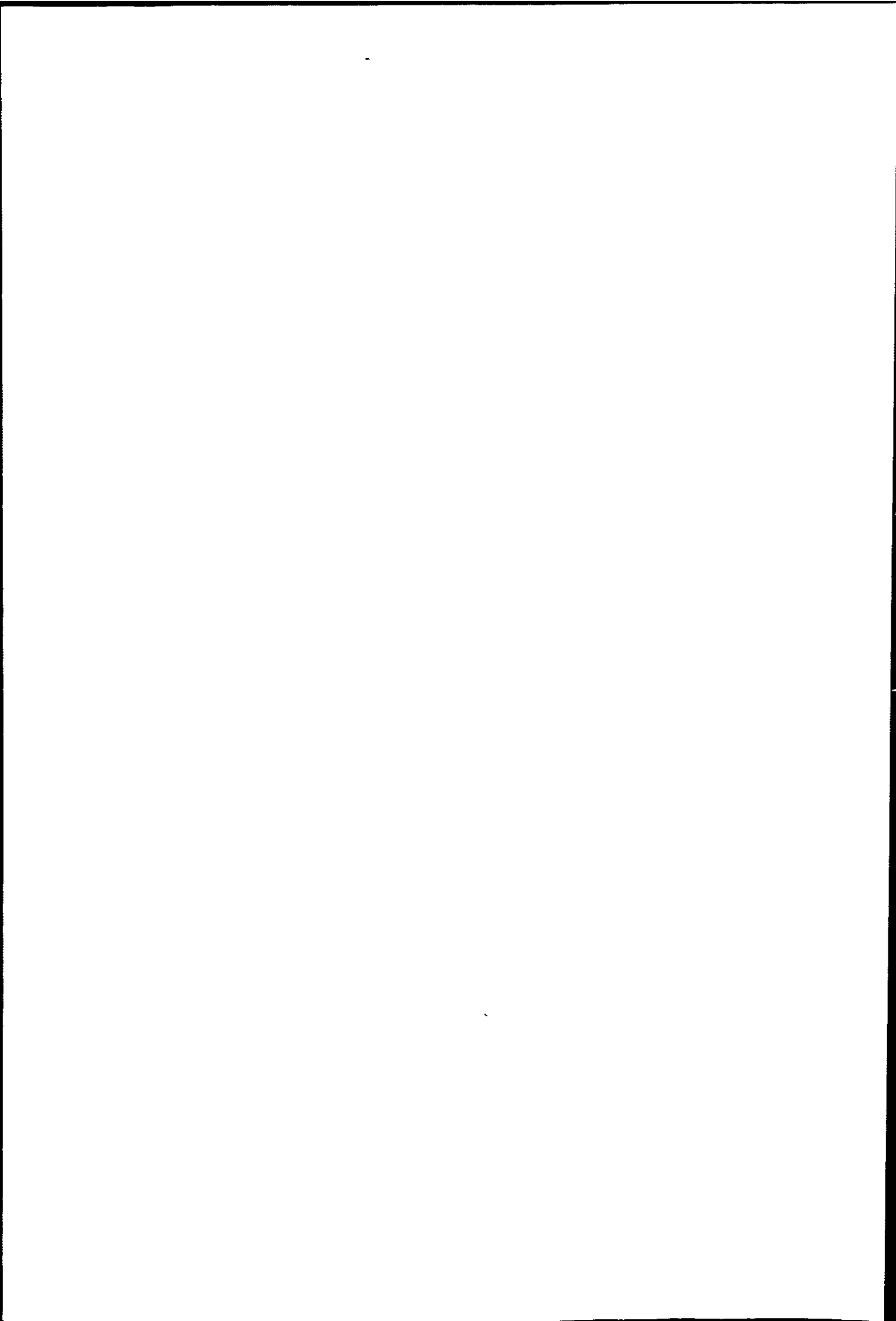
temperatures (1800-2800 K) Kimber and Gray[47] concluded that rate in oxygen was under diffusion control. With CO_2 and H_2O rates were at least one order lower and under partial diffusion control. The latter will diffuse further into the particle, at the same temperature than oxygen and relatively more burning take place internally. Faster burning of low rank coal chars than charcoal was attributed to a larger portion of the surface being accessible via larger (several μm) pores.

Mathematical treatment of rates of gasification of nineteen coal chars with steam at 850° and O_2 at $900\ ^{\circ}C$ is given by Kasaoka et al[48]. Fraction gasified α versus time t curves fitted closely the equation

$\alpha = 1 - \exp(-at^b)$ where a and b are constants, independent of coal rank. This equation was derived assuming that rate constant $k = a^{\frac{1}{b}}b(-\ln(1-\alpha)^{\frac{b-1}{b}})$

Using a normalised gasification time $\frac{t}{t_{1/2}}$ rate curves were fitted to a characteristic curve shown as

$$\alpha = 1 - \exp\left[-A\left(\frac{t}{t_{1/2}}\right)\right]^B$$ where A and B are constants.

Although useful in predicting the behaviour of chars from coals of particular fuel ratios, the constants do not relate to any reaction mechanism.

Dutta et al[49] studied the pyrolysis of several coals and the CO_2 reactivity of the chars produced from them at 840 to $1100\ ^{\circ}C$. Rate of weight loss versus fraction reacted curves show that each char had its own
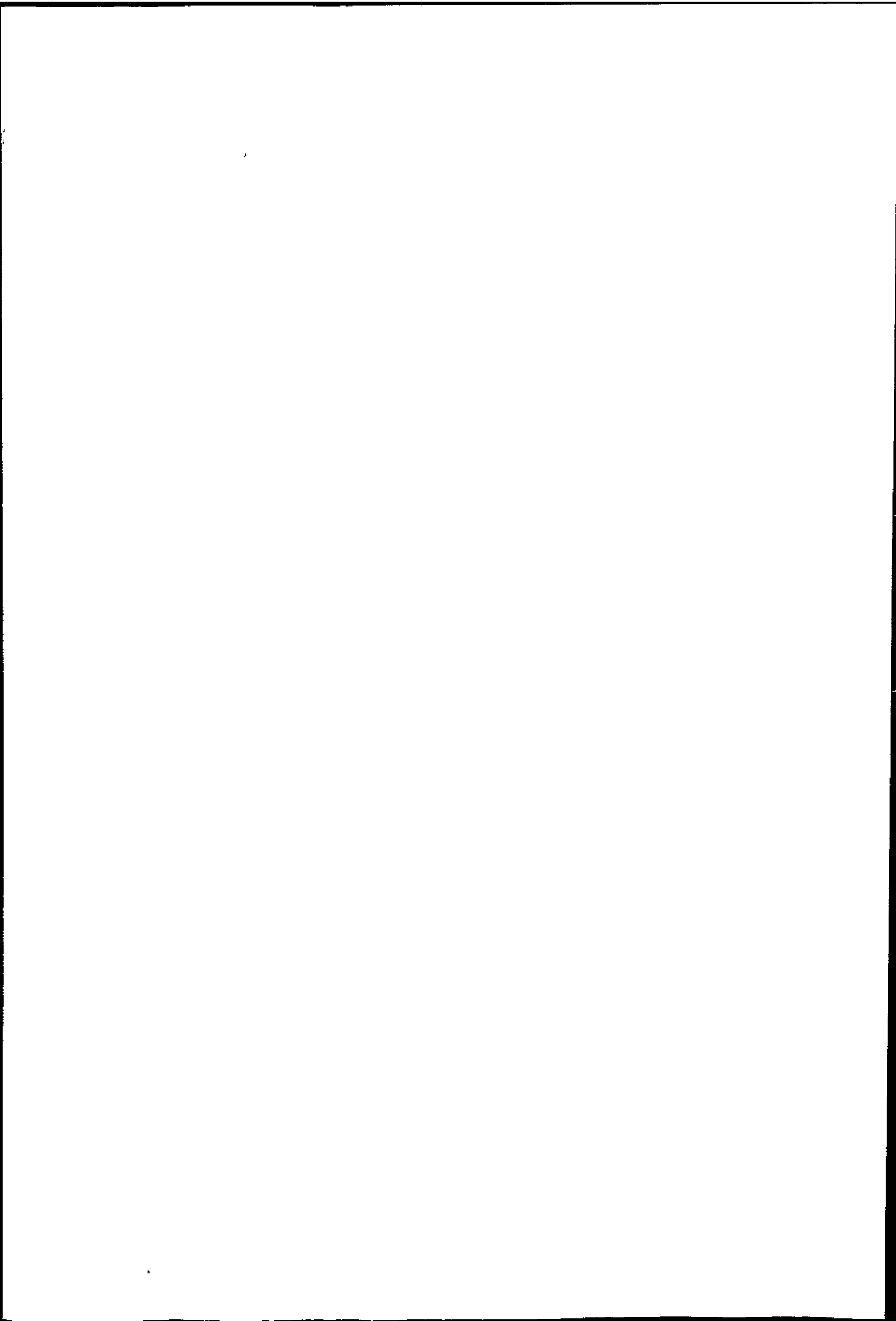
characteristic rate-conversion curve, attributed to the different pore structure and change of such with reaction. Char reactivity increased with decreasing rank of parent coal. Pore characteristics studied by SEM, mercury porosimetry and B.E.T. (N_2) adsorption showed that higher surface areas were due to a larger number of smaller pores, although only the fraction of surface with pores > 1-2 nm in radius may be available for reaction with CO_2. Reactivities were found to be approximately proportional to the surface due to pores above 1.5 nm in radius, and to have little relation to total surface area.

Kinetics of H_2O and CO_2 gasification of Swedish Shale char was investigated by Bjerle et al[50] in the temperature range 800° to 1000 °C. The reaction rate of fixed carbon was described by a modified Langmuir-Hinshlewood rate expression (K_3 was neglected). Retardation by CO and H_2 was observed for both reactions. Char reactivity was dependent on the pyrolysing conditions of the shale. That chars treated at 1200 °C are less reactive than those treated at lower temperatures is reported by Bradshaw et al[51] in a study on reactivity of coal chars to CO_2 at 900 to 1270 °C.

Thus kinetic studies are often intimately linked with porosity measurements. Some of the activation energies reported for the C/CO_2 reaction with coal chars are given in Table 2.5, and on other materials including cokes in Table 2.6. Values for the C/O_2 reaction on various carbons is summarised in Table 2.7.
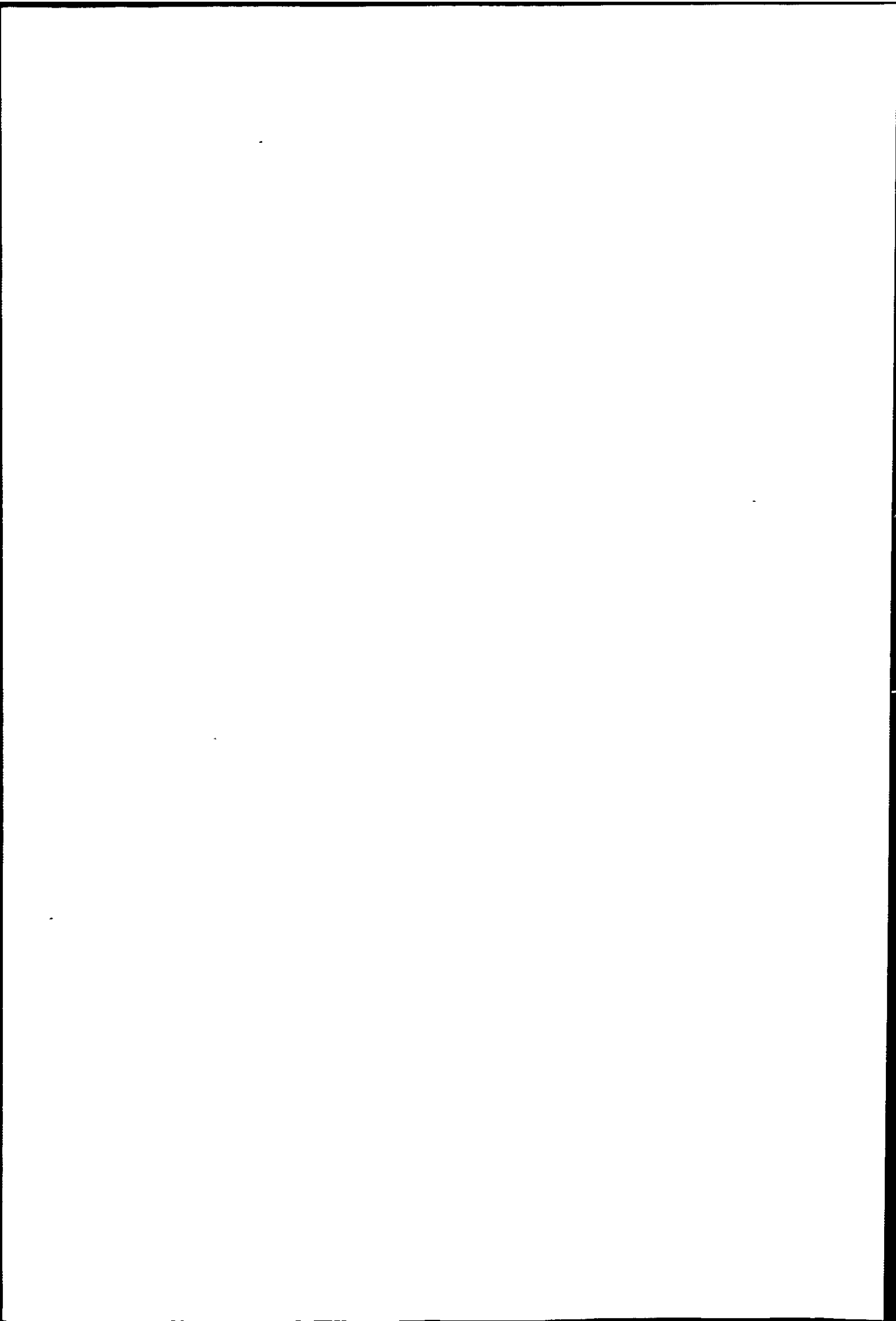
Table 2.5. Some Reported Activation Energies for the C/CO_2 Reaction on Coal Chars. (kJ mol^{-1}).

Author.	Activation Energy	Material	Reference
Gray & Misra	104.7	Brown coal chars from briquetted coal of light, medium and dark lithotype.	19
Knight & Sergeant	219 to 233	Chars from 4 Australian coals.	20
Dutta et al	247	Hydrane & Synthane chars derived from 2 U.S. coals under different gasification schemes.	49
Watson & Gray	214 to 238	Chars from a number of Australian sub-bituminous coals.	18
Bradshaw et al	194	Chars from Manvers and Barnburgh coals.	51

Table 2.6. <u>Some Reported Activation Energies for the C/CO_2 Reaction on other</u>
<u>Carbons (kJ mol^{-1})</u>

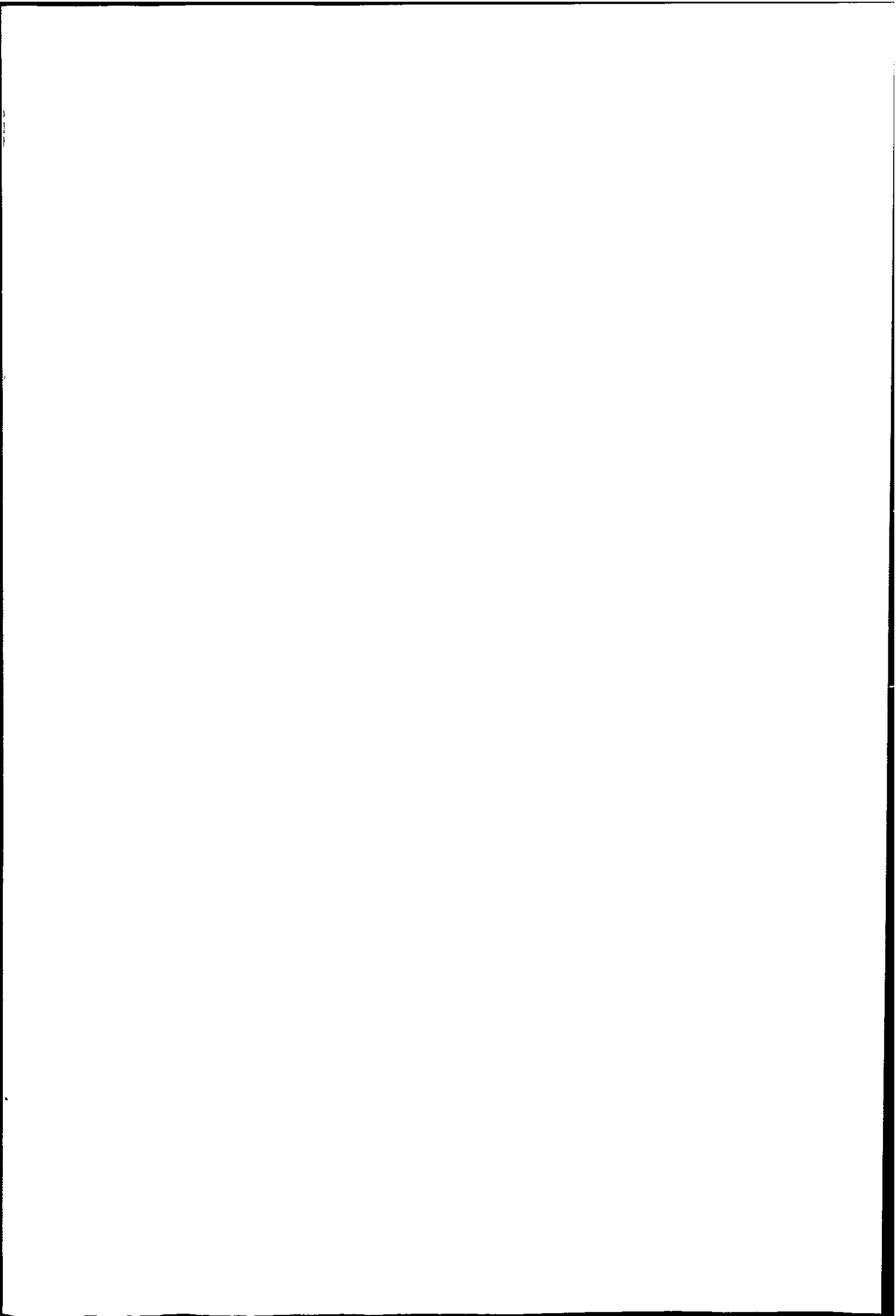| Author	Activation Energy	Material	Reference
Okstad & Hoy	364 (87 kcal mol^{-1}) 339 (81 ") 393 (94 ")	lignite (N.Z.) gas coke (England) metallurgical coke	8
Zuniga & Droguett	238	Coke from Chilean coal	70
Richards & Tandy	176 (at p_{CO_2} = 0.2)	Nantgarw coke	38
Walker & Rusinko	180 to 285	extruded carbon rods with coal tar pitch binder.	Chapter 1 ref. 66
Marsh & Taylor	230	graphitizing carbon from P.V.A.	43
DoVaston et al	250 170±20	polyacenaphthylene char triacetate chars.	41
McEnaney and Willis	261±24 to 171	cellulose triacetate carbons of various heat treatments (CO_2 at 1.33 k Pa)	42
Kawana	402 (96 kcal mol^{-1})	Coke from humic acid	69
Blake et al	239	Formed coke	87

Table 2.7. Some Reported Activation Energies for the C/O_2 Reaction (kJ mol^{-1}). (In the chemical control zone.)

Author	Energy of Activation	Material	Reference
McEnaney & Weedon	105 ± 12	Cellulose char, oxygen partial pressure 0.1	46
Lewis	180	Vitreous carbon, air oxidation	52
Navarro & Jenkins	161.5 ± 5	Air oxidation of glassy carbon from phenolic resins	53
Jones	167	Air oxidation of Spheron 9 (a non porous carbon black).	54
Young	146 to 165 135	Chars from Australian sub-bituminous coal petroleum coke.	88

2.3.1 <u>Thermal Analysis</u>. (TG and DTA) Thermal analysis involves the measurement of a parameter related to any physical or chemical property of a substance which is dependent upon temperature.

The technique of thermogravimetry (TG) is that in which the change in sample weight is recorded as a function of temperature or time. Weight loss measured at constant temperature (isothermal TG) has been the basis of many of the kinetic studies previously mentioned on cokes and chars. Relatively fewer workers have measured weight changes under an increasing linear temperature programme (dynamic TG) or used DTA or simultaneous TG/DTA.

The principles of thermoanalytical techniques are described by Wendlandt[55], giving experimental details, sources of error and applications.

The isothermal TG method is more suitable for slower reactions and is considered by some authors to be more accurate than the dynamic method. Rate of reaction at constant temperature is measured and a dimensionless quantity α, the "degree of transformation" is used in the evaluation of data, based on the assumption that the kinetics can be expressed by a formal equation

$\frac{d\alpha}{dt} = k(1-\alpha)^n$ where t is time, k the rate constant and n the order of reaction. The integrated form of this equation may be expressed as

$$\frac{1}{n} - \left[\frac{1}{(1-\alpha)^{n-1}} - 1 \right] = kt$$

or as $\alpha = 1 - \left[1 - kt(1-n) \right]^{(\frac{1}{1-n})}$

Values of $n = \frac{1}{2}$ and $\frac{2}{3}$ correspond to movement of a reaction boundary through cylindrical and spherically shaped particles respectively. For other values mathematical treatment is complicated by the non-linear appearance of n or α in the rate equation. Norris et al[56] discuss the application of numerical methods to the determination of k and n in solid-state reactions.

Reduced time plots ($\frac{t}{t \text{ of } \frac{1}{2} \text{ reaction}}$) used to recognise mechanisms in diffusion controlled reactions are discussed by Keattch and Dollimore[57].

The temperature dependence of k is given by the Arrhenius equation

$k = A \exp(\frac{-E_A}{RT})$ where A is the frequency factor R the gas constant and E_A the activation energy of the reaction. Thus the kinetic parameters A and E_A can be evaluated from a plot of log k versus $\frac{1}{T}$, obtained from isothermal TG measurements at a series of temperatures.

Mathematical analysis of dynamic TG curves is more complex. Again the formal kinetic equation is combined with the Arrhenius equation and expressions evaluated by differential, integral or approximate methods. Comparison and criticism of various methods is given by Wendlandt[55] and Blažek[58].

75
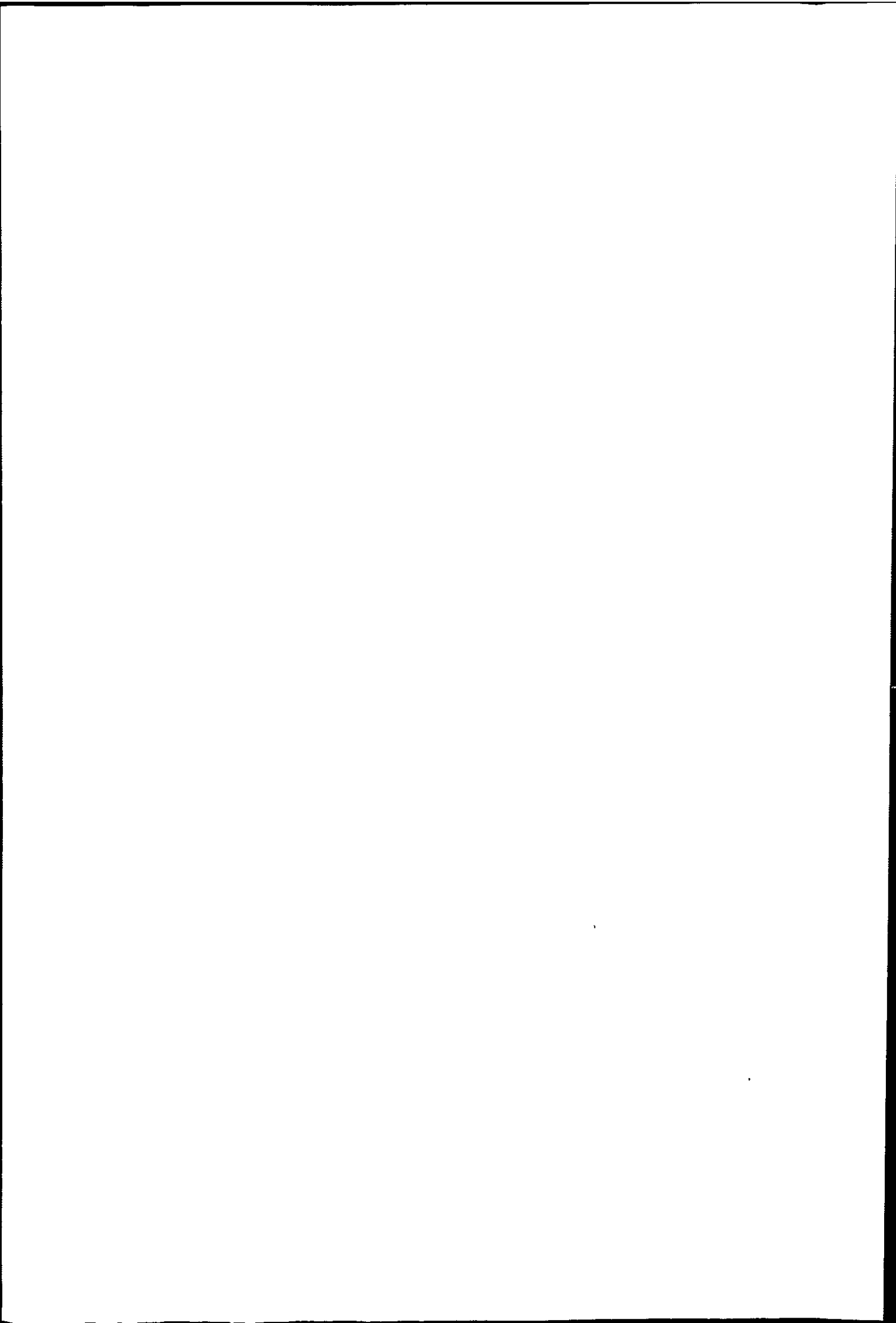
The first derivative of the TG curve - the DTG curve is a useful additional parameter. Although it gives no further information than the TG curve it is often useful in resolving overlapping peaks.

Differential thermal analysis (DTA) is the technique which measures the temperature difference between the sample and an inert reference material against temperature or time as the two specimens are subject to an identical temperature regime in an environment heated or cooled at a controlled rate. The method records all changes in enthalpy, i.e. physical and chemical changes. Results are more dependent on experimental conditions than they are in TG. Basic principles, apparatus and applications are given by Pope and Judd[59].

Kinetic information may be obtained from DTA, and many expressions have been derived involving rate of heating and peak maximum (or minimum) temperature, from which E_A and n can be calculated. These equations assume a constant heat capacity of the sample over the temperature range and that temperature gradients do not exist within the sample. The theoretical and experimental aspects of obtaining meaningful kinetic parameters from DTA are critically reviewed by Sharp[60], with application to solid state reactions. The effect of kinetic factors on the shape of a DTA curve is also described. These changes were noted by Kissinger[61] who related the shape of a DTA curve to the order of reaction by a "shape index".

76
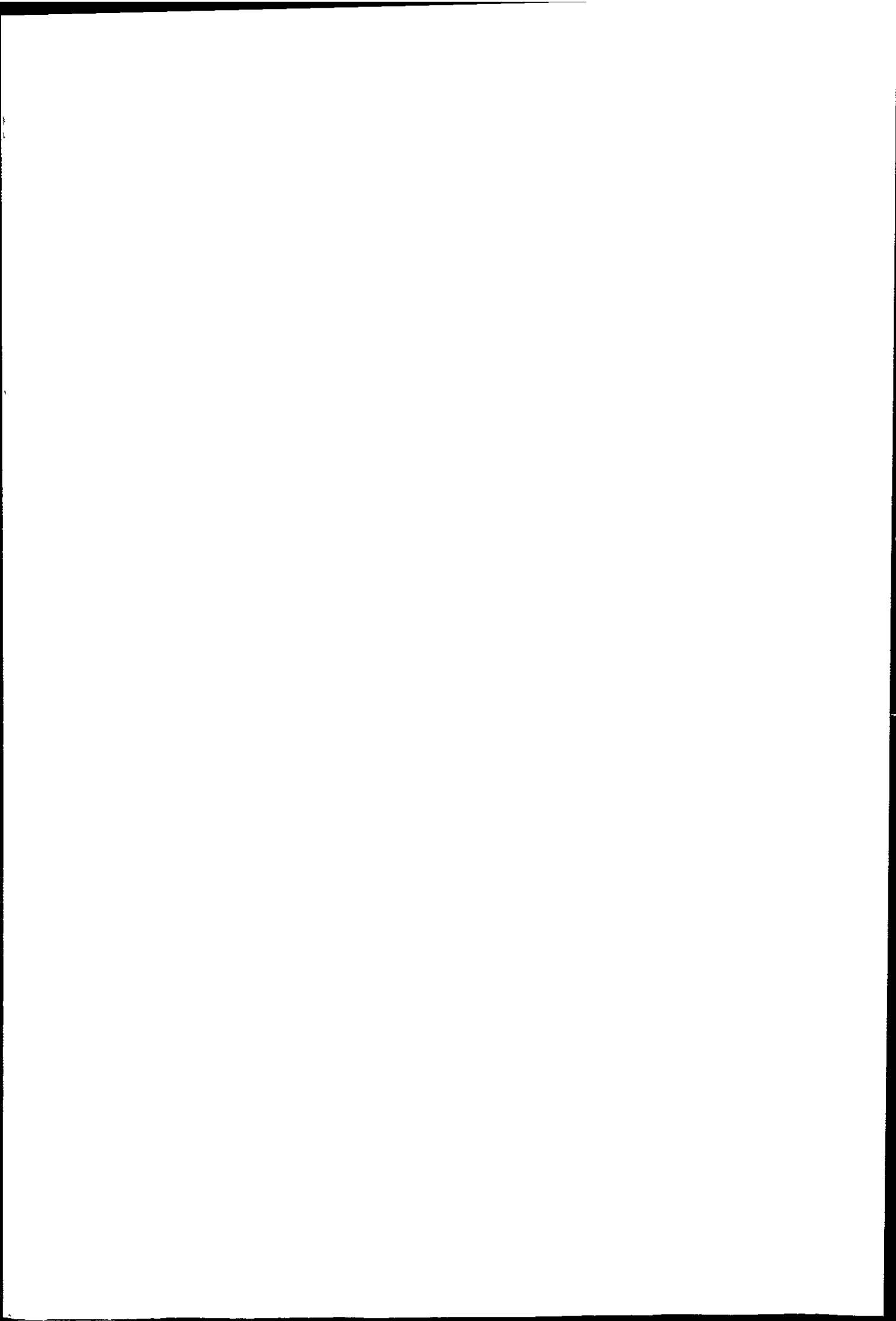
Thus TG and DTA represent powerful techniques in the study of reaction kinetics. The combination of a general rate expression

$$\frac{d\alpha}{dt} = k(1 - \alpha)^n \text{ and the Arrhenius equation}$$

leads to $\frac{d\alpha}{dt} = Af(\alpha)e^{-\frac{E_A}{RT}}$

It is assumed that $f(\alpha)$ is $(1-\alpha)^n$ in the analysis of experimental data by TG. A weight change gives the fraction of material reacted and the corresponding DTA peak area is proportional to the enthalpy of the reaction. The temperature difference ΔT developed between sample and reference is dependent on sample mass.

2.3.2 Review of Dynamic Thermoanalytical Studies

Marsh and Taylor[62] studied the kinetics of the C/CO_2 reaction by dynamic TG using a graphitizing carbon prepared from P.V.A. at heating rate of 0.5 K min^{-1}. The value of E_A compared well with that found isothermally, although the authors point out that agreement is not so good at higher heating rates.

In a programme designed to correlate coke testing with blast furnace performance Aderibigbe and Szekely[63] used dynamic TG, subjecting specimens to an environment where gas composition and temperature are time dependent (in an approximate manner to stack conditions). Samples were temperature programmed at fixed $\frac{P_{CO}}{P_{CO_2}}$ and at gradually decreasing P_{CO_2}.

77

At higher conversion levels (> 10% weight loss) the fractional weight loss was a linear function of time, i.e. the increase in temperature, decrease in CO_2 and structural changes appeared to balance each other. Reaction rates were slower where gas composition was fixed. It is suggested that reaction of a coke particle at lower temperatures has an activating effect, thus reactivity may vary markedly with furnace operation.

Doboviŝek et al[64] used DTA to study the combustion of solid fuels in flowing air at 20 $^{\circ}C$ min^{-1}. The exotherms for metallurgical coke began at about 550 $^{\circ}C$. For domestic coke (which had a high reactivity to CO_2 at 950 $^{\circ}C$) the exotherm began at 500 $^{\circ}C$, was broader and had two distinct maxima. Where DTA curves gave two maxima the author relates these to the cokes being made from a blend of two coals. Heats of combustion were evaluated from peak areas. Time from the beginning of the deviation of the DTA curve to its return was then determined at a series of temperatures. A plot of log (time of complete reaction) versus $\frac{1}{T}$ gave two straight line portions, showing a change from chemical to diffusion control of rate. This quite lengthy study shows the application of DTA, although similar results to the latter part could be obtained more easily from isothermal TG.

The use of DTA to identify and estimate carbonaceous materials is given by Swaine[65] based on the heat evolved during their air oxidation, at heating rates of 10 $^{\circ}C$ min^{-1}.

78
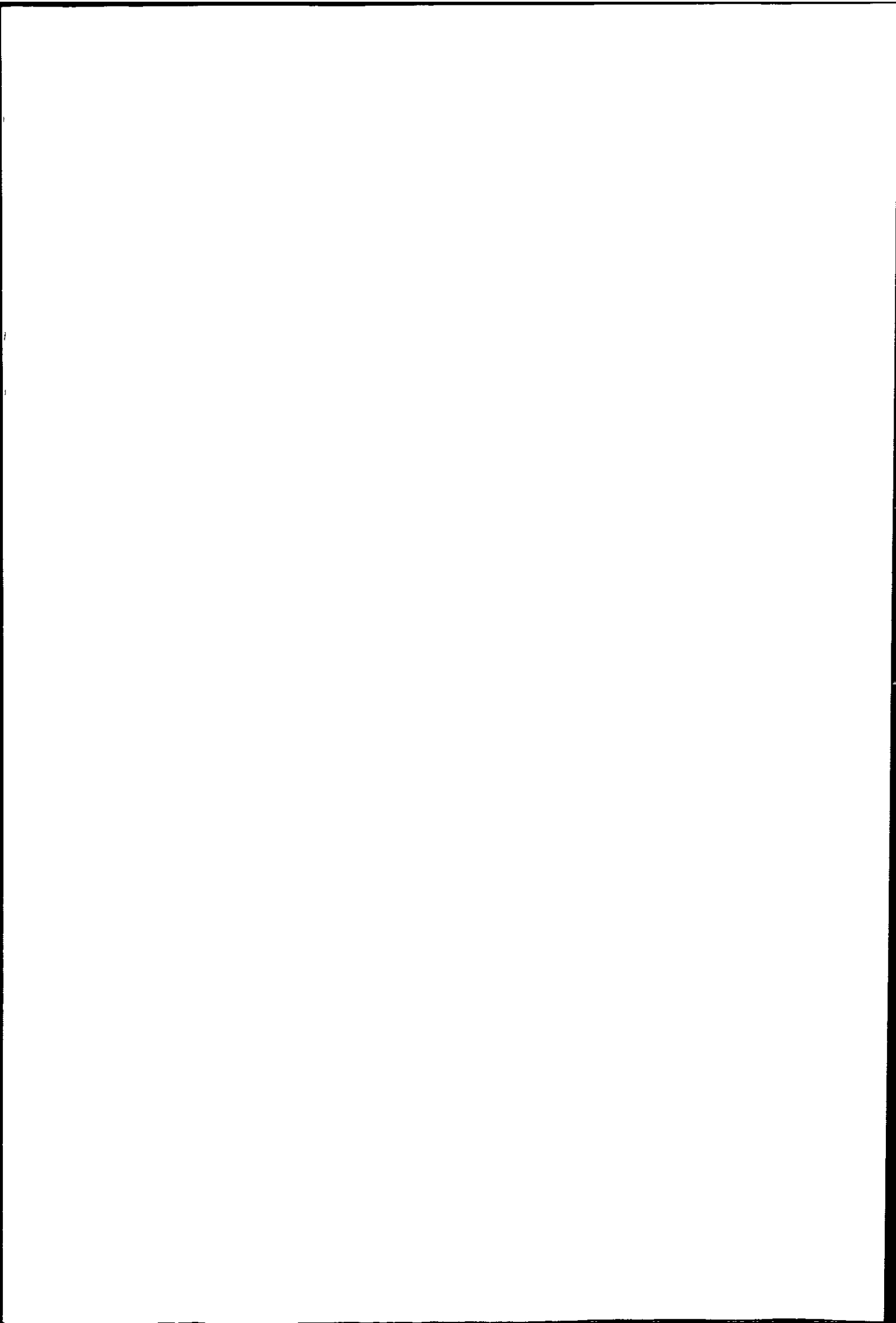
A quantitative method for the estimation of carbon in
flyash from the DTA peak area is described. Swain states
that where thermal behaviour was well separated two types
of carbon in a mixture could be determined by two peaks in
the DTA curve. This is criticised by Yang et al[66] in the
application of DTA to the O_2 and CO_2 reactivity of
carbonaceous materials. A birfurcated peak in the DTA
curve can be predicted by substituting the appropriate
functional form of $\frac{d\alpha}{dt}$ for various orders into

$\Delta T = k \left(\frac{d\alpha}{dt}\right)$ and setting $\frac{d\Delta T}{dt} = 0$

Three general equations are derived and solved
graphically showing that theoretically several peaks may
exist in a DTA curve, depending on the order of reaction.

Several carbons including coke were reacted by
these authors in air at 500-600 $^{\circ}C$ or CO_2 at 1050 $^{\circ}C$ i.e.
in the chemical controlled rate regime. From the rate of
reaction determined from TG the type of DTA curve was
predicted (one or several peaks) and compared with
experimental curves. Based on this analysis two peaks in
a DTA curve is not sufficient condition for the existence
of two types of carbonaceous material in a sample.

A detailed analysis by Yang and Steinberg[67] of
DTA curves for first order reactions shows that E_A and A
may be obtained from a single DTA curve from the peak maximum
when thermal transport effects are neglected. The treatment
is applied to the C/CO_2 reaction using nuclear graphite,
giving good agreement with results from isothermal TG.

DTA has also been used to estimate ignition
temperatures of carbons.

79·
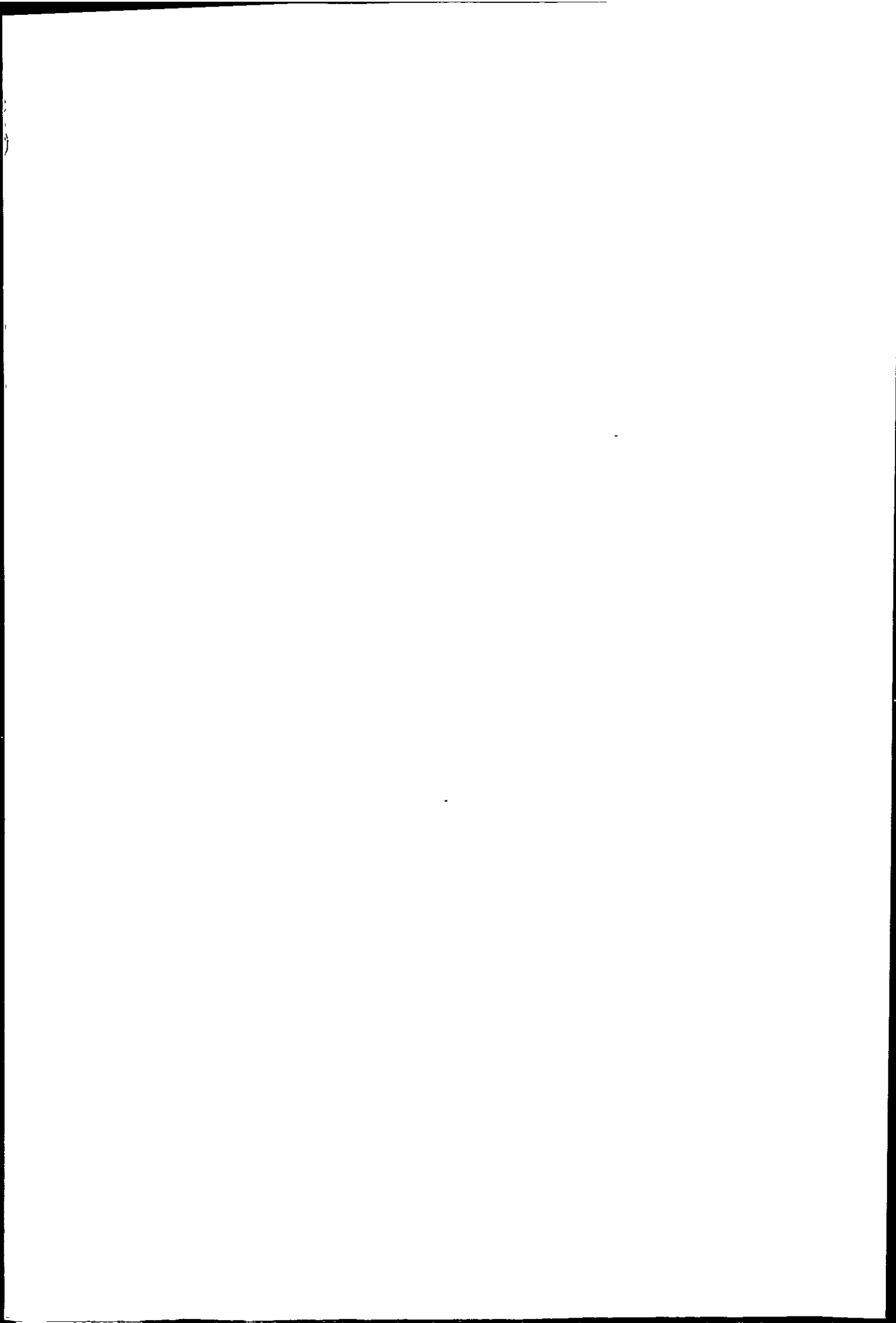
2.4.1   The Inhibition of Reactivity

Catalytic effects in the Boudouard reaction, in which the rate is enhanced have been much investigated. The activating effect of alkalis, iron and other transition metals has been reported for a wide variety of carbons. Solution treatment of cokes and enhanced reactivity to CO_2 is described by Lee[68], Kawana[69] and Zuñiga and Droguett[70].

In comparison the inhibition of the gasification of carbon has not received so much attention.

Inhibition by CO and H_2 in the gas phase is well known. Hedden et al[71] report the inhibiting effect of $POCl_3$, phosphorus vapour and some halogen containing compounds in the CO_2 gasification of various types of carbon. A reversible effect, which depended little on the form of the carbon was noted and an irreversible effect, which only occurred with the relatively strongly graphitised carbons. Mechanism is thought to be via the electron donating capacity of the chemisorbed species. Hawtin and Gibson[72] report that $POCl_3$ inhibits the air oxidation of graphite (at 450-500 ^{o}C) and Arthur and Bangam[73] report the same for cokes and charcoal.

Modification of the solid, i.e. the carbon surface will also lead to inhibition of reaction. The use of borates and phosphates as antioxidants of carbon is well known. Borates and silicates are used as inhibitors of oxidation and corrosion in metals[74].   Graphite is protected from air
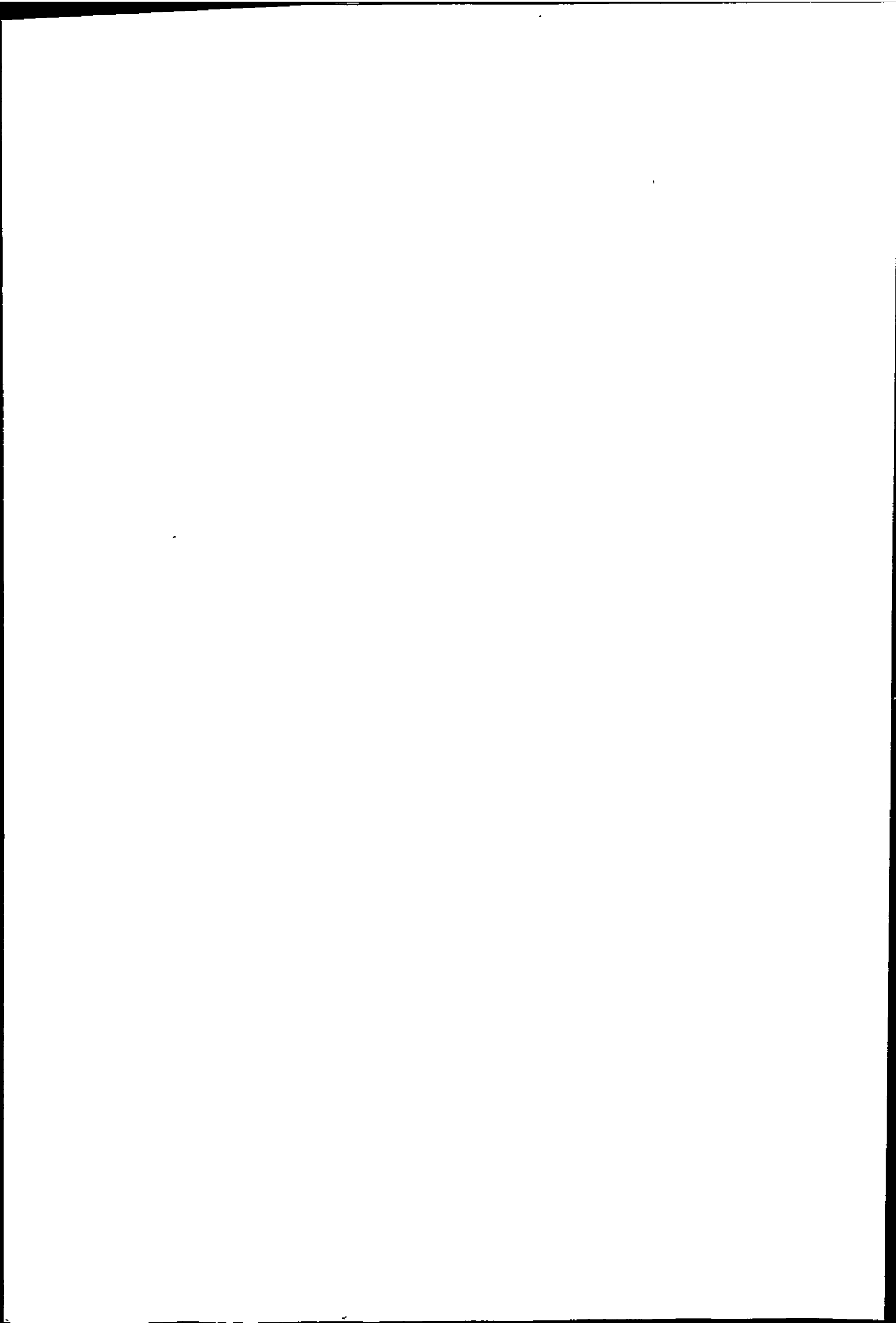
oxidation at temperatures up to 1600 $^\circ$C by silicides and alumina, forming refractory carbide layers with hot pressed samples. Magne et al[75] decomposed ammonium phosphate on a graphite surface and found the air oxidation at 600 $^\circ$C inhibited.

Boron is the only element of suitable size and electronegativity to substitute for carbon in the graphite lattice. It is an accelerator of graphitisation in carbon fibres and other forms of carbon. Graphites with substitutional and interstitial boron may be prepared by the addition of boron or B_4C to the carbon followed by graphitisition. Interstitial boron may be diffused away with heat treatment. Such materials were oxidised by O_2 in the temperature range 580 $^\circ$ - 780 $^\circ$C by Woodley[76]. The B_4C oxidised to B_2O_3 (at a slower rate than C/O_2 oxidation), which formed a physical barrier to diffusion and the oxidation rate of the graphite was reduced. The B_2O_3 acted by blocking pores and its removal by leaching in hot water resulted in a surface area increase and a subsequent increase in rate of oxidation.

The effect of substitutional boron on the kinetics of the C/O_2 and C/CO_2 reactions was investigated by Allardice and Walker [77,78]. In dry O_2 rate of gasification at 625 $^\circ$C and B.E.T. surface area decreased for doped graphites. This was considered to be due to progressive accumulation of B_2O_3 on the surface blocking active sites. The effect of different B/C ratios was

81
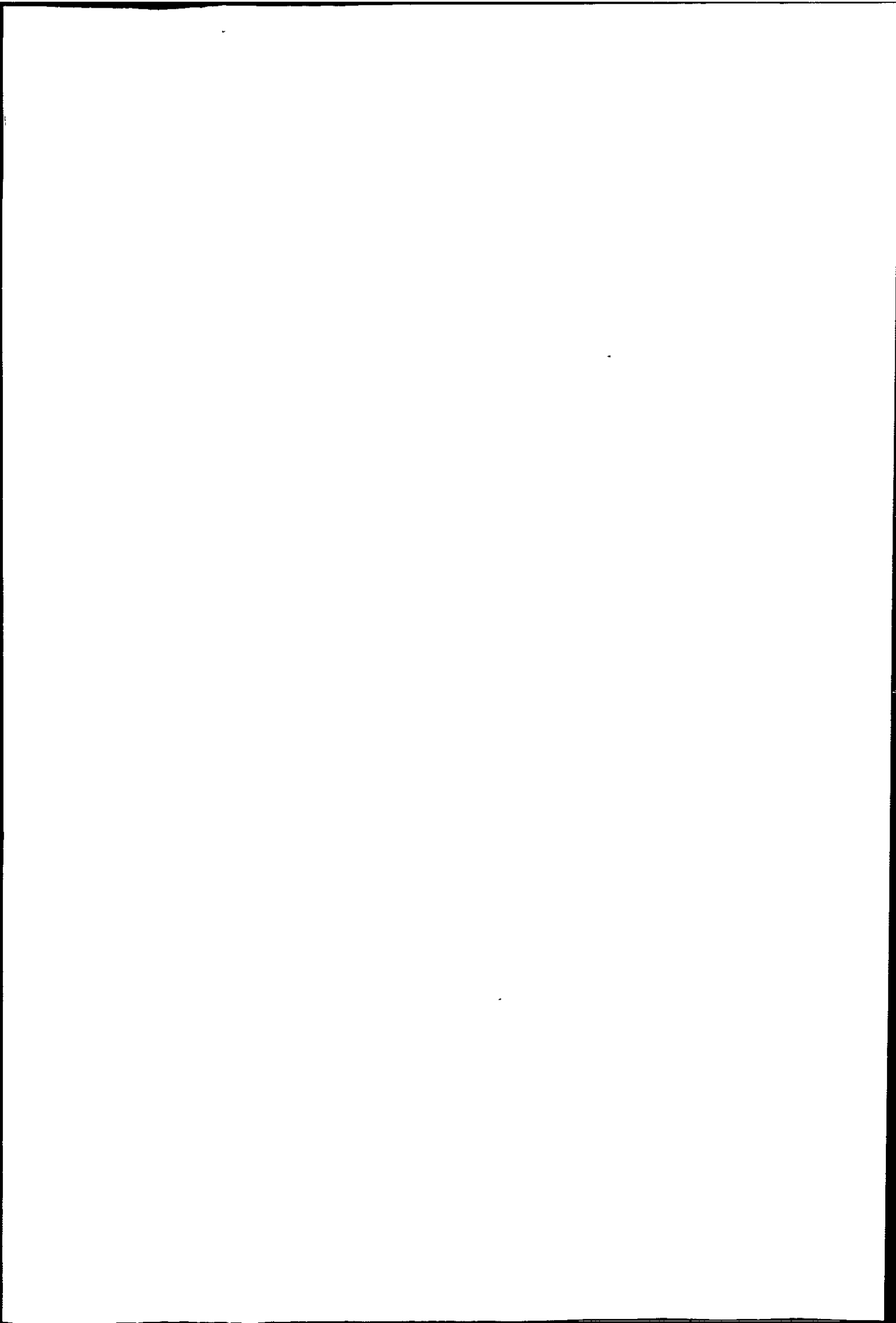
investigated and correlated with the electron acceptor properties of boron.

The rate of the doped graphite gasification by CO_2 at 925 - 1050 $^\circ$C was also less than undoped, although there was no accumulation of liquid B_2O_3 on the surface. The order of reaction changed with degree of boronation, although E_A was not affected, in contrast to the C/O_2 reaction. The authors suggest that boron acts by a chemical effect, rather than a physical one, in inhibiting the initial chemisorption step in the Boudouard reaction.

In these last three studies boron was an integral part of the solid structure and progressively accumulated on the surface as gasification proceeded. Thomas and Roscoe[79] studied the oxygen oxidation of single crystal graphite at 835 $^\circ$C on which boron had been introduced as a suspension of the element in acetone. Globules of B_2O_3 were seen on the surfaces, using a photomicrographic technique, forming over etch pits which grew by lateral expansion, the B_2O_3 thinning and redistributing. Rate of oxidation at hexagonal etch pits was less by a factor of five in the presence of the molten B_2O_3. Behaviour was different for oxidation by moist oxygen in the presence of boron.

Thus inhibition of graphite gasification by B_2O_3 appears to be effected by physical blocking of surface. A study of the inhibition of the CO_2 gasification of lump coke was required for which B_2O_3 seemed the most suitable

82
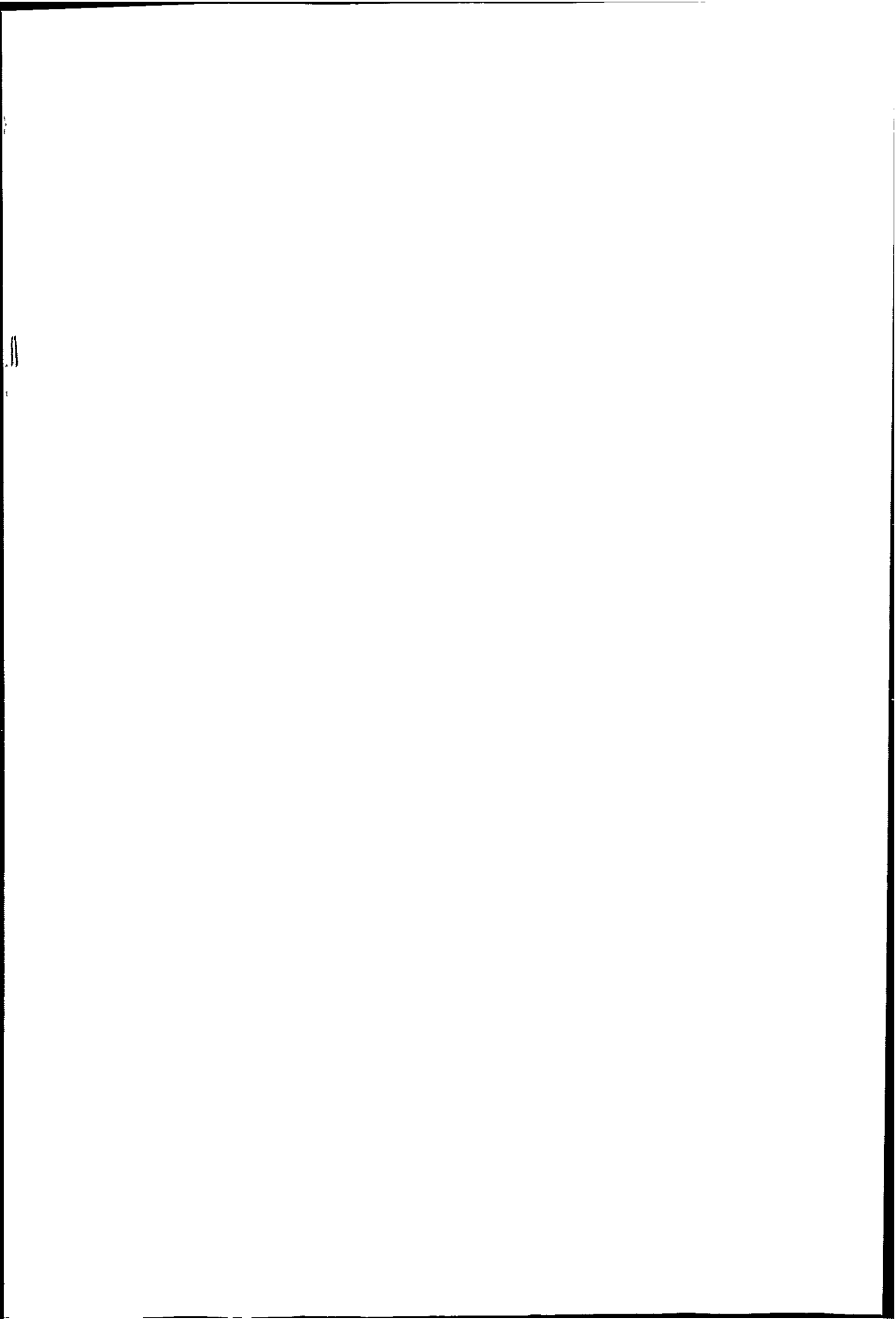
and economical compound. Alteration of a coking mix by

additives (such as the borides added to pitch coke

described by Hagio et. al.[80]) is not considered for Zn-Pb

production.

2.4.2 Summary of Industrial Work on Boronated Cokes

Trials were conducted at Lurgichemie[81] on three metallurgical cokes (0.5 to 1 mm granules) treated by drenching in ammoniacal boric acid solution. Reactivity to CO_2 at 1000 °C (ECE test method) was considerably reduced, even small amounts of B_2O_3 (0.3 mg g^{-1} coke) reducing reactivity to about 70% of untreated value. Increased treating of the coke (beyond 10 mg g^{-1}) did not further reduce reactivity, the maximum reduction being to about 25% of untreated value. Drenching lump coke followed by crushing also led to reduction.

Work on 15 oven cokes (including Cwm and Nantgarw) at I.S.P. by Bryson et al[82] used sections cut from lump coke, dipped in 2.5% boric acid at 30 °C and air dried. Reactivity to $CO2$ at 1000 °C (Nantgarw ratio test) was reduced, on average by about 34%.

Bryson et al[83] tested the reactivities of formed coke by solution treatment with separate compounds. Most were more effective reducers at 1000 °C than 1300 °C and those containing boron were the most successful. Boric acid, borax and "Polybor" were tried at different concentrations and 5, 10 and 15 second dipping times at 60 °C. Dipping time had little effect.

Work by Bryson and Illingworth[84] showed that dipping hot formed coke in boric acid powder also resulted in reactivity reduction. Further work by Illingworth[85,86] showed that boric acid added before briquetting had no
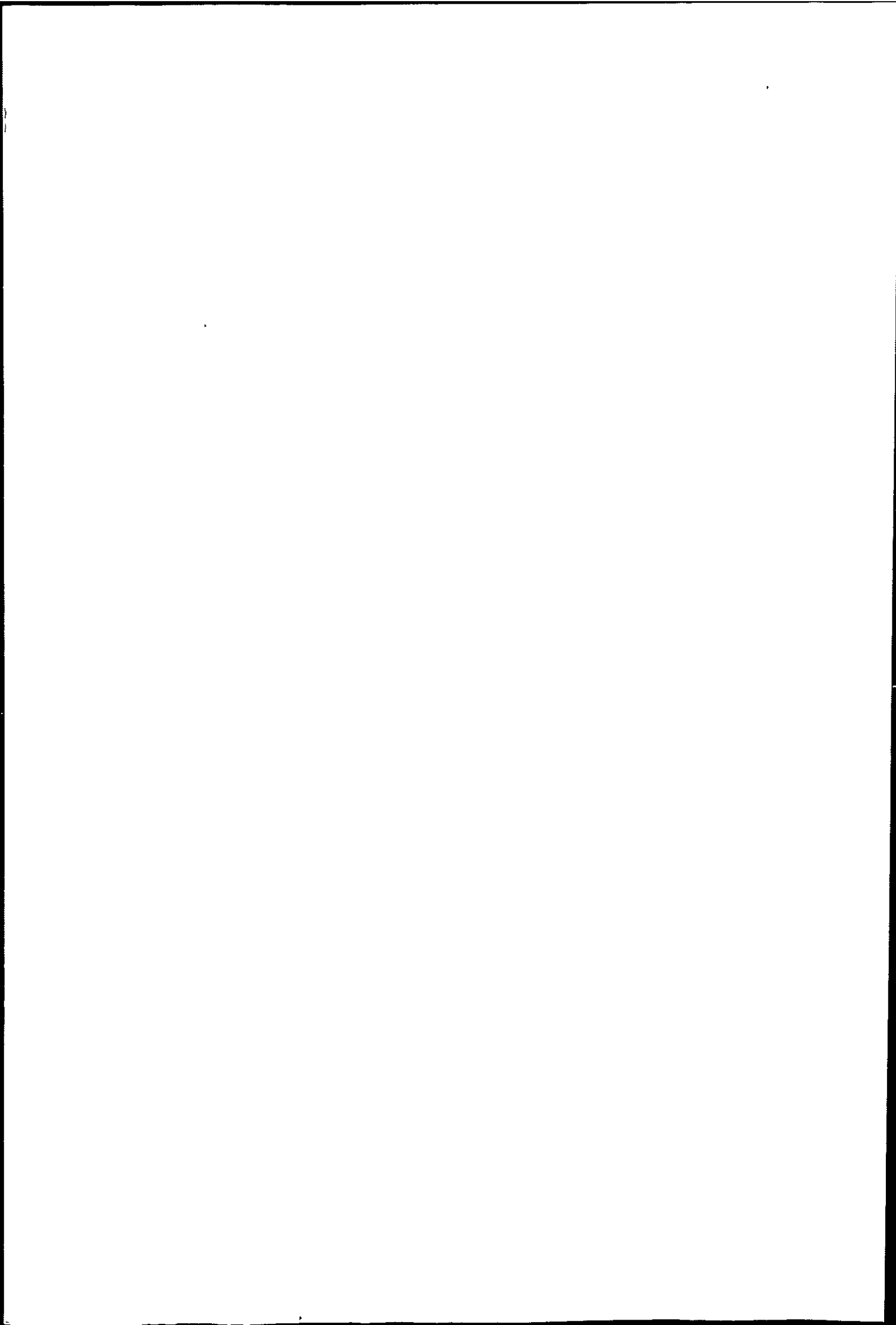
effect in reducing formed coke reactivity and solution
treatment before coking was not as effective in reducing
reactivity as dipping after coking.

It was concluded by I.S.P. that "Polybor", boric
acid and borax were viable inhibitors of reactivity,
solutions in cold water were adequate and that only
spraying or dipping was feasible in plant operation.
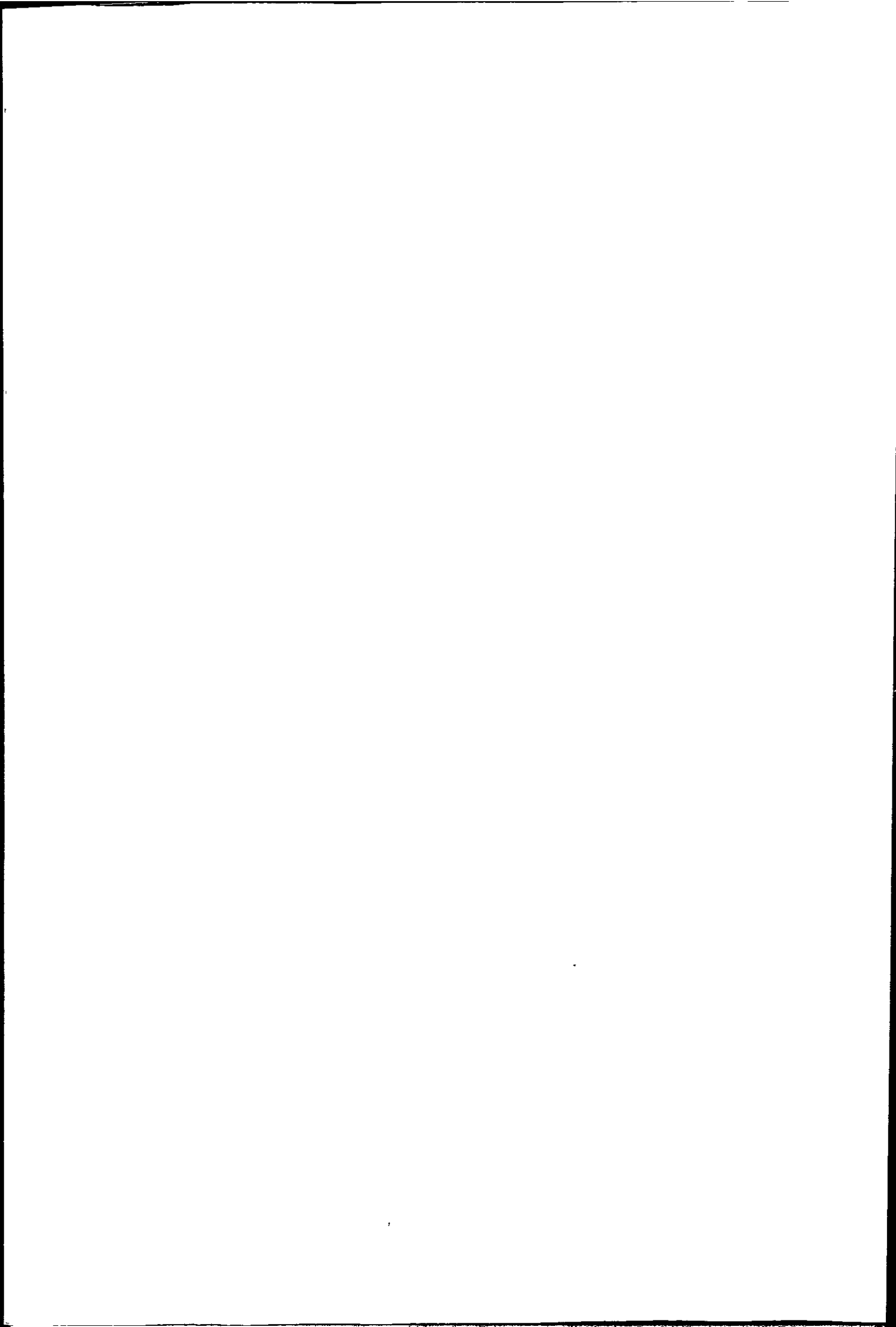
2.5 Aims of the Research

This work forms part of a wider study on the physico-chemical properties of coke. Previous workers in these laboratories have investigated the oxidation of zinc sulphide and lead sulphide and the present work looks at the reducing agent (coke) of the metal oxides in the Zn/Pb blast furnace. Other cokes used in the iron blast furnace are being studied in related projects.

It was hoped to gain insight to some aspects of coke reactivity by studying selected cokes and carbons of different pore structure (chars etc.). The nature of the inhibiting effect of B_2O_3 on coke reactivity was to be investigated.

Mathematical models were to be applied to rate studies and where possible correlated with surface structure obtained from microscopic examination.
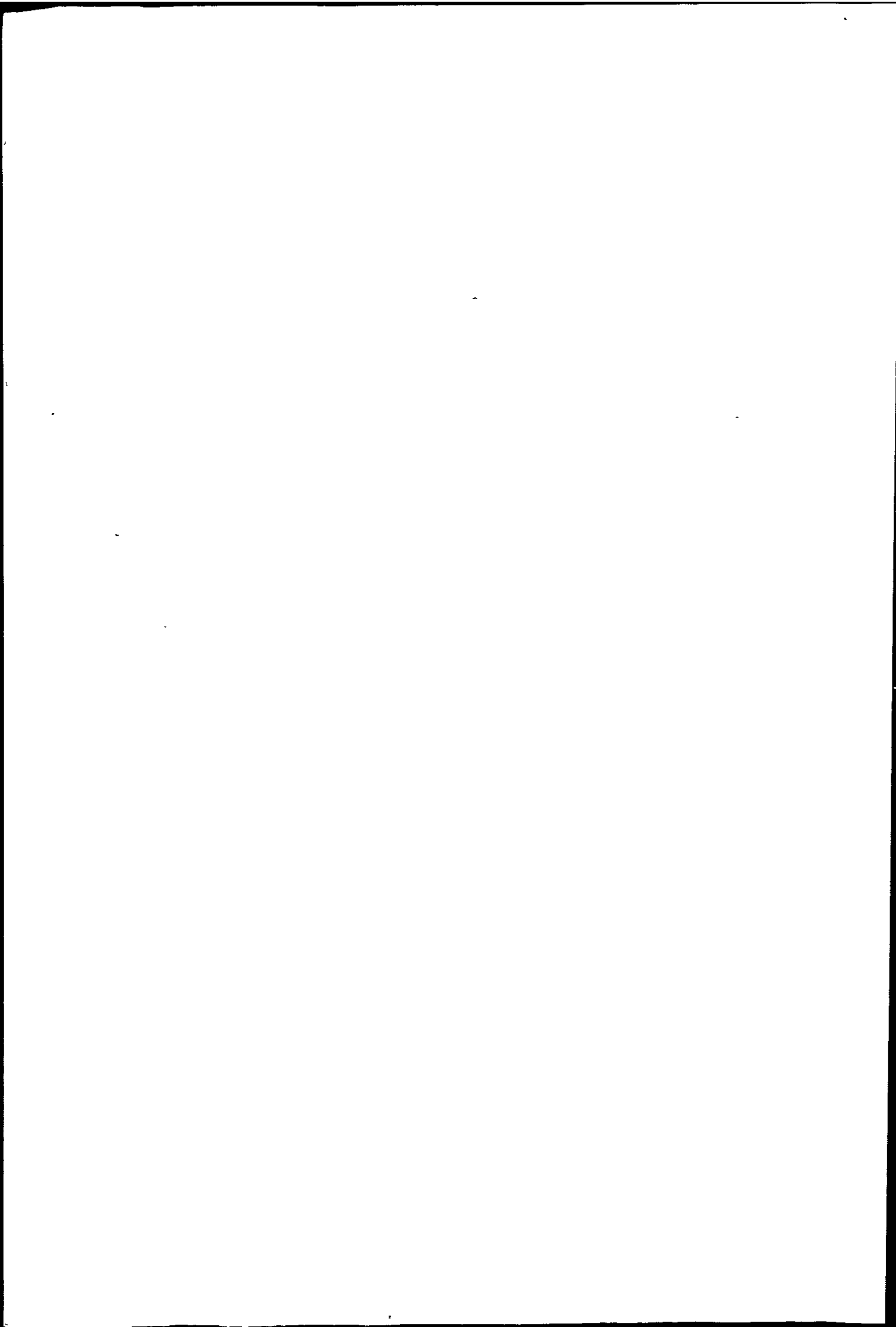
REFERENCES

1. H.P. Howland. Trans. Amer. Inst. Min. Eng.
    1916-17 56 339-64.

2. M. Mayers, Chapter 24 of "Chemistry of Coal
    Utilisation" Volume I, H.H. Lowry (Ed.) 1977
    John Wiley. Reprint of original title published in
    1945.

3. H.E. Blayden "Science in the Use of Coal" Conference
    Proceedings 1958, Published by the Institute of Fuel.

4. The Coke Oven Manager's Yearbook 1980. 131-151.

5. "Method of Measuring the Reactivity of Metallurgical
    Cokes". 1965. United Nations Publication ST/ECE/Coal/
    12.

6. Imperial Smelting Processes Ltd. Private communication.

7. J.G. King & J.H.Jones. J.Inst. Fuel. 1931, 5,
    39-55.

8. S. Banerjee & R.J. Sarjant. Fuel, 1951, 30,
    130-139.

9. S. Okstad & A. Høy. 2nd Conference Ind. Carbon and
    Graphite 1965. SCI, London 100-106.

10. I. Barbu & G. Reinhorn Metalurgia (Bucharest),
    1966, 18, (Pt. I), 620-1.

11. D.A. Reeve, Dept. of Energy, Mines and Resources.
    Mines Branch Ottawa Technical Bulletin TB 154, 1972.

12. N.L. Gol'dshtein, D.M. Zlatoustovskii, N.N.
    Zvereva & V.A. Zemlyanskov. Stal' 1975, 11, 977-81.
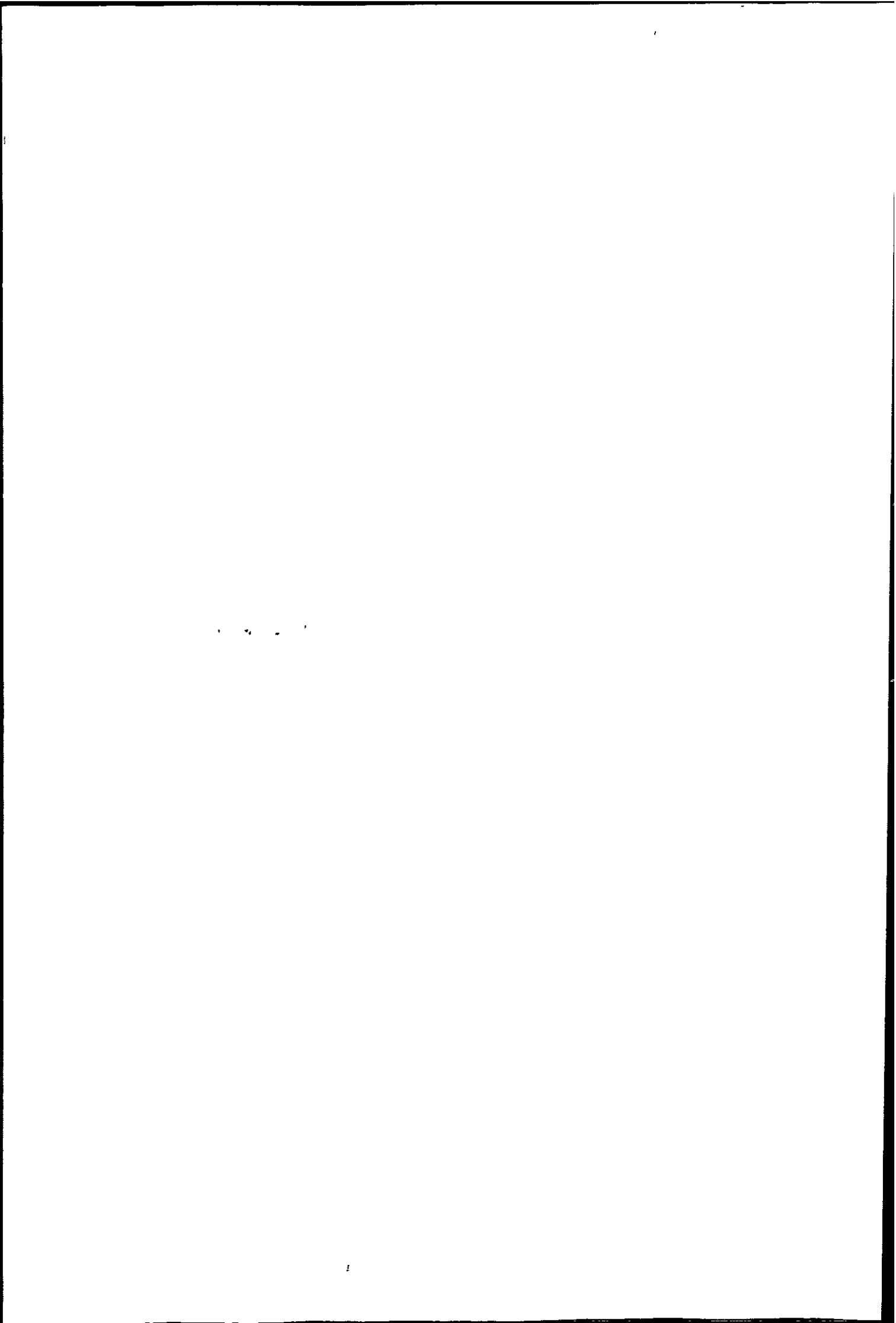
13. W-K Zu, G. Samaan & M. Uribe. Iron and Steelmaking, 1981, 24-31.

14. R.P. Donnelly, L.J. Brennan & A. Rouillard. Fuel, 1970, Series 49(1), 49-60.

15. C.R. Cross. The Coke Oven Managers Yearbook, 1980.

16. E. Hippo & P.L. Walker, Jr. Fuel, 1975, 54, 245-8.

17. P.L. Walker, Jr., O.P. Mahajan & M. Komatsu. Am. Chem. Soc. Div. Fuel Chemistry, 1979, 24, Part 3, 10-16.

18. D.J. Watson & V.R. Gray. N.Z. Journal of Science, 1980, 23, 313-17.

19. N.B. Gray & V.N. Misra. Proc. of Australia-Japan Extractive Metallurgy Symposium (Australia) 1980, 419-29.

20. A.T. Knight & G.D. Sergeant, Fuel, 1982, 61(2) 145-9.

21. R.G. Jenkins, S.P. Nandi & P.L. Walker, Jr., Fuel, 1973, 52, 288-93.

22. A.T. Knight & G.D. Sergeant. "Chemeca 82", Proc. 10th Aus. Chem. Eng. Conf. 1982, 243-7.

23. H. Marsh & J. Smith. "Analytical Methods for Coal and Coal Products", Volume 2, Chapter 30, 1978, Academic Press.

24. J.W. Patrick, M.J. Reynolds & F.H. Shaw. Fuel, 1973, 52, 198-204.

25. N. Schapiro & R.J. Gray, Blast Furnace and Steel Plant, 1963, 273-280.
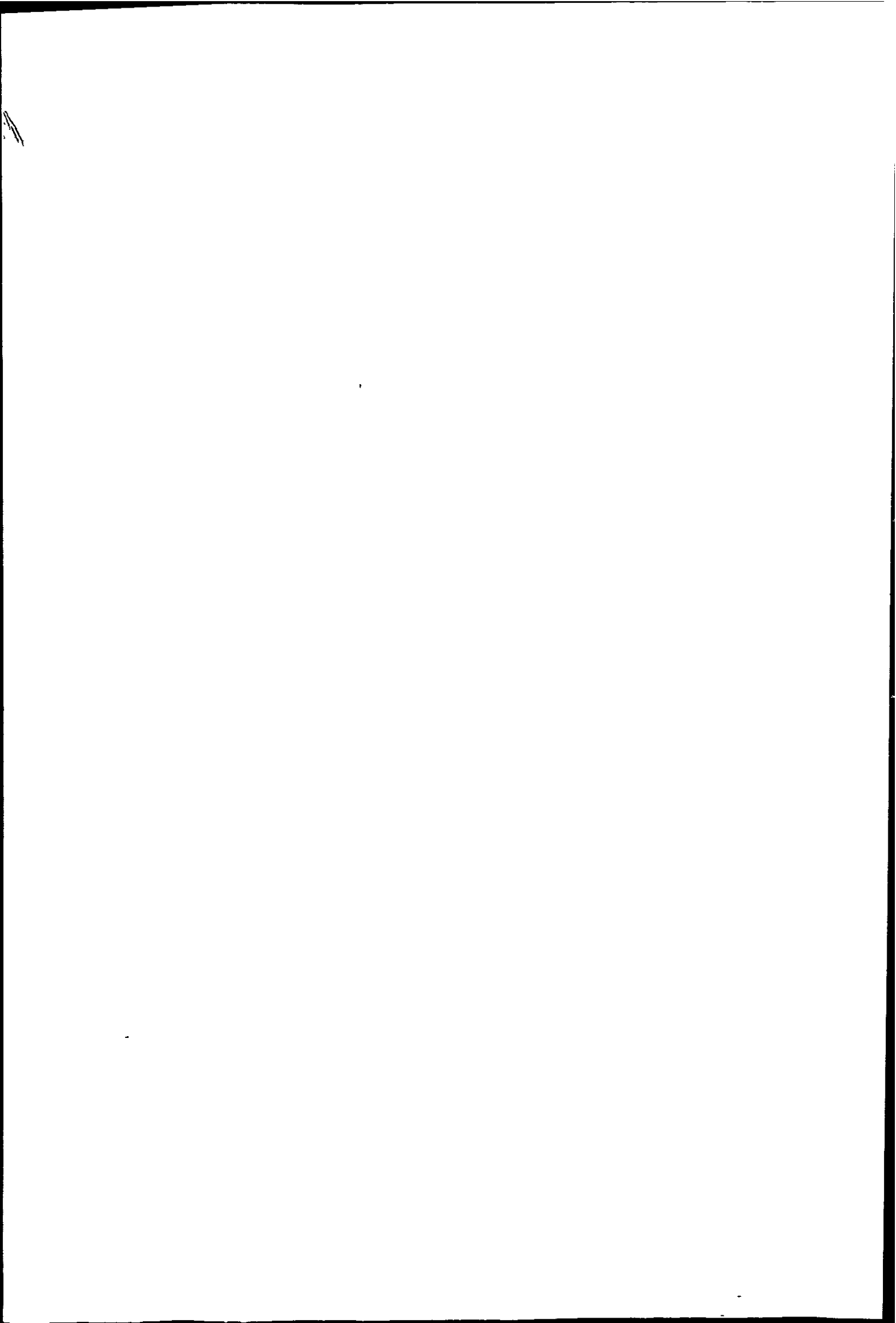
26. R.R. Thompson, A.F. Mantione & R.P. Aikman. Blast Furnace and Steel Plant 1971, 161-77.

27. L.G. Benedict & R.R. Thompson, Int. Jnl. of Coal Geology, 1981, 1(Pt.1) 19-34.

28. R.R. Thompson & L.G. Benedict. Proc. 34th Ironmaking Conference, Toronto, 1975, 122-32.

29. J.W. Patrick & H.C. Wilkinson, Coke Oven Managers Yearbook, 1980, 191-220.

30. S. Nishida, H. Fujita & M. Hijiriyama, Extended Abstracts, 15th Biennial Carbon Conference, 1981, 445-6.

31. W.W. Gill & C.D.A. Coin, Steel Times International, 1981, 81-92.

32. H. Fujita, M. Hijiriyama & S. Nishida. Nenryo Kyokaishi, 1982, 61(658), 109-17.

33. H. Fujita, M. Uba & S. Nishida, ibid. 1982, 61(661) 301-5.

34. H. Marsh, Journal of The Iron and Steel Institute 1973, 334-45.

35. D.A. Aderibigbe & J. Szekely, Ironmaking and Steel-making, 1981, 8 Pt.1, 11-19.

36. C. Heuchamps, Bulletin Societe Chimique de France, 1967, 4205-9.

37. E.T. Turkdogan & J.V. Vinters, Carbon 1970, 8, 39-53.

38. A.W. Richards & G.H. Tandy, Imperial Smelting Processes Ltd., Private communication.

39. L.L. Isaacs, Pre-prints of Papers, Am. Chem. Soc. Div. Fuel Chemistry, 1978, 23., Pt. 4, 215-23.

40. L. de Sinteza, Metalurgia (Bucharest) 1979, 31, Part 10-11, 551-4.

41. N.G. Dovaston, B. McEnaney & S.M. Rowan, Proc. 3rd Ind. Carbon and Graphite Conference, 1970, (SCI London) 212-9.

42. B. McEnaney & M.A. Willis, Proc. 5th London International Carbon and Graphite Conference, 1978, Volume I, 88-96, SCI London.

43. H. Marsh and D.W. Taylor, Fuel, 1975, 54, 218-9.

44. D. Dollimore and A. Turner, Trans. Faraday Soc., 1970, 66, 2655.

45. H. Marsh & D.W. Taylor. Extended Abstracts, 13th Biennial Carbon Conference. Am. Chem. Soc. 1977, Part 13, 132-3.

46. B. McEnaney & C.J. Weedon, Proceedings of 3rd Conf. Industrial Carbon and Graphite 1970, SCI London, 207-11.

47. G.M. Kimber and M.D. Gray, ibid. 278-81.

48. S. Kasaoka, Y. Sakatu, S. Kayano & Y. Masuoka Kaguka Kogaku Ronbunshu, 1982, 8(2), 174-80.

49. S. Dutta, C.Y. Wen & R.J. Belt, Ind. Eng. Chem. Process Des. Dev., 1977, 16 No. 1, 20-30.

50. I. Bjerle, H. Elkund, M. Linne & O. Svenson, ibid. 1982, 21 141-9.

51. D.I. Bradshaw, S.J. Peacock & G. Meir. Extended Abstracts 6th London Int. Carbon and Graphite Conference, 1982. SCI 106-8.

52. J.C. Lewis, Proc. 2nd Conf. Industrial Carbon and Graphite 1965, SCI London, 258-68.

53. M. Navarro and G.M. Jemkins, Extended Abstracts 4th London International Carbon and Graphite Conference 1974, SCI London, 116.

54. L.F. Jones, D. Dollimore and T. Nicklin, Thermal Analysis 2, Proceedings Third ICTA Davos, 1971.

55. W.W. Wendlandt, "Thermal Methods of Analysis", 1974, John Wiley & Sons.

56. A.C. Norris, M.I. Pope, M. Selwood and M.D. Judd. Thermal Anal. 1, Proceedings Fourth ICTA, Budapest 1974.

57. C.J. Keattch & D. Dollimore "An Introduction to Thermogravimetry" 2nd Edition 1975, Heyden & Son Ltd.

58. A. Blazek, "Thermal Analysis" 1973, Van Nostrand Reinhold.

59. M.I. Pope and M.D. Judd, "Differential Thermal Analysis", 1977, Heyden & Son Ltd.

60. J.H. Sharp, "Differential Thermal Analysis" Chapter 28, MacKenzie (Ed.) 1982, Academic Press.

61. H.E. Kissinger, Anal. Chem. 1957, 29 No.11, 1702-6.

62. H. Marsh & D.W. Taylor, Carbon, 1977, 15, 265-6.

63. D.A. Aderibigbe and J. Szekely, Metallurgical Transactions B, 1982, 13B, 513-5.

64. B. Dobovisek, N. Smajic and A. Rosina, Mikrochimica Acta 1967, Issue 4, 639-50.

65. D.J. Swaine, Thermal Analysis, Volume 2, 1969, Schwenker (Ed.) Academic Press, Proc. 2nd Int. Conf. 1968, 1377-86.

66. R.T. Yang, M. Steinberg & R. Smol, Anal. Chem. 1976, 48 No.12, 1696-9.

67. R.T. Yang & M. Steinberg, J. Phys. Chem. 1976, 80 No.9, 965-8.

68. G.W. Lee, Coke and Gas, October 1961, 398-405.

69. Y. Kawana, Bull. Chem. Soc. Japan 1954, 27 No.9, 574-8.

70. R. Zuniga & S. Droguett. Lat. Am. J. Chem. Eng. Appl. Chem. 1981, (Rev. latinoam ing. quim. quim. apl.) 11, 71-92.

71. K. Hedden, H.H. Kopper & V. Schulze. Z. Phys. Chem. 1959, 22, 23-62.

72. P. Hawtin & J.A. Gibson. Proc. 3rd Conf. Ind. Carbon and Graphite 1970, SCI London, 309-15.

73. J.R. Arthur and D.H. Bangham. J. Chim. Phys. 1950, 47, 559-62.

74. "Materials Science and Technology at N.P.L." 1981, Division of Materials Applications, National Physical Laboratory.

75. P. Magne, H. Amariglio & X. Duval. Bull.Sci. Chem. de France, 1971, 6, 2005-10.

76. R.E. Woodley, Carbon, 1968, 6, 617-26.

77. D.J. Allardice & P.L. Walker, Jr. Carbon 1970 8, 375-85.
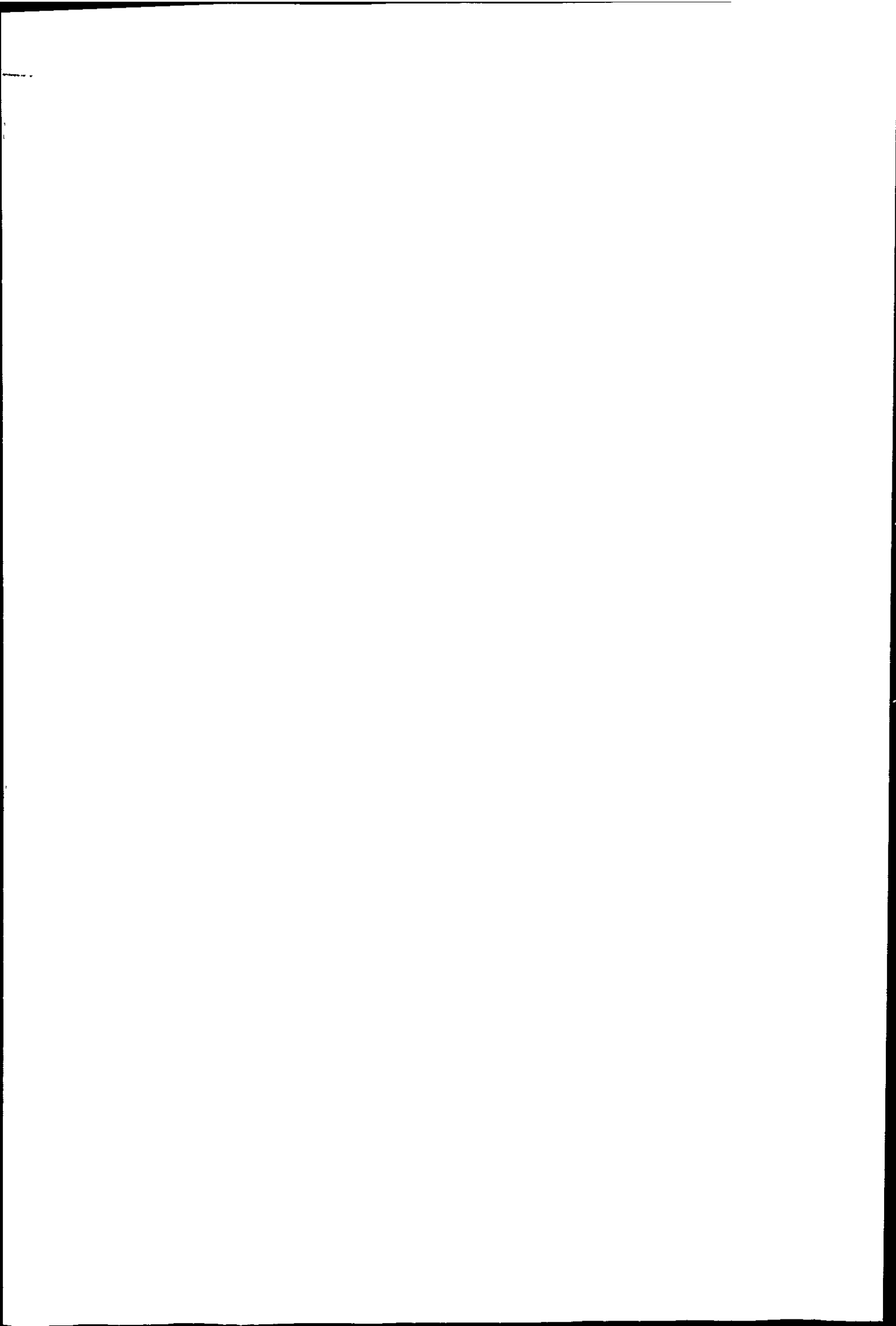
78. D.J. Allardice & P.L. Walker, Jr. Carbon, 1970, <u>8</u>, 773-80.

79. J.M.Thomas & C. Roscoe. Proc. 2nd Conf. Ind. Carbon and Graphite 1965, SCI London 249-57.

80. T. Hagio, K. Miyazaki & K.Kobayashi, Yogyo Kyokaishi 1979, <u>87(8)</u>, 416-22.

81. Lurgi Gesellschaft fur Warme - und Chemotechnik m.b.H. Private communication.

82. J.L. Bryson, W.R. Illingworth & J.P. Nash, Imperial Smelting Processes Ltd., Private communication.

83. J.L. Bryson, W.R. Illingworth & J.P. Nash, Imperial Smelting Processes Ltd., Private communication.

84. J.L. Bryson & W.R. Illingworth. Imperial Smelting Processes Ltd. Private communication.

85. W.R. Illingworth, Imperial Smelting Processes Ltd., Private communication.

86. W.R. Illingworth, Imperial Smelting Processes Ltd., Private communication

87. J.H. Blake, G.R. Bopp, J.F. Jones, M.G. Miller & W. Tambo, Fuel 1967, <u>46</u>, 115-25.

88. B.C. Young, Proc. International Conference on Coal Science. Dusseldorf 1981. (Publ. Verlag Gluckauf G.m.b.H. Essen 1981), 260-4.

CHAPTER THREE

EXPERIMENTAL TECHNIQUES

3.1   Thermal Analysis

3.1.1 The Massflow Thermal Balance

3.1.2 The STA 781 Thermal Analyser

3.2   Gas Sorption

3.2.1 The Nitrogen Sorption Balance

3.2.2 The Newer Gas Sorption Balance
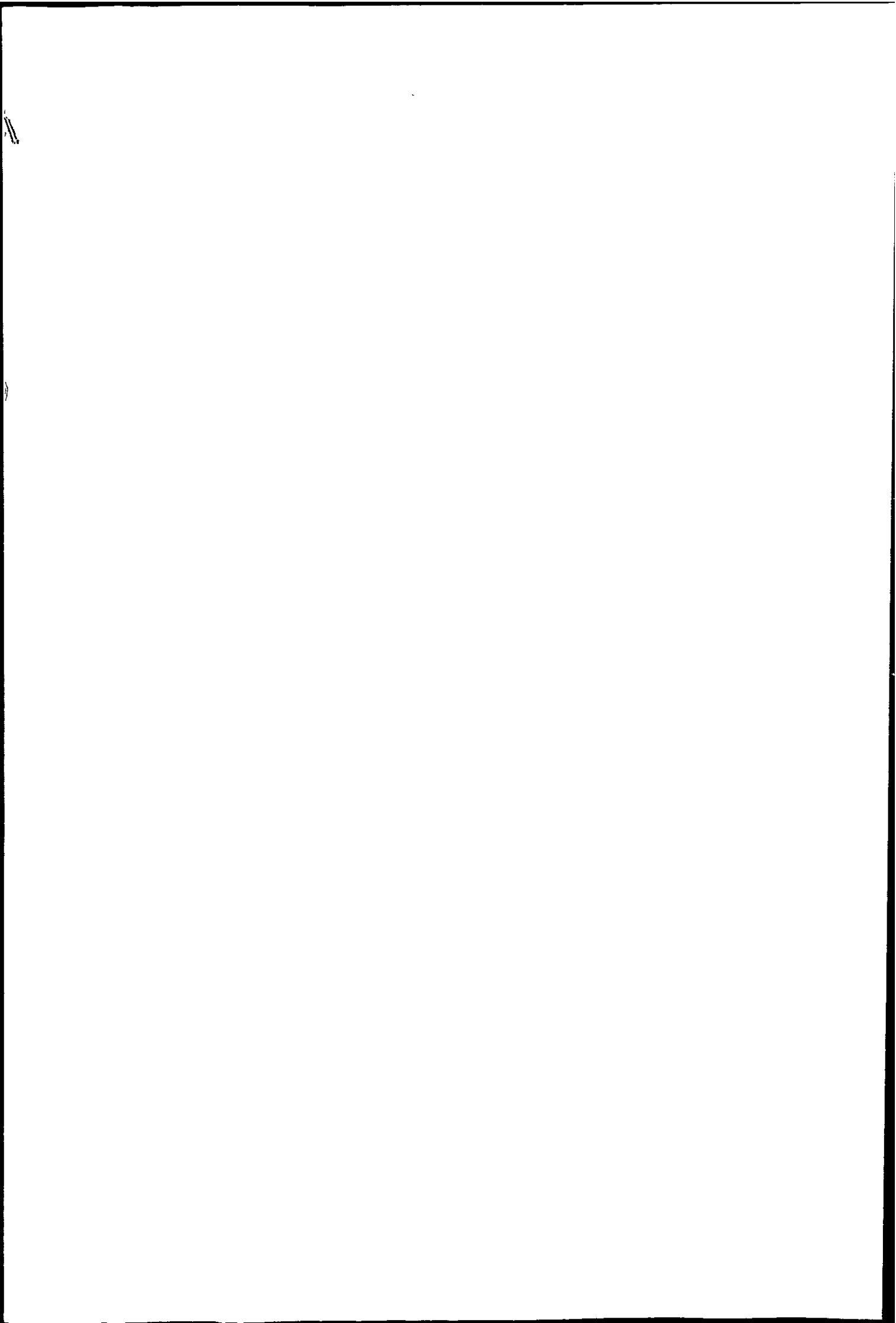
3.3   X Ray Diffraction

3.3.1 The X Ray Equipment

3.4   Microscopic Techniques

3.4.1 The Philips EM 300 Transmission Electron Microscope

3.4.2 The Jeol JSM-T20 Scanning Electron Microscope

3.4.3 Optical Microscopy

CHAPTER THREE

The coke and carbon reactivity study used thermal
analysis and gravimetric gas sorption as the main
experimental techniques. Transmission and scanning electron
microscopy were used to study the surface structure of the
materials and electron and optical microscopy to
investigate the coke and char mineral matter (ash). X ray
powder diffraction was also used to determine ash
constituents.

3.1   The principles of TG and DTA have been described in
Chapter 2.3.1, together with application to rate studies.
Two thermal balances were used in the present work.

3.1.1 The Massflow Thermal Balance

This is a Stanton Redcroft Massflow Thermobalance
model MF-H5 with some modifications, initially acquired
in 1974, and used with a Stanton Redcroft Eurotherm linear
temperature programmer model CA with programmed heating
rates between 2 to 40 ^{o}C min^{-1} and Leeds Northrup
"Speedomax W" chart recorder. A schematic diagram of the
balance and ancillary equipment is given in Figure 3.1.

The thermobalance design incorporates two beams, one
inside the chamber and the other outside, the two being
coupled by a magnetic link. Changes in weight occurring
on the inner beam are transferred to the outer beam,
detected electronically and indicated by an arm with a
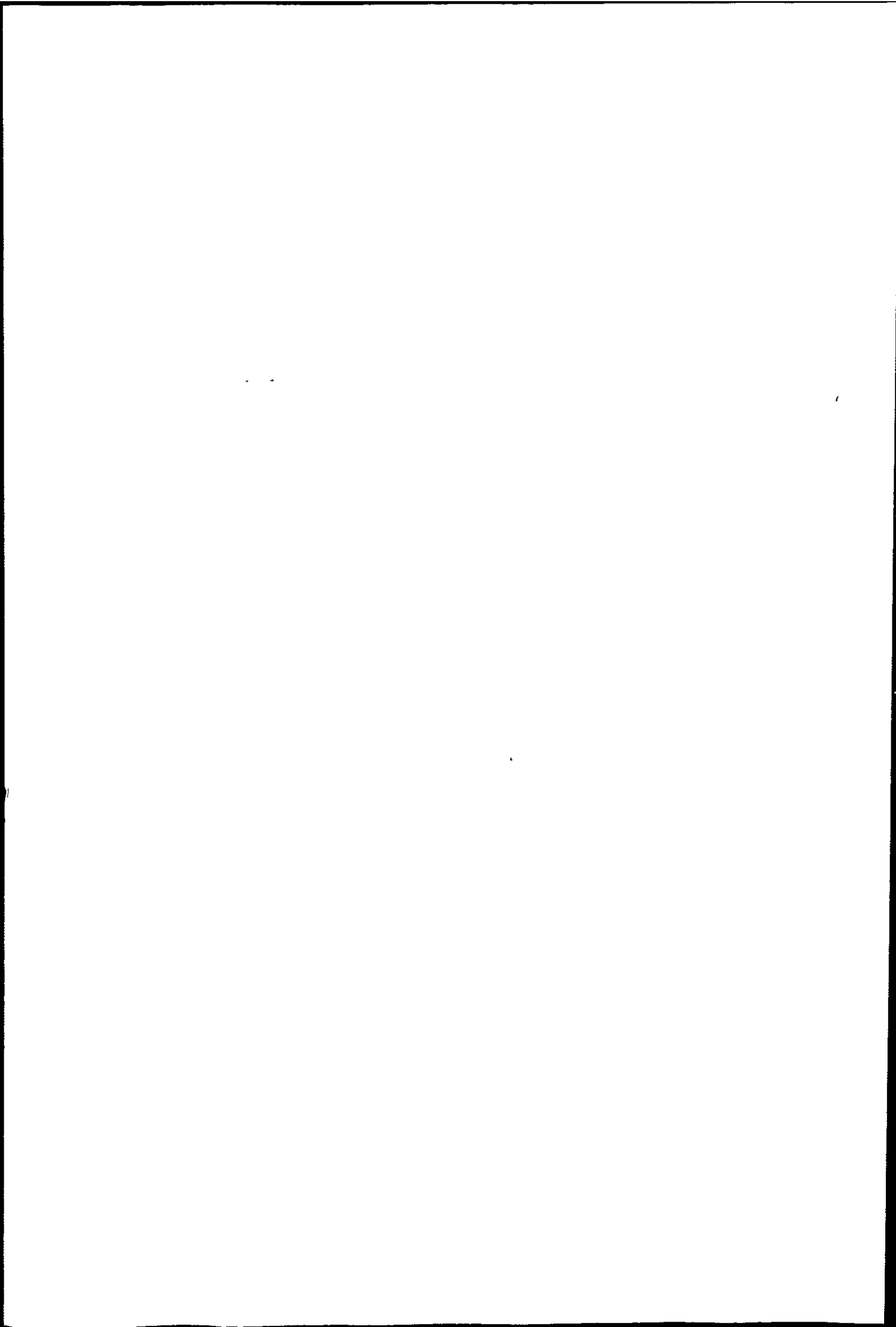full-beam deflection of 20 mg and sensitivity of 0.2 mg.

Schematic cross section of the balance chamber is
shown in Figure 3.2. The balance chamber is a 10-gauge

95

Mains power supply.
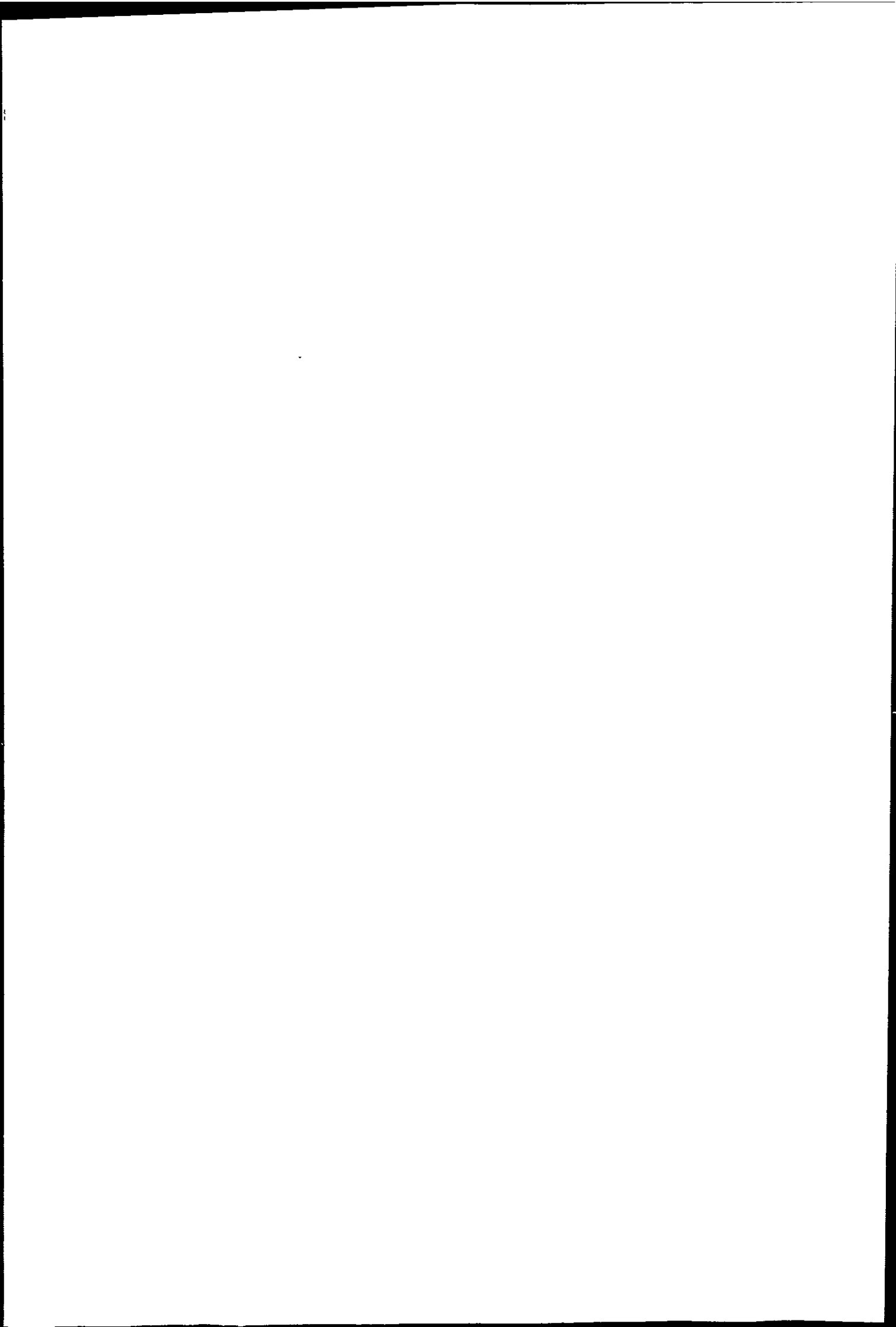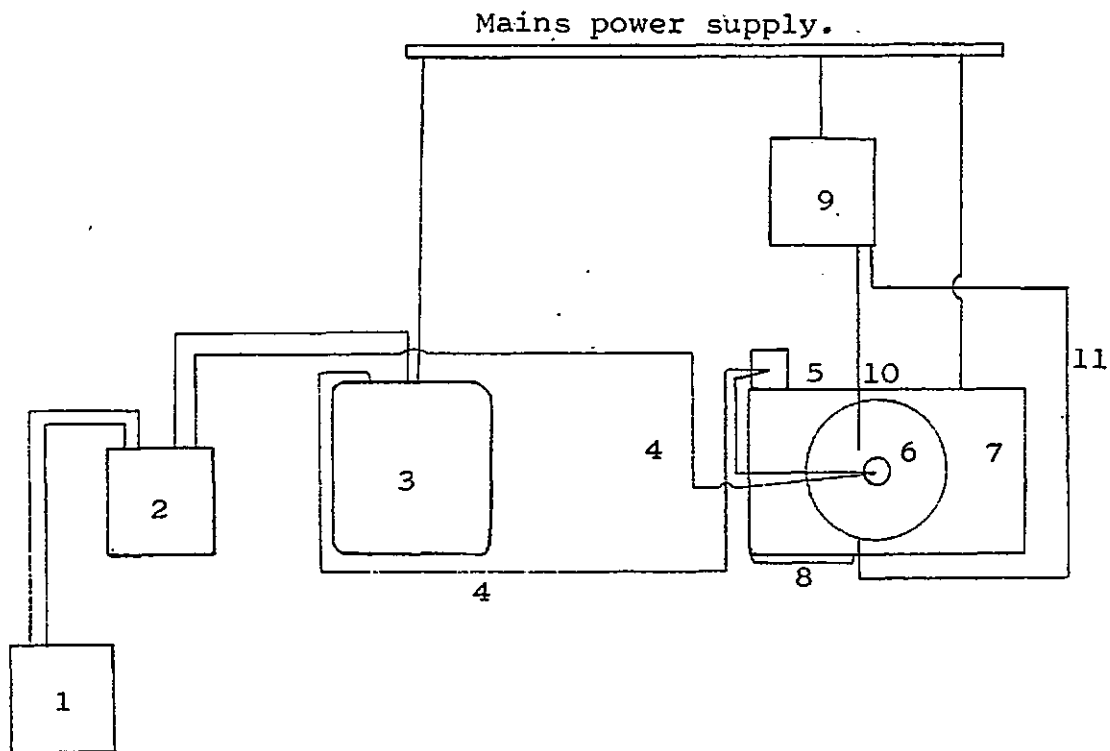
Key:
1. Chart recorder for ,T and ΔT

2. Signal switching unit forΔT and/or $\mathbb{T}$

3. D.C. amplifier 20-1000μ V range

4. Thermocouple of DTA head

5. Ice pot

6. Furnace

7. Thermobalance

8. TG record

9. Temperature programmer

10. Control thermocouple between furnace wall and mullite tube

11. Furnace load.

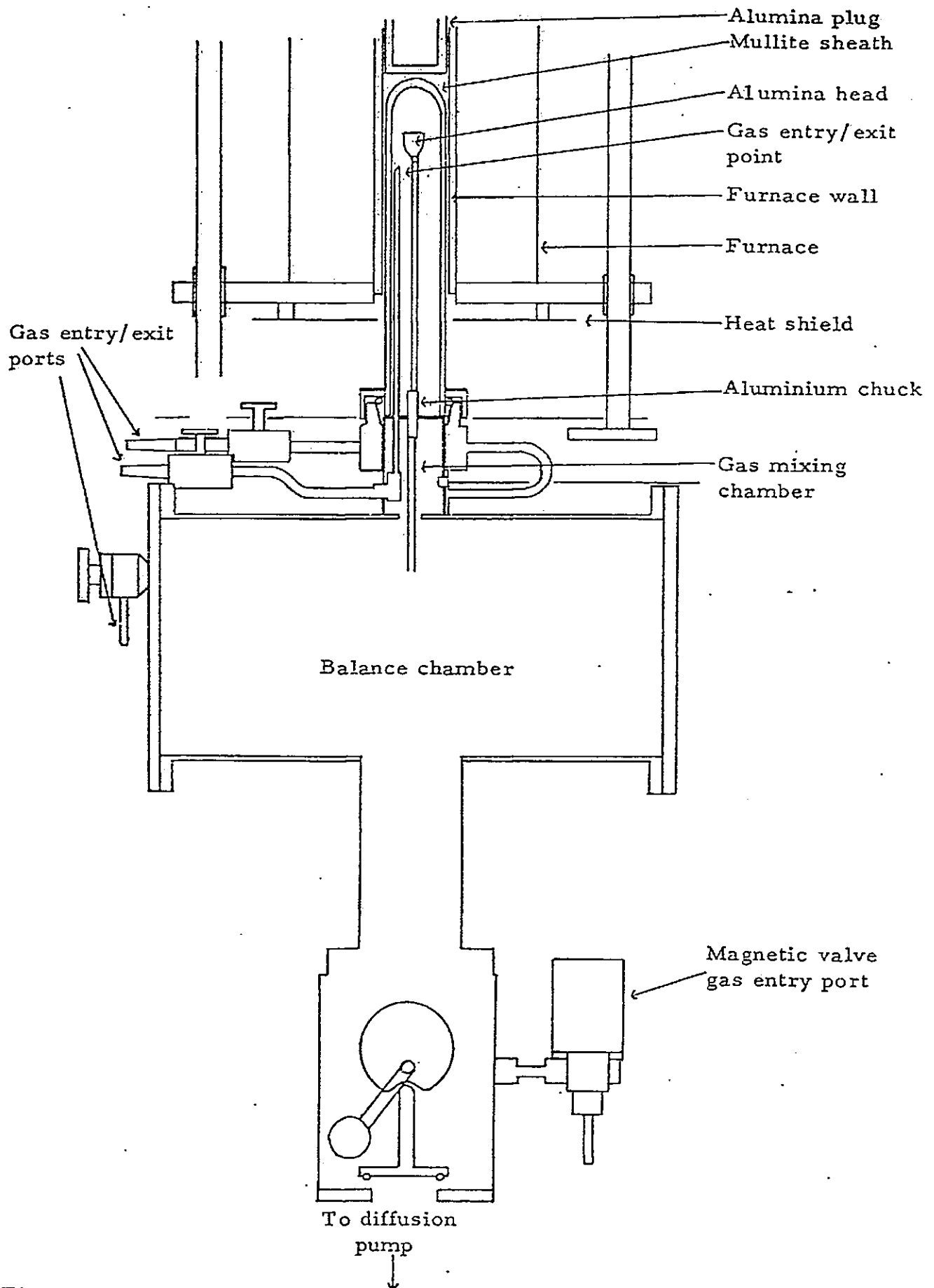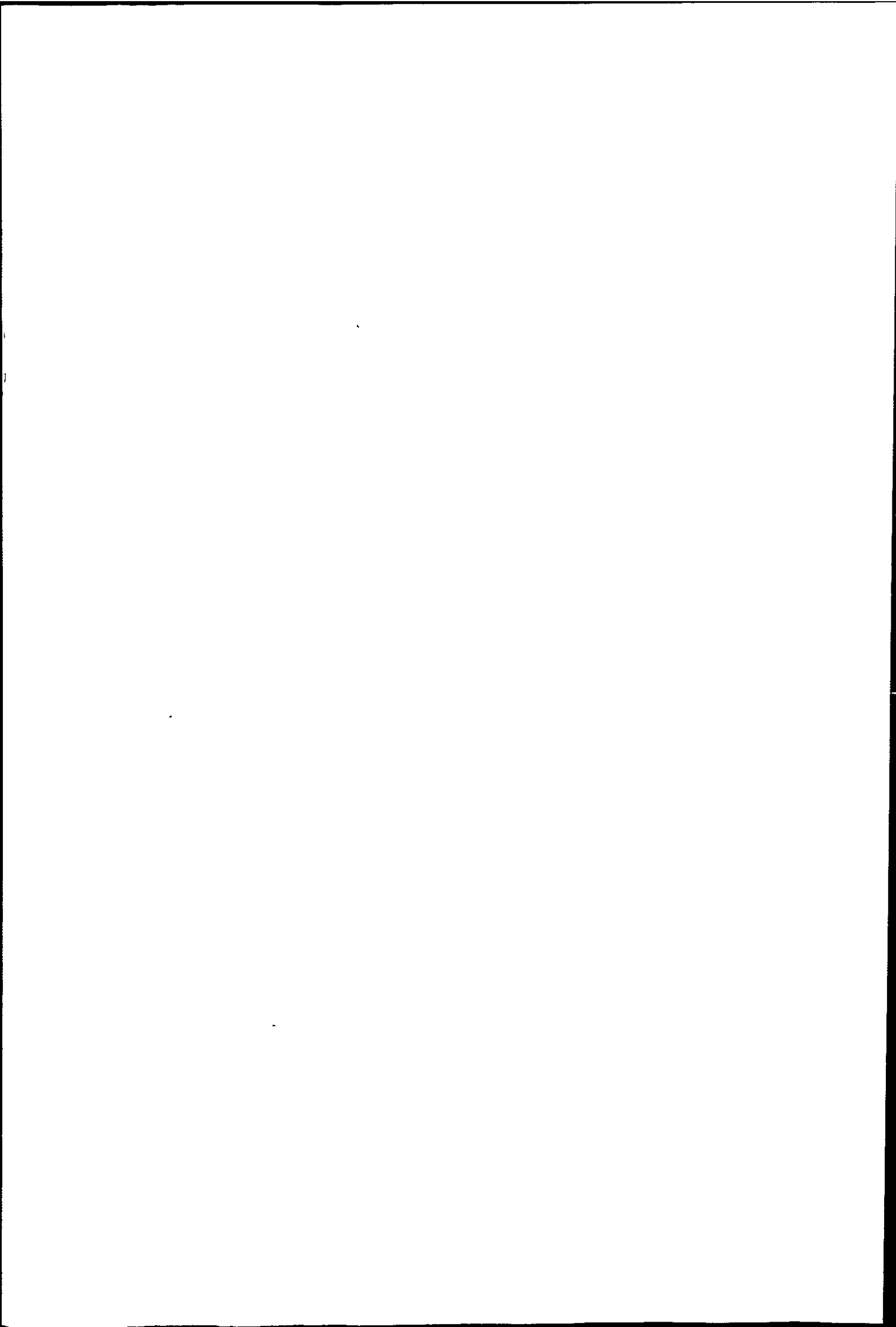Figure 3.1.   Massflow Thermobalance and Ancillary Equipment.

Alumina plug
Mullite sheath
Alumina head
Gas entry/exit point
Furnace wall
Furnace
Heat shield
Aluminium chuck
Gas mixing chamber

Gas entry/exit ports

Balance chamber

Magnetic valve gas entry port

To diffusion pump

Figure 3.2

Gas circuit of the Stanton-Redcroft Massflow Balance MF-H5

97

copper tube 178 mm diameter, silver brazed and epoxy-resin coated with doors 10 mm thick sealed with "O" rings. A water-cooled silicone "O" ring seals the mullite reaction tube to the chamber. There are four gas entry or outlet ports, two to the reaction tube and two to the main balance chamber. It is possible to keep a nitrogen atmosphere in the balance chamber and pass air containing corrosive gases over the sample. By means of the vacuum attachment, the system can be easily flushed out and known atmospheres introduced. The air for the oxidations under a flowing atmosphere was obtained from a pressurised cylinder and introduced via the two upper gas entry/exit ports, first passing through a rotameter where the rate of flow could be set. For the static air oxidations one of the entry ports was left open and the others closed.

Automatic electric weight loading increases the range of the instrument to the equivalent of ten full beam deflections of gain or loss without a decrease in sensitivity. This enables weight gains or losses of up to 200 mg to be followed.

During operation the balance automatically arrests and releases itself every 5 min to check that it is not sticking and to improve the sensitivity with very small weight changes.

The sample holder consists of an alumina block 20 mm diameter and 13 mm in depth with two wells each 6.5 mm diameter and 10 mm in depth to take the crucibles. The alumina head is coupled to the internal balance by alumina
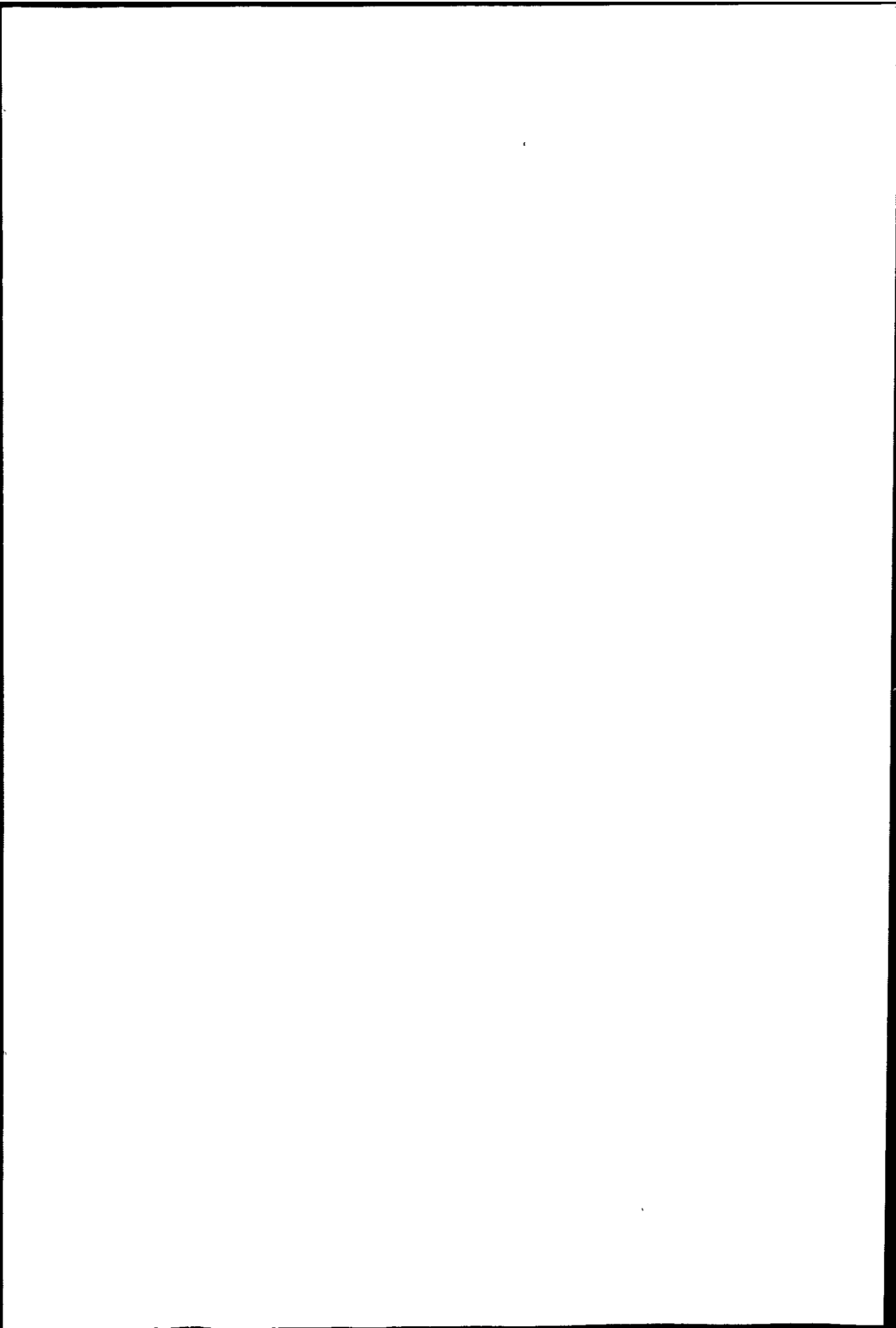
and silica rods joined by an aluminium chuck containing three adjustable screws by which the head is kept vertical.

Two matched (0.8g) platinum crucibles with dimples are used to contain the sample and reference material, as shown in Figure 3.3. The crucibles are placed in the 6.5 mm wells of the alumina head with the thermocouples sitting in the dimples and are thus surrounded by the sample. This leads to high sensitivity for the differential thermal output. Silica crucibles are limited in temperatures range due to reaction with alumina above 1000 $^{\circ}$C.

Two Pt/13% Rh Pt thermocouples are employed to detect the temperature difference between sample and reference ΔT and sample temperature T, as shown in Figure 3.4. The signal from the thermocouples is passed from the alumina head down the inside of the alumina and silica rods to the outside by 0.025 mm compensated platinum wires, which have a very small damping effect on the balance. Further compensated leads are employed to connect the signal with the DC amplifier and constant-reference-temperature ice-bath. The DC amplifier has seven pre-set ranges from 20-1000 μV; normally the 100 μV sensitivity setting is used. A single channel Leeds Northrup Speedomax W chart recorder is used with a switching unit enabling the differential output to be recorded for 4 min 55 s and then the temperature recorded for 5 s.

Calcined alumina was used as the thermally inert reference material. For isothermal work a shallow alumina crucible 24 mm diameter and 5 mm height was placed on the head and the switching unit used to record
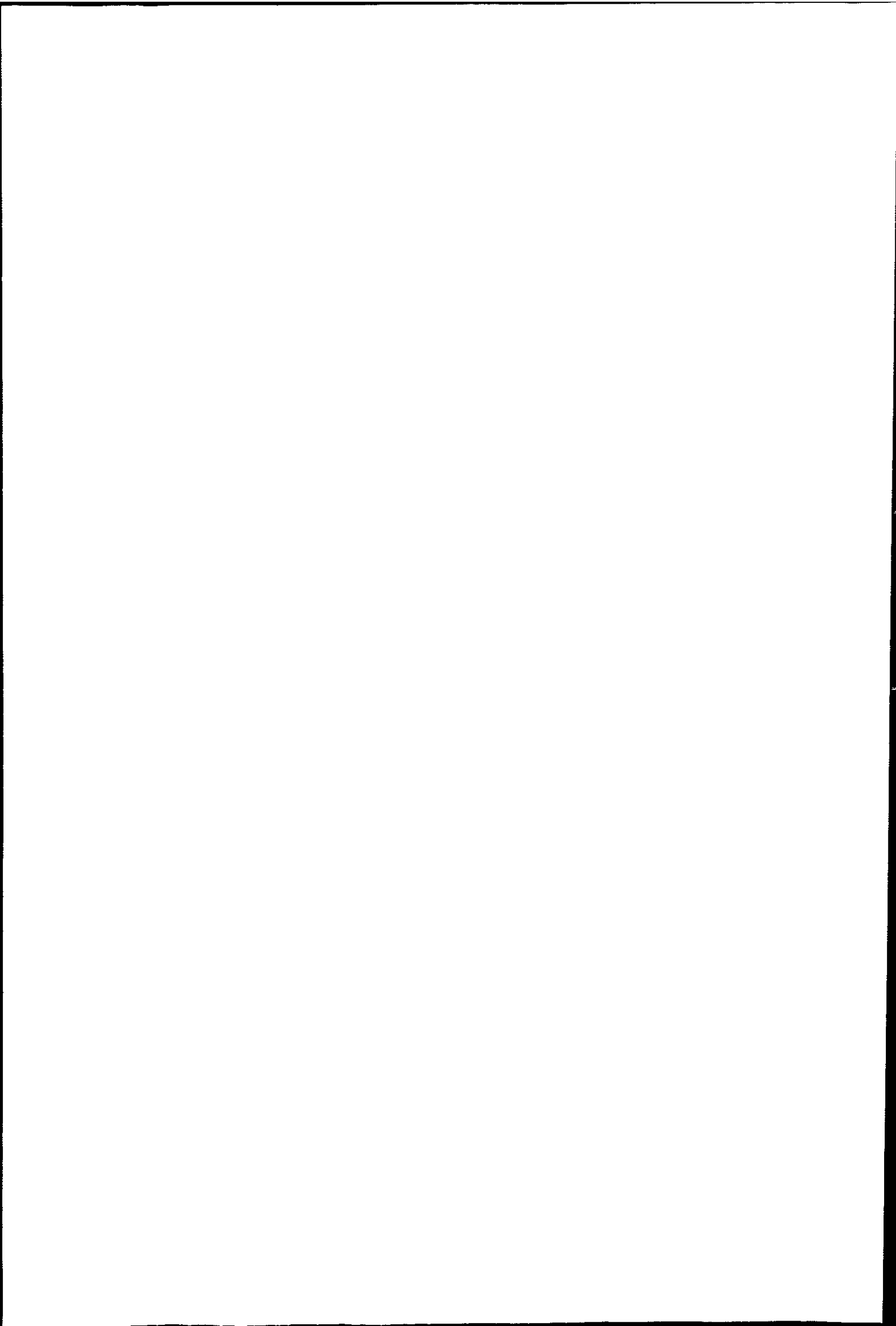
sample temperature, T, only.

The platinum-rhodium bifilar wound furnace has a 50 mm bore and is closed at the top with a 100 mm deep alumina plug filled with α-alumina powder. The furnace was rewound in 1981.

The temperature is controlled by a Stanton-Redcroft Eurotherm temperature controller with the sensing Pt/13% Rh Pt thermocouple trapped between the mullite reaction tube and the furnace wall. The controller enables the heating rate to be continuously varied from 2-20 ^{o}C min^{-1} with the maximum temperature (up to 1100 ^{o}C) pre-selected and subsequently held constant indefinitely (isothermal conditions).

Calibration curves were recorded, in static and flowing air, to determine buoyancy effect in TG and baseline drift in DTA, using alumina in both crucibles and a heating rate of 5 ^{o}C min^{-1}. The apparent weight increase was 1.5 to 2 mg and negligible after 200 ^{o}C. Buoyancy effect was also determined for isothermal TG using alumina in the shallow dish and preheating the furnace to 500, 700 and 900 ^{o}C. The effect was greater, although of shorter duration, the higher the furnace temperature. Correction for buoyancy was applied to all the TG work.
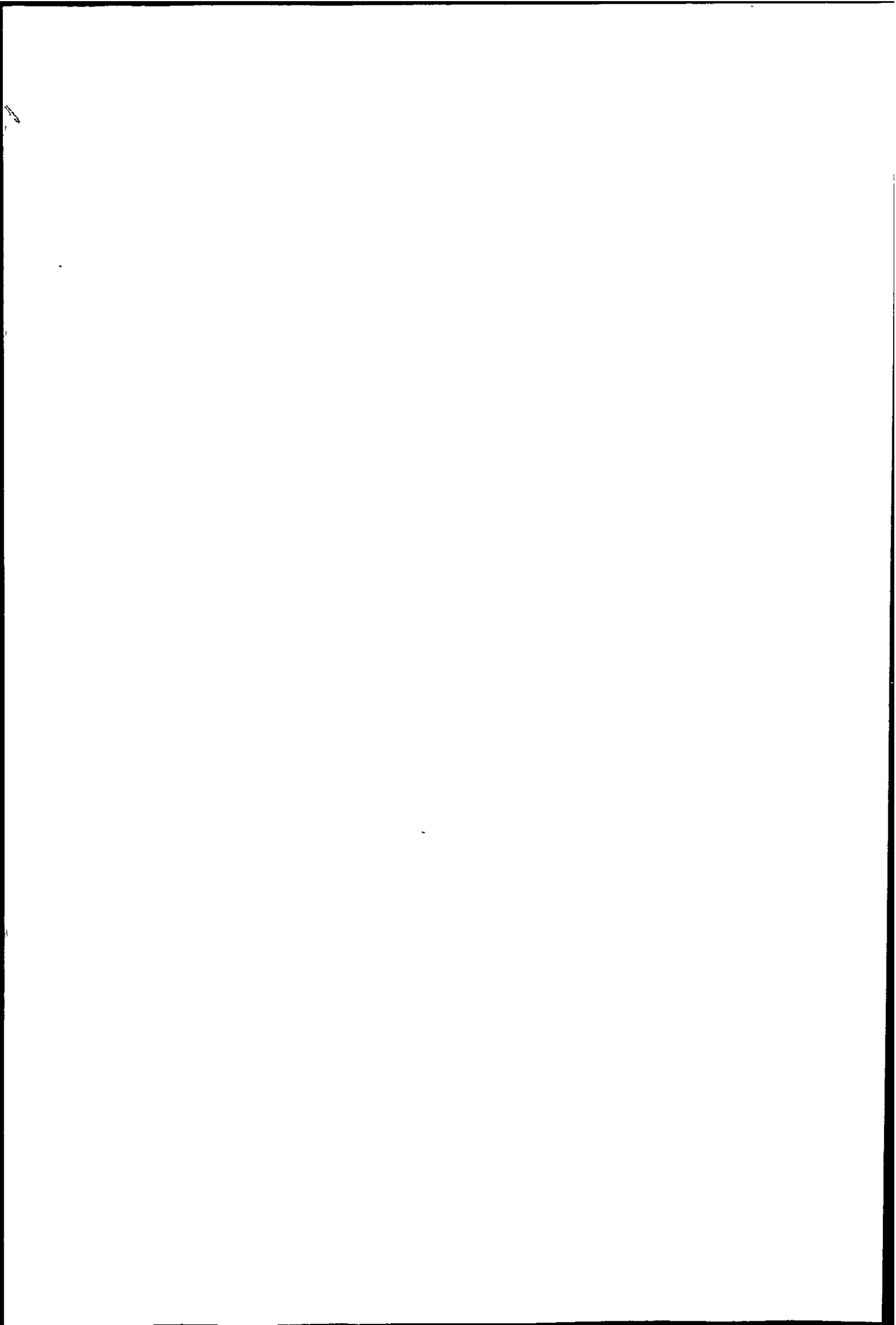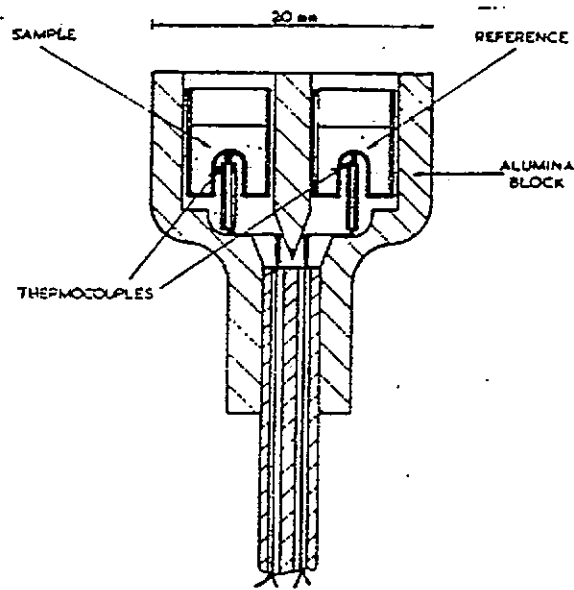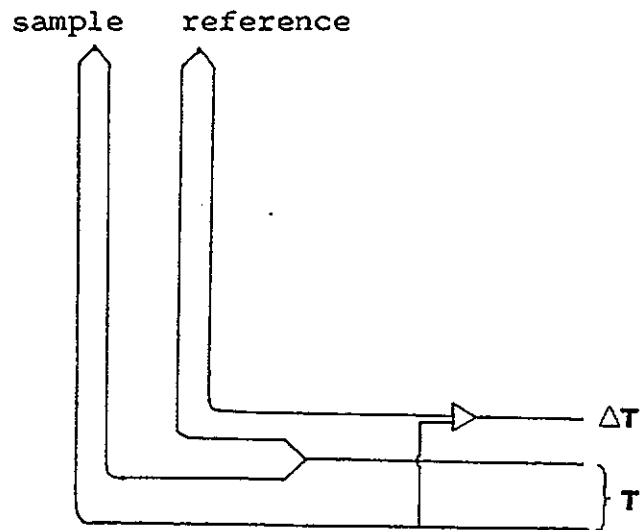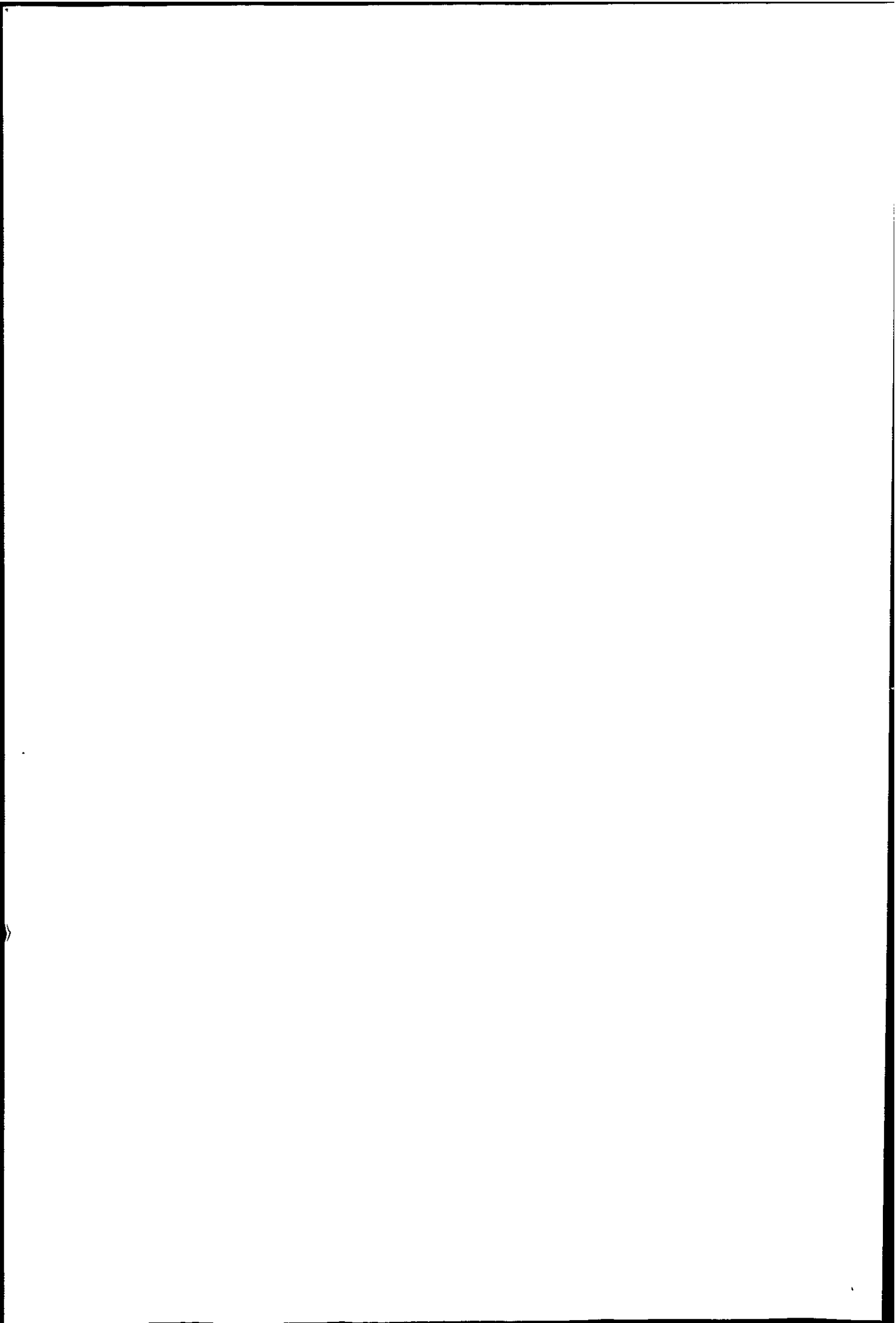
Figure 3.3 Massflow Thermobalance Sample Head.

Figure 3.4. Thermocouple arrangement of Sample Head.

3.1.2 The Stanton Redcroft 781 Thermal Analyser

The Stanton Redcroft[1] STA 780 series of thermal balances comprise of a range of equipment for TG and simultaneous TG/DTA. The STA 781 is the TG/DTG/DTA model working over the temperature range ambient to 1500 $^{\circ}$C. The complete assembly, together with the Linseis recorder (series LS4) is shown in Plate 3.1, with details of each module in the accompanying key. Schematic diagram is shown in Figure 3.5.

A 5 g capacity electronic microbalance is used with a digital control unit incorporating a microprocessor. Any desired weight range from 2 to 200 mg full scale deflection can be selected with a resolution of 1 μg in the range 2-20 mg and 10 μg in the range 2-200 mg. This facility makes it easy to display a selected percentage of the sample weight as full scale. Full digital taring, multiple inject and DTG facilities are incorporated.

Thermocouple connections are taken from the balance beam to measuring circuits using very fine wires made of the thermocouple materials. The ΔT signal is amplified by a low noise DC amplifier giving a maximum sensitivity of 10 μV full scale. Cold junction compensation and temperature linearisation are available for the sample temperature output.

The design of the gas-flow system in conjunction with the water-cooled finger enables runs to be carried out in flowing atmospheres without having to make a large weight correction, the magnitude of the latter generally being below 0.1 mg. Typical flow rates are normally in the range 25-75 cm^3/min^{-1}, with the flow meter calibrated for air discharging at atmospheric pressure. With other gases at the same outlet pressure the capacity varies inversely as

Procedure.

The sample was placed in an aluminium foil bucket suspended from the balance with a fine pyrex fibre (27 cm long). This enabled the sample to be at least 15 cm below the level of the liquid nitrogen contained in a Dewar flask, keeping the temperature to within ± 0.1 $^{\circ}C$ as previously determined by Glasson[7]. In practice, the sample is about 1 $^{\circ}$ warmer than the liquid nitrogen outside the balance limb (as determined by Glasson and Linstead-Smith[8]) using internal and external thermocouples.

The balance head was coupled by the taps and glass tubing to a two-stage rotary pump (enabling the pressure to be reduced to 10^{-3} Torr), and to a nitrogen reservoir and gauges, the nitrogen pressure being measured by the mercury manometers.

The cold trap was immersed in a Dewar flask of liquid nitrogen in order to aid outgassing of the sample and to reduce the effects of thermal transpiration.

The system was evacuated and the sample degassed at room temperature or by heating to 200 $^{\circ}C$ for at least 30 min. True sample weight (i.e. less adsorbed moisture and volatiles) was noted, the balance zero then set and the balance limb containing the sample immersed in liquid nitrogen.

A pressure of 30-50 mm Hg.(4000-6670 Pa) of nitrogen was introduced and the system allowed to attain equilibrium (30 min), when the nitrogen pressure and uptake were recorded. Six or seven readings were taken in the BET

115

range (0.05 to 0.30 relative pressure). Thereafter

pressures of 70-80 mm Hg (9.33-10.66 kPa) of nitrogen

were introduced, giving another seven readings up to the

maximum relative pressure obtainable (0.96).

Desorption points were determined by pumping out

similar pressures of nitrogen. Weight corrections for

buoyancy effects of the sample, container and suspension

were applied to the uptake readings.

3.2.2 The Newer Gas Sorption Balance

Plate 3.3 shows the gas sorption balance constructed in 1982. The design is essentially similar to that described above and the instrument was intended for use principally with nitrogen as adsorbate. CI microforce balance Mark 2 was used with a Mark 2C control unit. This has direct switching weight ranges 0-1 mg, 0-2.5 mg, 0-10 mg, 0-25 mg and 0-100 mg and is readily interchangeable with the Mark 2B unit.

The doser is of smaller volume allowing pressures of a few mm Hg(300 - 400 Pa) to be admitted. This balance was used for adsorption of CO_2 at 196 K, where additions at low relative pressures were desired.

For adsorption of N_2 at 77 K both sample limb and cold traps were surrounded by liquid nitrogen in Dewar flasks. For adsorption of CO_2 a slush of crushed CO_2/ether was used in the Dewar flasks. This was occasionally stirred with the addition of fresh crushed CO_2.

Sample weights were generally 0.25 g for coke samples and 0.1 g for charcoals and char. Where this amount was not available aluminium counterweights were added, making the appropriate buoyancy correction.

117

Plate 3.3. The Newer Gas Sorption Balance.

Key:

A   balance head unit

B   sample

C   doser

D   to gas cylinder

E   tap for independent flushing of doser and reservoir

F   gas reservoir

G   reservoir manometer

H   CI analogue control unit Mark 2C

J   manometers

K   cold trap

L   to vacuum pump

3.3   X-Ray Diffraction

Most solids are crystalline, i.e. consist of regular three-dimensional arrays of atoms in space, although the size of individual crystallites may be small. Points which have identical surroundings within a structure are known as lattice points. A collection of lattice points form a crystal lattice; when adjacent lattice points are joined together a unit cell is obtained. This is the smallest convenient repeating unit of the structure. The unit cell may be defined in a number of ways, and is characterised by three vectors, not in one plane, which are the edges of a parallelepiped. The general symbols for the unit cell vectors are a, b, c. while the directions of the sides of the unit cell are referred to as x, y and z axes. The interaxial angles of y∧z, z∧x, x∧y are denoted by α, β, γ.

On the basis of specialisation of their vectors crystal lattices can be referred to seven different systems, which are given in Table 3.2. Symmetry operations of reflection, rotation and inversion yield the 32 point groups, which fall into this system.
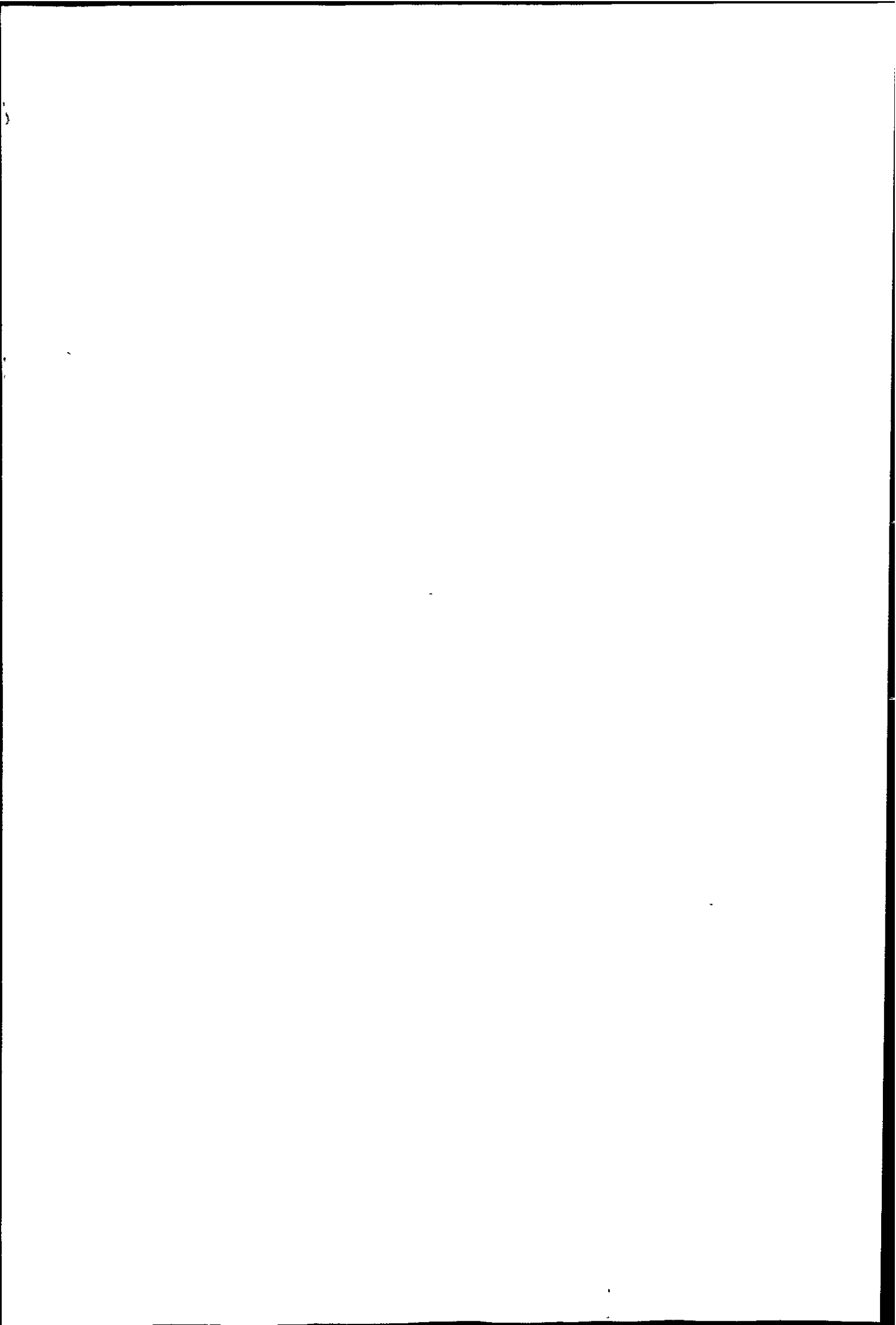
Table 3.2 Characteristic symmetry of the Crystal Systems

Crystal system	Conditions limiting cell dimensions		Minimum Symmetry
Cubic	$a = b = c$	$\alpha = \beta = \gamma = 90^{O}$	Four three-fold axes
Trigonal	$a = b = c$	$\alpha = \beta = \gamma \neq 90^{O}$	One three-fold axis
Tetragonal	$a = b \neq c$	$\alpha = \beta = \gamma = 90^{O}$	One four-fold axis
Hexagonal	$a = b \neq c$	$\alpha = \beta = 90^{O}, \gamma = 120^{O}$	One six-fold axis
Orthorhombic	$a \neq b \neq c$	$\alpha = \beta = \gamma = 90^{O}$	Two perpendicular two-fold axes or two perpendicular planes of symmetry
Monoclinic	$a \neq b \neq c$	$\alpha = \beta = 90^{O}, \gamma \neq 90^{O}$	One two-fold axis or (one plane of symmetry)
Triclinic	$a \neq b \neq c$	$\alpha \neq \beta \neq \gamma \neq 90^{O}$	None

Various sets of parallel planes may be drawn through the lattice points. Each set of planes can be completely described by three intergers ($\underline{h}$, $\underline{k}$, $\underline{l}$), the Miller indices, corresponding to the three axes ($\underline{a}$, $\underline{b}$, $\underline{c}$) respectively. Index $\underline{h}$ is the reciprocal of the fractional value of the intercept made by the set of planes on the $\underline{a}$ axis etc. From the observation of sets of h, k, l reflections that are systematically absent the lattice type can be deduced.

When point group symmetry is applied to infinite lattices the "space groups" are obtained; there being 230 possible in three dimensions.

As the dimensions of a crystal lattice are of the same order of magnitude as X-ray wavelength the lattice behaves as a three-dimensional diffraction grating, and diffraction is governed by Bragg's Law

$$n\lambda = 2d \sin\theta$$

where λ is the wavelength of the radiation

n the order (generally 1)

d the interplanar spacing

and θ the angle of diffraction

d is related to the unit cell dimensions by the Miller indices.

With the powder diffraction method small crystalline particles are in random orientation and produce reflections from those planes that happen to be at the correct angle θ to the incident X ray beam.

The intensity and distribution of the diffracted beams with respect to the Bragg angle is characteristic

121
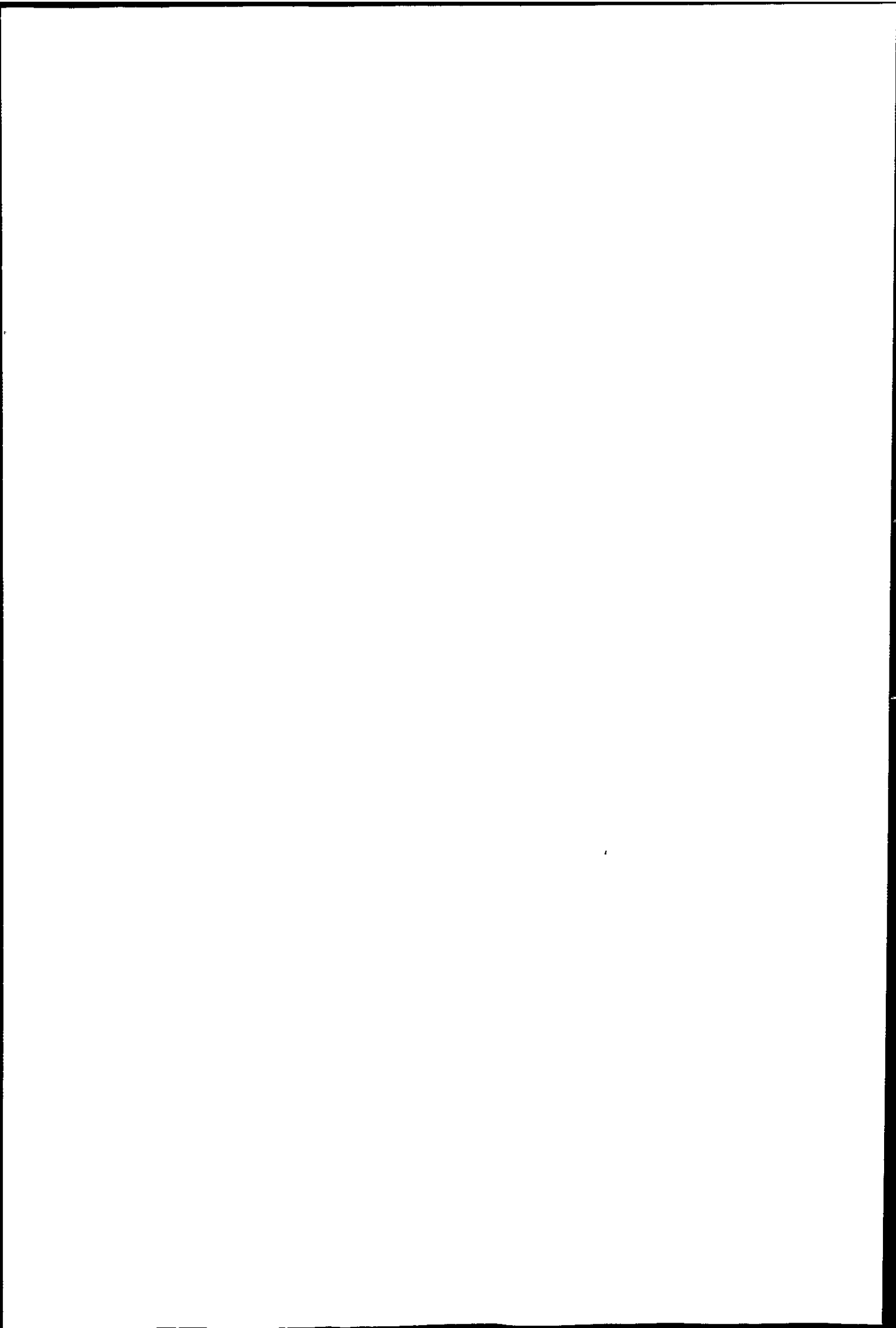
of a particular structure and may be used to identify the phases present. Diffraction patterns for the majority of crystalline compounds are listed in the A S T M tables.

3.3.1 The X-ray Equipment

A Hilger and Watts Y90 X-ray generator was used, fitted with a Philips X-ray tube and copper target. Voltage and current were set at 36 kV and 18 mA respectively. The X-rays generated were filtered with a nickel foil to reduce the K_β component and passed through a collimator and slits before impinging on the sample mounted vertically at the centre of the 50 cm Berthold diffraction table. The diffracted X-rays were detected by a Berthold LB 2560 gas-filled proportional counter connected to a discriminator/ratemeter and the trace recorded on a Curken 250-2 chart recorder.

The table had been aligned and calibrated with a single calcite crystal. Samples of lightly powdered ash or coarsely crushed coke were fixed in a microscope cover slip with a drop of "Durafix" and mounted in the path of the beam.
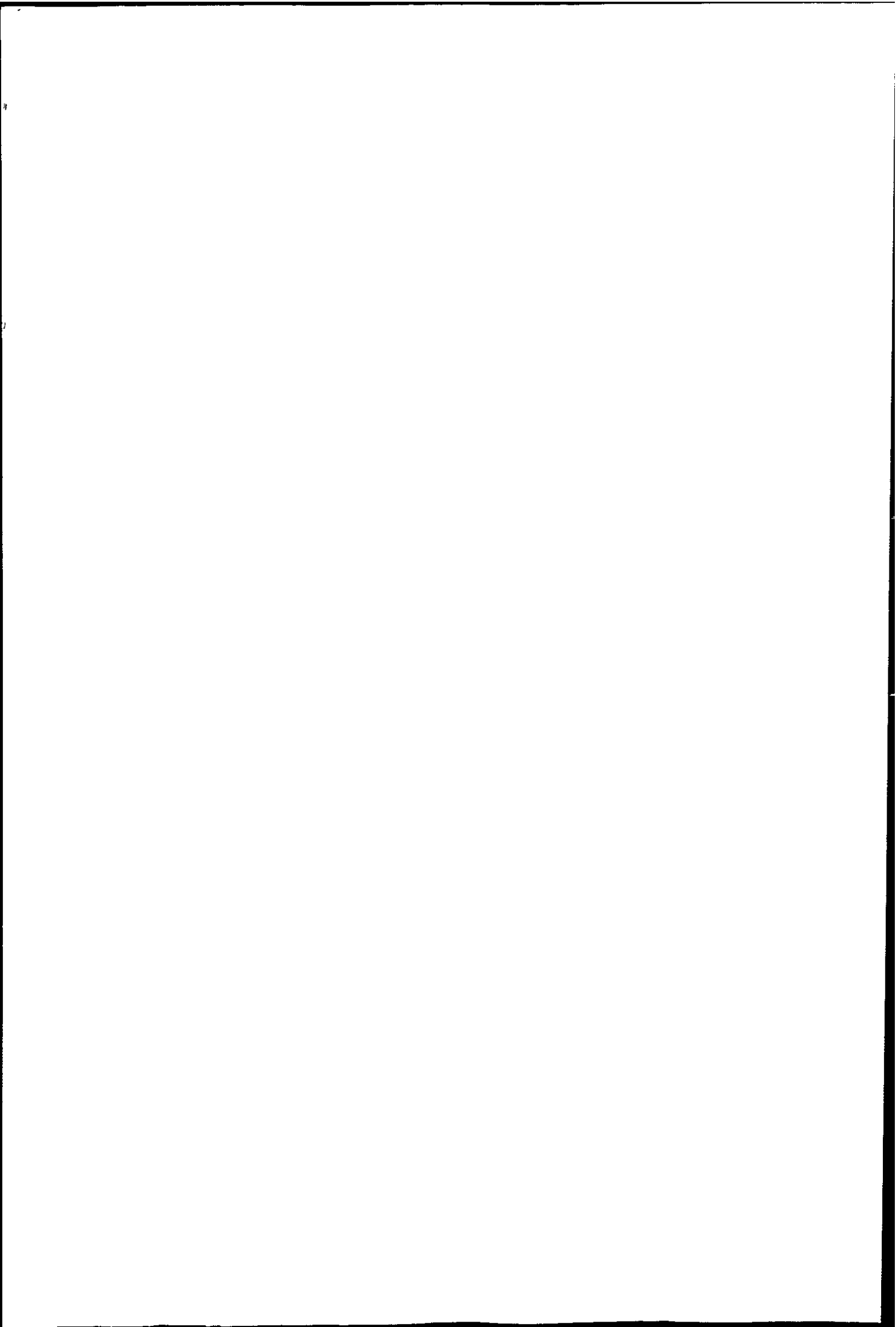
3.4 Microscopic Techniques

Optical and electron microscopy were used in the present study. The resolving power of a microscope depends ultimately on the wavelength of radiation employed, and the optical microscope has a maximum resolution between 200 and 300 nm. Optical microscopy can reveal surface defects, grain boundaries and gross morphology of solids but detail on the atomic scale was not possible until the advent of electron microscopy.

The wave-particle duality of electrons is expressed in the de Broglie equation

$$\lambda = \frac{h}{mu}$$

where m is the mass of the electron, u its velocity, λ the associated wavelength and h Planck's constant.

When an electron is accelerated through a potential difference of V volts the energy imparted is eV, where e is the charge on the electron. This is equivalent to the kinetic energy $^1/_2 \, mu^2$.

Thus $mu = \sqrt{2eV}$ and the wavelength associated with the accelerated electron may be calculated.

Due to the high velocities attained by the electrons, relativistic corrections are necessary.

The wavelength of electrons accelerated by a potential difference of 80 kV is 0.0043 nm (4.3 pm), so by the use of an electron beam and a thin (1 μm) specimen a much greater resolving power is possible. However, artefacts caused by electron beam irradiation and high vacuum affect the interpretation of the image formed in transmission
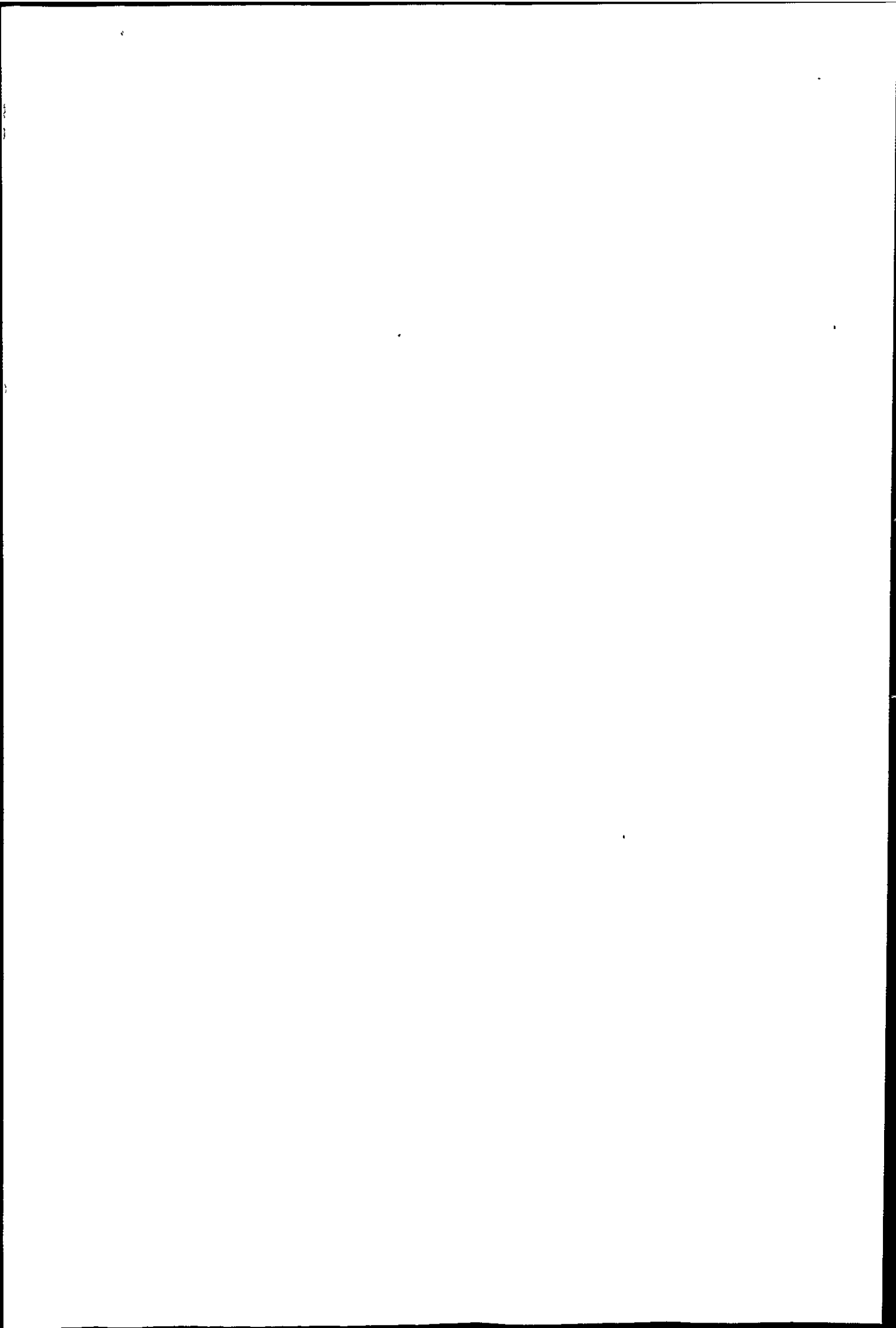
electron microscopy. The theoretical limit of resolution (∼1 pm) is in practice much lower due to lens aberrations caused by:- mechanical asymmetry, magnetic inhomogeneities and deposits on the lens surfaces. Nevertheless resolving powers of 0.2 to 0.5 nm are attainable and the use of high voltage electron microscopy with thinner specemins has led to better resolution. Theory and application of transmission electron microscopy to surface chemistry is given by Fryer[9], with many references to carbons and graphite.

In scanning electron microscopy the image is formed by secondary electrons reflected from the sample surface. The limit on sample size and thickness thus depends only on the dimensions of the sample chamber. The range of magnifications overlap those of optical and transmission electron microscopy and maximum resolution lies around 20 nm. Principles and applications are described in the text by Goldstein et al[10].

3.4.1   The Philips EM 300 Transmission Electron Microscope
 (TEM).

A TEM basically consists of five sections, viz 1. the electron gun, 2. a condenser system of magnetic lenses, 3. a specimen chamber, 4. a magnification system of lenses and 5. an image-recording device.

Figure 3.8 is a schematic diagram of the Philips EM 300 transmission electron microscope, and the following a brief description.

The gun provides a beam of electrons and is composed of a hairpin tungsten filament enclosed by a Wehnelt cylinder. The electrons are accelerated by a high voltage through a hole in the Wehnelt cylinder which is negatively biased to converge the beam to a diminished virtual image of the filament-a short distance in front of the filament. The beam current is controlled by varying the bias voltage applied to the Wehnelt cylinder (Emission control).

Lens (1) focusses the diminished virtual image of the electron source, to a greater extent than that produced by the Wehnelt cylinder. Lens (2) focusses the beam in the specimen plane. Usually the first lens is operated at constant current, and the current varied in the second lens changing the focal length and thus the area of illumination.

To minimize spherical aberrations, the objective lens must be operated with small acceptance angles (10^{-2} - 10^{-3} rad.); this is achieved by placing an aperture in the beam in front of the lens. This lens determines the ultimate resolving power of the instrument and produces a real image of the specimen, which is further magnified by
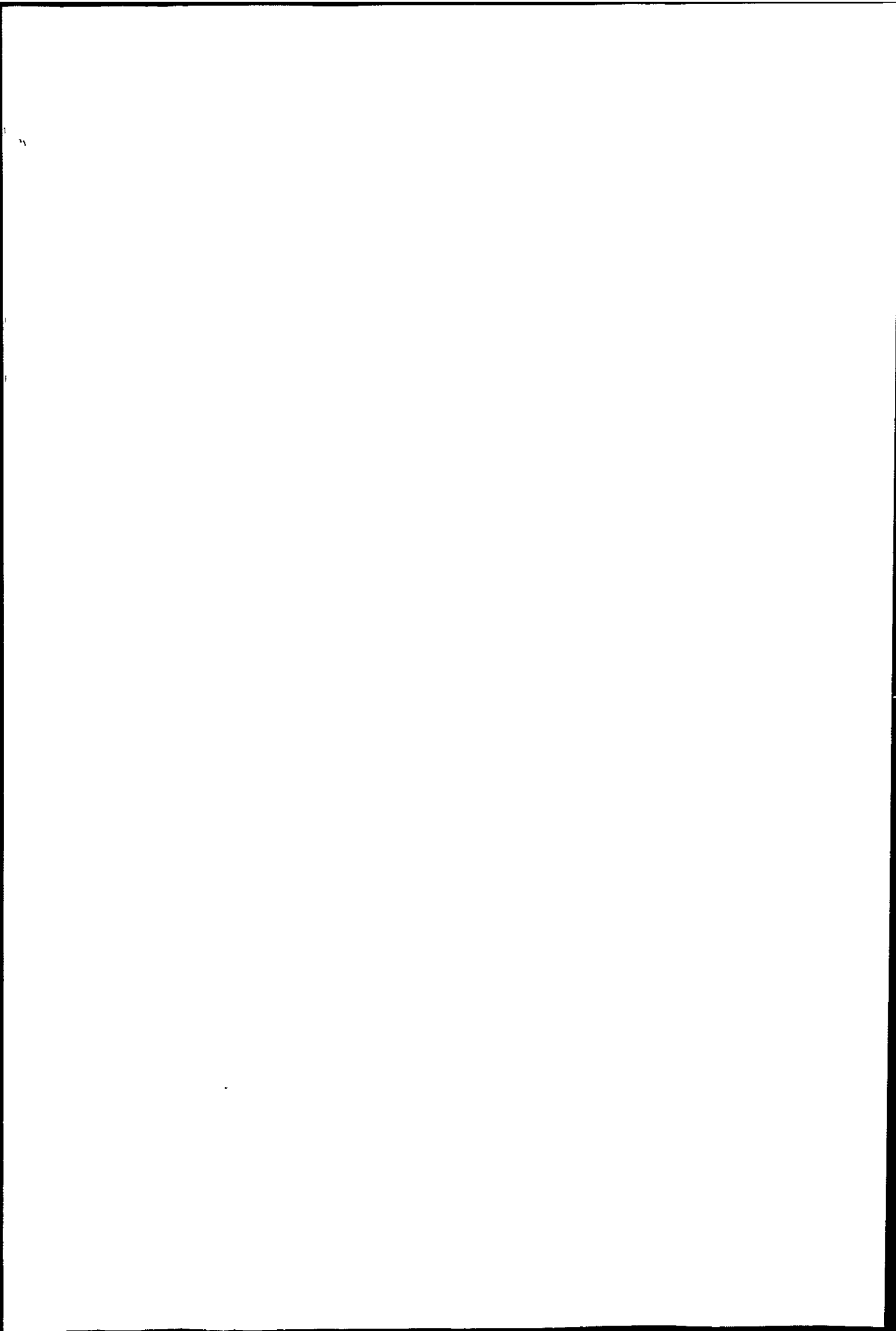
the projector lens system.

The three lenses give a wider range of distortion-free magnification than is possible with one. Usually the intermediate lens is kept under constant current conditions for low magnification work (1000 X) and the projector lens current varied; for higher magnifications vice versa. The third lens, the diffraction lens, enables variations to be made in the magnification of the specimen area selected for electron diffraction without needing to adjust the objective lens which has been used to focus the specimen.

An electromagnetic lens invariably suffers from astigmatism, due to asymmetry of the magnetic field strength about the lens axis caused by foreign bodies deposited on the pole pieces and electrostatic charging. To counteract these effects, stigmators are used in conjunction with the condenser and objective lenses.
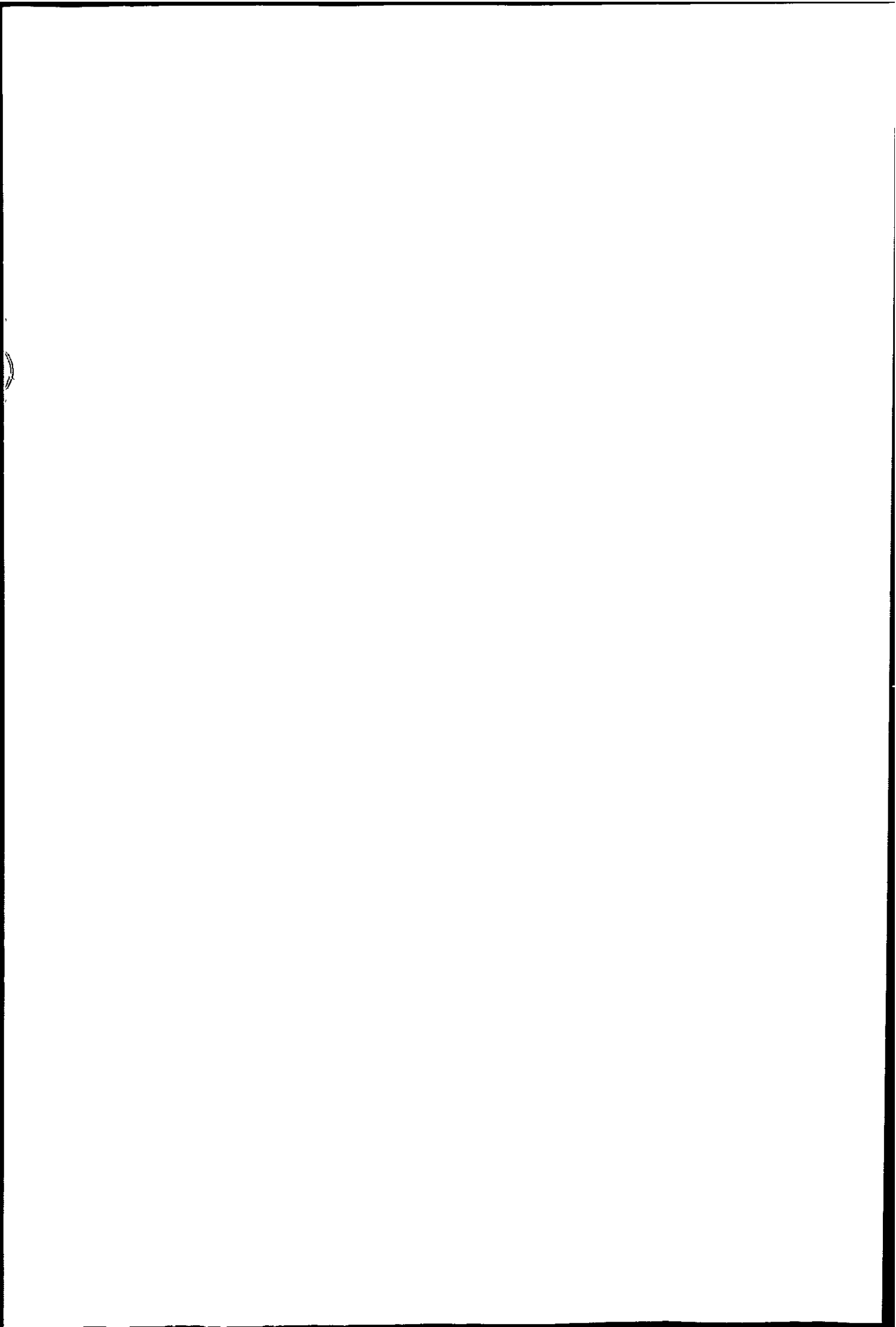
Astigmatic conditions of the objective lens are checked by observing Fresnel interference fringes seen around a small object at high magnification, if the lens is astigmatic the fringe is not even. To correct this the objective stigmators are used.

Condenser lens astigmatism is checked by focussing the condenser so that a bright spot is seen; if the spot does not expand symmetrically when the condenser is defocussed the illumination system is astigmatic, and the stigmator is used to correct it.

126
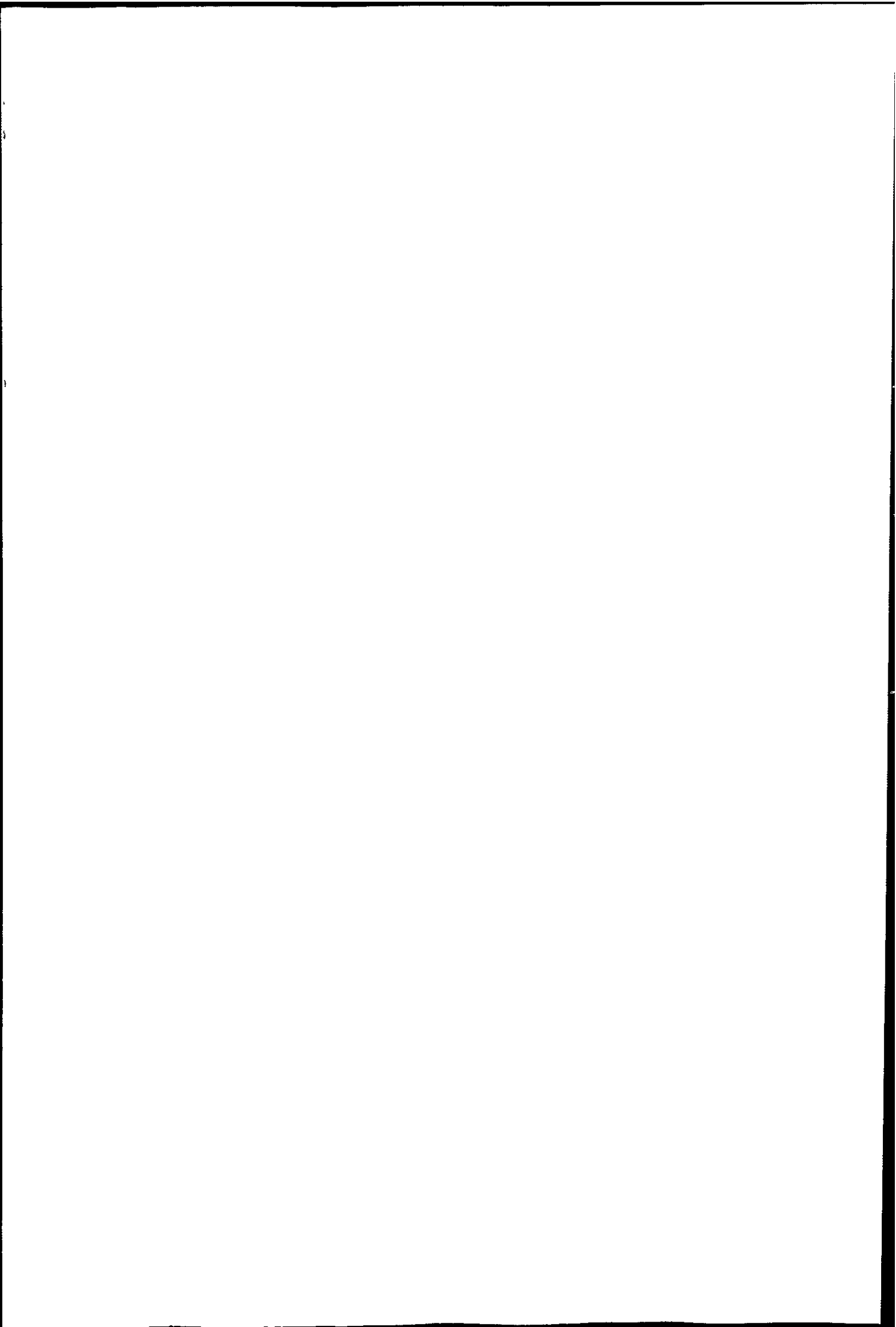
Samples were mounted on a copper grid with carbon film and the specimen grid mounted in the holder and introduced to the microscope through the objective lens. A voltage of 80 kV was selected and the filament adjusted to saturation current. After alignment of the beam and correction for condenser lens astigmatism, the scanning mode was selected and the grid scanned for a suitable section of specimen. When found, the instrument was set to the magnification mode and the appropriate magnification factor selected. The image was then carefully focussed and photographed after adjusting the illumination and exposure time. $3\frac{1}{8}$" by 4" plates were employed to record the images.

The charcoals dusted directly onto the grid were too coarse to examine in this way, but TEM was used for milled coke and coal char, and ash materials, made into suspensions.
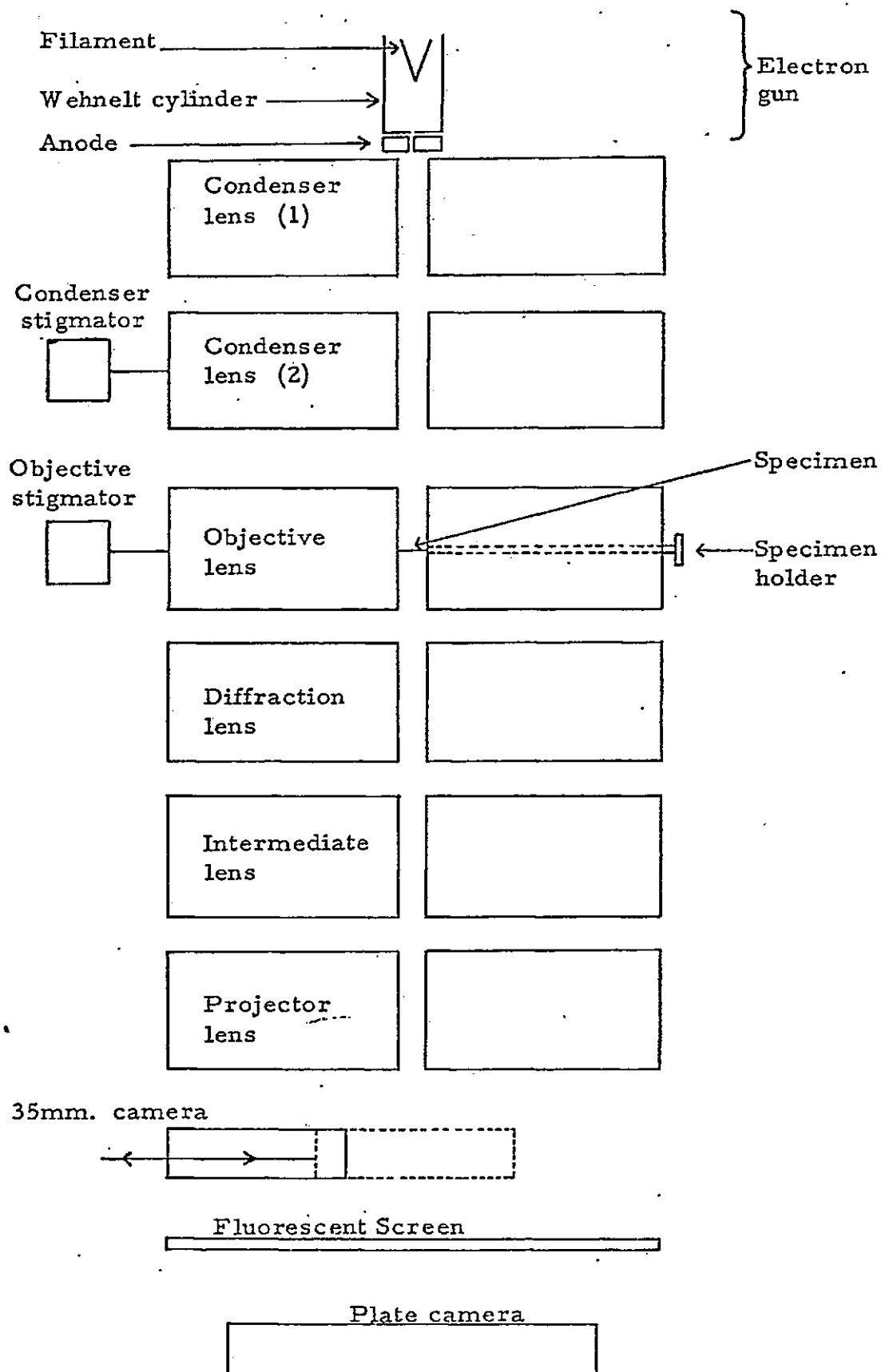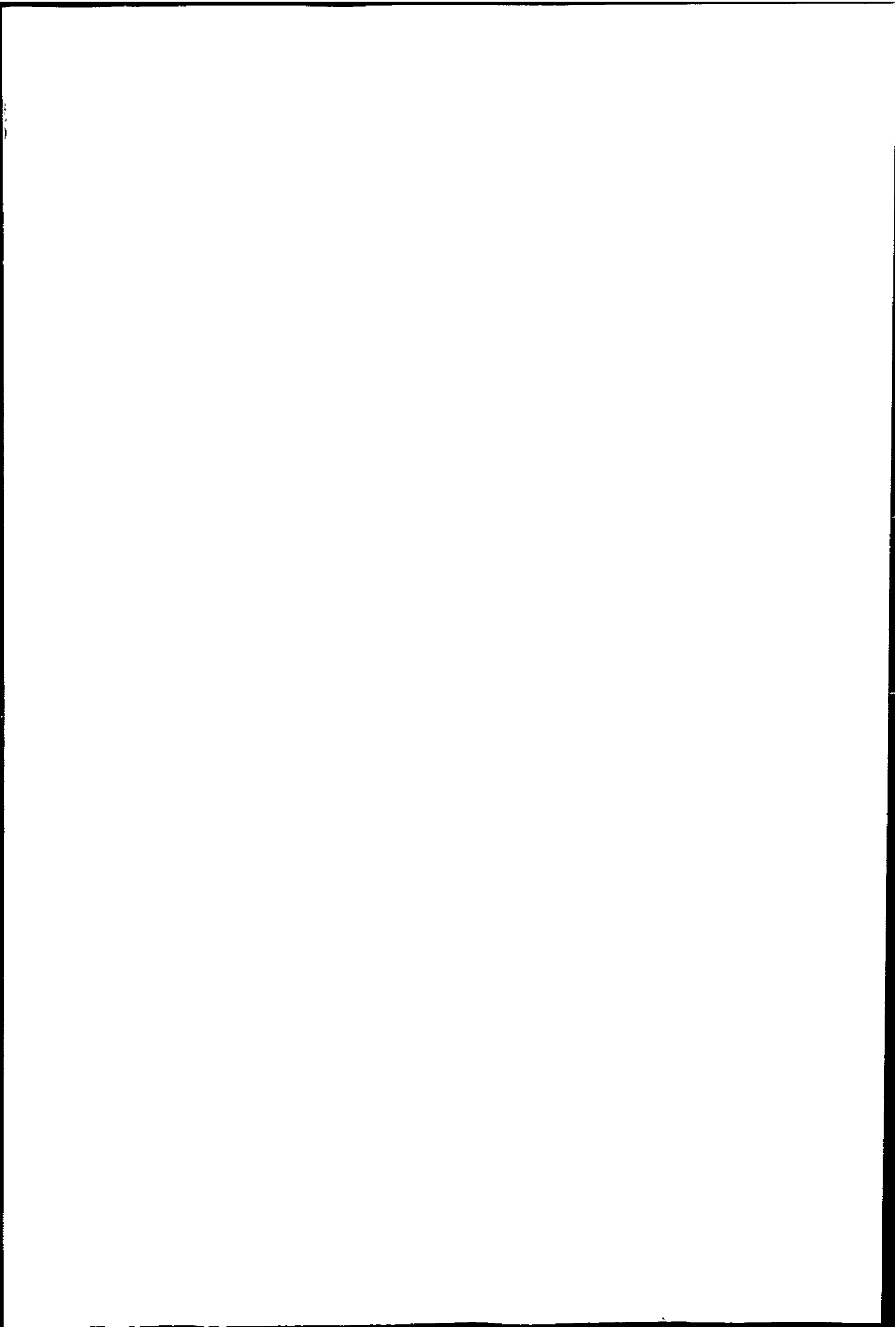
Filament

Wehnelt cylinder

Anode

Electron
gun

Condenser
lens (1)

Condenser
stigmator

Condenser
lens (2)

Objective
stigmator

Objective
lens

Specimen

Specimen
holder

Diffraction
lens

Intermediate
lens

Projector
lens

35mm. camera

Fluorescent Screen

Plate camera

Figure 3.8. Philips E. M. 300 Electron Microscope

128

3.4.2   The Jeol Model JSM-T20 Scanning Electron Microscope

   (SEM).

   In the SEM an area to be examined is irradiated with

a finely focussed electron beam, which may be static, or

swept in a raster across the surface of the specimen. This

produces secondary electrons, back scattered electrons,

Auger electrons, characteristic X rays and photons of

various energies. The secondary and backscattered electrons

vary as a result of surface topography as the electron

beam sweeps across the specimen. The microscope has a

large depth of field giving the image the appearance of a

three dimensional structure with detailed surface relief.

   As the secondary electron emission comes only from a

volume near the beam impact area the use of a finely

focussed beam results in a high resolution.

   The JSM-T20 was developed for easy operation and

maintenance with a resolution of 20 nm (200 $\overset{o}{A}$) and

magnifications 35 x to 10,000 x in 16 steps.   Both

secondary electron image and backscattered electron image

can be selected.

   The electron optic system has an electron gun with

accelerating voltage of 19 kV and a 3-stage reducing lens

system (2 condensers and one objective). On the console

three scanning mode buttons allow the selection of wave-

form (suitable for adjusting gun filament and focussing

image), Y modulated image or the secondary electron image.

Three scanning speed buttons allow the selection of image

size.   "Contrast" and "brightness" controls determine the
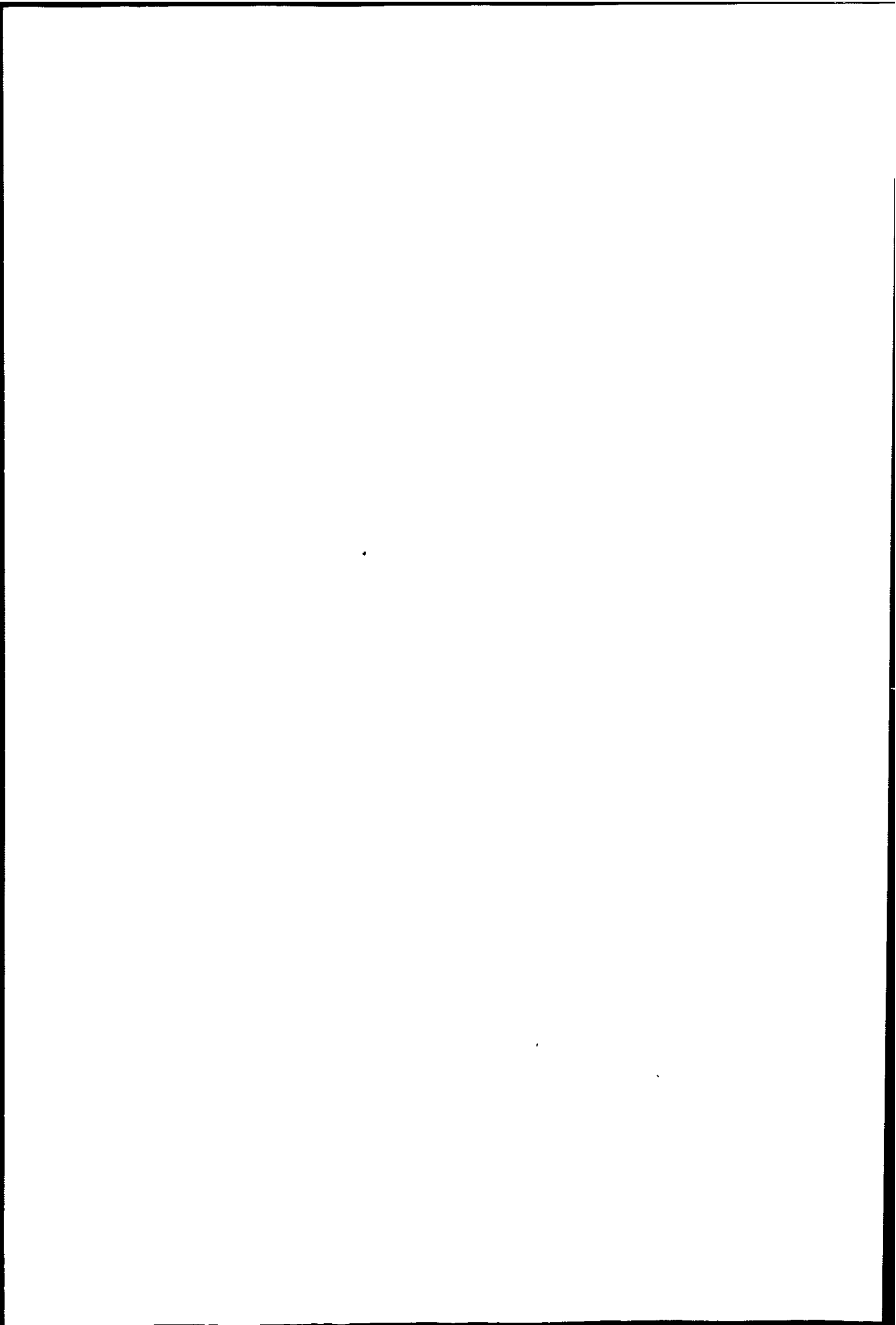
correct exposure for the camera attachment.

Figure 3.9 shows a schematic diagram of a scanning electron microscope.

The fine-beamed electron probe scans the specimen, and an image is displayed on the cathode ray tube (CRT). The image magnification is determined by the ratio of scanning amplitude of CRT to that of the electron probe.
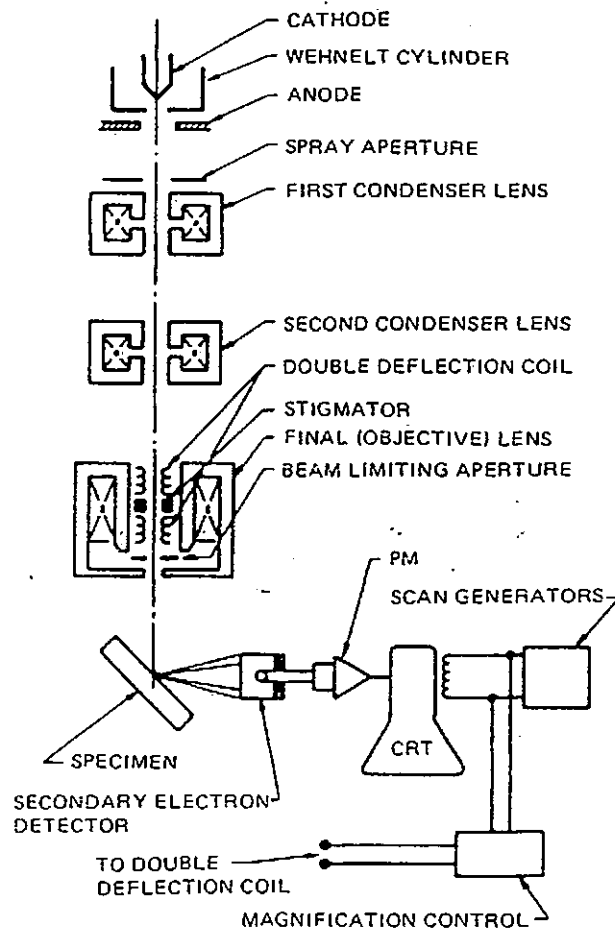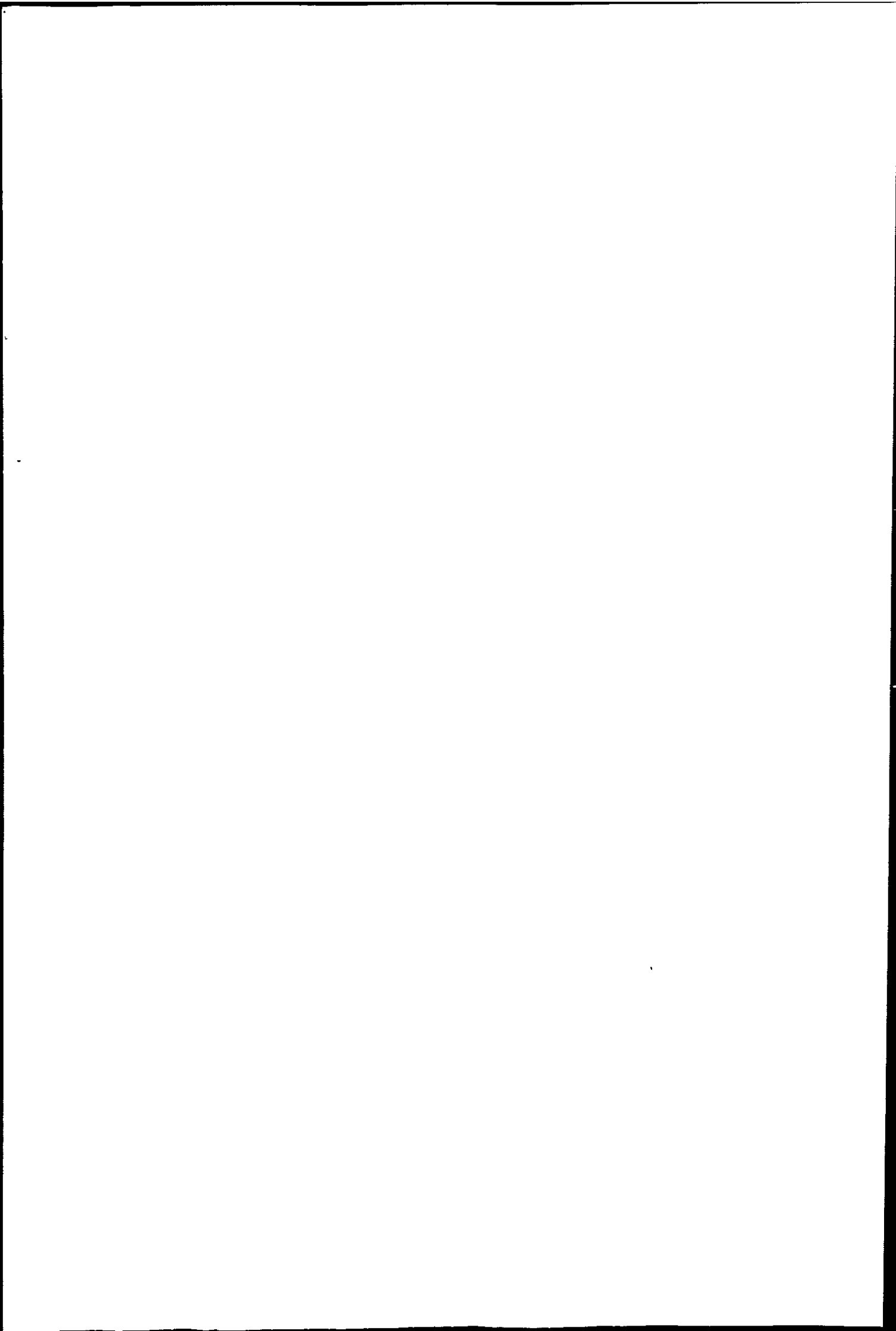

Figure 3.9. Schematic drawing of a SEM (after reference 10).

The beam from the electron gun passes through a series of lenses which demagnify the electron beam, the final lens focussing the beam on the specimen. The

resolving power of the microscope can not be less than the electron beam diameter. A set of scanning coils are mounted above the final lens; and within the bore of the lens is located a stigmator and a set of three movable apertures. These apertures determine the angular aperture subtended by the electron beam at the specimen surface. At the base of the lens column is a large specimen chamber. The whole system is evacuated by means of a pumping system.

The secondary electrons are detected by a scintillator/photomultiplier system (PM) the resulting signal being further amplified and applied to the cathode ray display tube. Additional electronic equipment is needed to supply the current for the lenses, the accelerating voltage, control systems for the cathode ray displays and ancillary equipment associated with signal detection and amplification.

All samples for examination by SEM were mounted on aluminium stubs and gold coated to 12 nm in a Polaron SEM coating unit E5100 to ensure electrical conductivity.

3.4.3 Optical microscopy

A Zeis Photomicroscope III with camera attachment was used to study the well sintered coke ash from high temperature burn offs. The main disadvantage is the insufficient focal depth.
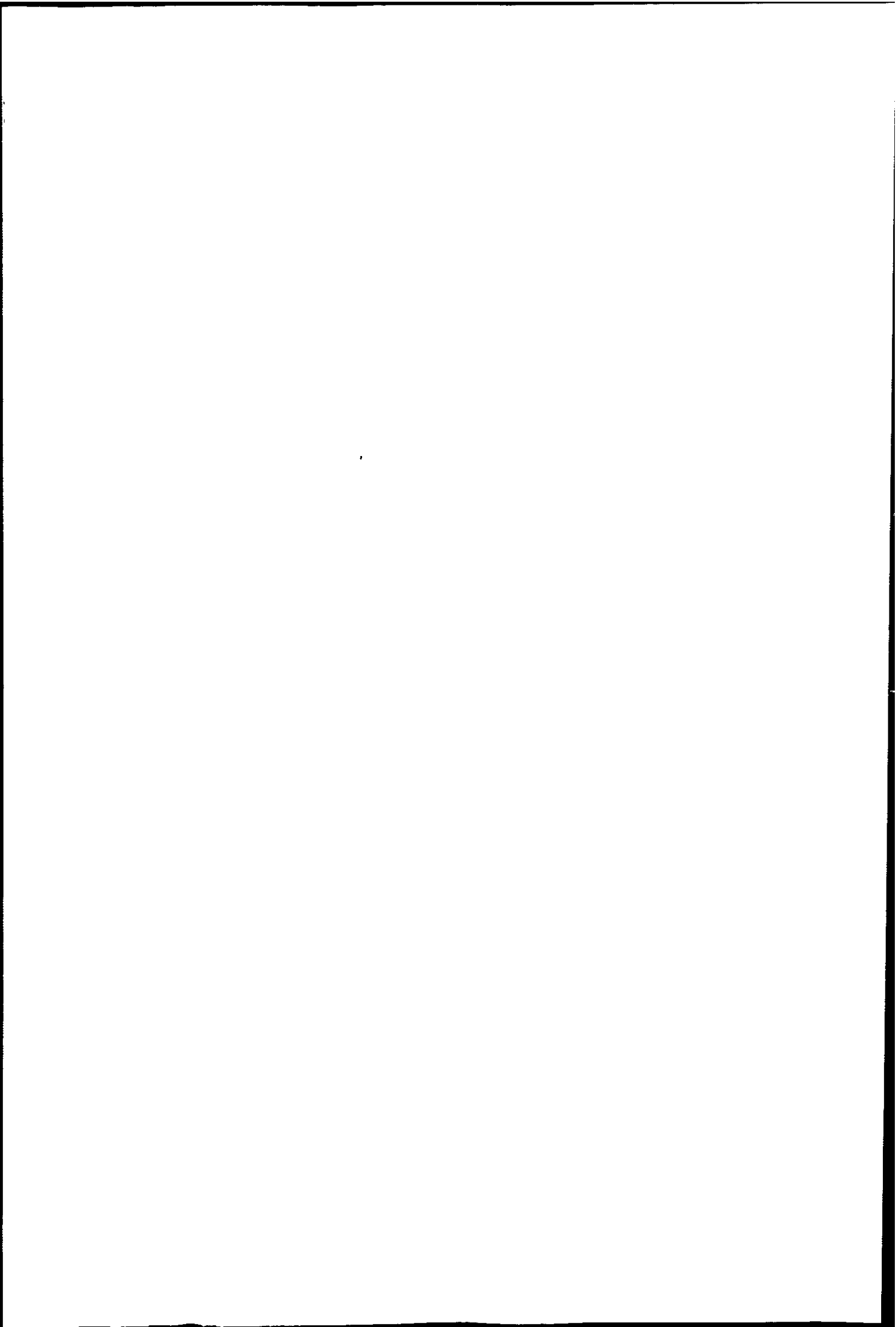
References.

1. Stanton Redcroft Ltd., Copper Mill Lane, London SW17 OBN.

2. R.E. Dodd & P.L. Robinson "Experimental Inorganic Chemistry", 1954, Elsevier.

3. S. Brunauer, L.S. Demming, W.S. Demming & E. Teller. J. Amer. Chem. Soc., 1940, $\underline{62}$, 1723.

4. S. Brunauer, P.H. Emmett & E. Teller. J. Amer. Chem. Soc. 1938, $\underline{60}$, 309-19.

5. B.C. Lippens, B.G. Linsen & J.H. de Boer. J. Catalysis 1964, $\underline{3}$, 32.

6. C.I. Electronics Ltd., Brunel Road, Churchfields, Salisbury, Wiltshire.

7. D.R. Glasson, J. Chem. Soc., 1956, 1506.

8. D.R. Glasson & D.E.B. Linstead-Smith. "Progress in Vacuum Microbalance Techniques" Volume 2, 1973, Heyden, 209.

9. J.R. Fryer, "The Chemical Applications of Transmission Electron Microscopy", 1979, Academic Press.

10. J.I. Goldstein, D.E. Newberry, P. Echlin, D.C. Joy, C. Fiori & E. Lifshin, "Scanning Electron Microscopy and X-ray Microanalysis", 1981, Plenum Press.

CHAPTER FOUR

PRELIMINARY CHARACTERISATION OF THE COKES,

CHAR AND OTHER CARBONS

4.1　Introduction

    4.1.1　Introduction

    4.1.2　Boric oxide doping and solution treatment

    4.1.3　Coke and char ash
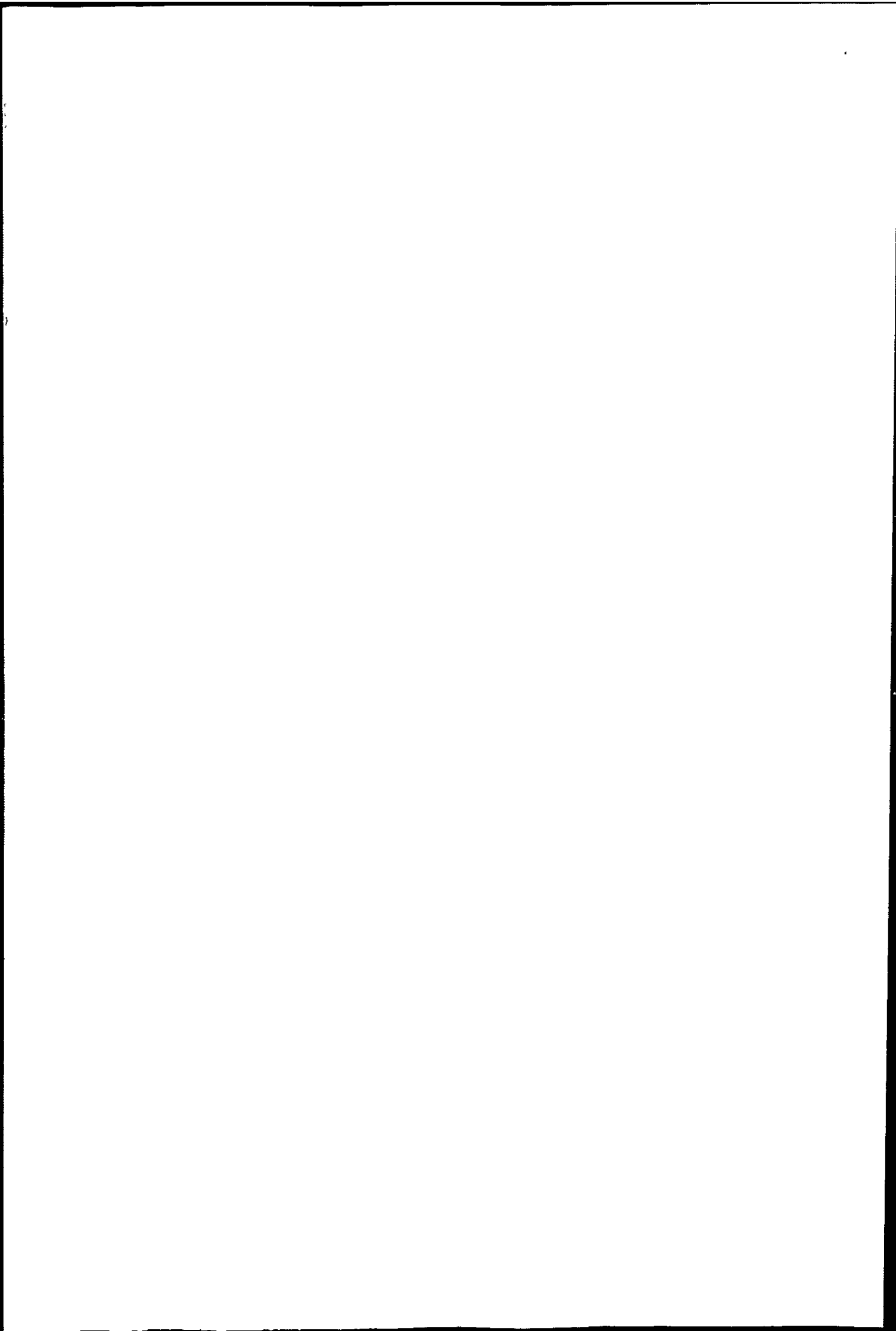
4.2　Experimental Procedures

4.3　Results

    4.3.1　Investigation of the carbons

    4.3.2　Investigation of the coke ash and brown coal

          char ash.

4.4　Discussion

    4.4.1　Characterisation of the carbons

   4.4.2　Nature of the coke and char ashes.

4.1.1   Introduction

The characterisation of several carbons, including metallurgical cokes and an Australian brown coal char, by density measurements, X ray diffraction, gas sorption and microscopic examination was first undertaken. The cokes were the main interest of the present study, the other carbons being far removed from cokes in physical properties, although providing some comparative information. Doping with boric oxide solution was achieved easily with the char and activated charcoal for gas adsorption, providing carbons of very different porosity from the cokes with a boric oxide additive.

Blast furnace coke is a very heterogeneous material, as previously outlined in Chapter 2. The ash content of the cokes and char were also studied by the above techniques and by TG/DTA. The reactivity of the carbon is the subject of subsequent chapters.

Optical and scanning electron microscopy (SEM) were not used quantitatively. A thorough study of porosity by microscopic methods requires many measurements and a detailed statistical analysis of data. Optical microscopy was useful for doped coke ash particles too large for SEM; and SEM gave the gross surface structure of the carbons and cokes. The combination of optical and SEM on cokes has been very informative, as described by Marsh and Smith. (Reference 23, Chapter 2.)
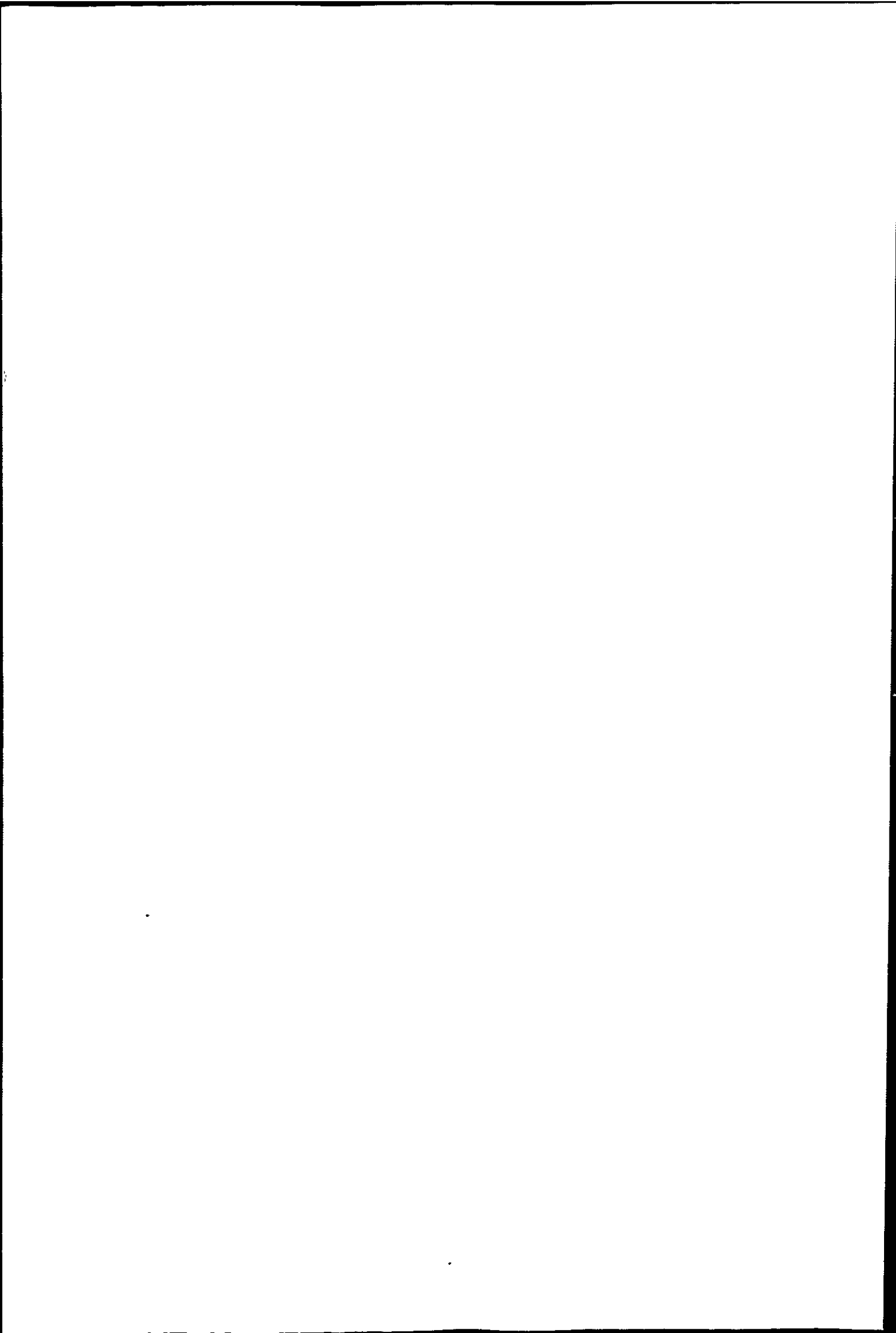
Adair et al[1] used SEM to study blast furnace coke
gasified by O_2 and CO_2, revealing surface changes. In a
graphitic material lamellae are projected more edge-on
to the surface. As rates of gasification are greater in
directions parallel to the basal planes, extensive
fissuring results on coke oxidation. The topographical
changes induced in polished sections of metallurgical coke
on CO_2 gasification at 1173 K were studied by French and
Marsh[2] using optical and scanning electron microscopy and
monitoring the same area before and after gasification.

The initial surfaces of the three cokes of this study
were initially deeply pitted and fissured. Changes induced
by gasification could not be followed unless the same area
was monitored. For needle cokes, where gold coating is not
absolutely necessary, Downing et al[3] have used SEM to study
surface changes in air oxidation at two temperatures.

The gas sorption techniques are described more fully
in Chapter 6.

When examined by X ray powder diffraction techniques
cokes generally show diffuse maxima at scattering angles
corresponding to the dominant graphite peaks. Analysis
of diffraction patterns uses the equations of Bragg (to
obtain d spacing) and Scherrer (to obtain mean crystallite
size from the line broadening). Poorly crystalline carbons
are pictured as an assemblage of crystallites within which
the atoms are in planes with the structure of the graphite
hexagonal layer, but the planes are stacked in a "turbo-
stratic" manner, i.e. the layers have random rotational
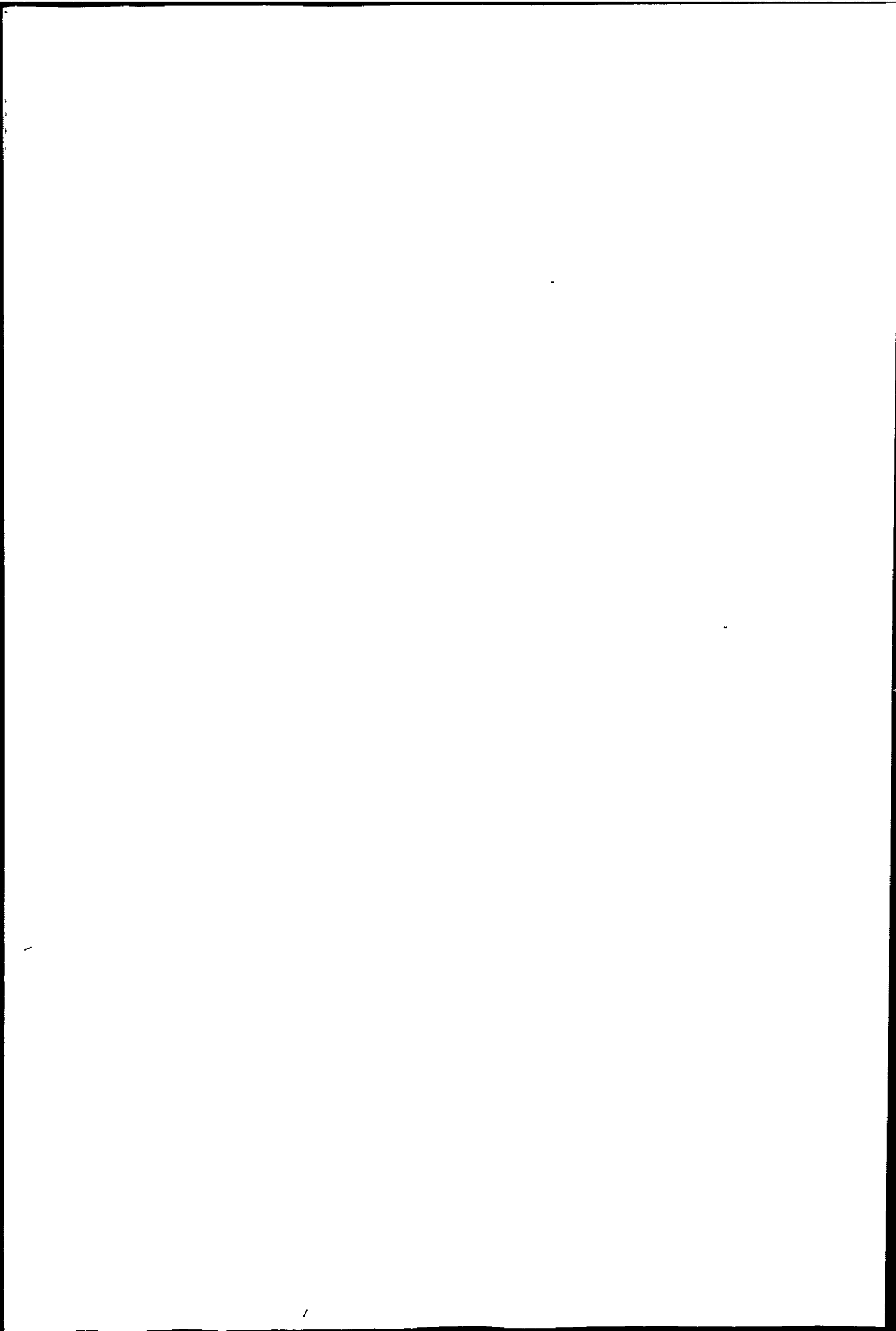
orientation about the c axis. A more refined structural model is given by Strong.[4]
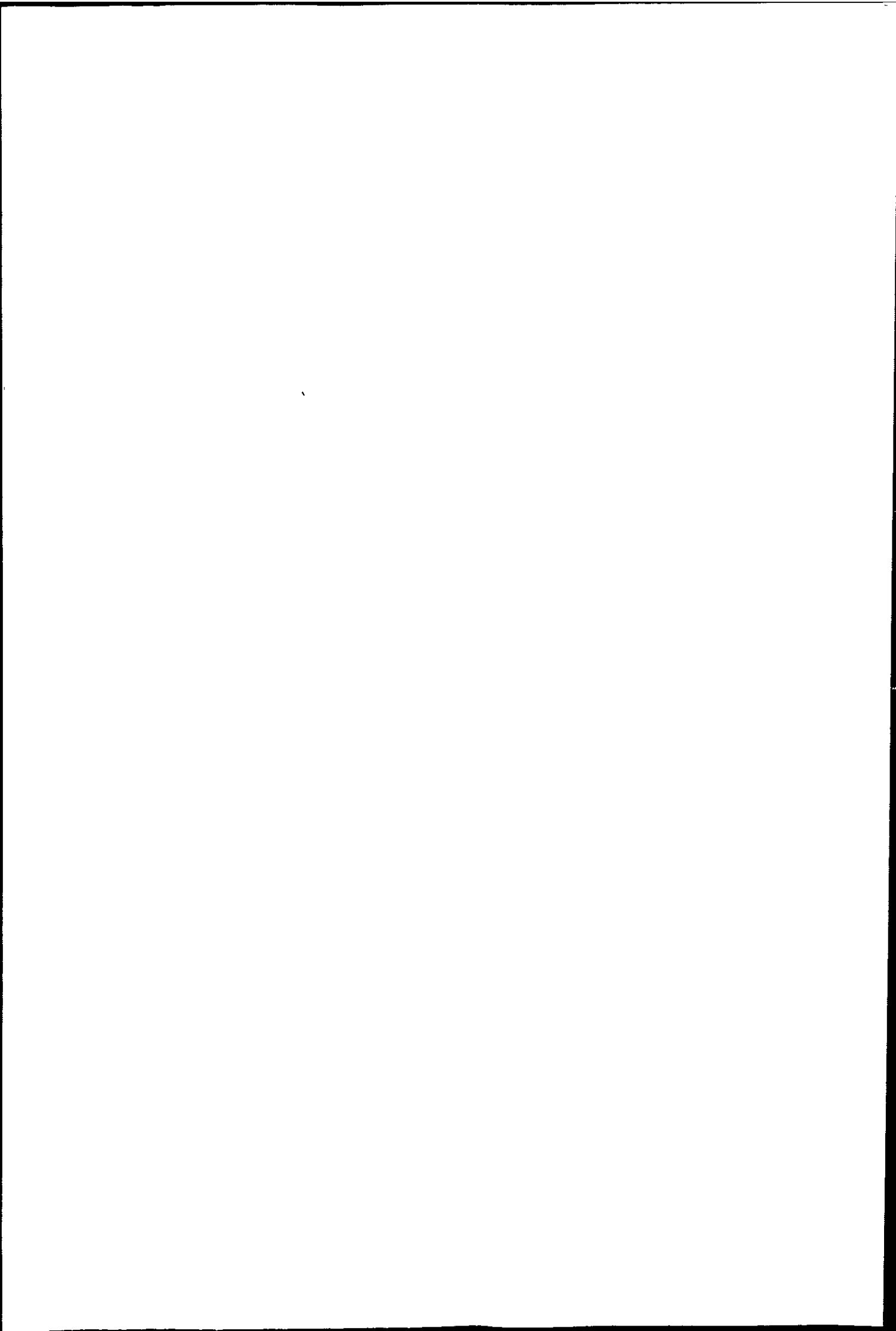
4.1.2 Boric Oxide Doping and Solution Treatment.

Lump coke has a surface dust of fine particles, which can be washed away. When the cokes of the present study were soaked in B_2O_3 solution, drained and dried no net increase in weight was found. Rolling hot coke in B_2O_3 or pouring molten B_2O_3 over coke lumps proved unsatisfactory. By heating Nantgarw coke to about 200 $^{\circ}$C and pouring on a saturated solution of B_2O_3 (2.5%), a weight gain of about 2% of original coke weight was achieved. On heating this coke to 500 $^{\circ}$C for a few minutes the surface coating melted in and became B_2O_3. If the coke was preheated to 400 $^{\circ}$C more B_2O_3 was retained, the maximum doping achieved being 2.3% for Nantgarw, 2.4% for Cwm and 1.4% for Polish cokes. However, at this higher temperature the solution sputtered, and a 200 $^{\circ}$C preheating was adopted as the standard doping technique, giving B_2O_3 additive of approximately 1.5% of coke weight for Nantgarw coke.

The dry brown coal char adsorbed from B_2O_3 solution at room temperature. On soaking, draining and drying at 110 $^{\circ}$C the weight increase (as H_3BO_3) was 2 to 3%.

The dried charcoal activated for gas adsorption on similar treatment gave a weight increase of 12%. The solution probably remains in the pores of the char and charcoal and on drying the H_3BO_3 is deposited.

Solution treatment of coke is not in general operation, although several workers have used alkali and transition metal salt solutions to enhance coke reactivity. Das[5] impregnated coke with Cu and Fe by boiling the coke to

dryness with a solution of a soluble salt. Nand and Mann[6] soaked lignite char in alkali salt solutions overnight (1 to 20% concentrations).

Other workers have incorporated finely divided catalyst powders into carbons prior to heat treatment, e.g. the work of Jalan and Rao[7] using carbon blacks and Mitra et al[8] using "ferrocoke".

Natural and nuclear graphites, and chars have been solution treated by surface deposition in studies of catalysts (activators) of the Boudouard reaction. The energies of activation for this and the C/O_2 reaction are generally lowered, although the amount varies widely, as described by Walker et al[9].

Holmes and Emmett[10] found added impurities catalysed the conversion of small to large pores in the gasification of charcoals. This effect was also reported by Marsh and Rand[11] for Ni and Fe doped polyfurfuryl alcohol char. Gasification in CO_2 was catalysed only in the vicinity of the metal agglomerate resulting in little change in micropore structure but development of macro and transitional pores.

The presence of B_2O_3 as an inhibitor (negative catalyst) may have the opposite effect in the gasification of a microporous carbon, i.e. lead to a greater development of micropores, in comparison with the original material.
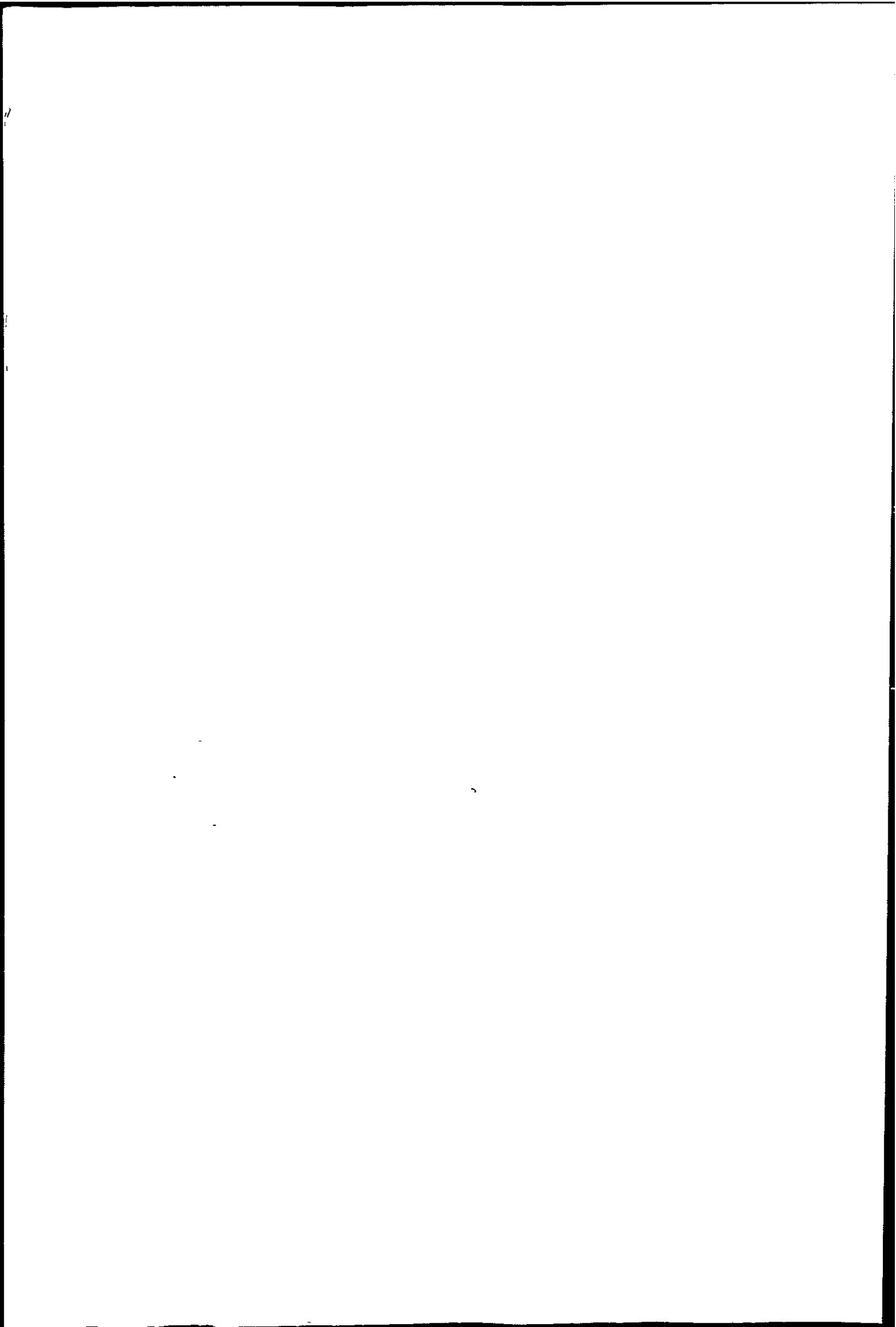
4.1.3 Coke and Char Ash.

The ash content arises due to (i) the inorganic constituents of coal-forming plants, (ii) accumulation of minerals during coalification. Some decomposition of the mineral matter of coal occurs during carbonisation so cokes generally contain less ash than coals. (equivalent amounts)

The nature of coal ash in terms of solid state properties, composition and geochemistry has been extensively studied. Coke ashes have not been so well investigated. In the hearth region of the blast furnace the ash is molten, forming the slag, the acidity or basicity of which is important in metal-gas-slag equilibria. The amount of ash present affects the economy of metal production. Comparative data is given by Chatterjee et al[12] for blast furnaces operating with high ash coke.

The ash contains catalysts of the Boudouard reaction and acid leaching to remove ash minerals from chars is frequently used in comparative reactivity studies. It is often difficult to distinguish between the catalyst effects of mineral matter and effects due to changes in the porosity of the carbon. Re-addition of ash to washed char does not restore initial reactivity (Chapter 2, ref. 22). Similarly in cokes the mineral matter is an integral part of the macrostructure.
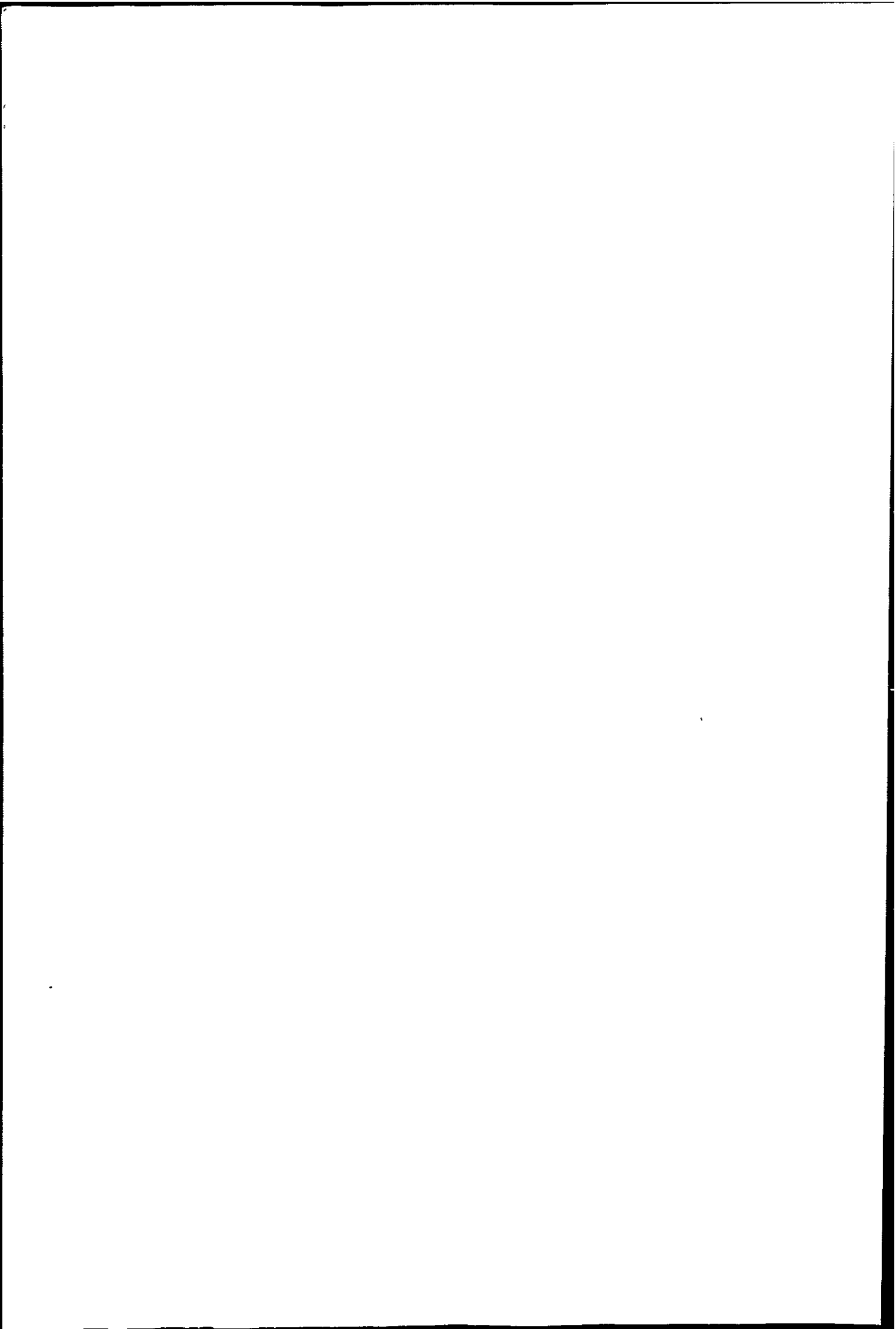
4.2 Experimental procedures.

Liquid densities were found from the volume of acetone displaced by a weighed sample, and gas densities for the cokes from displacement of nitrogen at room temperature using the vacuum balance described in Chapter 3.2.1. This was done conveniently before determination of N_2 adsorption isotherm at 77 K.

CO_2 adsorption at 196 K was carried out using the vacuum balance described in Chapter 3.2.2, with approximately 0.5 to 1.0 g dry sample. The buoyancy effect was neglected in N_2 and CO_2 adsorption for the char and charcoals as uptake of adsorbate was high.

Samples examined by SEM (charcoals, char, cokes and ashes) were gold coated to 12 nm and studied with the Jeol T20 scanning electron microscope.

Char and coke samples for transmission electron microscopy were crushed and vibration milled for several hours as a slurry using an agate ball mill. The slurry was diluted and placed in an ultrasonic bath for several minutes. A drop of supernatant liquid was placed on a 200 mesh copper grid with carbon film and allowed to evaporate. Grids were examined using the Philips EM300 microscope at 80 KV accelerating voltage. Ash samples were crushed, dispersed in acetone and placed in the ultrasonic bath and examined as above.

X ray powder diffraction traces for the carbons, cokes and ashes were obtained using the equipment described in Chapter 3.3.1, using Cu K_α radiation. and tube current
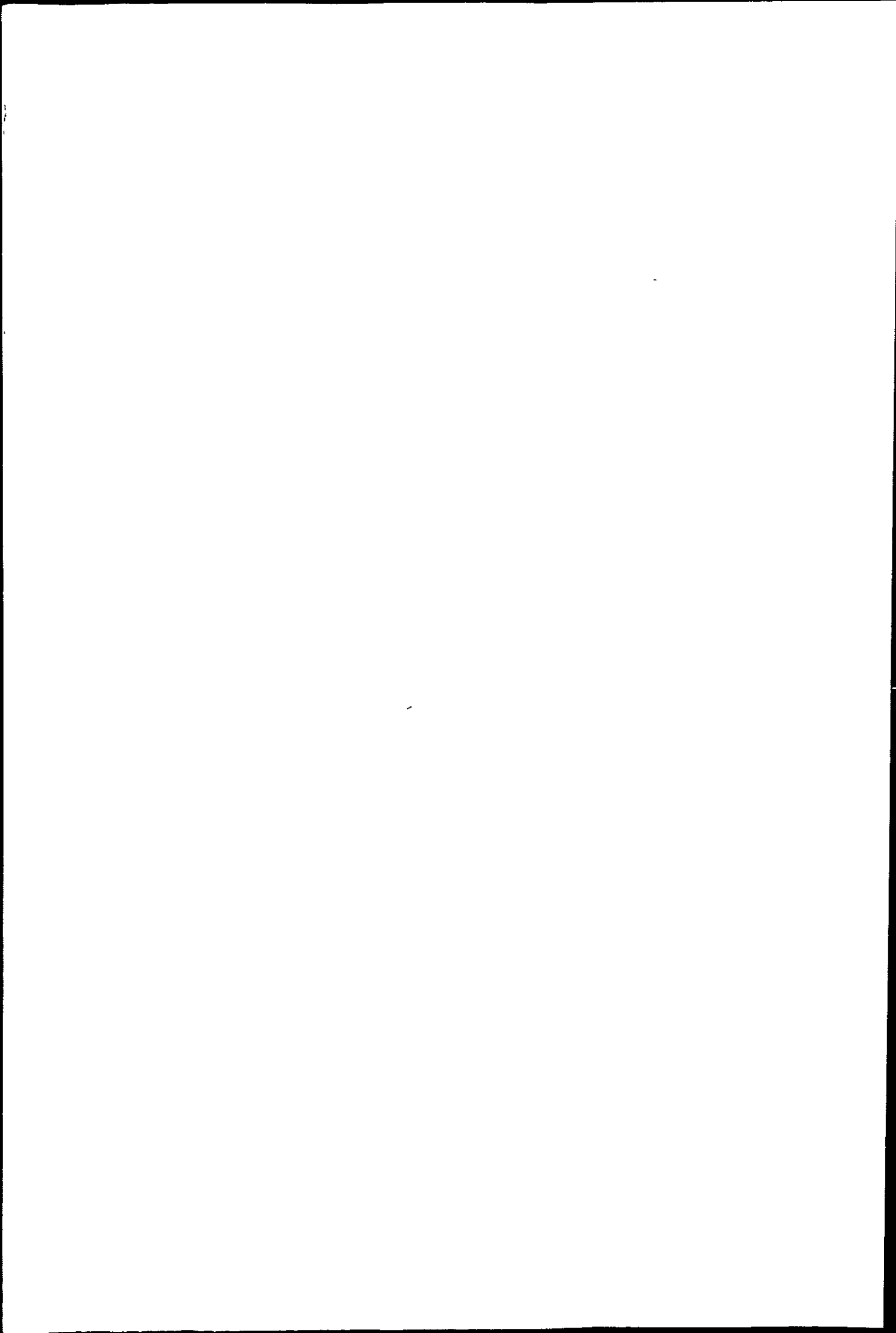
and voltage of 18 mA and 36 kV respectively. The table was rotated at 1.0 ^{o}min^{-1}. Detector counts were 3 x 10^3 per second with a 1 second time constant. Chartspeed of 2 cm min^{-1} gave a trace with 8 cm between the 4 ^{o} markers.

Optical micrographs were obtained from the Zeis Photomicroscope III. Ash samples were placed directly on a glass slide and examined using direct light and a magnification of 78.75. Several Nantgarw coke lumps were vacuum embedded in epoxy resin, sectioned, attached to a microscope slide and lapped down to 30 μm. The thin section was examined at 31.25 magnification.

Coke and char ash samples were prepared in a muffle furnace. Those prepared at > 1000 ^{o}C were the residues from isothermal TG work.

Ash samples were examined by TG/DTA using the Stanton-Redcroft 781 thermal balance under a static air atmosphere. Approximately 10 mg were taken using the Pt/Rh crucibles. TG range was 10% of sample weight and DTA amplifier sensitivity 40 μV.

Chemical analysis for Ca, Mg and sulphate was under-taken on the Nantgarw coke ash from 1000 ^{o} and 500 ^{o}C burn offs, by standard methods as given by Vogel[13].

Approximately 0.25 g of the 1000 ^{o}C burn off ash was accurately weighed and boiled with 50 cm^3 water. The solution was filtered on a prepared Gooch crucible. The crucible was dried at 110 ^{o}C and ignited at 1000 ^{o}C. This gave the water soluble ash fraction. The filtrate was made up to 100 cm^3. 25 cm^3 aliquots were titrated with 0.01 M
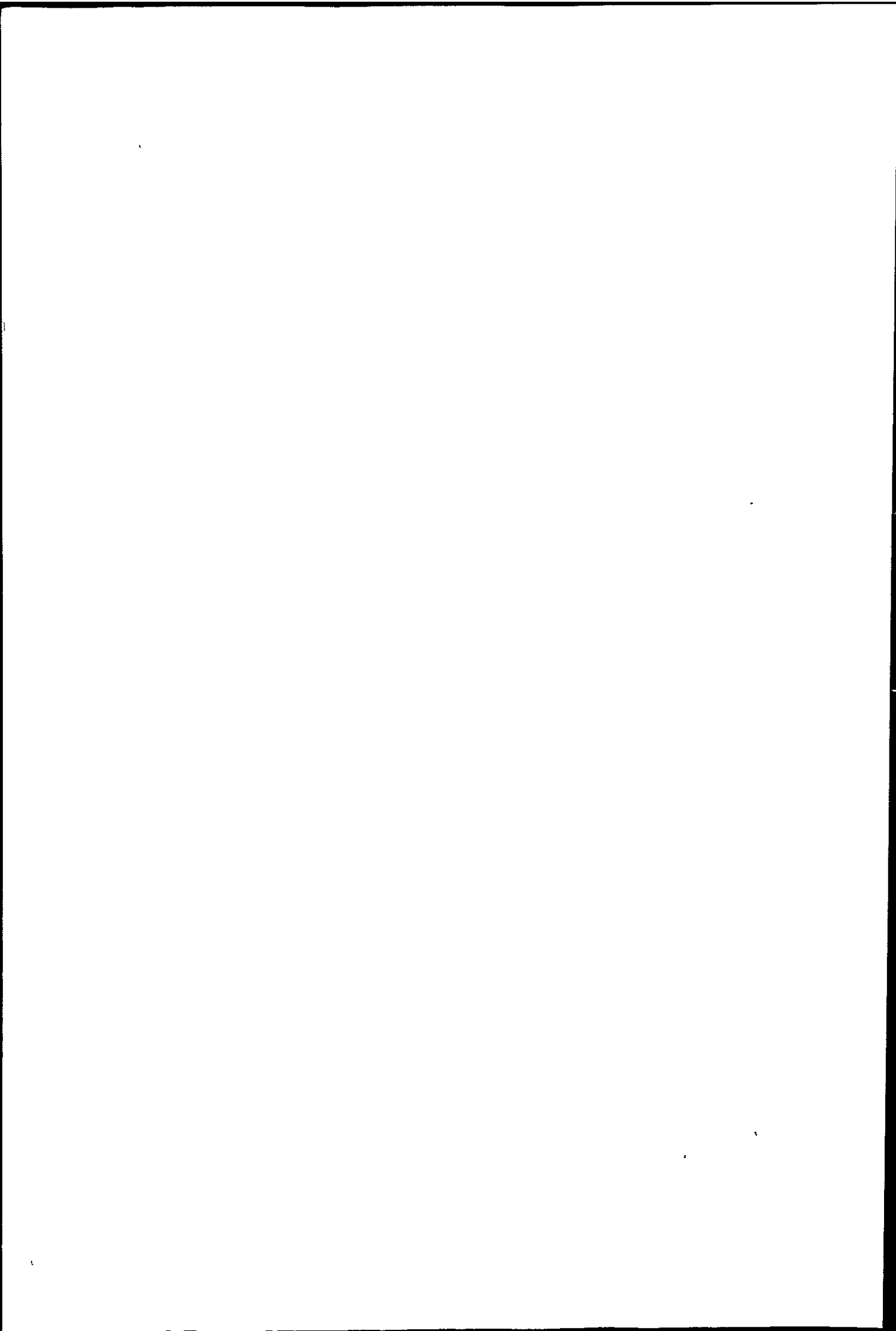
EDTA for Ca and Mg and for Mg only by suitable adjustment of pH. To the remaining 50 cm^3 was added 25 cm^3 of 5% $BaCl_2$ and 2 cm^3 dilute HCl. The sulphate was determined gravimetrically.

Two 0.05 g samples of the 500 ^{o}C ash were accurately weighed. The first sample was boiled with 50 cm^3 of 5 M HCl giving a pale lemon solution and a deep brown residue. 50 cm^3 water were added, the residue filtered on a prepared Gooch crucible dried at 110 ^{o}C and weighed. The crucible was heated to 1000 ^{o}C and re-weighed. This gave the acid insoluble portion and its weight loss in heating to 1000 ^{o}C.

The second sample was boiled with 50 cm^3 water and analysed for Ca and Mg titrimetrically and sulphate gravimetrically as above.
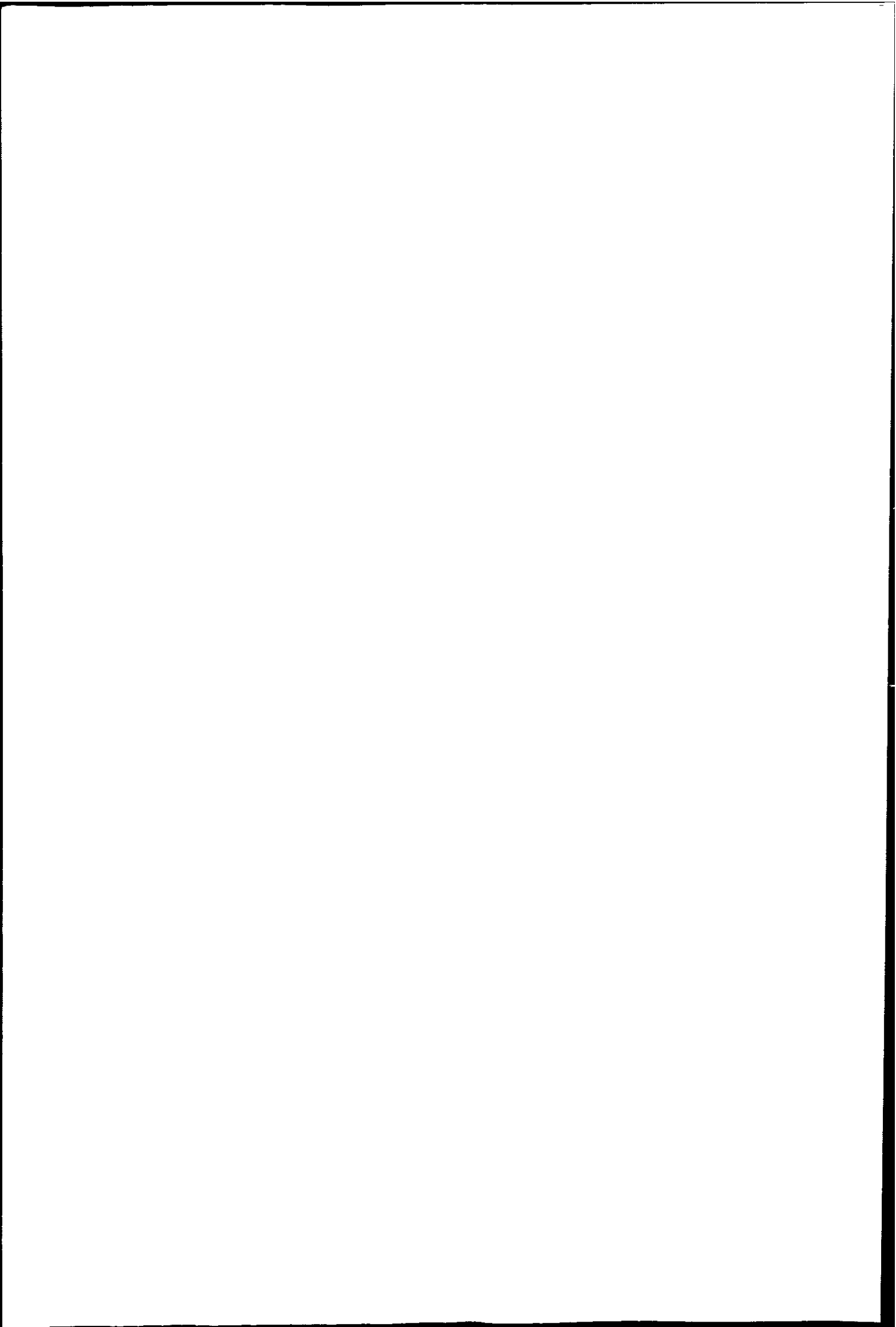
4.3 Results.

### 4.3.1 Investigation of the Carbons

Proximate analysis of the three metallurgical cokes is given in Table 4.3.a, as supplied by ISP. Cwm and Nantgarw cokes are made from coal blends as detailed in Table 4.3.b. Proximate analysis of the Australian brown coal char is given in Table 4.3.c.

The charcoals were supplied by Hopkin and Williams. Activated charcoal for gas adsorption was in the form of granules 1.4 to 2.8 mm. The decolourising and chromatography charcoals were very fine powders, (approximately 55μ m). Decolourising charcoal and purified "Norit GSX", which is also sold as a decolourising charcoal, were examined. ("Norit" is the trademark of Norit U.K. Ltd.) Norit activated charcoals are produced from sawdust which is mixed with phosphoric acid and carbonised in rotary kilns.[14] They have a surface area of 1200-1500 m^2 g^{-1} and wide use in refining, pharmaceuticals and air filters.

PMC graphite is used as a source of high purity carbon and consists of the turnings from graphite electrodes used in the steel industry. Specifications are given in Table 4.3.c, as supplied by PMC Carbon Ltd. Brown coal char (ex. Australia) is also used to a limited extent as a carburiser in U.K. iron foundries, as described by Coates.[15]

The scanning electron micrographs of Plates 4.1 to 4.4 show the gross surface structure of these materials.

Nitrogen adsorption isotherms at 77 K are shown in Figure 4.1.; that of Nantgarw coke is given in Figure 6.4.g. of Chapter 6.
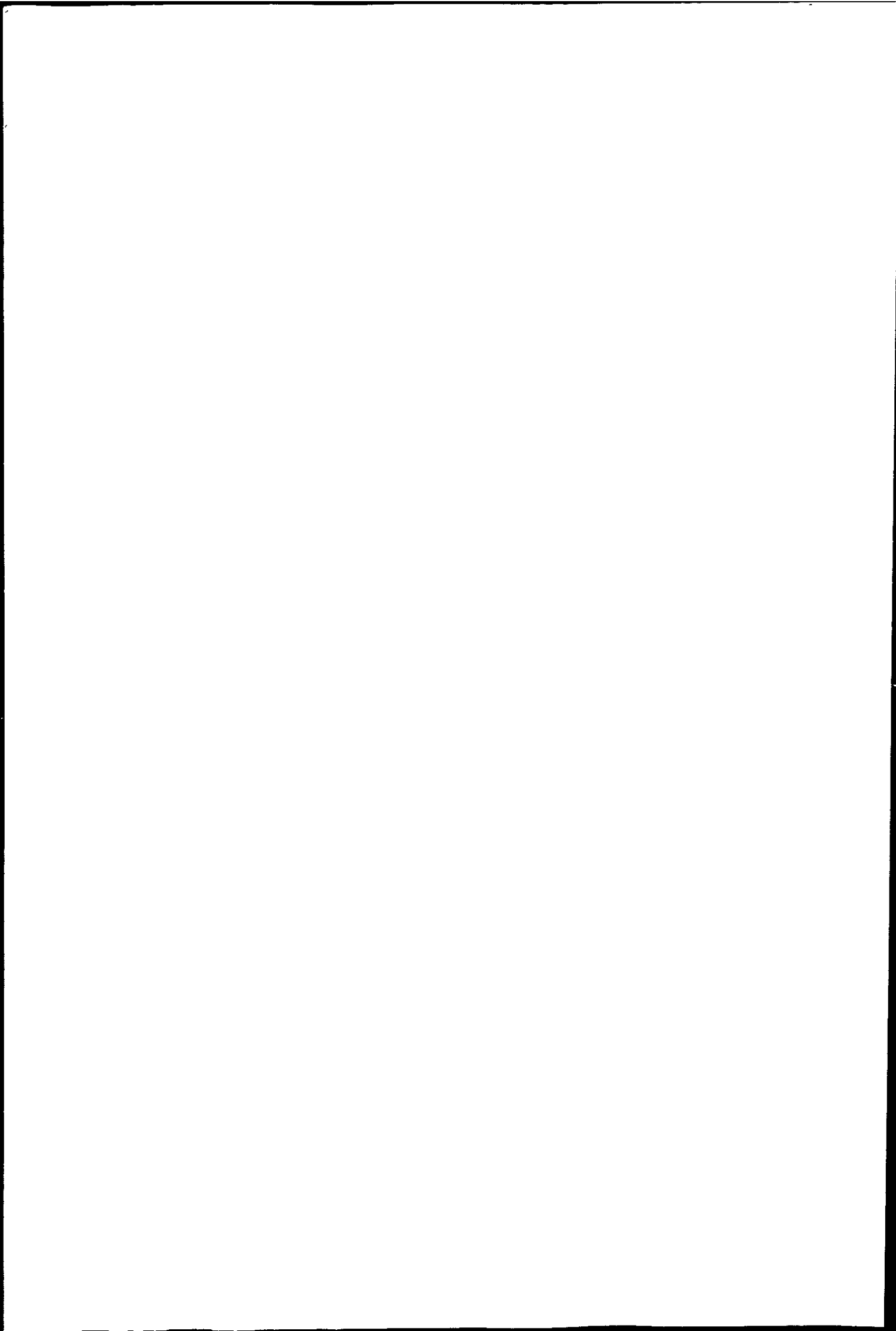
The PMC graphite had a low uptake of nitrogen, giving a type 2 isotherm with no hysteresis. Where a type 1 isotherm was found the specific surface area was calculated from the Langmuir equation (i.e. for the char and the activated charcoal for gas adsorption). For the cokes and other carbons specific surface area was calculated from the BET equation. These values are presented in Table 4.3.d together with specific surface areas from adsorption of CO_2 at 196 K, calculated in the same way. The Dubinin-Radushkevich plots for adsorption of CO_2 at 196 K for the chromatography, decolourising and activated charcoals are shown in Figures 4.2 and 4.3, plotted on semi log scale.

The Australian brown coal char and the cokes gave a broad X-ray diffraction peak at $12.75°$ to $13.0°$ and a smaller broad peak at 21.5 to $21.7°$ as shown in Figure 4.4. No peaks were recorded for the charcoals. A small peak at $15°$ was also recorded for the char.

Liquid and gas densities of the cokes are also given in Table 4.3.d. For cokes the values assessed industrially are apparent density, bulk density and real density, as described by Patrick and Wilkinson (Chapter 2, ref.29) and % porosity is evaluated as $100(1- \frac{apparent\ density}{true\ density})$. Volume porosity was calculated here in a similar manner using the X-ray density of carbon (2.266 g cm^{-3}) as "true density" and the liquid displacement as the apparent density, for the industrial materials.
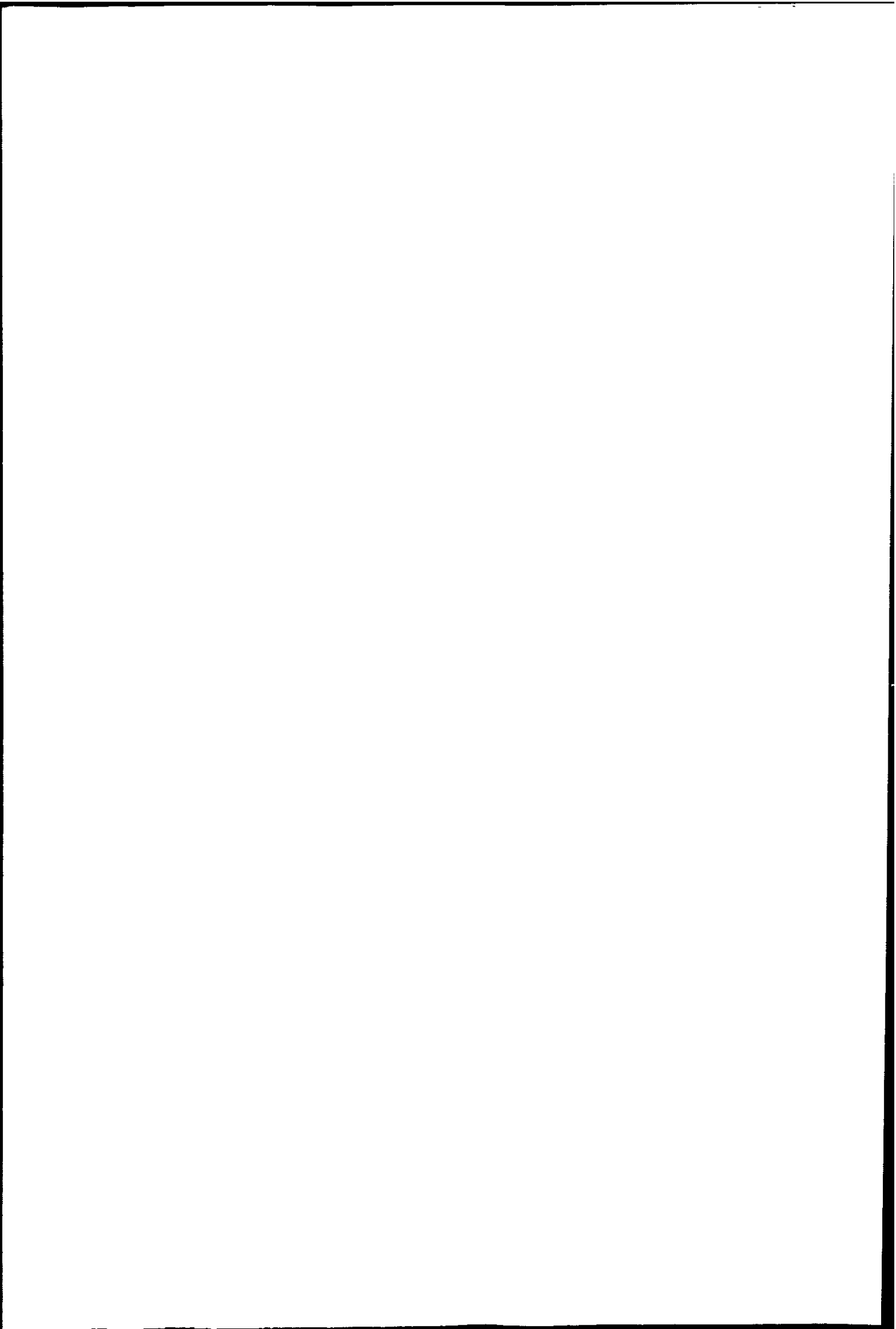
Optical micrographs of a thin section of Nantgarw coke are shown in Plate 4.5 and transmission electron micrographs of a milled sample of Nantgarw coke in Plate 4.6.

The charcoals contained some volatile material; the activated charcoal for gas adsorption and the brown coal char contained considerable quantity. On outgassing at room temperature the powdered charcoals lost about 0.6% weight and the charcoal for gas adsorption 8% weight. Loss of moisture and volatiles for Australian brown coal char is shown by TG in Figure 4.5.

B_2O_3-doped Nantgarw and Cwm cokes and B_2O_3-doped brown coal char, after burn off in CO_2 are shown by SEM in Plate 4.7.

Table 4.3.a.

Proximate analysis of the Metallurgical Cokes.

	Nantgarw	Cwm	Polish
Moisture	$< 1\%$		
ash (dry basis)	9.36%	7.94%	11.32%
volatiles (dry basis)	0.90%	1.01%	1.33%
sulphur	0.90%	0.77%	1.11%
reactivity to CO_2 at 1000 ^{O}C			
(Nantgarw ratio	1.0	1.55	3.06
(ECE test	0.11	0.19	0.43

Table 4.3.b.

Composition of the Welsh Cokes.

(i) Nantgarw (from 5 coals)

Coal	Rank	%
Bedwas	301	20
Bargoed	204 & 301	25
Nantgarw/ Windsor	301	20
Wolstanton	501	15
Marine	301	20

(Wolstanton is the only English coal)

(ii) Cwm (from 4 coals & coke breeze)

Coal	Rank	%
Cwm	301	40
Cymawr	201	20
Nantgarw/ Windsor	301	24
Newport Abercàrn	301	10
Dry breeze	-	6
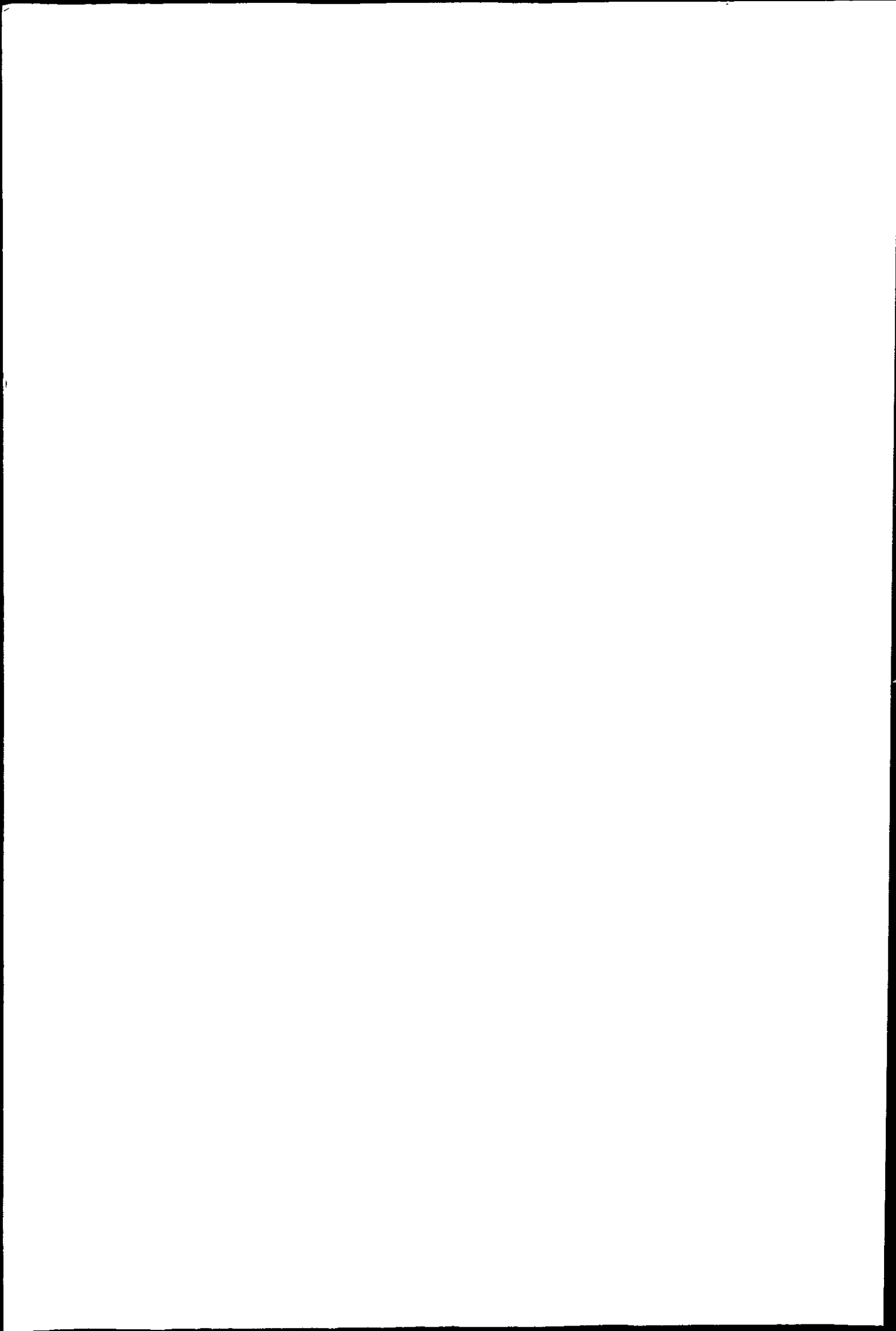
Table 4.3.c.

(i)   Proximate Analysis of Australian Brown Coal Char.

Moisture	~ 4%
ash	1.84% (dry basis)
volatiles	3.41% (" ")
sulphur	0.3%

(ii)   Specifications of PMC graphite (reference 30)

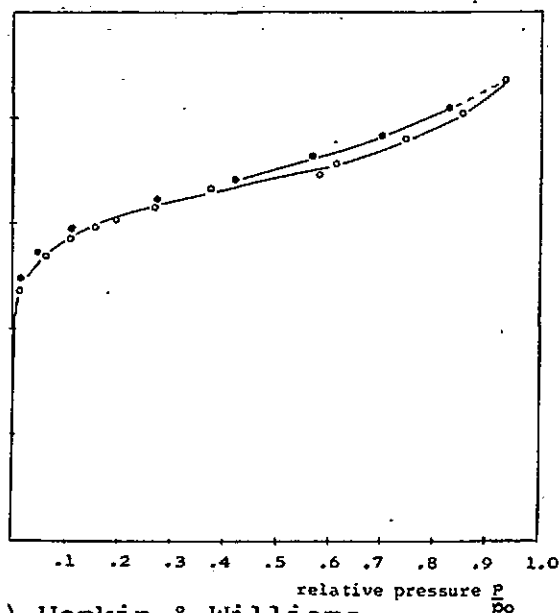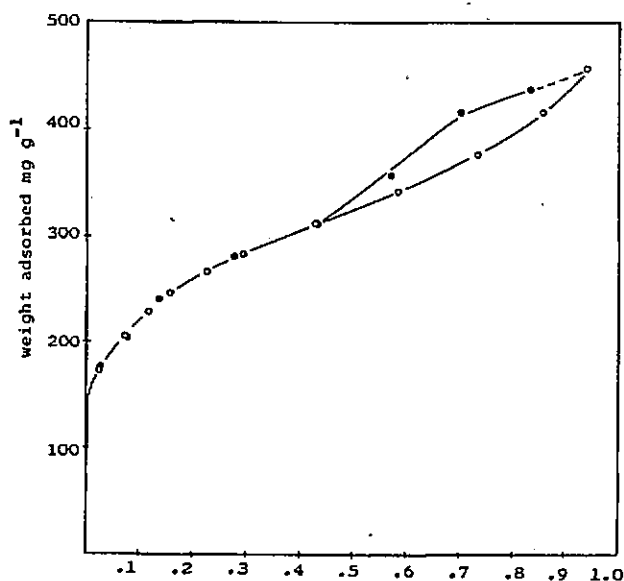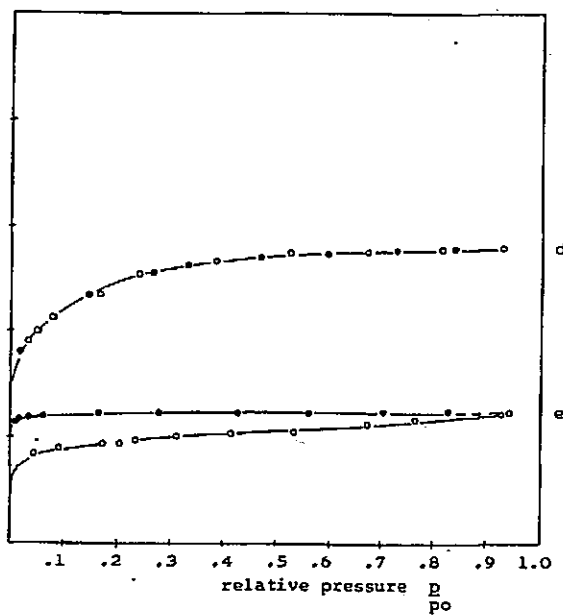|	
fixed carbon	99.50%
sulphur	0.05%
Nitrogen	0.02%
ash	0.40%
volatiles	NIL
moisture	0.10%
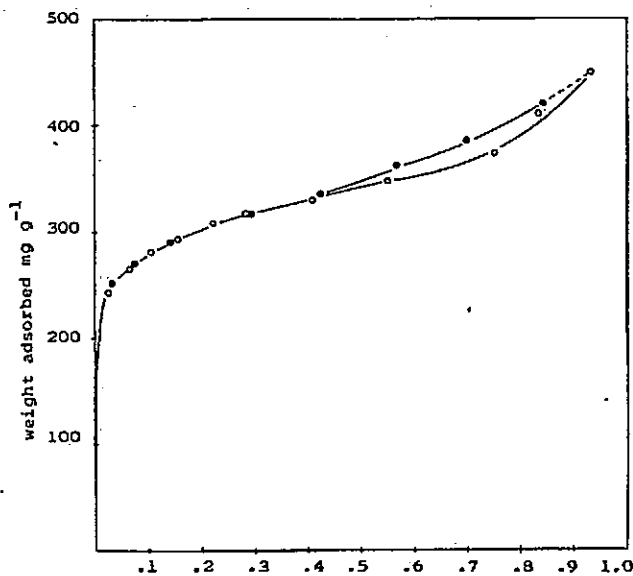
(a) Hopkin & Williams charcoal
    for chromatography

(b) Hopkin & Williams
    decolourising charcoal
    "Norit GSX"

(c) Hopkin & Williams charcoal
    for decolourising

(d) Hopkin & Williams charcoal
    activated for gas
    adsorption.

(e) Australian brown coal char.

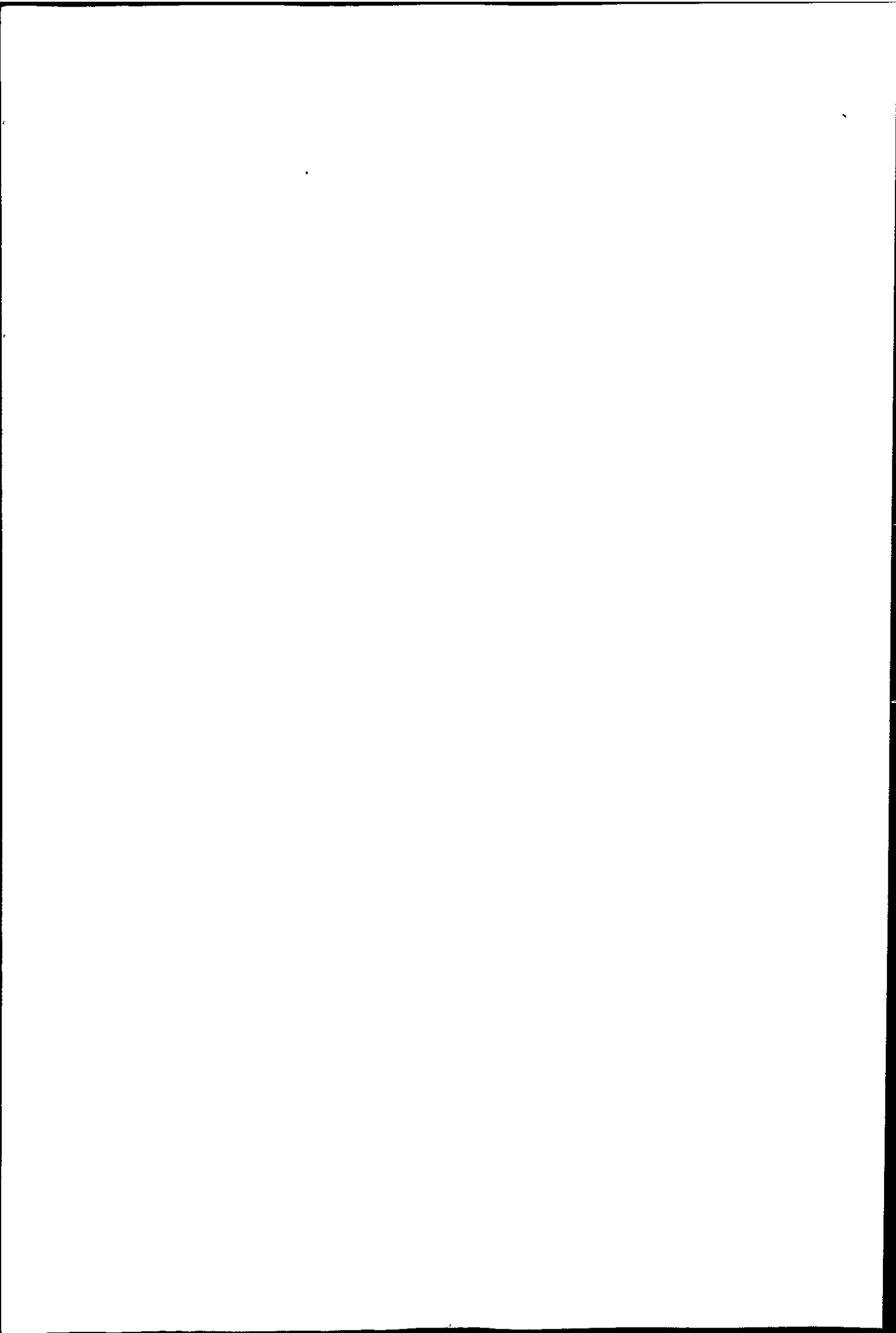Figure 4.1. N_2 adsorption isotherms at 77 K.

Table 4.3.d.

carbon	Isotherm type from N_2 sorption at 77 K	Specific surface area in $m^2\ g^{-1}$ from:		Crystallite size (equivalent spherical diameter) in nm, from gas sorption		density (g cm^{-3})*		% porosity
		N_2 at 77 K	CO_2 at 196 K	N_2 at 77 K	CO_2 at 196 K	liquid dis-placement	gas dis-placement	
PMC graphite	2	1.40	-	1891	-	1.95	-	13.9
Hopkin & Williams charcoal for chromatography	2	824	813	3.21	3.26	1.82	-	
Hopkin & Williams decolourising charcoal	2	698	761	3.79	3.48	1.94	-	
Hopkin & Williams Norit GSX decolourising charcoal	2	824	847	3.21	3.13	1.82	-	
Hopkin & Williams charcoal activated for gas adsorption	1	995	1139	2.66	2.33	2.01	-	
Australian brown coal char	1	410	527	6.44	5.02	2.15	-	5.1
Nantgarw metallurgical coke	2	3.60	-	736	-	1.38	1.48	39.1
Cwm metallurgical coke	2	1.19	-	2225	-	1.30	1.40	42.6
Polish metallurgical coke	2	1.61	-	1645	-	1.30	1.40	42.6

*Density and porosity of cokes different from industrial values due to sample size.
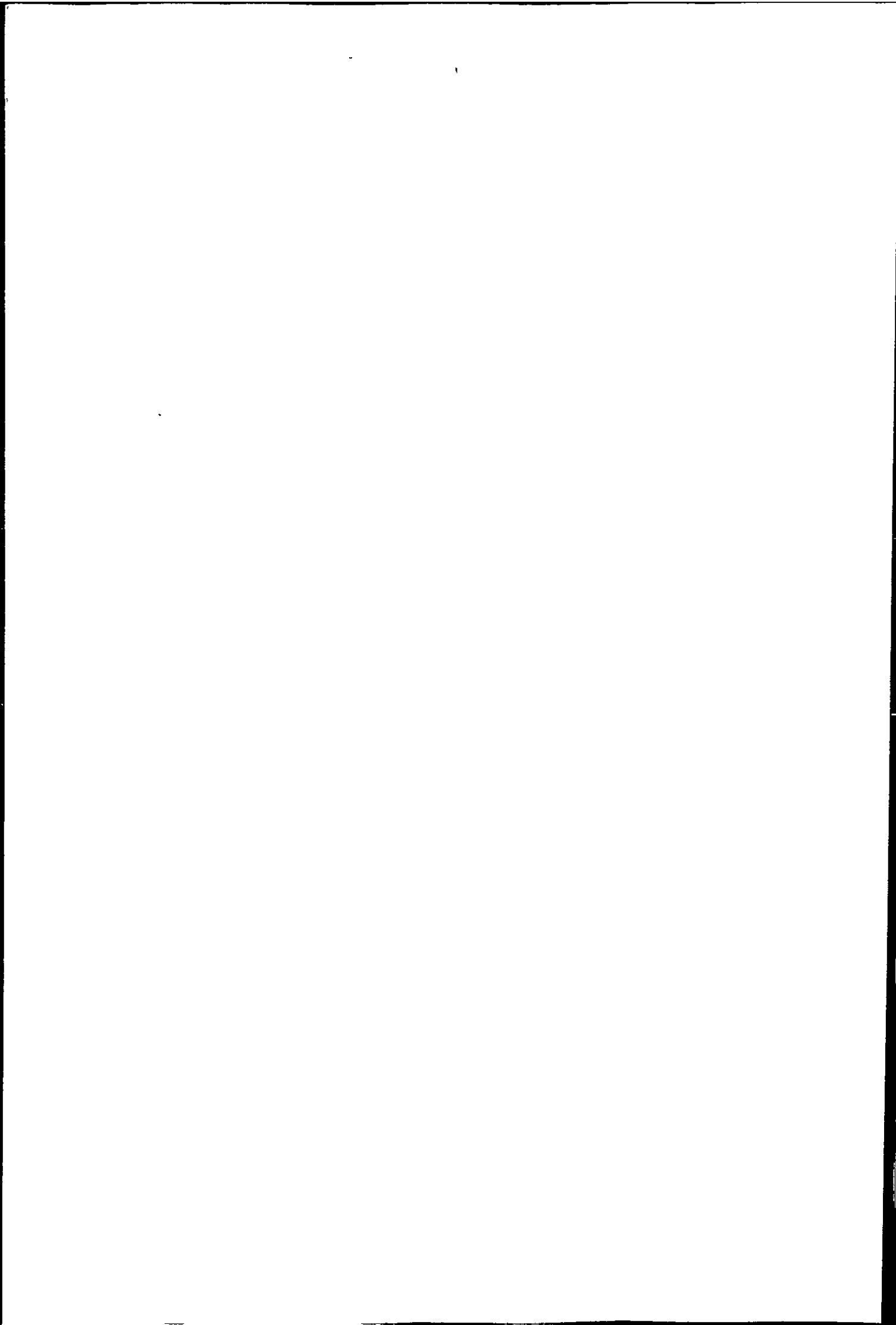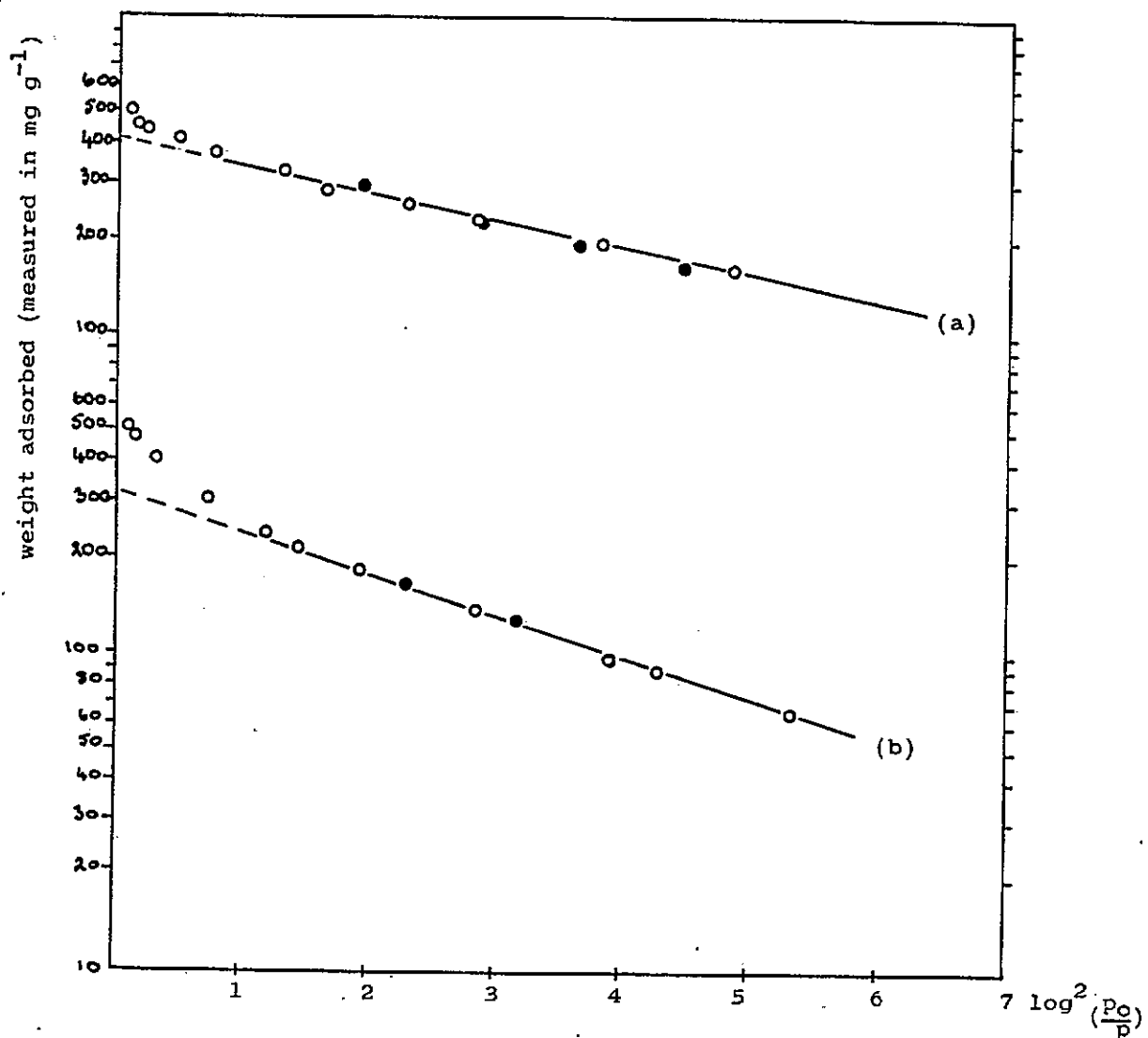
Figure 4.2. Dubinin-Radushkevich plots from adsorption of CO_2 at 196 K for (a) Hopkin & Williams charcoal for chromatography and (b) Hopkin and Williams decolourising charcoal.

154
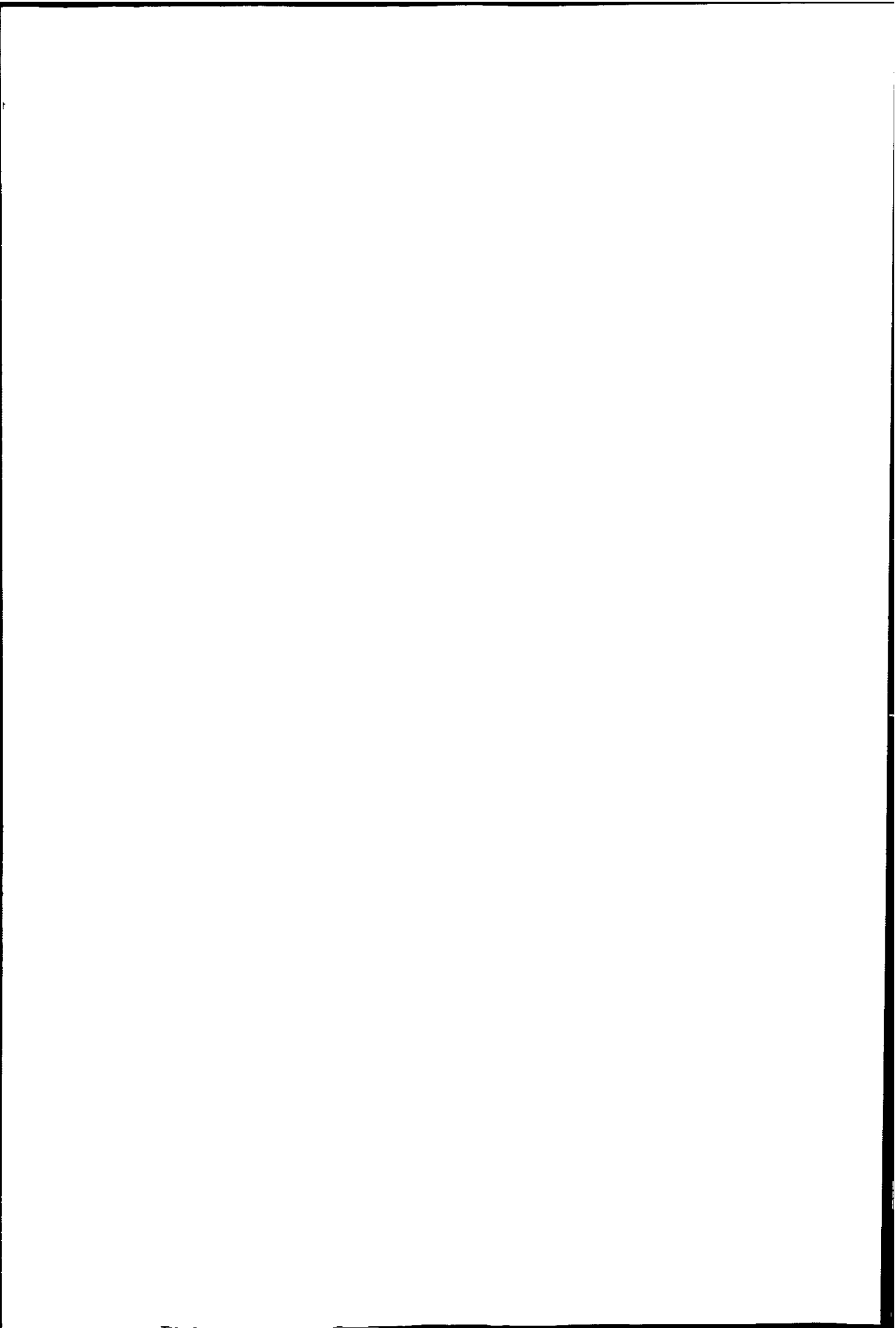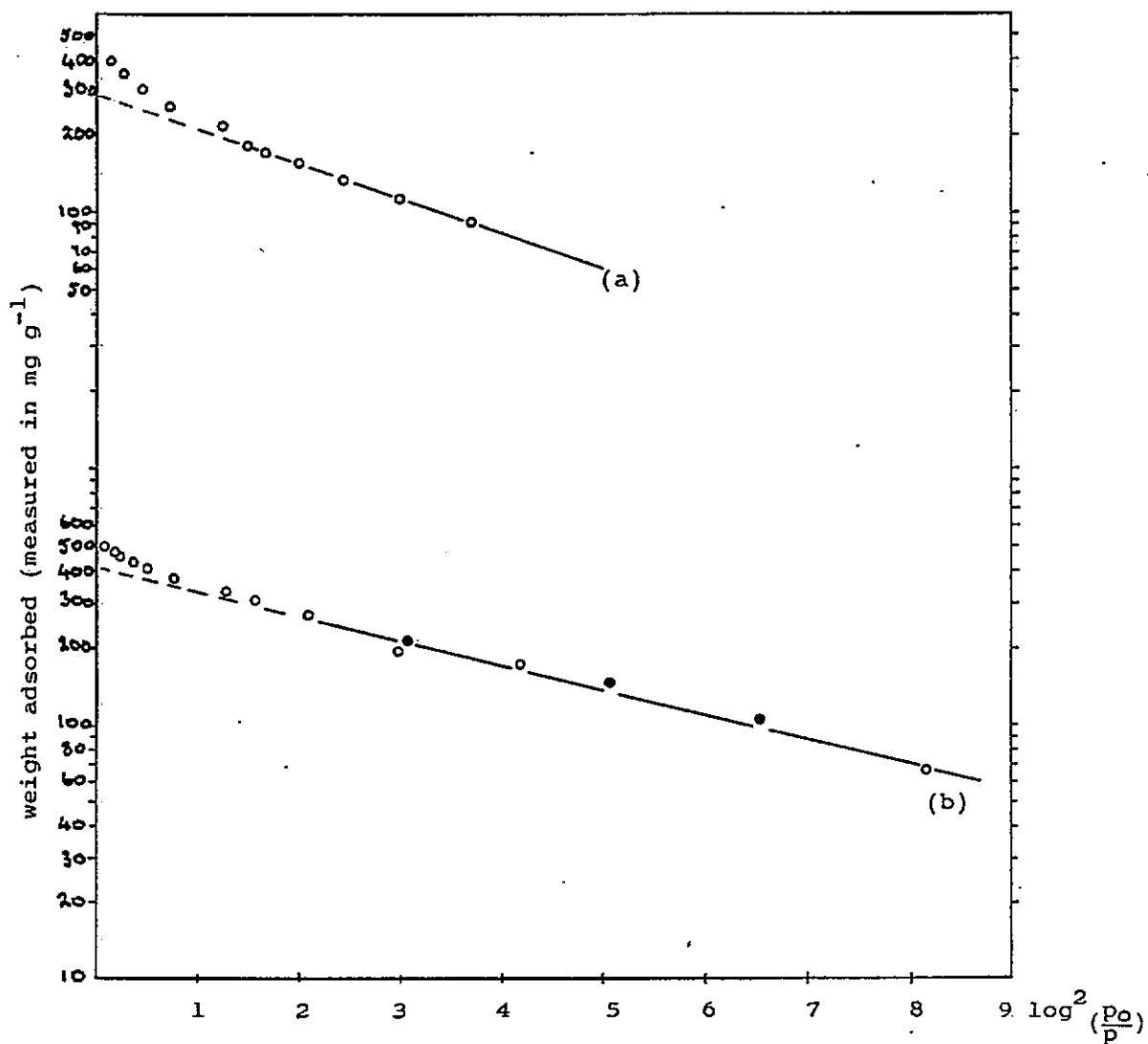
Figure 4.3. Dubinin-Radushkevich plots from adsorption of CO_2 at 196 K for (a) Hopkin & Williams charcoal activated for gas adsorption and (b) Hopkin & Williams charcoal "Norit GSX".

155

Figure 4.4. X ray Powder Diffraction Traces for the Cokes and Australian Brown Coal Char.

156

intensity ——→

Australian brown coal char

Polish coke

Cwm coke

Nantgarw coke dust

Nantgarw coke

24 °   20 °   16 °   12 °   8 °   4 °

Diffraction angle θ
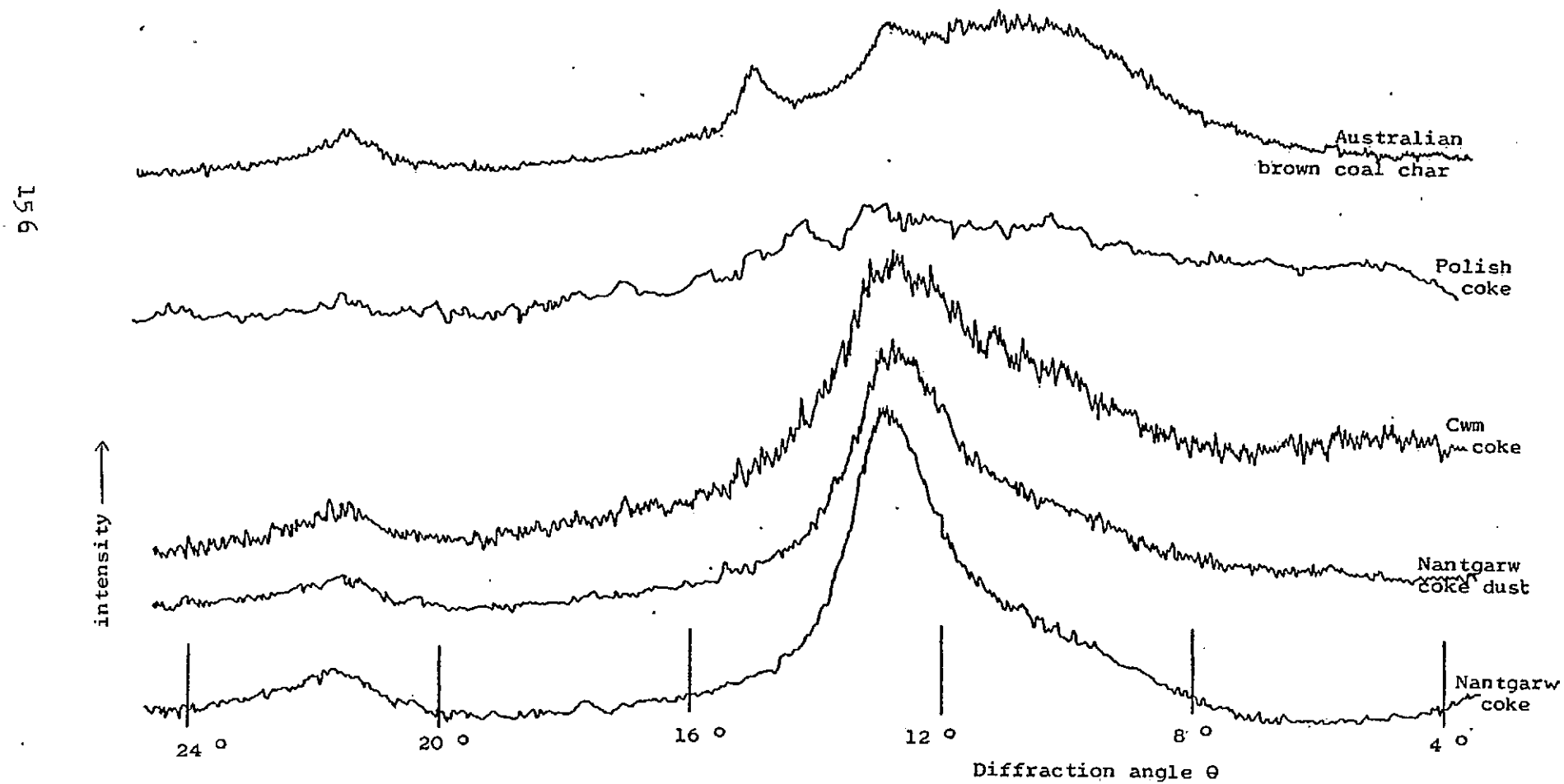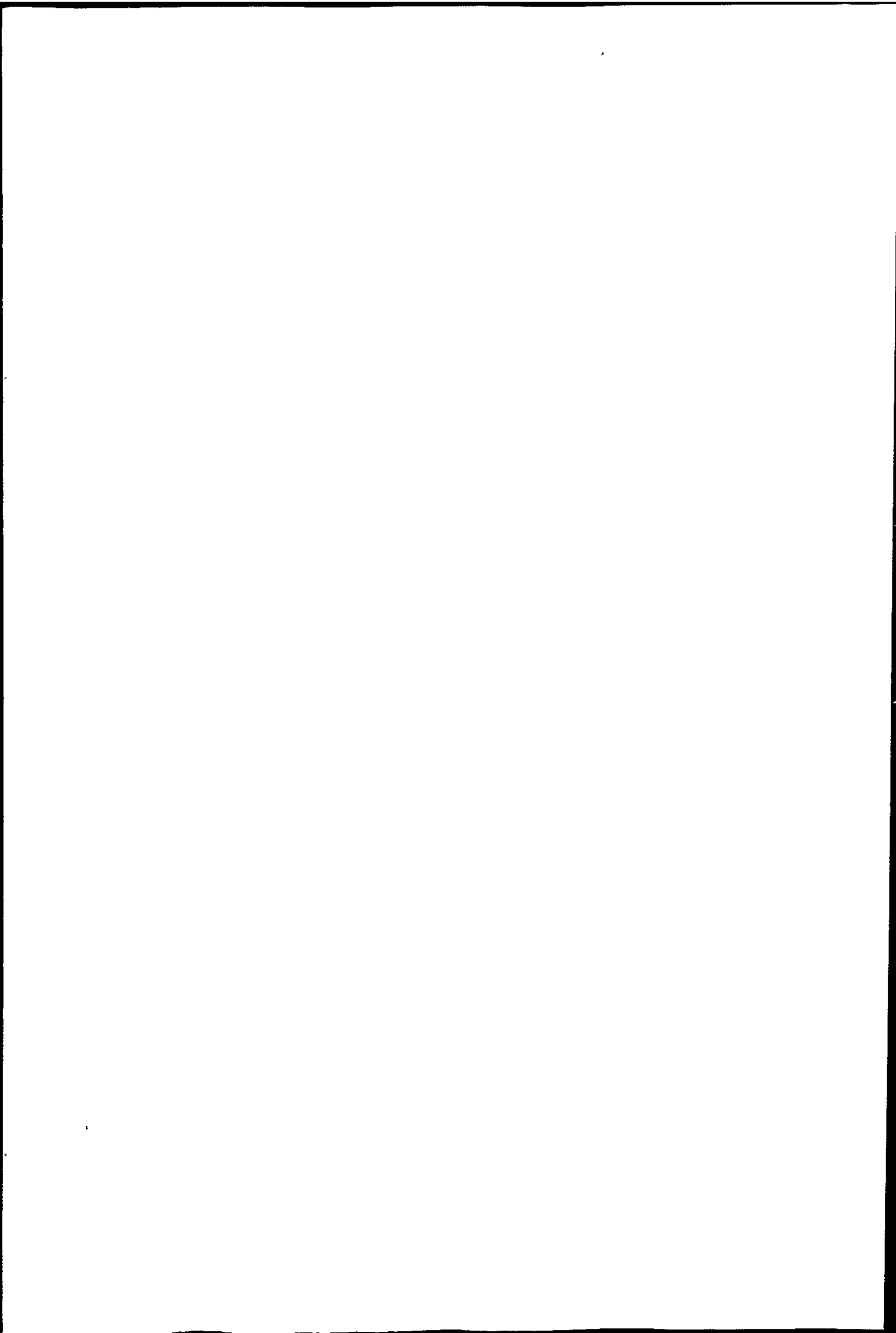
Figure 4.5: Loss of moisture and volatile material on heating Australian Brown Coal Char
in flowing nitrogen at 10 °C min⁻¹ (Sample weight 166.5 mg)

4.3.2   Investigation of the Coal Char and Coke Ashes.

Coke ash composition as supplied industrially is given in Table 4.3.e.

X-ray powder diffraction traces of ash from Nantgarw coke burnt off in air at 500 $^{\circ}$C and 1000 $^{\circ}$C are shown in Figure 4.6 and similarly for the char ashes in Figure 4.7. The d spacings and possible assignment of peaks is given in Tables 4.3.f and 4.3.g for Nantgarw coke ash and Tables 4.3.h and 4.3.i for Australian brown coal char ash. Results for the coke ash are summarised in Table 4.3.j.
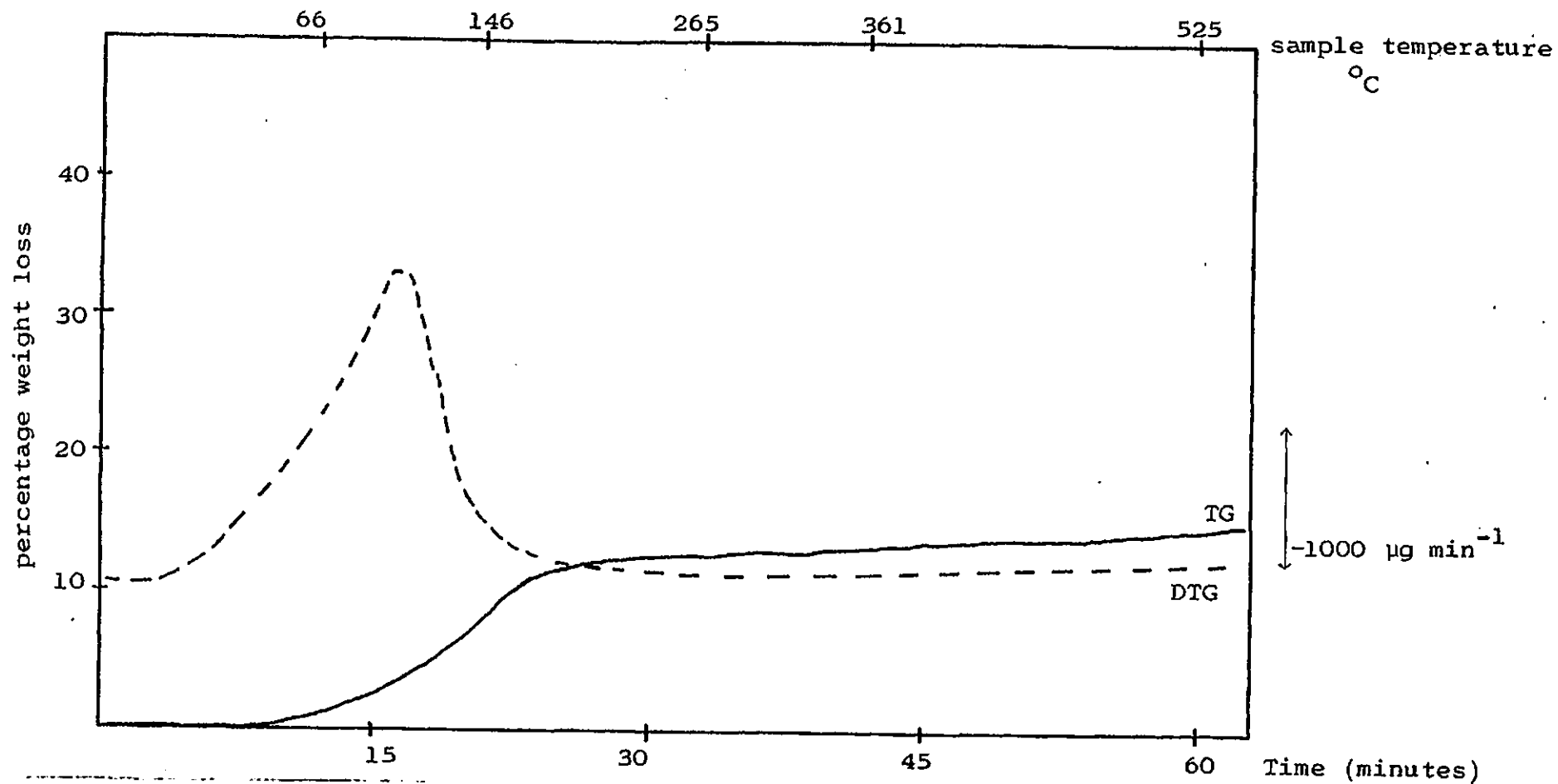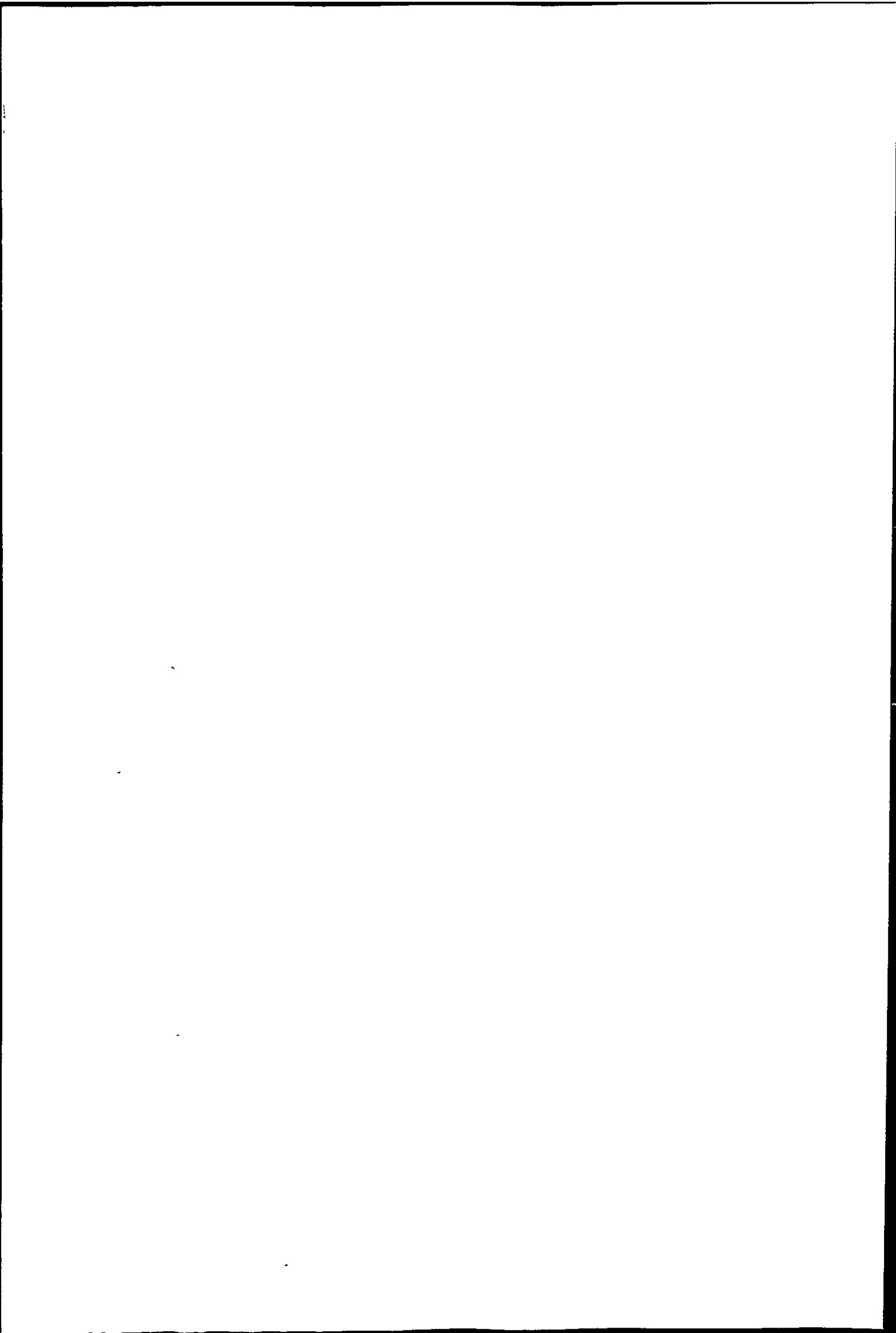
Following XRD, some chemical analysis of the Nantgarw coke ashes was undertaken and results are summarised in Table 4.3.k.

Nitrogen adsorption isotherms at 77 K of the coke and char ashes from 500 $^{\circ}$C burn off are shown in Figure 4.8. Scanning and transmission micrographs of these materials are shown in plates 6.1 and 6.2 of Chapter 6. Optical micrographs of the 1000 $^{\circ}$C and higher temperature burn off Nantgarw coke ashes are shown in Plate 4.8.

TG/DTA traces of the coke and char ashes from 500 $^{\circ}$C burn off are shown in Figures 4.9 and 4.10 on heating to 1500 $^{\circ}$C at 5 $^{\circ}$C min^{-1} and 10 $^{\circ}$C min^{-1} respectively,

The ash from B_2O_3-doped Nantgarw coke was also examined. This contained black lumps which could be picked out by hand under a magnifying lens. Their X ray powder diffraction pattern is shown in Figure 4.11 and results tabulated in 4.3.1. The data for possible iron borates from A.S.T.M. index is summarised in Table 4.3.m giving

161

the d spacings and relative intensity of the three strongest peaks.

The appearance of the doped Nantgarw coke 1000 $^{\circ}$C ash under the optical microscope is shown in Plate 4.8 and one of the black aggregates. The surface of the latter material is also shown in the scanning electron micrographs of Plate 4.9.
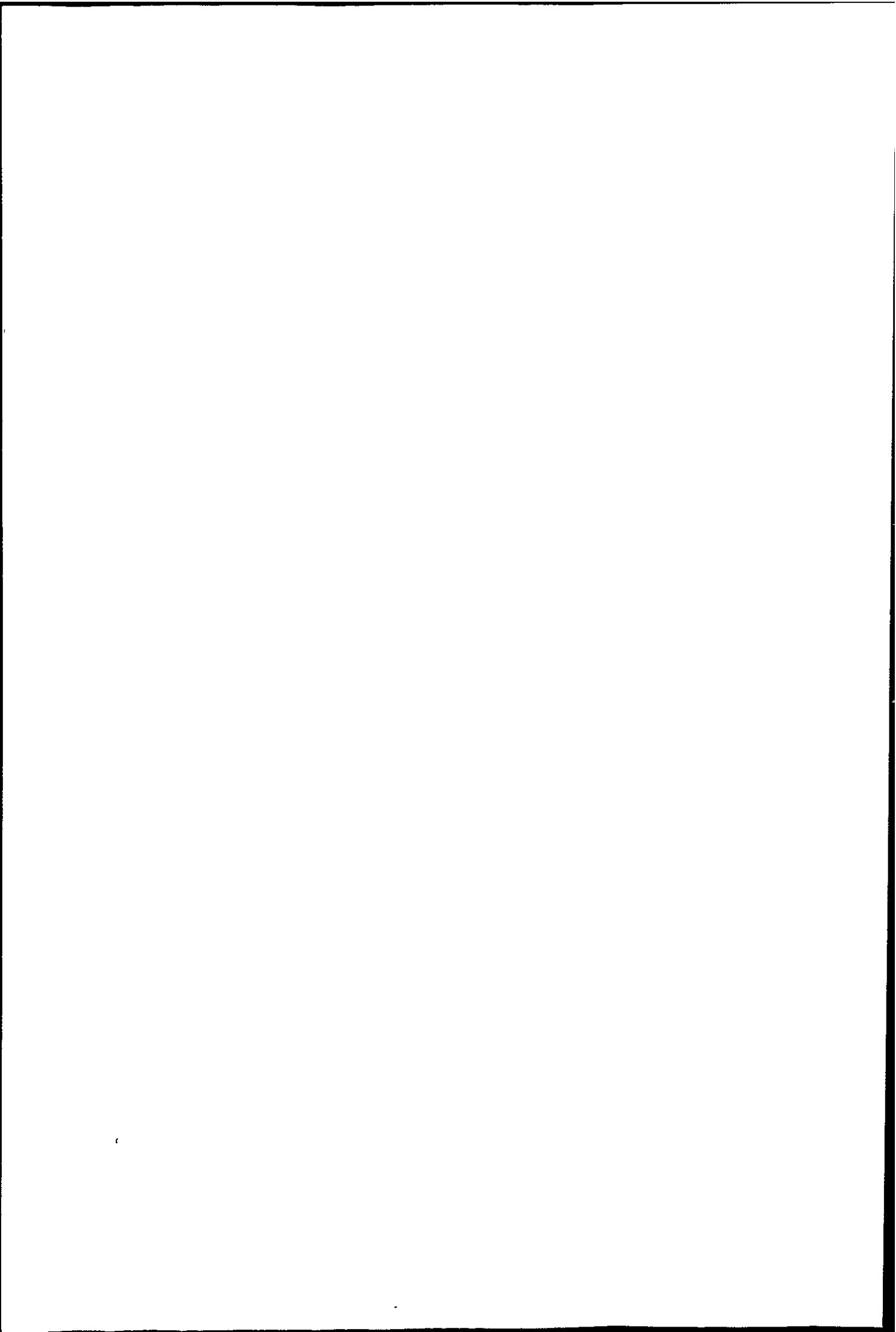
Table 4.3.e.

Coke ash composition (percentages)

	Nantgarw	Cwm	Polish
Al_2O_3	31	32.1	27.8
SiO_2	43	36.9	41.1
Fe_2O_3	9	8.8	11.4
C_aO	3	5.9	4.4
MgO	1	1.4	2.5
Na_2O	2	2.8	1.5
K_2O	4	3.5	2.3
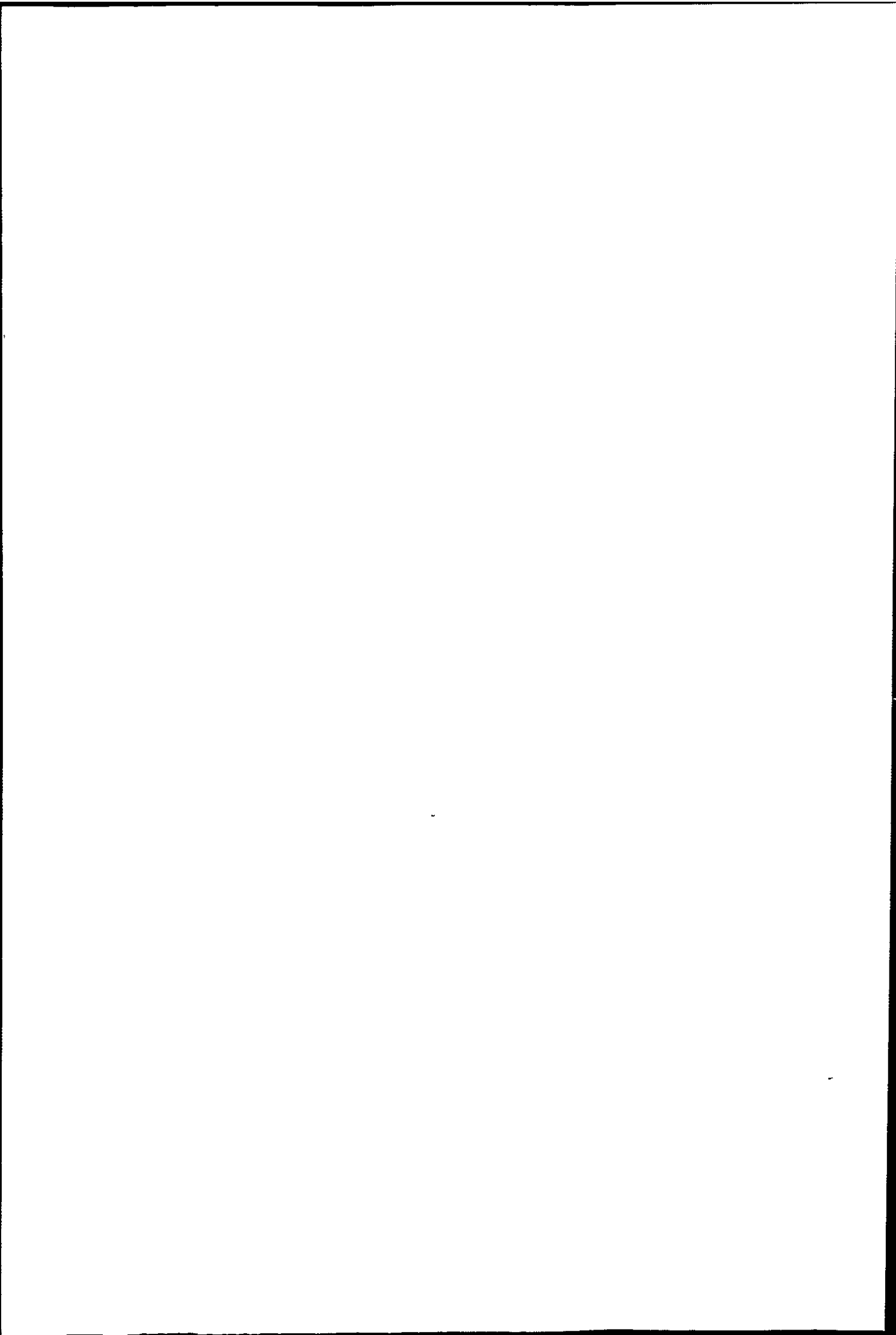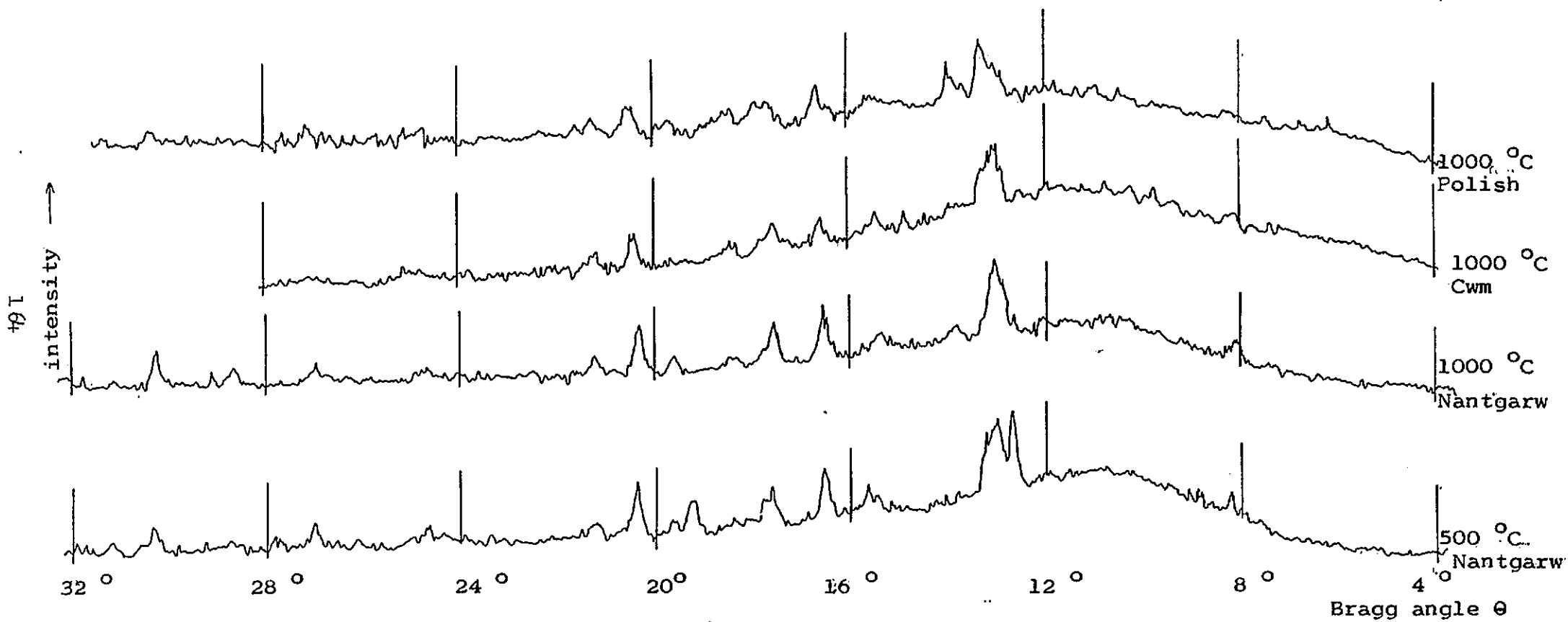
Figure 4.6. X ray powder diffraction traces of coke ash from air burn offs.
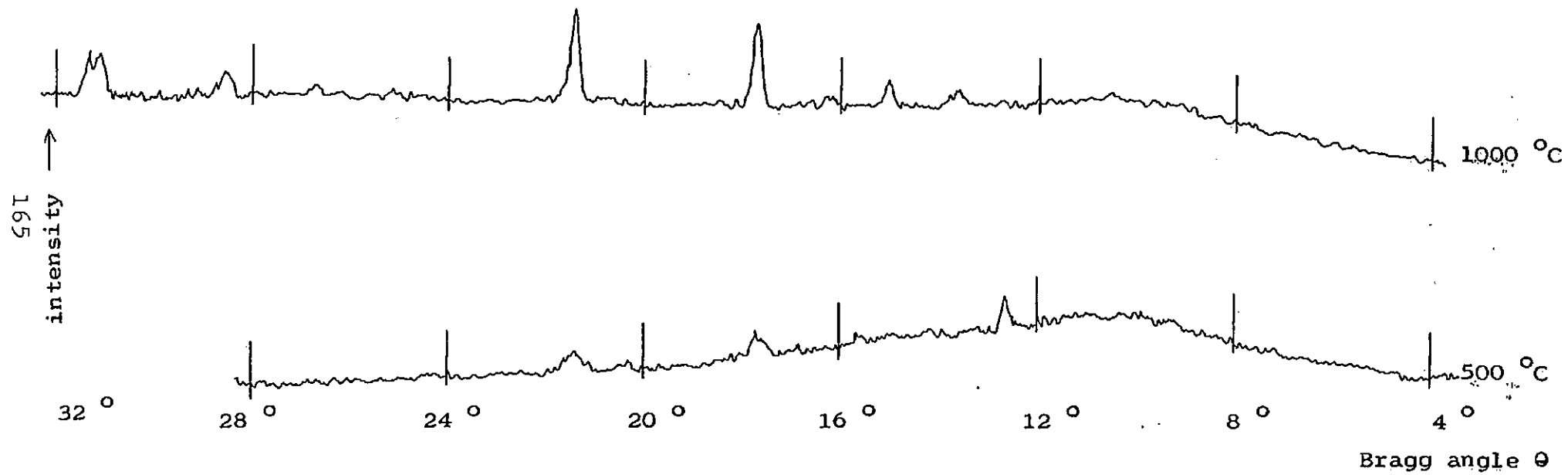
Figure 4.7. X ray powder diffraction traces of ash from air burnt off Australian brown coal char.

Table 4.3.f.

Assignment of X ray powder diffraction peaks for 500 $^{\circ}$C burn off Nantgarw coke ash.

	$\theta(^{\circ})$	$d(\overset{\circ}{A})$	Assignment	$d(\overset{\circ}{A})$ ASTM	I/I_1	hkl
w	8.20	5.407	sillimanite	5.35	70	110
s	12.70	3.508	$CaSO_4$	3.49	100	002,020
s	12.95	3.428	sillimanite	3.41	90	120
w	15.45	2.895	sillimanite, γFe_2O_3 $CaSO_4$	2.88 2.95 2.849	70 34 35	002 220 210
w	15.65	2.859	sillimanite	2.88	70	002
s	16.55	2.707	"	2.67	80	220
m	17.60	2.551	"	2.53	90	112
m	17.75	2.530	γFe_2O_3 Fe_3O_4	2.52 2.53	100 100	311
m	19.25	2.339	$CaSO_4$	2.328	20	202,220
w	19.65	2.293	sillimanite	2.30	30	022
s	20.40	2.213	"	2.20	100	122
w	21.25	2.128	"	2.10	60	230
w	24.65	1.849	"	1.829	60	312
w	27.00	1.699	"	1.690	60	322
w	27.80	1.654	"	1.679	70	420
w	30.30	1.529	"	1.516	90	332
w	31.15	1.491	γFe_2O_3 Fe_3O_4	1.48 1.48	53 85	440

Table 4.3.g.

Assignment of X ray powder diffraction peaks for 1000 $^{\circ}$C burn off Nantgarw coke ash.

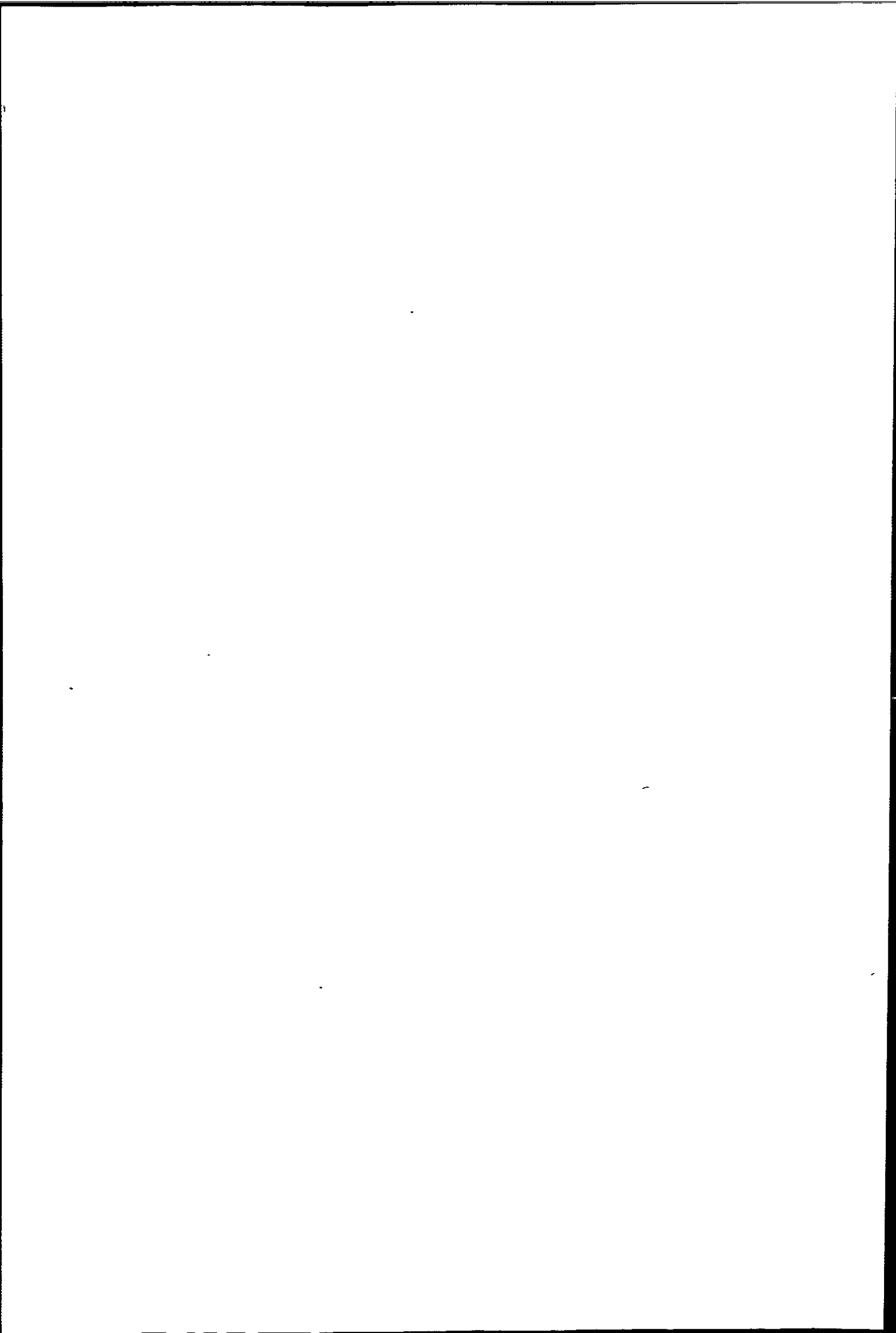|	$\Theta(^{\circ})$	$d(\text{Å})$	Assignment	$d(\text{Å})$ ASTM	I/I_1	hkl
w	8.05	5.51	sillimanite	5.35	70	110
s	13.05	3.42	"	3.41	90	120
w	13.85	3.22	anorthite	3.20	100	$\bar{2}04$
broad w	15.3 to 15.4	2.91 ± .01	sillimanite	2.88	70	002
m	16.50	2.715	sillimanite αFe_2O_3	2.67 2.69	80 100	220 104
m	17.55	2.558	sillimanite	2.53	90	112
broad w	18.3 to 18.5	2.46 to 2.43	"	2.42	60	130
w	19.60	2.299	"	2.30	30	022
m	20.30	2.223	"	2.20	100	122
w	21.25	2.128				
w	24.70	1.846	"	1.829	60	312
w	26.95	1.702	" αFe_2O_3	1.705 1.69	50 60	240 116
w	28.70	1.606	sillimanite αAl_2O_3	1.595 1.601	70 80	042 116
m	30.25	1.531	sillimanite	1.535	20	412

Table 4.3.h.

Assignment of X ray powder diffraction peaks for 500 $^{\circ}$C burn off Australian brown coal char ash.

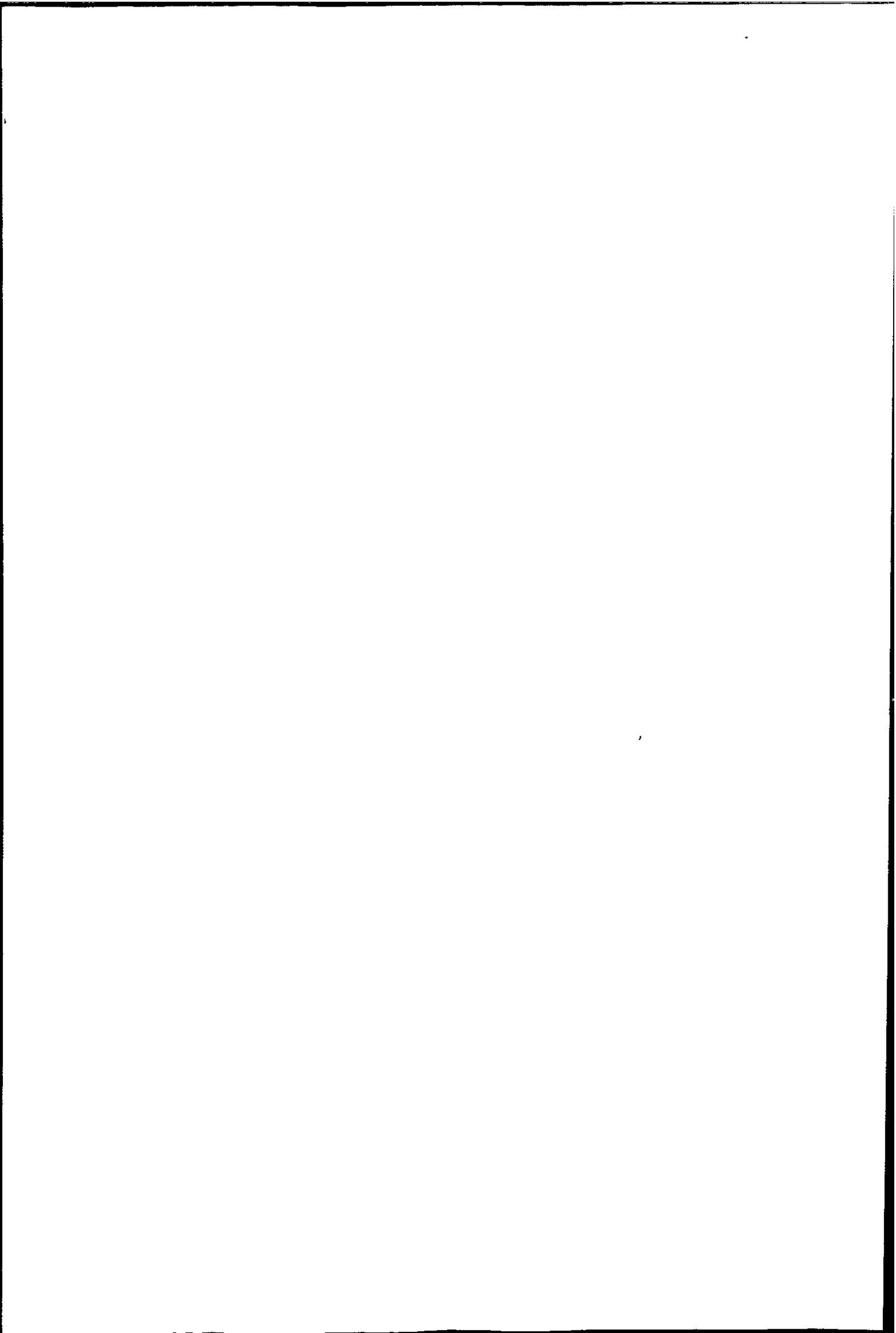| $\Theta(^{\circ})$	$d(\text{Å})$	Assignment	$d(\text{Å})$ from	I/I_1 ASTM
m 12.65	3.522	$CaSO_4$	3.49	100
w 15.60	2.868	γFe_2O_3	2.95	34
		$Mg(AlFe)_{.91.09}O_4$	2.87	80
m 17.70	2.537	αAl_2O_3	2.552	90
		γFe_2O_3 Fe_3O_4	2.52	100
w 20.35	2.218	sillimanite	2.20	100
m 21.40	2.114	αAl_2O_3	2.085	100
		MgO	2.11	100

Table 4.3.i.

Assignment of X ray powder diffraction peaks for 1000 $^{\circ}$C burn off Australian brown coal char ash.

$\Theta(^{\circ})$	$d(\text{Å})$	Assignment	$d(\text{Å})$	I/I_1
w 13.65	3.268	impure SiO_2	3.38	100
m 15.05	2.970	sillimanite	2.88	70
		$Mg(Al\,Fe)O_4$	2.87	80
w 16.20	2.764	sillimanite	2.67	80
s 17.75	2.530	αFe_2O_3	2.51	50
		αAl_2O_3	2.552	90
		Fe_3O_4	2.53	100
s 21.45	2.109	αAl_2O_3	2.085	100
		MgO	2.11	100
w 25.15	1.815	impure SiO_2	1.84	60
w 26.70	1.716	αFe_2O_3	1.69	60
m 28.55	1.614	αAl_2O_3	1.601	80
		Fe_3O_4	1.61	85
m 31.10	1.493	MgO	1.49	52
m 31.35	1.482	Fe_3O_4	1.48	85
		γFe_2O_3	1.48	53
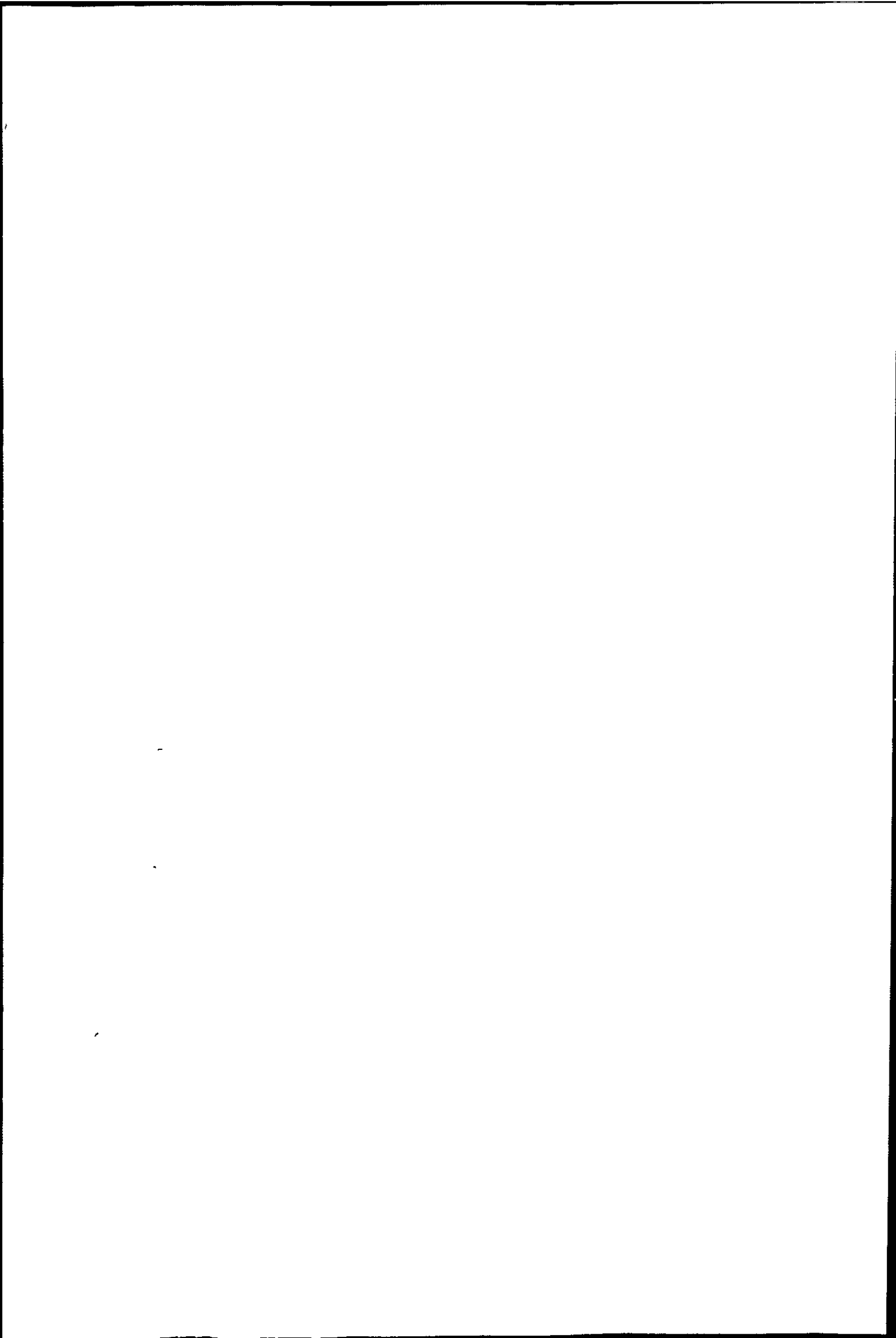
Table 4.3.j.

Principal constituents of Nantgarw coke ash.

500 °C ashing		1000 °C ashing	
sillimanite	$Al_2O_3SiO_2$	sillimanite	$Al_2O_3SiO_2$
anhydrite	$CaSO_4$	anorthite	$CaO.Al_2O_3.2SiO_2$
iron III oxide	γFe_2O_3	iron III oxide	αFe_2O_3
iron II III oxide	Fe_3O_4		

Table 4.3.k.

Chemical analysis of Nantgarw coke ashes.

	acid soluble	water soluble	sulphate	CaO	MgO
500 °C ash	23% losing 6% of sample weight on heating to 1000 °C	11% losing 4% of sample weight on heating to 1000 °C	4% (estimated as $CaSO_4$)	2.40%	0.73%
1000 °C ash		2%	nil	0.280%	0.301%

169
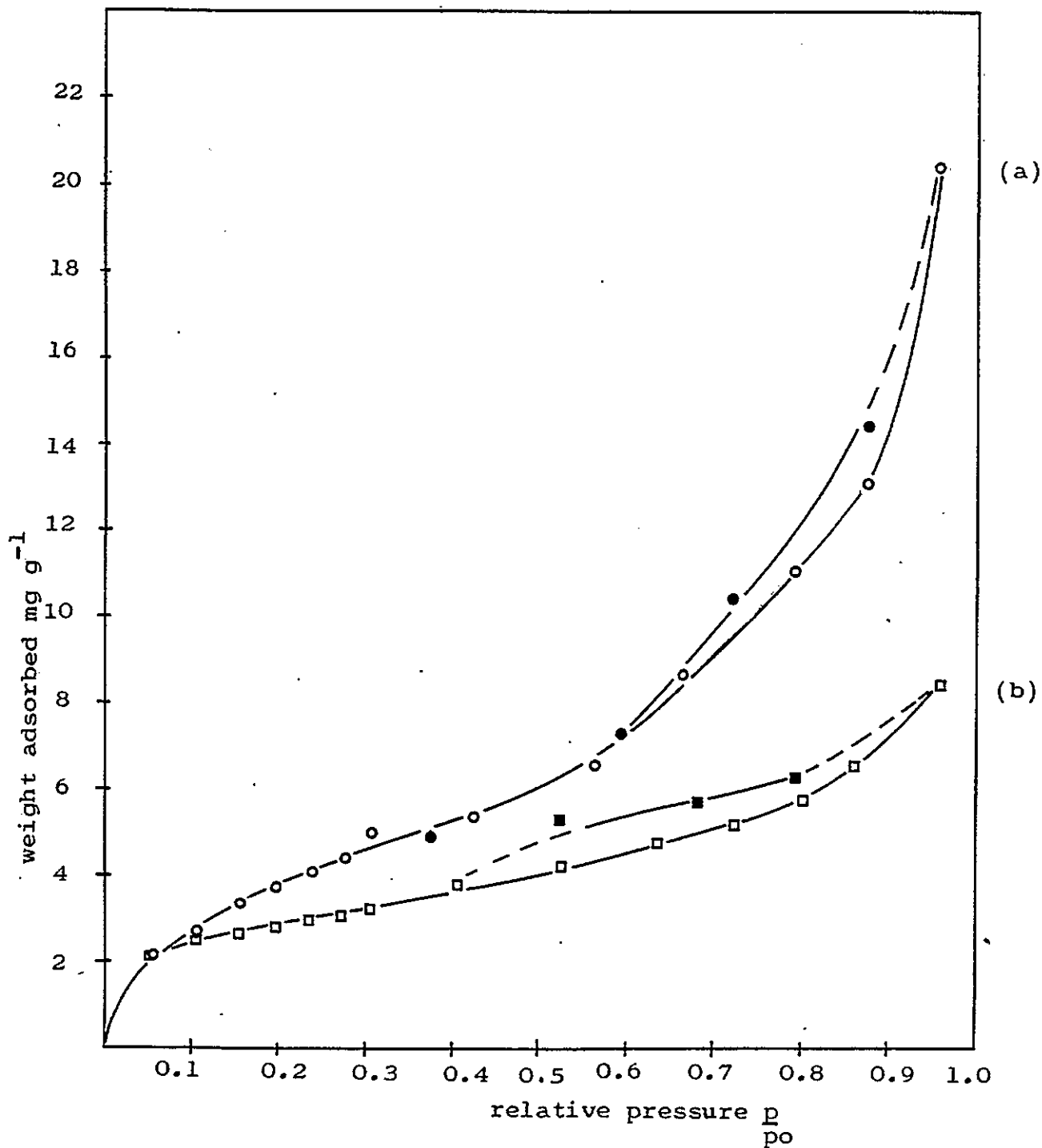
Figure 4.8. Nitrogen adsorption isotherms at 77 K on ashes from 500 °C burn off of (a) Australian brown coal char and (b) Nantgarw metallurgical coke.

170
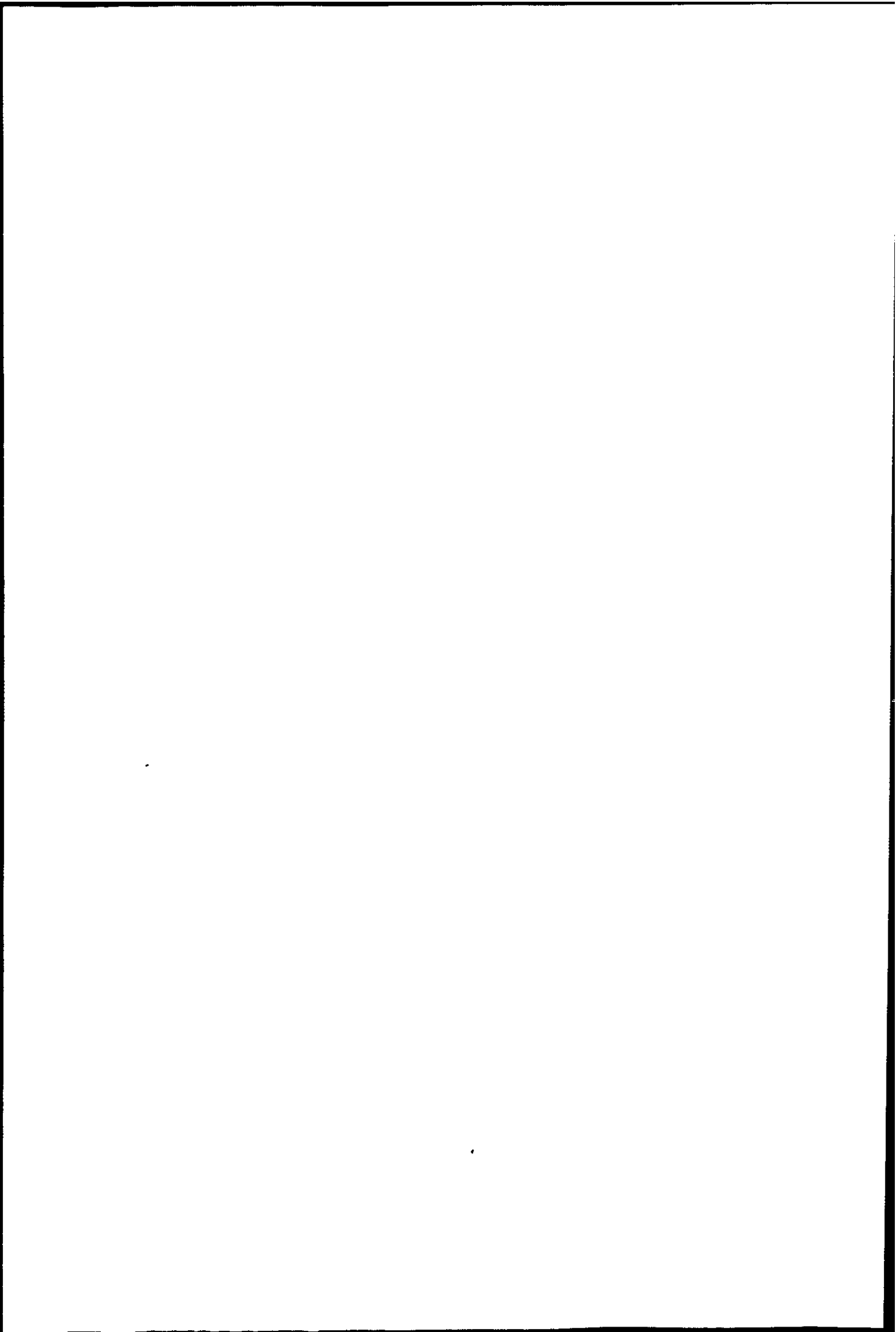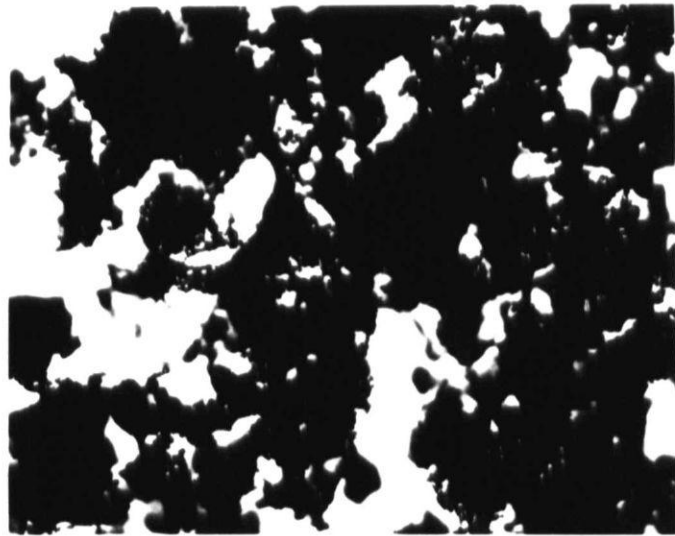
(i) Ash from 1000 ^{o}C air burn off.   Typical material.

(ii) Ash from 1000 ^{o}C air burn off of B_2O_3-doped coke.

Plate 4.9. Optical Micrographs of Nantgarw Coke Ash
Magnification 31.3x

171

(iii) Part of black aggregates in 1000 °C air burn off B_2O_3-doped coke ash.
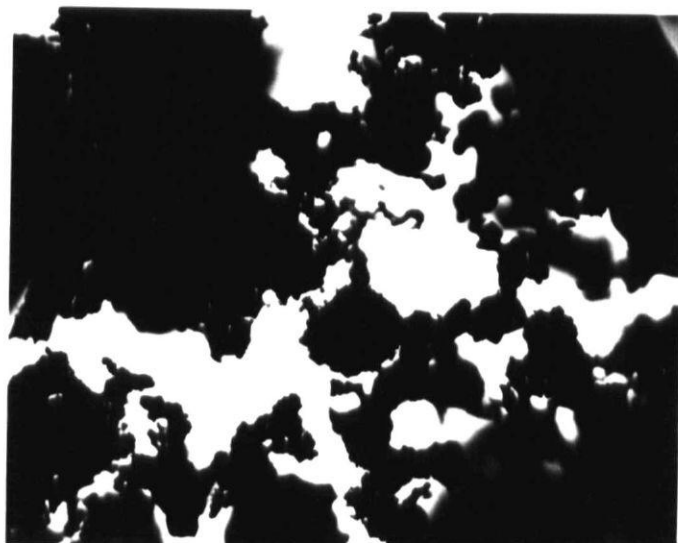
(iv) Ash from 1350 °C burn off in CO_2. Finest material.

Plate 4.8 (continued). Optical Micrographs of Nantgarw Coke Ash.

Magnification 31.3x

172
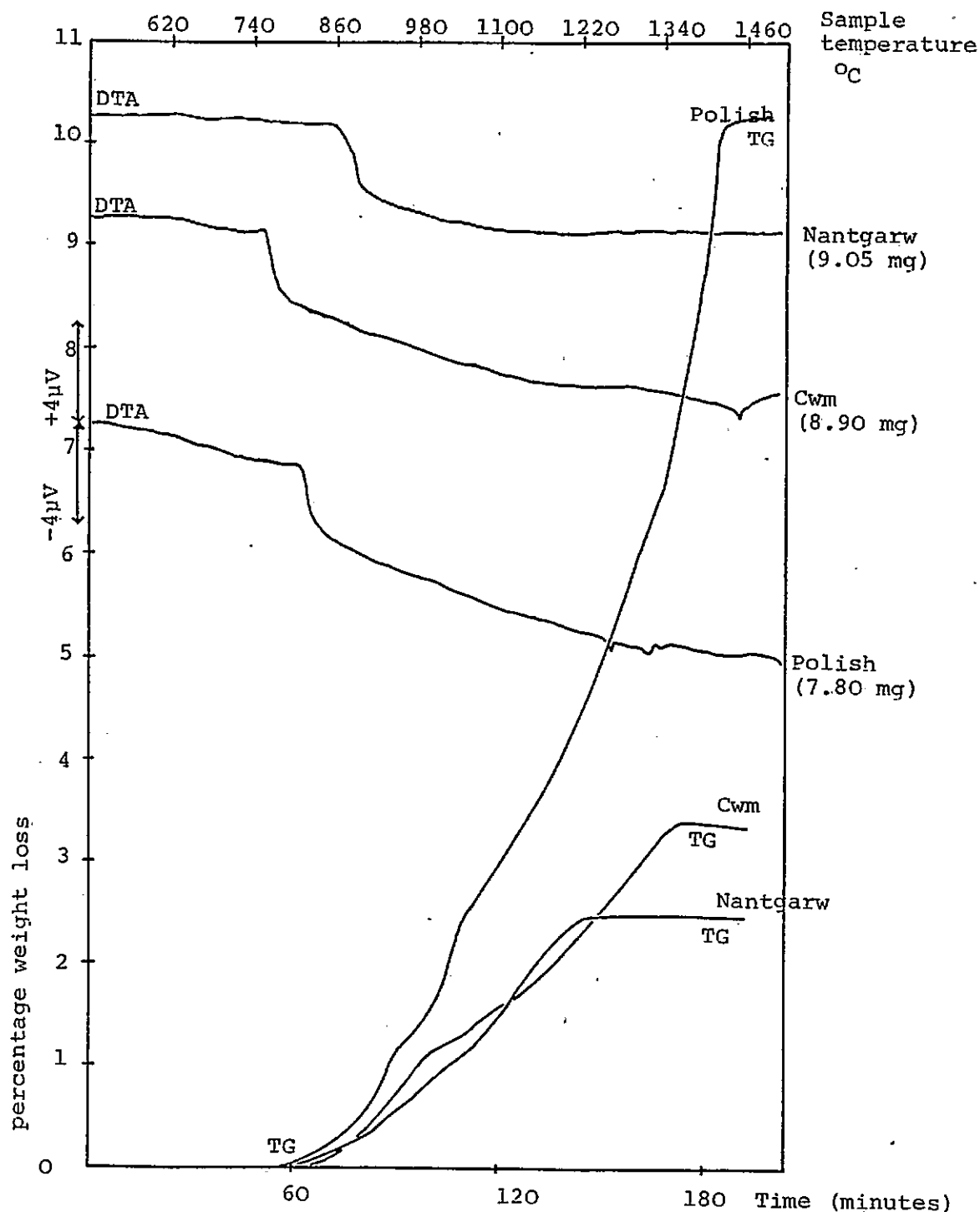
Figure 4.9. TG/DTA of ashes from three metallurgical cokes burnt off at 500 °C, on heating to 1500 °C at 5 °C min⁻¹. (Pt/Rh crucibles, static air atmosphere).

173
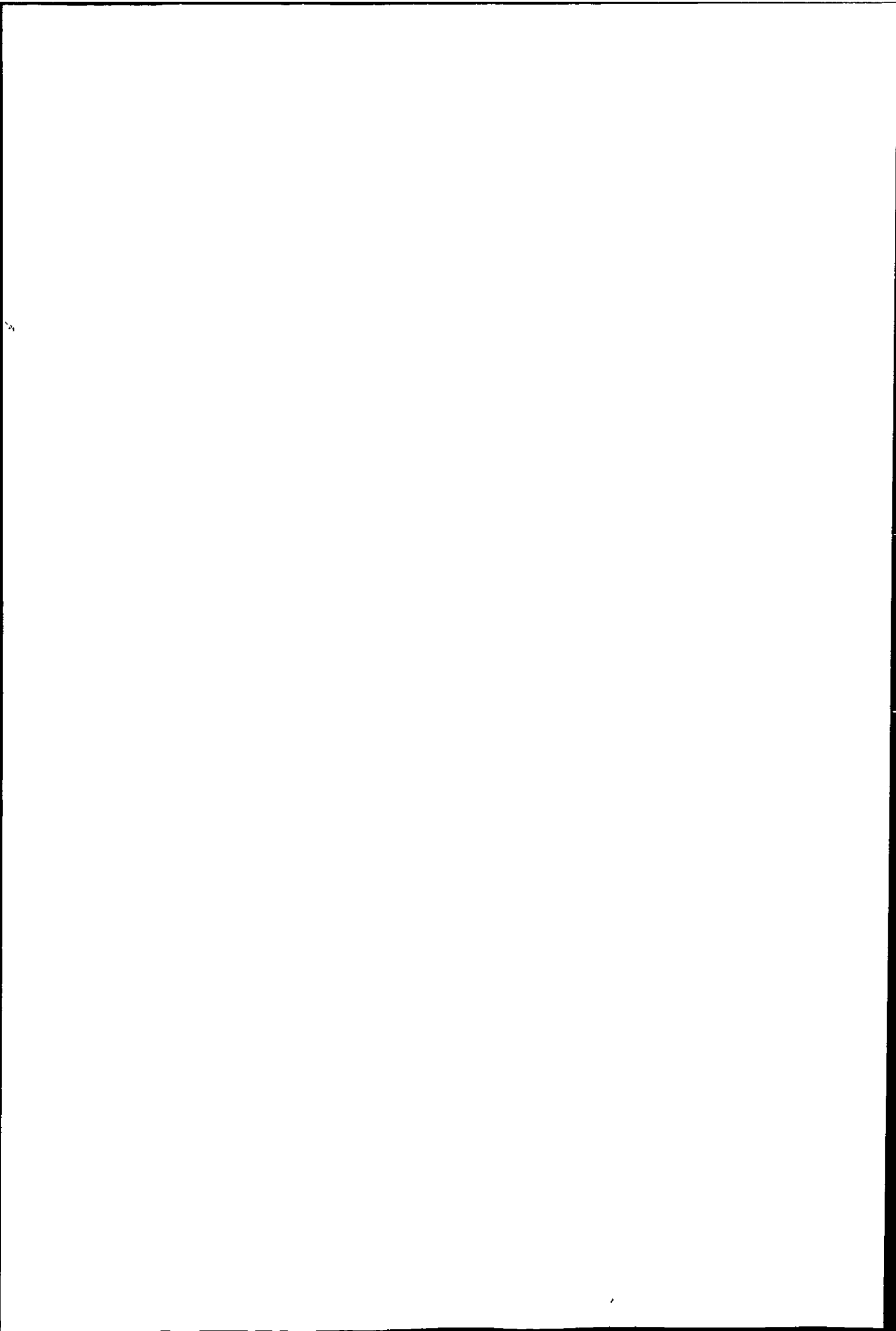
Figure 4.10. TG/DTA of Australian brown coal char ash (from 500 °C burn off) on heating to 1500 °C at 10 °C min⁻¹ (Pt/Rh crucibles, static air atmosphere).

174
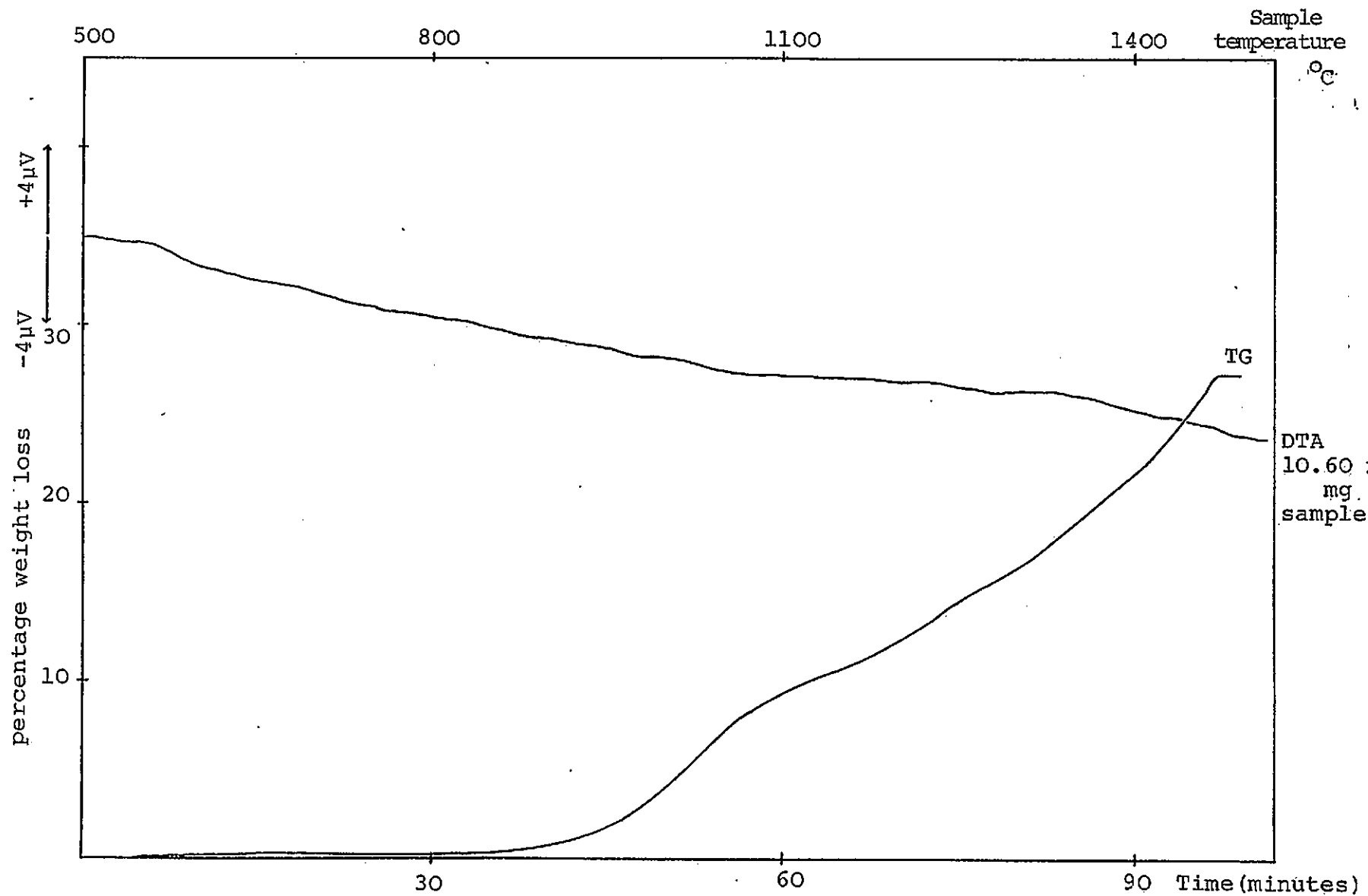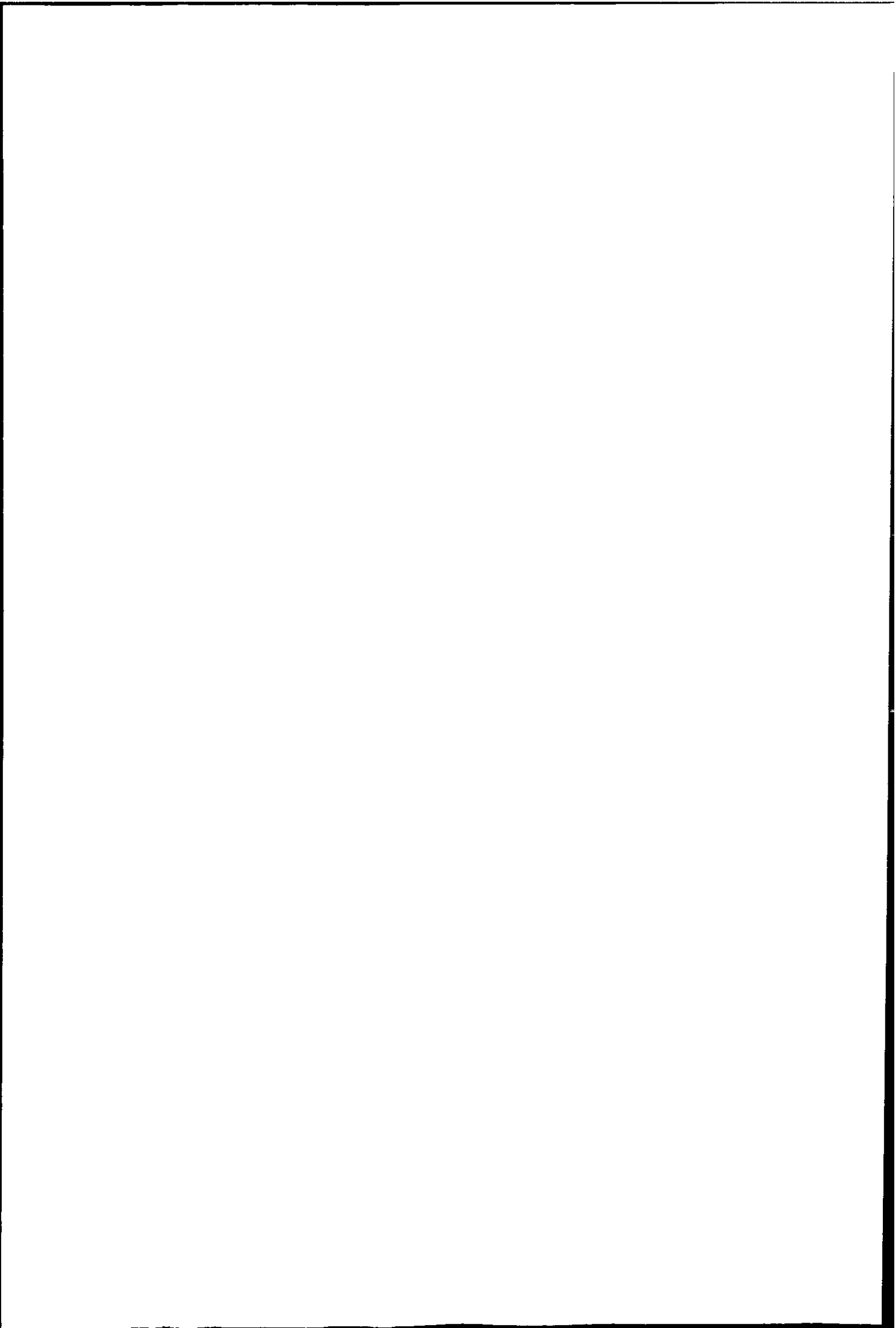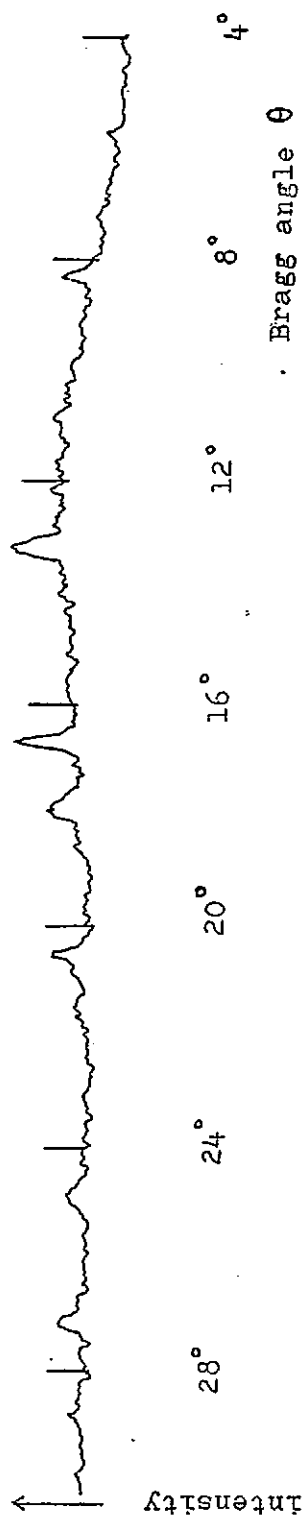
Figure 4.11. X ray powder diffraction trace of black
lumps from B_2O_3 doped Nantgarw coke ash.

175

Table 4.3.l.

X ray powder diffraction of black aggregates from
B_2O_3-doped Nantgarw coke ash.

$\theta°$	$d(Å)$	possible assignment
m 8.30	5.342	sillimanite
s 13.20	3.377	$FeBO_3$, sillimanite
s 16.65	2.692	$FeBO_3$, αFe_2O_3
m 17.90	2.509	αFe_2O_3
m 20.55	2.197	$FeBO_3$, sillimanite
m 24.85	1.835	sillimanite
m 27.15	1.690	αFe_2O_3.

Table 4.3.m.

Data for strongest peaks for iron borates from ASTM index.

					origin	ASTM reference
iron II metaborate $Fe(BO_2)_2$	$d(Å)$	4.48	2.64	2.83	fusion of FeO & B_2O_3	
	I/I_1	100	100	70		3-0186
iron III orthoborate $FeBO_3$	$d(Å)$	2.68	3.50	2.08	–	21-423
	I/I_1	100	60	30		
iron II tetraborate FeB_4O_7	$d(Å)$	5.5	4.2	3.49	stable 250 – 700 $°C$	21-422
	I/I_1	100	90	60	with 50% B_2O_3 concentration	
iron III borate Fe_3BO_6	$d(Å)$	2.96	3.69	2.56	–	18-636
	I/I_1	100	60	60		
iron II III borate Fe_3BO_5	$d(Å)$	2.58	5.16	2.37		13-572
	I/I_1	100	50	25	natural sample	
paigeite Fe_3BO_5	$d(Å)$	2.58	5.17	2.18	natural sample	"
	I/I_1	100	55	20		

4.4 Discussion

4.4.1 Characterisation of the Carbons

Plate 4.1(i) shows the irregular surface of a Nantgarw coke lump from the 710 to 500 μm sieved fraction used in TG work. Larger lumps had an essentially similar appearance. Micrograph 4.1(ii) is a portion of the same lump at higher magnification. Cwm and Polish cokes as shown in plates 4.2(ii) and (iii) showed similar portions of surface with this lamellar flow-type structure. In a gasified coke lump, as in plate 4.2(i) these areas are deeply fissured and cracks are developing across the smoother areas. Lumps of inert material, as shown in plate 4.1(iii) are also present in the coke. The closed porosity and texture of Nantgarw coke are shown in the optical micrographs of plate 4.5, where regions of different closed porosity adjoin. When a mixture of coals is carbonised very little mutual diffusion in the plastic phase occurs and boundaries remain between the characteristic textures of the coals. Cokes made from blends are held together by adhesion rather than true mixing. The inert lumps often seen in micrographs may be coke breeze, inertinite, or shale and have an important influence on coke strength.

Examination of milled Nantgarw coke by transmission electron microscopy revealed particles with a folded structure as seen in TEMs of graphite. However, sample preparation had destroyed the initial surface and porosity in the range of interest and this technique was not further used for the study of the cokes.

Plates 4.3 and 4.4 show the surface detail of the charcoals and the Australian brown coal char. The moisture and volatile matter in the char was found to be high and the latter could not be removed completely even after several successive heat treatments. Leaving the char under flowing nitrogen would remove some volatiles and most were evolved by about 150 °C as shown in Figure 4.5 when the char was heated at 10 °C min^{-1} in flowing N_2.

Brown coals are described[16] as similar to bituminous coals, based on heating value and moisture. Soft brown coals shrink dramatically when dried and their porosity is described by Wagenfeld et al.[17]

The type 1 isotherms for the char and activated charcoal from N_2 adsorption at 77 K are typical of micro-porous materials. The hysteresis loop for the char reveals the presence of a range of pore sizes from micro to macro-pores (radii <1 nm to >25 nm). Type 2 isotherms were obtained for decolourising charcoal, charcoal for chroma-tography and "Norit GSX". When this type of isotherm is observed for powdered samples the approach to infinite film thickness is actually due to interparticle condensation, as described by Adamson.[18] The Dubinin-Radushkevich plots for these materials from CO_2 sorption at 196 K show a considerable micropore volume.

At 77 K penetration of nitrogen into micropores is very slow as discussed for microporous cokes by Roques et al[19], leading to low surface area values. The specific surface areas calculated for all the carbons, except the charcoal

for chromatography, are higher from adsorption of CO_2 at 196 K than N_2 at 77 K.

A value of 17.0 Å^2 for the cross sectional area of CO_2 at 196 K was taken. There is some variation in literature values for the cross sectional areas of adsorbates, depending on means of calculation and nature of the adsorbent, as described by McClelland and Harnsberger.[20] Robens[21] gives 21.0 Å for the cross sectional area of CO_2 at 196 K.

Particle size was calculated from the surface area value, S. Where it is assumed that the particles have the same size and shape the mean particle length, l, may be calculated from $S = \frac{f}{\rho l}$ where ρ is the density of the material and f a parameter which is 6 for cubes and spheres, 4 for rods and cylinders and 2 for plates. The length l is then a mean minimum size of crystallites.

The broad X ray diffraction peak at 13 $^{\circ}$ given by the char and cokes is due to diffraction from the 002 planes of the graphite crystallites. PMC graphite gave a sharp peak at 13.25 $^{\circ}$ (d = 0.337 nm). From the peak width at half height an average crystallite size of 22 Å was calculated for Nantgarw coke. This is much smaller than that calculated from gas sorption.

The line broadening treatment assumes a non porous solid and a non-Gaussian distribution of crystallite sizes can be taken. Thus lower values than those estimated from specific surface areas are often found.

In a study of graphite, coke and charcoal, Turkdogan et al[22] found that the mean crystallite size (determined from line broadening) had no effect on rate of oxidation, the essential parameter being the "effective surface areas". In the present work the CO_2 "reactivities" of the three cokes from Table 4.3.a bear no relationship to their (initial) surface areas or crystallite size from Table 4.3.d. Open porosity however gives an indirect measure of the surface available for gaseous attack. Rates of reaction to CO_2 for the char and other carbons from Table 5.4.j. of Chapter 5, shows that at 910 $^\circ$C the Australian brown coal char is the most reactive, followed by the decolourising charcoal. The total surface area is thus no guide to CO_2 "reactivity". It must be the "available surface area" that is important and which an effective inhibitor of coke reactivity would need to reduce.

After oxidation in CO_2, B_2O_3-doped cokes and coal char show surface globules (Plate 4.7). At the low percentage coke burn off these cannot be ash and were attributed to the B_2O_3. These globules did not wet the surface and were not evenly distributed. B_2O_3 may run preferentially into the finer grain, more reactive areas of the coke surface, making a small amount an effective inhibitor. Microscopic examination of the doped coke at the temperature of reaction would be useful.

4.4.2 Coke and Char Ashes.

The unwanted portion of the blast furnace charge separates as the liquid slag. Fluxes are added to combine with gangue minerals and lower melting points and viscosity. Slag composition and slag reactions are discussed by Turkdogan.[23] Many compounds have been identified from examination of solid slag, and phase diagrams constructed for liquid slag, as given by Hopkins (Chapter 1, ref. 28). Ash composition (for coals and cokes) is generally given as percentage oxides as in Table 4.3.e, although the principal constituent of Nantgarw, Cwm and Polish coke ashes is probably sillimanite Al^{*} Al^{**} SiO_5 . Minerals of this group were formed from kaolinite under high temperature and pressure.

$$Al_2O_3 \cdot 2SiO_2 \cdot 2H_2O \longrightarrow Al_2O_3SiO_2 + SiO_2 + 2H_2O$$
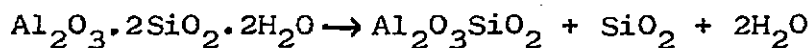
Phase diagrams and crystallographic data are given by Kukolev[24] who describes the form of sillimanite as "fibrous". Under the optical and electron microscopes fibrous portions of the ash were often seen, as in the transmission electron micrograph of Plate 6.2(ii) and the scanning electron micrograph of Plate 4.9(iii). White lumps which could be picked out by hand were also present in the 1000 ^{o}C char and coke ashes. These gave an X ray powder diffraction pattern of impure silica. Hadan and Studemann[25] investigated a brown coal ash by X ray powder diffraction and consider the transformations of kaolin, mica, pyrite etc. on heating. Clay minerals are a large part of most coal ashes, together with pyrite and pyrrhotite, as described

* 6 coordinate Al ** 4 coordinate Al

182

by Wert and Hsieh[26]. On heat treating coal to a coke Huffman et al[27] consider that there is significant transformation of the clay minerals, that ferrous clay changes to ferrous glass and that inorganic sulphur retention in coke is determined by the reduction of pyrite and the reaction of calcite to form calcium sulphide.

The ash from coke burnt off at 500 $^{\circ}$C was pinkish and finely powdered, that from 1000 $^{\circ}$C was pale yellow and coarser. The same difference in texture was seen in the pale yellow 400 $^{\circ}$C char ash and the dark red-brown 1000 $^{\circ}$C char ash. From a consideration of the Tammann temperatures of the ash minerals, the coke ash from 500 $^{\circ}$C burn off is unlikely to have sintered. This is borne out by the scanning and transmission micrographs of plates 6.1 and 6.2. (Chapter 6.) The 1000 $^{\circ}$C coke ash shows the rounded surface and coalescence of smaller particles in strings, typical of sintered material. The 1000 $^{\circ}$C char ash was of similar appearance. Ash from higher temperature burn offs was rather coarse for SEM.

The effect of sintering is also shown by the specific surface areas of the ashes from 500 $^{\circ}$C burn offs, calculated from N_2 adsorption at 77 K. That of the char ash was 12.56 m^2g^{-1} and that of the coke ash 8.93 m^2g^{-1}. A much lower value (<1 m^2g^{-1}) was obtained for the 1000 $^{\circ}$C ashes. The effect of build up of coke ash as carbon is burnt away is considered in Chapter 6.

From table 4.3.e the ash constituents of Nantgarw coke total 93%. If the calcium and magnesium were present as

183

sulphates rather than oxides then 3% CaO would be 7.3% as $CaSO_4$ and 1% MgO would be 3% as $MgSO_4$, making a total of 99.3%.
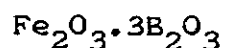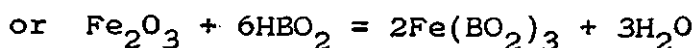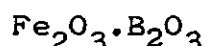
The amounts of Al_2O_3 and SiO_2 are 31% and 43% of the ash respectively. The Al_2O_3 would require 18% SiO_2 in sillimanite and 8% would be in the anorthite. If Na and K were present as silicates this would incorporate a further 5% of the SiO_2. Thus 31% of the SiO_2 may be present in silicates and some (12%) as free SiO_2. At 1000 ^{o}C MgO could form $MgSiO_3$, and $CaSO_4$ become anorthite, leaving little Ca or Mg in the water soluble part of the 1000 ^{o}C ash.

Proximate analysis of Nantgarw coke shows a sulphur content of 0.9% and an ash content of 9.3%. Thus the Fe_2O_3, CaO and MgO content of coke may be calculated as 0.84%, 0.28% and 0.09% respectively. If these are calculated on the basis of FeS_2, CaS and MgS instead, then the sulphur content due to these sulphides becomes 0.67%, 0.16% and 0.07% of the coke. This totals 0.91% and may indicate the combination of the sulphur.

If the $CaSO_4$ and $MgSO_4$ (estimated as 7.3 and 3% of the ash) become sulphides the amount of sulphur in the ash would be 2.5% or 0.23% of the coke. Insufficient CaO or MgO is present in the coke mineral matter to retain sulphur and the coke loses sulphur during ashing. The sulphur content of coke has a deleterious effect in metal production, (as described in reference 29 of Chapter 2).

184

The TG/DTA results of Figures 4.9 and 4.10 show that some endothermic decomposition of the low temperature ashes occurs on heating to about 1500 $^\circ C$. All the ashes had melted by this temperature although no sharp melting points were obtained from the DTA trace.

The ash contains iron and alkalis which are catalysts of the Boudouard reaction. Iron is particularly effective when present as the metal or carbide as reported by Zuniga and Droguett (Chapter 2, reference 10) in a study of cokes treated with solutions of metal salts. The possible effect of B_2O_3 in combining with the iron content of the ash was considered. The iron content of Nantgarw coke, estimated as Fe_2O_3 is 0.84%. This could form iron borates

$$Fe_2O_3 + 2H_3BO_3 = 2FeBO_3 + 3H_2O$$

$$Fe_2O_3 \cdot B_2O_3$$

or $$Fe_2O_3 + 6HBO_2 = 2Fe(BO_2)_3 + 3H_2O$$

$$Fe_2O_3 \cdot 3B_2O_3$$
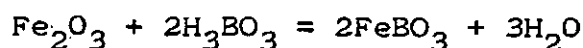
The requirement of $3B_2O_3 \cdot Fe_2O_3$ would necessitate 11 mg B_2O_3 g^{-1} coke. Alkalis in the ash could also form borates and borosilicates. Based on 2% Na_2O and 4% K_2O the maximum amount of B_2O_3 needed in all would be 13.3 mg g^{-1} coke. Solution treatment of Nantgarw coke, giving 1 to 1.5% of sample weight increase, achieves this amount of B_2O_3.

Complete burn off in air or CO_2 of doped Nantgarw coke gave ashes which contained round black lumps, the higher the ashing temperature the coarser these particles. The optical micrograph of plate 4.8(iii) shows one such aggregate. The surface could be studied by low power SEM as shown in plate 4.9, where globules seem to have melted into other portions of ash. From the d spacings found (Table 4.3.1) these lumps may consist of $FeBO_3$ and αFe_2O_3. Attempts to prepare an iron borate by fusion of stiochiometric amounts of Fe_2O_3 and B_2O_3 did not yield identifiable products. Mellor[28] reports the failure of earlier attempts.

Of the ash constituents Fe_2O_3 has the lowest Tammann temperature (630 $^{\circ}$C) and is able to combine with the liquid B_2O_3. The catalytic effect of iron oxide, due to the formation of iron under reducing conditions, was much less when silica was added to coke. Donnelly et al[29] consider this to be due to the formation of iron silicate.

The preliminary investigation thus gave information on the texture and porosity of the cokes and coal char. The mineral matter, which forms a considerable portion of the coke weight, cannot be neglected in assessing the action of B_2O_3.

Polish coke has the ash of highest iron content and Cwm coke that of highest alkalis and alkaline earths. These two cokes also retained less B_2O_3 on doping than Nantgarw coke.

References

1. R.R. Adair, E.H. Boult & H. Marsh. Fuel, 1972, 51, 57-63.

2. M. French & H. Marsh, Proc. 5th London Internation Carbon and Graphite Conference, 1978, 1, 123-6, SCI.

3. R.S. Downing, G.M. Mulder & D.A. Borger. "Carbon 82", Proc. 6th London International Carbon and Graphite Conference 1982, 129-31, SCI.

4. S.L. Strong, Proc. 4th London International Carbon and Graphite Conference 1974, SCI, 175-6.

5. S. Das. J. Mines Metals and Fuels, 1977, 25, part 9, 277-8.

6. S. Nand & R.S. Mann, Proc. 64th CIC Coal Symposium, 1981 (Can.Soc.Chem.Eng.) 499-506.

7. B.P. Jalan & Y.K. Rao, Carbon, 1978, 16, 175-184.

8. P.K. Mitra, B.K. Sharma, D.K. As, D.N. Tewary & K. Raja. Current Science, 1981, 50, No.3, 130-1.

9. P.L. Walker, Jr., M. Shelef & R.A. Anderson, "Chemistry and Physics of Carbon", 4, 1968, P.L. Walker Jr. (Ed.), Marcel Dekker.

10. J.Holmes & P.H. Emmett. J. Phys.Colloid.Chem. 1947, 51, 1276-1307.

11. H. Marsh & B. Rand, Carbon, 1971, 9, 63-77.

12. A. Chatterjee, B.N. Singh, L.M. Chatterjee & P.K. Chakravarty, Steel Times International, 1981, 94, 94-102.

13. A.I. Vogel, "Quantitative Inorganic Analysis", 3rd Edition, 1961, Chapter IV, p.439 using NH_4OH/NH_4Cl buffer for Ca & Mg determination. Chapter V, p.462 for sulphate determination.

14. Chemistry in Britain, 1982, 18 no.7, p.488.

15. R. B. Coates, "The British Foundryman", August 1979.

16. "Analytical Methods for Coal and Coal Products", I, 1978. Chapter 3, Academic Press.

17. H.K. Wagenfeld, M. Setek, L. Kiss & W.O. Stacy, Proc.Int.Conf. on Coal Science. Düsseldorf 1981, Verlag Glückauf GmbH Essen 1981. 869-74.

18. A.W. Adamson, "The Physical Chemistry of Surfaces", 3rd Ed, 1976. John Wiley.

19. M. Roques, J. Weber & M. Bastick. Proc. 3rd Conf. Industrial Carbons and Graphite 1970, SCI London, 226-9.

20. A.L. McClelland & H.F. Harnsberger, J. Colloid & Interface Science, 1967, 23, 577-99.

21. E. Robens, "Microweighing in Vacuum and Controlled Environments", Chapter 4, p.157. Czanderna & Wolsky (Eds.). Elsevier, 1980. Volume 4 of Methods and Phenomena. Their applications in Science and Technology.

22. E.T. Turkdogan, R.G. Olsson & J.V. Vinters. Carbon, 1970, 8, 545-64.

23. E.T. Turkdogan, Met. Trans. 1978, 9B, 163-79.

24. G.V. Kukolev, "The Chemistry of Silicon and the Physical Chemistry of the Silicates", 2, Chapter 8, 1971, National Lending Library for Science and Technology.

25. M. Hadan & K. Stüdemann. Chemische Technik, 1982, 34(2). 94-96.

26. C.A. Wert and K.C. Hsieh. Proc.Int.Conf. on Coal Science. Düsseldorf, 1981, Verlag Glückauf GmbH Essen 1981, 780-5.

27. G.P. Huffman, F.E. Higgins & R.J. Lee, ibid, 835-40.

28. J.W. Mellor. "A Comprehensive Treatise on Inorganic and Theoretical Chemistry", 1946, Longmans. Chapter 32, p.113.

29. R.P. Donelly, R. Broadbent and B.J. O'Leary, Fuel, 1952, 31, 418-28.

30. PMC Carbon Ltd., TR House, 134-138 Borough High Street, London SE1 1LB.

CHAPTER FIVE

ISOTHERMAL OXIDATION STUDIES OF

METALLURGICAL COKE AND AUSTRALIAN BROWN COAL CHAR

5.1   Introduction

5.2   Experimental Procedure

5.3   Air Oxidations

5.3.1   Results

5.3.2   Discussion

5.4 CO_2 Oxidations

5.4.1   Results

5.4.2   Discussion

5.5   Mathematical Analysis

CHAPTER FIVE

5.1 Introduction

Isothermal TG permits the oxidation to be continuously monitored up to complete burn-off. Where weight loss curves permit the calculation of a rate constant then its variation with temperature may be given in the form of an Arrhenius plot, enabling the kinetic parameters A and E_A to be calculated from the intercept and slope.

Air and CO_2 oxidations of Nantgarw coke and Australian brown coal char, and of B_2O_3-doped material were performed. Initial air oxidations were carried out on the Stanton Redcroft Massflow balance MF-H5 under static atmosphere conditions. As the temperature limit of the furnace is approximately 1000 $^{\circ}C$ the Boudouard reaction could not be studied. A grant from the S.E.R.C. (No.GR/B/87689) enabled the purchase of the Stanton Redcroft STA 781 thermal analyser. Air oxidations at higher temperatures were studied, and some of the lower temperature runs were repeated. The Boudouard reaction could be studied up to the temperature limit of the furnace (approximately 1500 $^{\circ}C$).

It was expected that at some temperature the air oxidation and perhaps the Boudouard reaction would become diffusion controlled, giving the temperature ranges over which comparison could be made of the actual oxidation curves with the appropriate mathematical expressions for the surface geometries described in Chapter 1.3.1. Comparison of metallurgical cokes could also be made by a "reactivity test" similar to that used industrially (Chapter 2, ref. 6).

5.2 Experimental

The work was carried out on the two thermal balances described in Chapter 3.1. B_2O_3 doped coke and char were prepared as described in Chapter 4. Lump coke and coke and char granules were sieved from the bulk sample. Air oxidations under static conditions were first performed on the Massflow balance with the sample contained in a shallow alumina crucible (approximately 24 mm diameter and 5 mm high), resting on the ceramic TG/DTA block. The crucibles within the block were too small to take lump coke samples. Approximately 120 to 100 mg of Nantgarw coke in the form of one or two lumps were used; ~ 180 mg of char was sufficient to give a single layer on the base of the crucible. 60 mg samples of char were also used. Particle size of the char varied from 1.4 mm to 0.71 mm. With the furnace raised the TG pen was positioned on the scale by the addition of suitable counterweights to the balance pan. The furnace was heated at as rapid a rate as possible and when it had reached the set temperature lowered carefully over the Mullite tube. Environment temperature was constantly recorded on the Leeds Northrup recorder, with the DTA signal switched off. The buoyancy correction for the appropriate conditions was applied to the data. Results were obtained for coke oxidations up to approximately 950 $^{\circ}$C, and for the char up to approximately 750 $^{\circ}$C.

Similar sample weights of lump coke were oxidised in air in the Stanton-Redcroft 781 thermal balance using the

TG only hangdown. The small volume of the furnace and sample environment meant that reactions in static air were prevented by reactant starvation, so air flowing at 43.5 cm^3 min^{-1} was used. The Pt sample bucket was used throughout with the TG on the X1 (200 mg limit) scale. Approximately 30 mg of coke granules and 60 mg char granules gave a single layer on the crucible base. The sample was weighed into the bucket, the furnace raised and gas flow adjusted. The furnace was programmed to the set temperature at as fast a rate as possible (48 ^{o}C min^{-1}). Where some reaction was likely to take place before this temperature was reached (for the coke approximately 850 ^{o}C in air and 1100 ^{o}C in CO_2) the sample was preheated under N_2.

Nantgarw coke lumps ($\sim$ 5 mm diameter) and granules (500-710 μm) and char granules were oxidised in CO_2 (dried by passage through $MgClO_4$) flowing at 35.2 cm^3 min^{-1}. By choice of a suitable range on the balance control module of the STA 781, percentage weight loss could be directly recorded on the TG trace.

At certain temperatures runs with different sample weights were performed on the Massflow balance and the effect of varying the gas flow rate was investigated with the STA 781. Coke granules of 500-710 μm are of similar size range to that specified in the "Nantgarw ratio" test (-0.7 mm + 0.42 mm). A comparison of Nantgarw, Cwm and Polish coke granules from their air oxidation at higher (977 ^{o}C) and lower (520 ^{o}C) temperatures was made on the STA 781 and from their CO_2 oxidation at 955 ^{o}C.

Rate of oxidation in CO_2 for the Hopkin and Williams charcoals and PMC graphite was also determined using the STA 781.
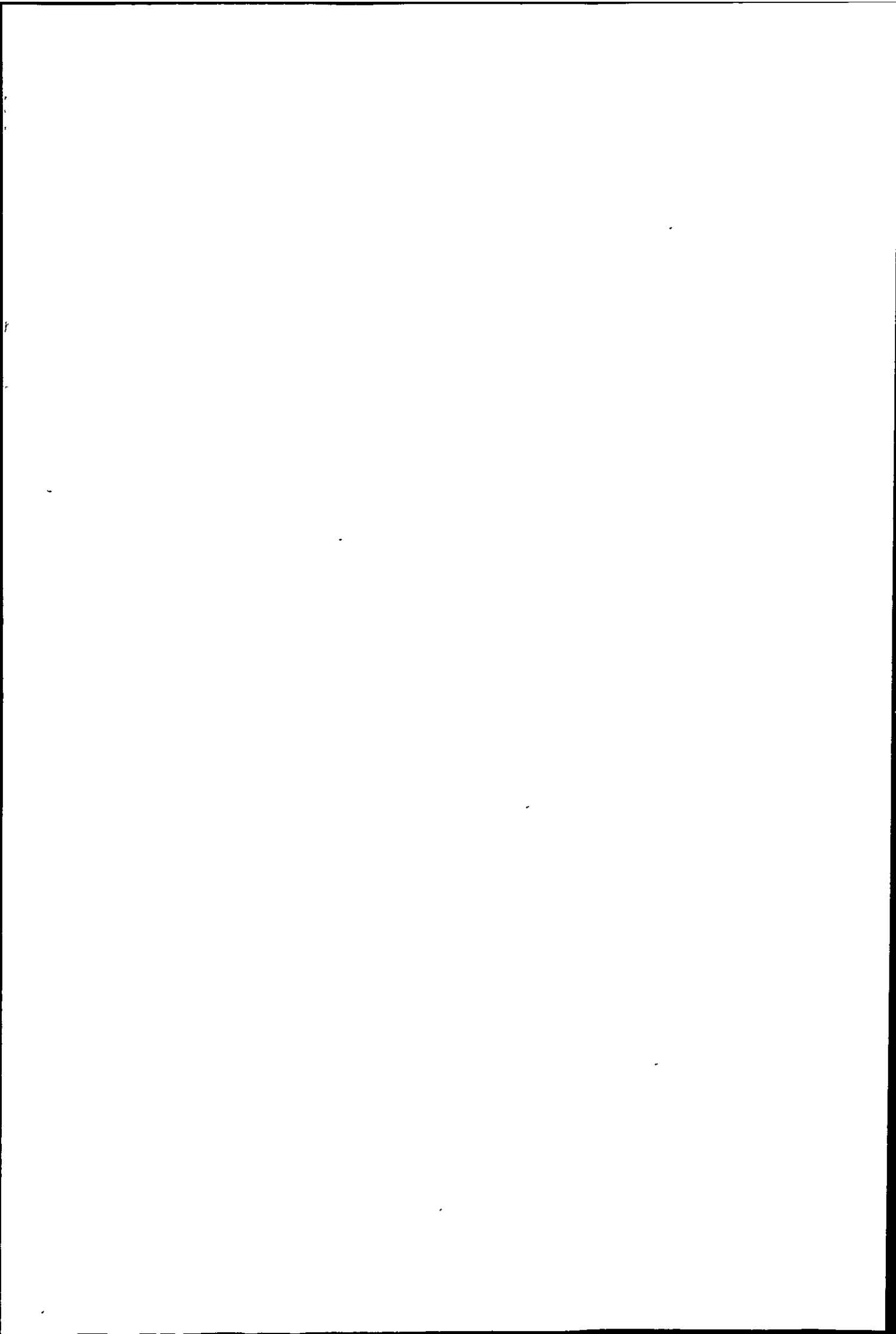
5.3 Air Oxidations

5.3.1 Results

Typical weight loss curves for the air oxidation of Nantgarw coke lumps and Australian brown coal char granules are shown in Figures 5.3.a and 5.3.b. These were obtained using the Massflow thermal balance and have been corrected for the buoyancy effect. This effect was determined using calcined Al_2O_3 in the shallow crucible and was of greater magnitude, but shorter duration the higher the temperature. The data for the coke presented as percentage weight loss are given in Figure 5.3.c. Some of the percentage weight loss curves for the oxidation of Nantgarw coke lumps in flowing air on the Stanton Redcroft 781 thermal balance are shown in Figures 5.3.d and 5.3.e. Similar sets of curves were obtained for the coke granules and for B_2O_3-doped coke lumps above 620 $^{\circ}$C. At lower temperatures the rate of weight loss of B_2O_3-doped coke increased to a maximum and then slowed to a lower rate with time as shown in the two lower curves of Figure 5.3.f. As the coke and char contain some mineral matter the percentage carbon weight loss is also given.

From the maximum rate of weight loss, which generally extended over a considerable portion of the burn off, a rate of reaction was calculated as weight loss per second per initial sample weight on an ash free basis. This was taken as a rate constant, k. Values of log k versus $\frac{1}{T}$ were plotted.
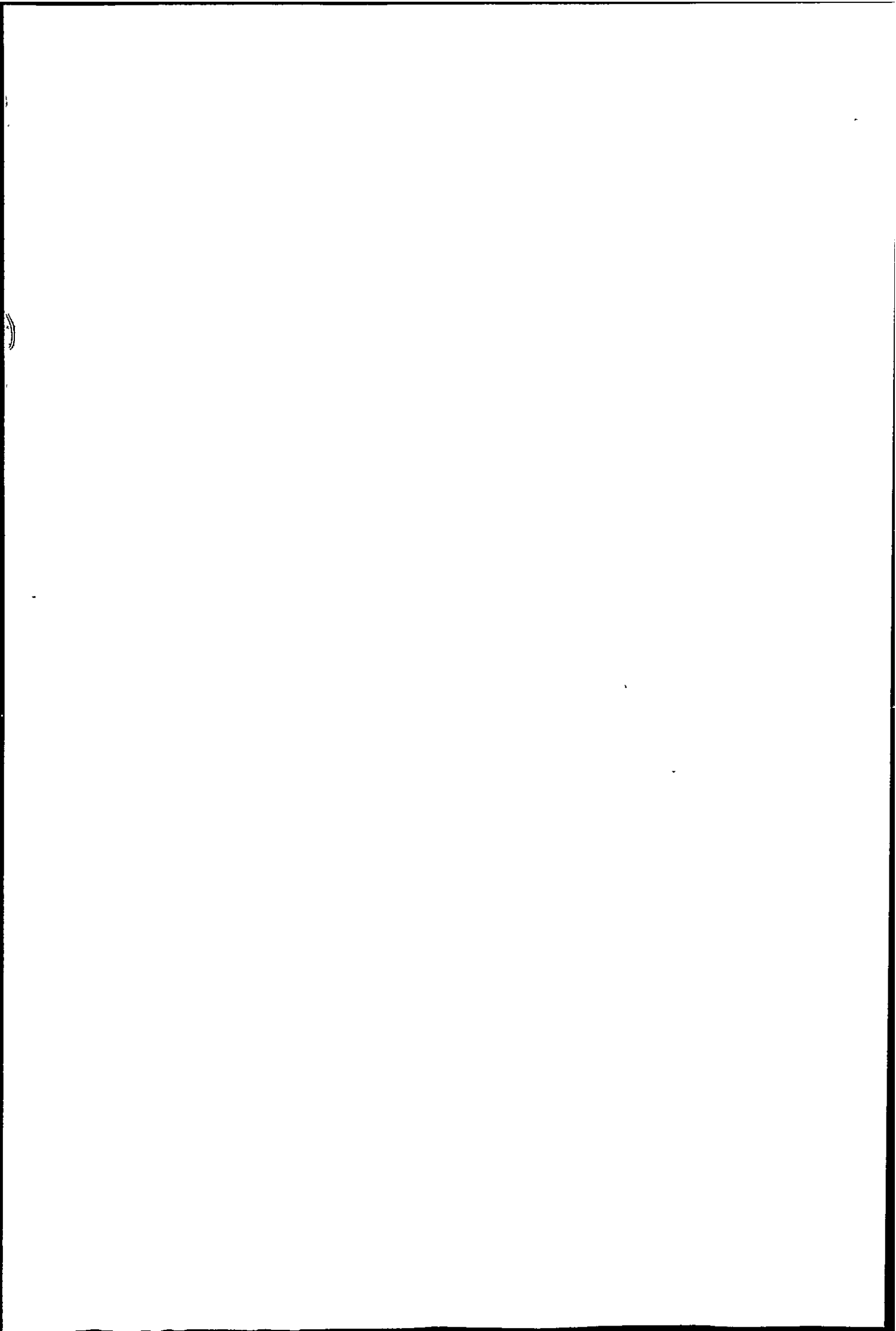
Results obtained on the Massflow balance for Nantgarw coke and doped Nantgarw coke are given in Table 5.3.a and Table 5.3.b. These are combined in the Arrhen s plot in Figure 5.3.g.

Results for the Australian brown coal char are similarly shown in Table 5.3.c, and for the doped char in Table 5.3.d; these are plotted in Figure 5.3.h. Some runs with larger sample weights were done with the char and the results are given in Table 5.3.e.

Flowing air oxidation results are given in Table 5.3.f for coke lumps, Table 5.3.g for doped lump coke and Table 5.3.h for coke granules. Corresponding Arrhen s plots are shown in Figures 5.3.i and 5.3.j. Flowing air results for the char are given in Table 5.3.i and are also plotted in Figure 5.3.j.

The effect of different air flow rates on the oxidation of Nantgarw coke lumps at 975 $^\circ$C is shown in Figure 5.3.k and on the char oxidation at two temperatures in Figure 5.3.1. The DTG function at a suitable sensitivity was used. This is upset by alterations in the gas flow, so the furnace was heated rapidly (the air being at the set flow rate) to the required temperature. Some oxidation has taken place before the temperature limit was reached.

Cwm, Polish and Nantgarw coke granules were oxidised in air flowing at 43.5 cm^3 min^{-1}. Rates of reaction at 977 and 522 $^\circ$C are given in Table 5.3.j, using $\sim$ 33 mg samples.

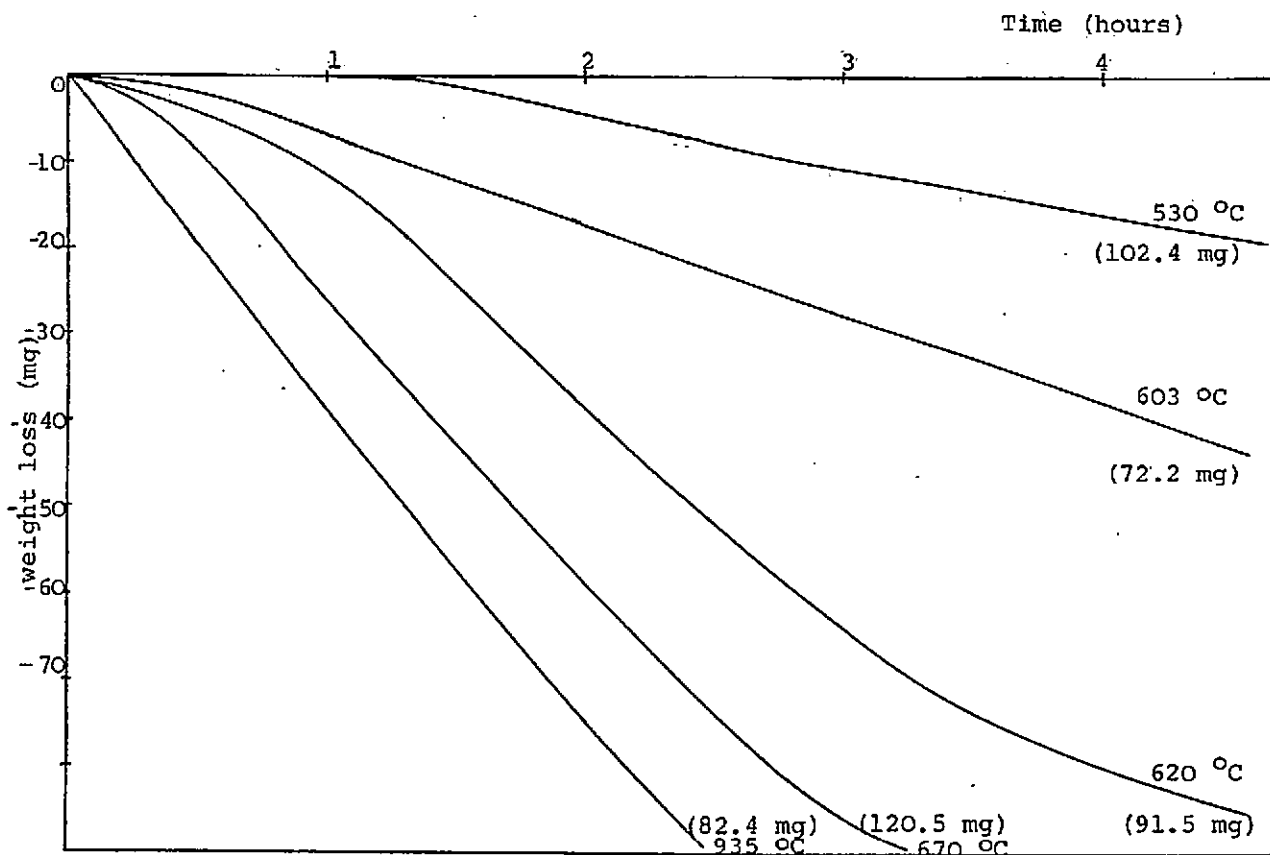Figure 5.3.a. Oxidation of Nantgarw coke lumps in static air.
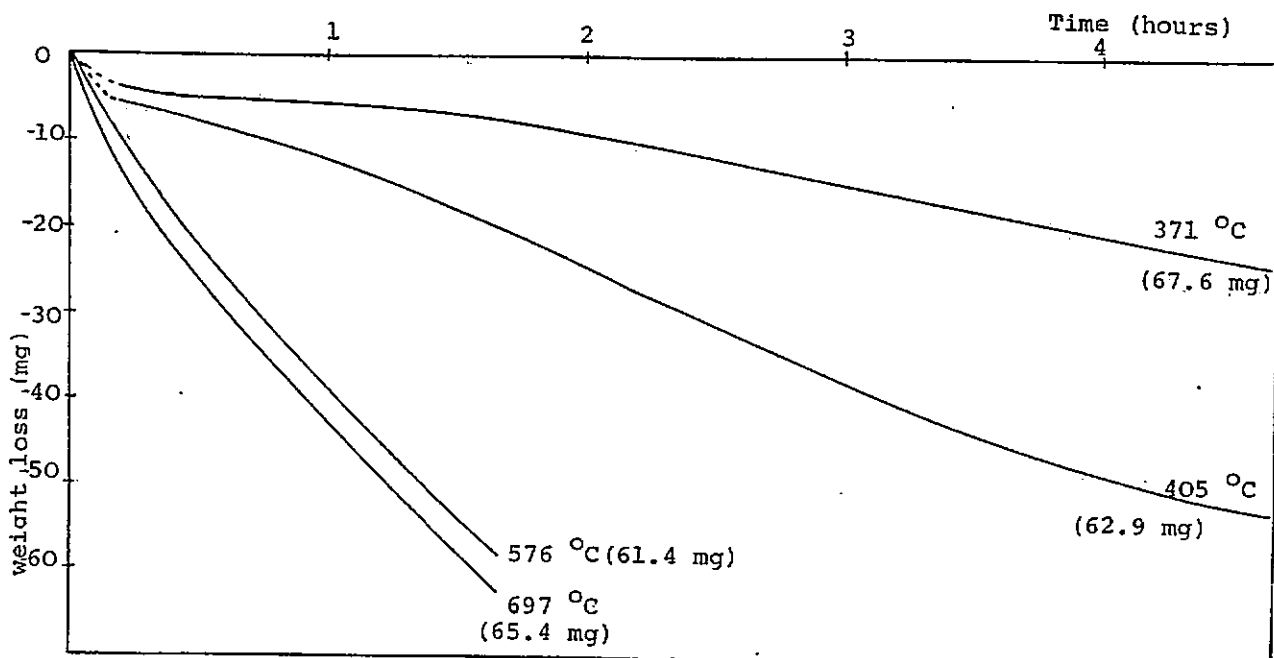
Figure 5.3.b. Oxidation of Australian Brown Coal Char in static air.

Initial sample weights in brackets.

Figure 5.3.c.   Static Air Oxidations of Nantgarw Metallurgical Coke on Massflow Thermal
                 Balance MF H5

Figure 5.3.d. Flowing Air Oxidations of Nantgarw Metallurgical Coke (43.5 cm^3 min^{-1} flow rate)

199
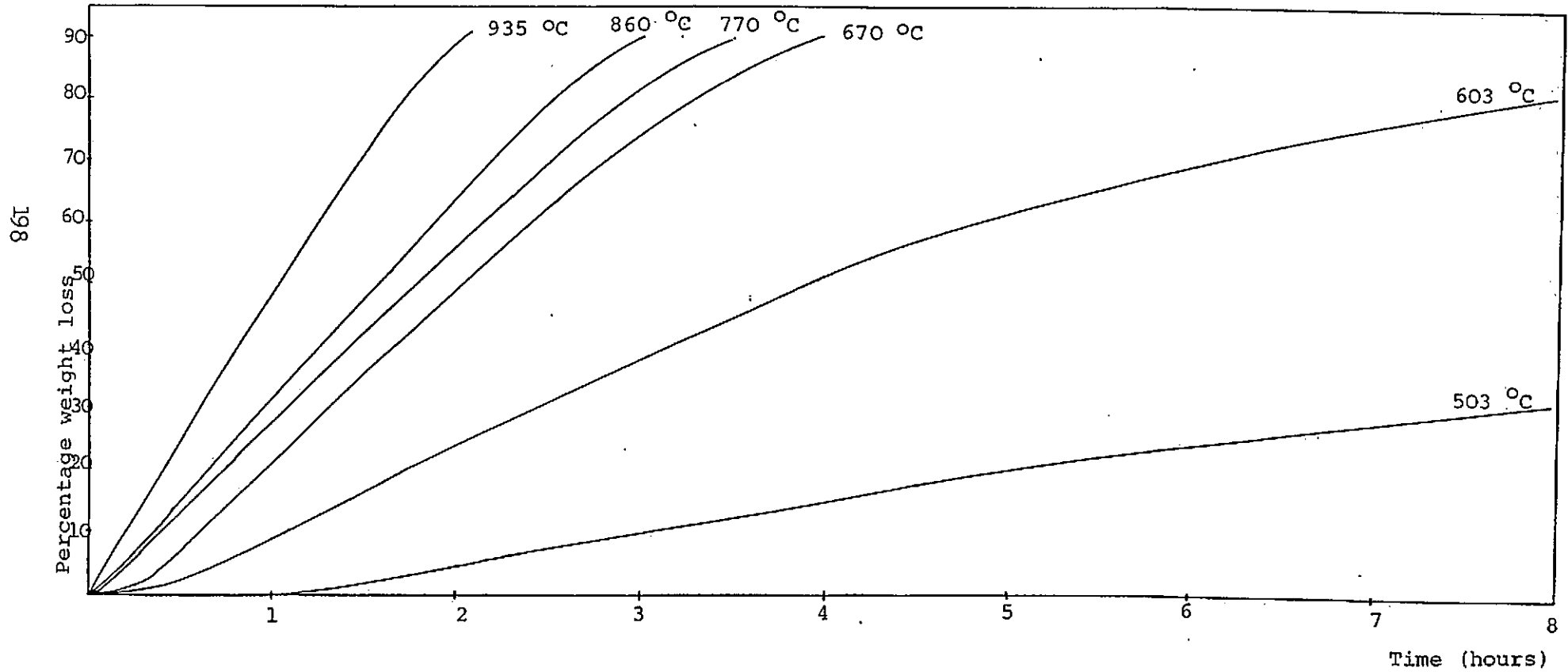
Figure 5.3.e. Flowing Air Oxidation of Nantgarw Metallurgical Coke. (43.5 cm^3 min^{-1} flow rate).

Figure 5.3.f. Flowing Air Oxidations of B_2O_3-doped Nantgarw Metallurgical
Coke (43.5 cm^3 min^{-1} flow rate).

Table 5.3.a.

Static Air Oxidation of Nantgarw Coke (lumps).

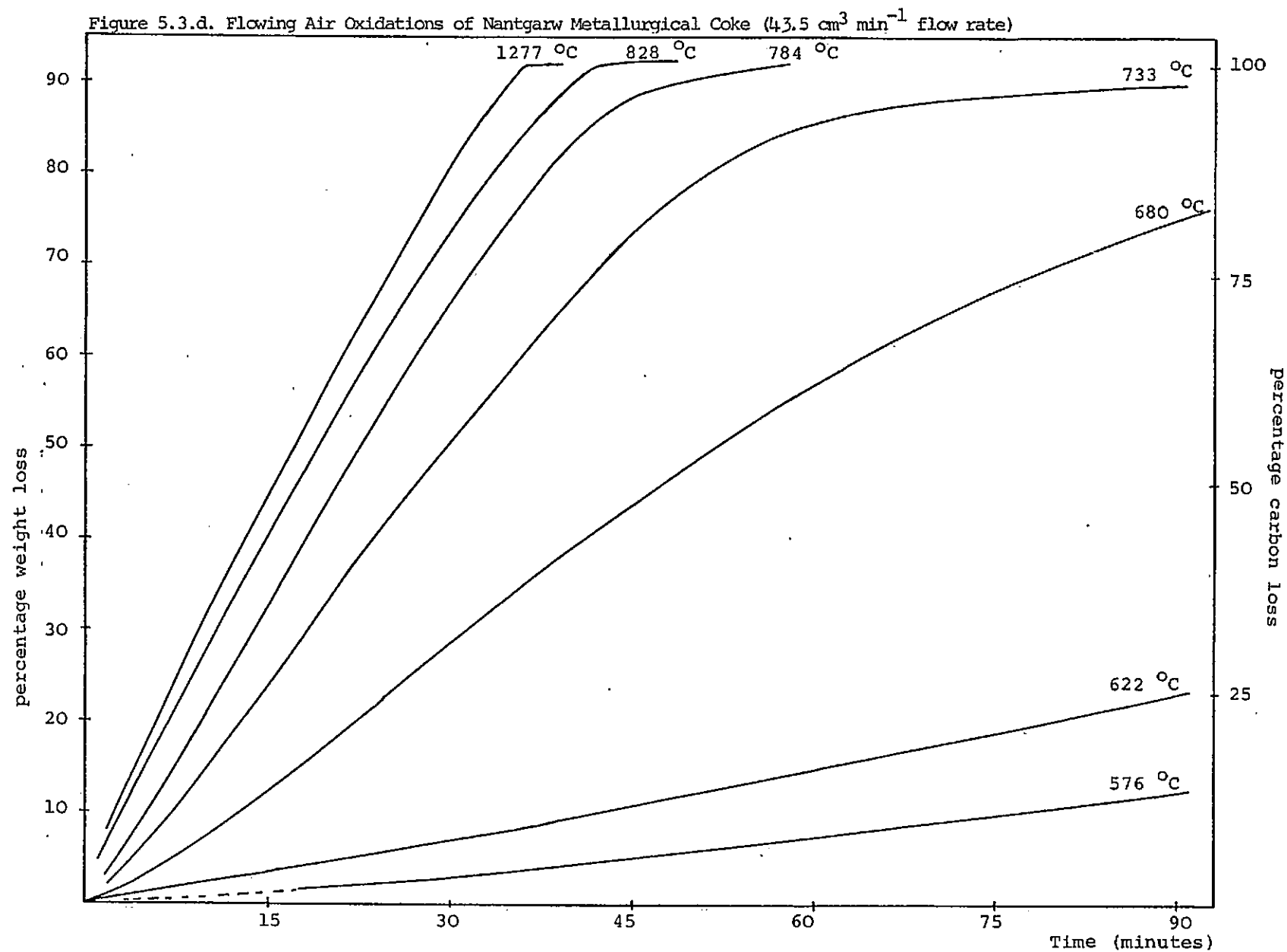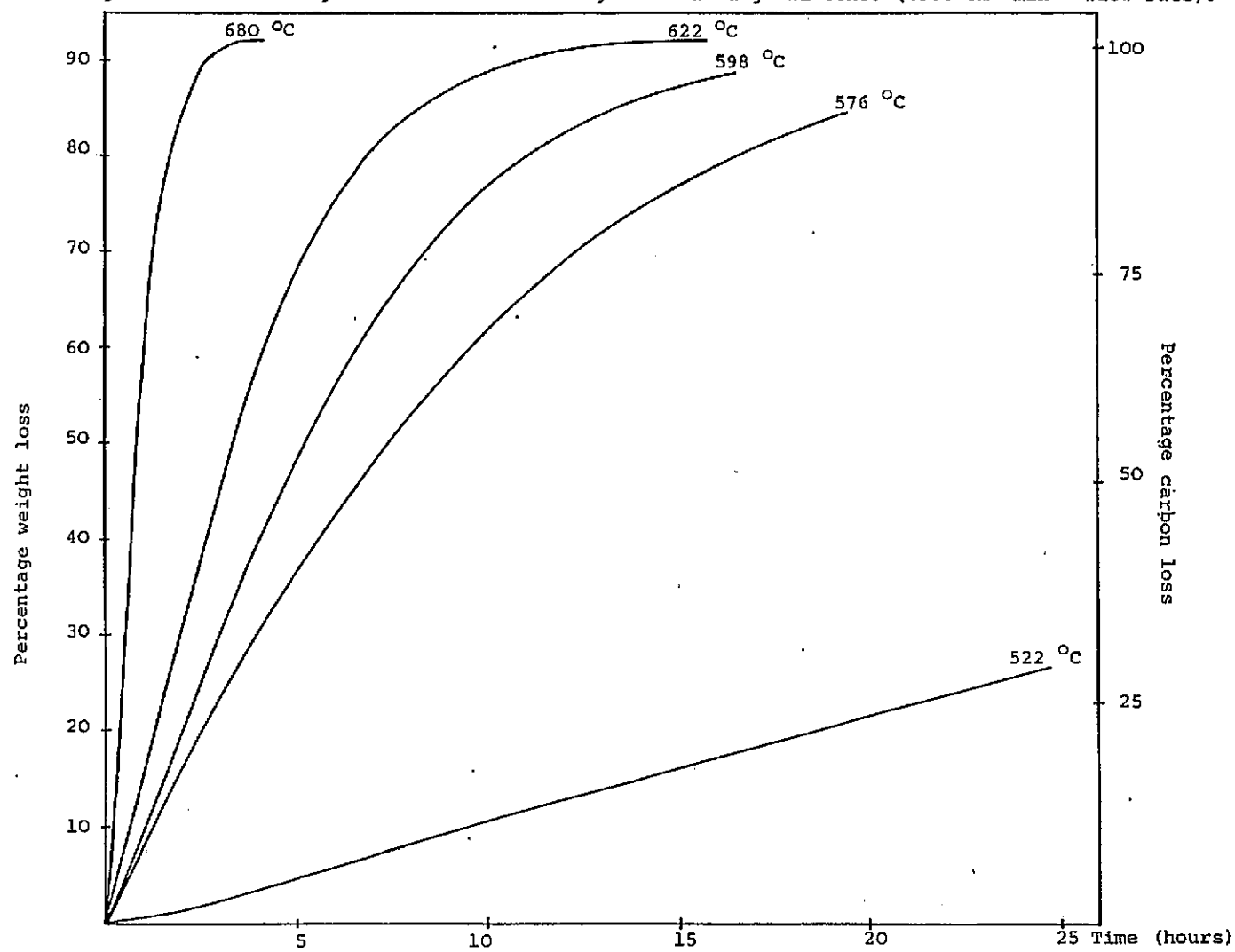| Temperature		Rate of oxidation x 10^5 (g s^{-1} g^{-1})	log (10^5 x rate)	10^3 x reciprocal temperature (K^{-1})
°C	K			
530	803	1.580	0.199	1.245
550	823	1.356	0.132	1.215
603	876	4.263	0.630	1.142
620	893	7.648	0.884	1.120
670	943	8.101	0.909	1.061
770	1043	8.531	0.931	0.959
860	1133	9.767	0.990	0.883
935	1208	12.55	1.099	0.828

Table 5.3.b

Static Air oxidation of B_2O_3 doped Nantgarw Coke Lumps.

Temperature		Rate of oxidation x 10^5 (g s^{-1} g^{-1})	log (10^5 x rate)	10^3 x reciprocal temperature (K^{-1})
°C	K			
624	897	0.599	-0.223	1.115
637	910	1.946	0.289	1.099
690	963	6.235	0.795	1.038

Figure 5.3.g. Variation of Reaction Rate Constant
with Temperature for the Air Oxidation
of Nantgarw Coke (Static Atmosphere).

Table 5.3.c

Static Air Oxidation of Australian brown coal char.
(60 mg samples).

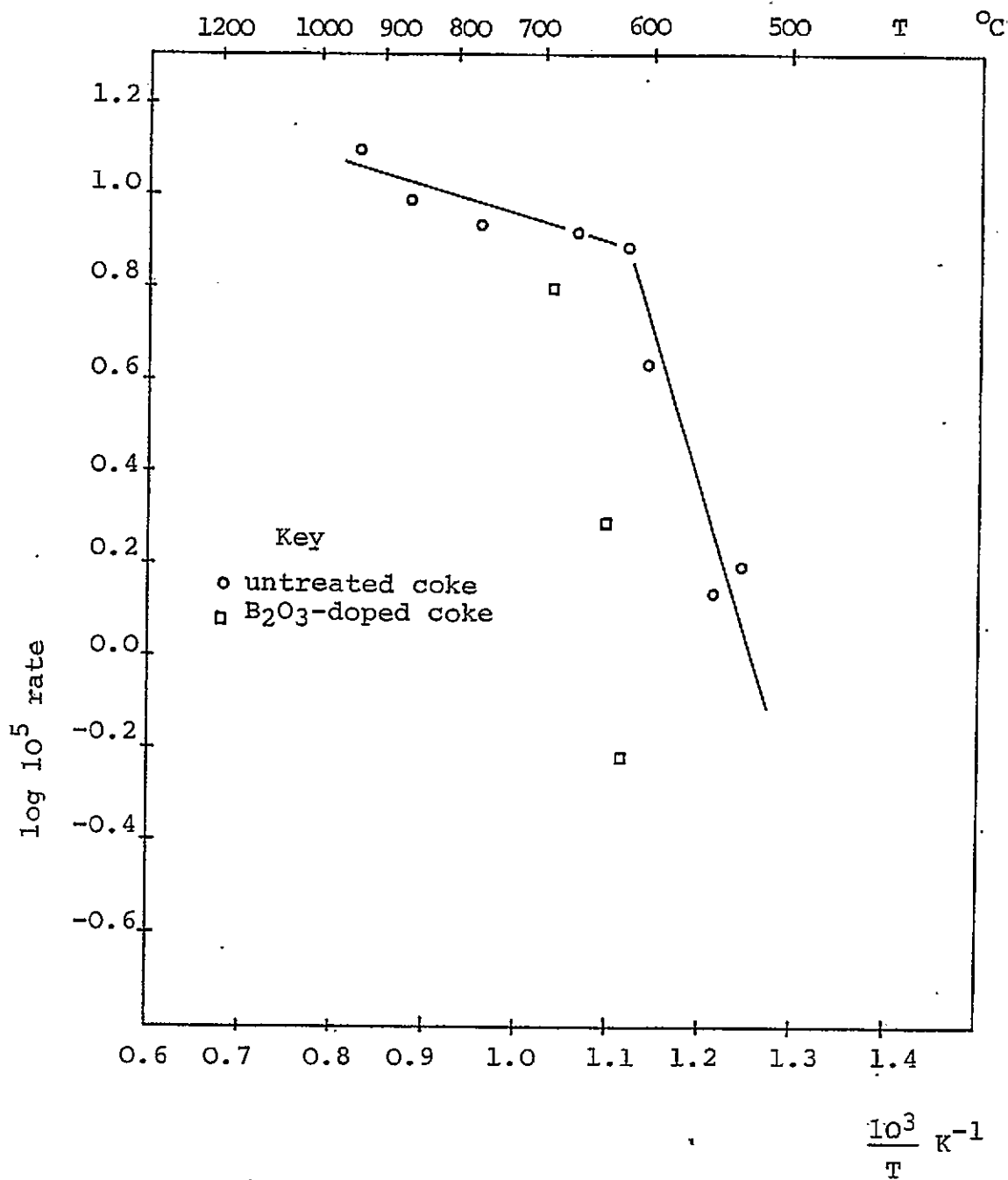| Temperature		rate of oxidation x 10^5 g s^{-1} g^{-1}	log (10^5 x rate)	10^3 x reciprocal temperature (K^{-1})
°C	K			
321	594	0.518	-0.286	1.684
371	644	2.318	0.365	1.553
405	678	5.719	0.757	1.475
485	758	14.18	1.152	1.319
494	767	12.76	1.106	1.304
576	849	15.36	1.186	1.178
615	888	15.64	1.194	1.126
697	970	13.88	1.142	1.031
755	1028	15.89	1.201	0.973

Table 5.3.d

Static Air Oxidation of B_2O_3 solution treated char
(60 mg samples).

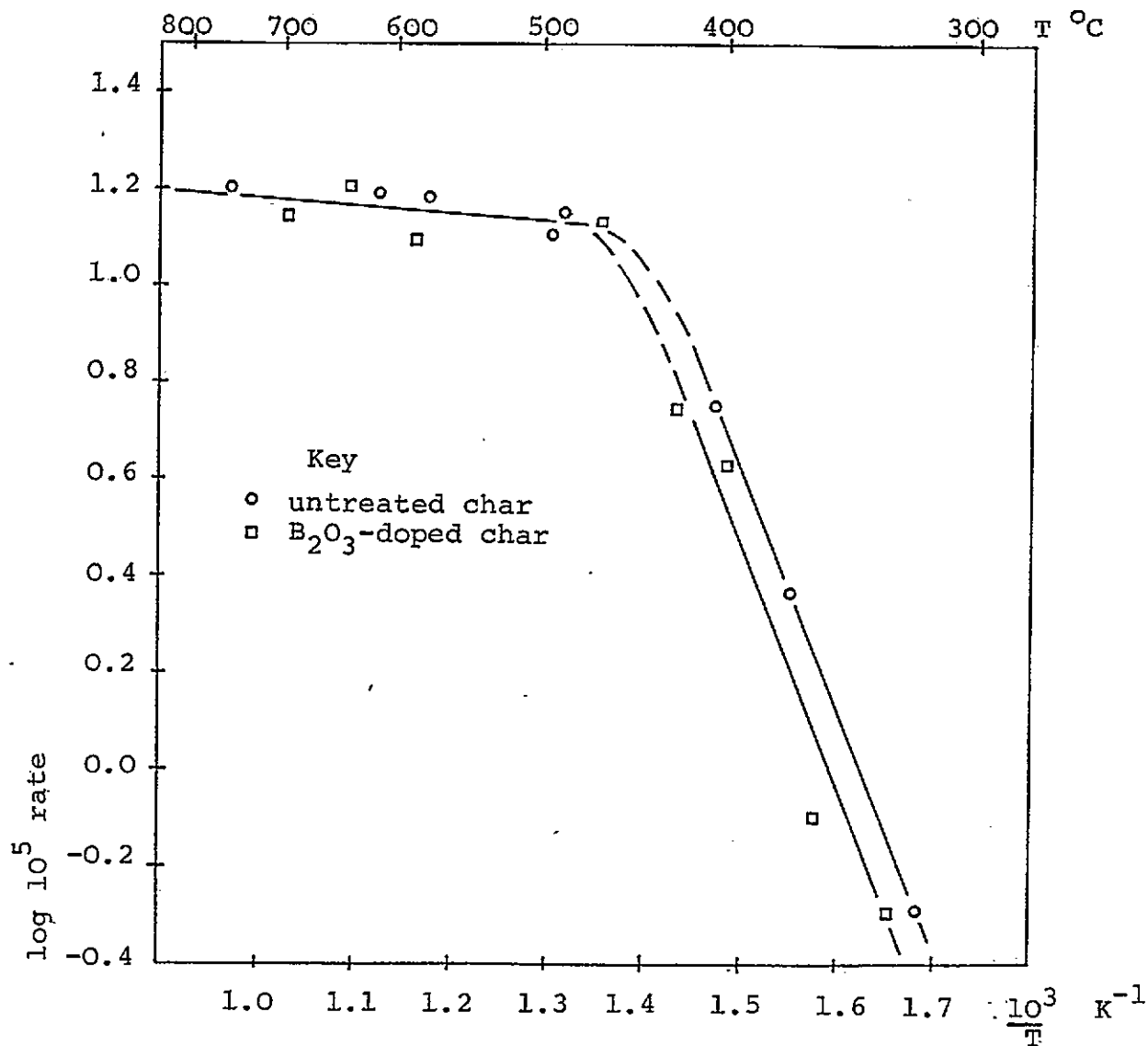| Temperature		Rate of oxidation x 10^5 g s^{-1} g^{-1}	log (10^5 x rate)	10^3 x reciprocal temperature (K^{-1})
°C	K			
331	604	0.519	-0.285	1.656
361	634	0.799	-0.097	1.577
400	673	4.268	0.630	1.486
425	698	5.535	0.743	1.433
465	738	13.70	1.137	1.355
585	858	12.46	1.096	1.166
640	913	15.90	1.202	1.095

Figure 5.3.h. Variation of Reaction Rate Constant with Temperature for the air oxidation of Australian Brown Coal Char (static atmosphere).
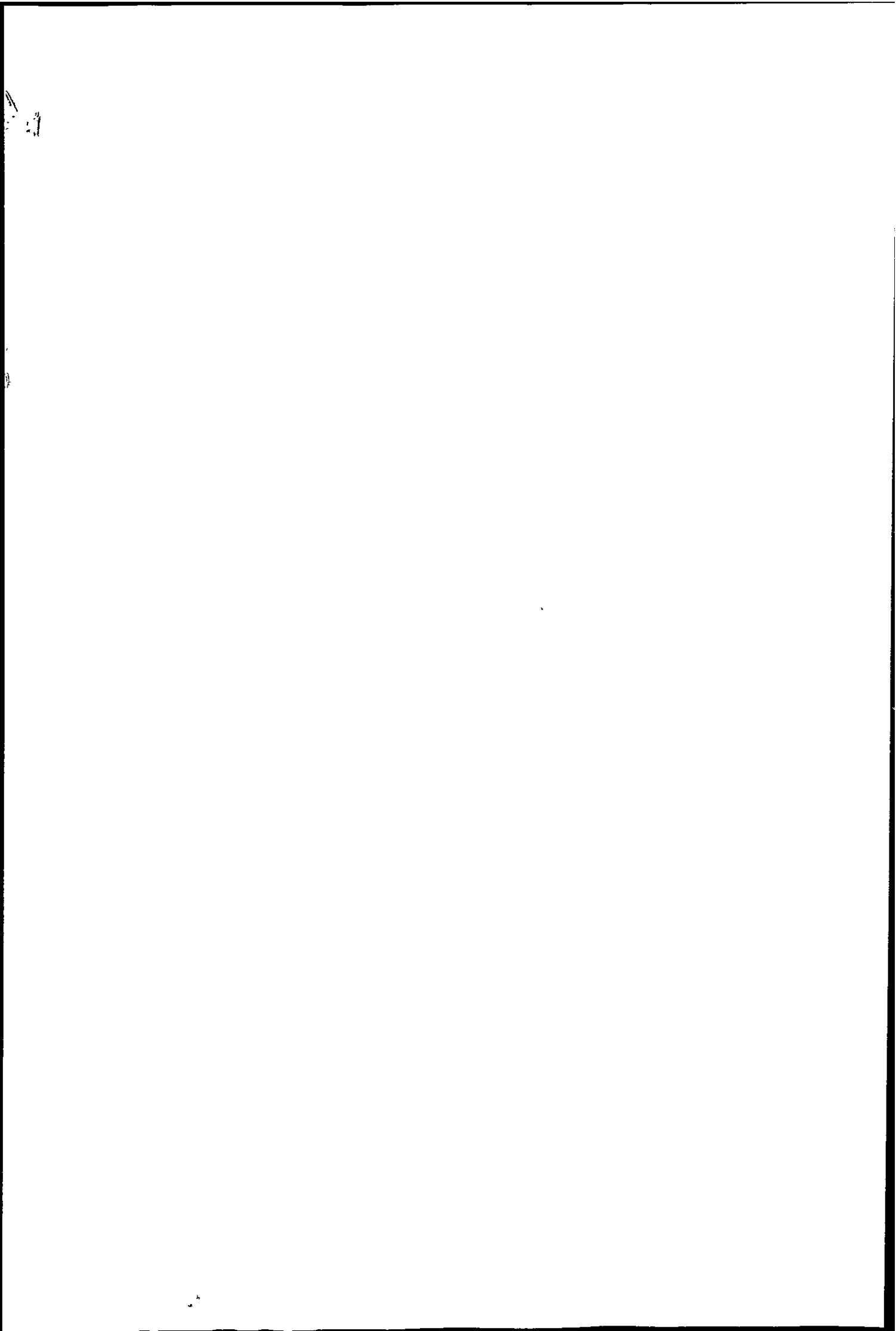
Table 5.3.e

Air Oxidation of Australian Brown Coal Char with

different sample weight.

Sample weight (mg)	Temperature ($^{\circ}$C)	rate (g s^{-1} x 10^6)	rate (g s^{-1}g^{-1} x 10^5)
169.5	689	9.052	5.438
65.4	697	8.915	13.88
182.3	494	9.044	5.052
64.7	494	8.108	12.76

Table 5.3.f

Flowing Air Oxidation of Nantgarw Coke Lumps

(100 mg samples)

Temperature $^{\circ}$C	K	rate of oxidation x 10^5 g s^{-1} g^{-1}	log (10^5 x rate)	10^3 x reciprocal temperature (K^{-1})
522	795	0.3210	-0.493	1.258
576	849	2.361	0.373	1.178
598	871	3.056	0.485	1.148
622	895	4.306	0.634	1.117
680	953	16.106	1.207	1.049
733	1006	29.442	1.469	0.994
784	1057	36.779	1.566	0.946
828	1101	41.667	1.620	0.908
884	1157	48.148	1.683	0.864
927	1200	54.444	1.736	0.833
977	1250	47.778	1.679	0.800
1074	1347	47.593	1.678	0.742
1169	1442	46.669	1.669	0.694
1277	1550	44.722	1.651	0.645
1383	1656	59.261	1.773	0.604

Table 5.3.g

Flowing Air Oxidation of B_2O_3 doped Nantgarw Coke Lumps.

(100 mg samples)

Temperature		rate of oxidation x 10^5	log (10^5 x rate)	10^3 x reciprocal temperature
^oC	K	g s^{-1} g^{-1}		(K^{-1})
570	843	0.311	-0.507	1.186
625	898	0.806	-0.094	1.114
667	940	3.195	0.505	1.064
697	970	5.555	0.745	1.031
722	995	9.306	0.969	1.005
775	1048	16.667	1.222	0.954
828	1101	38.333	1.584	0.908
872	1145	44.997	1.653	0.873
923	1196	43.555	1.639	0.836
970	1243	36.110	1.558	0.805
1067	1340	44.443	1.648	0.746
1166	1439	43.885	1.642	0.695
1267	1540	47.777	1.679	0.649

Table 5.3.h.

Flowing Air Oxidation of Nantgarw Coke Granules

(30 mg samples * 120 mg sample).

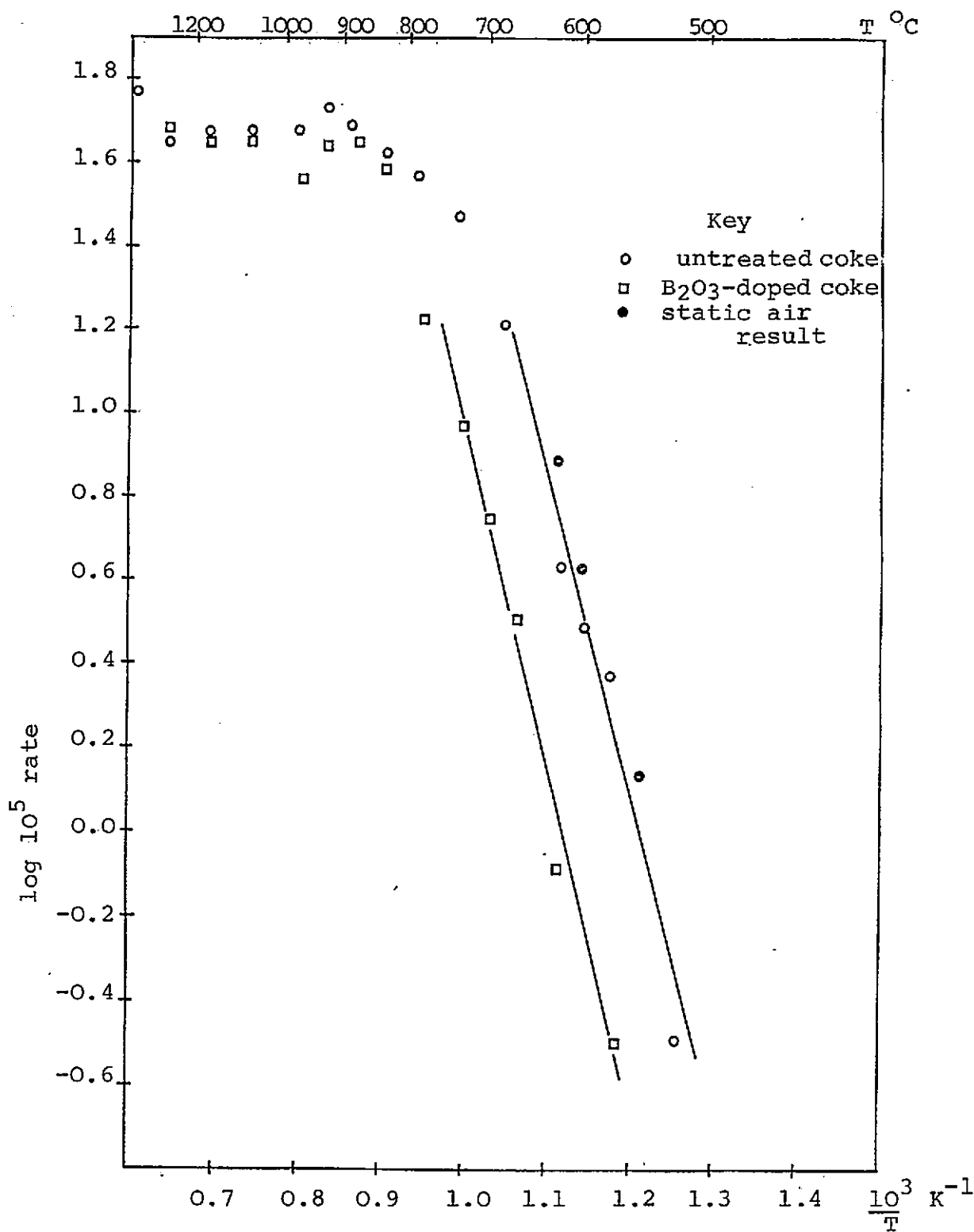| Temperature		rate of oxidation x 10^5	log (10^5 x rate)	10^3 x reciprocal temperature
^{o}C	K	g s^{-1} g^{-1}		K^{-1}
568	841	1.527	0.184	1.189
573*	846*	2.083*	0.319*	1.182*
598	871	4.306	0.634	1.148
629	902	6.389	0.806	1.109
676	949	18.402	1.265	1.054
726	999	39.456	1.596	1.001
775	1048	71.649	1.855	0.954
826	1099	120.87	2.082	0.910
873	1146	131.93	2.120	0.873
977	1250	120.82	2.082	0.800
1067	1340	126.34	2.102	0.746
1169	1442	140.84	2.149	0.694
1270	1543	136.10	2.134	0.648
1376	1649	148.63	2.172	0.606

Figure 5.3.i. Variation of Reaction Rate Constant with
Temperature for the Air Oxidation of Nantgarw Coke Lumps.
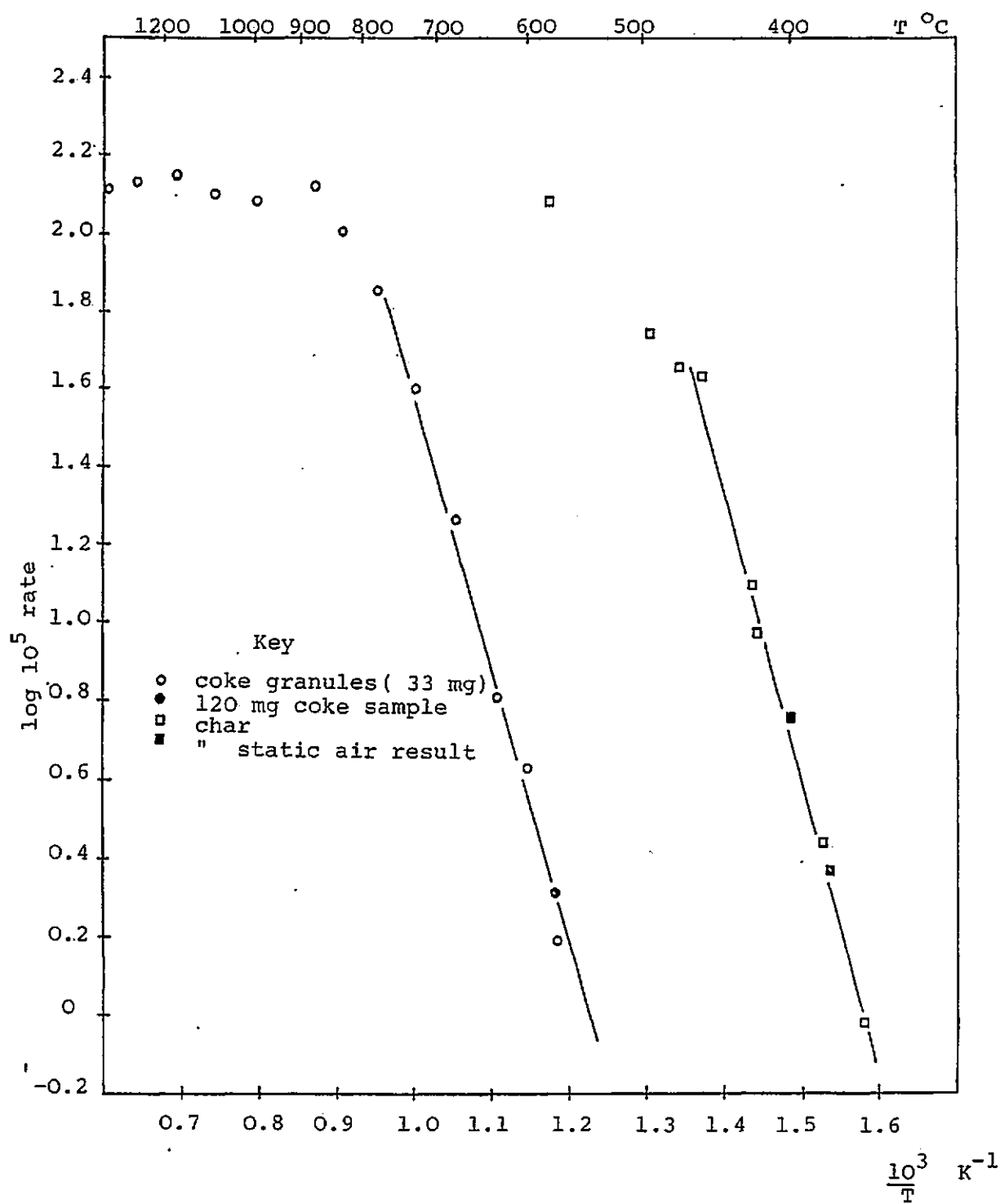(flowing atmosphere).

Figure 5.3.j. Variation of Reaction Rate Constant with
Temperature for the Air Oxidation of Australian Brown Coal
Char and Nantgarw Coke Granules (flowing atmosphere).

Table 5.3.i.

Flowing Air Oxidation of Australian Brown Coal Char

(50 mg samples)

Temperature		rate of oxidation x 10^5 g s^{-1} g^{-1}	log (10^5 x rate)	10^3 x reciprocal temperature
°C	K			
359	632	0.944	-0.025	1.582
381	652	2.750	0.439	1.529
420	693	9.333	0.970	1.443
422	695	12.361	1.092	1.439
457	730	43.056	1.634	1.370
472	745	45.417	1.657	1.342
494	767	55.556	1.745	1.304
578	851	122.22	2.087	1.175

Table 5.3.j.

Flowing Air Oxidation of three cokes.

Coke.	Temperature °C	rate of oxidation x 10^5 g s^{-1} g^{-1}	"Nantgarw Ratio"
Nantgarw	977	120.9	
Cwm	977	118.1	
Polish	977	123.6	
Nantgarw	522	0.972	1
Cwm	522	2.431	2.50
Polish	522	4.815	4.95

Figure 5.3.k. Air Oxidation of Nantgarw Metallurgical Coke at 975 °C at different air flow rates. (~105 mg samples).

Key:- solid line TG
broken line DTG

(i) Air oxidation of Australian Brown coal char at 381 °C
(54 mg samples).

(ii) Air oxidation of Australian Brown Coal Char at 594 °C
(53.4 mg samples).
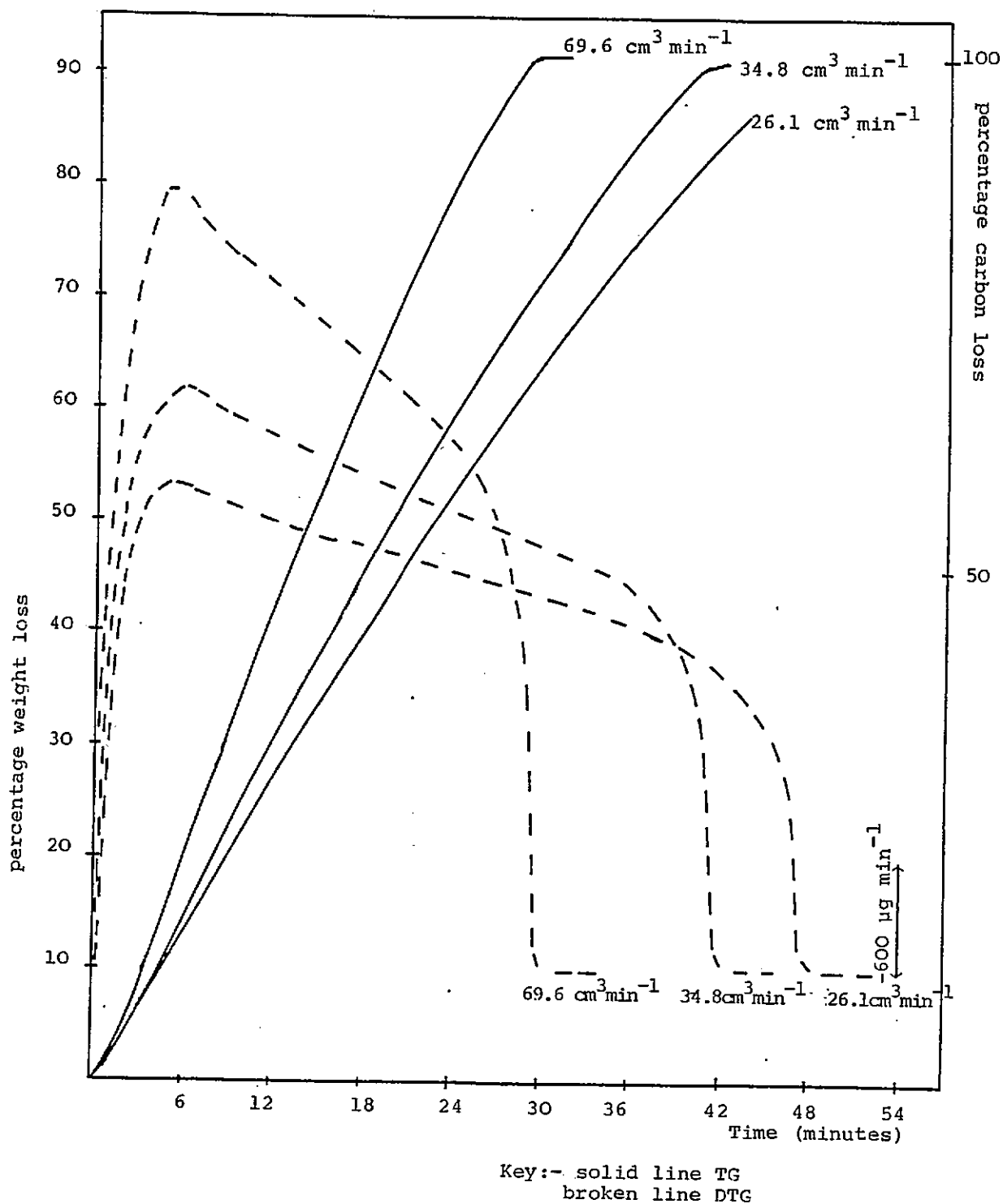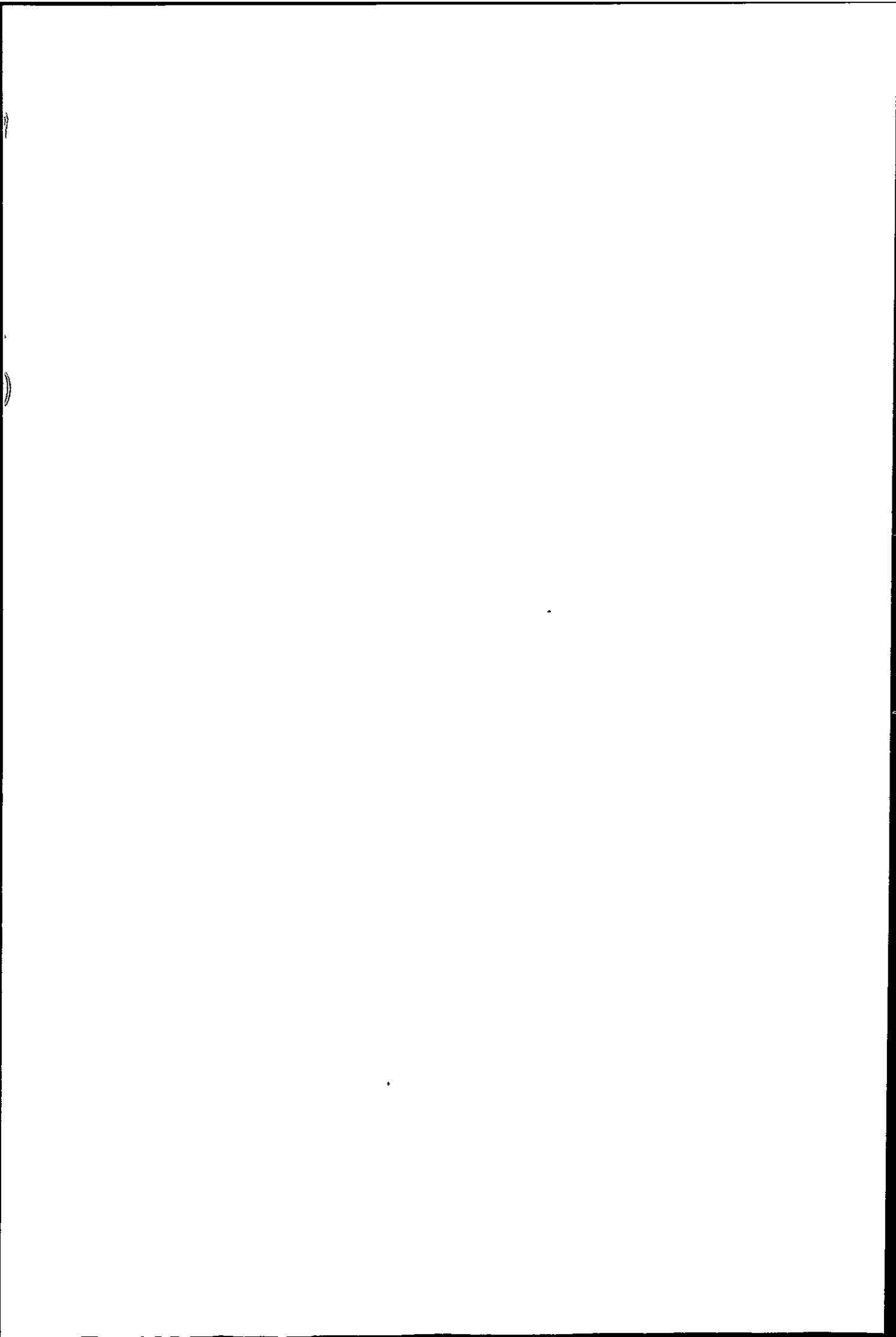
Figure 5.3.1. Air oxidations of Australian Brown Coal Char at different
Flow Rates

213

5.3.2 Discussion

The weight loss curves for the coke and char show a considerable time interval over which the rate of weight loss appears linear. The char contains an appreciable amount of volatile material, which accounts for the weight loss before the oxidation begins.
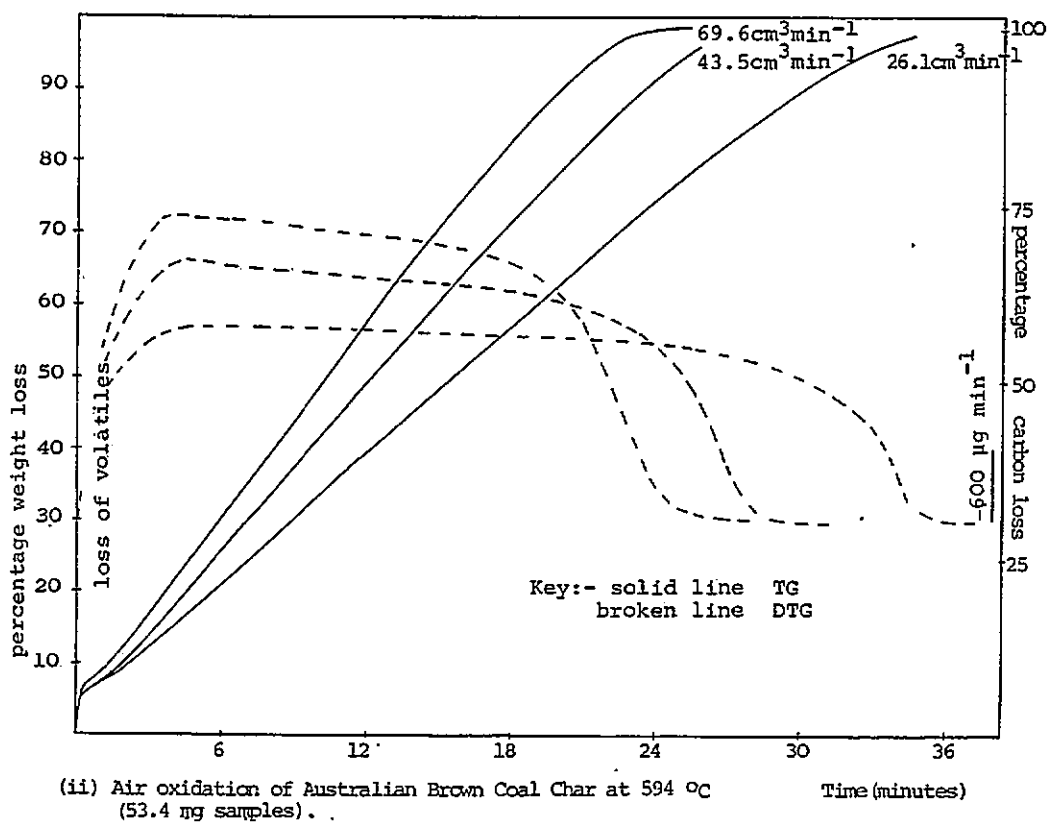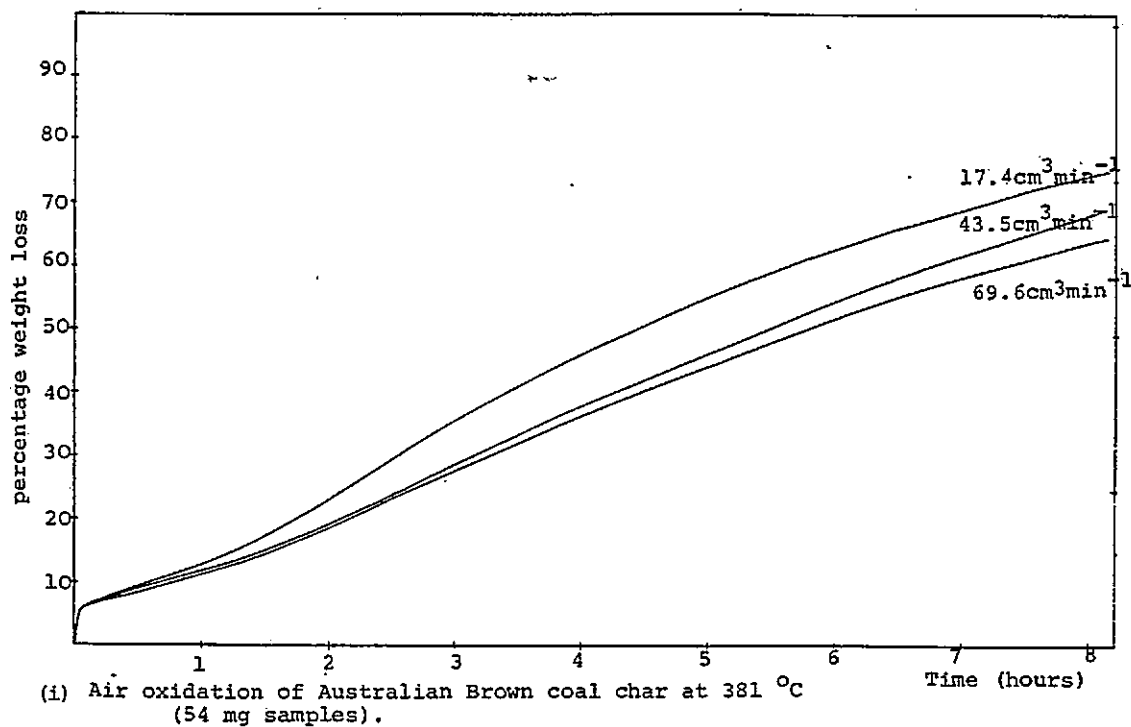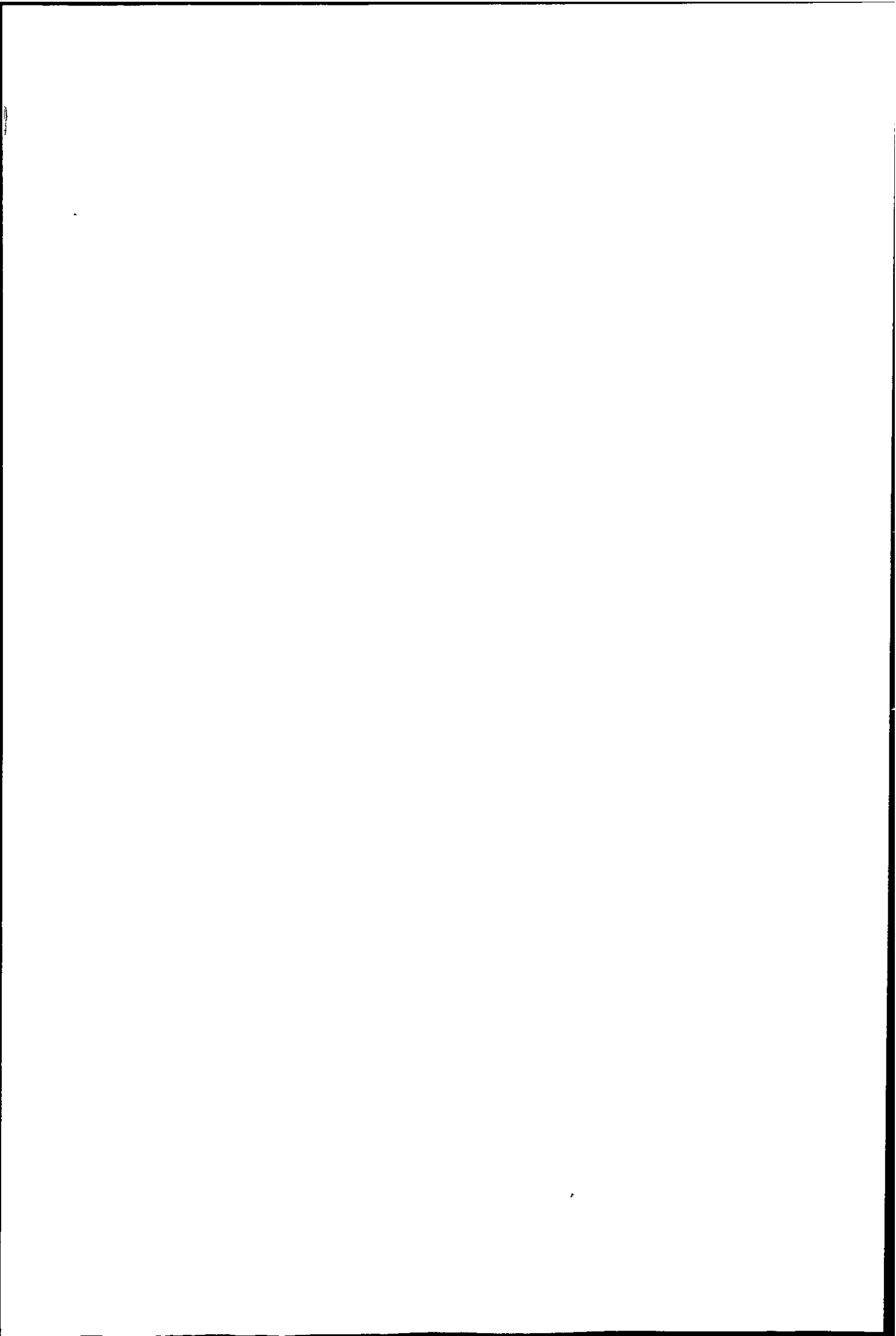
When plotted as percentage weight loss the oxidation curves in Figure 5.3.c, d and e have a similar form. The rate of weight loss may appear linear by a choice of time scale, e.g. the curves at 622 $^{\circ}$ and 680 $^{\circ}$C of Figure 5.3.d when plotted in Figure 5.3.e. The DTG results of Figures 5.3.k and l show that the rate of weight loss passes through a maximum which is maintained longer for the char than the coke.

The maximum rate of weight loss is not achieved at once in the lower temperature runs. At higher temperatures the initial part of the TG curve was not recorded because the pen is deflected as air exchanges for N_2. Similar sets of oxidation curves were obtained for the Nantgarw coke granules and B_2O_3-doped lumps above 620 $^{\circ}$C, and for the Australian brown coal char.

At temperatures below about 620 $^{\circ}$C the rate of oxidation of the doped coke reached a maximum then slowed as shown in Figure 5.3.f. This could be due to higher viscosity of B_2O_3 leading to slower spreading. The viscosity of B_2O_3 at 900 $^{\circ}$C is almost three times that at 1100 $^{\circ}$C as given by Mellor[1].

The Arrhenius plots of the results obtained for the coke and the char on the Massflow balance show two linear regions (Figures 5.3.g and h), interpreted as Zones I and III as described in Chapter 1, reference 40.

In Zone III rate of reaction is determined by the thickness of the gas layer at the surface of the carbon, i.e. it is independent of the amount of carbon present, but depends on the crucible and furnace geometry. Hence, rate of oxidation expressed as $g \, s^{-1}$ should be independent of sample starting weight, but the rate expressed as $g \, s^{-1} \, g^{-1}$ should vary. This is seen to be so with the char at 690 ^{o}C and 494 ^{o}C from Table 5.3.e. The same sample weight could not be achieved so easily with the coke lumps as with the char and so there is a greater spread of results in the diffusion controlled zone.

The slope of the Zone I region indicates an energy of activation of about 100 kJ mol^{-1}. In this region the char oxidises at about ten times the rate for the coke, although their final reactivities tend to the same diffusion-limited value. The change to diffusion control appears about 650 ^{o}C for the coke and between 420 and 480 ^{o}C for the char. Diffusion is expected to limit the rate at lower temperatures for microporous materials. (Chapter 1 reference 41.) B_2O_3 treatment lowers the reactivity of both the coke and the char in this Zone.

Figures 5.3.i and j show similar Arrhenius plots from data obtained under flowing air on the STA 781 using coke lumps, as before and coke granules. The diffusion limited rate is higher and the change from Zone I to Zone

215

III occurs between 680 to 850 $^\circ$C for coke lumps, and between about 780 to 850 $^\circ$C for coke granules. The higher limiting temperature and rate for granules reflects the easier access of gas to the surface of the smaller particles. For the char, diffusion seems to be rate-limiting at about 460 $^\circ$C and the rate would probably tend to a similar value to that for the coke granules.

In Zone I, where rate depends on the chemical reactivity of the surface, the rate of reaction as $g\ s^{-1}\ g^{-1}$ should be independent of starting weight, and was found to be so using 120 mg of coke granules. Rate of reaction is little different for lumps and granules and close to results obtained in the Massflow balance where sample environment was different.

As seen in Figure 5.3.k an increase in air flow rate increases the rate of coke oxidation at 975 $^\circ$C (Zone III) and a similar effect was found at 550 $^\circ$C (Zone I).

For the char, however, an increase in air flow rate at 381 $^\circ$C (Zone I) decreases the rate of oxidation and must indicate the difference in porosity between the two materials. At 594 $^\circ$C (Zone III) an increased air flow increases the rate of oxidation.

The values obtained for the activation energy E_A of the C/O_2 reaction and for the frequency factor A, from the slope and intercept of the Arrhenius plots are tabulated below. (For the chemical control zone.)

216

Kinetic Parameters for the C/O_2 reaction in flowing air.

Material	$E_A(kJ\ mol^{-1})$ $\pm\ 20$	$A(g\ s^{-1}\ g^{-1})$
Nantgarw coke lumps	147	5.0×10^4
Nantgarw coke granules	133	3.2×10^3
B_2O_3-doped Nantgarw coke lumps	155	1×10^4
Australian brown coal char	142	4.0×10^6

Kinetic Parameters for the C/O_2 reaction of Australian Brown Coal Char and Nantgarw coke in Static Air.

Material	$E_A(kJ\ mol^{-1})$	$A(g\ s^{-1}\ g^{-1})$
original char	96	2.5×10^3
B_2O_3-doped char	97	6.3×10^2
Nantgarw coke	126	2.8×10^3

The activation energy values are useful only for comparison, the unit mol^{-1} entering the value only because R is used in the calculation.

B_2O_3 treatment of the coke and the char does not appear to alter the activation energy for the air oxidation. The B_2O_3 probably acts by physical blocking of surface, owing its efficiency to its ability to spread.

Values of E_A were similar for the coke and the char but the frequency factor was much greater for the more reactive char.

In runs where char samples were not oxidised to complete burn off it was often noticeable that some lumps were ashed, while others appeared little burnt. Selective oxidation in the C/O_2 reaction has been noted by workers on polymer chars, and could be enhanced in coal chars by the catalytic effect of the mineral matter. Coke lumps also often had portions where ash had built up preferentially.
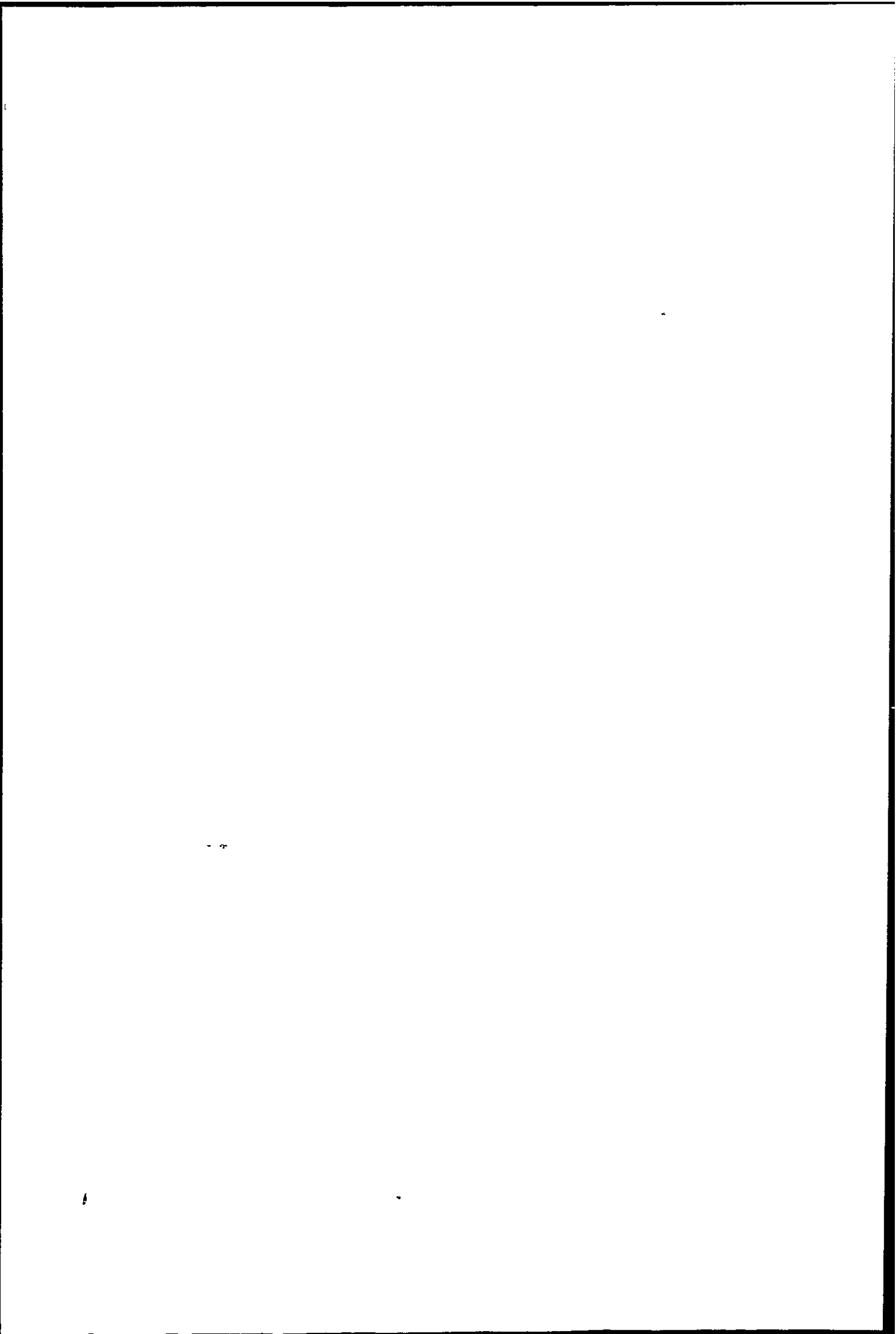
5.4 CO_2 Oxidations.

5.4.1 Results

Isothermal weight loss curves for the CO_2 oxidation of Nantgarw coke lumps are shown in Figure 5.4.a. Maximum rates of reaction are given in Table 5.4.a and shown as an Arrhenius plot in Figure 5.4.b.

The effect of different coke sample weight at higher and lower temperatures (under the same CO_2 flow rate) is given in Table 5.4.b, and the effect of varying the CO_2 flow rate at 1264 ^{o}C with the same sample weight is given in Table 5.4.c. At lower temperatures, increasing the CO_2 flow rate had little effect on rate of reaction of the coke.

Results for the B_2O_3 doped coke lumps are given in Table 5.4.d and also plotted in Figure 5.4.b. Some of the weight loss curves for the CO_2 reaction with doped Nantgarw coke are given in Figure 5.4.c.

The rates of reaction for isothermal CO_2 oxidations of Australian brown coal char and B_2O_3 doped char are given in Tables 5.4.e and f and combined in the Arrhenius plot of Figure 5.4.d. Typical weight loss curves are shown in Figure 5.4.e, the initial portion being loss of volatile matter.

The oxidation of Cwm, Polish and Nantgarw coke granules (500-710μ m) at 955 ^{o}C in CO_2 flowing at 17.6 cm^3 min^{-1} is shown in Figure 5.4.f. From the average rate of reaction for each successive 10% burn off, Figure 5.4.g was constructed, in order to compare the relative

reactivities of the cokes throughout the entire CO_2 burn off. These rates are given in Table 5.4.g and their ratios in Table 5.4.h.

Polish and Cwm coke lumps were doped in B_2O_3 and burnt off in CO_2 at 955 $^{\circ}C$. Rates of reaction are given in Table 5.4.i together with that of Nantgarw coke at 1004 $^{\circ}C$ which had been soaked for 2 hours in B_2O_3 solution, drained and air dried.

The rates of reaction at 910 $^{\circ}C$ of PMC graphite (35 mg sample) and the Hopkin and Williams charcoals characterised in Chapter 4 (20 mg samples) to CO_2 flowing at 38.8 cm^3 min^{-1} are given in Table 5.4.j. This temperature was chosen in order to minimise diffusion effects. Results for Nantgarw coke and the Australian brown coal char, already presented, are included in Table 5.4.j for comparison.

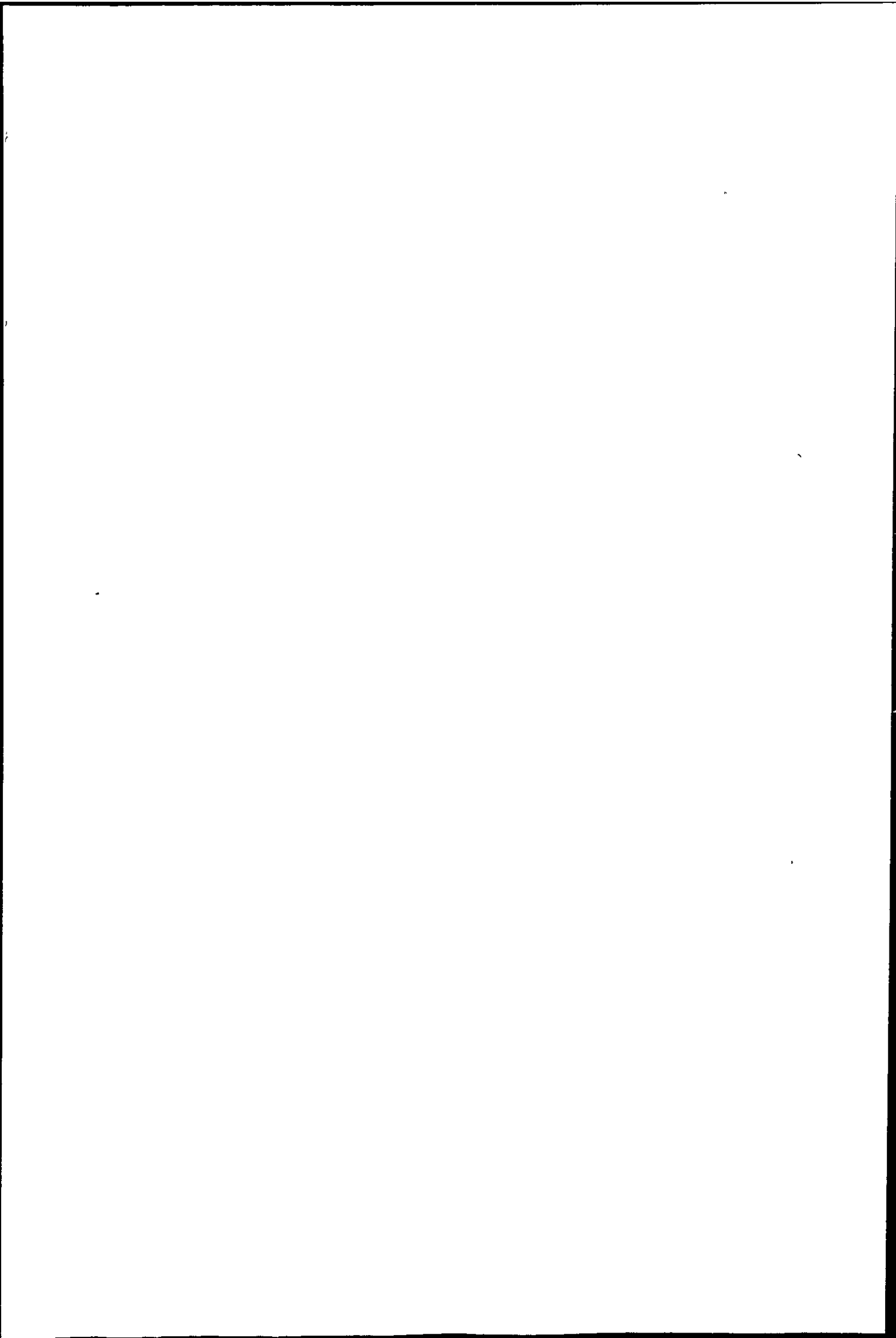Figure 5.4.a. CO_2 oxidations of Nantgarw Metallurgical Coke
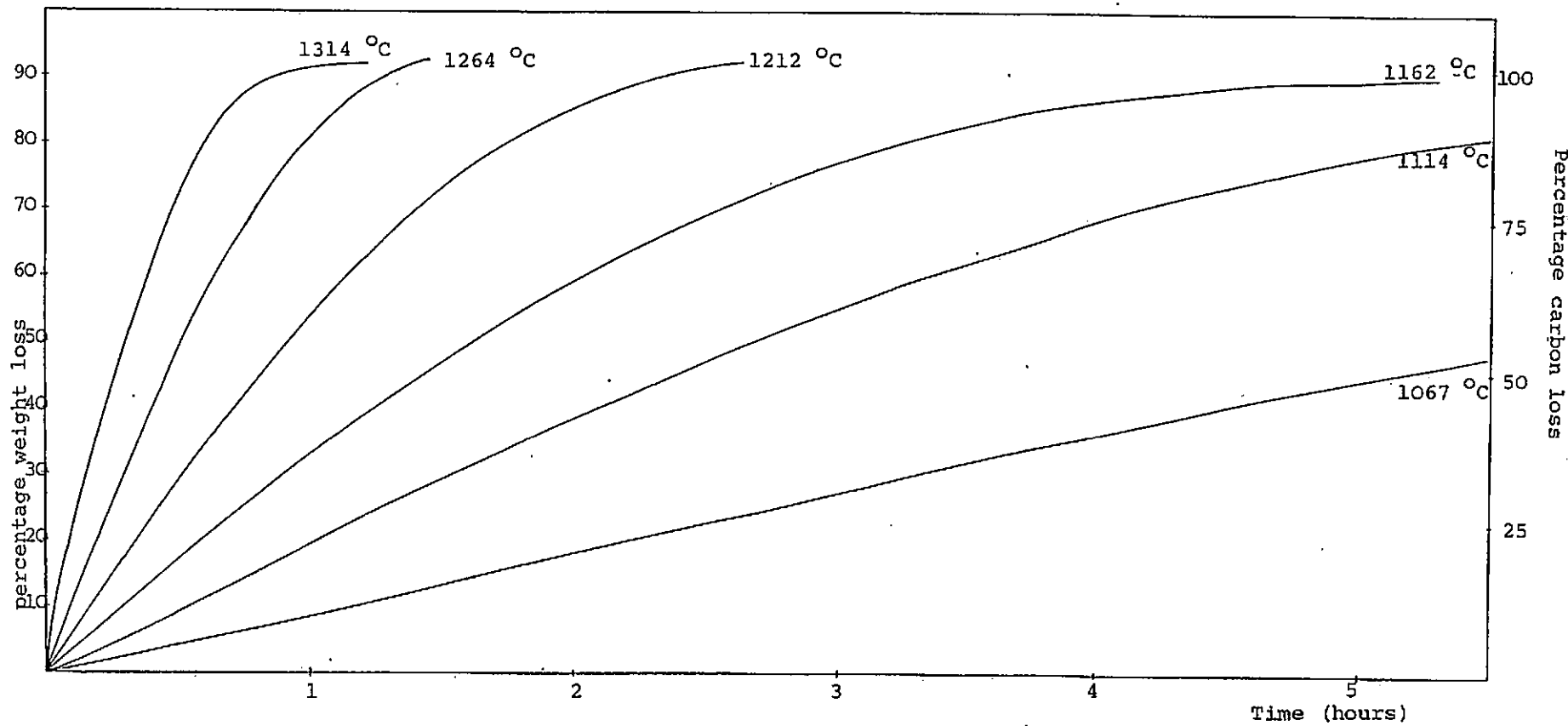
Table 5.4.a

CO_2 Oxidation of Nantgarw coke lumps

(80 mg samples. CO_2 flow 35.2 cm^3 min^{-1})

Temperature		rate of reaction x 10^6 $g\ s^{-1}\ g^{-1}$	log (10^6 x rate)	10^3 x reciprocal temperature K^{-1}
^{o}C	K			
909	1182	3.385	0.530	0.846
961	1234	7.219	0.859	0.810
1013	1286	16.948	1.229	0.778
1067	1340	24.726	1.393	0.746
1114	1387	43.614	1.640	0.721
1162	1435	78.467	1.895	0.697
1212	1485	148.61	2.172	0.673
1264	1537	261.12	2.417	0.651
1314	1587	380.53	2.580	0.630

Table 5.4.b.

CO_2 Oxidation of Nantgarw coke lumps

(flow rate 35.2 cm^3 min^{-1})

Sample weight (mg)	Temperature (^{o}C)	rate of reaction x 10^6 $g\ s^{-1}$	rate of reaction x 10^6 $g\ s^{-1}\ g^{-1}$
77.06	1264	20.12	261.12
37.56	1264	8.660	230.56
79.24	961	0.572	7.219
46.60	961	0.324	6.953
34.20 (granules)	961	0.266	7.778

222

Table 5.4.c

CO_2 Oxidation of Nantgarw coke lumps at 1264 $^\circ C$

Sample weight (mg)	CO_2 flow rate cm^3 min^{-1}	rate of reaction x 10^6 g s^{-1}	rate of reaction x 10^6 g s^{-1} g^{-1}
37.56	35.2	8.660	230.56
38.15	14.1	7.522	197.18

Table 5.4.d.

CO_2 Oxidation of B_2O_3 doped Nantgarw Coke lumps

(80 mg samples. CO_2 flow 35.2 cm^3 min^{-1})

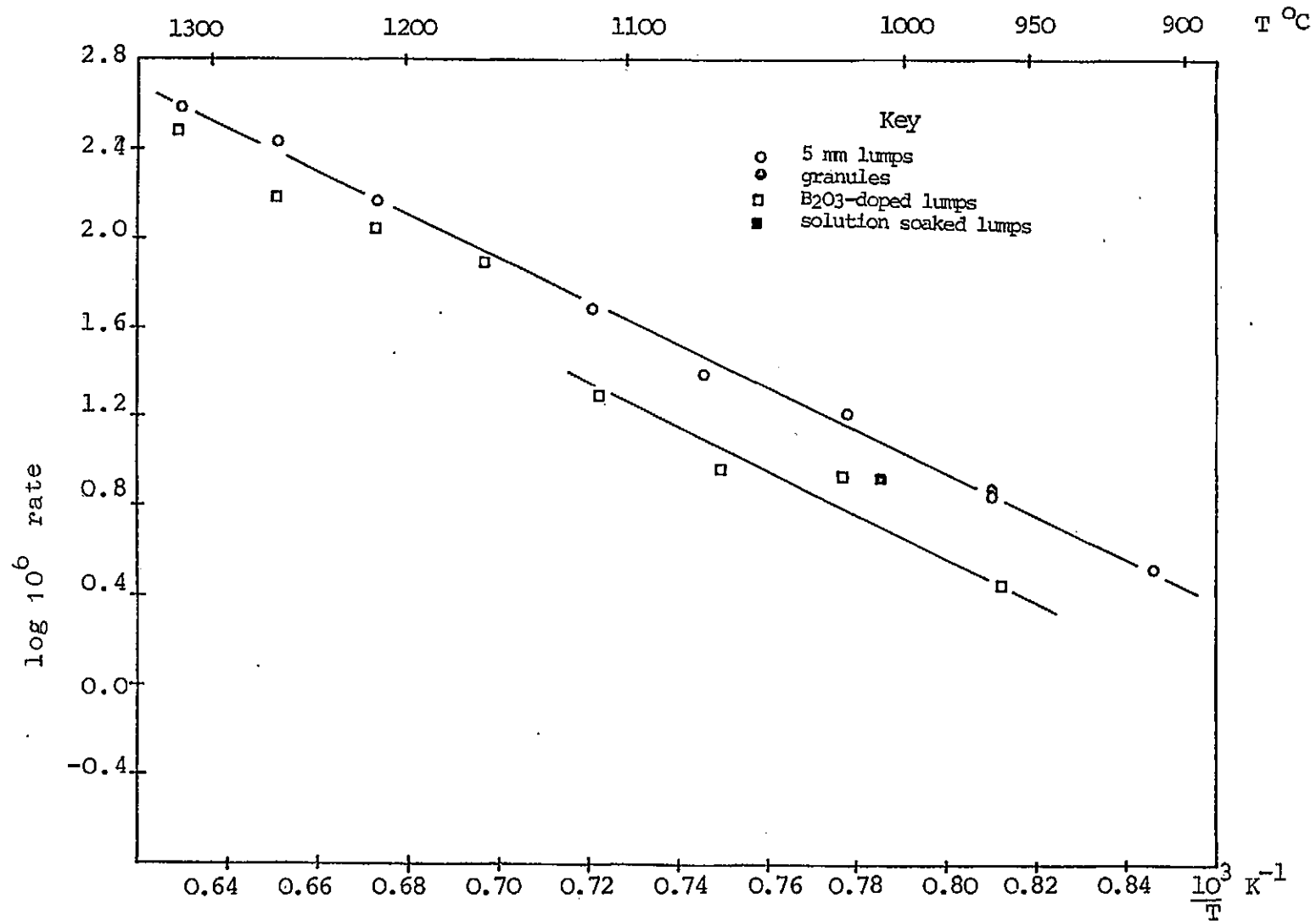| Temperature		rate of reaction x 10^6	log (10^6 x rate)	10^3 x reciprocal temperature
$^\circ C$	K	g s^{-1} g^{-1}		K^{-1}
959	1232	2.862	0.457	0.812
1014	1287	8.889	0.949	0.777
1063	1336	9.259	0.967	0.749
1111	1384	19.445	1.289	0.723
1162	1435	79.861	1.902	0.697
1213	1486	111.11	2.046	0.673
1263	1536	151.39	2.180	0.651
1317	1590	297.27	2.473	0.629

Figure 5.4.b. Variation of Reaction Rate Constant with Temperature for
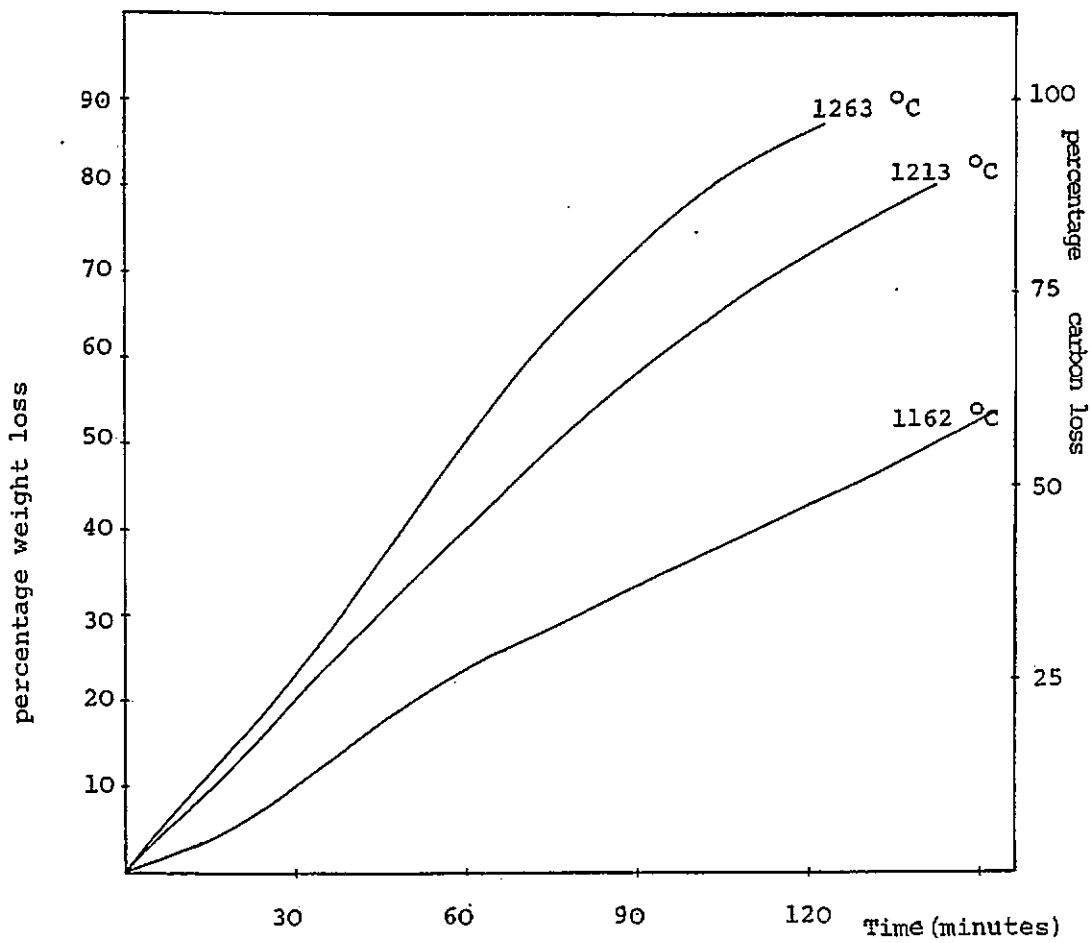Nantgarw Coke in the Boudouard Reaction.

Figure 5.4.c. Oxidation of B_2O_3-doped Nantgarw coke in CO_2.

Table 5.4.e.

Isothermal CO_2 oxidation of Australian brown coal char.

(40 mg samples. CO_2 flow 35.2 cm^3 min^{-1}).

Temperature		rate of reaction x 10^6	$\log(10^6 \times rate)$	10^3 x reciprocal temperature
$^\circ C$	K	g s^{-1} g^{-1}		K^{-1}
663	936	2.778	0.444	1.068
696	969	6.261	0.797	1.032
718	991	11.482	1.060	1.010
767	1040	34.994	1.544	0.962
789	1062	63.888	1.805	0.942
864	1137	205.55	2.313	0.880
907	1180	402.75	2.605	0.848
956	1229	888.94	2.949	0.814
1014	1287	972.31	2.988	0.777
1056	1329	1611.2	3.207	0.753
1111	1384	2223.1	3.347	0.723
1157	1435	2778.6	3.444	0.697
1263	1536	3167.9	3.501	0.651
1369	1642	2378.8	3.516	0.609

Table 5.4.f.

CO_2 oxidation of B_2O_3-doped Australian Brown Coal Char

(40 mg samples CO_2 flow 35.2 cm^3 min^{-1}).

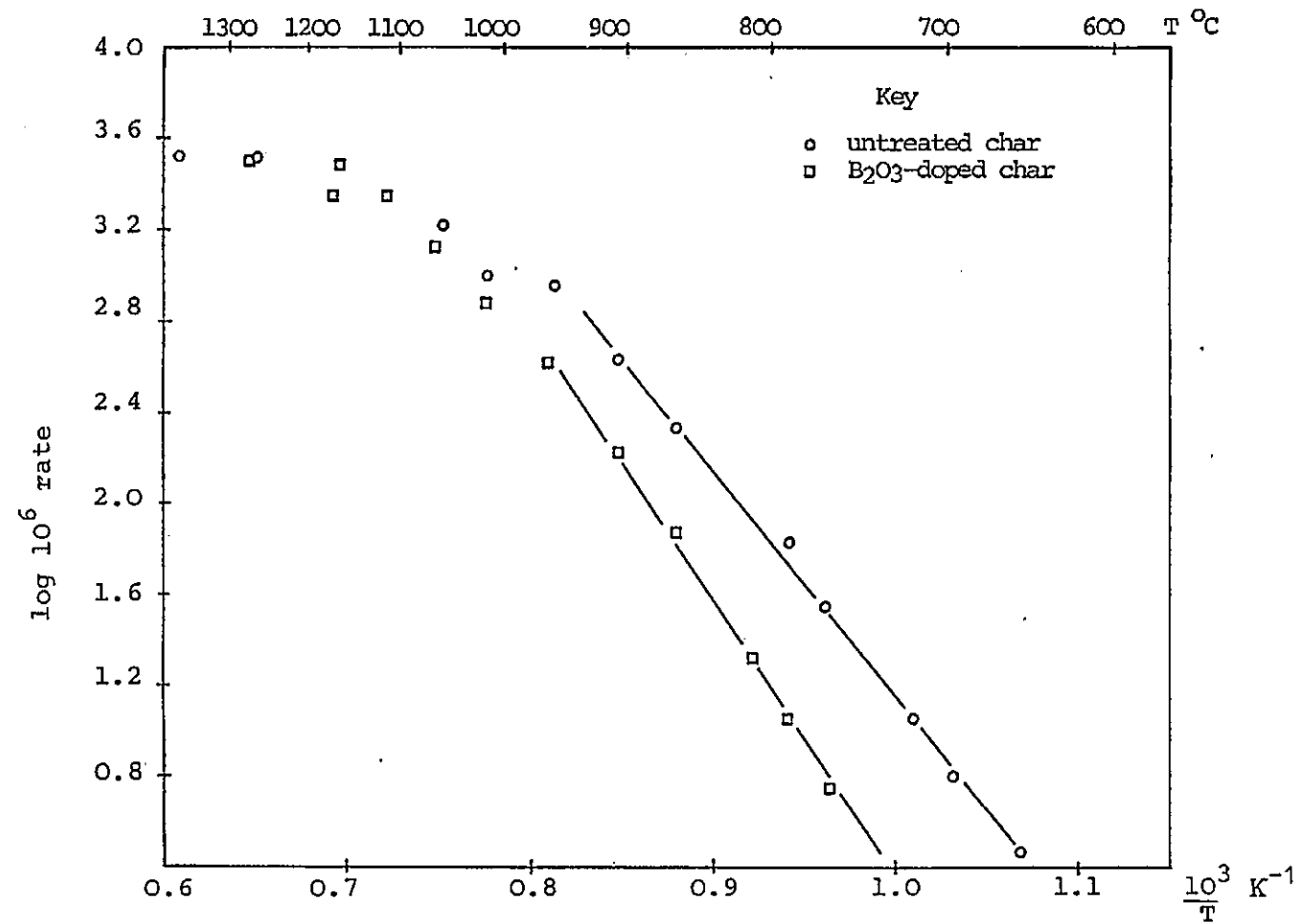| Temperature		rate of reaction x 10^6	$\log(10^6 \, rate)$	10^3 reciprocal temperature
$^\circ C$	K	g s^{-1} g^{-1}		K^{-1}
763	1036	5.556	0.745	0.965
790	1063	11.458	1.059	0.941
812	1085	21.181	1.326	0.922
864	1137	73.611	1.867	0.880
907	1180	167.77	2.225	0.848
961	1234	402.84	2.605	0.810
1014	1287	750.01	2.875	0.777
1063	1336	1333.3	3.125	0.749
1169	1442	2222.2	3.347	0.694
1270	1543	3267.2	3.514	0.648

Figure 5.4.d. Variation of Reaction Rate Constant with Temperature for Australian Brown Coal Char in the Boudouard Reaction.
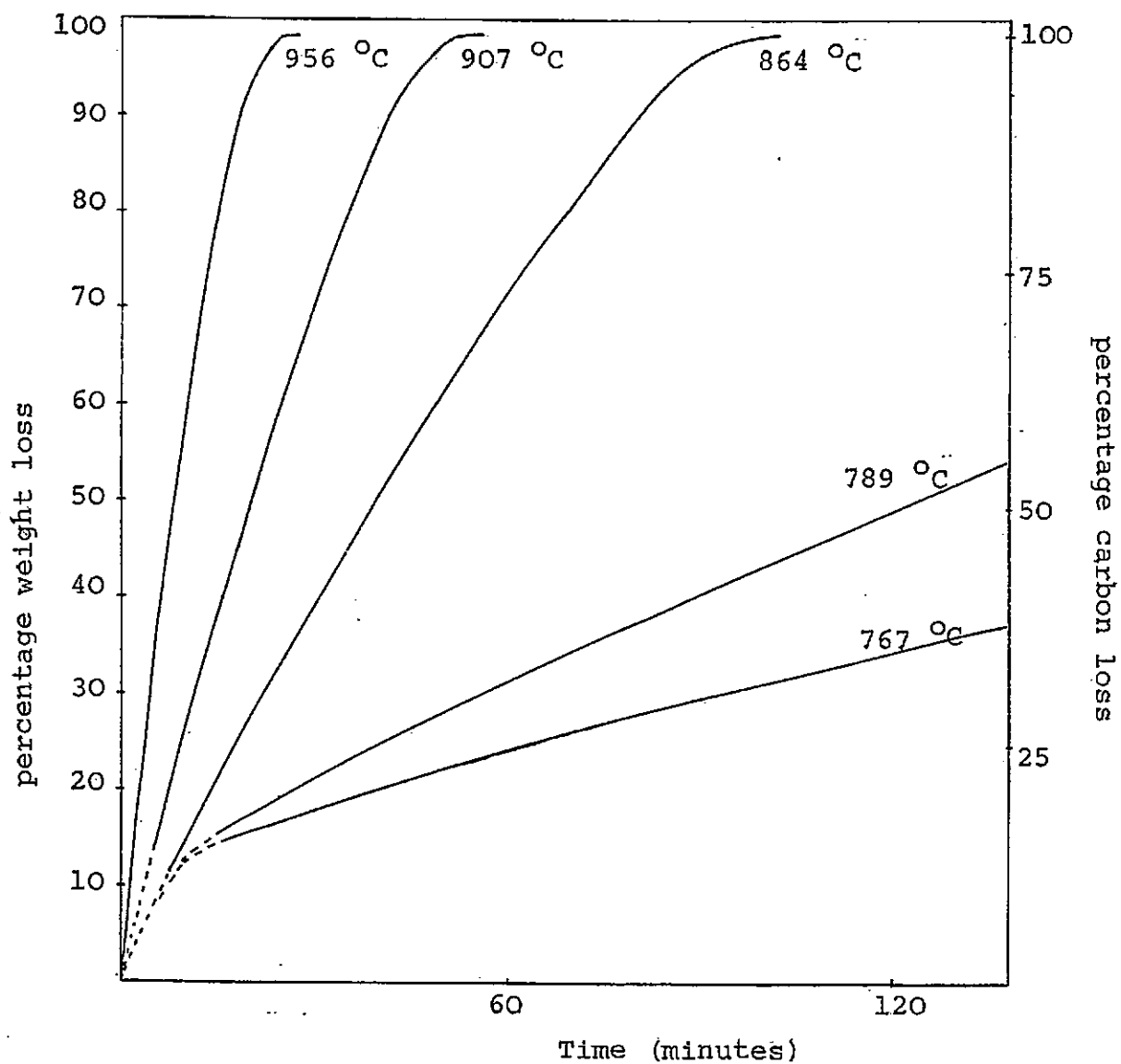
227

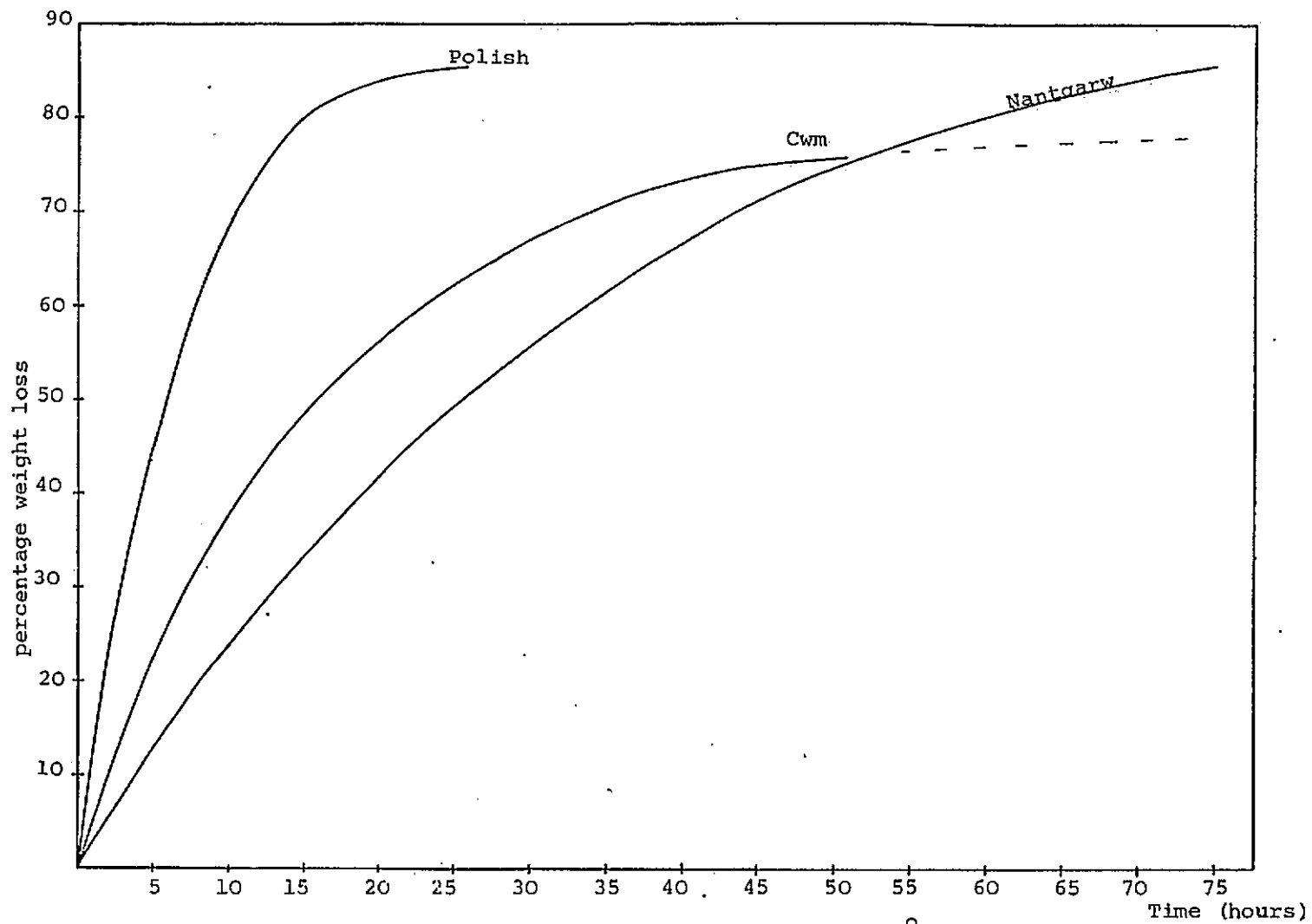Figure 5.4.e. Oxidation of Australian Brown Coal Char in CO_2.

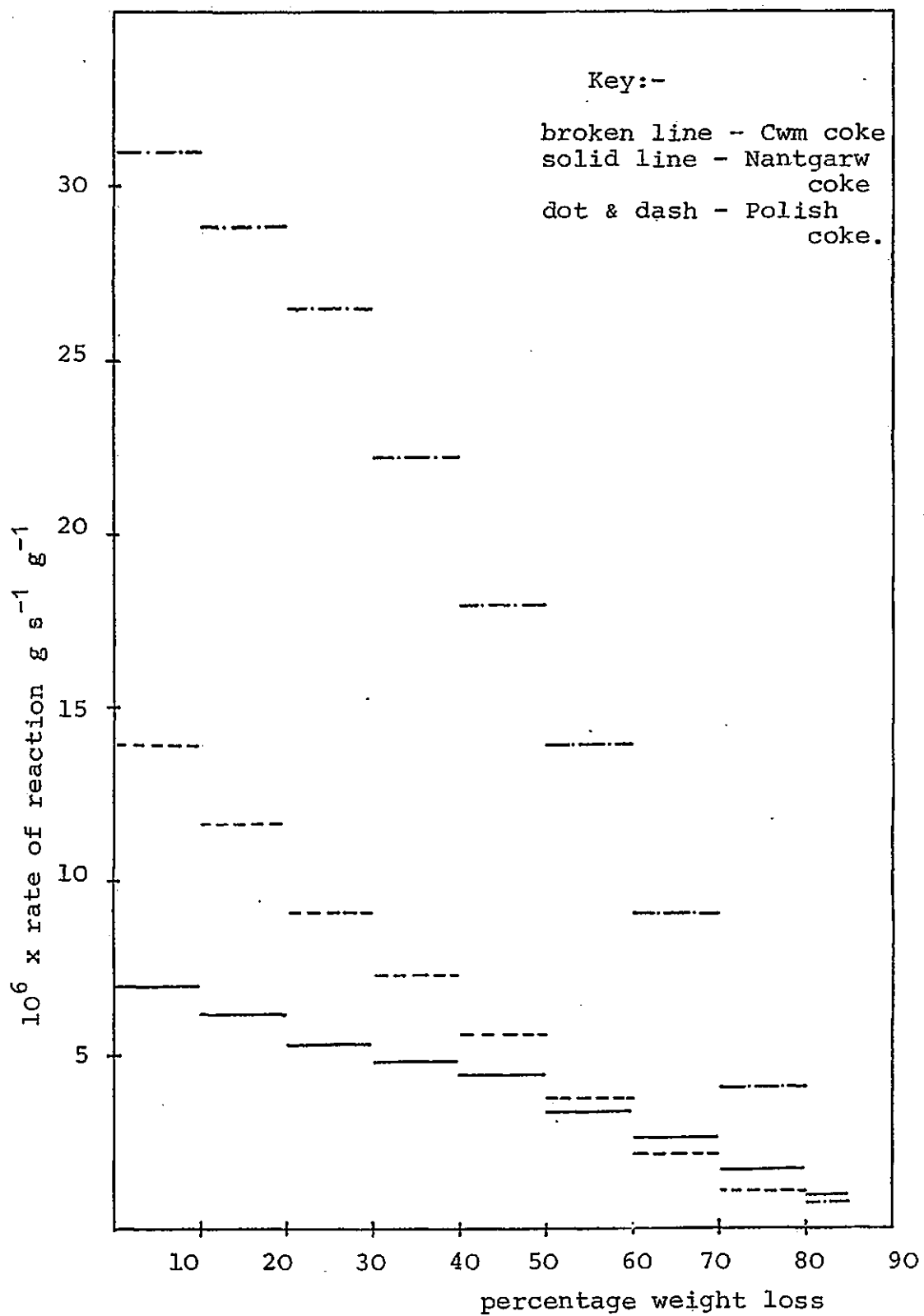Figure 5.4.f. Oxidation of Three Metallurgical Cokes at 955 $^{\circ}$C in CO_2.

Figure 5.4.g. Variation in rate of oxidation of Three Metallurgical Cokes at 955 $^{\circ}$C in CO_2 with Percentage Weight Loss.
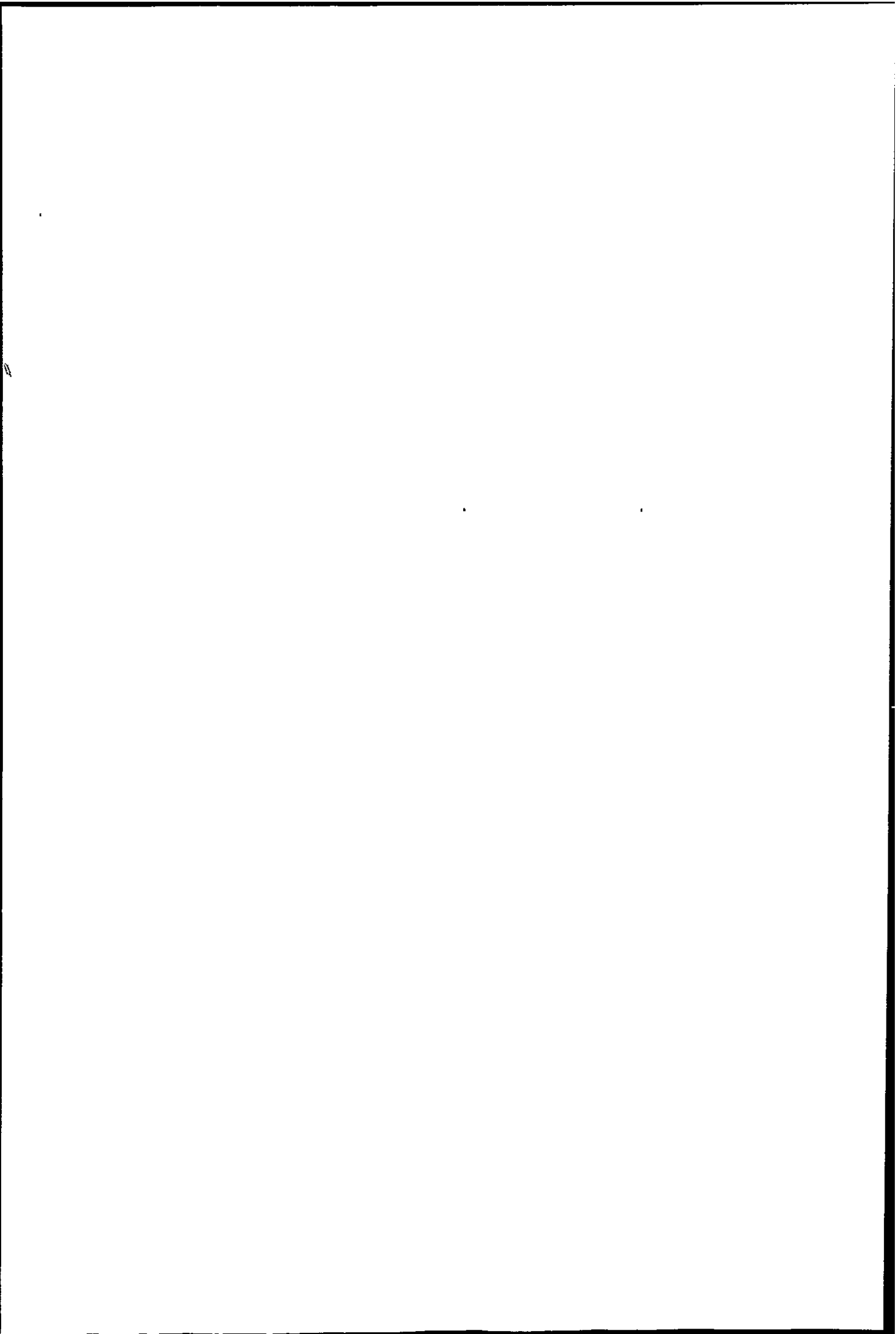
Table 5.4.g.

Rates of oxidation of three metallurgical cokes in CO_2 at 955 °C. ($g\ s^{-1}\ g^{-1} \times 10^6$)

% burn-off	0-10	10-20	20-30	30-40	40-50	50-60	60-70	70-80	>80
Nantgarw	6.96	6.18	5.30	4.85	4.44	3.37	2.71	1.73	0.99
Polish	30.88	27.76	26.45	22.21	17.92	13.90	9.27	4.12	0.77
Cwm	13.89	11.57	9.11	7.31	5.58	3.83	2.22	1.26	0.93

Table 5.4.h.

"Nantgarw Ratio" throughout burn-off for Cwm and Polish Cokes.

% burn-off	0-10	10-20	20-30	30-40	40-50	50-60	60-70	70-80
Polish	4.44	4.49	4.99	4.58	4.04	4.13	3.42	2.38
Cwm	2.00	1.87	1.72	1.51	1.26	1.14	0.82	0.73

Table 5.4.i.

Rates of reaction of doped cokes in CO_2 at 955 °C (CO_2 flow 35.2 $cm^3\ min^{-1}$).

| Coke (lumps)	Rate of reaction x 10^6 $g\ s^{-1}\ g^{-1}$
Nantgarw	2.86
Cwm	variable results (3 to 10)
Polish	14.24
Nantgarw (soaked) reacted at 1004 °C	8.24

231

Table 5.4.j.

Rates of reaction of several carbons at 910 $^{\circ}$C in CO_2.

Material	maximum rate of reaction x 10^6 (g s^{-1} g^{-1})
Australian brown coal char.	446.7
Hopkin & Williams charcoal for decolourising	166.65
Hopkin & Williams charcoal "Norit GSX"	69.44
Hopkin & Williams charcoal for chromatography	67.78
Hopkin & Williams charcoal activated for gas sorption	30.28
Nantgarw coke	3.39
PMC graphite	2.78

5.4.2. Discussion

Rates of reaction for the brown coal char and for Nantgarw coke were approximately ten times slower than the corresponding air oxidations. Several lower temperature runs were not taken to complete burn-off. Ash had not built up as a surface layer and the partially gasified lumps were dull and brittle. In oxidations above 1260 ^{O}C the coke ash had melted.

The Arrhenius plot of Figure 5.4.b. shows a single linear region. Gaseous diffusion is not becoming rate limiting for Nantgarw coke in the Boudouard reaction up to at least 1400 ^{O}C. The value of E_A calculated from the slope is 186 kJ mol^{-1}. Richards and Tandy (Chapter 2, reference 38) give a value of 176 kJ mol^{-1} and a comparison of their results with the present work is given below.

Temperature ^{O}C	Rate of reaction of Nantgarw coke (mol min^{-1} atm^{-1} g^{-1})	
	Richards & Tandy	Present work (calculated from Figure 5.4.b.)
1000	3.8×10^{-5}	5.61×10^{-5}
1100	2.1×10^{-4} (1.3×10^{-4} at lower gas flow).	2.13×10^{-4}
1200	4.0×10^{-4}	6.29×10^{-4}
1300	–	13.45×10^{-4}
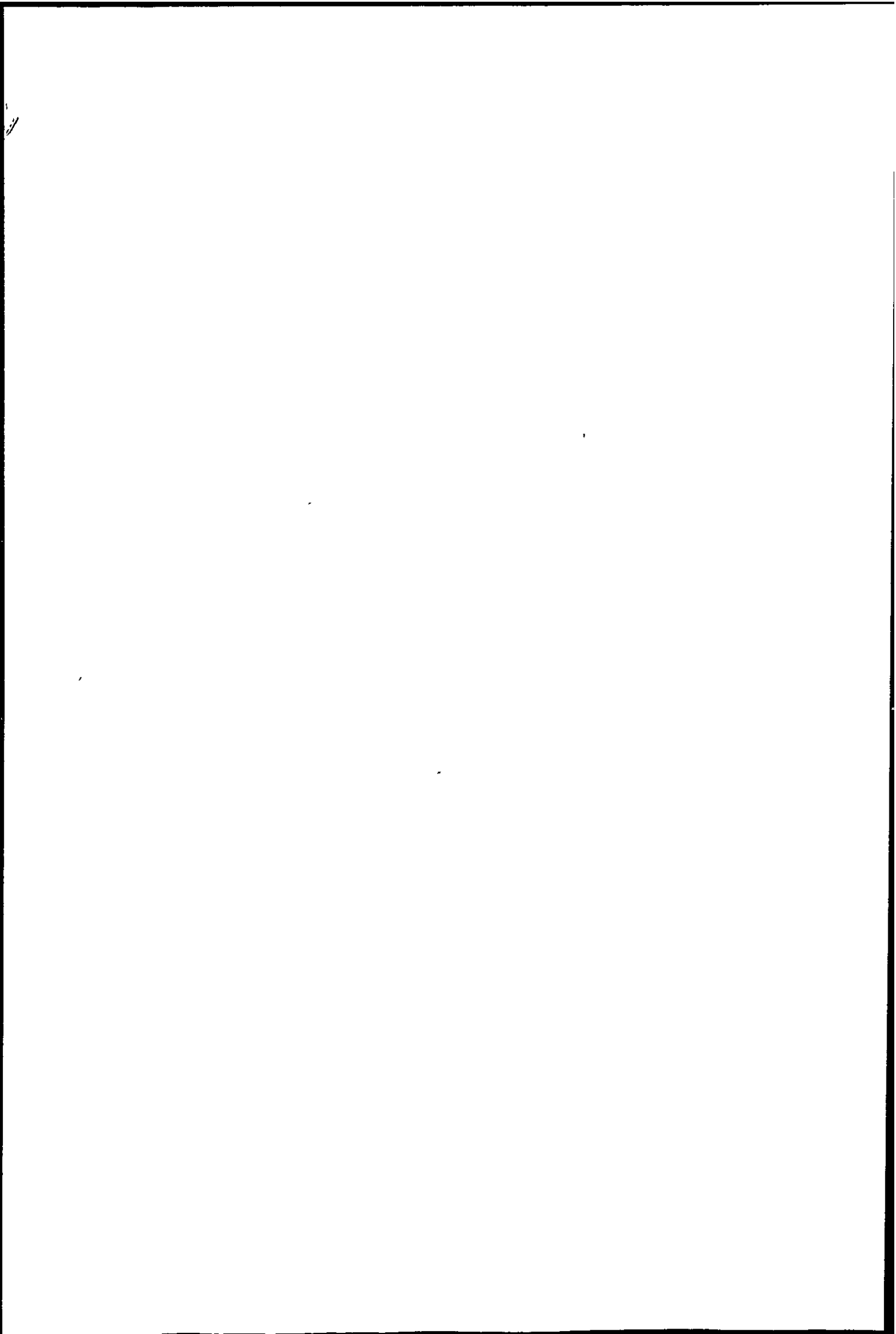
Richards and Tandy used CO_2/CO mixtures, extrapolating the rates to zero p_{CO}, which might account for the higher values of the present work.

The rate of reaction of B_2O_3 doped coke at lower temperatures (1162 ^oC) reached a maximum then fell. Above 1213 ^oC the oxidation curves were of similar shape to those of the undoped coke, and as seen in Figure 5.4.b the rate of reaction of the doped coke approached that of the untreated. The value of E_A calculated from the lower temperature results is 192 kJ mol^{-1}.

Above about 1150 ^oC the inhibiting effect of B_2O_3 diminishes. Below this temperature B_2O_3 treatment greatly reduces the reactivity of Nantgarw coke. Lumps which have merely been soaked in B_2O_3 solution show a reduced rate of reaction to CO_2 at 1000 ^oC. The rates of reaction of Cwm and Polish coke are also greatly reduced by B_2O_3 doping. Rates at 955 ^oC can be compared (Tables 5.4.g and i.) as lumps and granules react similarly at this temperature.

In the CO_2 gasification of the Australian brown coal char Figure 5.4.d shows diffusion becoming rate limiting at about 950 ^oC. B_2O_3 doping reduces the char reactivity in the zone of predominantly chemical control of rate, but as to be expected has no effect when diffusion of CO_2 becomes rate limiting. If the inhibition is less at higher temperatures the effect is hidden by the control of in-pore diffusion.

Values of the kinetic parameters for the coke and the char are summarised in Table 5.4.k. The great difference in coke and char reactivity is reflected in the values of the pre-exponential factor A. The difference in E_A values between doped and untreated material, although greater for the char, is within the possible experimental error in determining E_A. Thus the presence of B_2O_3 does not appear to significantly alter the activation energy of the Boudouard reaction.

Material	E_A(kJ mol^{-1}) $\pm$ 20 kJ mol^{-1}	A(g s^{-1} g^{-1})
Nantgarw coke	186	4×10
B_2O_3-doped Nantgarw coke	192	1.3×10^2
Australian brown coal char	194 (in chemical control zone)	6.3×10^4
B_2O_3-doped char	231 (in chemical control zone)	2.5×10^6

Table 5.4.k. Kinetic Parameters for the Boudouard Reaction.

It has been stated (Chapter 2, reference 2) that at high enough temperatures all cokes have equal reactivities. This is likely to be when the nature of the carbon surface does not govern the rate of reaction, i.e. when diffusion of CO_2 does govern the rate. Comparing the coke and char results (plotted together in Figure 5.4.h) this may happen at about 1600 $^{\circ}$C, which may

be reached in the hearth zone of the blast furnace. Thus 1000 $^{\circ}$C is chosen for coke "reactivity" tests as it is the lowest temperature at which rate of reaction may be measured in a convenient time and where diffusional effects are a minimum.

Thus it would be expected that in the air oxidation of cokes they would have equal "reactivities" above about 650 $^{\circ}$C and this is borne out for Nantgarw, Cwm and Polish cokes as shown in Table 5.3.j.

Figure 5.4.g compares the three cokes in the Boudouard reaction at 955 $^{\circ}$C, the initial rate of reaction being similar to the industrial reactivity test value (where moist CO_2 is used). The "Nantgarw ratio" is maintained for Polish coke but decreases for Cwm coke. Above 60% burn off the build up of ash is likely to affect the rates of oxidation.
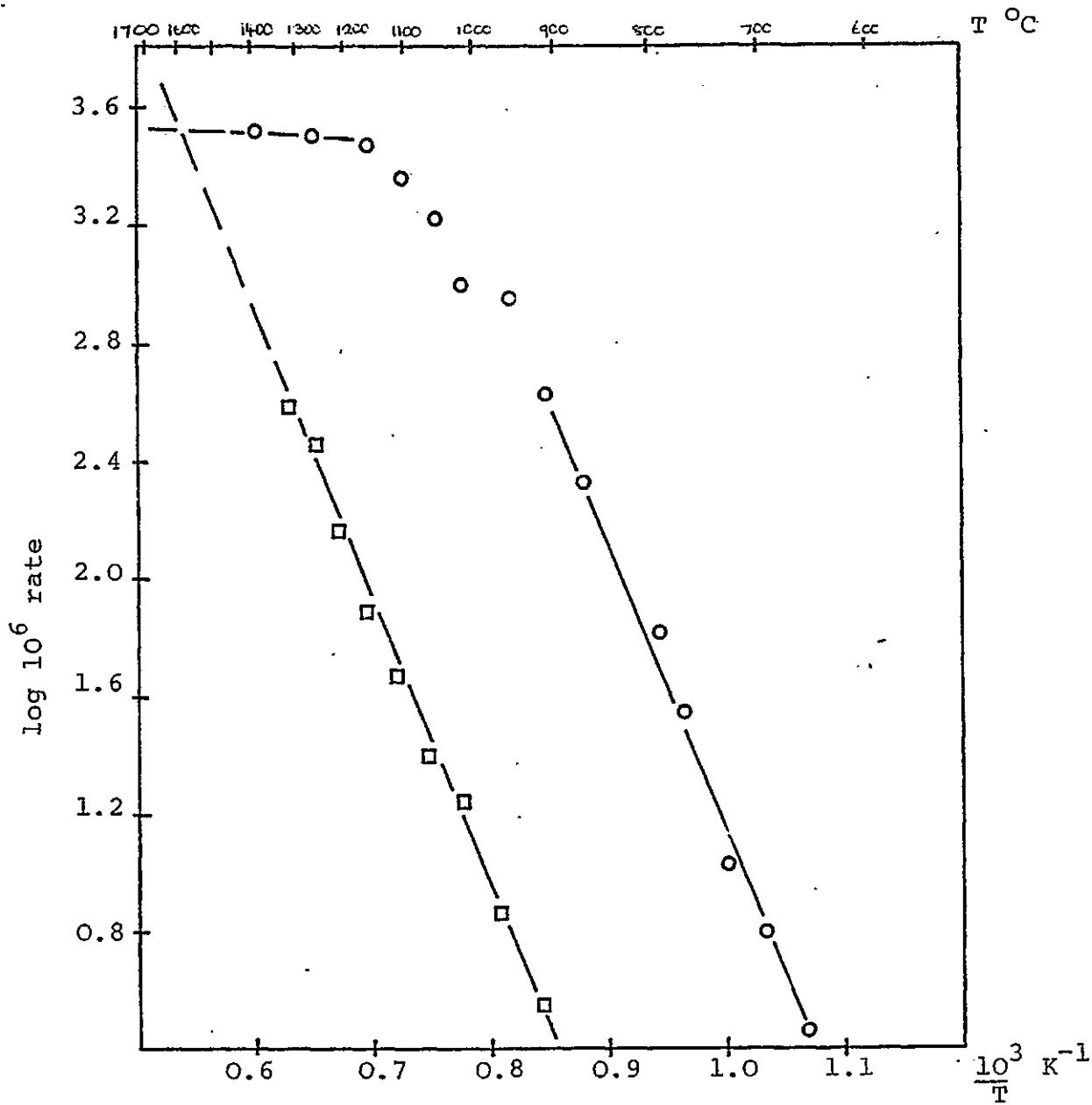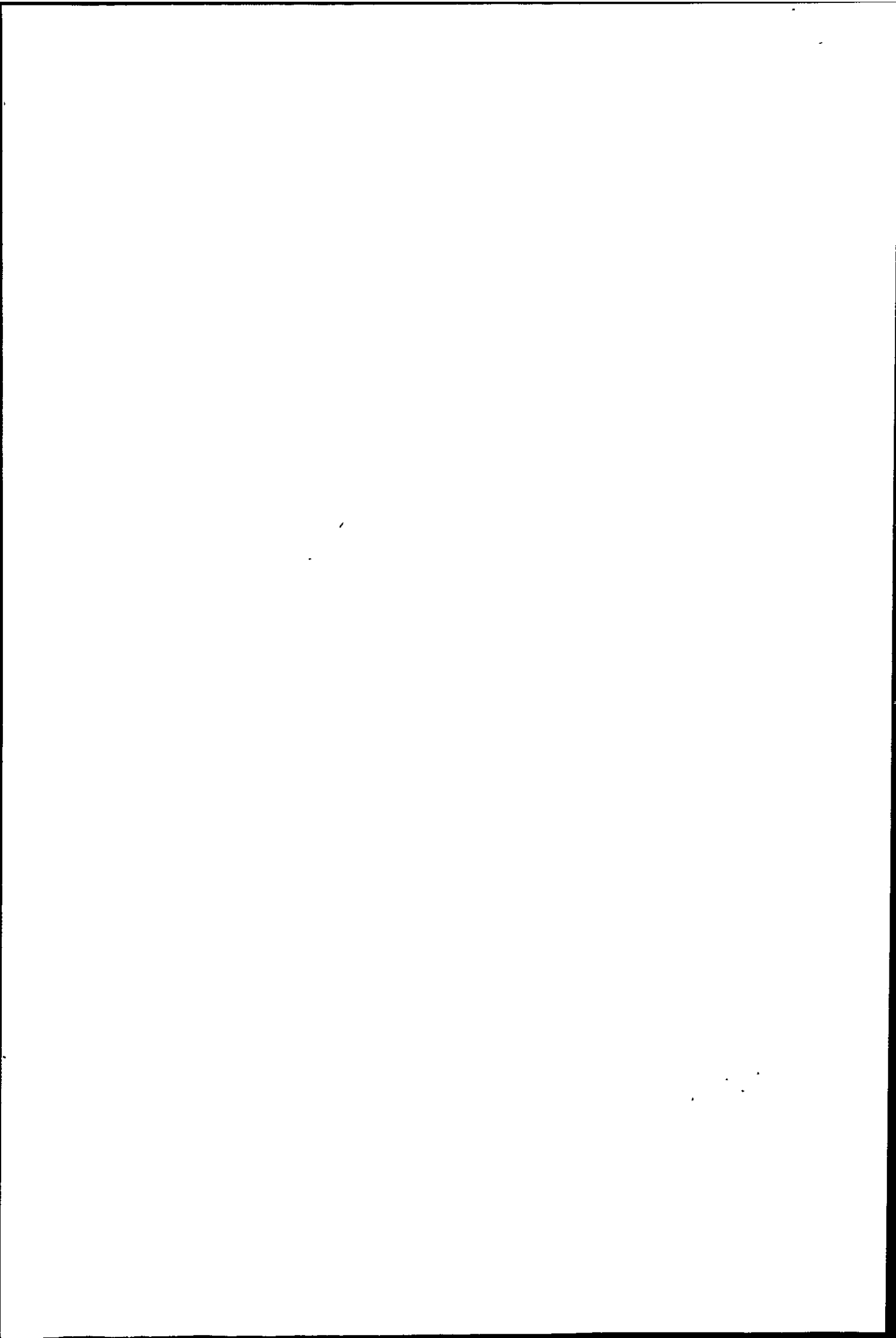
Figure 5.4.h. Estimation of Isokinetic Temperature for
Coke and Char in the Boudouard Reaction.

squares — Nantgarw metallurgical coke
circles — Australian brown coal char.

5.5 Mathematical Analysis

The previous results have indicated over what temperatures chemical or diffusion control operates for Nantgarw coke and Australian brown coal char oxidation in air and in CO_2.

Under chemical reaction control, for shrinking non-porous particles, the "conversion function" of time/(time of complete reaction) is given by $1-(1-X)^{1/F}$ where X is the fraction reacted and F a shape factor which is 1, 2 and 3 for infinite slabs, long cylinders and spheres respectively, as discussed in Chapter 1.3.1. The surface of the coke lumps, as shown by SEM (Plate 4.1) contains regions of cylinder-like geometry. In the first half of the burn-off, before surface ash accumulates, it is possible to compare the experimental oxidation values (from the appropriate temperatures) of air or CO_2 burn off with those calculated from this equation.

The formulae for diffusion control with the same surface geometries also given in Chapter 1.3.1.

An arbitrary time of complete reaction of 15 hours was chosen and for values of X from 0.05 to 0.95 at 0.05 intervals the reaction time t was calculated and values of X versus t plotted for the 3 surface geometries under both chemical and diffusion control. The programme for the calculation was written in Fortran 77 (Appendix 1) on the PRIME system and the data plotted by a Calcomp plotter. The curves for the models under chemical and diffusion control are shown in Figures 5.5.a and b respectively.
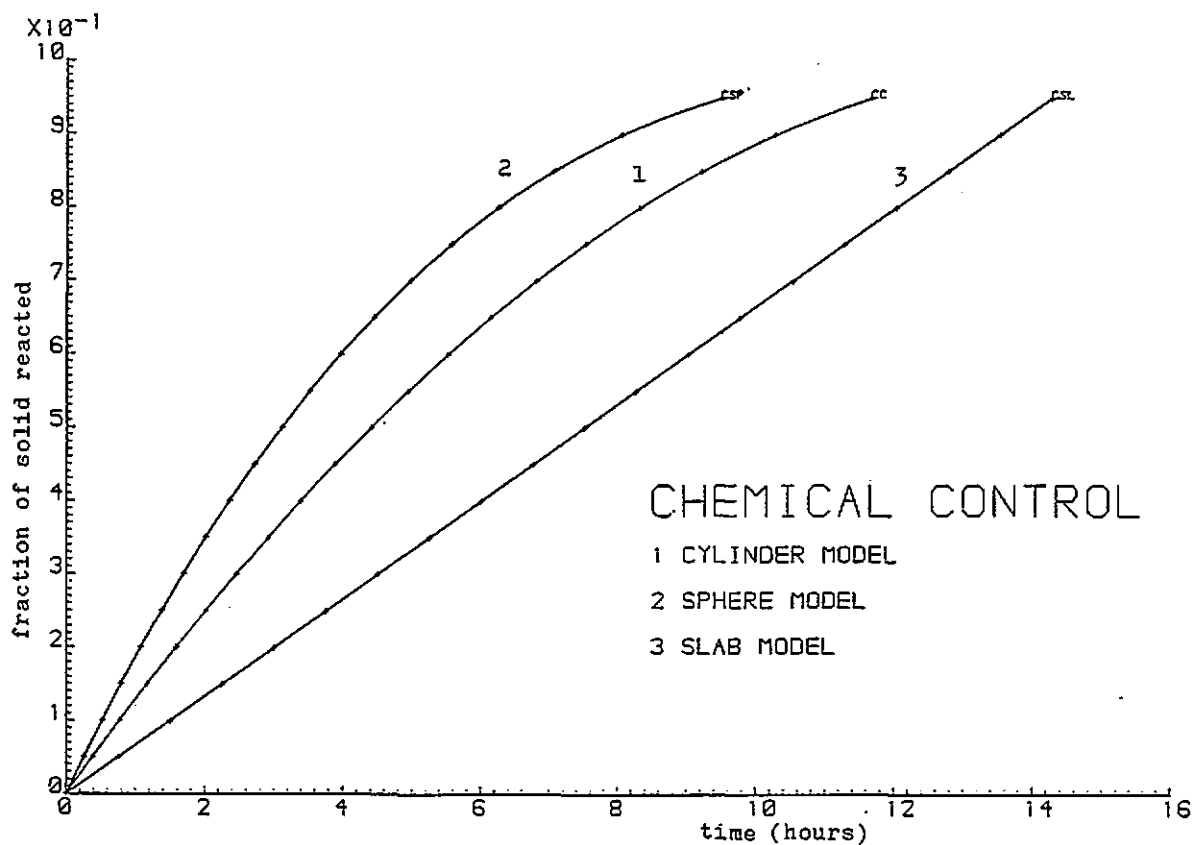
238

Figure 5.5.a. Fractional conversion of a non porous
solid with time, for different surface geometries,
when rate of gasification is under chemical control.
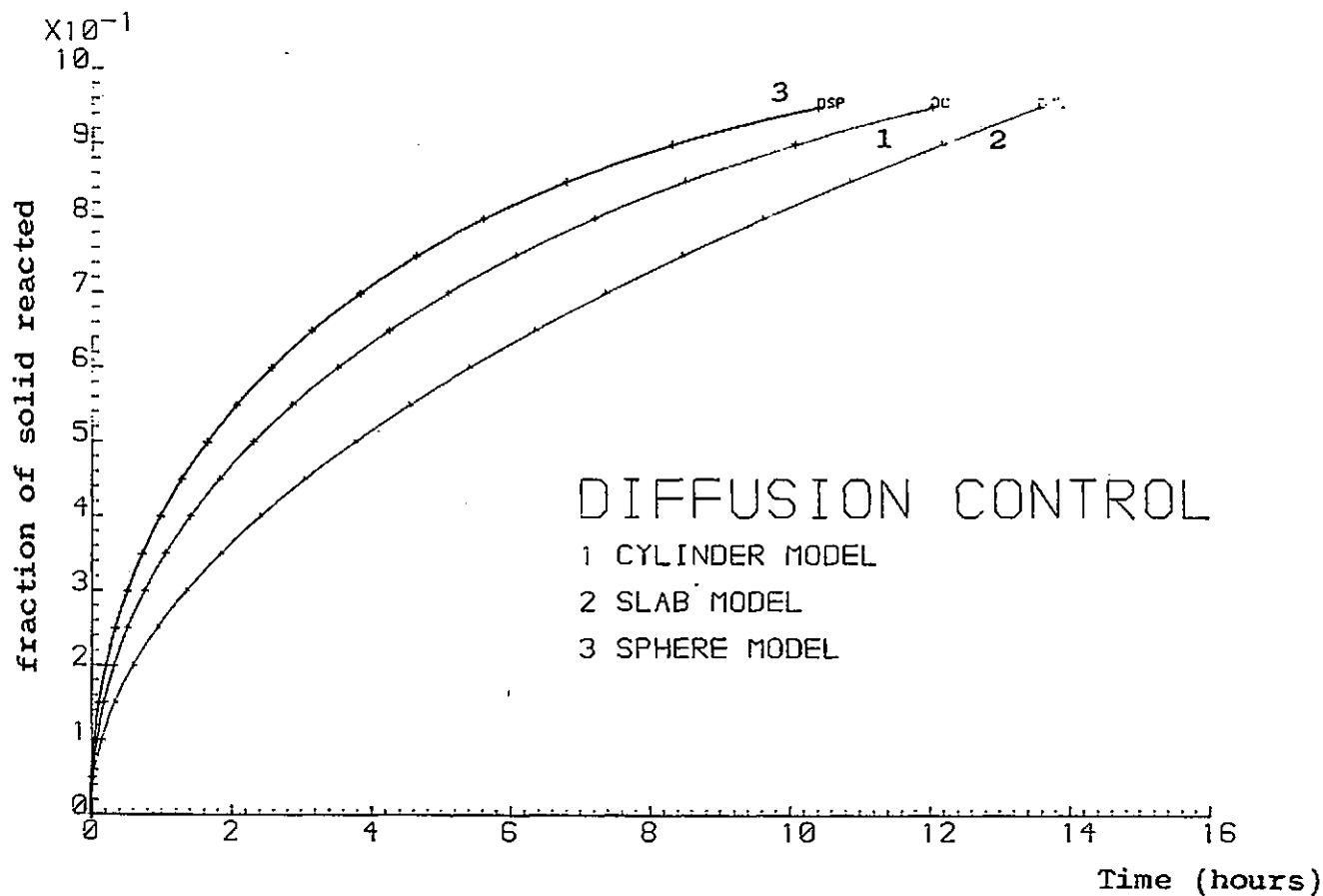(Time of complete reaction taken as 15 h.)

Figure 5.5.b. Fractional conversion of a non-porous solid with time, for different surface geometries, when rate of gasification is under diffusion control. (Time of complete reaction taken as 15 h .)

Because the ratio of the original surface area to volume of the particle enters the chemical control equation (in a linear fashion) the time to burn off a particular fraction can be seen to be shortest for spheres and longest for slabs. The time of complete reaction is also proportional to the initial size of the particle. For diffusion control the time taken to burn off a particular fraction is shortest for spheres and longest for slabs.

From the oxidation curve of CO_2 gasification of Nantgarw coke at 1212 $^{\circ}C$ the times taken to react fractions 0.05 to 0.50 at 0.05 intervals were tabulated. Time of complete reaction was 2.70 hours, giving a time of half reaction of 51 min. Values of reduced time were then plotted versus the functions for cylinders and spheres under chemical control of rate as shown in Figure 5.5.c. Similar graphs were obtained for the air oxidation of Nantgarw coke below 670 $^{\circ}C$. Better correlation is seen from the cylinder than the sphere model, although the latter gives a linear plot above 0.15 fraction reacted. In this initial burn off the maximum surface develops for Nantgarw coke, as described in Chapter 6, and the assumption of a non-porous solid is probably least justified in the initial part of the burn off.

Similar correlation with the cylinder model in the air oxidation of graphite flakes under diffusion control was obtained by Ozgen and Rand[2].

Although the surface of the coke is very irregular the application of the models for simple geometries can be useful.
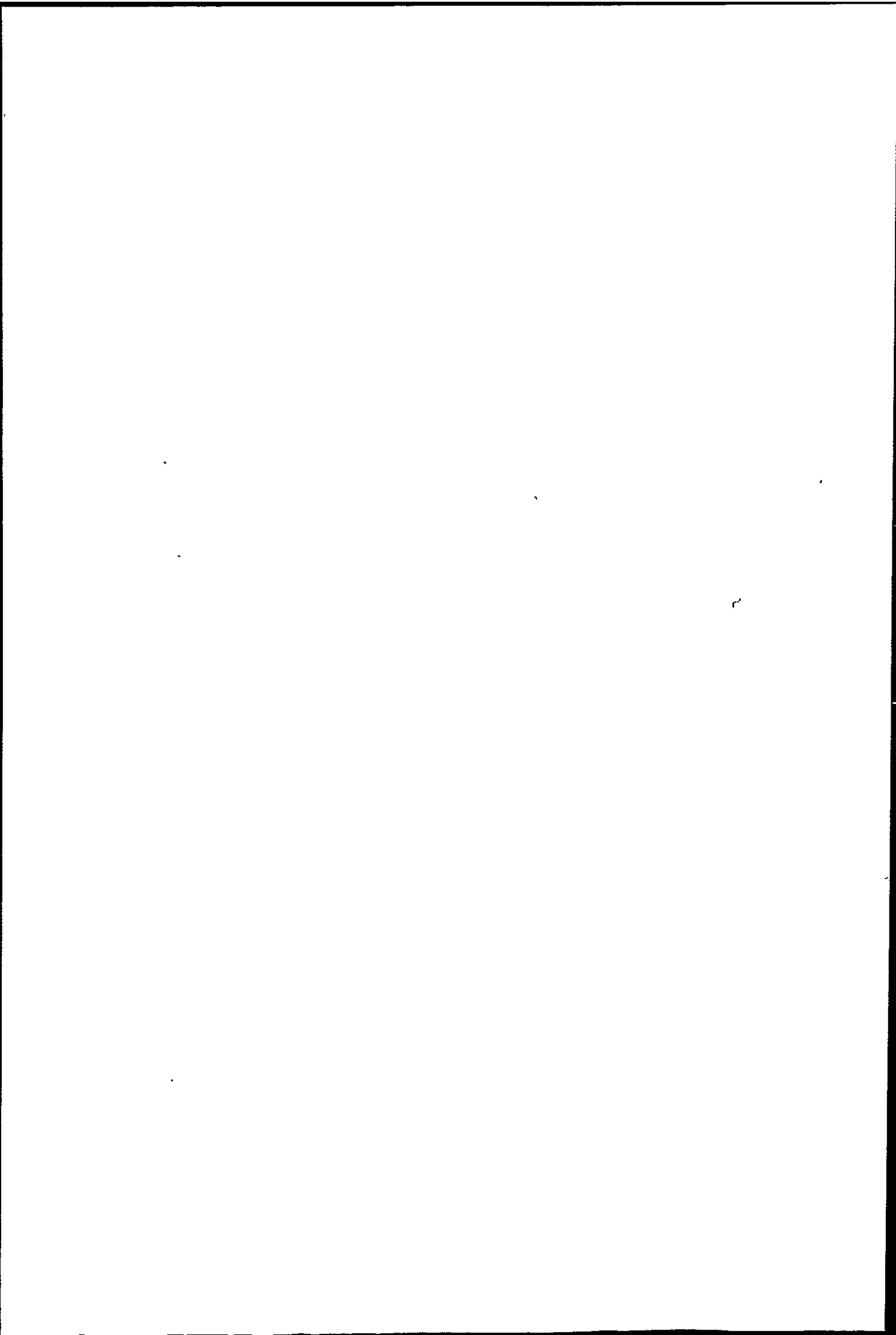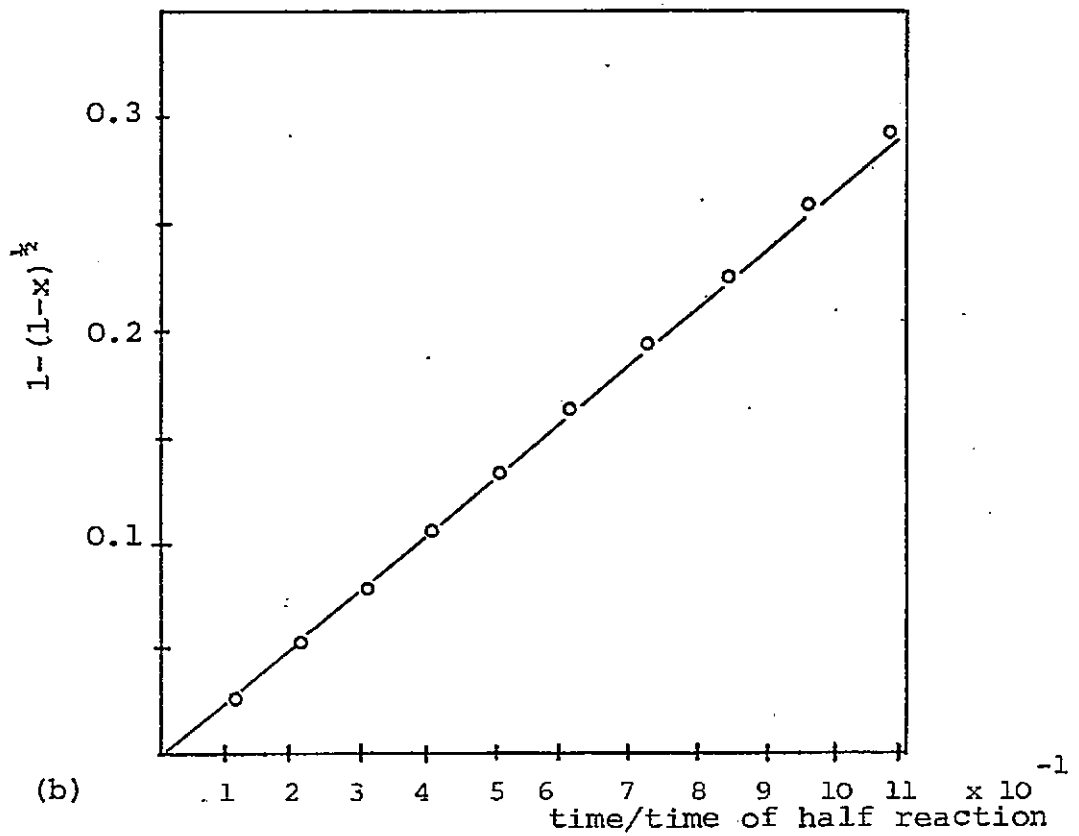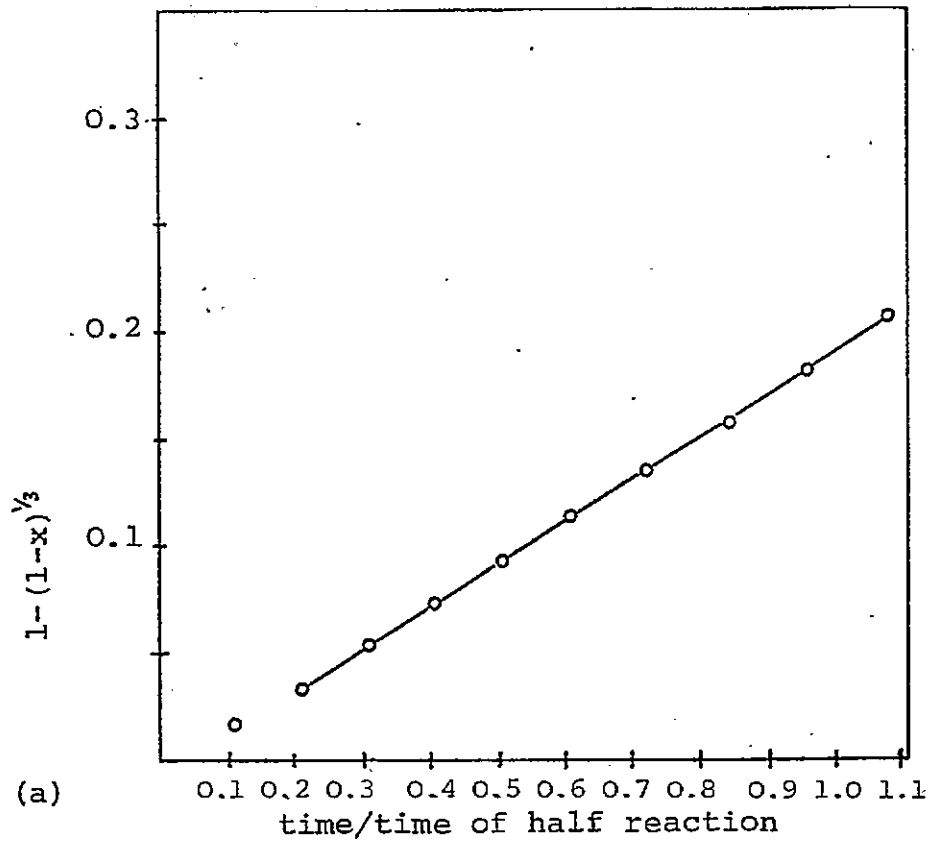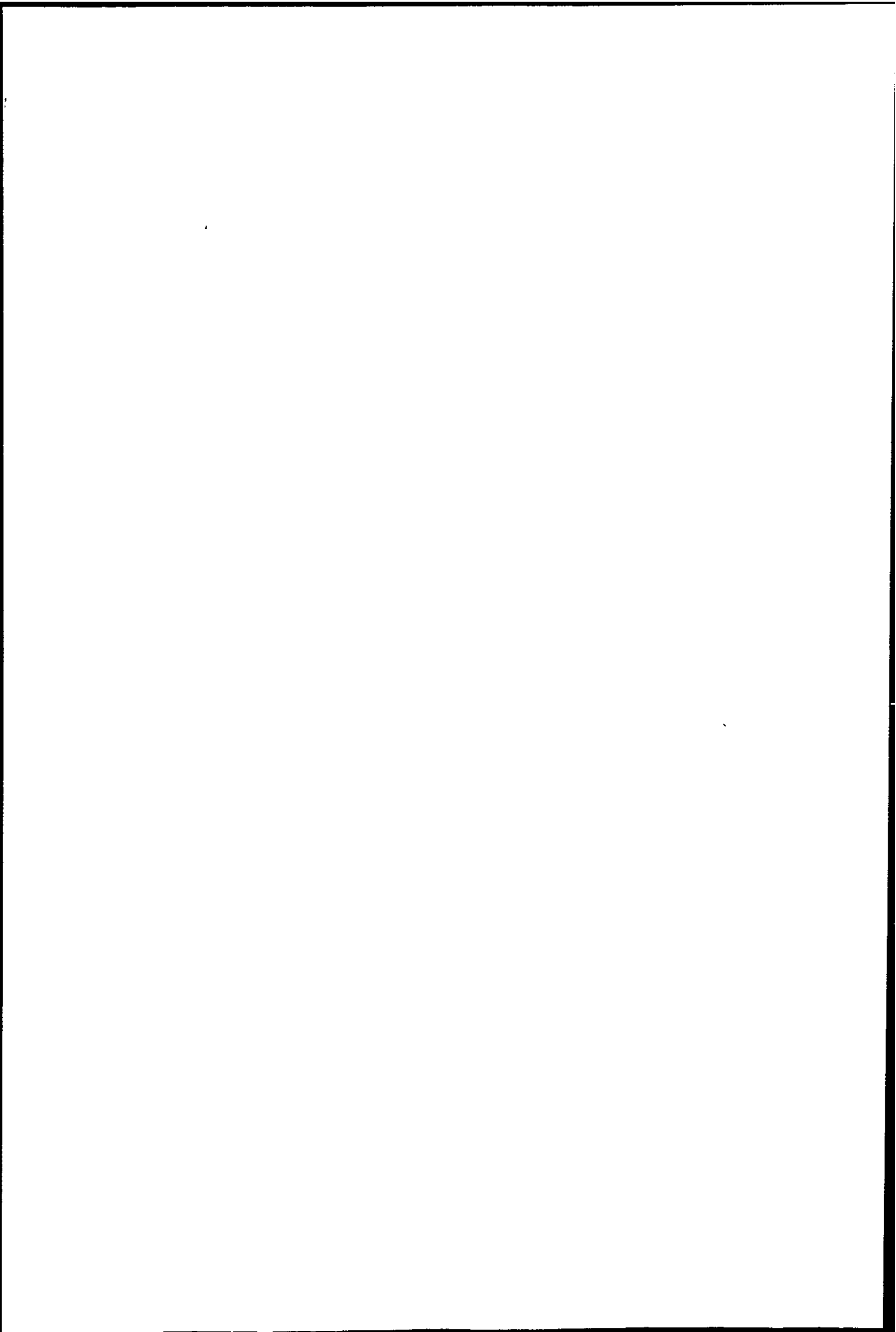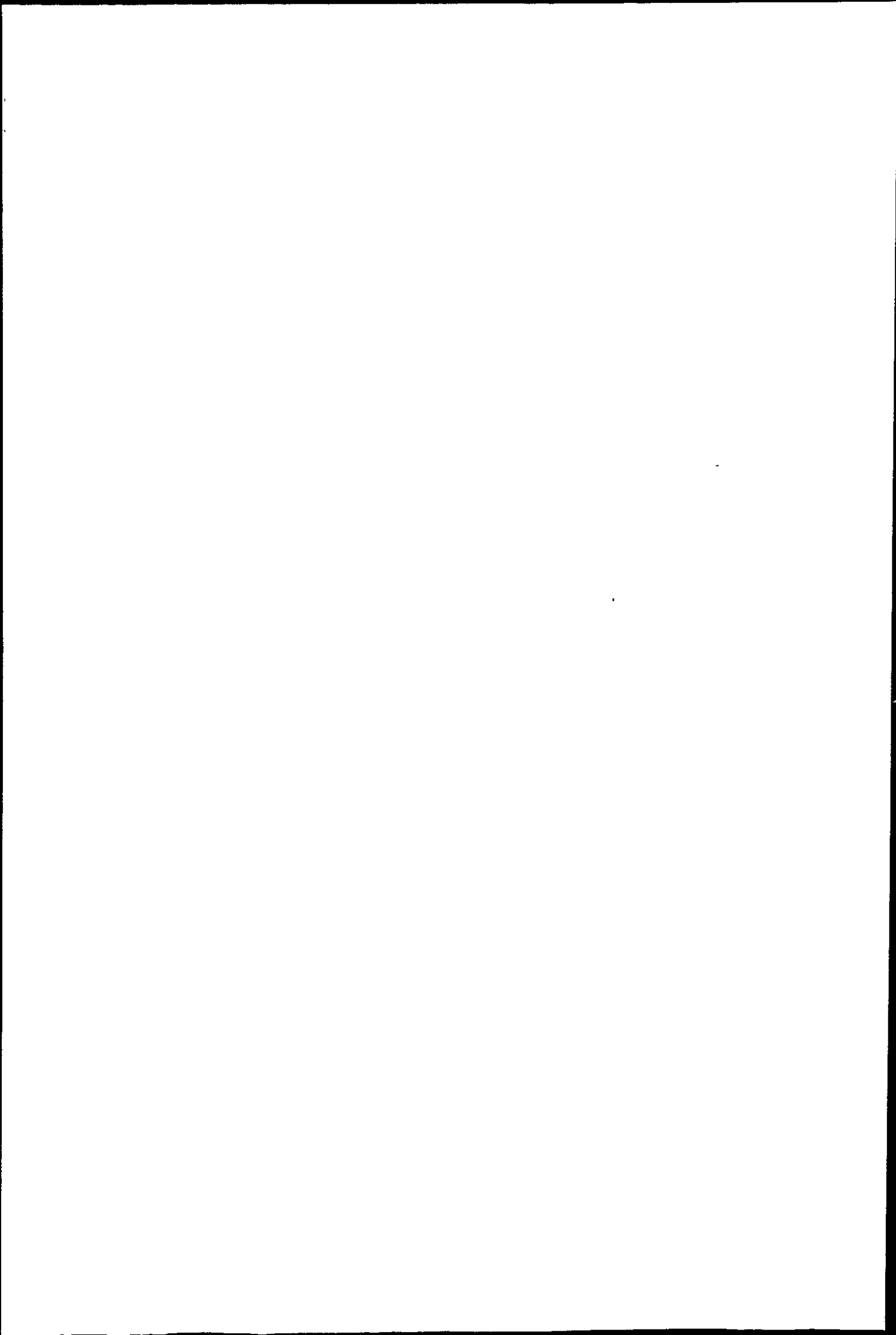
Figure 5.5.c Reduced Time Plots for CO_2 oxidation of
Nantgarw Coke lumps at 1212 $^{\circ}C$.

(a)   Sphere model
(b)   Long cylinder model

REFERENCES

1. J.W. Mellor "Inorganic and Theoretical Chemistry",
    Longmans, 1946, Vol.5. Chapter 32, p.41.

2. S. Ozgen and B. Rand, "Carbon '82", extended abstracts
    of papers, 6th London International Carbon and
    Graphite Conference. 1982, SCI London, 139-41.

CHAPTER SIX

SURFACE AREA CHANGES OF GASIFIED

COKES AND COAL CHAR

6.1   Introduction

6.2   Review of Surface Area Studies on Cokes and
        Brown Coal Chars.

6.3   Experimental Procedure.

        6.3.1   Nantgarw Coke Study

        6.3.2   Comparative Coke Reactivity Study

        6.3.3   Brown Coal Char Study

6.4   Surface Area of original and B_2O_3-doped
        Nantgarw Coke Gasified under Various Regimes.

        6.4.1   Results

        6.4.2   Discussion

6.5   Comparative Reactivity Study of Three Metallurgical
        Cokes.

        6.5.1   Results

        6.5.2   Discussion

6.6   Surface area Study of Australian Brown Coal Char.

        6.6.1   Results

        6.6.2   Discussion

6.1   Introduction.

Coals, cokes and chars are highly porous materials. For the quantitative characterisation of internal pore structure, the pore volume, surface area and pore size distribution need to be estimated. A large pore volume does not always imply a large surface area, since this is dependent on the pore size distribution. Pores are classified as macro ($r \geqslant 25$ nm), meso ($r = 1$ to 25 nm) and micro ($r \leqslant 1$ nm) where r is the pore radius.[1]

Active carbons differ in properties from other porous materials in that

(i) they have a wide range of pore sizes,

(ii) due to the non-polar nature of carbon, dispersion

forces play a large part in adsorption.

Measurement of surface area by gas sorption rests on the determination of the monolayer capacity (x_m). When this quantity is multiplied by the area occupied by a single adsorbed molecule (A_m) the surface area in $m^2 g^{-1}$ is calculated from $S = \dfrac{x_m \, NA_m \times 10^{-20}}{M}$ when A_m is in square Angstrom units, N is the Avogadro constant, M is the molecular weight of adsorbate, and x_m is expressed in g adsorbate per g of solid. It is assumed that the adsorbate molecules close pack on the surface. Calculation of adsorbate cross sectional areas (from liquid density, critical constant data etc.) is discussed by Gregg & Sing[2] and with respect to carbons by Sutherland.[3] Values of 16.2 $\overset{o}{A}^2$ for N_2 and 17.0 $\overset{o}{A}^2$ for CO_2 were taken in the

present work, at 77 K and 196 K respectively.

In characterising a solid by physical adsorption measurements, some model of the adsorption process must be applied. In Langmuir's original treatment a kinetic approach led to the isotherm.

$$x = \frac{x_m b p}{1+bp}$$ where b is an adsorption coefficient

and x is the amount sorbed per g adsorbent at equilibrium pressure p. The same isotherm may be derived on statistical mechanical grounds. Thus a graph of $\frac{p}{x}$ versus p is linear and x_m may be calculated from the slope. Langmuir's equation was used in the present work to evaluate surface areas of the original, burnt off and doped Australian brown coal char, where Type I isotherms were obtained (described in Chapter 4). The equation cannot be used successfully on non-porous or wide pore adsorbents due to multilayer formation and/or capillary condensation.

For the cokes studied in this work where Type 2 isotherms were found, surface areas were estimated from the BET equation using N_2 sorption at 77 K. Derivation and discussion of the BET equation is given by Gregg[4] and by Lowell[5]. The equation was used in the form

$$\frac{p}{x(P_o-p)} = \frac{1}{x_m c} + \frac{(c-1)}{x_m c} \frac{p}{P_o}$$

where x is the amount sorbed per g adsorbent at equilibrium pressure p, p_o the S.V.P. of the adsorbate and c is a constant equal to $\exp(\frac{E_1-E_2}{RT})$. E_1 is the heat of adsorption of the first layer and E_2 that of subsequent

layers (and taken as the heat of liquifaction of the adsorbate).

Thus a plot of $\frac{p}{x(p_0-p)}$ versus $\frac{p}{p_0}$ should give a straight line of slope $\frac{(c-1)}{x_m c}$ and intercept $\frac{1}{x_m c}$. Adding slope and intercept gives $\frac{1}{x_m}$.

Adsorption onto porous materials often gives rise to hysteresis, i.e. the desorption branch of the isotherm differs from the adsorption. Observation of a reproducible isotherm hysteresis can be associated with a certain type of porosity in the adsorbent. The relationship between shape of hysteresis loop and pore geometry is classified by de Boer[6], who distinguishes 5 basic types based upon 15 idealised pore geometries.

Adsorption into wide pores can be treated by assuming that bulk condensation occurs in the pores and this is governed by the Kelvin equation. The S.V.P., p above a curved surface of a liquid in a capillary will be lower than that of the open surface p_0 and

$$\ln \frac{p}{p_0} = -\frac{2\gamma V}{rRT} \cos \theta$$

where γ is the surface tension of the liquid, V the molar volume, r the radius of the capillary and θ the angle of contact of liquid and solid. Often θ is taken as zero. In practice a finite desorption step is considered, giving a method of calculating pore size distribution. For non-intersecting cylindical pores the mean pore radius $r = \frac{2V_p}{S}$ where V_p is the total pore volume and S the surface area of the pores. The use of this formula fails to give a real value of r below a certain minimum as x_m

247

(in volume units) $\rightarrow V_p$.

The concept of surface area for microporous adsorbents is often criticised. Instead of layer by layer filling (implied in the BET treatment), Dubinin[7] suggested that adsorption results in volume filling of pores, due to an adsorption force field in the entire volume of micropores. This is based on the approach of Polanyi to the force of adsorption as an intermolecular potential gradient. The adsorption potential at a point at or near the surface of the adsorbent being defined as the isothermal work done by the adsorption forces in bringing a molecule from the bulk gas to that point. Micropores are commensurate with the size of adsorbed molecules and the adsorption must depend on the nature of the system as a whole. The fundamental equation of the Dubinin approach is

$$W = W_o \exp\left(- \frac{A}{E}\right)^n$$

where A is $RT \ln(\frac{Po}{p})$, W_o is the mass of gas adsorbed when all the micropores are filled and W the mass of gas adsorbed at a particular relative pressure. E is a characteristic free energy, depending on the system and n is a small integer. No physical meaning is ascribed to n. When n=2 the equation becomes the well known Dubinin-Radushkevich (D-R) equation

$$W = W_o \exp\left\{- B\left(\frac{T}{\beta}\right)^2 \log^2\left(\frac{Po}{p}\right)\right\}$$

where B is a structural constant and β an affinity constant ie quantities that depend on the nature of the adsorbate and adsorbent.
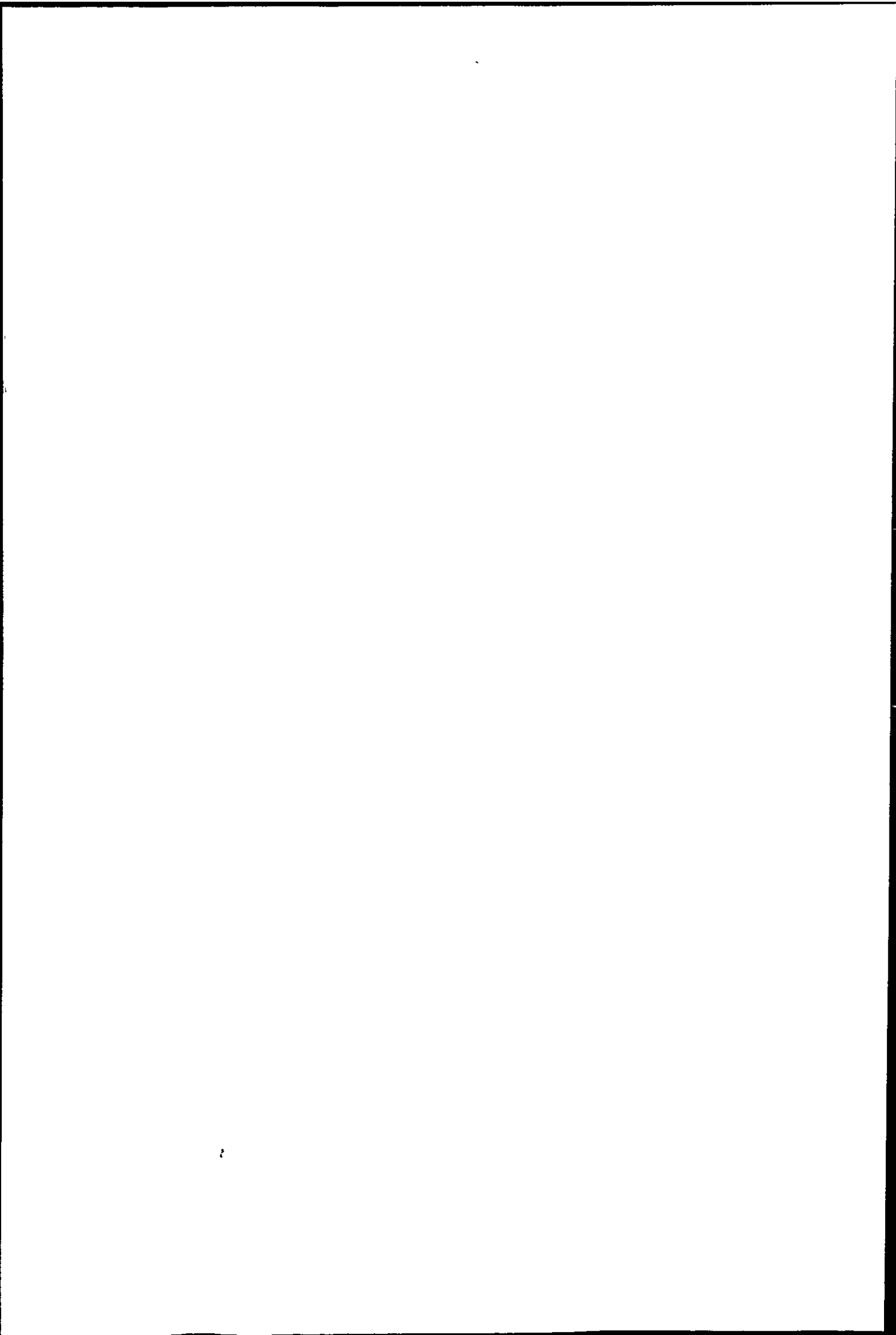
In the present work open micropore volume of the char was calculated using the equation in the form

$$\log W = \log W_o - D \log^2(\frac{P_o}{P})$$

where $D = 2.303 \frac{BT^2}{\beta^2}$.

Thus W_o was evaluated from the intercept of a plot of $\log W$ versus $\log^2(\frac{P_o}{P})$. To obtain the micropore volume from W_o the liquid density was used. The D-R equation applies to a homogeneous system of micropores and strictly should be summed for the contributions for each class of micropore.

6.2 Review of Surface Area Studies on Cokes and Brown Coal Chars.

Microporosity in carbonaceous materials is reviewed critically by Marsh and Rand[8], who consider coals and their resultant cokes as "essentially microporous materials". N_2 adsorption at 77 K is considered to give unrealistically low values of surface area and CO_2 at 195 K not completely satisfactory results. Two linear portions of the Dubinin-Radushkevich plot are often found for cokes, coals and polymer carbons depending on degree of burn off.

The inadequacy of N_2 at 77 K to obtain surface areas of coal products is discussed by Marsh[9], Lamond and Marsh[10] and Marsh and Wynne-Jones[11]. Anderson[12] et al compare N_2, CO_2 and methanol as adsorbates on carbons and coals, computing surface areas from the BET or Langmuir equation.

Chiche et al[13] examined the porosity of two cokes by CO_2, H_2O and methanol adsorption in relation to that of the parent coals. Carbonisation was performed more slowly and at a lower temperature than that used industrially, resulting in cokes with some microporosity. The D-R equation was used to evaluate pore changes on carbonisation.

Surface area changes of several cokes on gasification by CO_2 and H_2O at 1000 °C were studied by Bastick and Guerin[14] by N_2 adsorption at 77 K, up to 60% burn off. Specific surface area passed through a maximum at about 20% burn off, which was somewhat greater for H_2O than CO_2

gasification. This surface area development was greater for coke granules (0.75 mm) than coke lumps (15 mm). From a consideration of pore size distribution surface area increased by disappearance of separating walls between the smaller pores.

The surface area of a metallurgical coke on reaction with O_2 at 475 ^{o}C and 550 ^{o}C and CO_2 at 875 ^{o}C and 950 ^{o}C was measured by Grillet and Guerin[15] at 10%, 25% and 50% burn off. Surface area development was essentially the same, being greatest for the 25% burn off and least for the 50% samples.

Formed coke and a calcined char were reacted in CO_2 at 900 ^{o}C and surface area changes investigated by Blake et al.[16] as part of a reactivity study. Specific surface area, determined by BET N_2 sorption was initially high (200 m^2g^{-1}) and increased continuously up to approximately 60% burn off.

Rates of gasification in CO_2 at 950 ^{o}C and surface area development were investigated by Fassotte and Saussez[17] in a comparative study of metallurgical and formed cokes. Surface areas were determined by H_2O adsorption at 25 ^{o}C. The low reactivity of metallurgical coke was attributed to low initial surface area which developed only slightly during gasification, in contrast to that of the formed cokes.

Thus coke surface areas have been measured after partial gasification by several workers. Changes in surface area may be expected to reflect structural changes

251

by the oxidising gas and be useful in assessment of coke degradation in the blast furnace.

Many studies have been made on porosity and surface area changes in gasification of polymer chars and coal chars. Cameron and Stacy[18] describe the pore structure of brown coal chars as made up of two distinct pore systems.

The development of porosity in brown coal chars on activation with CO_2 between 1123 K and 1273 K was studied by Berger et al[19] by benzene and CO_2 sorption at 298 K and mercury porosimetry. High surface area was associated with micropores and very narrow mesopores. Activation resulted in a well developed macropore system. The reactivity of coal chars in general is influenced by the level of macro and transitional porosity. Chars which contain a high proportion of these "feeder" pores allow reactant gas to diffuse to the internal surface of the micropores. Gray and Misra[20] consider macropore structure to primarily determine char reactivity by controlling rate of access of CO_2 to the internal surface.
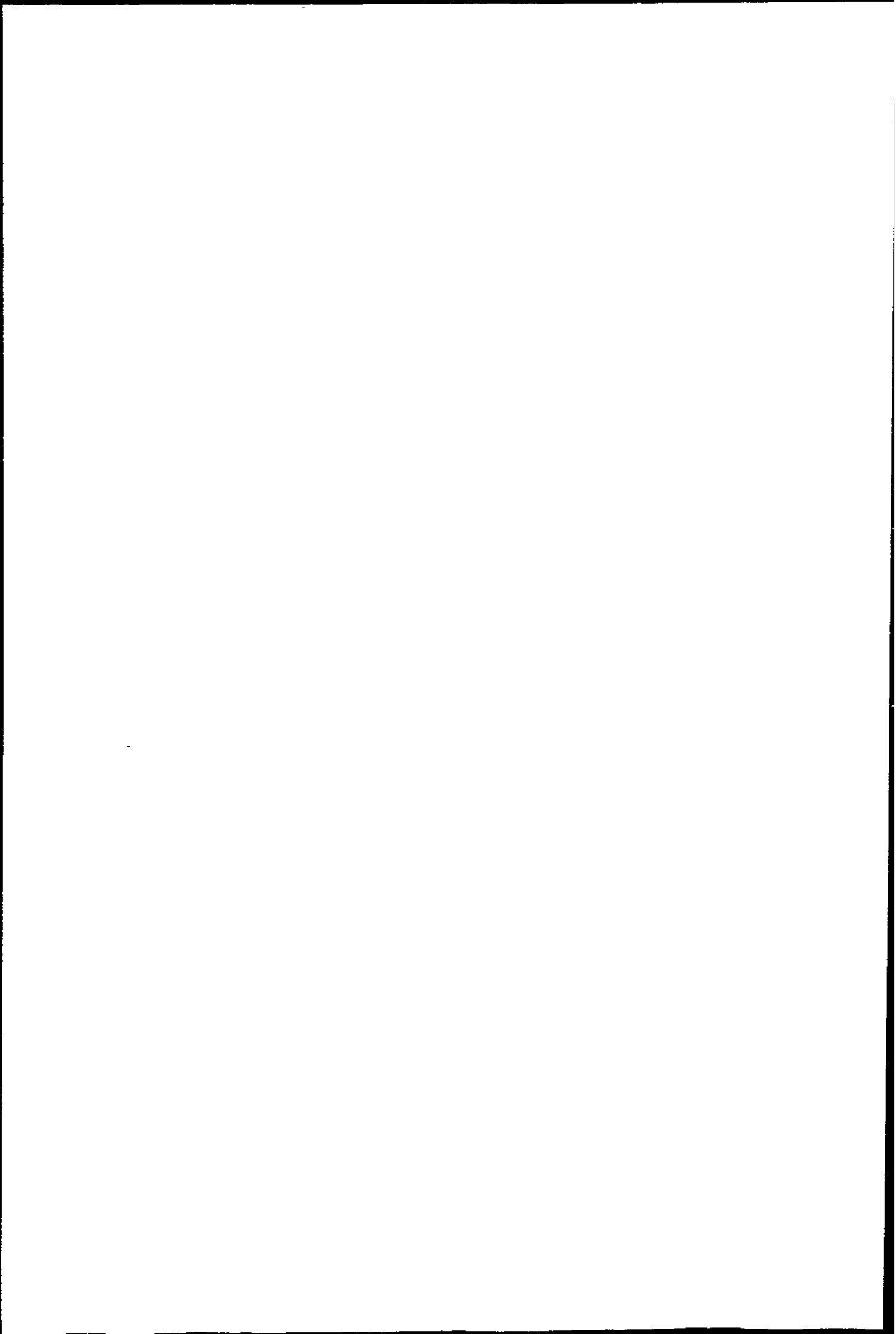
## 6.3 Experimental Procedure

6.3.1 Nantgarw Coke Study

Surface areas of 5 mm Nantgarw coke lumps and B_2O_3 doped coke lumps gasified by air or CO_2 at several temperatures were determined by N_2 sorption at 77 K using the BET equation. Measurements were made using the apparatus described in Chapter 3.2.1. The SVP of nitrogen at 77 K was taken as 1 atmosphere plus a small correction (26 mm Hg) for thermal loss, which had been determined by previous calibration. The cross sectional area of N_2 was taken as 16.2 $\overset{o}{A}^2$ at this temperature, thus the area occupied by 1 g is 3.483×10^3 m^2. Where 0.25 g of sample was not available aluminium counterweights were added to the sample bucket and the appropriate buoyancy calculated for each sample. The vacuum balance was first calibrated using N_2 at room temperature to determine the volume displaced by counterweight, bucket and pyrex hangdown threads. The buoyancy correction was particularly important on samples of low surface area (~1 m^2g^{-1}), its effect often outweighing the gas uptake especially at higher relative pressures. Samples were outgassed at room temperature for at least 40 min., although loss on pumping out was small (0.1 mg).

Samples of Nantgarw coke and doped Nantgarw coke were burnt off to various extents in air at 500 ^{o}C and 1000 ^{o}C in a muffle furnace using shallow alumina boats. A sample burnt off under static air on the Mass flow balance was used also.
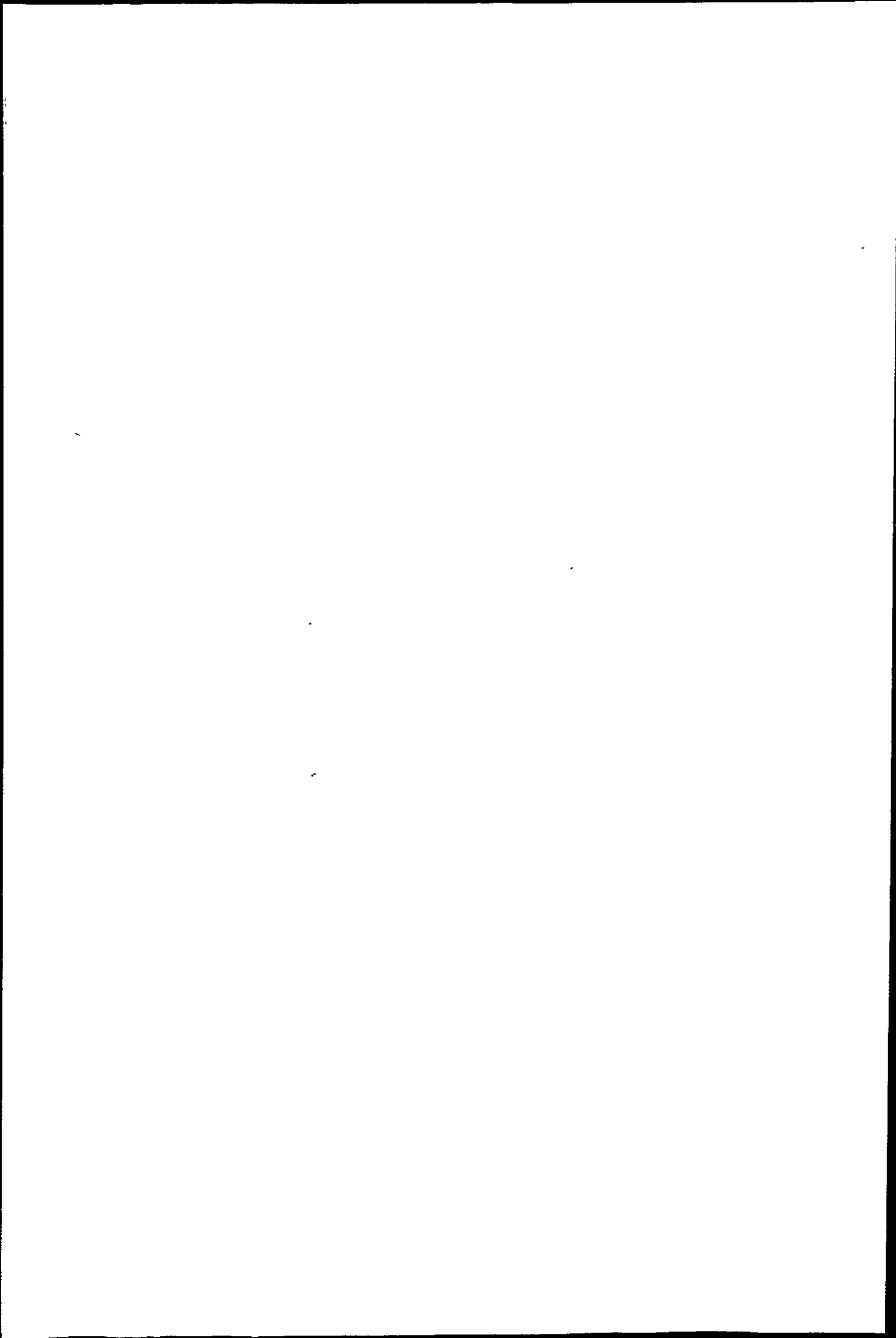
Samples were burnt off in dried CO_2 flowing at
40 cm^3 min^{-1} using the furnace of the Massflow balance
at 1000 ^{O}C, or a tube furnace at 1400 ^{O}C. Temperature
of the latter was checked with an optical pyrometer.
Several samples were heated at 500 ^{O}C, 1000 ^{O}C or 1400 ^{O}C
under nitrogen to determine the effect of heat treatment
alone.
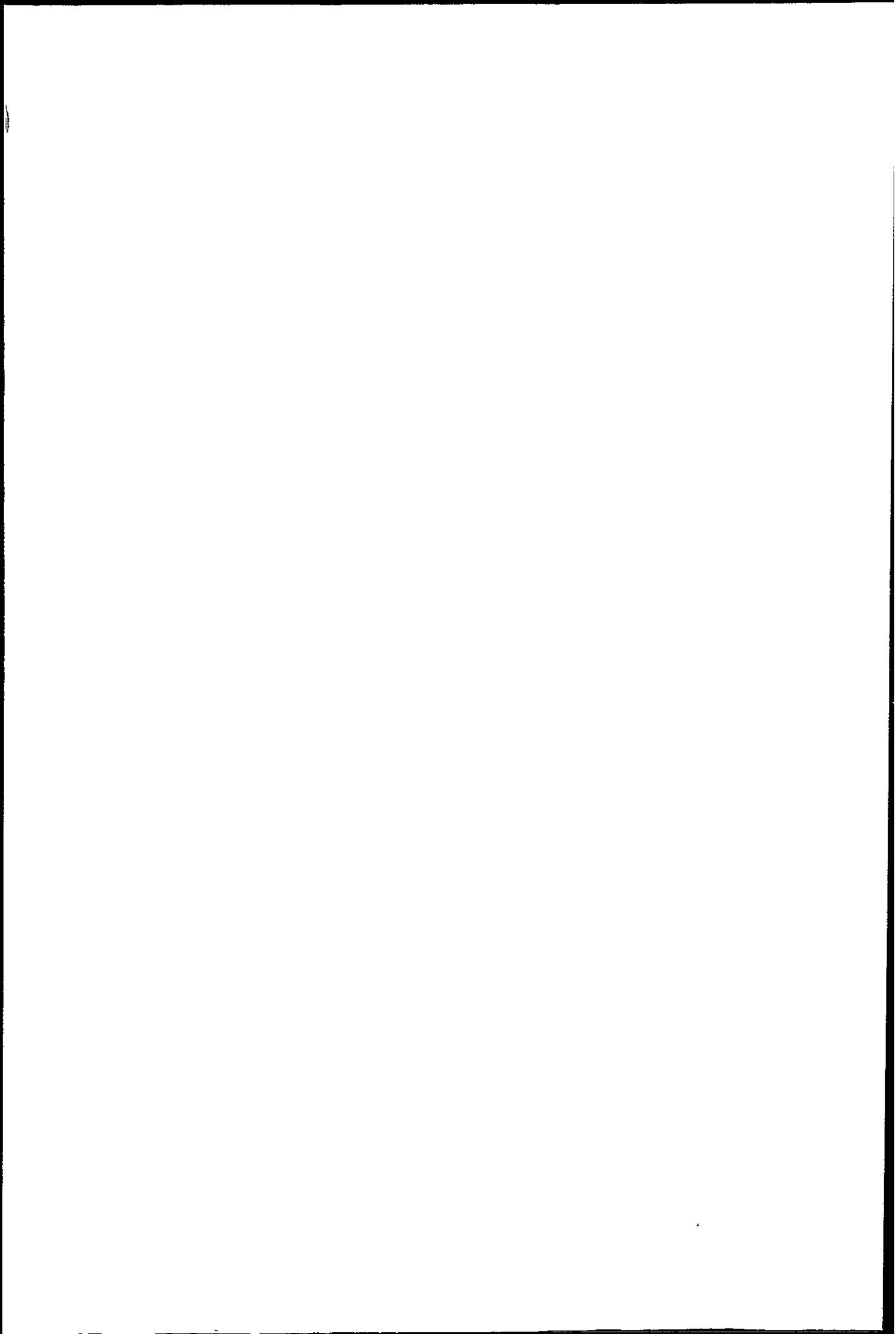
6.3.2 Comparative Coke Reactivity Study

Two other metallurgical cokes supplied by Imperial Smelting Processes (Cwm and Polish cokes) were studied. Initial surface area was determined after outgassing at 200 $^{\circ}$C. Adsorption work was performed on the vacuum balance described in Chapter 3.2.2, by N_2 sorption at 77 K. This balance had also been calibrated using N_2 at room temperature.

Samples for air oxidation were prepared in a muffle furnace. CO_2 burn off samples were prepared on the STA 781 thermal balance using the TG only hangdown and furnace at 1000 $^{\circ}$C. All subsequent CO_2 burn off samples were prepared on this instrument, where burn off was continuously monitored, allowing preparation of a better spaced set of burn off samples.

Doped samples were from the same batch, prepared as described in Chapter 4.

Burnt off samples were outgassed at room temperature and the complete adsorption isotherm determined for most of them.
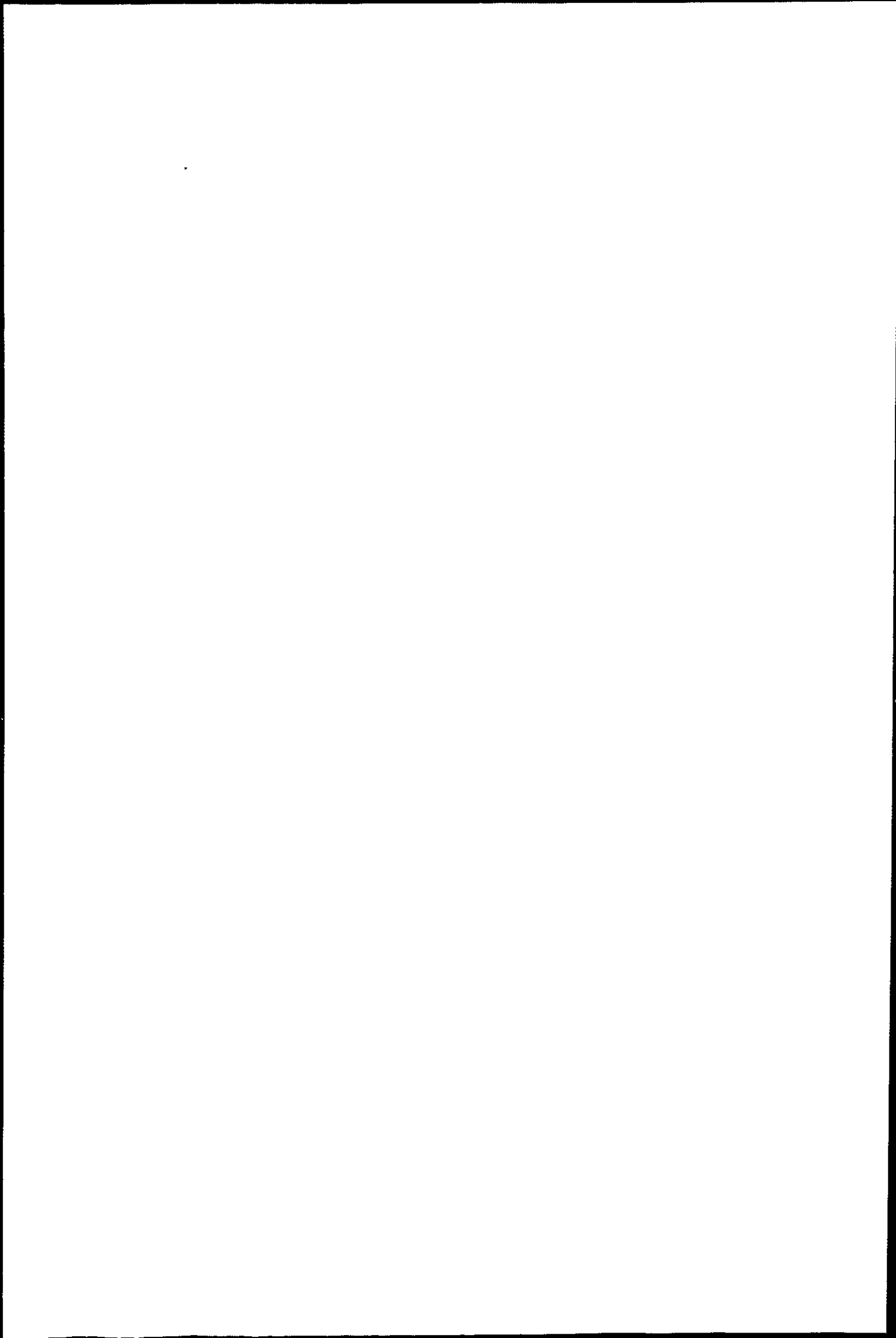
6.3.3 Brown Coal Char Study.

Nitrogen adsorption isotherms at 77 K of the original, doped and heat-treated char were determined using the vacuum balance described in Chapter 3.2.1. The char was heat treated under nitrogen using the furnace of the Massflow balance.

Samples of char (1.4 to 0.71 mm) and of B_2O_3 doped char were prepared to various degrees of burn off in CO_2 at 910 $^{\circ}C$ on the STA 781 thermal balance (furnace set to 950 $^{\circ}C$) using the TG only hangdown.

CO_2 adsorption at 196 K was measured for these materials on the vacuum balance described in Chapter 3.2.2, using approximately 0.1 g samples. The low temperature was achieved with an ether/crushed CO_2 slush bath, keeping the solid CO_2 constantly replenished. Samples were out-gassed for several hours at room temperature and held in vacuo overnight. As the uptake of CO_2 was about 200 mg g^{-1} the buoyancy, which was calculated as about -200 μ g atm^{-1}, was neglected. The cross sectional area of CO_2 at 196 K was taken as 17.0 $\overset{\circ}{A}^2$ giving a surface area for 1 g of CO_2 of 2.326 x 10^3 m^2.

Surface areas were determined from Langmuir or BET plots and the micropore volume from CO_2 adsorption using the Dubinin-Radushkevich equation.

SVP of CO_2 at 196 K was taken as 1.86 atmospheres. The cross sectional area and SVP are values calculated from the liquid density at -56 $^{\circ}C$ and the extrapolated liquid vapour pressure as described by Anderson et al.[12]

A value for the liquid density as 1.23 g cm^{-3} for CO_2 at 195 K is given by Dovaston et al[21]. The value of 1.14 g cm^{-3}, as given by Keattch and Dollimore[22] was taken in the present work.
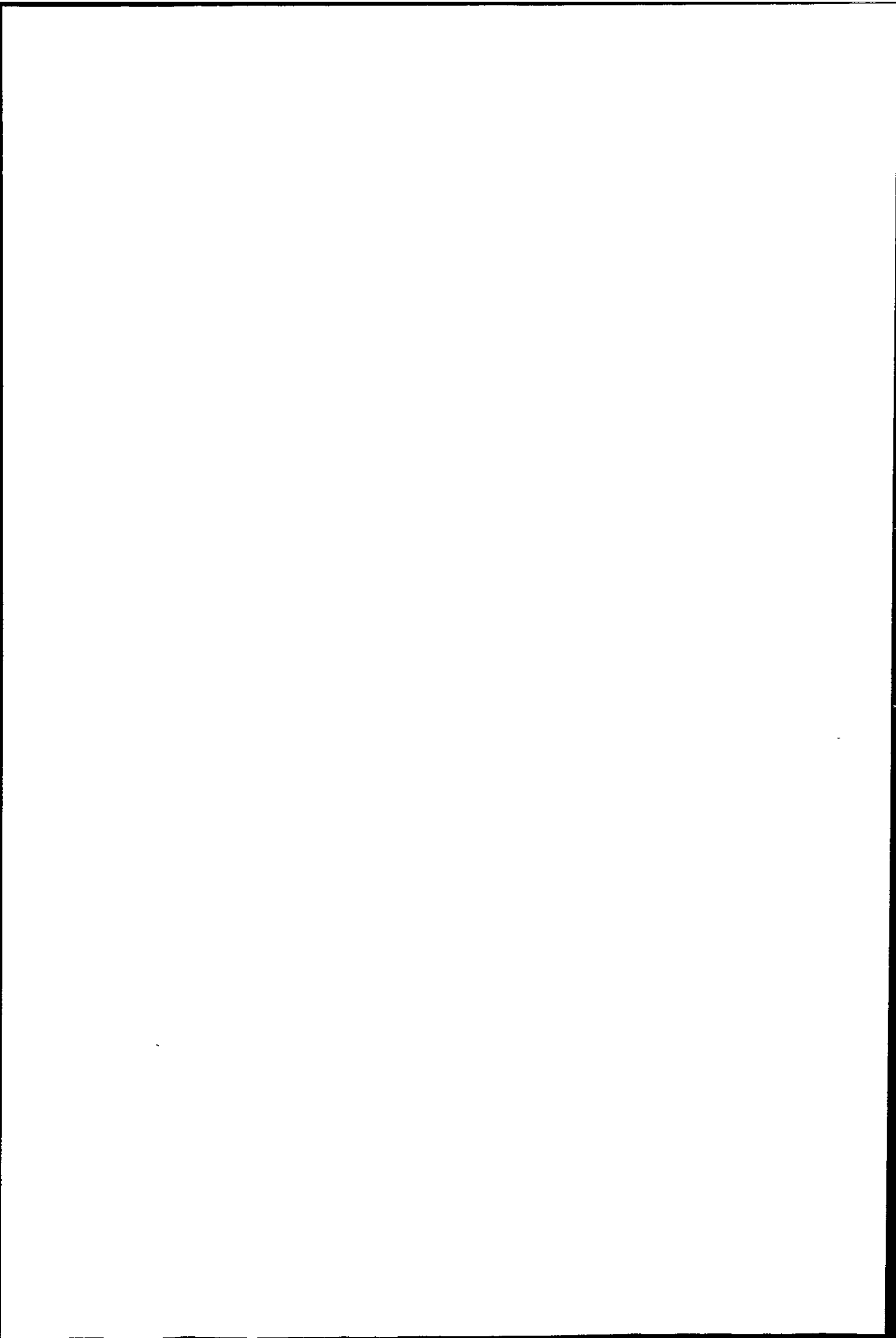
6.4 Surface Area of Nantgarw coke and B_2O_3 doped

Nantgarw coke gasified under various regimes.

6.4.1 Results

The surface areas of Nantgarw metallurgical coke (initially approximately 5 mm diameter lumps) burnt off in air at 500 °C and 1000 °C are given in Tables 6.4a and 6.4.b and presented graphically in Figures 6.4a and 6.4.b. Data for the B_2O_3 doped coke burnt off in air is similarly given in Table 6.4.c (500 °C burn off) and Table 6.4.d (1000 °C burn off), and plotted with the original coke results. Doped samples were all from the same batch. Complete burn off for doped Nantgarw coke was at 90.2% weight loss, the 1.4% difference from the undoped coke being the weight of B_2O_3. Percentage carbon burn off, rather than percentage burn off is plotted in all the coke results.

The buoyancy effect was approximately -600 µg atmosphere^{-1} using about 0.2 g of coke sample and taking the density as 1.48 g cm^{-3}. For samples over 50% burn off the effect of the ash was calculated using a value for ash density of 3.0 g cm^{-3}. The buoyancy then became -400 to -330 µg atmosphere^{-1}. The contribution of approximately 1% B_2O_3 on doped samples made a difference of about 4 µg atmosphere^{-1} less to the buoyancy correction, ie, although included in the calculation, it was not significant.

Surface area per g of starting material was calculated as specific surface area x $\frac{(100 - wt.\ loss)}{100}$,

258

and is tabulated with the specific surface areas determined experimentally. Linear BET plots were always obtained, and where the whole isotherm was determined it was of Type 2. Figure 6.4.c shows the complete isotherm for two 500 $^{\circ}C$ air burn off samples together with that of the original coke.

The specific surface areas of Nantgarw coke burnt off in CO_2 at 1000 $^{\circ}C$ and 1400 $^{\circ}C$ are given in Tables 6.4.e and 6.4.f and plotted in Figures 6.4.d and 6.4.e. Values for B_2O_3 doped coke burnt off at 1000 $^{\circ}C$ and 1400 $^{\circ}C$ are given in Tables 6.4.g and 6.4.h and plotted with those of the undoped coke.

The ash had melted in the 1400 $^{\circ}C$ burn off samples and some remained as globules in the alumina boat.

Several complete isotherms for 1000 $^{\circ}C$ CO_2 burnt off samples are given in Figure 6.4.f. Open circles represent adsorption points; closed circles desorption points.

The specific surface areas of heat treated coke and doped heat treated cokes are given in Table 6.4.i and the complete isotherms of original and heat treated doped coke are plotted in Figure 6.4.g.

The particle size of the coke ash from 500 $^{\circ}C$ and 1000 $^{\circ}C$ burn off is shown by electron microscopy in Plates 6.1 and 6.2.

Table 6.4.a

Specific surface area variation of Nantgarw coke lumps burnt off in air at 500 $^{\circ}$C.

% burn off	% carbon burn off	specific surface area $(m^2 g^{-1})$	surface per g starting material $(m^2 g^{-1})$
0	0	3.60	3.60
6.9	7.5	6.42	5.98
13.9	15.2	10.92	9.40
28.2	30.8	3.73	2.68
37.9	41.4	3.78	2.35
60.2	65.7	4.12	1.64
71.9	78.5	5.88	1.65
91.6	100	8.93	0.75
23(on massflow)	25	24.95 (static air burn off)	

Table 6.4.b.

Specific surface area variation of Nantgarw coke lumps burnt off in air at 1000 $^{\circ}$C

% burn off	% carbon burn off	specific surface area $(m^2 g^{-1})$	surface per g starting material $(m^2 g^{-1})$
0	0	3.60	3.60
14.9	16.3	4.08	3.47
29.3	32.0	4.33	3.06
52.2	57.0	4.36	2.08
63.4	69.2	3.03	1.11
76.2	83.2	2.19	0.52
91.2	100	0.1	

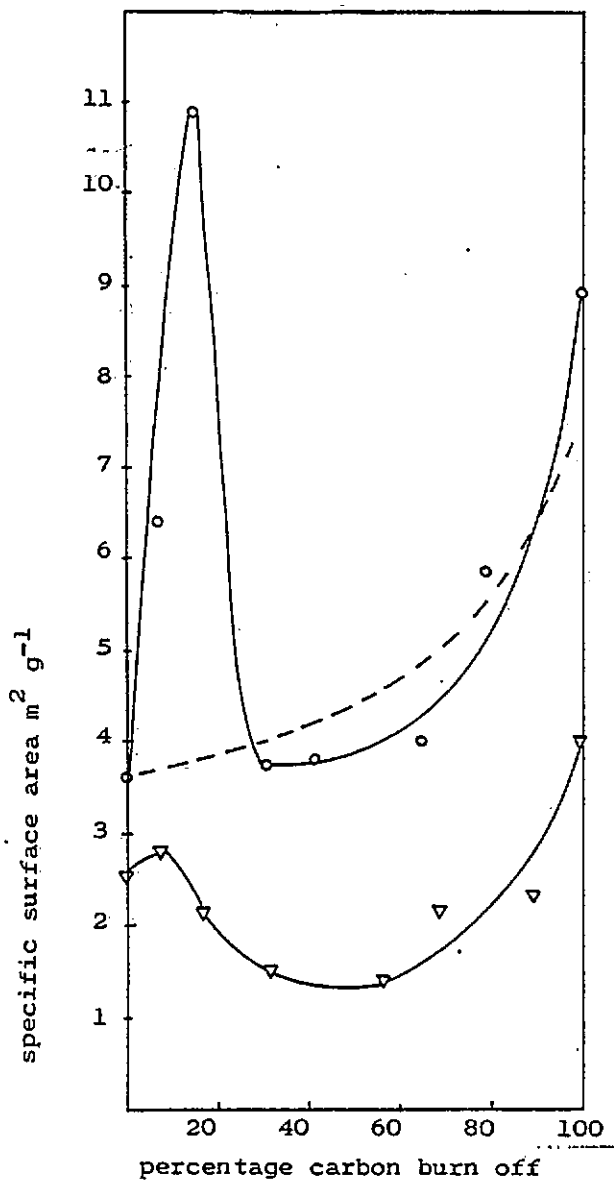specific surface area $m^2 g^{-1}$

percentage carbon burn off

Figure 6.4.a.(above)

Variation of specific surface area on burn off in air at 500 °C for Nantgarw Metallurgical Coke.

Key: Circles:-original coke
triangles:-B_2O_3 doped coke
broken line:- contracting
sphere model

Figure 6.4.b.(below)
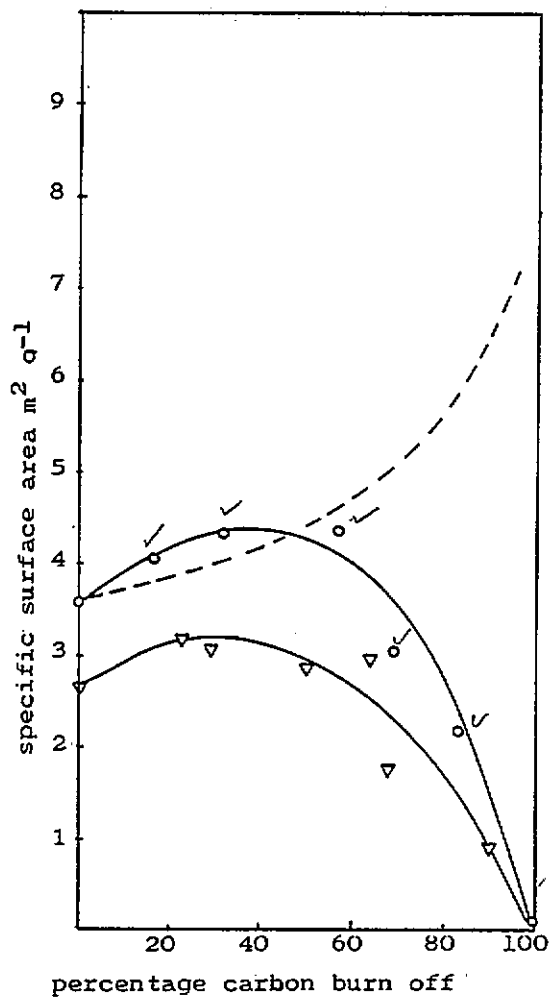Variation of specific surface area or burn off in air at 1000 °C for Nantgarw Coke.

specific surface area $m^2 g^{-1}$
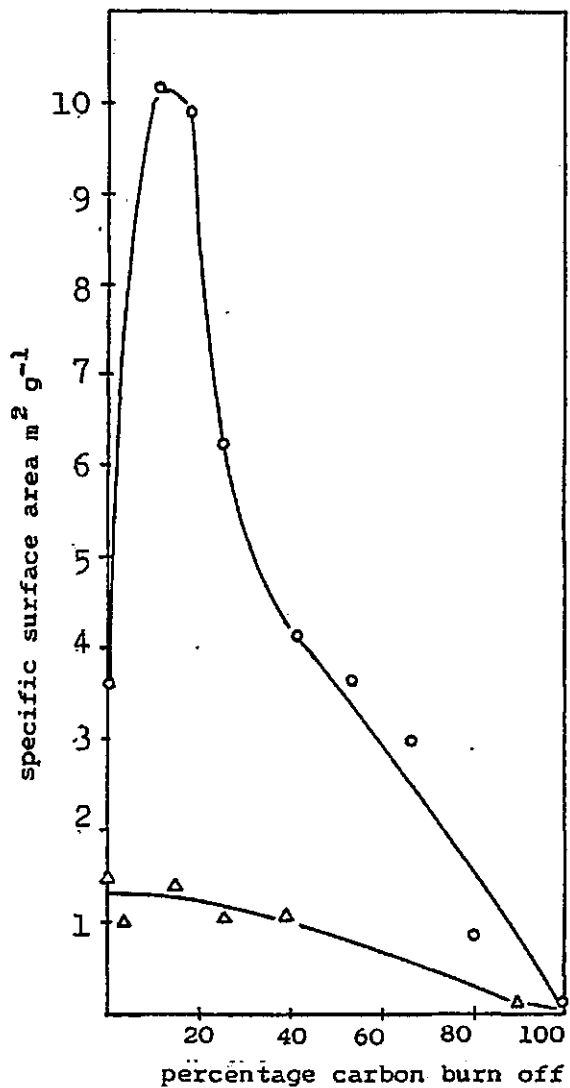
percentage carbon burn off

Table 6.4.c.

Specific surface area variation of B_2O_3 doped Nantgarw coke lumps burnt off in air at 500 $^\circ$C.

% burn off	% carbon burn off	specific surface area ($m^2 g^{-1}$)	surface per g starting material($m^2 g^{-1}$)
0	0	2.61	2.61
7.3	8.1	2.76	2.56
15.3	17.0	2.16	1.83
29.2	32.4	1.51	1.07
52.4	58.1	1.36	0.65
62.8	69.6	2.15	0.80
82.9	91.9	2.39	0.41
90.2	100	3.98	

Table 6.4.d.

Specific surface area variation of B_2O_3 doped Nantgarw coke lumps burnt off in air at 1000 $^\circ$C.

% burn off	% carbon burn off	specific surface area ($m^2 g^{-1}$)	surface per g starting material($m^2 g^{-1}$)
0	0	1.46	1.46
20.7	23.0	3.19	2.53
26.4	29.3	3.04	2.24
45.8	50.8	2.83	1.53
58.6	65.0	2.95	1.22
60.1	66.6	1.74	0.69
82.9	91.9	0.91	
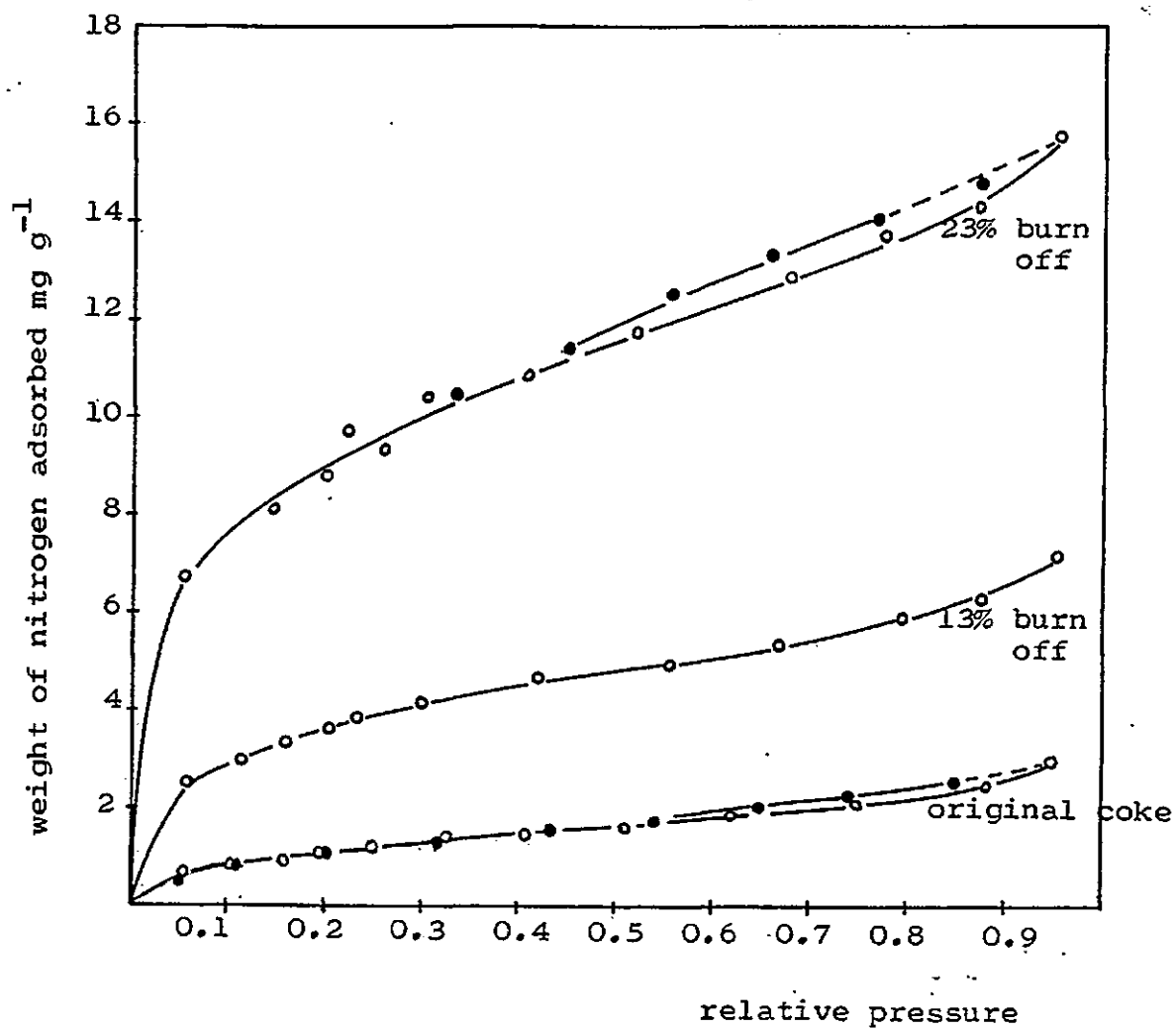
Figure 6.4.c. Nitrogen adsorption isotherms at 77 K for Nantgarw Coke burnt off in air at 500 $^{\circ}$C.

Table 6.4.e.

Specific surface area variation of Nantgarw coke burnt off in CO_2 at 1000 °C.

% burn off	% carbon burn off	specific surface area ($m^2 g^{-1}$)	surface per g of starting material($m^2 g^{-1}$)
0	0	3.60	
10.0	10.9	10.19	9.17
18.3	20.0	9.90	8.09
22.3	24.4	6.25	4.86
37.7	41.2	4.16	2.59
48.3	52.7	3.66	1.89
60.5	66.1	2.97	1.17
75.7	82.6	0.88	0.21
91.6	100	0.1	

Table 6.4.f.

Specific surface area of Nantgarw coke burnt off in CO_2 at 1400 °C.

% burn off	% carbon burn off	specific surface area ($m^2 g^{-1}$)	surface area per g of starting material($m^2 g^{-1}$)
0	0	1.43	
9.8	10.7	0.75	0.68
24.0	26.2	1.04	0.79
32.6	35.6	2.22	1.50
58.2	63.5	6.39	2.67
69.3	75.7	3.06	0.94
88.3	96.4	0.7	0.08

Figure 6.4.e.(below).
Variation of specific
surface area on burn off
in CO_2 at 1400 °C for
Nantgarw Coke.

Figure 6.4.d.(above).

Variation of specific surface
area on burn off in CO_2 at
1000 °C for Nantgarw coke.

Key: circles. original coke
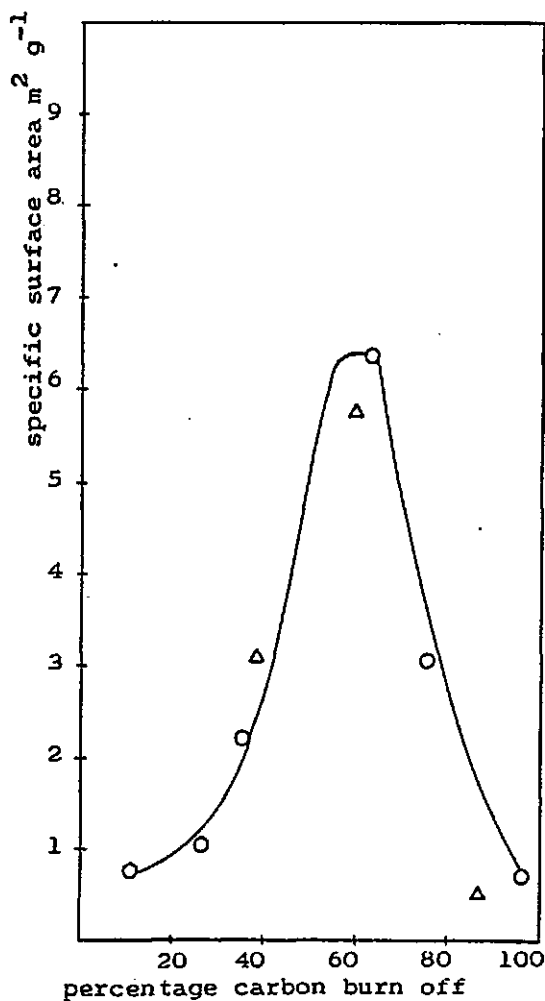triangles. B_2O_3 doped
coke

265

Table 6.4.g.

Specific surface areas of B_2O_3-doped Nantgarw coke burnt off in CO_2 at 1000 °C.

% burn off	% carbon burn off	specific surface area (m^2 g^{-1})
0	0	1.46
3.3	3.7	1.00
14.2	15.7	1.37
24.1	26.7	1.01
35.9	39.8	1.07

Table 6.4.h.

Specific surface areas of B_2O_3-doped Nantgarw coke burnt off at 1400 °C in CO_2.

% burn off	% carbon burn off	specific surface area($m^2 g^{-1}$)	surface area per g of starting material($m^2 g^{-1}$)
35.0	38.8	3.11	2.02
55.0	61.0	5.75	2.59
79.3	87.9	0.53	0.11

Table 6.4.i.

Specific surface areas of Heat Treated Nantgarw Coke.

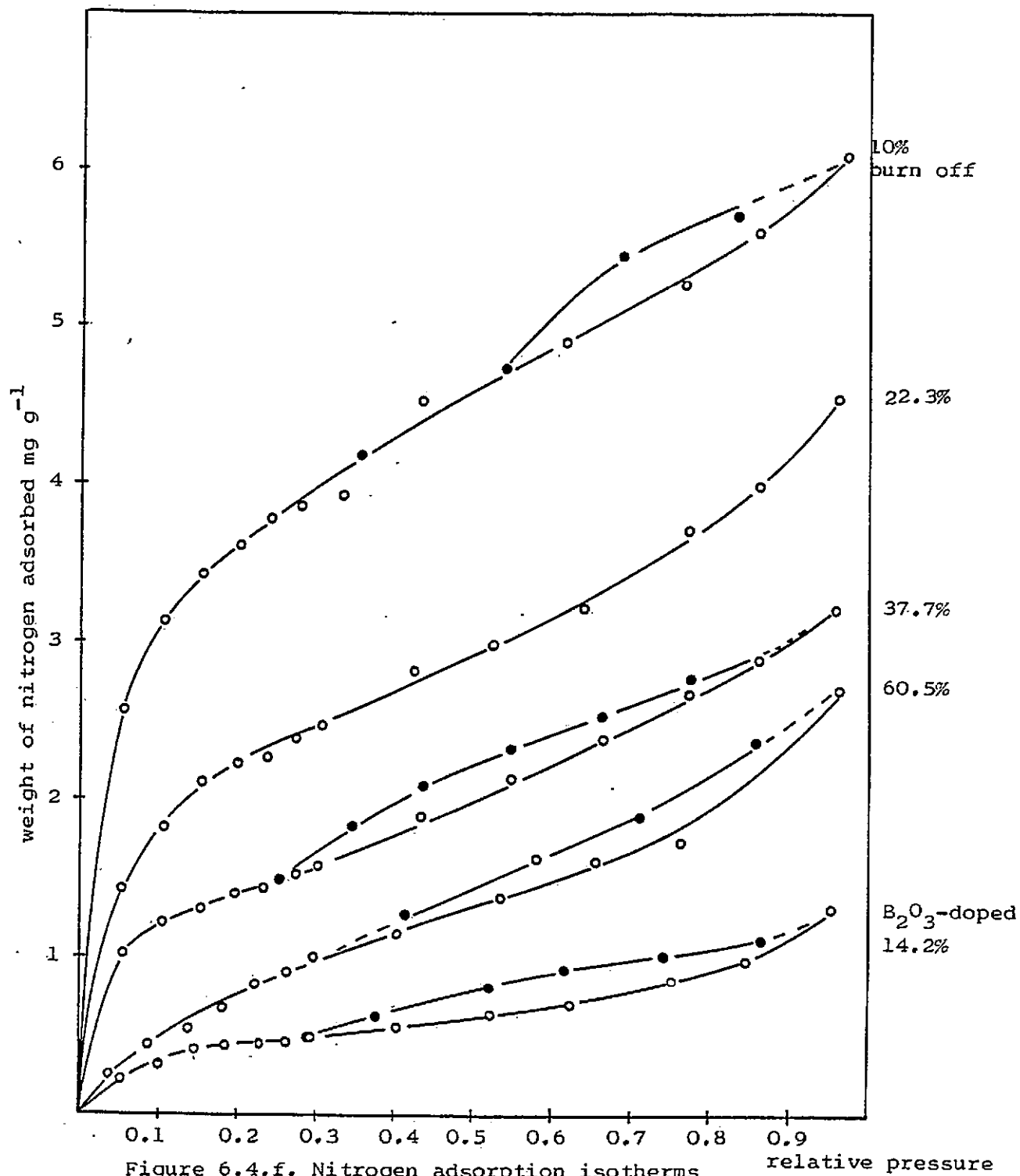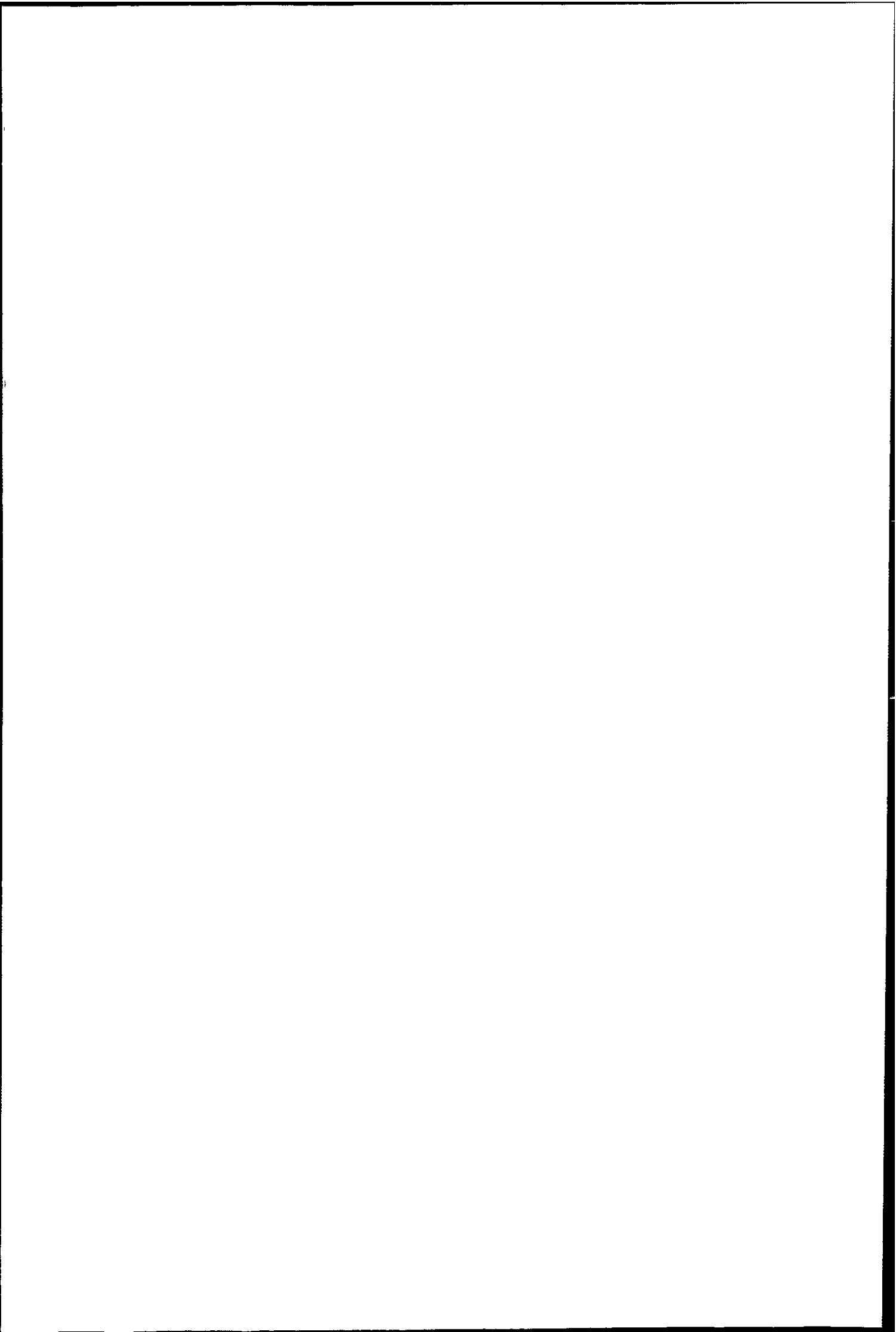| Heat treatment temperature °C	specific surface area (m^2 g^{-1})
500 (B_2O_3-doped)	2.61
1000 (" ")	1.46
1400 (original)	1.43
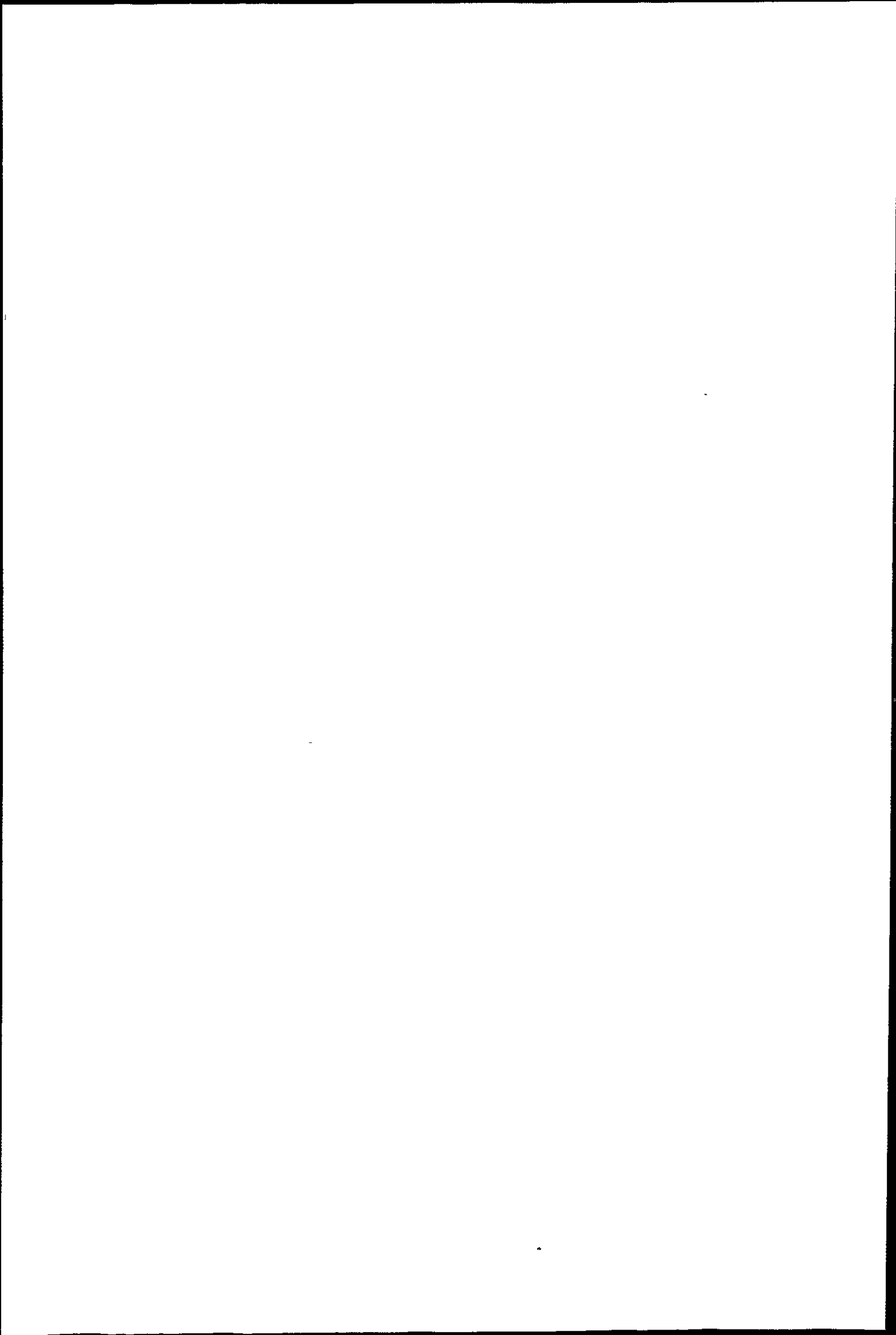
Figure 6.4.f. Nitrogen adsorption isotherms at 77 K for Nantgarw Coke Burnt off in CO_2 at 1000 ^oC.
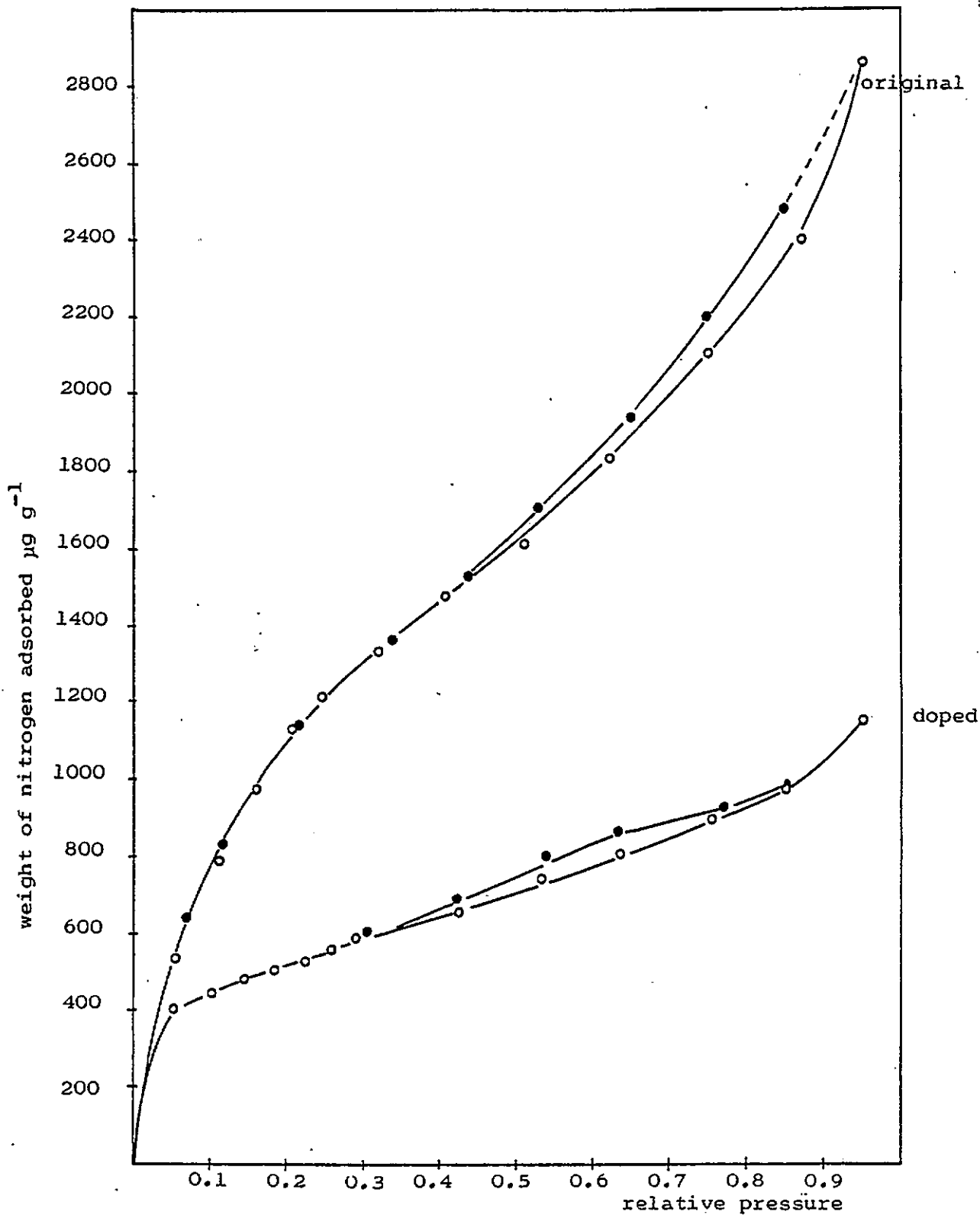
Figure 6.4.g. Nitrogen adsorption Isotherms at 77 K of original and B_2O_3 doped Nantgarw Coke.

6.4.2 Discussion

The development of specific surface area with degree of burn.-off for Nantgarw coke depends on temperature and gasifying agent. The ash content of Nantgarw coke was found as 8.4%, so as the carbon is burnt away the amount of ash remaining on the coke surface can be calculated, eg, in Table 6.4.j for the 1000 $^{\circ}$C air burn off samples. The percentage ash on the coke surface plotted against percentage carbon burn off, Figure 6.4.h, shows that after about 50% burn off, surface ash builds up rapidly. In the blast furnace coke is descending, and moving rapidly in the region of the raceways. In the laboratory samples surface ash was left on the coke and so during the latter half of the burn off will affect the surface area. From the Tammann temperatures of the principal ash constituents (Table 4.3.j of Chapter 4), it can be seen that Nantgarw coke ash is likely to sinter at an appreciable rate at 1000 $^{\circ}$C but not at 500 $^{\circ}$C. Thus the specific surface area of the 1000 $^{\circ}$C ash was very low and its progressive build up greatly lowered the coke surface area, as seen in Figure 6.4.b. The specific surface area of the 500 $^{\circ}$C ash however was almost 9 m^2g^{-1} and its build up on the coke during the latter part of the burn off tended to increase specific surface area.

Transmission electron micrographs of the 500 $^{\circ}$C and 1000 $^{\circ}$C ashes, shown in Plate 6.2, illustrate the difference in particle size induced by sintering. Surface morphology is shown in the scanning electron micrographs of Plate 6.1, and

271

Table 6.4.j.

Surface Ash on Burn-off for 1 g of Nantgarw Coke.

(assuming 91.6% carbon 8.4% ash).

% burn off	% carbon burn off	carbon lost (g)	separated ash (g)	coke remaining + surface ash (g)	surface ash as % of material remaining
14.9	16.3	0.149	0.014	0.851	1.65
29.3	32.0	0.293	0.027	0.707	3.82
52.2	57.0	0.522	0.048	0.478	10.04
63.4	69.2	0.634	0.058	0.366	15.85
76.2	83.2	0.762	0.070	0.238	29.41
91.6	100	0.916	0.084	0.084	100
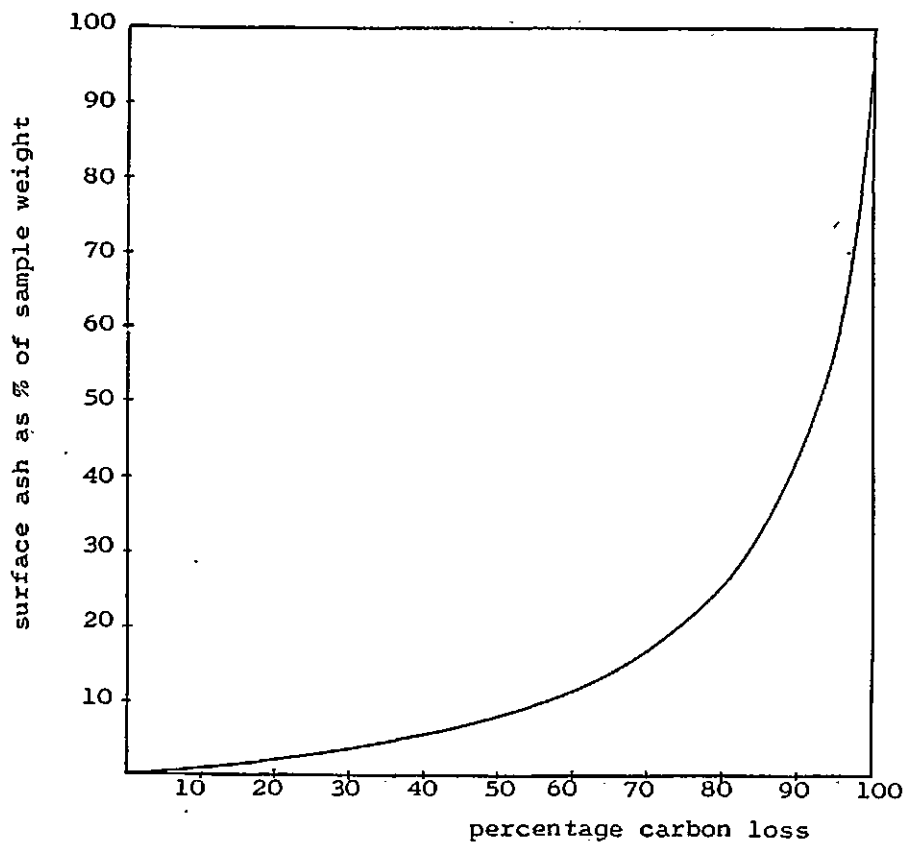
Figure 6.4.h.   Accumulation of Surface Mineral for a Coke of 8.4% ash content.

similarly reveals the larger aggregate size and rounded

surface of the particles of the 1000 $^{\circ}$C sintered ash.

The presence of B_2O_3 in the 500 $^{\circ}$C ash lowers its specific

surface area. Although B_2O_3 constitutes only 1 to 1.5%

of the initial coke weight, it represents about 12% of

the ash material when the carbon has burnt away. The

B_2O_3 might be expected to lower surface area and stick

ash lumps together. This is shown in the scanning electron

micrographs of Plate 4.9.

Thus during the latter part of the burn off the ash

plays a role in blocking available surface. When

oxidation takes place above the Tammann temperature of the

ash (ie in all CO_2 burn off, and in air burn offs above

650 $^{\circ}$C) the accumulating ash greatly lowers surface area.

In the first half of the burn off this effect is minimal

and the temperature regime more important.

Isothermal oxidations in air (Chapter 5) have shown

that 500 $^{\circ}$C is in the zone of chemical control of rate

and 1000 $^{\circ}$C in the diffusion controlled zone. In CO_2

both 1000 $^{\circ}$C and 1400 $^{\circ}$C are in the zone of predominantly

chemical control.

Assuming that the coke lumps are non porous

contracting spheres or cylinders, the surface areas on

burn off can be calculated, as these values are proportional

to $r^{1/3}$ and $r^{1/2}$ respectively, where r is the radius. The

changes in specific surface area (for a material with an

initial value of 3.60 m^2g^{-1}) for the contracting sphere

and contracting cylinder models are plotted in Figure

6.4.i. The values for the two models diverge rapidly after about 40% burn off.

In air at 1000 $^\circ$C specific surface area increases up to about 50% burn off almost in keeping with the non-porous model (Figure 6.4.b). Oxidation is taking place at the coke surface resulting in progressive surface ablation and loss of surface area per g of starting material. The B_2O_3 doped coke shows a similar trend.

However for burn off in air at 500 $^\circ$C the specific surface area of the coke (Figure 6.4.a) increases rapidly up to about 15% burn off. This may be explained as due to opening of closed pores. The specific surface area then falls back to almost the original value as pore walls are consumed. The sample burnt off in static air conditions on the Mass flow balance gave a much higher specific surface area than any of the samples prepared in the muffle furnace.

Surface area development for the B_2O_3 doped samples on air burn off at 500 $^\circ$C is much reduced, the values falling even lower than those of the 1000 $^\circ$C air burn off samples. B_2O_3 does not have a sharp melting point but softens at about 400 $^\circ$C and although its ability to spread may not be so great at the lower temperature, the time to achieve the same percentage burn off is much longer.

Figures 6.4.d and 6.4.e show that the surface area of Nantgarw coke gasified in CO_2 increases during burn off both at 1000 $^\circ$C and 1400 $^\circ$C. The 1000 $^\circ$C burn off

is similar to the 500 $^{\circ}$C air burn off, as noted by Grillet and Geurin[15], resulting in a maximum surface area at about 15% burn off. The isotherms of Figures 6.4.c and 6.4.f indicate pore development in the macro and mesopore range, the area of the hysteresis loop representing cumulative pore volume. The hysteresis loop closes at a relative pressure of 0.30 to 0.35. The minimum pore radius, calculated from the Kelvin equation then lies between 0.79 nm and 0.91 nm.

B_2O_3 doping again reduces surface area of coke burnt off in CO_2 at 1000 $^{\circ}$C and to a greater extent than in the air burn off at 1000 $^{\circ}$C or at 500 $^{\circ}$C. Rates of reaction in air and CO_2 at 1000 $^{\circ}$C differ by a factor of ten and rates in CO_2 at 1000 $^{\circ}$C and air at 500 $^{\circ}$C are comparable. (Chapter 5.)

At 1400 $^{\circ}$C the specific surface area does not increase markedly until about 40% carbon burn off (Figure 6.4.e), and its maximum is less than at 1000 $^{\circ}$C. Rate of reaction is very much faster and more carbon must be lost from the external surface, creating less porosity. This creation of internal surface as reactant gas diffuses into the pores is responsible for the loss of coke strength, as noted by many workers (eg. Chapter 2, reference 27).

B_2O_3 doping does not lower specific surface area on CO_2 burn off at 1400 $^{\circ}$C, and is probably running off the coke surface. Its effect on rate of reaction also diminishes at this temperature, as shown by isothermal TG.

Thus the effectiveness of B_2O_3 in reducing surface area is illustrated in this series of results. Heat treatment of doped coke leads to a lower specific surface area (Table 6.4.i), which is maintained during burn off, except at 1400 $^{\circ}$C.

Comparison of the isotherms of original Nantgarw coke and the heat treated doped coke (Figure 6.4.g) would suggest that B_2O_3 blocks macropores and larger mesopores, although it is not possible to determine this at reaction temperatures.
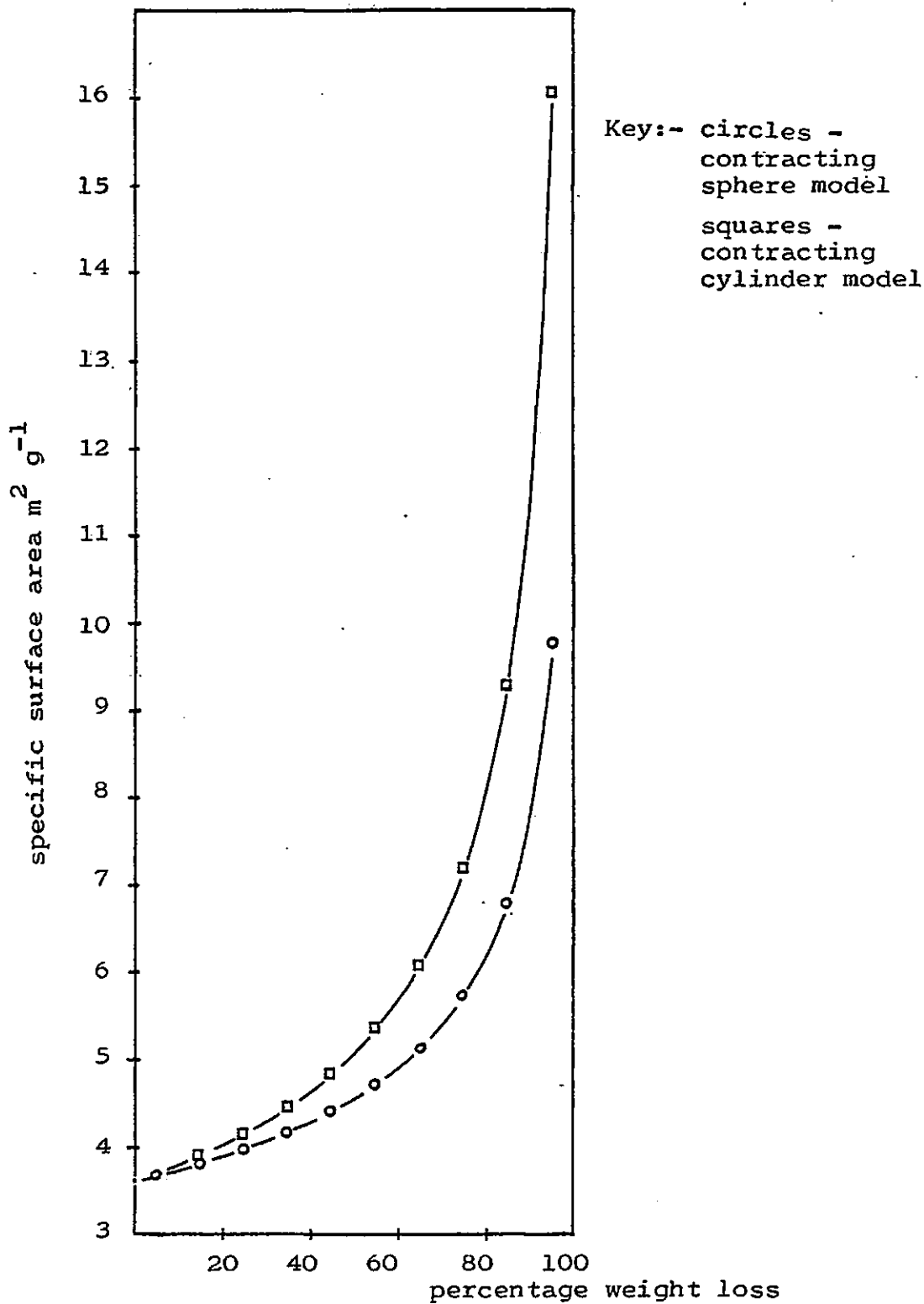
Key:- circles –
contracting
sphere model

squares –
contracting
cylinder model

Figure 6.4.i. Variation of Specific Surface area with weight loss for two non-porous models of Initial specific surface area 3.6 m^2 g^{-1}

277

6.5 Comparative Reactivity Study of Three Metallurgical Cokes.

6.5.1 Results

The ash content of Cwm and Polish cokes was found to be 8.8 and 10.9% respectively and their gas densities in N_2 as 1.40 g cm^{-3}.

The surface areas of Polish coke burnt off in CO_2 are given in Table 6.5.a and plotted in Figure 6.5.a. The initial value was 1.61 m^{2}g^{-1} after outgassing at 200 ^{O}C and only 0.35 m^{2}g^{-1} after outgassing at room temperature.

The initial specific surface area of Cwm coke was 1.19 m^{2}g^{-1} after outgassing at 200 ^{O}C. The variation on burn off in CO_2 at 955 ^{O}C is given in Table 6.5.b and plotted in Figure 6.5.a, which also shows the results for Nantgarw coke at 1000 ^{O}C burn off on the same scale.

Nitrogen adsorption isotherms at 77 K are shown, for various degrees of CO_2 burn off in Figures 6.5.b and and 6.5.c for Polish coke and in Figure 6.5.d for Cwm coke.

Surface areas of air burnt off Cwm and Polish cokes are given in Table 6.5.c and values for B_2O_3-doped, burnt off samples (in air and CO_2) in Tables 6.5.d and 6.5.e.

Adsorption isotherms of doped Cwm and Polish cokes burnt off 15% in CO_2 at 955 ^{O}C are shown in Figure 6.5.e.

278

Table 6.5.a.

Surface area of Polish coke burnt off in CO_2 at 955 $^{\circ}$C.

% burn off	% carbon burn off	specific surface area $(m^2\ g^{-1})$	surface area per g of starting material
0	0	1.61	1.61
5	5.62	12.08	11.48
15	16.83	44.46	37.79
25	28.09	55.95	41.96
35	39.33	58.84	38.25
45	50.56	58.28	32.05
55	61.80	49.49	22.27
65	93.03	14.67	5.14
89	100	1.20	0.13

Table 6.5.b.

Surface area of Cwm coke burnt off in CO_2 at 955 $^{\circ}$C

% burn off	% carbon burn off	specific surface area $(m^2\ g^{-1})$
0	0	1.19
5	5.48	23.01
8	8.77	18.55
15	16.45	20.74
20	21.93	40.38
24	26.32	18.78
35	38.38	28.70
45	49.34	14.59
51	55.92	29.01
60	65.79	13.29
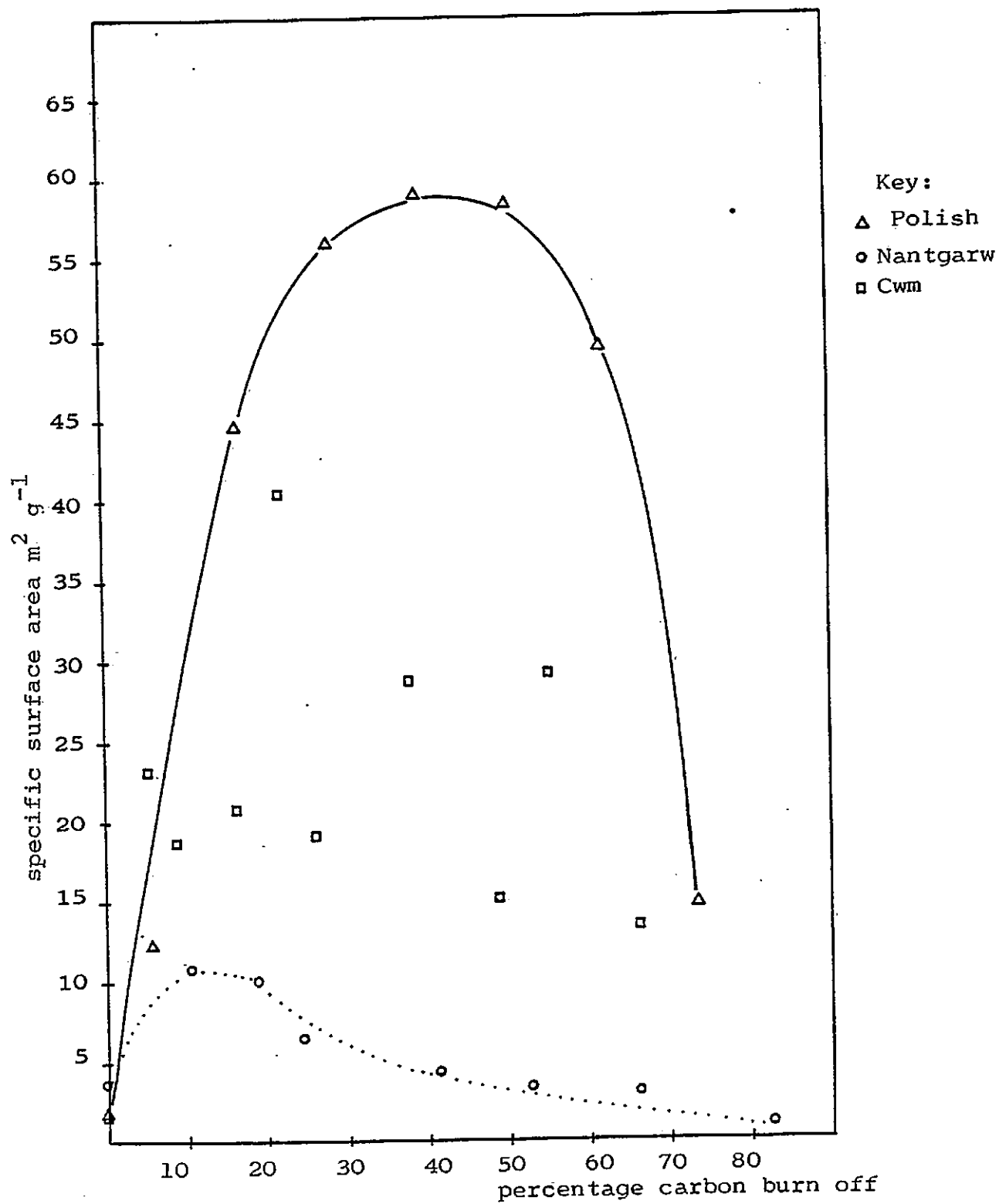
Figure 6.5.a. Variation of Specific Surface Area with Burn off in CO_2 for Cwm, Nantgarw and Polish cokes.

280
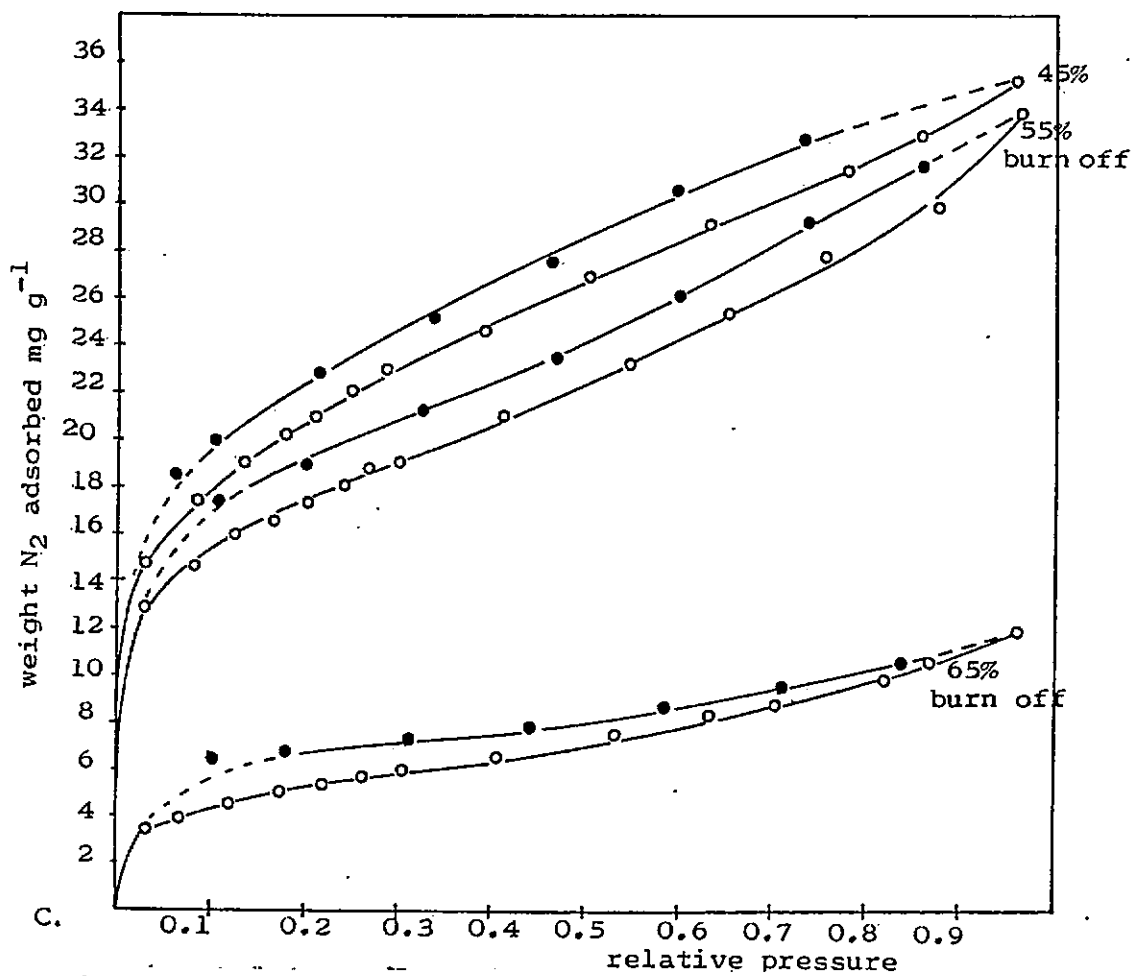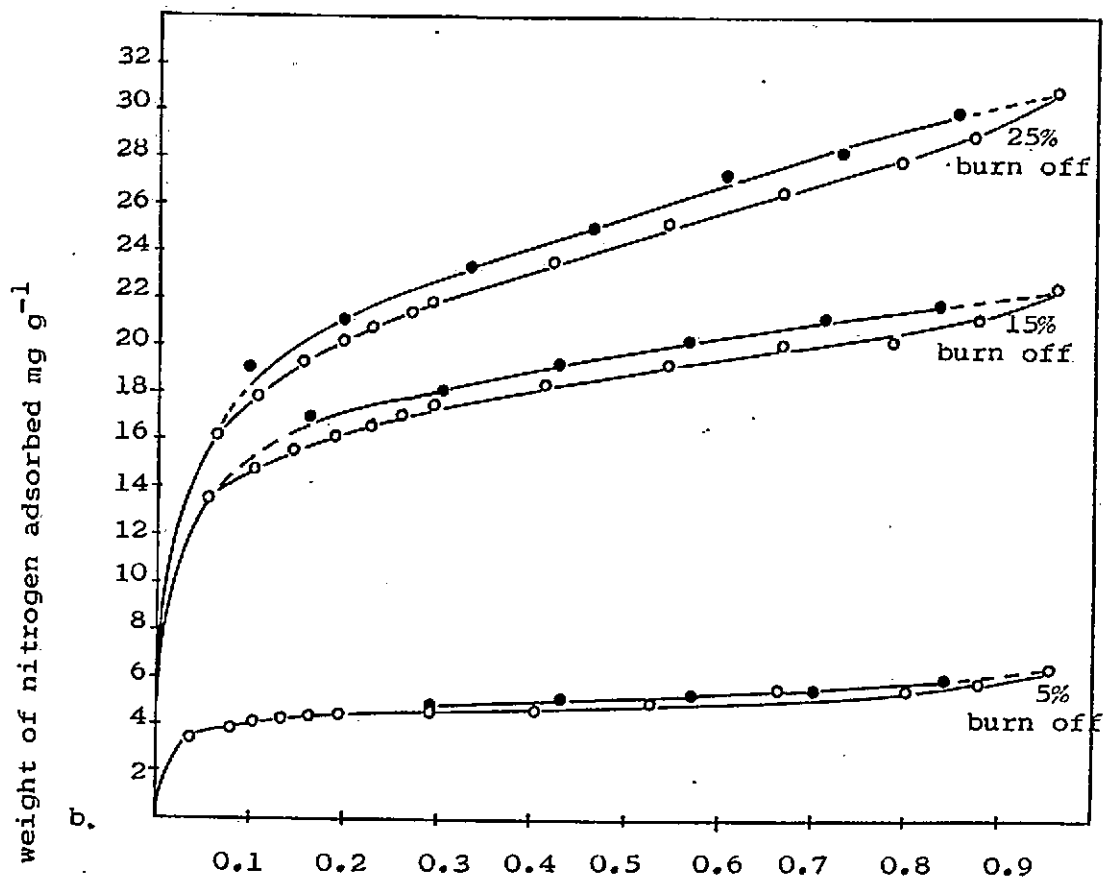
Figures 6.5.b. and 6.5.c. Nitrogen adsorption Isotherms
at 77 K for Polish coke burnt off in CO_2
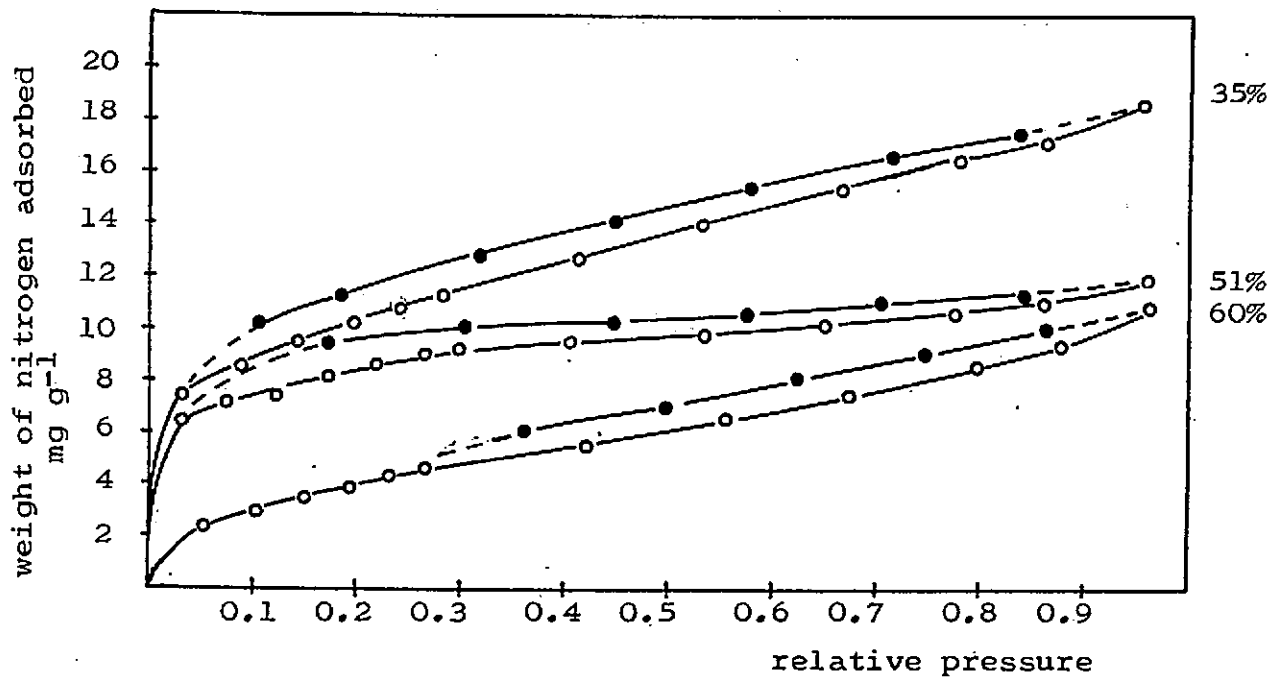
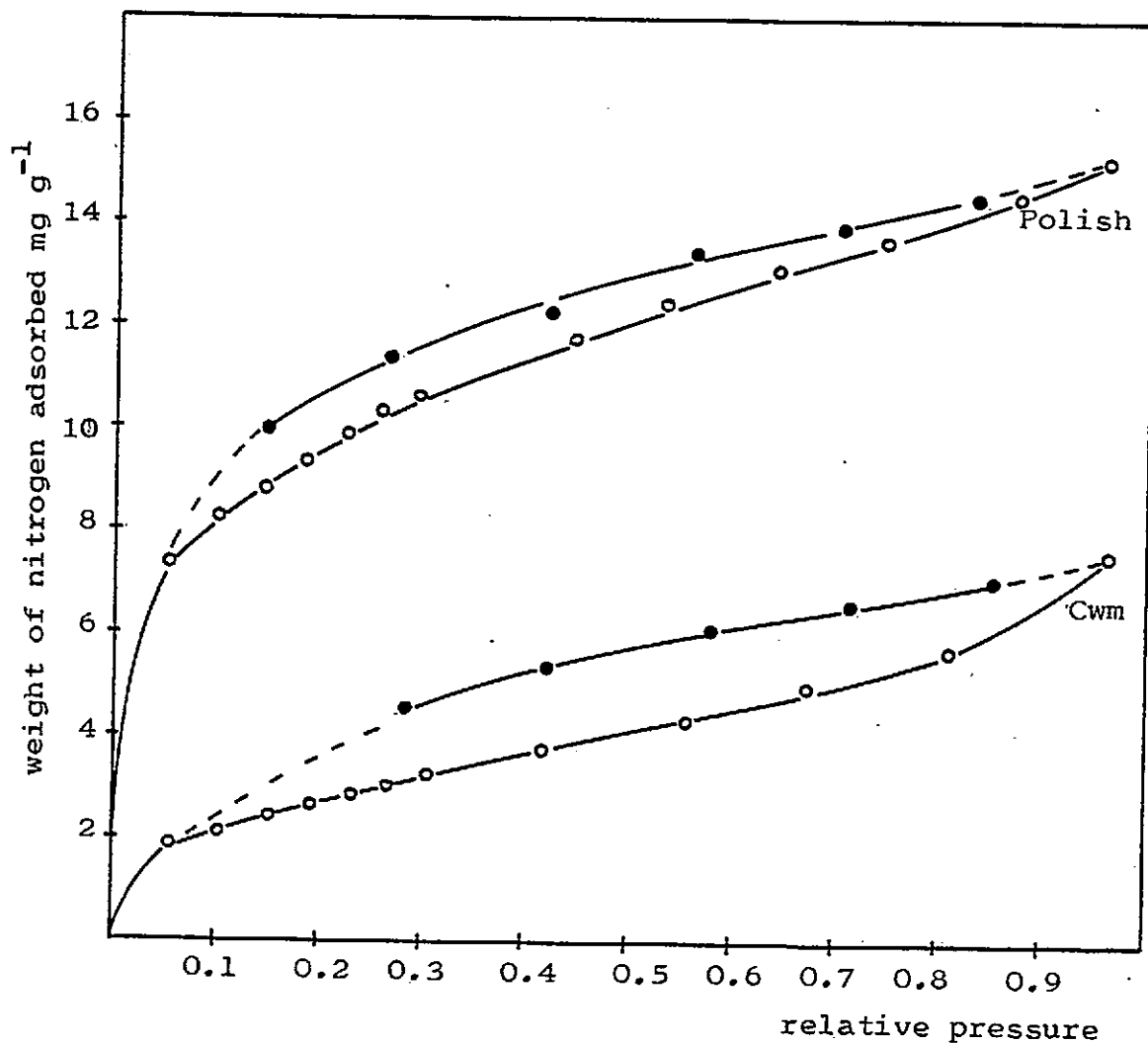Figure 6.5.d. Nitrogen adsorption Isotherms at 77 K for Cwm coke burnt off in CO_2

Figure 6.5.e. Nitrogen adsorption isotherms at 77 K for B_2O_3 doped Cwm and Polish cokes burnt off 15% in CO_2

282

Table 6.5.c.

Specific surface area of Cwm and Polish Coke Burnt off
in air at 1000 $^{\circ}$C.

	% burn off	specific surface area m^2 g^{-1}
Cwm coke	36.0	17.45
Polish coke	36.2	34.10

Table 6.5.d.

Specific surface areas of burnt off B_2O_3-doped Cwm coke.

% burn off	specific surface area m^2 g^{-1}
33.6% in air at 1000 $^{\circ}$C	6.51
15.0% in CO_2 at 955 $^{\circ}$C	8.90

Table 6.5.e.

Specific surface areas of Burnt off B_2O_3-doped Polish coke.

% burn off	specific surface area m^2 g^{-1}
37.9% in air at 1000 $^{\circ}$C	16.12
15.0% in CO_2 at 955 $^{\circ}$C	27.15

6.5.2 Discussion

The initial specific surface areas of Nantgarw, Cwm and Polish cokes are 3.60, 1.19 and 1.61 m^2g^{-1} respectively. They thus bear no relationship to their industrial "reactivity" (Table 4.3.a.).

Burn off in CO_2 at 955 $^\circ$C was expected to increase the specific surface area of Cwm and Polish coke, with accumulating ash lowering surface area at higher burn offs. The ash content of Polish coke is greatest, but still only about 12% of sample weight by 50% burn off.

For Polish coke, values followed a smooth curve. Maximum specific surface area was reached by about 35% burn off and this was maintained until half the carbon burn off. Considering surface area per g of starting material (Table 6.5.a) it can be seen that surface is initially increasing despite carbon being removed. The area and point of closure of the desorption branch of the isotherms of Figures 6.5.b and 6.5.c would indicate that this extra surface is generated through the development of a whole range of pore sizes. At 5% burn off only meso and macro pores are present. These increase in cumulative volume and smaller pores develop by 25% burn off. This porosity is increased at 45% burn off, maintained at 55%, and is diminishing at 65% burn off. The sharper "knees" of the 45% and 55% burn off isotherms show that the pore size distribution is displaced to the fine pore end of the size range.

The specific surface area values for Cwm coke gave
a greater spread of results, seeming to represent two
series of samples, although prepared from the same batch.
Cwm may be a more heterogeneous coke. Both Cwm and Nantgarw
are made from coal blends. The isotherms of Figure 6.5.d
again show the increase in porosity due to a range of pore
sizes.

In a study of blast furnace coke of similar physical
properties, Aderibigbe and Szekely[23] measured total
porosity as a function of burn off. Pores contributing to
molecular diffusion ($d > 35 \mu m$) increased with increasing
burn off, whilst those contributing to Knudsen diffusion
($d < 32$ nm) decreased slightly at first and then increased.
It was concluded that the increase in porosity of the coke
was due to the enlarging of large pores. It was not possible
to study the total porosity of the coke in the present
work.

The maximum specific surface area for Nantgarw, Cwm
and Polish cokes in CO_2 burn off is at 15, 25 and 43%
carbon burn off respectively. From this the mean maximum
pore radius $\bar{r}$ may be calculated (Appendix 2).

Results are summarised in Table 6.5.f., where it can
be seen that this pore radius is smaller for Cwm and
Polish than Nantgarw coke. The calculation assumes
cylindrical pores and a maximum development of porosity,
but the values are useful for comparison.
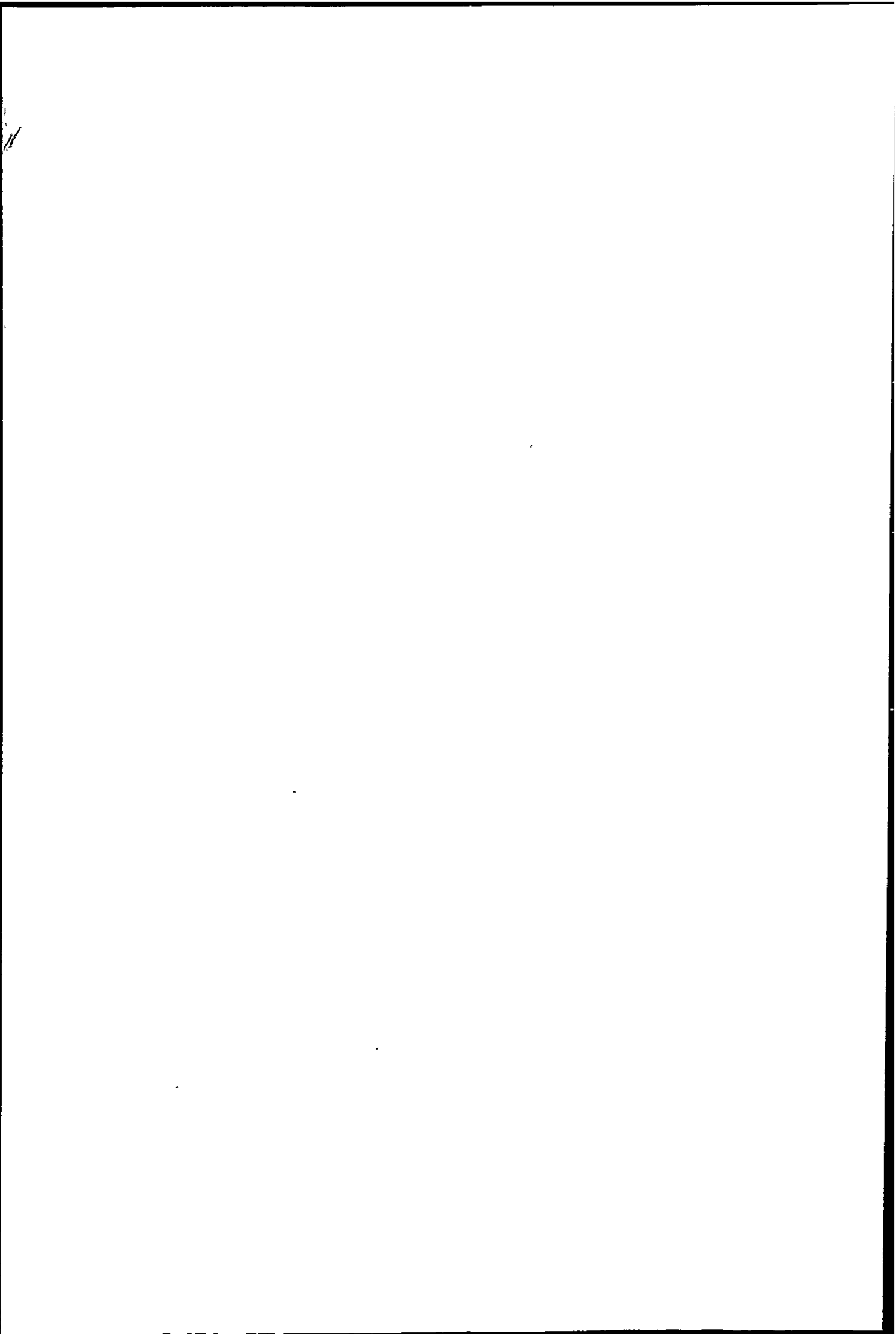
The mean free path, λ, for CO_2 at 1000 °C is calculated as 0.57 μm (570 nm).[23] When the Knudsen number $\frac{\lambda}{2\bar{r}} \geqslant 10$ gaseous diffusion proceeds mainly by the Knudsen mechanism, but when this is $\leqslant 0.01$ molecular diffusion predominates. Thus Cwm and Polish cokes have pores where Knudsen diffusion operates, although it is not known what fraction this is of the total porosity.
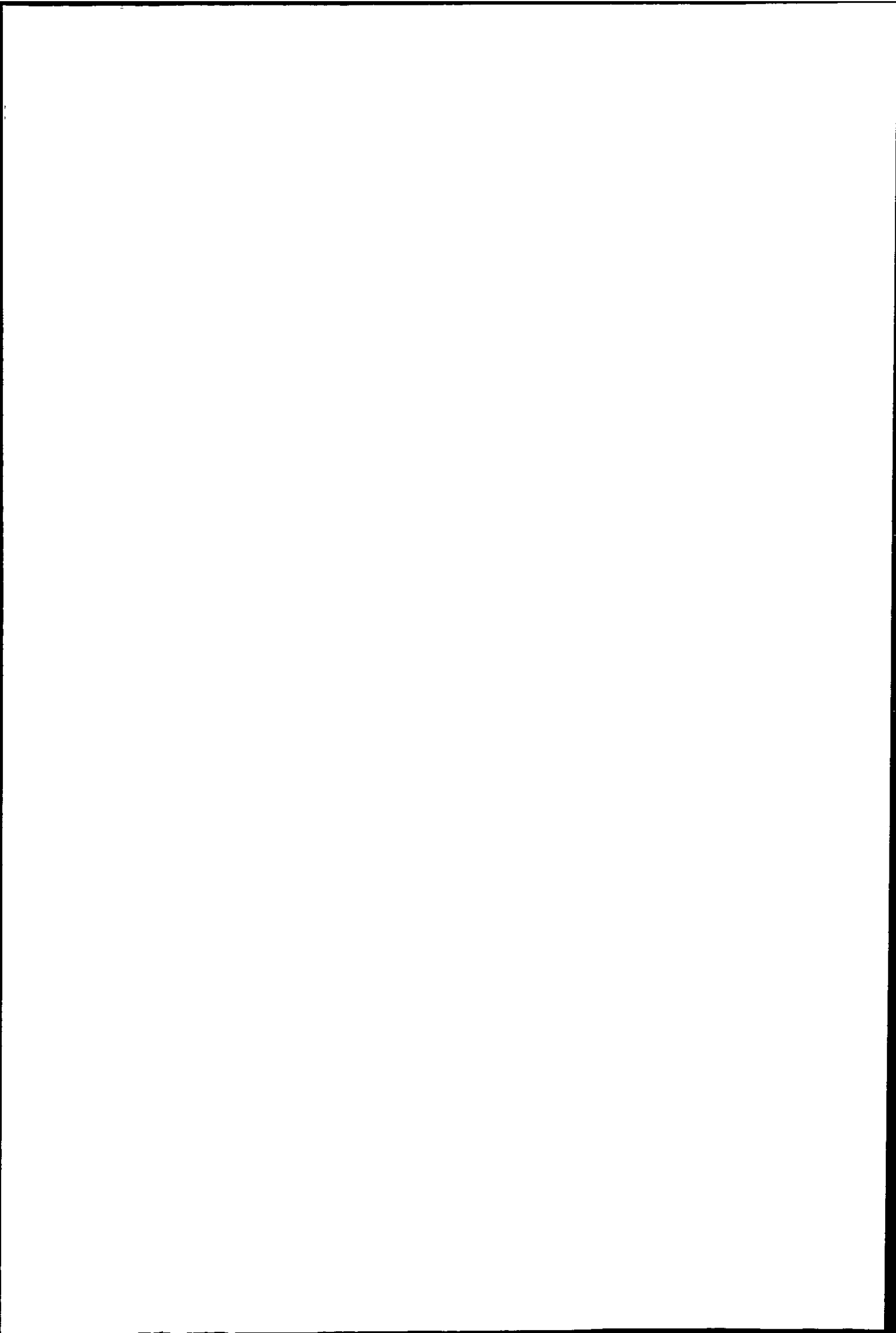
Table 6.5.f.

Pore Development of Three cokes on CO_2 gasification.

Coke	Mean maximum pore radius (nm)	Knudsen number
Nantgarw	33.4	8
Cwm	15.8	30
Polish	15.3	30

Although the initial specific surface area of the cokes bear no relation to "reactivity", its development does. The surface area is greatest for the most "reactive" coke, as summarised in Table 6.5.g., taking a mean value for Cwm coke.

Table 6.5.g.

Coke	Reactivity by Nantgarw ratio test.	Rate of reaction in CO_2 at 955 °C $\times 10^6$ g s^{-1} g^{-1} (From Table 5.4.g)	Maximum specific area m^2 g^{-1}
Nantgarw	1	6.96	10
Cwm	1.55	13.89	28
Polish	3.06	30.88	59

Thus a coke of high "reactivity" is one where specific surface area can develop and be maintained. The curves of Figure 6.5.a after about 10% burn off, follow the pattern of the DTG curves of Figure 5.4.g.

Although a large specific surface area may develop, not all of it may be accessible to reactant gas. The specific surface area increases by approximately 1:3:6, but the actual rate of reaction in CO_2 only increases by approximately 1:2:4.

When Polish and Cwm cokes are burnt off in air at 1000 $^{\circ}$C some surface develops (Table 6.5.c), although this is in the zone of diffusion control of oxidation and the specific surface area of Nantgarw coke increases little. This is probably the maximum 1000 $^{\circ}$C air burn off increase.

The specific surface area of the doped cokes burnt off in CO_2 is reduced, as expected. The amount of B_2O_3 retained by Cwm and Polish cokes is less than for Nantgarw and the percentage surface area reduction is also less, as shown in Table 6.5.h. Reduction in rate of reaction in CO_2 at 955 $^{\circ}$C is considerable (from Table 5.4.i.) even for the small amount of B_2O_3 retained. Rate of reaction of doped Cwm coke was more variable than the other two.

Table 6.5.h.

Coke	% B_2O_3 retained	% reduction in specific surface area at 15% burn off in CO_2	% reduction in rate of CO_2 oxidation at 955 °C
Nantgarw	1.1 to 1.5	86	58.9
Cwm	0.8	57	variable (80% to 30%)
Polish	0.2	39	53.9

The results of this work suggest that the effectiveness of B_2O_3 as an inhibitor of the Boudouard reaction on coke is due to its ability to block available carbon surface, which is not the same as the total surface. Blocking of larger pores, ie those where gasification mainly takes place, is the important factor in reducing rate of reaction.

6.6 Surface Areas of Brown Coal Char.

6.6.1 Results

Figure 6.6.a shows the N_2 adsorption isotherms at 77 K for the original and B_2O_3 doped char. Specific surface area values are given in Table 6.6.a for these and for heat treated material, estimated from Langmuir plots.

Typical Langmuir plots for CO_2 adsorption at 196 K on the burnt off char are shown in Figure 6.6.b. Dubinin-Radushkevich plots for the same results are given in Figure 6.6.c using semi log graph paper. The intercept on the W axis gives the weight of CO_2 in the micropores (in mg g^{-1} char) and open micropore volume is calculated from this using 1.14 g cm^{-3} as the liquid density of CO_2 at 196 K. Results are tabulated in 6.6.b with specific surface areas, calculated from Langmuir's equation.

Dubinin-Radushkevich plots for the doped char burnt off at 910 ^{o}C in CO_2 are shown in Figure 6.6.d, and results are tabulated in 6.6.c, with specific surface area values, from CO_2 adsorption at 196 K.

The variation in specific surface area with weight loss in CO_2 at 910 ^{o}C is plotted for the original and doped char in Figure 6.6.e and the variation in open micropore volume similarly in Figure 6.6.f.
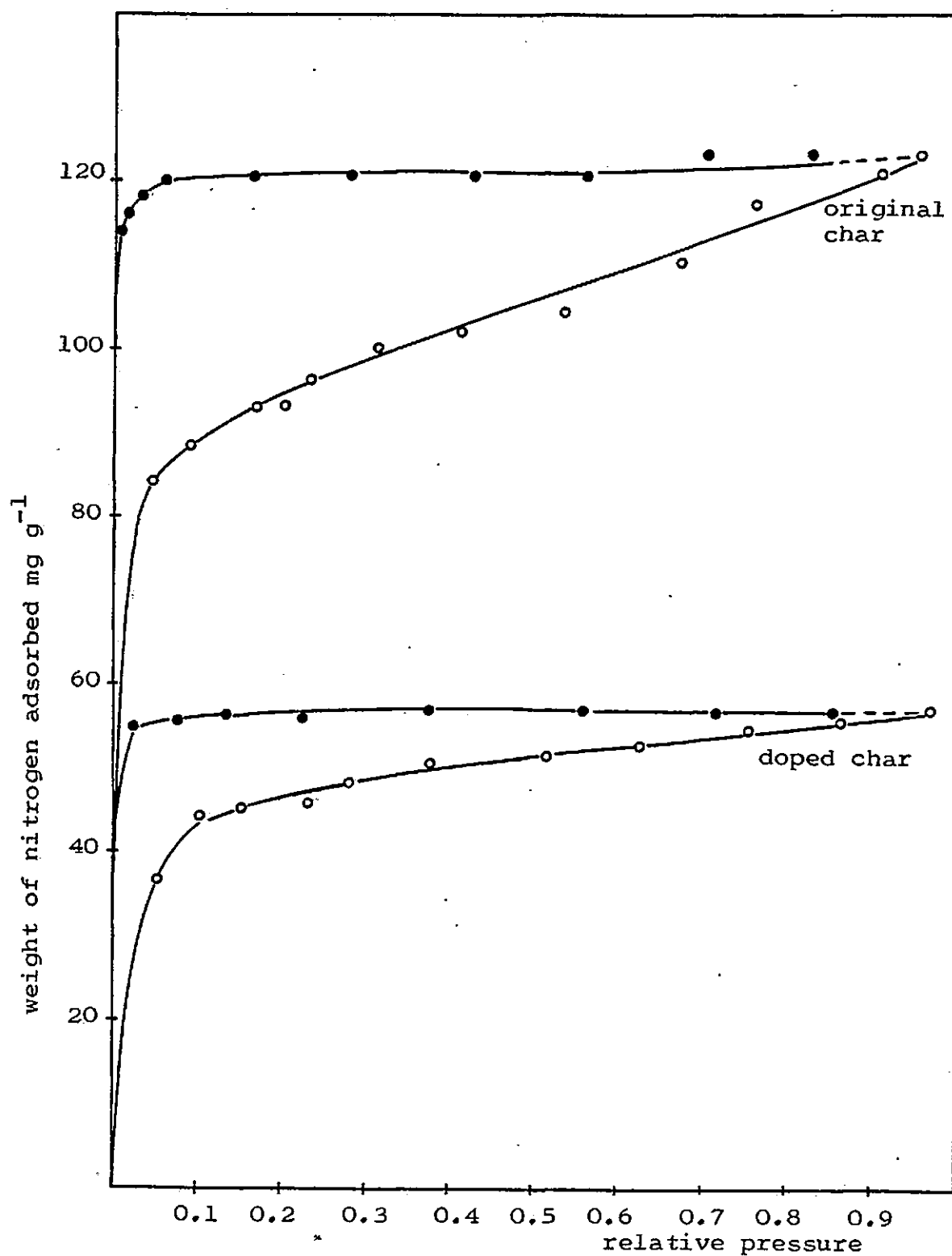
Figure 6.6.a. Nitrogen adsorption isotherms at 77 K
for Australian Brown Coal Char and B_2O_3-doped
Australian Brown Coal Char.
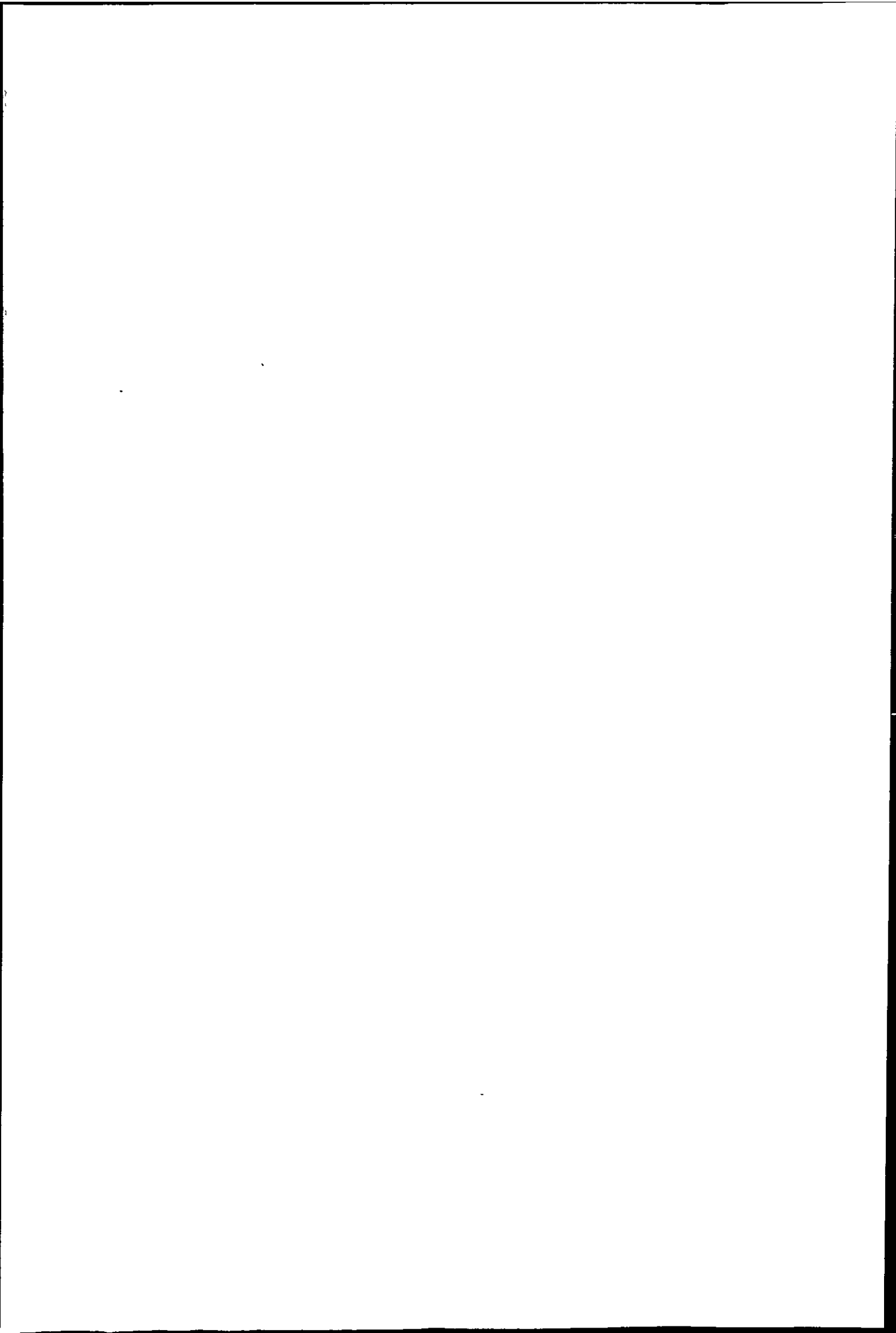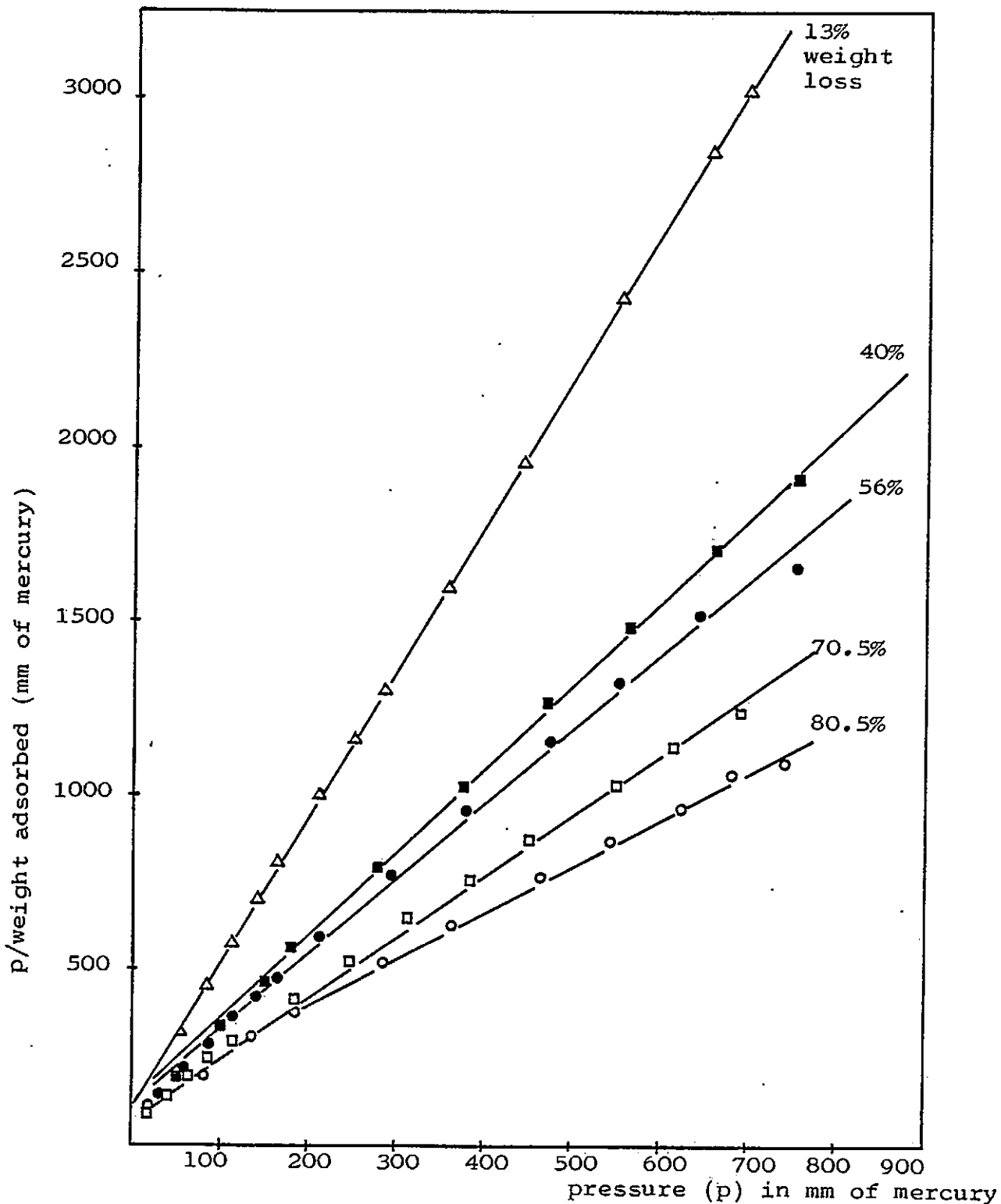
Figure 6.6.b. Langmuir Plots from CO_2 adsorption at
196 K on Australian Brown Coal Char Burnt off in CO_2
at 910 °C.

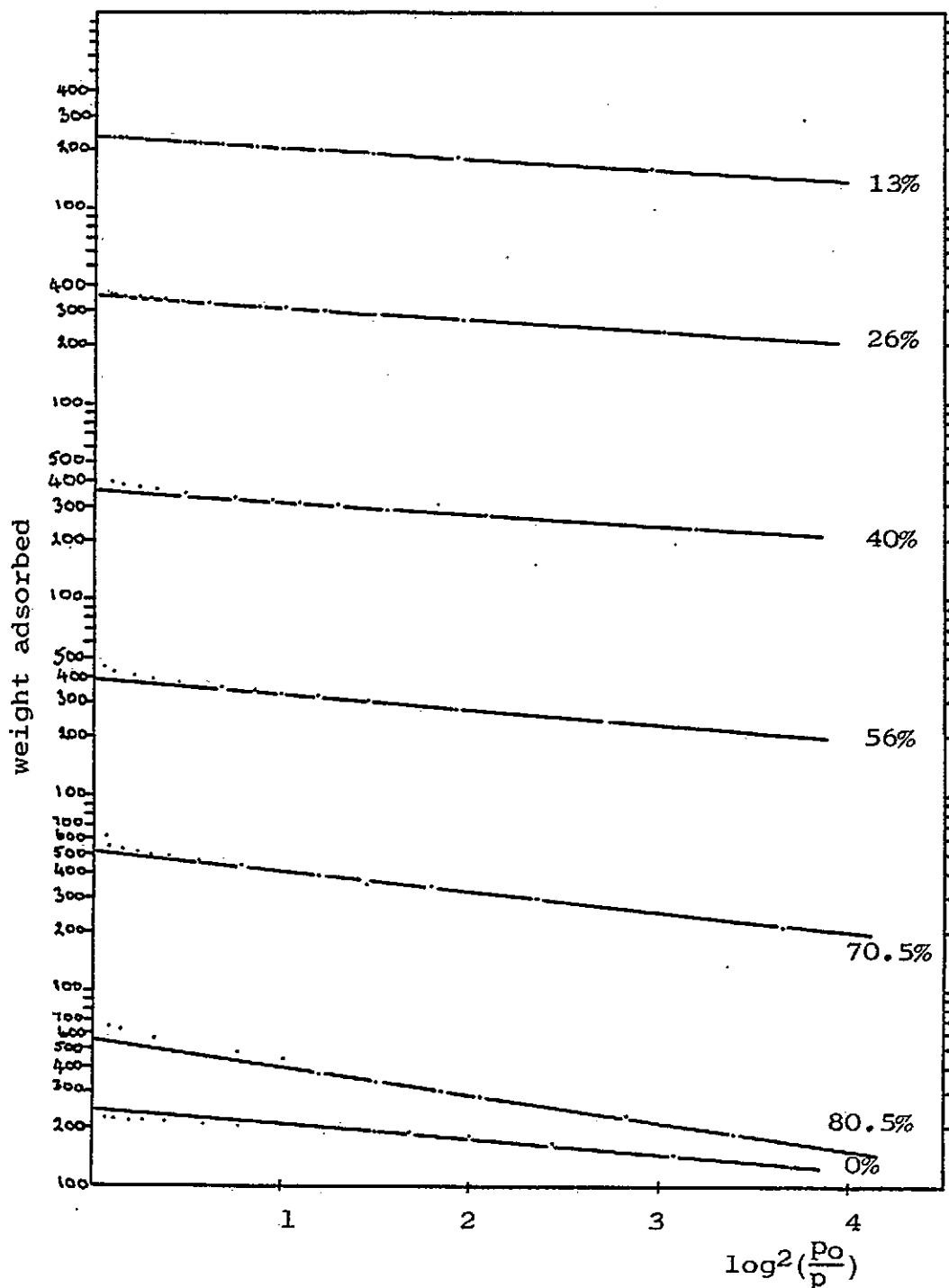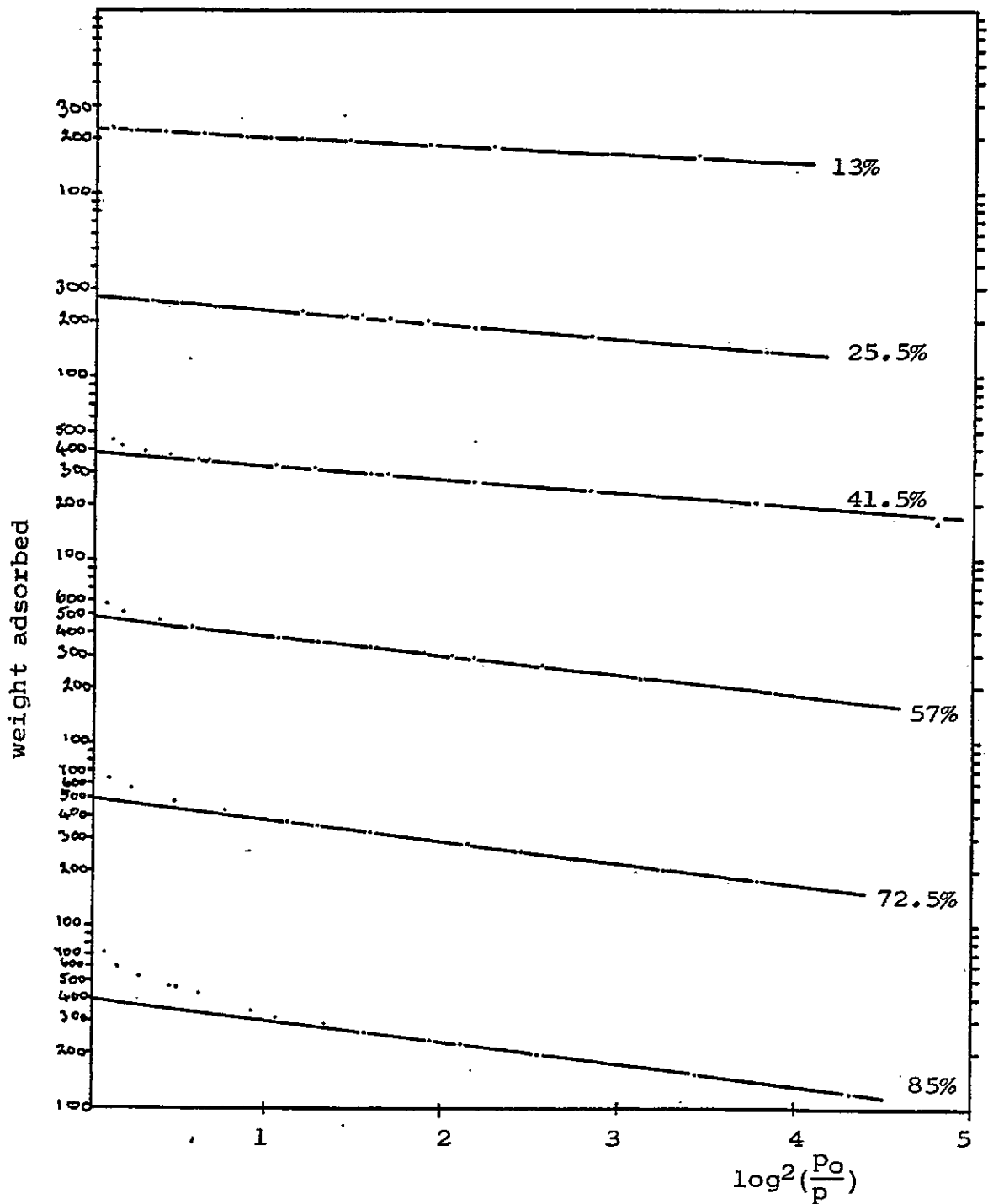(Weight adsorbed has been measured in g CO_2 g^{-1} sample)

Figure 6.6.c. Dubinin-Radushkevich plots from CO_2 adsorption at 196 K on Australian Brown Coal Char burnt off various amounts in CO_2 at 910 $^{\circ}C$

(Weight adsorbed has been estimated in mg g^{-1})

Table 6.6.a

N_2 sorption by Australian Brown Coal Char at 77 K.

Material	Specific surface area m^2 g^{-1}	Material	Specific surface area m^2 g^{-1}
original char	440	B_2O_3 doped char	206
original char heat-treated at 500 °C under N_2	542 (BET 396)	doped char heat-treated at 500 °C under N_2	483

Table 6.6.b.

CO_2 sorption by Australian Brown Char Coal at 196 K.
* burn off at 710 °C

% weight loss at 910 °C in CO_2	% carbon burn off	Specific surface area m^2 g^{-1}	Surface area per g original material m^2 g^{-1}	Wo mg CO_2 g^{-1}	Open micropore volume cm^3 g^{-1}
0	0	527	527	240	0.211
13	1.2	554	547	230	0.202
26	16.3	853	714	350	0.307
40	32.6	938	632	355	0.311
40*	32.6*	930*	627*	375*	0.329*
56	51.2	1045	510	390	0.342
70.5	68	1313	420	510	0.447
80.5	79.7	1662 (BET 1129)	337	550	0.483
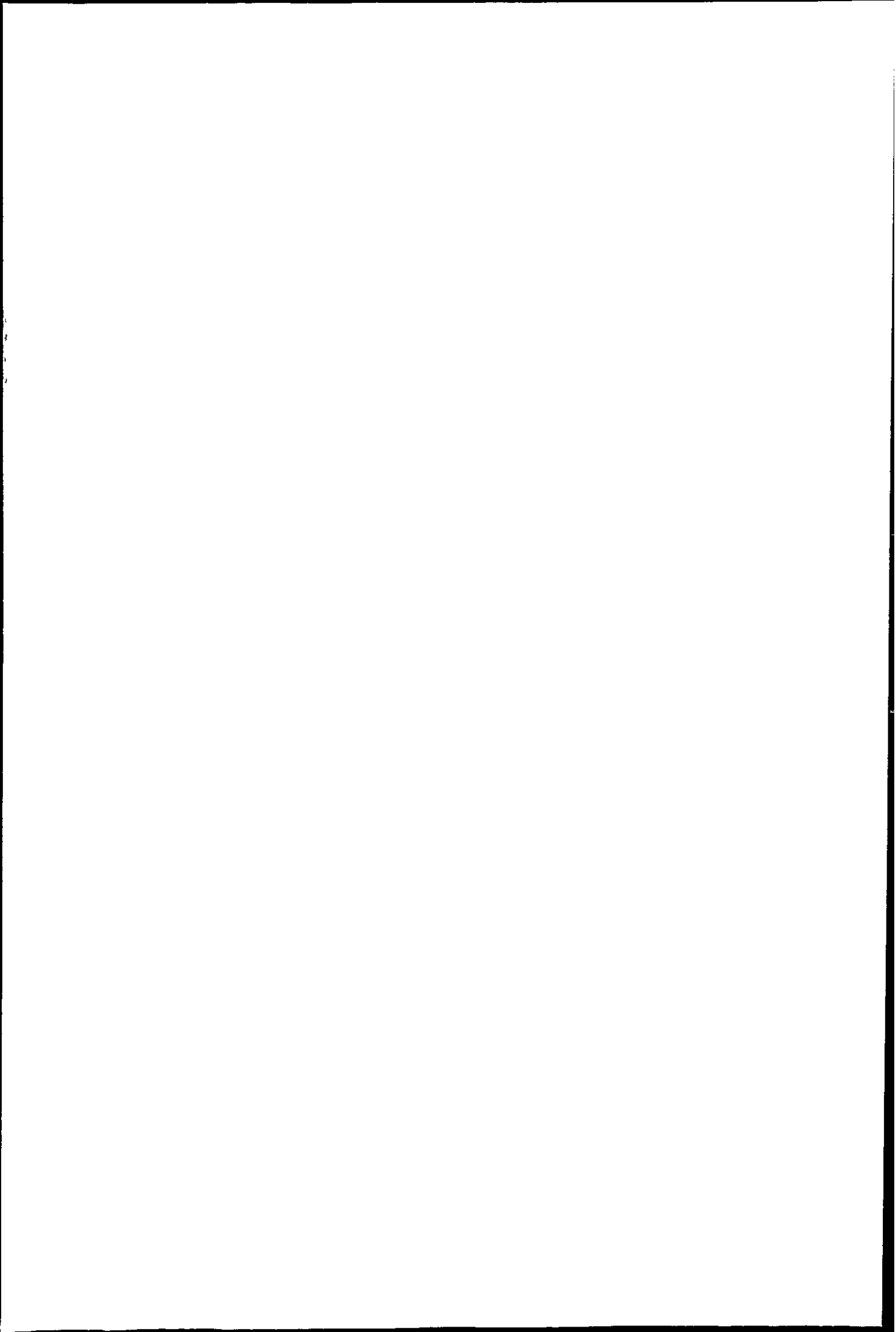
Figure 6.6.d. Dubinin-Radushkevich plots from CO_2 adsorption at 196 K on B_2O_3-doped Australian Brown Coal Char burnt off various amounts in CO_2 at 910 °C.

(Weight adsorbed was estimated in mg CO_2 g^{-1} char)

Table 6.6.c

CO_2 sorption at 196 K by B_2O_3 doped Australian Brown Coal Char.

% weight loss in CO_2 at 910 °C	Specific surface area $m^2 g^{-1}$	Wo mg CO_2 g^{-1} char	Open Micropore volume $cm^3 g^{-1}$
O	490		
13.0	533	230	0.202
25.5	632 (BET 483)	270	0.237
41.5	1121 (BET 695)	380	0.333
57.0	1551 (BET 849)	485	0.425
72.5	1776 (BET 930)	500	0.439
81.0	1861 (BET 952)	400	0.351
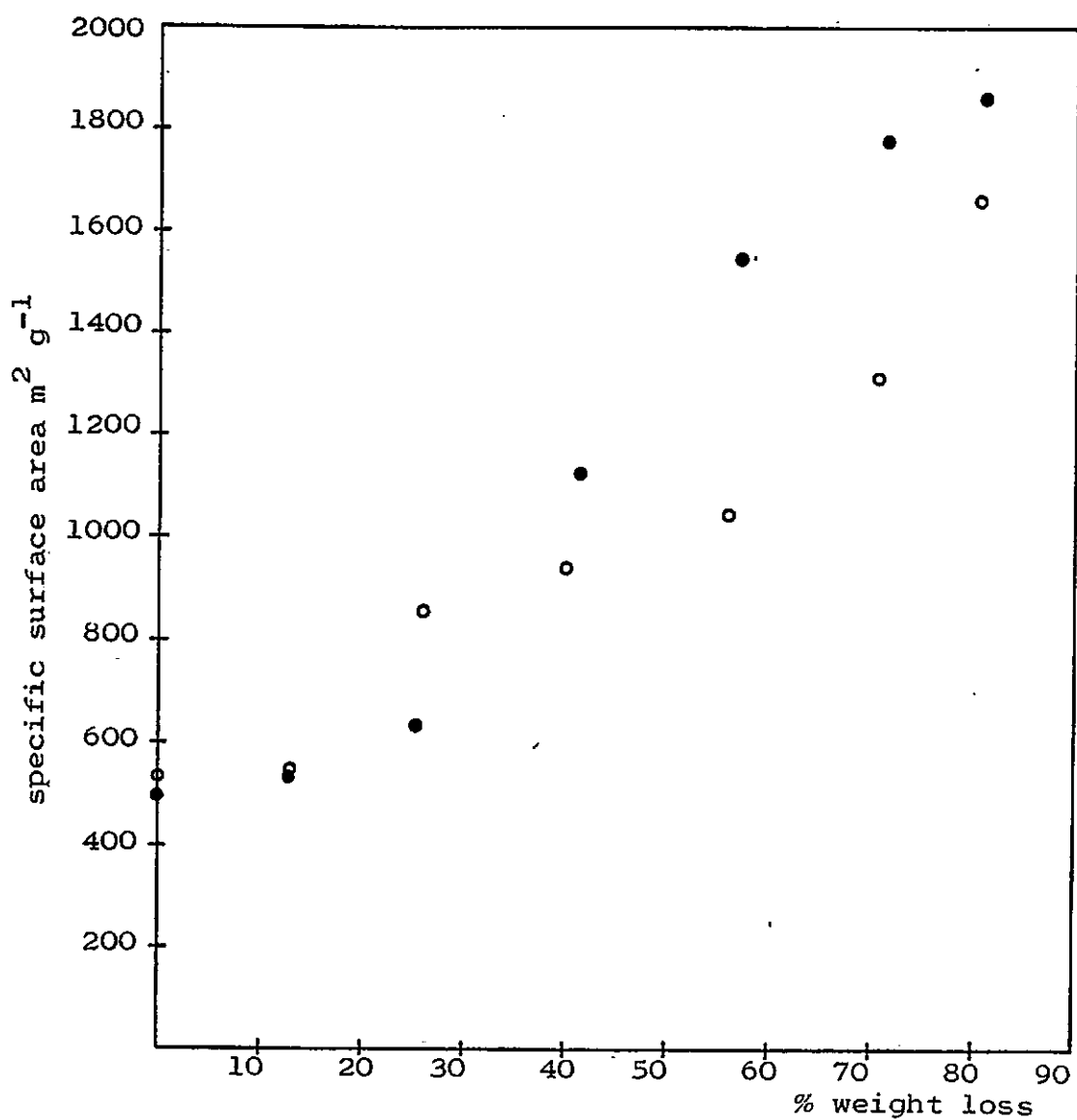
Figure 6.6.e. Variation of Surface Area with Burn off in CO_2 for Australian Brown Coal Char.

open circles :- char
closed circles :- B_2O_3-doped char
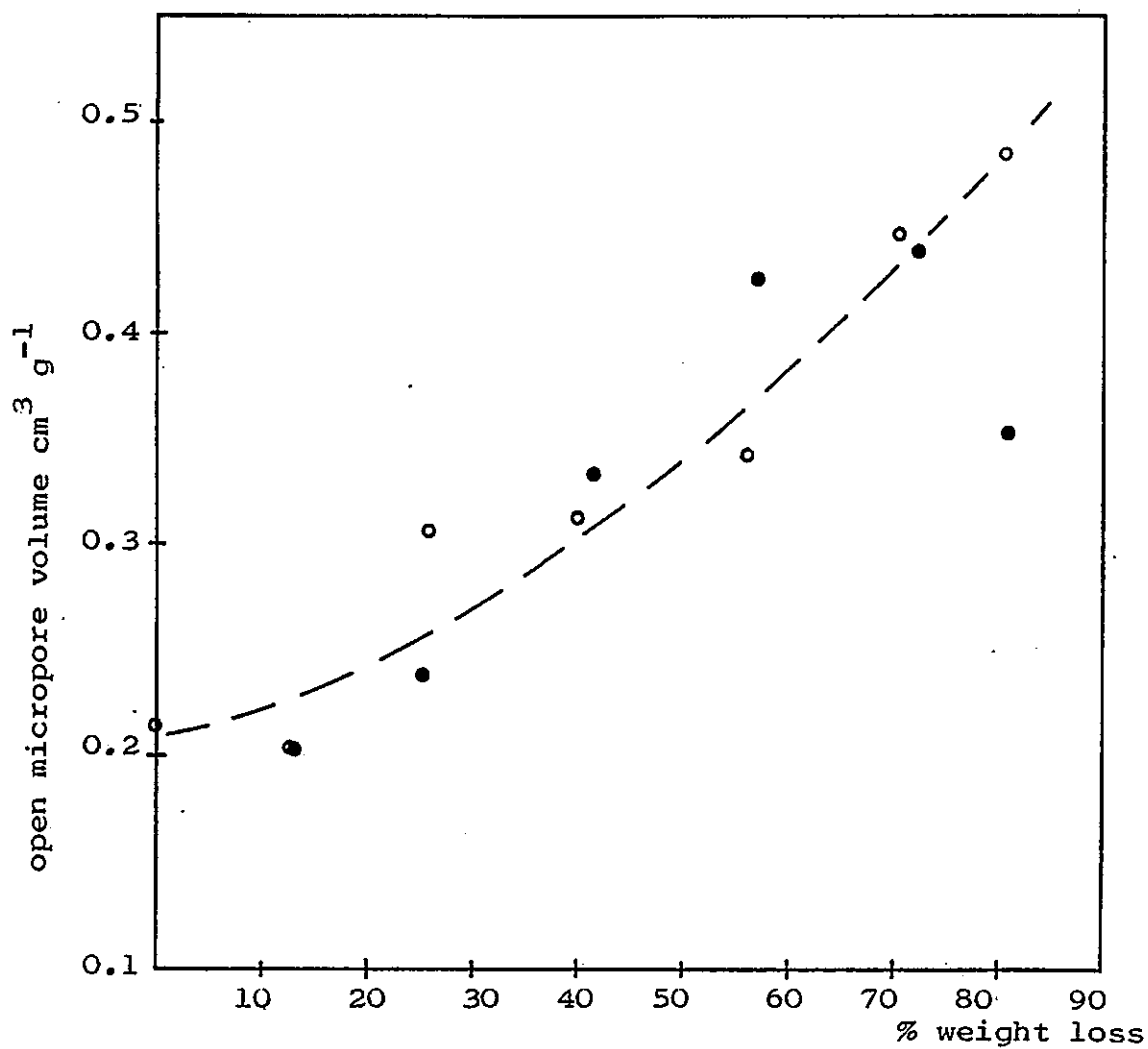
Figure 6.6.f. Variation in Open Micropore Volume with Burn off in CO_2 for Australian Brown Coal Char.

open circles :- char

closed circles :- B_2O_3-doped char

6.6.2 Discussion.

Preliminary investigation of the char had shown that heat treatment never completely removes volatile matter, and in this work the char had only been dried at 110 $^{\circ}C$ for pretreatment. Thus the first 12% weight loss represents the volatile matter. Percentage carbon weight loss is calculated on this basis and allowing for 2% ash content and, in doped samples, 2% B_2O_3.

Surface area per g of original char (specific surface x $\frac{100 - \text{percentage carbon loss}}{100}$) is seen to increase during the initial part of the burn off despite carbon being removed from the surface. (Table 6.6.b.) The specific surface area increases by 200%, but the open micropore volume by about 130%. This would suggest that additional surface is created by the enlargement of meso and macropores. Isothermal studies have shown that 910 $^{\circ}C$ is within the zone of chemical control of rate. These porosity measurements would suggest that reaction of CO_2 occurs within the larger pores of the char.

The Langmuir plots of Figure 6.6.b show linear regions. At low pressures (<50 mm Hg) some curvature is seen, which was more pronounced for the burnt off doped samples. As wider pores form a larger fraction of the total porosity as burn off increases, the Langmuir equation may not be applicable due to multilayer formation and/or capillary condensation. The validity of surface areas calculated from this equation is open to question due to the simplified picture of the surface and the idea of

298

localised adsorption, but the treatment is useful here in comparing the doped and original chars.

.As seen in Figure 6.6.e B_2O_3 treatment has not reduced the specific surface area of the char on burn off in CO_2. Values are even higher after 40% weight loss than for the undoped material.

For a material of 2% inerts (volatile free char) and 4% inerts (volatile free doped char) the build up of surface ash is not significant until about 80% weight loss, as plotted in Figure 6.6.g. The specific surface area of the doped char is levelling off at 81% weight loss due to this accumulation of surface material, whereas that of the undoped char is still increasing.

The reduction in rate of reaction in CO_2 at 907 $^{\circ}C$ by B_2O_3 treatment is from 403×10^{-6} g $s^{-1}g^{-1}$ to 168×10^{-6} g $s^{-1}g^{-1}$ (Chapter 5.4). Thus it is not the total surface area that is important, but that fraction of it containing pores greater in size than micropores.

The time taken to burn off a particular weight of carbon is much greater for the doped samples. If some of the larger pores are blocked an increase in open micropore volume compared with the undoped char may occur. The open micropore volumes, as plotted in Figure 6.6.f are similar although a greater increase in that of the doped char does occur between 40 and 70% weight loss.

The maximum relative pressure obtainable was about 0.54 using CO_2 at 196 K. Nitrogen sorption at 77 K can attain a relative pressure of 0.96 and the isotherms of
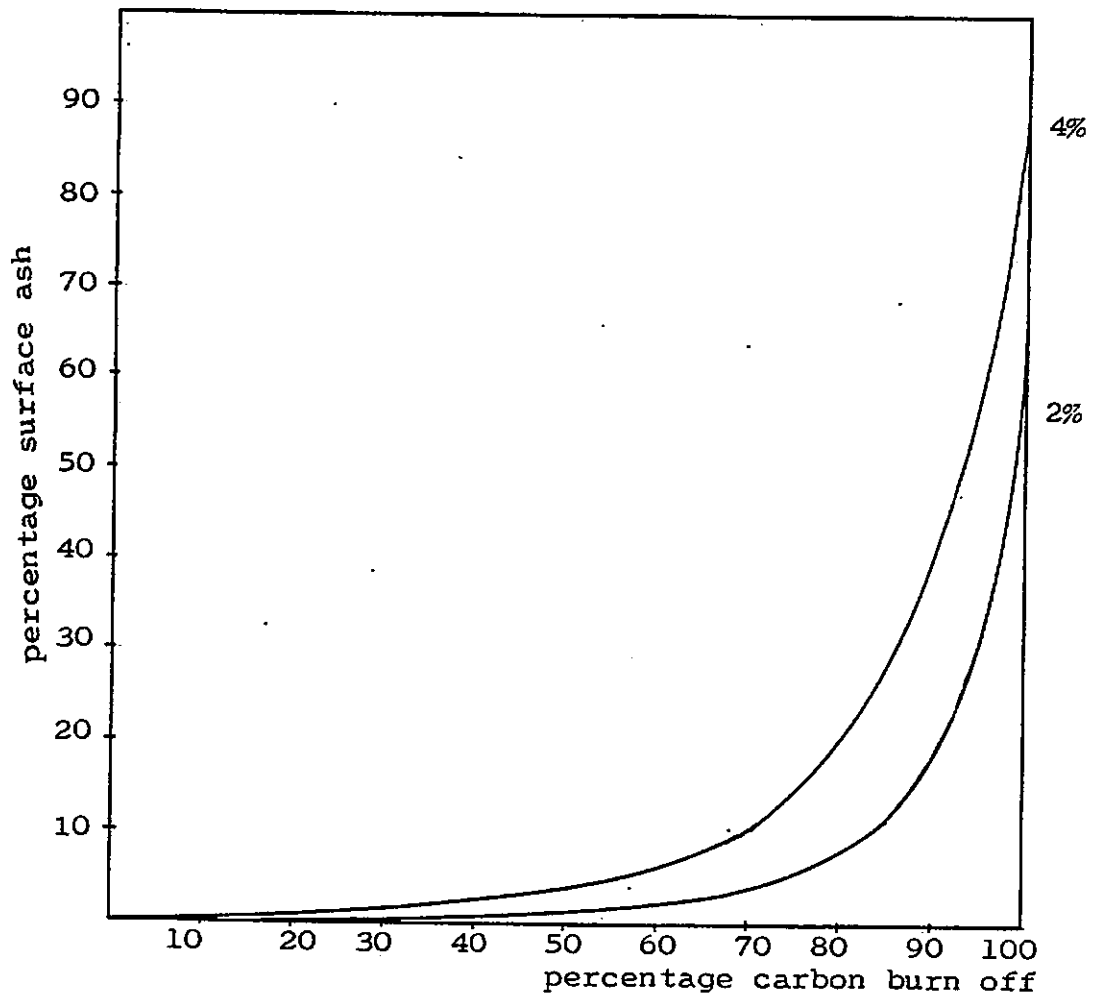
Figure 6.6.g. Accumulation of surface mineral matter
for a Carbon of 4% and 2% mineral content

Figure 6.6.a show that a complete range of pore sizes exists in the char, and the doped char. Before heat treatment the additive is present as H_3BO_3.

The calculated specific surface areas (from Langmuir plots), given in Table 6.6.a are lower than those obtained from CO_2 sorption, as discussed in Chapter 4.

From the specific surface areas determined by nitrogen sorption B_2O_3 doping reduces 542 m^2 g^{-1} to 483 m^2 g^{-1}, a reduction of 10.9%. The comparable CO_2 sorption results give a reduction of 554 m^2 g^{-1} to 533 m^2 g^{-1}, ie 3.8%. Although the nitrogen results may underestimate the specific surface area (by micropores not being accessible to N_2 at this temperature) the blockage of the larger pores by B_2O_3 is indicated.

References

1. "Microweighing in Vacuum and Controlled Environments"

   p.163, Czanderna & Wolsky (Eds.), 1980, Elsevier.

   Volume 4 of 'Methods and Phenomena. Their

   Applications in Science and Technology."

2. S.J. Gregg & K.S.W. Sing. "Adsorption, Surface Area and
   Porosity", 1967, Academic Press.

3. J.W. Sutherland. "Porous Carbon Solids". R.L. Bond

   (Ed.), Academic Press, 1967.

4. S.J.Gregg. "The Surface Chemistry of Solids",1961,
   Chapman and Hall.

5. S. Lowell. "Introduction to Powder Surface Area",1979,Wiley.

6. J.H. de Boer, Adv. Catalysis, 1956, $\underline{8}$, 18.

7. M.M. Duninin. Chem. Rev. 1960, $\underline{2}$, 235.

8. H. Marsh & B. Rand, Proc. 3rd Conf. Industrial

   Carbons and Graphite, 1970, SCI London, 172-83.

9. H. Marsh, Fuel, 1965, $\underline{44}$, 253-68.

10. T.G. Lamond & H. Marsh, Carbon, 1964, $\underline{1}$, 281-92.

11. H. Marsh & W.F.K. Wynne-Jones, Carbon, 1964, $\underline{1}$,

    269-79.

12. R. B. Anderson, J. Bayer & L.J.E. Hofer, Fuel,

    1965, $\underline{44}$, 443-52.

13. P. Chiche, H. Marsh & S. Pregermain, Fuel, 1967,

    $\underline{46}$, 341-50.

14. M. Bastick & H. Guerin, J. Chim. Phys. et Phys.

    Chim. Biol. 1961, $\underline{58}$, 97-105.

15. Y. Grillet & H. Guerin. Comptes Rendus - Academie

    des Sciences Paris - Serie C 1970, $\underline{270}$ pt. 9,

    757-60.

16. J. H. Blake, G.R. Bopp, J.F. Jones, M.G. Miller
    & W. Tambo, Fuel, 1967, 46, 115-25.

17. W. Fassotte & M. Saussez. Institut National des
    Industries Extractives. Bull. Tech. No.42, 1973.

18. A. Cameron & W.O. Stacy. Aus. J. Appl. Science,
    1959, 10(4), 449-57.

19. J. Berger, T. Siemieniewska & K. Tomkow, Fuel, 1976,
    55, 9-15.

20. N.B. Gray & V.N. Misra. Proc. Australia-Japan Extractive
    Metallurgy Symposium (Australia) 1980, 419-29.

21. N. G. Dovaston, B. McEnaney & S.M. Rowan, Proc. 3rd
    Conf. Industrial Carbon and Graphite, 1970, SCI
    London 212-8.

22. C.J. Keattch & D. Dollimore, "An Introduction to
    Thermogravimetry", 2nd Edition, 1975, Heyden, p.95

23. D.A. Aderibigbe & J. Szekely, Metallurgical
    Transactions B, 1982, 13B, 513-5.

CHAPTER SEVEN

DYNAMIC TG/DTA STUDIES

7.1 Introduction

The previous chapters have described experimental work on carbons and cokes at constant temperature, pressure and gas composition. Under industrial conditions coke lumps are subject to a time-dependent temperature and gas composition during their descent in the blast furnace. Thus it is more realistic to employ dynamic thermal analysis methods in studying their reactions.

By dynamic methods a whole temperature range can be studied quickly and continuously. With a sensitive thermal balance the sample size can be small and heating rate slow, reducing thermal gradients in the sample. Simultaneous TG/DTA was carried out on the Massflow thermal balance for air oxidations of the carbons. The higher furnace temperature of the STA 781 thermal balance allowed an investigation of air and CO_2 oxidation of the materials; it gave also simultaneous DTG data.

Dynamic thermal methods have been applied to the oxidation of lead sulphide[1] and zinc sulphide[2] for the Zn/Pb blast furnace, and to the oxidation of nickel ore concentrates by Jayaweera and Dunn[3]. There have been relatively few applications of dynamic methods to the oxidation of coke, in contrast with the large number of isothermal studies.

Dynamic TG and DTA have been used to obtain kinetic parameters, although practical and theoretical difficulties arise, as discussed in Chapter 2.3.1, particularly for

solid state reactions. No quantitative kinetic analysis from TG data was attempted in the present work, but the effect of rate of heating and gas flow were investigated. The effect of fast heating rate on a TG curve is generally to increase the temperature at which a reaction appears to start and to extend the range over which a weight loss is observed. Rates of 5 to 10 $^{o}C\ min^{-1}$ are commonly employed.

A DTA curve is usually characterised by the temperature of the start of a change (the temperature of the point of intersection of baseline with extended straight line of the ascending side), the temperature of the peak, the temperature at the maximum rate of reaction and the temperature at the end of the change. These are complex functions, as described by Blazek (Chapter 2, reference 58). Kinetic factors are known to influence the shape of a DTA peak. Variations in activation energy and frequency factor change the position and size of a peak but have little change on shape. Change in order of reaction greatly affects the shape of a DTA curve, the higher the order the broader and more symmetrical the peak.

For first order reactions Kissinger[4] developed a method for obtaining kinetic parameters from the variation in peak temperature with heating rate, and extended this to reactions of any order, provided the latter does not change during the course of the reaction.[5]

Based on heat flow equations of the form

$$\frac{\partial T}{\partial t} = \frac{k}{\rho c} \nabla^2 T$$

(where $\nabla^2 T$ is the 2nd derivative of temperature T, with respect to dimensional coordinates, t the time, k the thermal conductivity, ρ the density and c the specific heat capacity) in combination with the Arrhenius equation, Kissinger derived

$$d(\ln \frac{\phi}{T_m^2}) = - \frac{E_A}{R} d(\frac{1}{T_m})$$

where ϕ is the heating rate $(\frac{dT}{dt})$ and T_m the temperature at which rate of reaction is greatest, which temperature he took as the peak temperature of the DTA curve.

Several DTA curves are recorded at the same sensitivity and sample weight but different heating rates. Peak temperatures are recorded and a graph is plotted of $\ln(\frac{dT}{dt}/T_m^2)$ versus $\frac{1}{T_m}$. A straight line is obtained of slope $- \frac{E_A}{R}$.

The premise that the DTA peak temperature coincides always with the maximum rate of reaction is incorrect and the above method is widely criticised. However the simultaneous TG/DTG/DTA functions of the STA781 thermal balance had shown that in the air and CO_2 oxidation of Nantgarw coke and Australian brown coal char these temperatures were very close. Isothermal studies had shown that diffusion was not rate limiting for the CO_2/Nantgarw coke reaction at least to 1350 ^{o}C so an unchanging order of reaction could be assumed. It was hoped that this method would give useful comparative information on the reaction of the B_2O_3 treated coke and char. Isothermal studies rely on determination of amount

of material burnt off. The DTA curve made no assumptions as to degree of burn off and in fact does not yield such information.

A comparative study of Nantgarw, Cwm and Polish cokes was also made by dynamic thermal methods.

7.2 Experimental Procedures

7.2.1 Initial air oxidations were carried out on the Massflow balance described in Chapter 3.1.1, applying the appropriate buoyancy correction to the TG curve (which had been determined by finding the apparent weight gain at various heating rates using Al_2O_3 in reference and sample crucibles.) TG chart speed of 12" h^{-1} was used and the weight loss calculated and replotted. The chart full width was set at 20 mg and it was possible to achieve a sensitivity of 0.1 mg. Silica crucibles were used with calcined Al_2O_3 as DTA reference material. DTA amplifier sensitivity was 100 μV full scale except for graphite when 250 μV was used and the trace was replotted. DTA baseline was made as linear as possible by adjusting the three screws of the ceramic head containing the crucibles and the DTA chart was run at 3" h^{-1}. Flowing air was introduced from the lower inlet port after passing through a rotameter, adjusting the flow to 1 l min^{-1}.

Air and CO_2 oxidations were carried out on the STA 78.1 thermal balance described in Chapter 3.1.2. Pt/Rh crucibles were used with calcined Al_2O_3 as DTA reference material. TG buoyancy effect was negligible. DTA baseline was set by adjusting the feet of the balance unit and the gas flow was adjusted on the integral flow meter. CO_2 was first dried by passage through $MgClO_4$. Recorder chart speeds of 100 and 200 mm h^{-1} were found to be suitable. DTA amplifier range and DTG range had to be found before a set of experiments, by trial and error.

For the investigation of particle size a char sample was crushed and sieved fractions taken. Coke was more difficult to crush and samples of greater particle size range (< 180 μm) were used. In all other runs single coke lumps or char granules 1.4 to 0.71 mm were used. The crucibles limited the coke lump size to about 3 mm diameter.

7.2.2 In the study of variation in peak temperature with heating rate, approximately 3 mm diameter lumps of Nantgarw coke were used, giving samples of about 13 mg. The CO_2 flow was set at 50 (35.2 cm^3 min^{-1}) and the furnace heated at 45 ^{o}C min^{-1} until a sample temperature of 900 ^{o}C was reached. The temperature programme was then selected. DTA amplifier sensitivity of 40 μV and recorder chart speed of 100 mm hr^{-1} were used. 500-710 μm coke granules were similarly treated using the same sample weight.

3 mm lumps of Nantgarw coke were doped with B_2O_3 as previously described, 1.56% of sample weight being retained for that batch. It was not possible to completely burn off the doped coke at rates higher than 8 ^{o}C min^{-1} before the completion of the temperature programme, so fewer results were obtained than for undoped lumps.

Australian brown coal char granules 1.4 to 0.71 mm were similarly studied using approximately 12 mg samples and the same CO_2 flow rate, and by heating the sample at 45 ^{o}C min^{-1} to 500 ^{o}C before selecting the temperature programme. The programme limit was set at 1200 ^{o}C. Recorder chart speed of 100 mm h^{-1} and DTA sensitivity of 40 μV, and 80 μV for heating rates above 6 ^{o}C min^{-1} were used, (the DTA amplifier ranges having been previously zeroed).

Doped char from the same batch as used in isothermal work was similarly studied.

7.2.3 Cwm and Polish coke lumps of approximately 3 mm diameter were selected and reacted in CO_2 at two heating rates, treating them as for Nantgarw coke. The temperature programme was selected when a sample temperature of 800 $^{\circ}C$ had been reached (on heating the furnace at 45 $^{\circ}C$ min^{-1}).

A value of R of 8.314 JK^{-1} mol^{-1} was taken in the calculations.

7.3   Results

7.3.1 Coke and Carbon Oxidations

Static air oxidations at $5\ ^{\circ}C\ min^{-1}$ of Nantgarw coke, PMC graphite, Australian brown coal char and the Hopkin and Williams charcoals characterised in Chapter 4 are shown in the TG curves of Figure 7.1 and simultaneous DTA curves of Figure 7.2. Flowing air oxidation TG and DTA results of the materials are given in Figures 7.3 and 7.4 at the same heating rate.

The reaction of these carbons with CO_2 at a heating rate of $10\ ^{\circ}C\ min^{-1}$ and gas flow $21.1\ cm^3\ min^{-1}$ is shown by TG in Figures 7.5 and 7.6 and the corresponding DTA curves are given in Figure 7.7. These results were obtained using the STA 781 thermal balance as were the following air oxidations.

TG/DTA/DTG results for air oxidation of Nantgarw coke (lump) heated at $10\ ^{\circ}C\ min^{-1}$ and air flow $43.5\ cm^3$ min^{-1} are shown in Figure 7.8 and TG/DTA results for the coke heated at $5^{\circ}C\ min^{-1}$ at two different air flow rates in Figure 7.9.

TG/DTA/DTG results for two of the Australian brown coal char samples of different particle size, oxidised in air flowing at $17.4\ cm^3\ min^{-1}$ and heated under a temperature programme of $5\ ^{\circ}C\ min^{-1}$ are given in Figure 7.10 and the thermal analysis of this material (as a single lump) at the same heating rate but air flow of $43.5\ cm^3\ min^{-1}$ in Figure 7.11.

Key: (Figure 7.1)

A — decolourising charcoal
B — charcoal for chromatography
C — charcoal "Norit GSX"
D — charcoal activated for gas sorption
E — Australian brown coal char
F — Nantgarw coke
G — PMC graphite
H — B_2O_3-doped char
I — B_2O_3-doped Nantgarw coke.
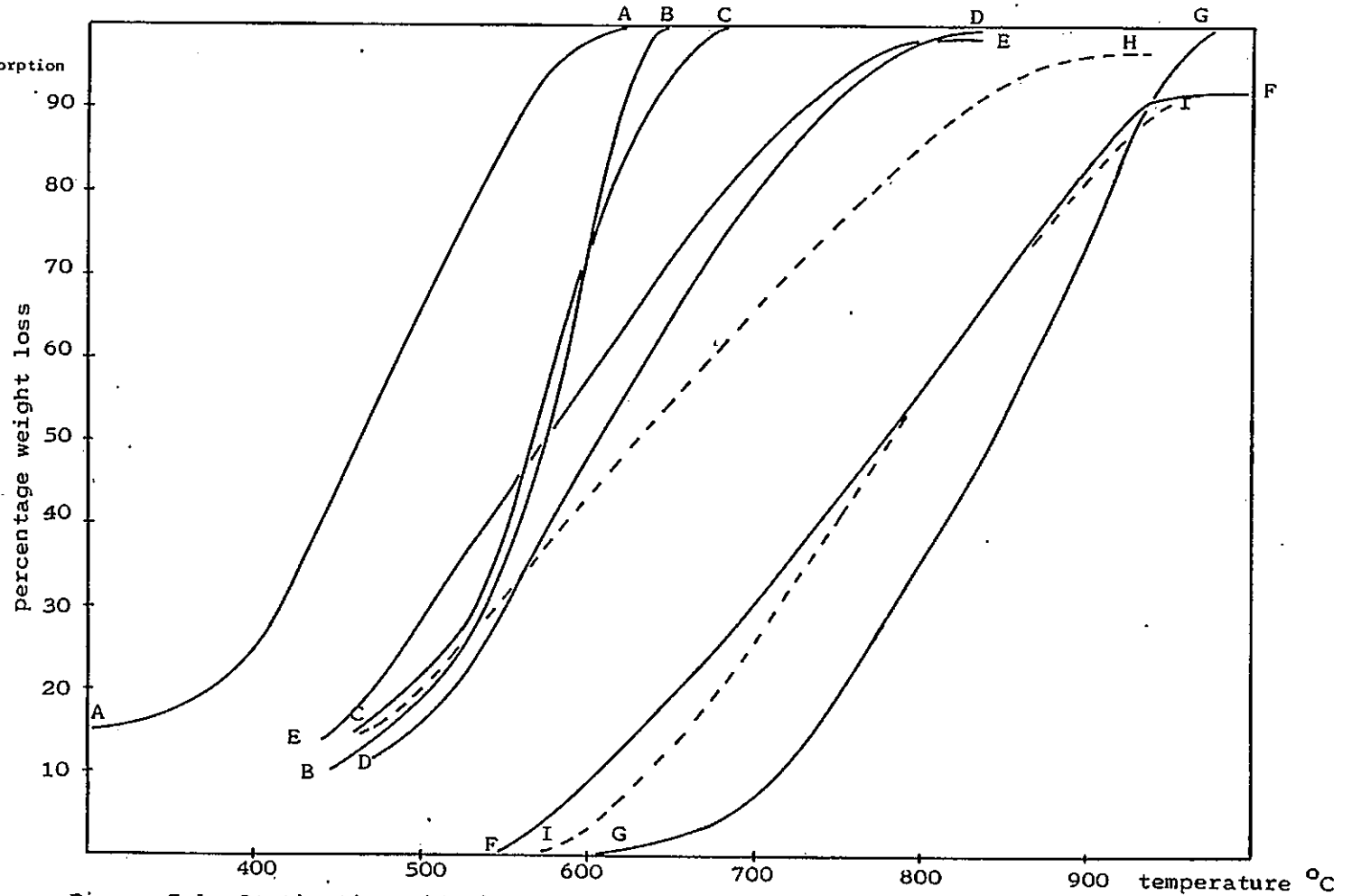
Figure 7.1. Static Air oxidation of Coke, Char and Carbons at a Heating Rate of 5 ^{o}C min^{-1}.

PMC graphite
18.4 mg

Australian brown
coal char lumps
22.4 mg

Australian brown
coal char lumps
71.8 mg

+10µV

crushed <180 µm

−10µV

Nantgarw
coke
26.2 mg

lump

Nantgarw
coke
31.8 mg

charcoal activated
for gas adsorption
13.0 mg

charcoal "Norit GSX"
12.3 mg

charcoal for
chromatography 8.0 mg

decolourising
charcoal 13.2 mg

18   120   204 361   522 611 715 812 911 1007
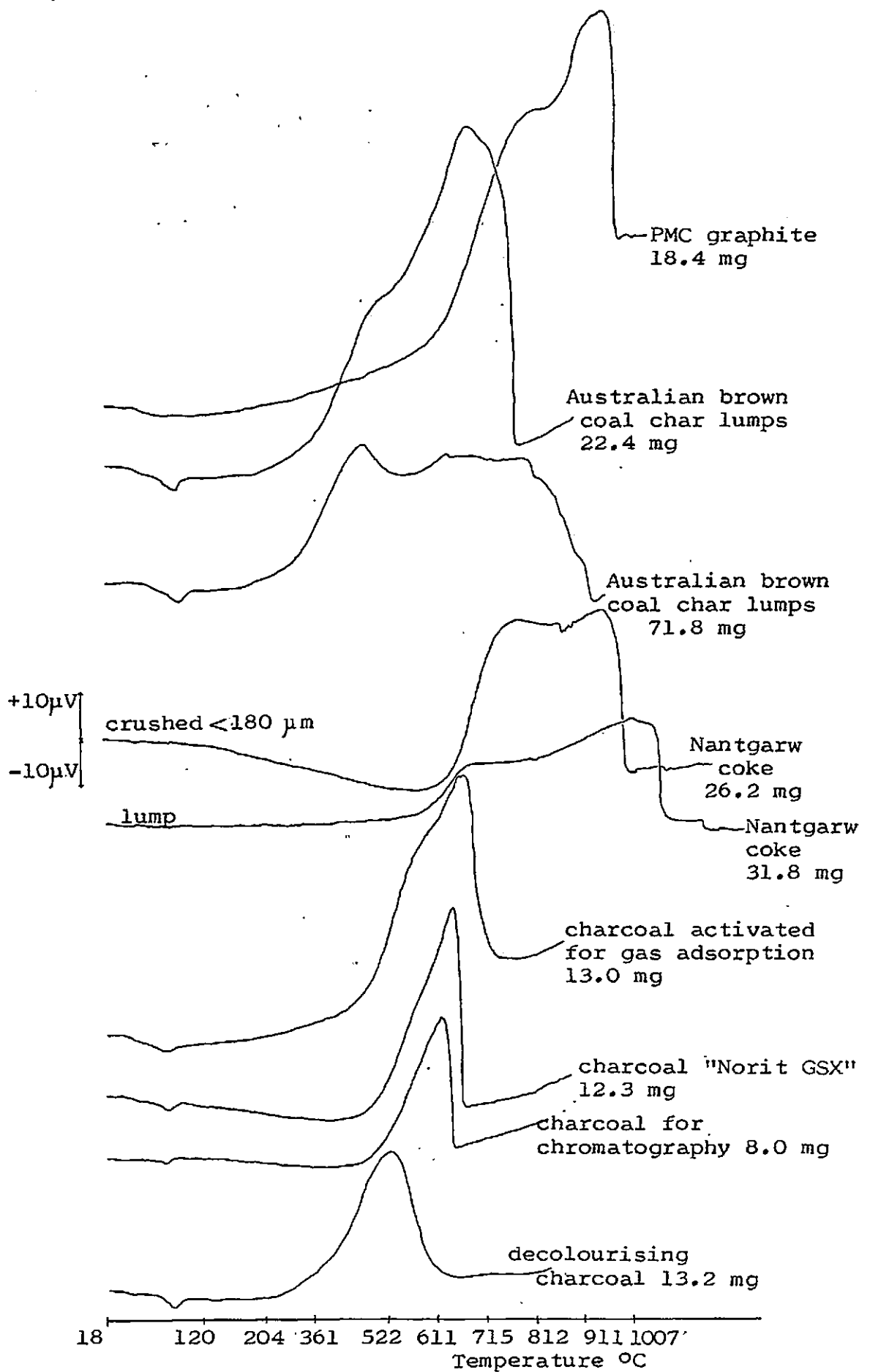
Temperature $^{\circ}$C

Figure 7.2. DTA of Static Air oxidation of Coke, Char,
Charcoals and Graphite under a temperature programme of
5 $^{\circ}$C min^{-1}.   315

Key: (Figure 7.3.)

A - decolourising charcoal
B - charcoal "Norit GSX"
C - charcoal activated for gas sorption
D - Australian brown coal char
E - Nantgarw coke
F - PMC graphite.
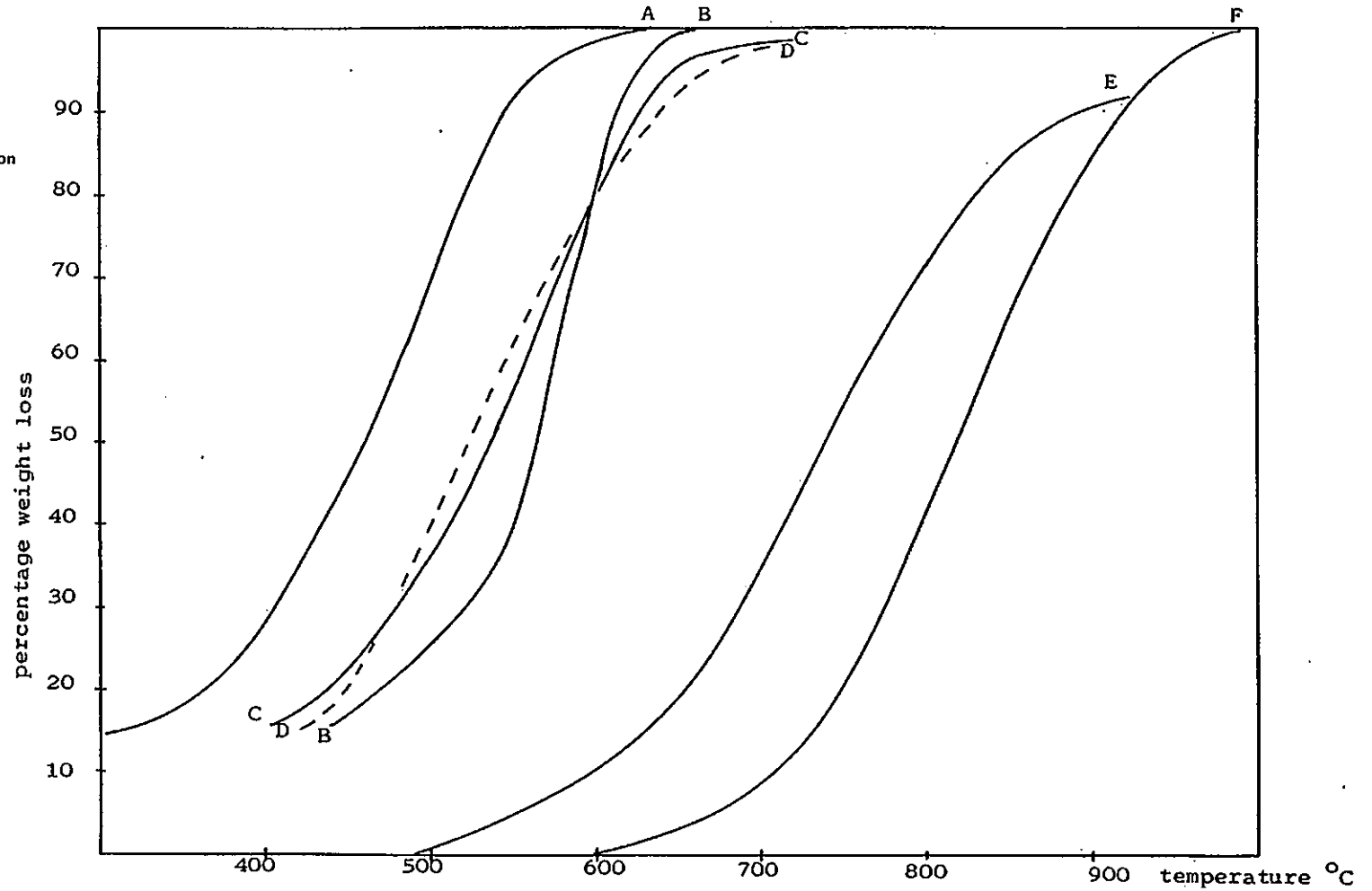
Figure 7.3. Flowing air oxidation of Coke, Char and Carbons at a Heating Rate of 5 °C min-1
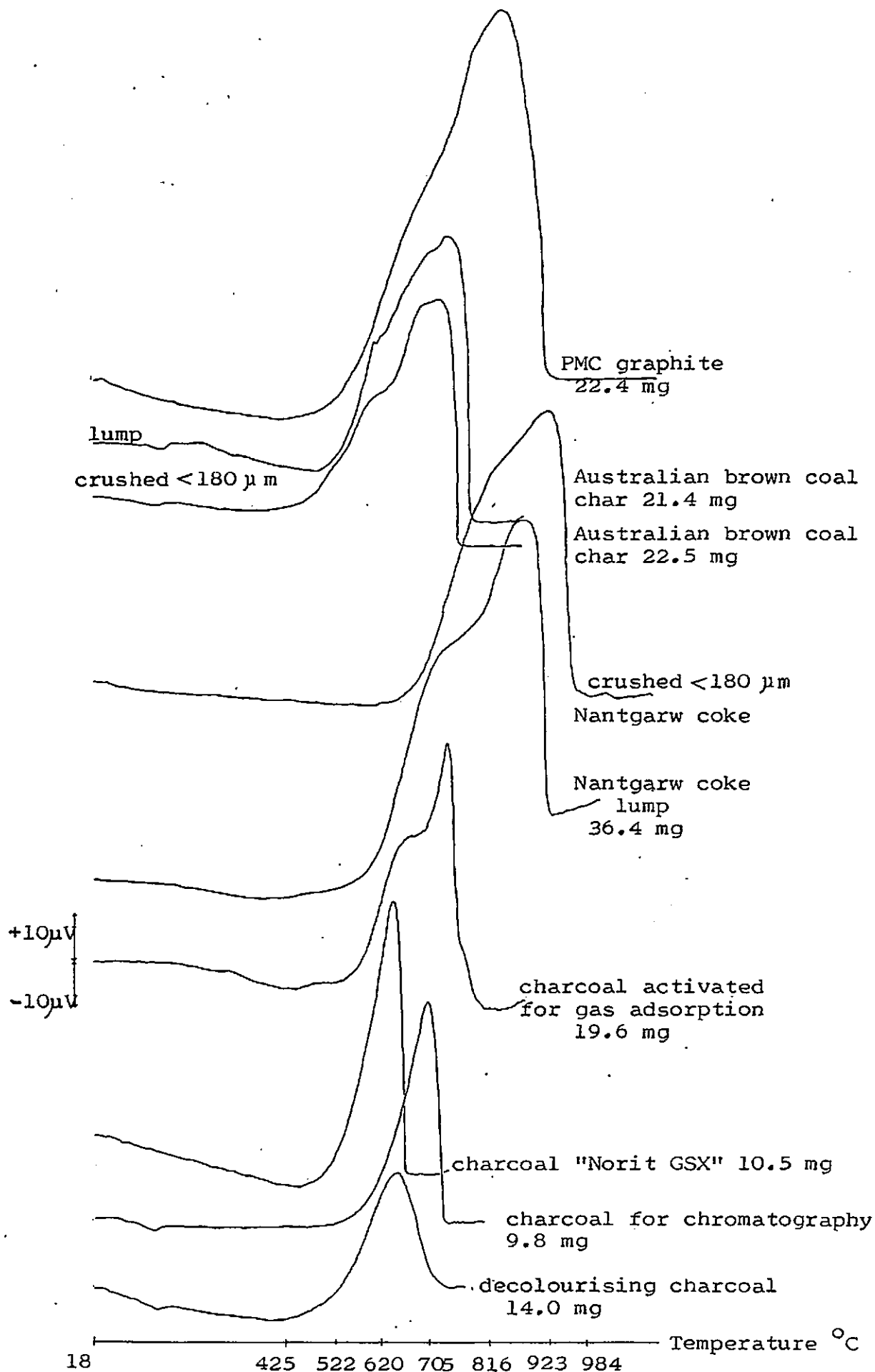
Figure 7.4. DTA of Flowing Air (1 l min^{-1}) oxidation of Coke, Char, Charcoals and Graphite under a temperature programme of 5 °C min^{-1}. 317
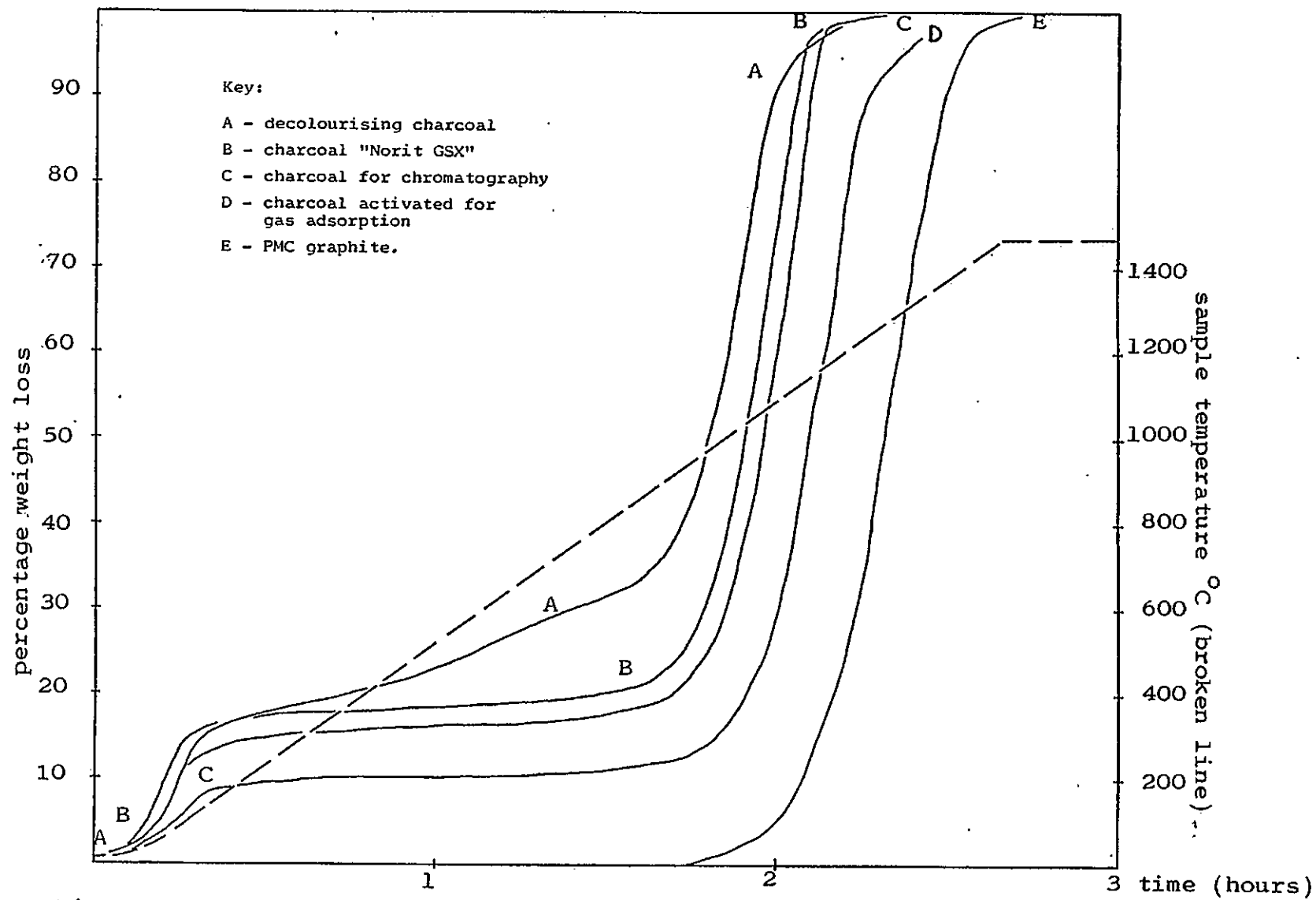
Figure 7.5. CO_2 oxidation of Charcoals and Graphite at a Heating Rate of 10 °C min-1
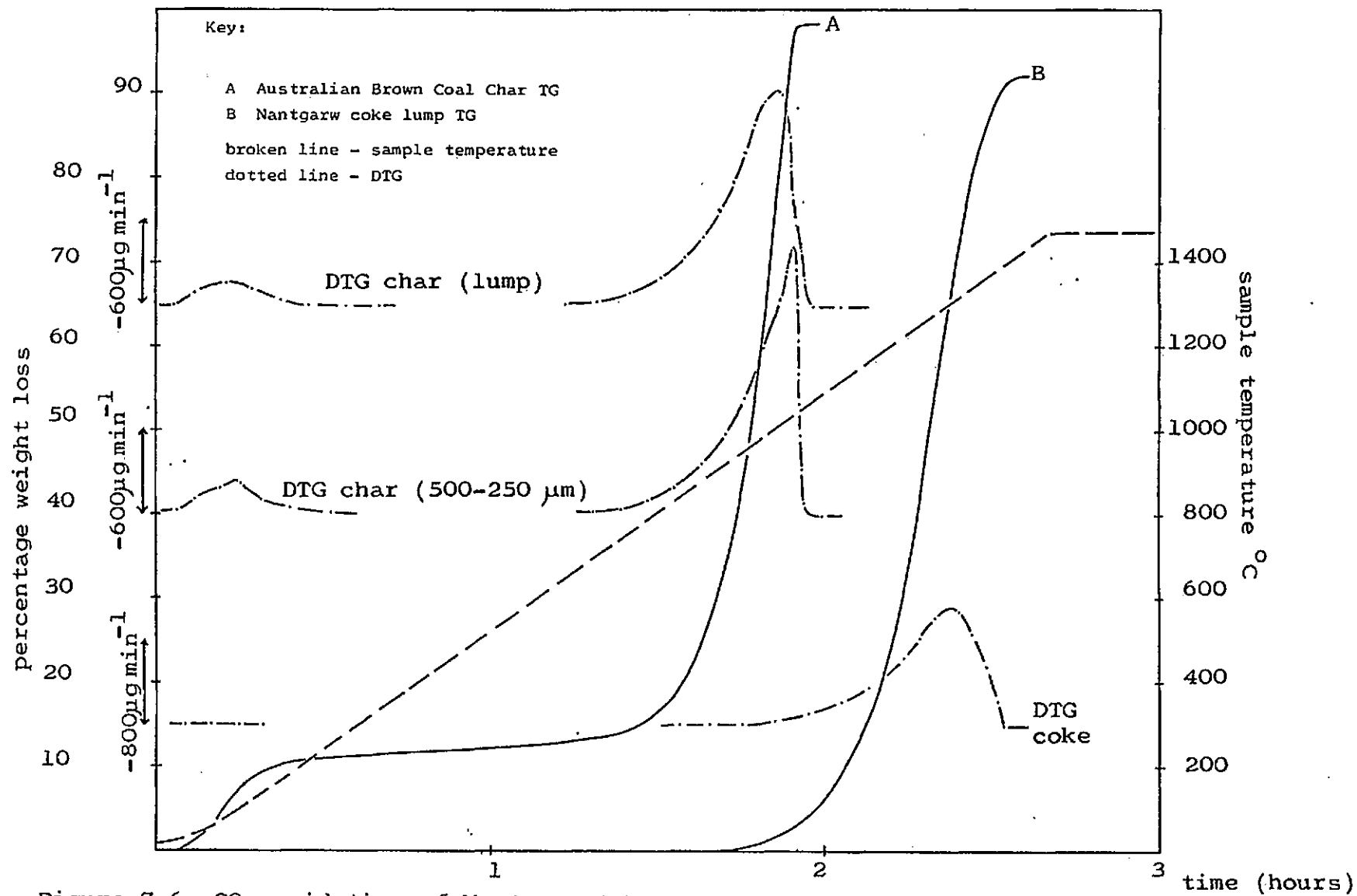
Figure 7.6. CO_2 oxidation of Nantgarw Coke and Australian Brown Coal Char at a Heating Rate of 10 °C min-1

Key:

A   Australian Brown Coal Char TG
B   Nantgarw coke lump TG

broken line – sample temperature
dotted line – DTG

DTG char (lump)

DTG char (500–250 μm)

DTG coke
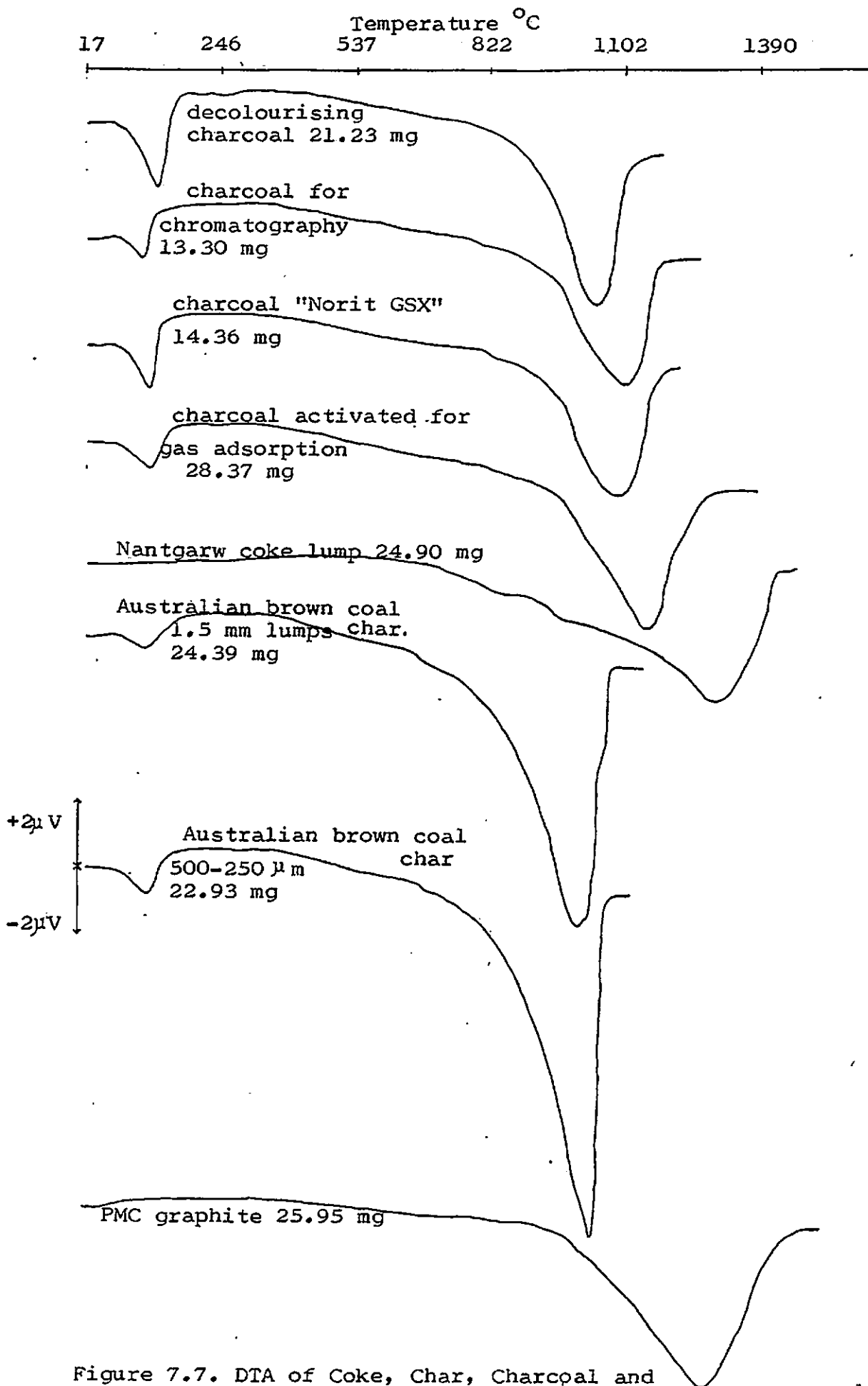
Figure 7.7. DTA of Coke, Char, Charcoal and
Graphite oxidation in CO_2 at a heating rate of 10 ^{o}C min^{-1}
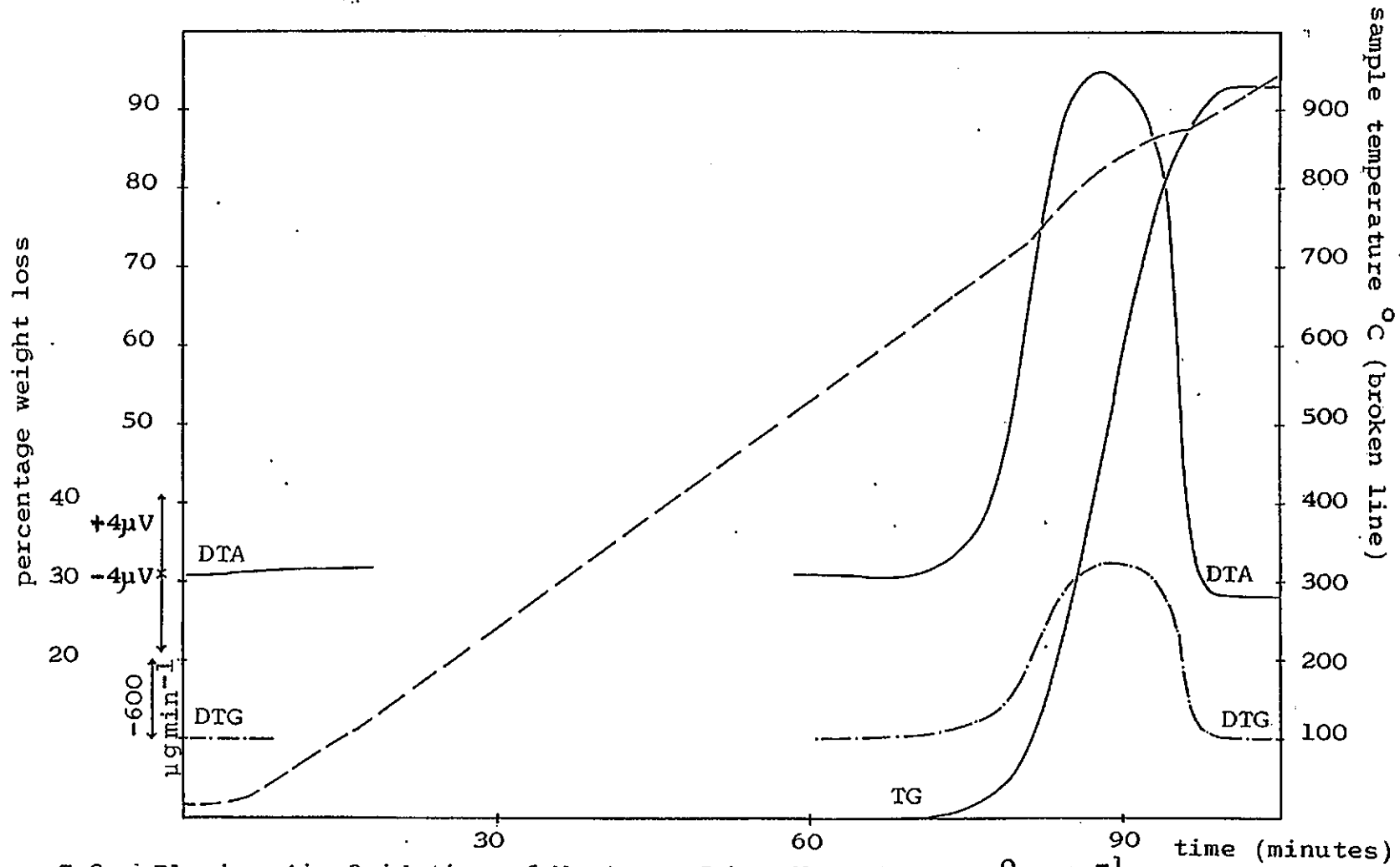
Figure 7.8. Flowing Air Oxidation of Nantgarw Coke Heated at 10 $^{\circ}C\ min^{-1}$. Simultaneous TG/DTG/DTA.
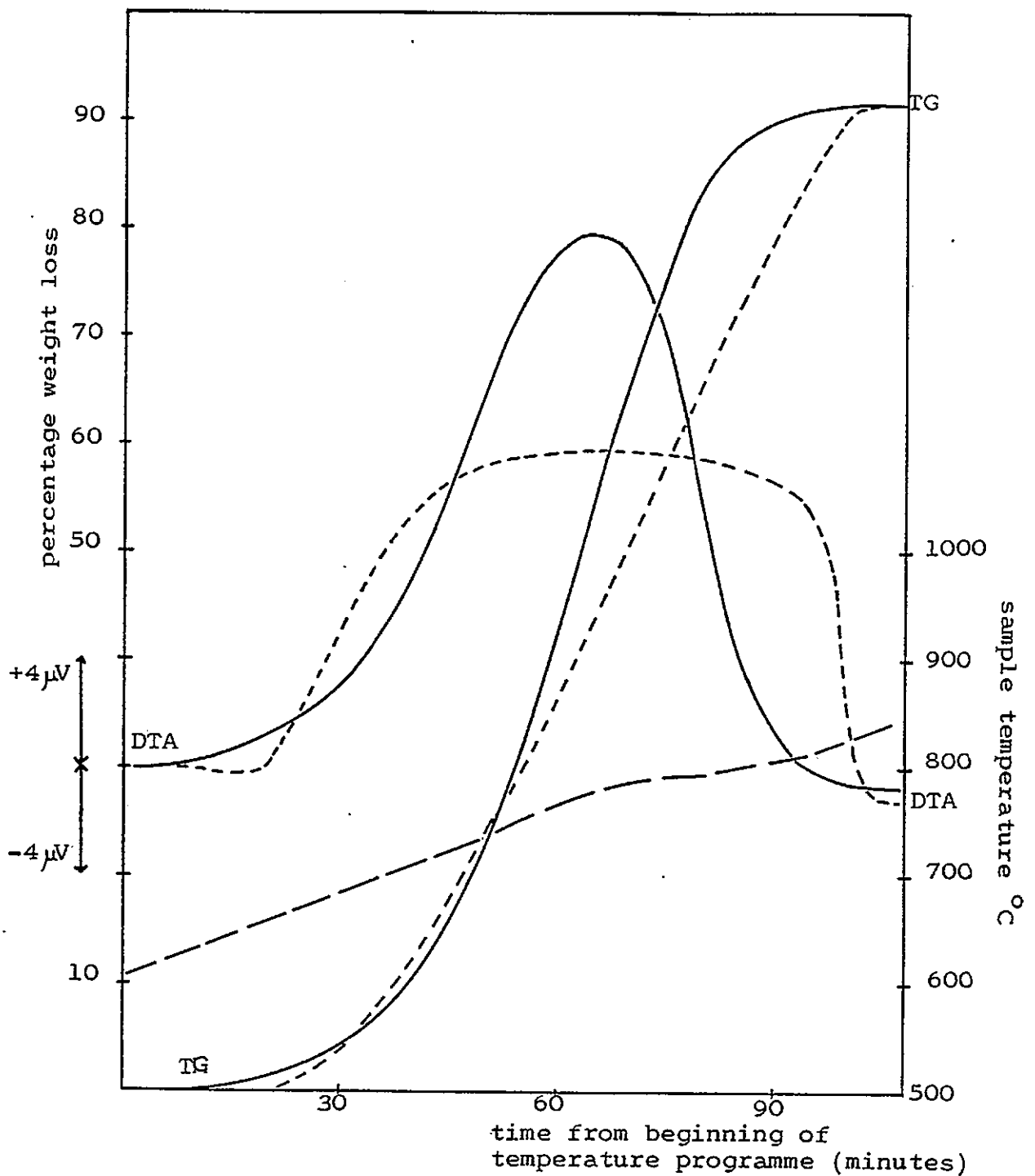
Figure 7.9. Air Oxidation of Nantgarw coke heated at 5 $^\circ$C min^{-1} with Different Air Flow Rates. Simultaneous TG/DTA.

Key:
solid line - air flow 26.2 cm^3 min^{-1}
dotted line - air flow 13.1 cm^3 min^{-1}
broken line - sample temperature
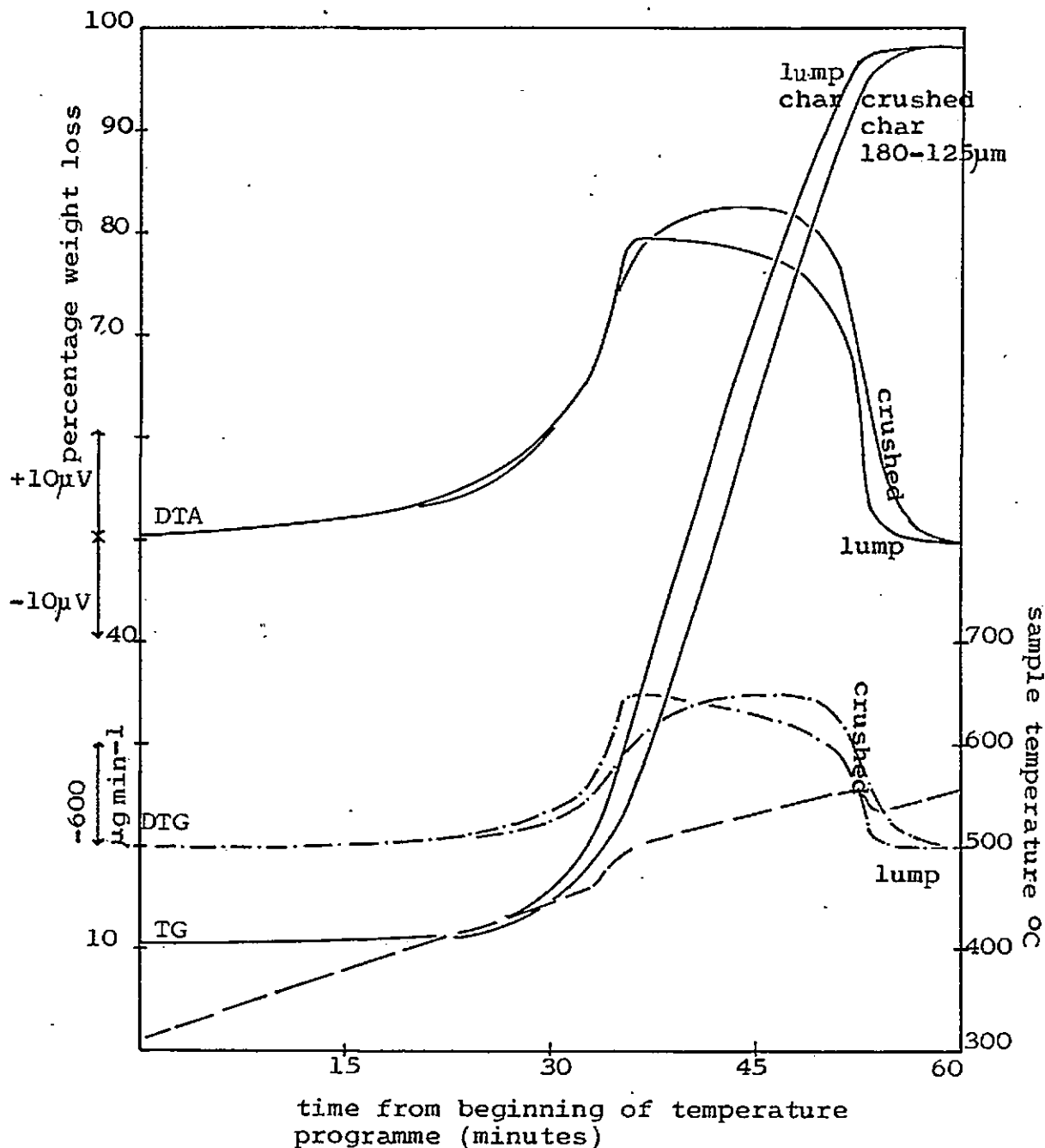
Figure 7.10. Air oxidation of Australian Brown Coal
Char. 19.40 mg samples of different particle size
heated at 5 ^{o}C min^{-1} in air flowing at 17.4 cm^3 min^{-1}
Simultaneous TG/DTG/DTA.

Broken line corresponds to sample temperature
Dot and dash   "   "   "   DTG.
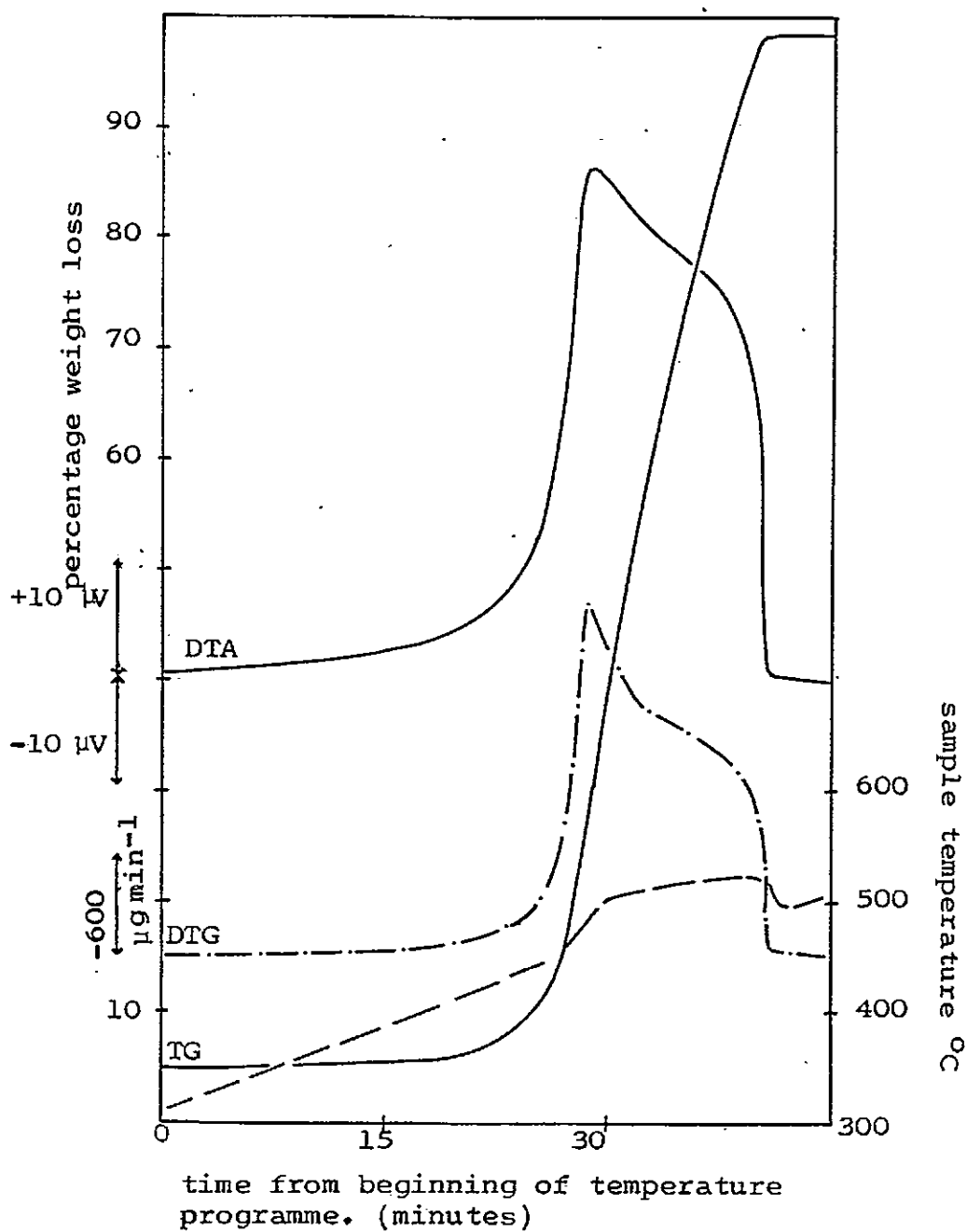
Figure 7.11. Air oxidation of Australian Brown Coal Char (20.0 mg lump) at a heating rate of 5 °C min^{-1} and 43.5 cm^3 min^{-1} air flow rate. Simultaneous TG/DTG/DTA.

(Broken line corresponds to sample temperature).

324

7.3.2 <u>Quantitative DTA in the Boudouard Reaction</u>

The TG curves for the oxidation of Nantgarw coke lumps in CO_2 flowing at 35.2 cm^3 min^{-1} are given in Figure 7.12 and the simultaneous DTA curves in Figure 7.13. Similar results were given by the 500-710μ m granules, although the DTA curves were slightly flattened. 2 to 12 $^\circ C$ min^{-1} were the heating rates between which it was possible to obtain a measurable rate of reaction and to complete the reaction before the temperature limit of the furnace was reached (a sample temperature of about 1450 $^\circ C$ under flowing atmosphere conditions). Values of the temperature by which burn-off was complete for the heating rates employed are given in Table 7.1.

The TG and DTA curves for the B_2O_3 doped Nantgarw coke are given in Figures 7.14 and 7.15 respectively. The DTA curves are replotted, with a common temperature axis in Figure 7.16 for Nantgarw coke lumps and Figure 7.17 for the B_2O_3-doped Nantgarw coke, where the shift in temperature of peak minimum may be more easily seen. Values for the heating rates employed are given in Table 7.2 for Nantgarw coke lumps, Table 7.3 for 500-710μ m granules and Table 7.4 for doped lumps, together with calculated values of $\ln\left(\frac{dT}{dt}\Big/T_m^2\right)$ and $\frac{1}{T_m}$.

Results for different particle sizes in the CO_2 oxidations of Nantgarw coke at 6 $^\circ$ min^{-1} are given in Table 7.5. The temperature at which the TG curve is first seen to deviate depends upon the sensitivity of the balance, and the extrapolated onset temperature was found

from the DTA curve as the intersection of the tangent to the greatest slope of the leading edge and the projection of the baseline. The time of complete burn off was the same for each sample.

The DTA traces for the oxidation of Australian brown coal char at heating rates 2 to 15 $^{\circ}C$ min^{-1} in CO_2 at the same flow rate are shown in Figure 7.18 and for the B_2O_3 doped char in Figure 7.19. The results are replotted on a common temperature axis in Figures 7.20 and 7.21 respectively.

Temperatures of complete burn off for these heating rates are given in Table 7.6 for the char and 7.7 for the doped char.

The sample temperature at peak minimum (T_m) of the DTA curve for the several heating rates ($\emptyset$) are presented for the char in Table 7.8 and for the doped char in Table 7.9 together with the calculated values of $\ln(\frac{\emptyset}{T_m^2})$ and $\frac{1}{T_m}$.

The effect of particle size of the char on the CO_2 oxidation at a heating rate of 4 $^{\circ}C$ min^{-1} is tabulated in 7.10. The time of complete reaction was again the same for each sample.

TG results for the coke and char at several heating rates and for doped material, plotted on a common temperature axis are shown in Figure 7.22.
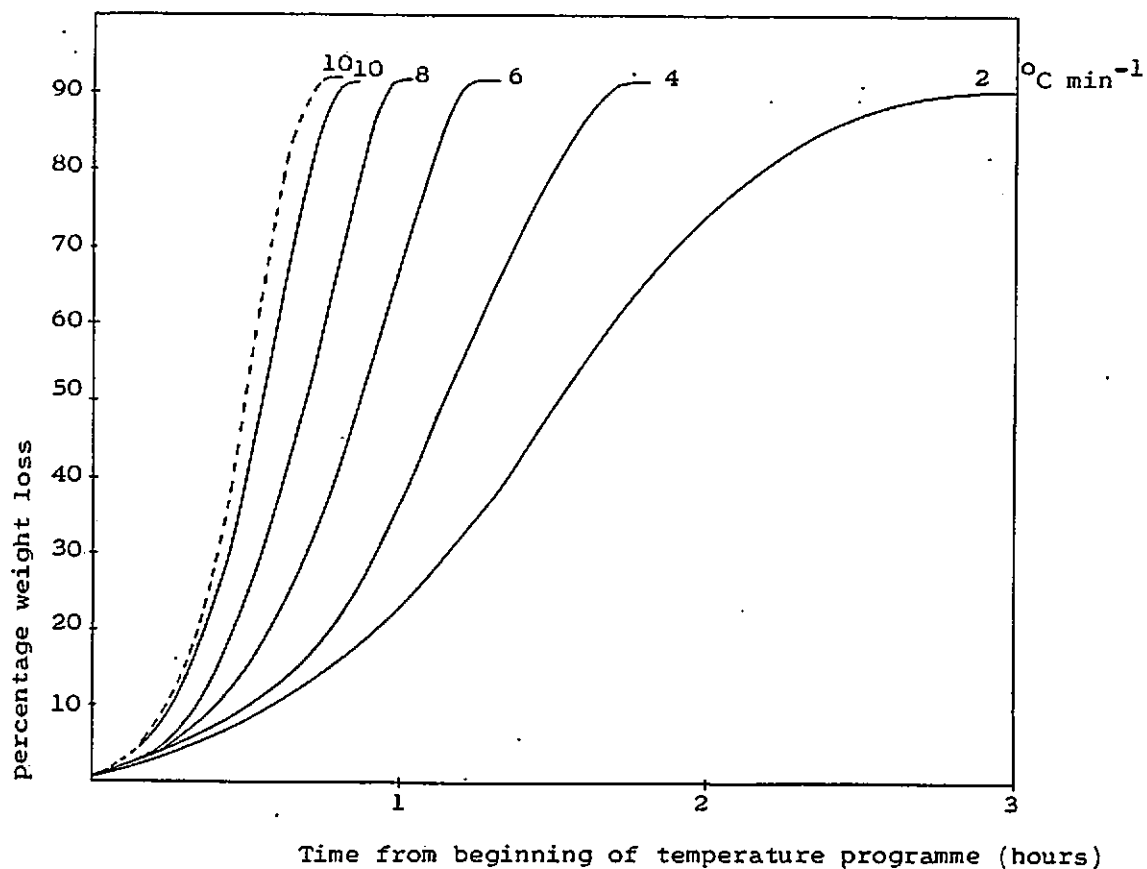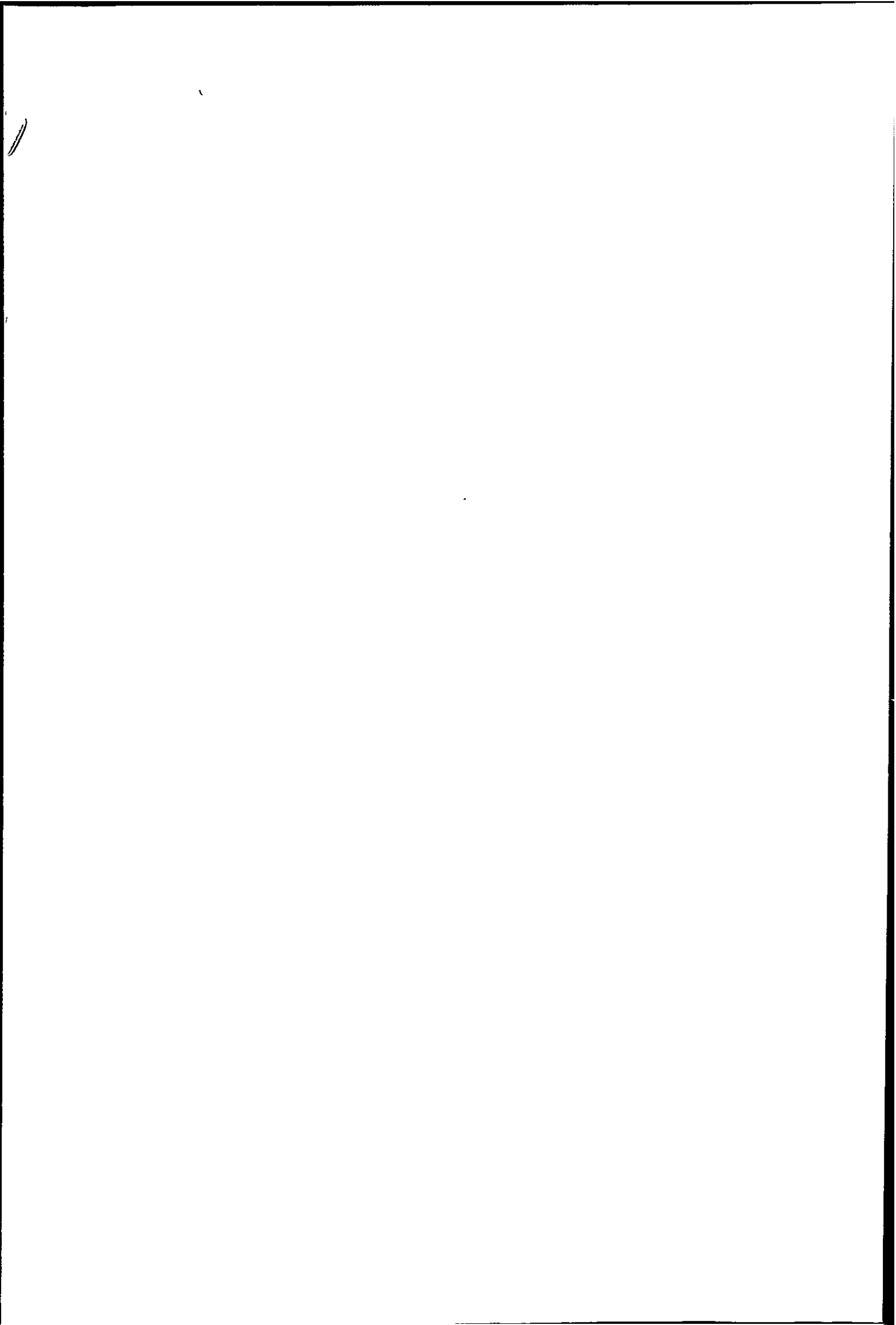
Figure 7.12. CO_2 oxidation of Nantgarw coke under several temperature programmes (after rapid pre-heating to 990 ^{O}C).
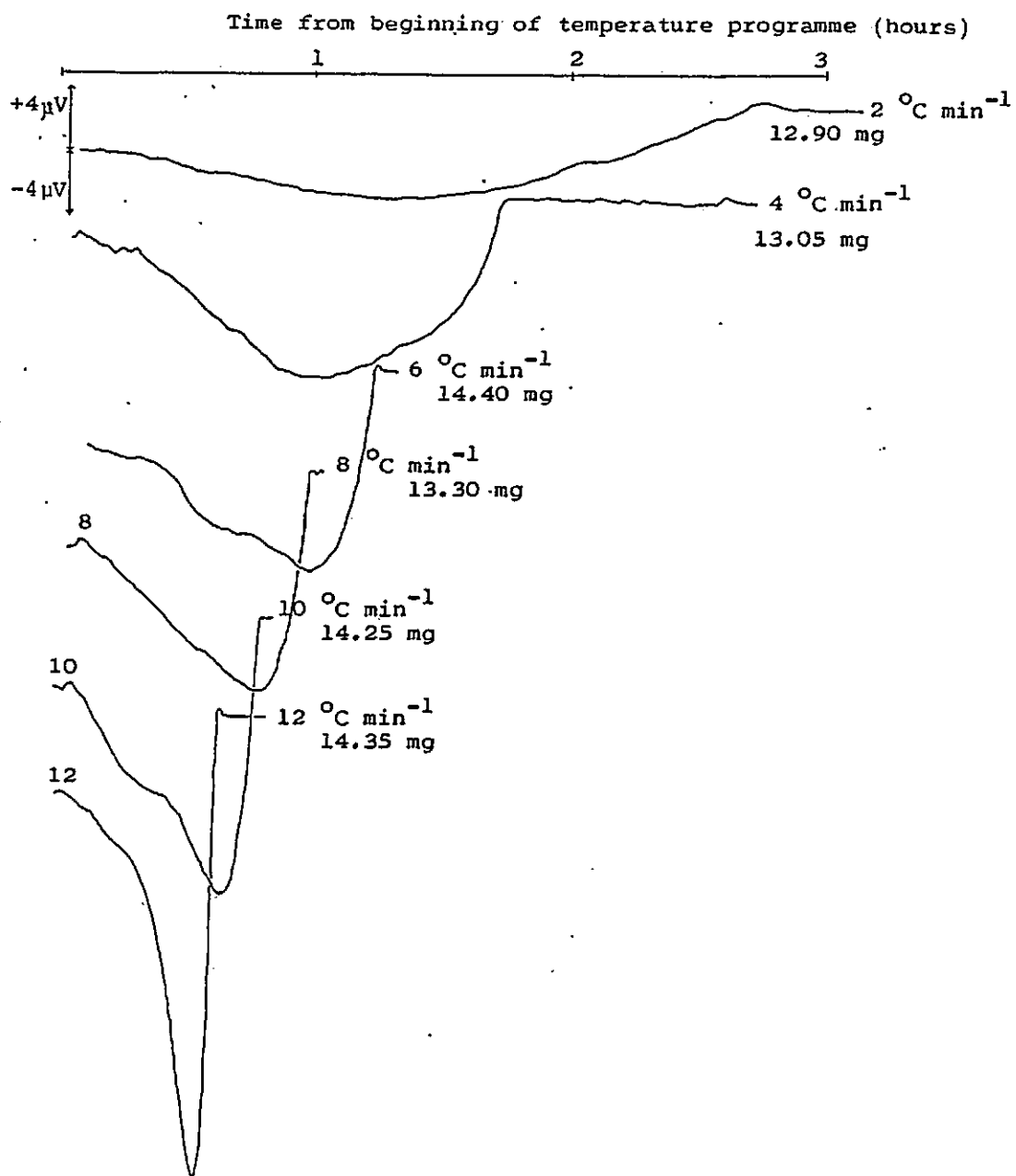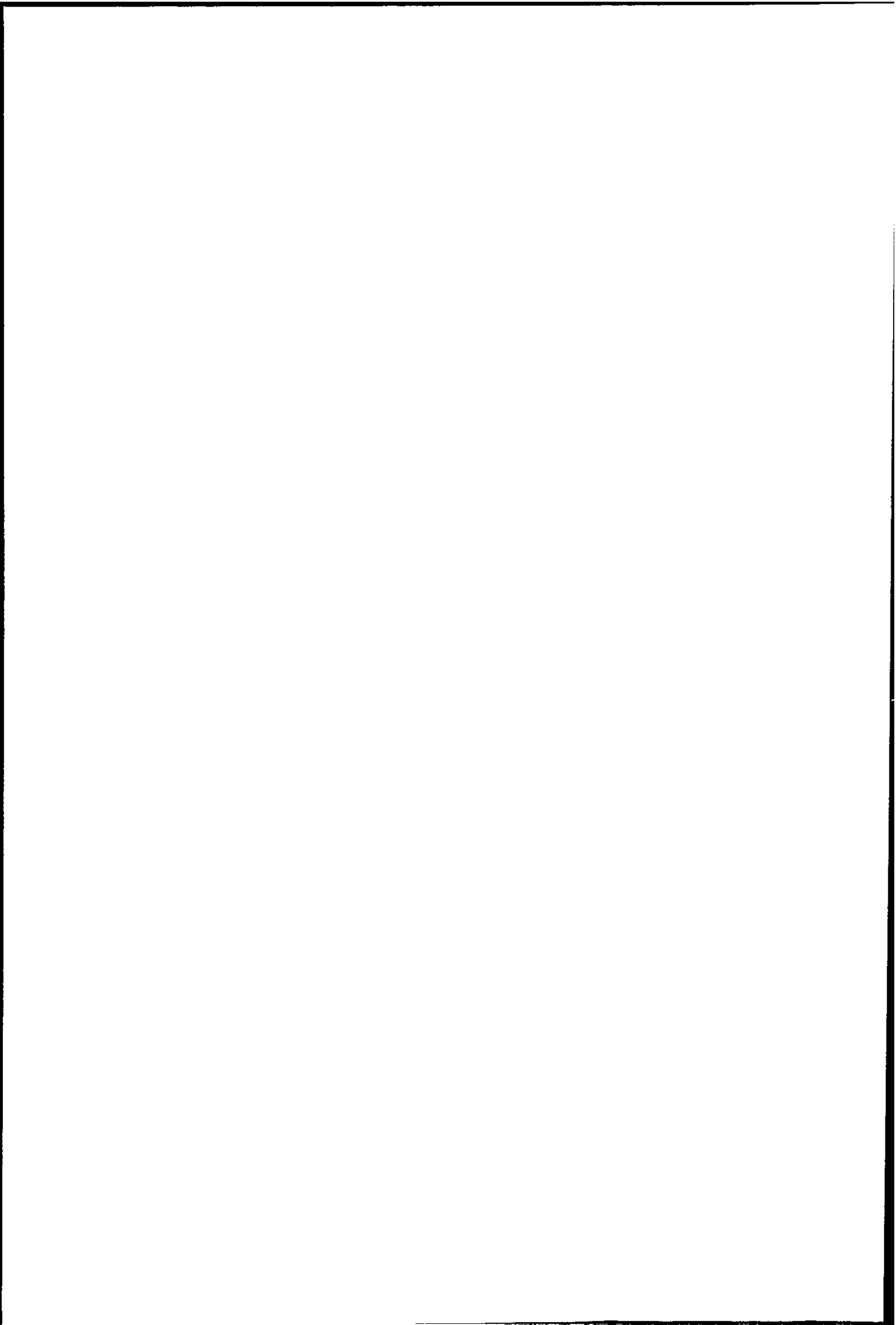Dotted line - result from Figure 7.6 at 10 ^{O}C min^{-1} heating rate.

Figure 7.13. DTA of CO_2 oxidation of Nantgarw coke lumps under different temperature programmes, after rapid pre-heating to 990 °C.

Table 7.1

Variation in temperature of complete burn off with
heating rate for Nantgarw coke in CO_2.

Temperature $^{\circ}C$	Heating Rate $^{\circ}C \ min^{-1}$
1263 lumps	2
1256 granules	2
1309 lumps	4
1342 granules	4
1373 granules	5
1407 lumps	6
1380 granules	6
1425 lumps	8
1428 granules	8
1450 lumps	10
1449 granules	10
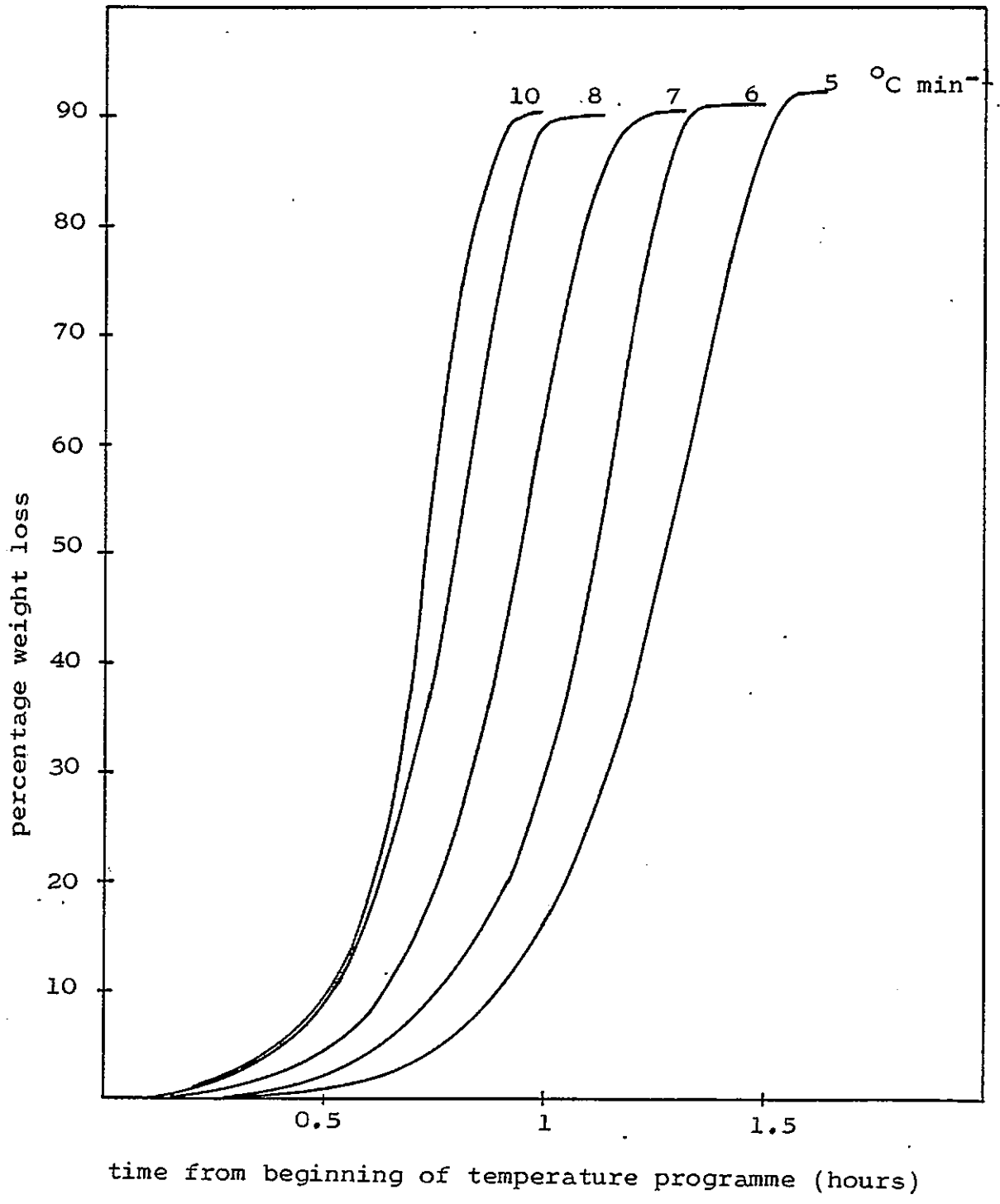
Figure 7.14. CO_2 oxidation of B_2O_3-doped Nantgarw coke under several temperature programmes (after rapid pre-heating to 990 ^{o}C)
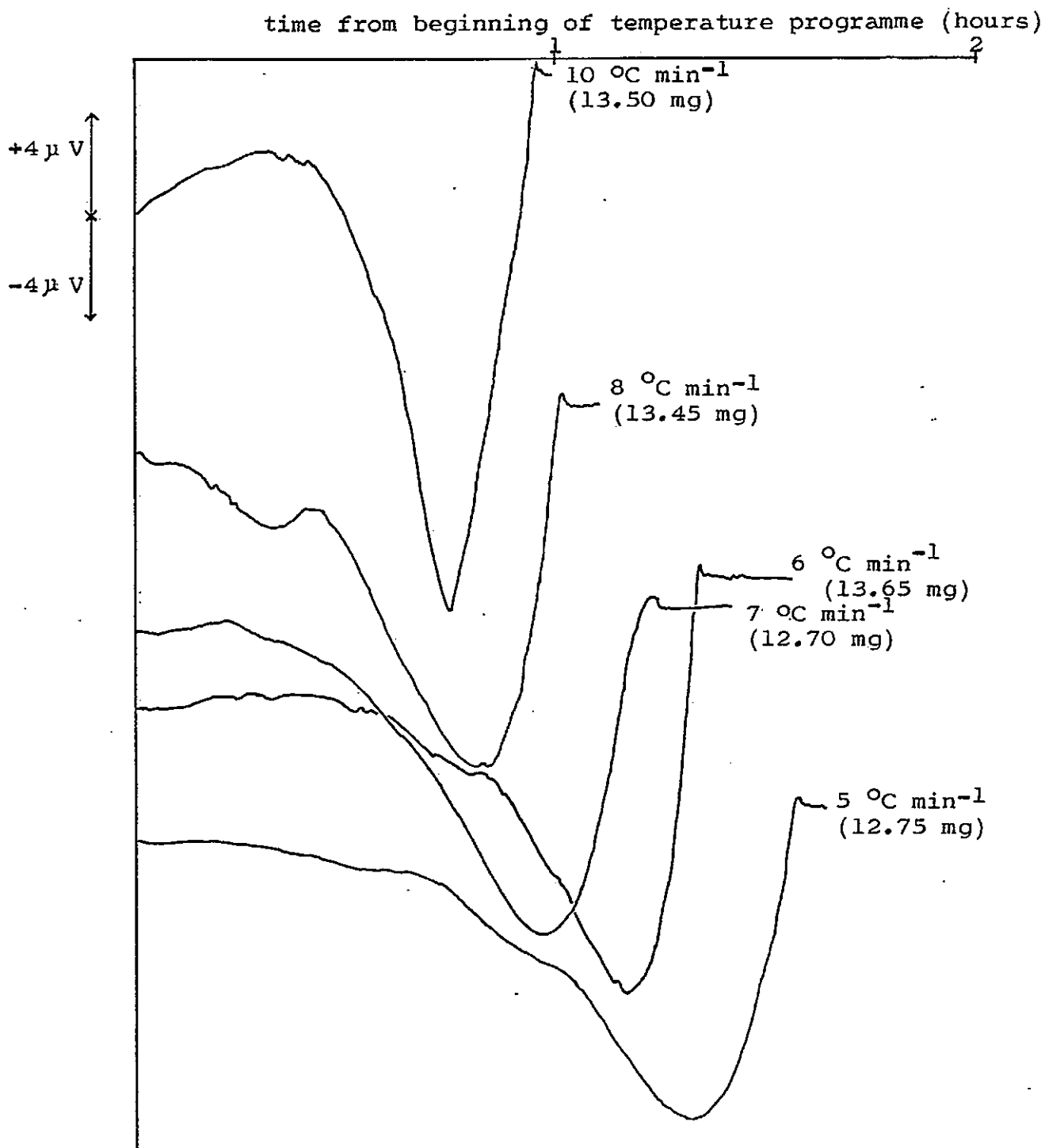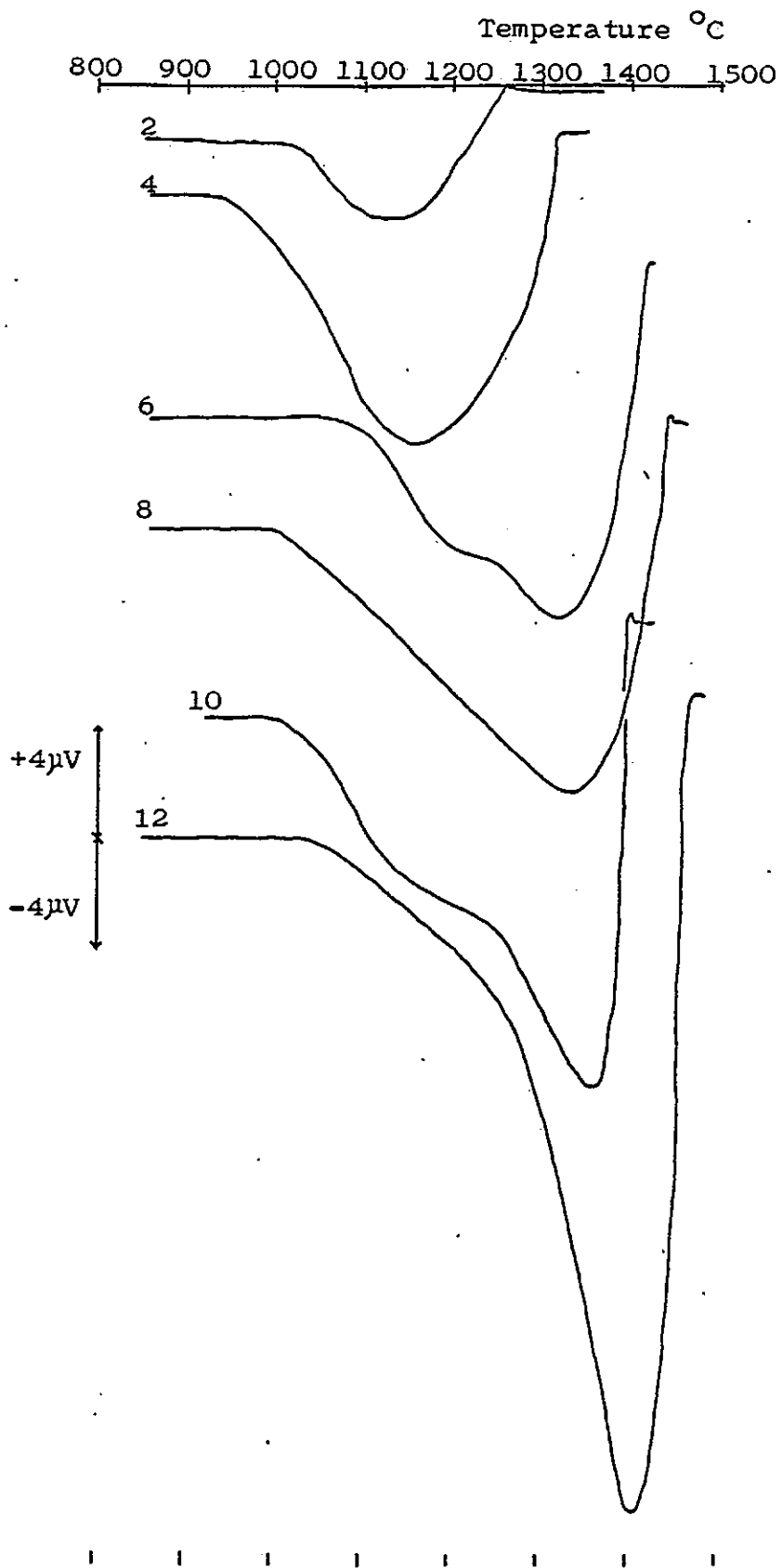
Figure 7.15. DTA of CO_2 oxidation of B_2O_3-doped Nantgarw coke under several temperature programmes, after rapid pre-heating to 990 $^{\circ}C$.

7.16. DTA of CO_2 oxidation of Nantgarw coke
lumps under several temperature programmes
(^{o}C min^{-1})

Temperature $^{\circ}C$

800　900　1000　1100　1200　1300　1400　1500

5

6

7

8

+4 μV

10

-4 μV
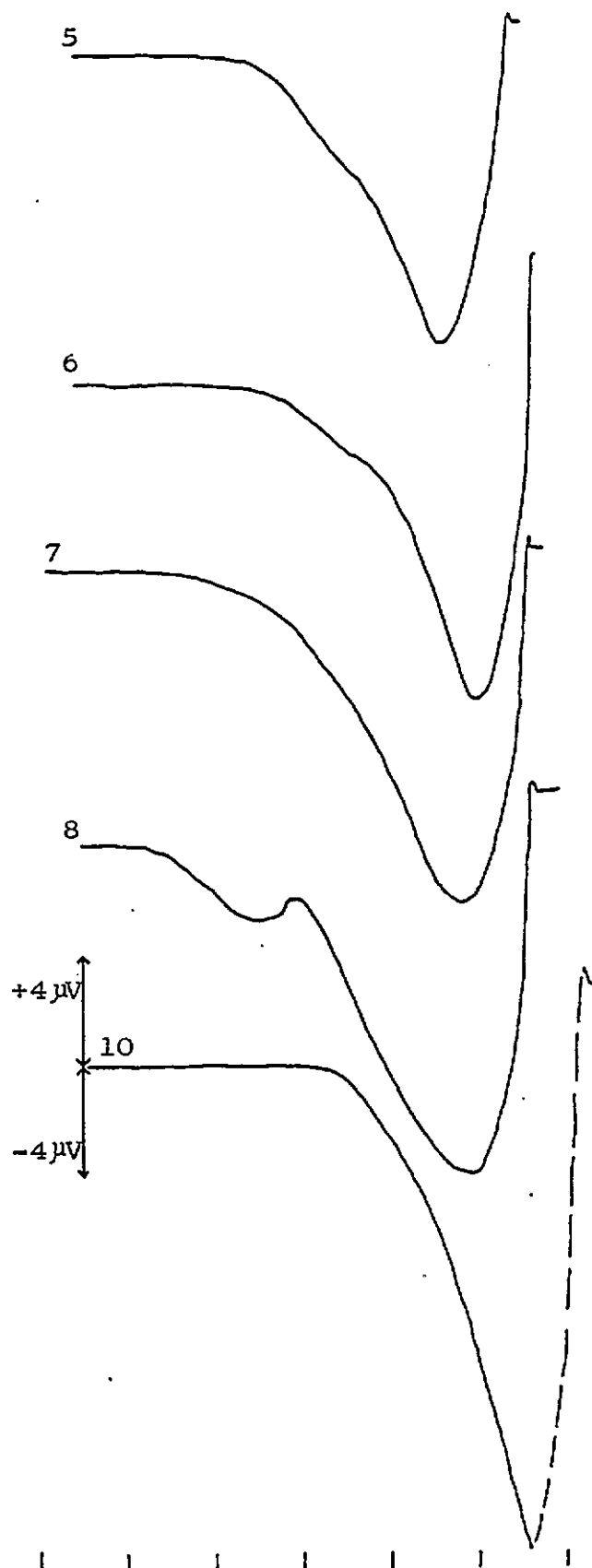
Figure 7.17. DTA of CO_2 oxidation of B_2O_3-doped Nantgarw coke under several temperature programmes ($^{\circ}C$ min^{-1})

333

Table 7.2.   Nantgarw Coke Lumps in the Boudouard Reaction

Rate of heating $\frac{dT}{dt}$ ($^\circ$C min^{-1})	Temperature of Peak minimum ($^\circ$C)	Temperature of Peak minimum T_m (K)	$\frac{dT}{dt}/T_m^2$ (min^{-1}K^{-1})	$\ln(\frac{dT}{dt}/T_m^2)$	$\frac{10^4}{T_m}$ (K^{-1})
12	1404	1677	4.267×10^{-6}	−12.365	5.963
10	1362	1635	3.741×10^{-6}	−12.496	6.116
8	1341	1614	3.071×10^{-6}	−12.694	6.196
6	1317	1590	2.373×10^{-6}	−12.951	6.289
4	1234	1507	1.761×10^{-6}	−13.250	6.636
2	1206	1479	0.914×10^{-6}	−13.905	6.761

334

Table 7.3.   Nantgarw Coke Granules in the Boudouard Reaction

Rate of heating $\frac{dT}{dt}$ (^{o}C min^{-1})	Temperature of Peak minimum (^{o}C)	Temperature of Peak minimum T_m (K)	$\frac{dT}{dt}/T_m^2$ (min$^{-1}K^{-1}$)	$\ln\left(\frac{dT}{dt}/T_m^2\right)$	$\frac{10^4}{T_m}$ (K^{-1})
14	1411	1684	4.9368×10^{-6}	-12.219	5.938
12	1369	1642	4.4508×10^{-6}	-12.322	6.090
10	1352	1625	3.787×10^{-6}	-12.484	6.154
8	1324	1597	3.137×10^{-6}	-12.672	6.262
6	1298	1571	2.431×10^{-6}	-12.927	6.365
5	1263	1536	2.119×10^{-6}	-13.064	6.510
4	1213	1486	1.811×10^{-6}	-13.221	6.730
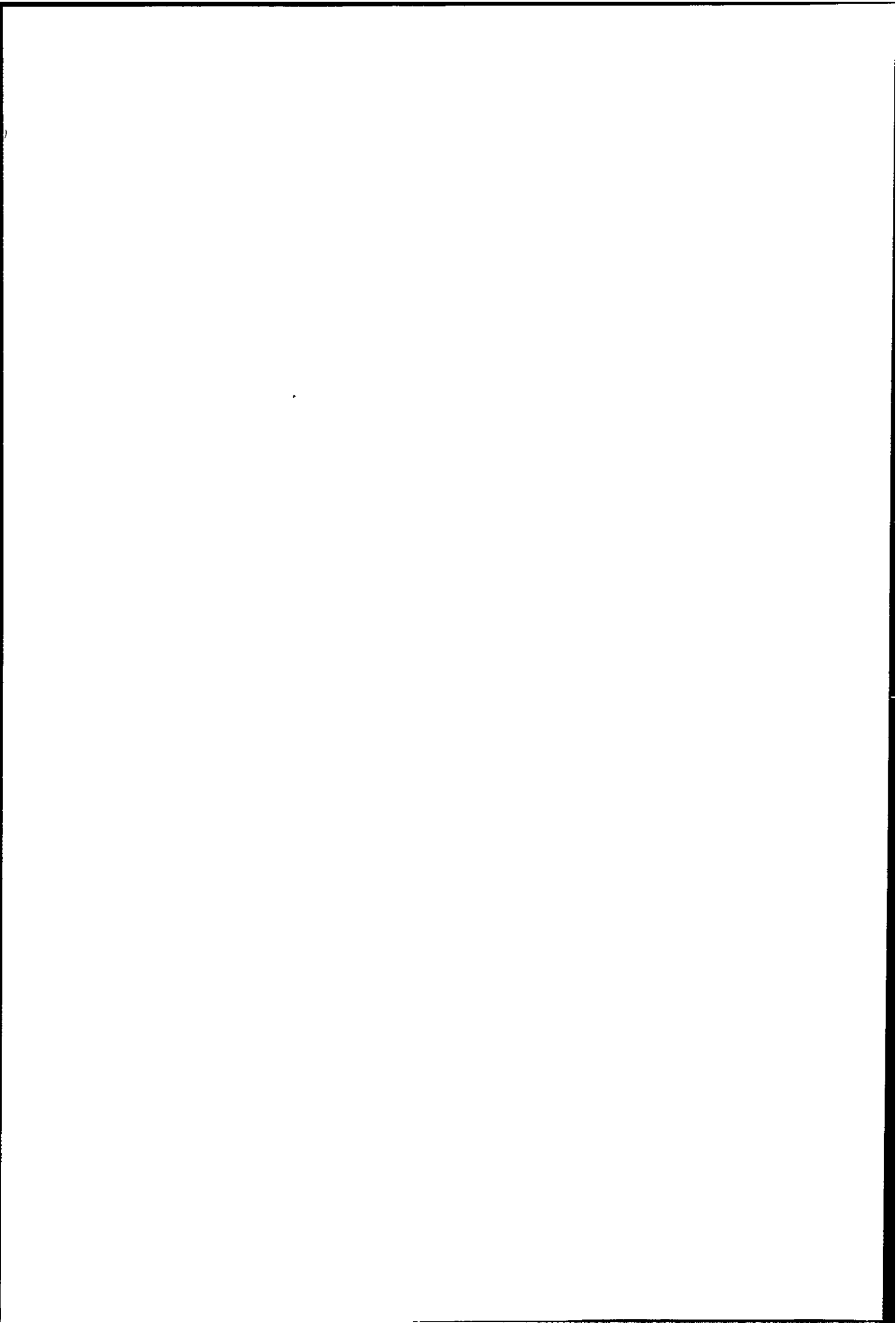
Table 7.4. B_2O_3 Doped Nantgarw Coke in the Boudouard Reaction

Rate of Heating $\frac{dT}{dt}$ ($^{\circ}$C min^{-1})	Temperature of Peak Minimum ($^{\circ}$C)	Temperature of Peak Minimum T_m (K)	$\frac{dT}{dt}/T_m^2$ (min^{-1}K^{-1})	$\ln(\frac{dT}{dt}/T_m^2)$	$\frac{10^4}{T_m}$ (K^{-1})
10	1459	1732	3.334×10^{-6}	-12.612	5.774
8	1397	1670	2.869×10^{-6}	-12.762	5.988
7	1383	1656	2.553×10^{-6}	-12.878	6.039
6	1397	1670	2.151×10^{-6}	-13.049	5.988
5	1366	1639	1.8613×10^{-6}	-13.194	6.101
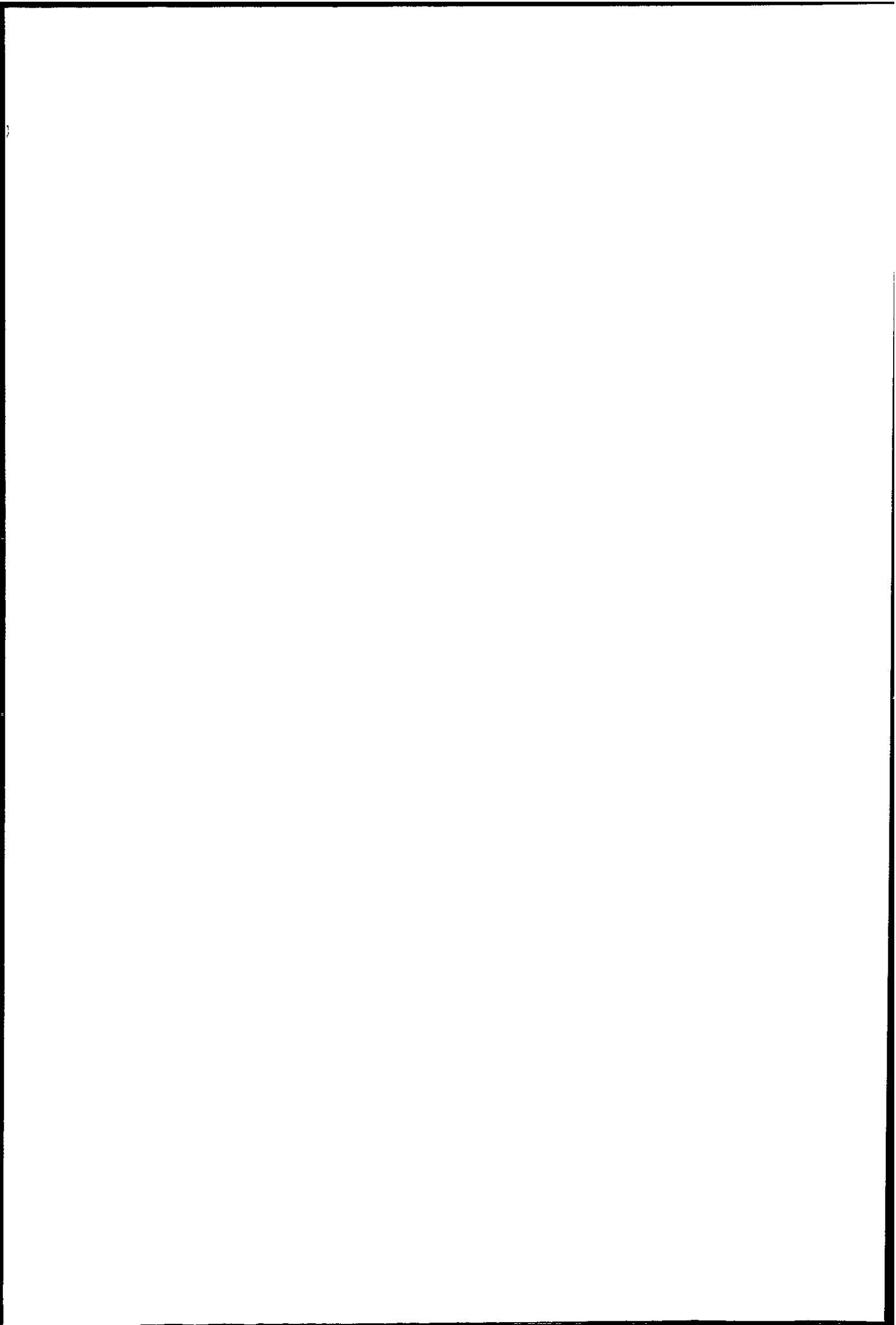
Table 7.5. Effect of Sample Division in the CO_2 oxidation of Nantgarw Coke at 6 ^{o}C min^{-1} (for 12.5 mg samples)

Particle Sizes	Temperature of First Deviation of TG curve ^{o}C	Extrapolated onset temperature from DTA curve ^{o}C
3 mm diameter lumps	1045	1111
500-710 μm granules	1029	1096
crushed coke particles < 180 μm	899	997
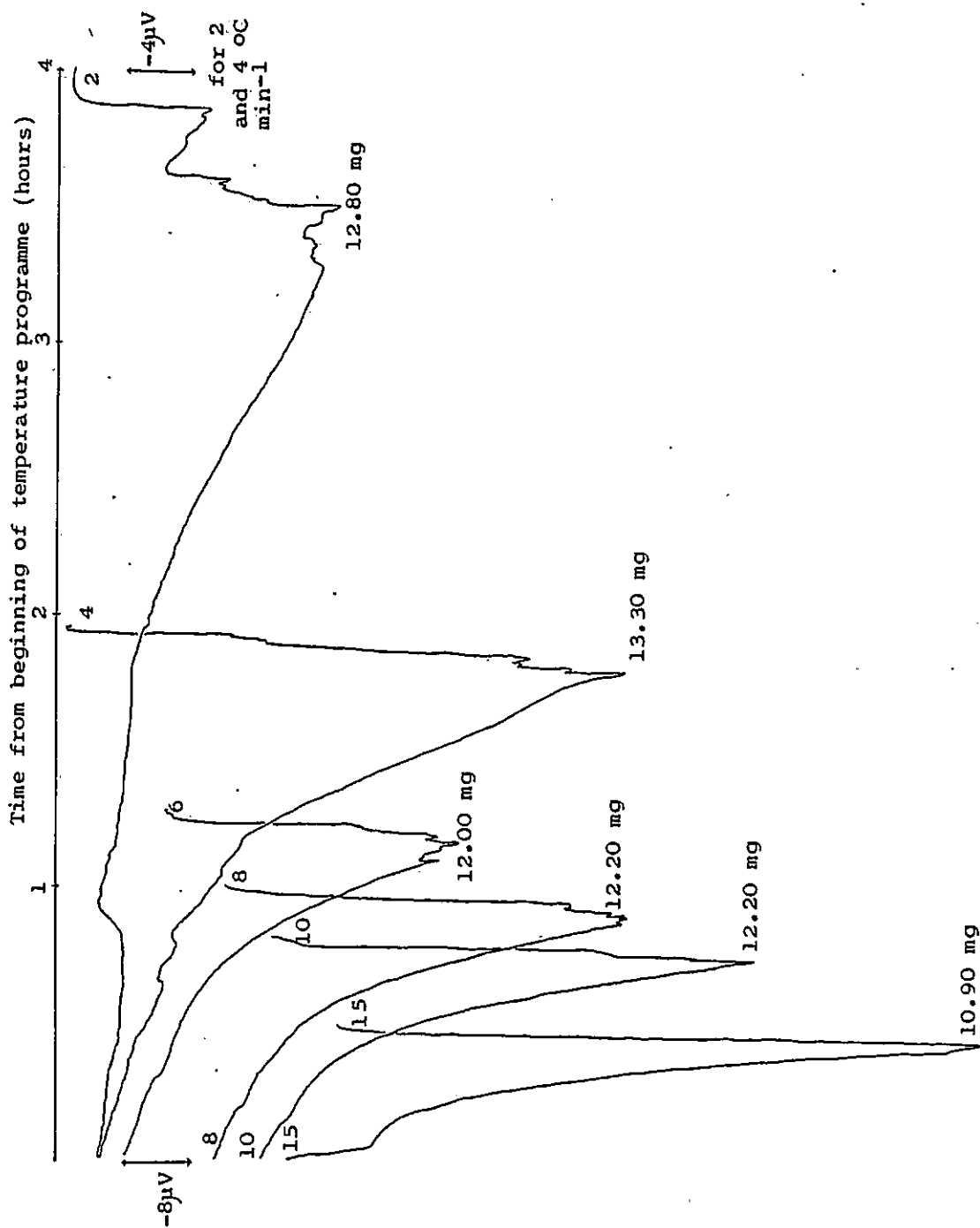
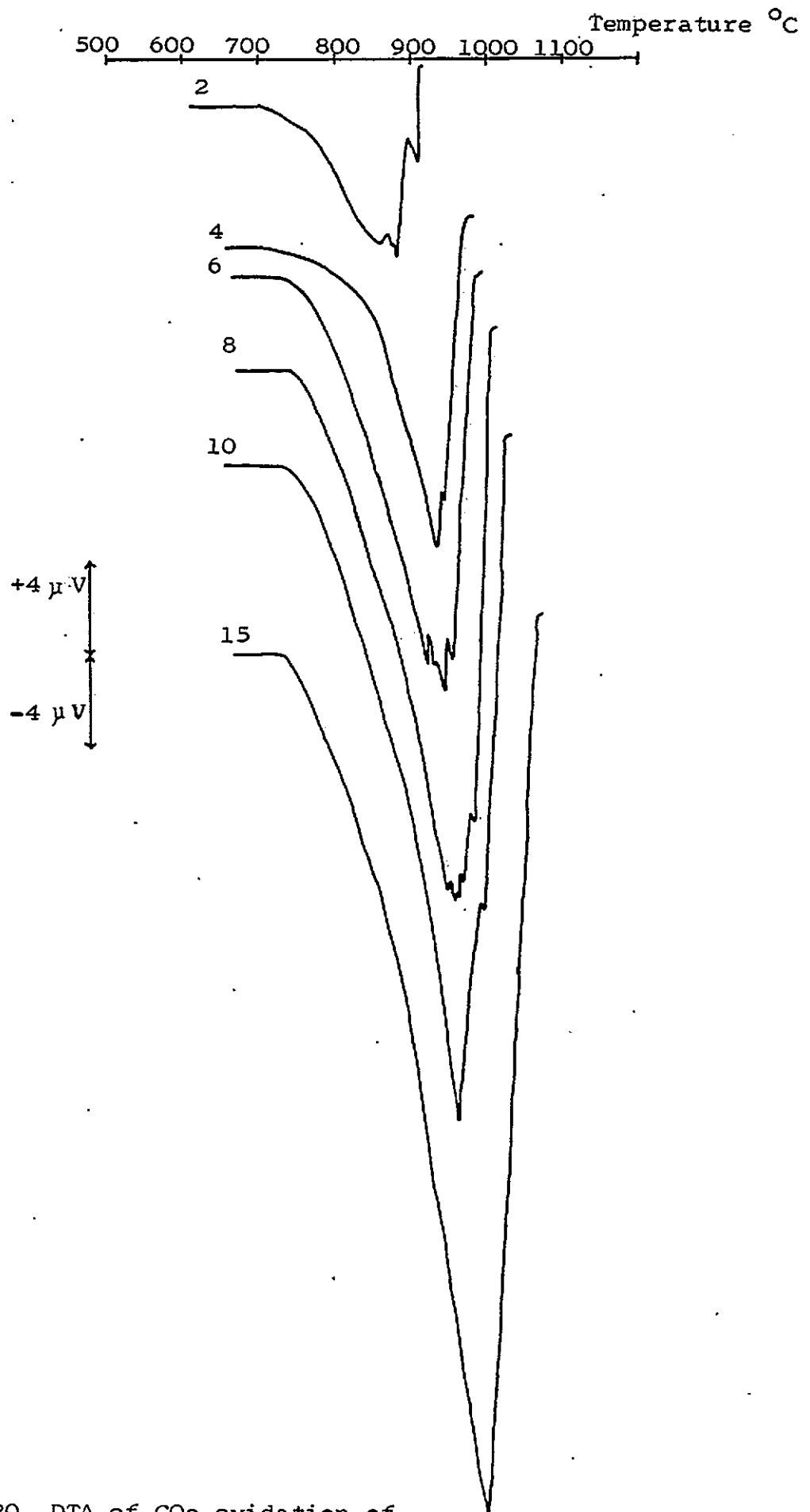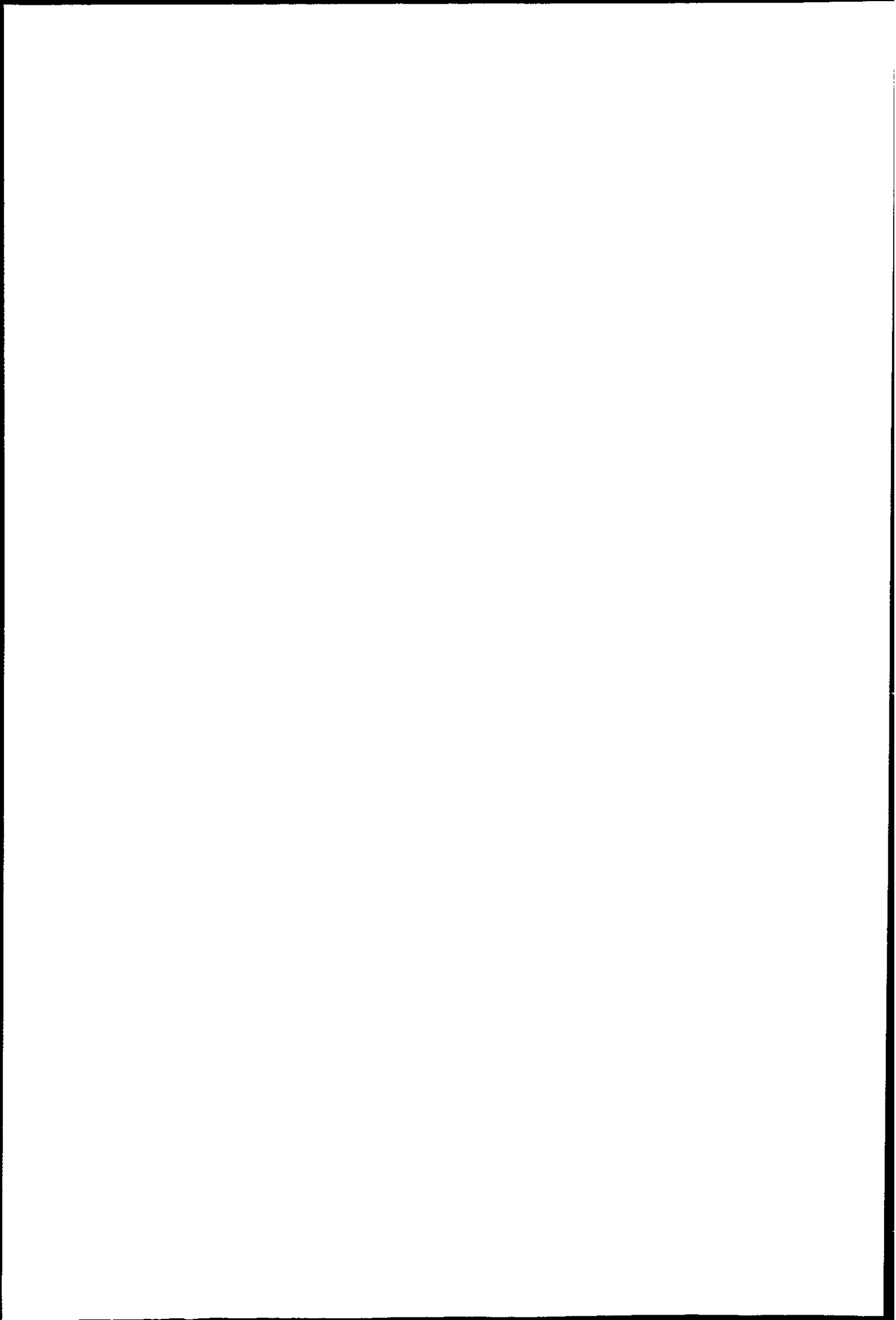Figure 7.18. DTA of CO_2 oxidation of Australian Brown Coal Char under several temperature programmes (^{O}C min-1)
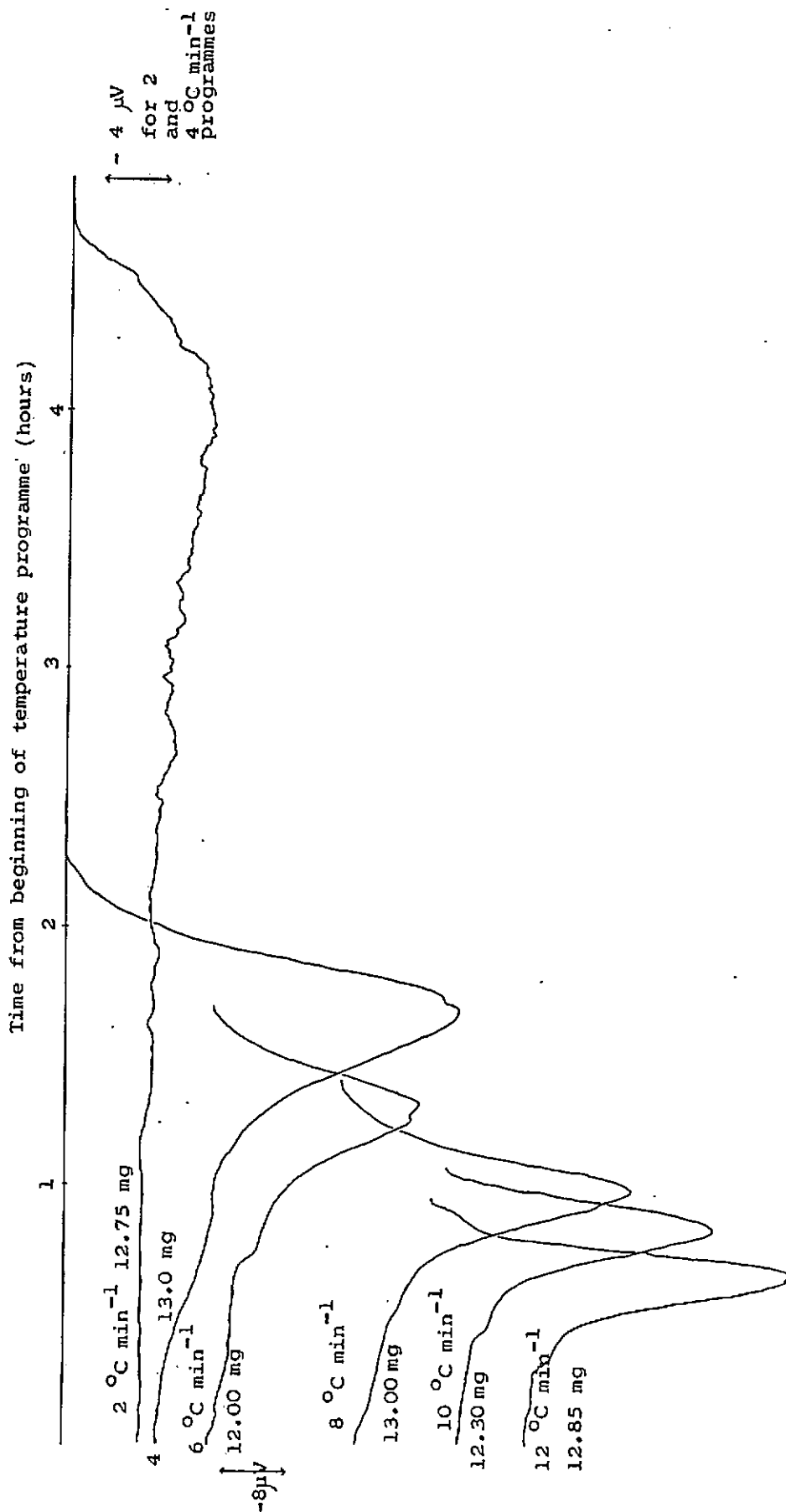
Figure 7.19. DTA of CO_2 oxidation of B_2O_3 doped Australian Brown Coal Char under several temperature programmes.

Figure 7.20. DTA of CO_2 oxidation of
Australian Brown Coal Char under several
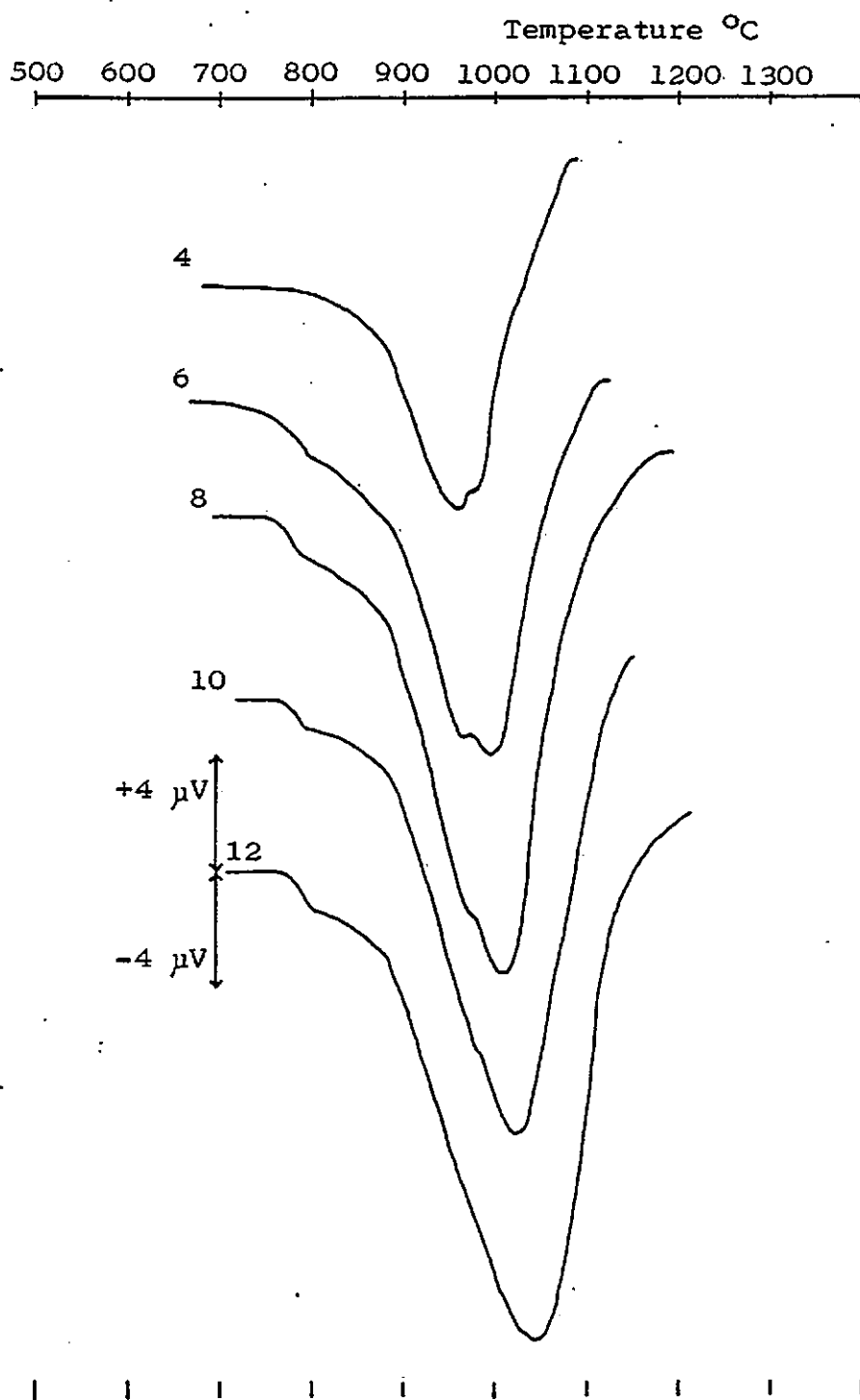temperature programmes ($^{\circ}C$ min^{-1})

Figure 7.21. DTA of CO_2 oxidation of B_2O_3-doped Australian Brown Coal Char under several temperature programmes (^oC min^{-1})
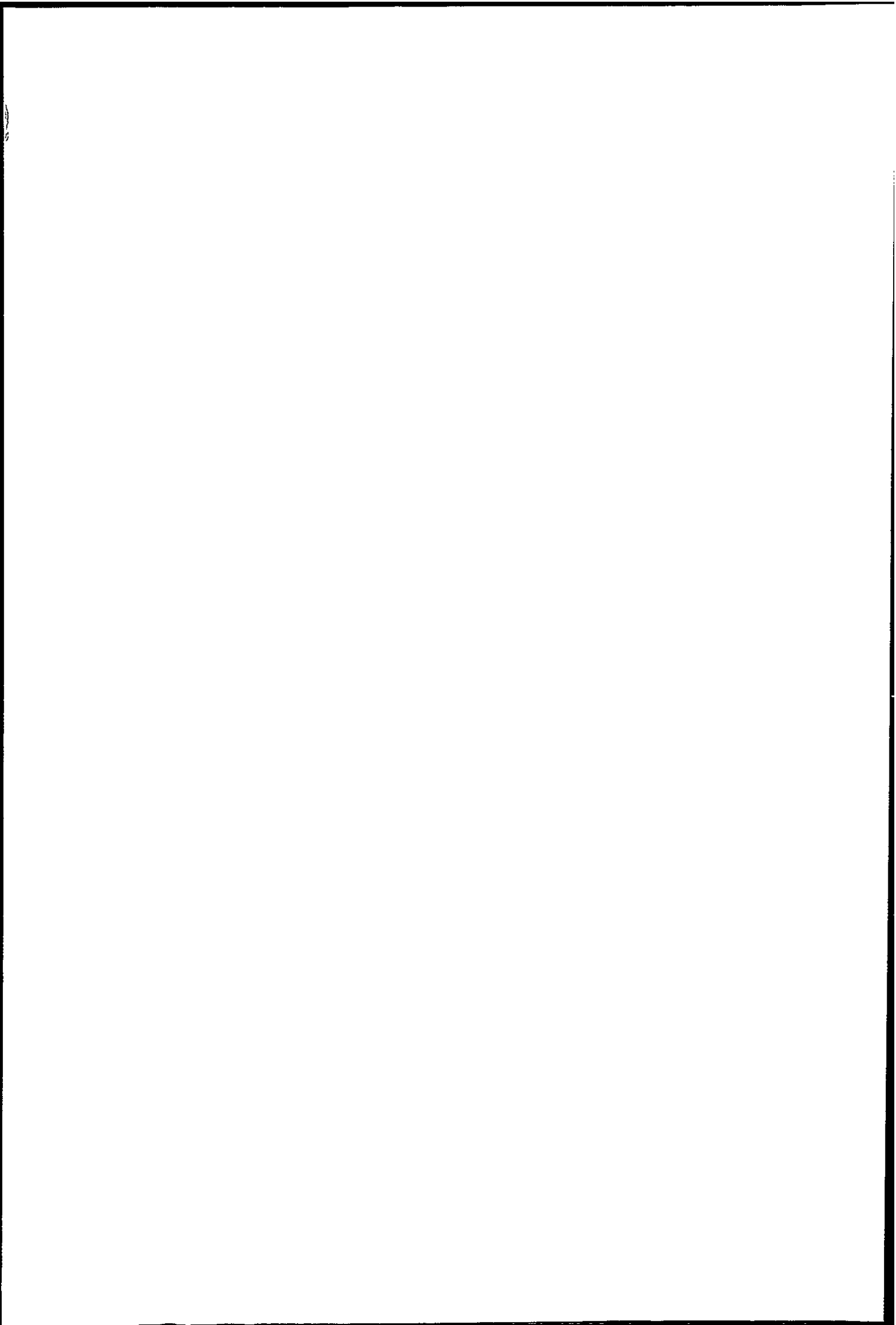
Table 7.6. Variation of temperature of complete burn off with heating rate, for Australian Brown Coal Char in CO_2.

Temperature $^{\circ}C$	Heating rate $^{\circ}C$ min^{-1}
913	2
971	4
982	6
1002	8
1032	10
1065	15

Table 7.7. Variation of temperature of complete burn off with heating rate for B_2O_3-doped Australian Brown Coal Char in CO_2

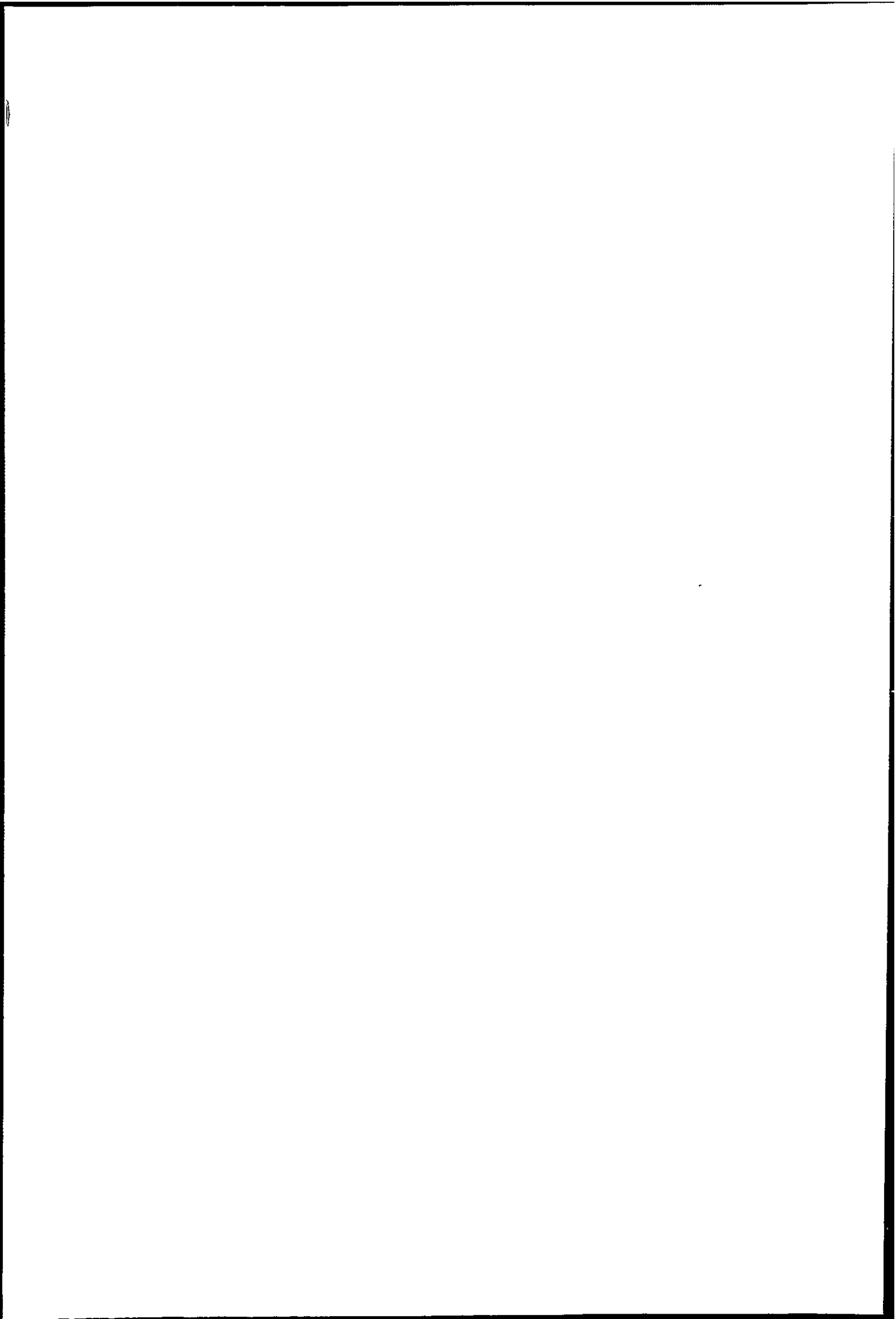| Temperature $^{\circ}C$	Heating rate $^{\circ}C$ min^{-1}
1007	2
1081	4
1136	6
1155	8
1188	10
1213	12

Table 7.8. Australian Brown Coal Char in the Boudouard Reaction

Rate of Heating $\frac{dT}{dt}$ ($^{\circ}$C min^{-1})	Temperature of Peak Minimum ($^{\circ}$C)	Temperature of Peak Minimum T_m K	$\frac{dT}{dt}/T_m{}^2$ (min^{-1}K^{-1})	$\ln(\frac{dT}{dt}/T_m{}^2)$	$\frac{10^4}{T_m}$ K^{-1}
15	995	1268	9.329×10^{-6}	-11.582	7.886
10	961	1234	6.567×10^{-6}	-11.933	8.104
8	954	1227	5.314×10^{-6}	-12.145	8.150
6	942	1215	4.064×10^{-6}	-12.413	8.231
4	936	1209	2.737×10^{-6}	-12.809	8.271
2	879	1152	1.507×10^{-6}	-13.405	8.681

Table 7.9. B_2O_3 doped Australian Brown Coal Char in the Boudouard Reaction.

Rate of Heating $\frac{dT}{dt}$ ($^{\circ}$C min^{-1})	Temperature of Peak Minimum $^{\circ}$C	Temperature of Peak Minimum T_m K	$\frac{dT}{dt}/T_m^2$ (min^{-1}K^{-1}) x10^6	$\ln(\frac{dT}{dt}/T_m^2)$	$\frac{10^4}{T_m}$ (K^{-1})
12	1041	1314	6.950	-11.877	7.610
10	1022	1295	5.963	-12.030	7.722
8	1006	1279	4.891	-12.228	7.819
6	994	1267	3.738	-12.497	7.893
4	958	1231	2.640	-12.845	8.124
2	915	1188	1.417	-13.467	8.418

Table 7.10   Effect of Sample Division in the CO_2 oxidation of Australian Brown Coal Char at 4 $^{\circ}C$ min^{-1} (for 112 mg samples.)

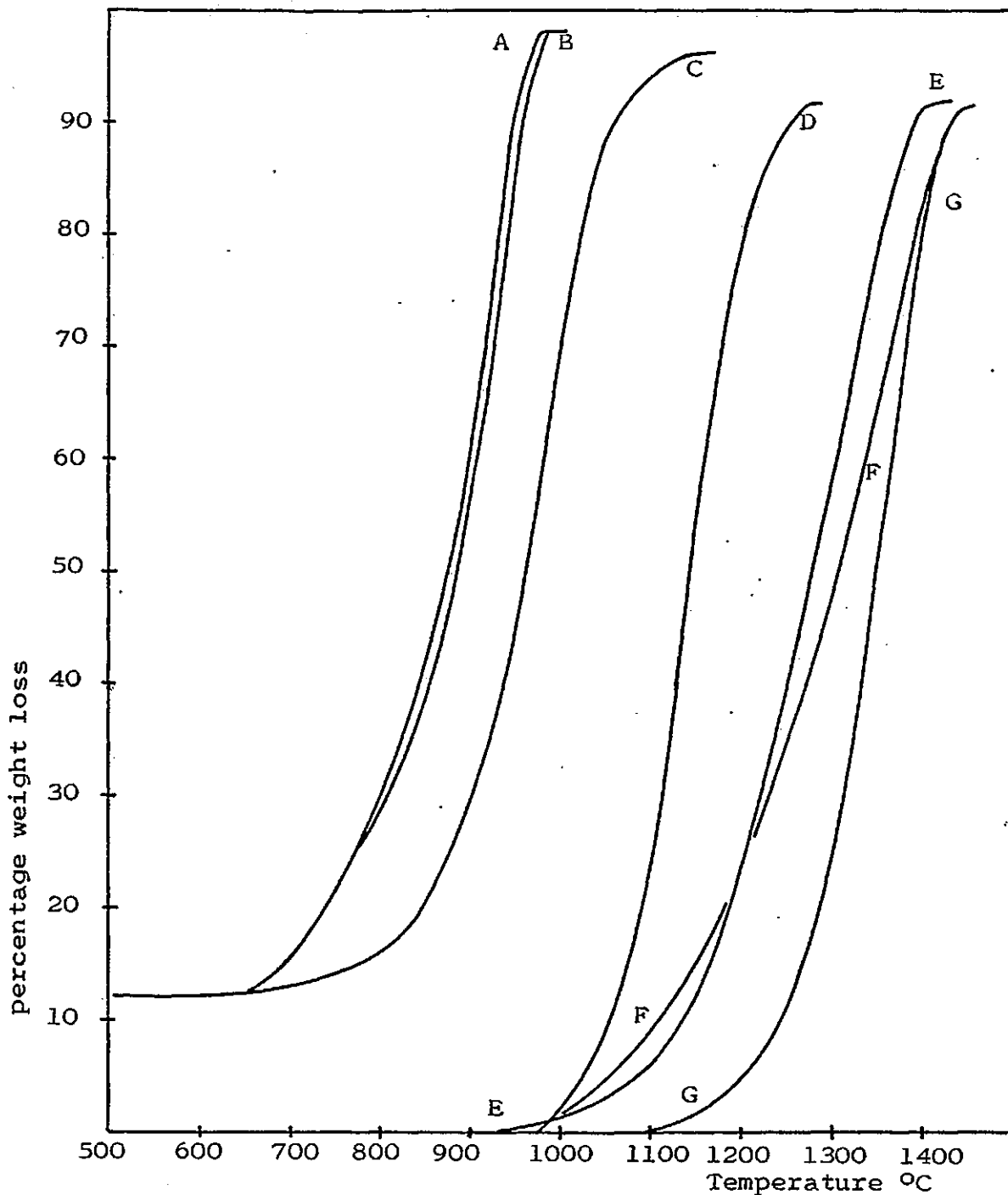| Particle Size	Temperature of First Deviation of TG curve $^{\circ}C$	Extrapolated onset temperature from DTA curve $^{\circ}C$
1.4 - 0.71 mm	697	798
125 - 75 μm	670	766
< 63 μm	666	744

345
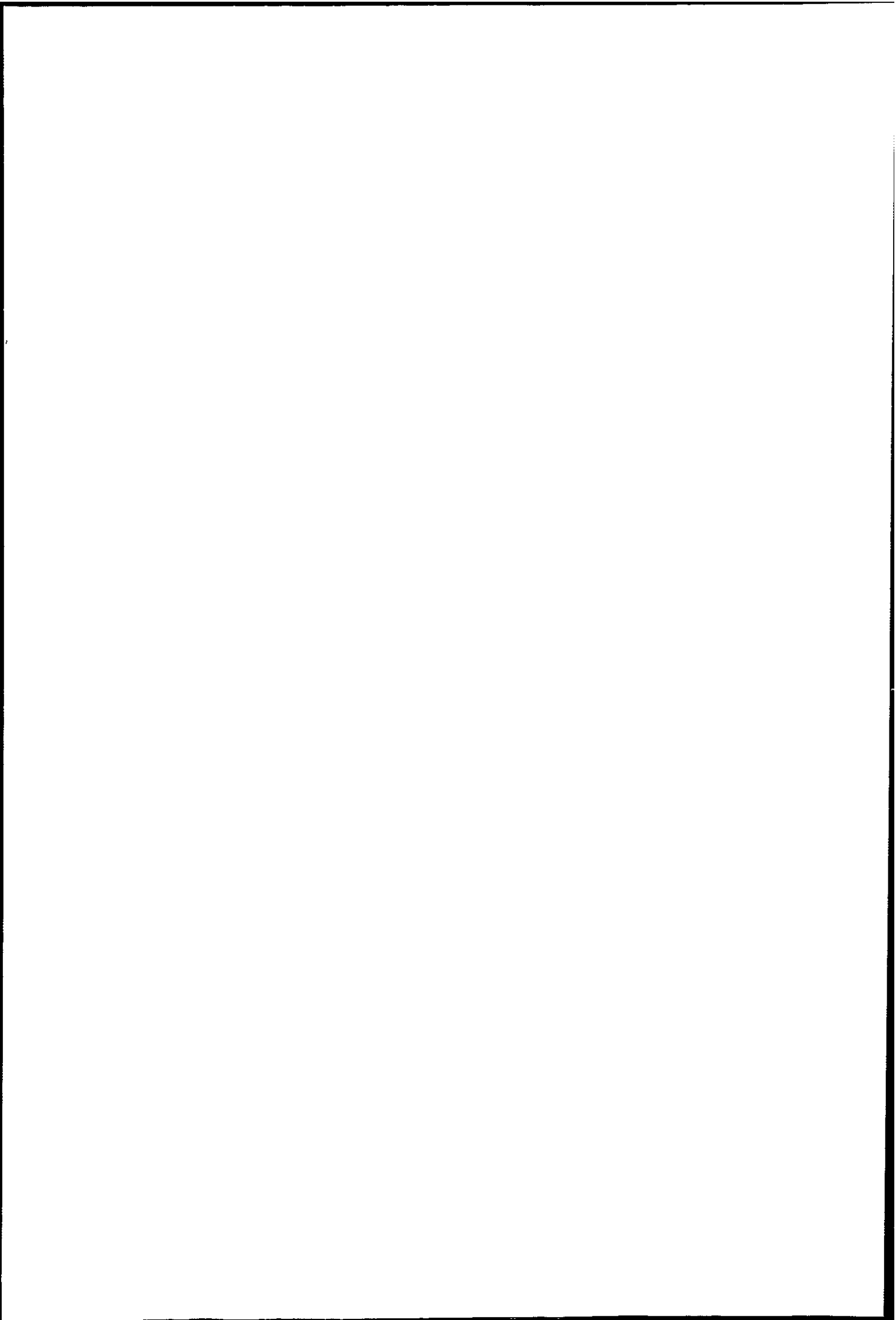
Figure 7.22. CO_2 oxidation of Nantgarw coke and Australian
Brown Coal Char and of B_2O_3-doped material, by TG.

Key :
A - Australian brown coal char. Heating rate 4 $^{\circ}C$ min^{-1}
B - "   "   "   "   "   " 6 $^{\circ}C$ min^{-1}
C - B_2O_3-doped Australian brown coal char. Heating rate 6 $^{\circ}C$ min^{-1}
D - Nantgarw coke. Heating rate 2 $^{\circ}C$ min^{-1}
E - "   "   "   " 6 $^{\circ}C$ min^{-1}
F - "   "   "   " 10 $^{\circ}C$ min^{-1}
G - B_2O_3-doped Nantgarw coke. Heating rate 5$^{\circ}C$ min^{-1}

346
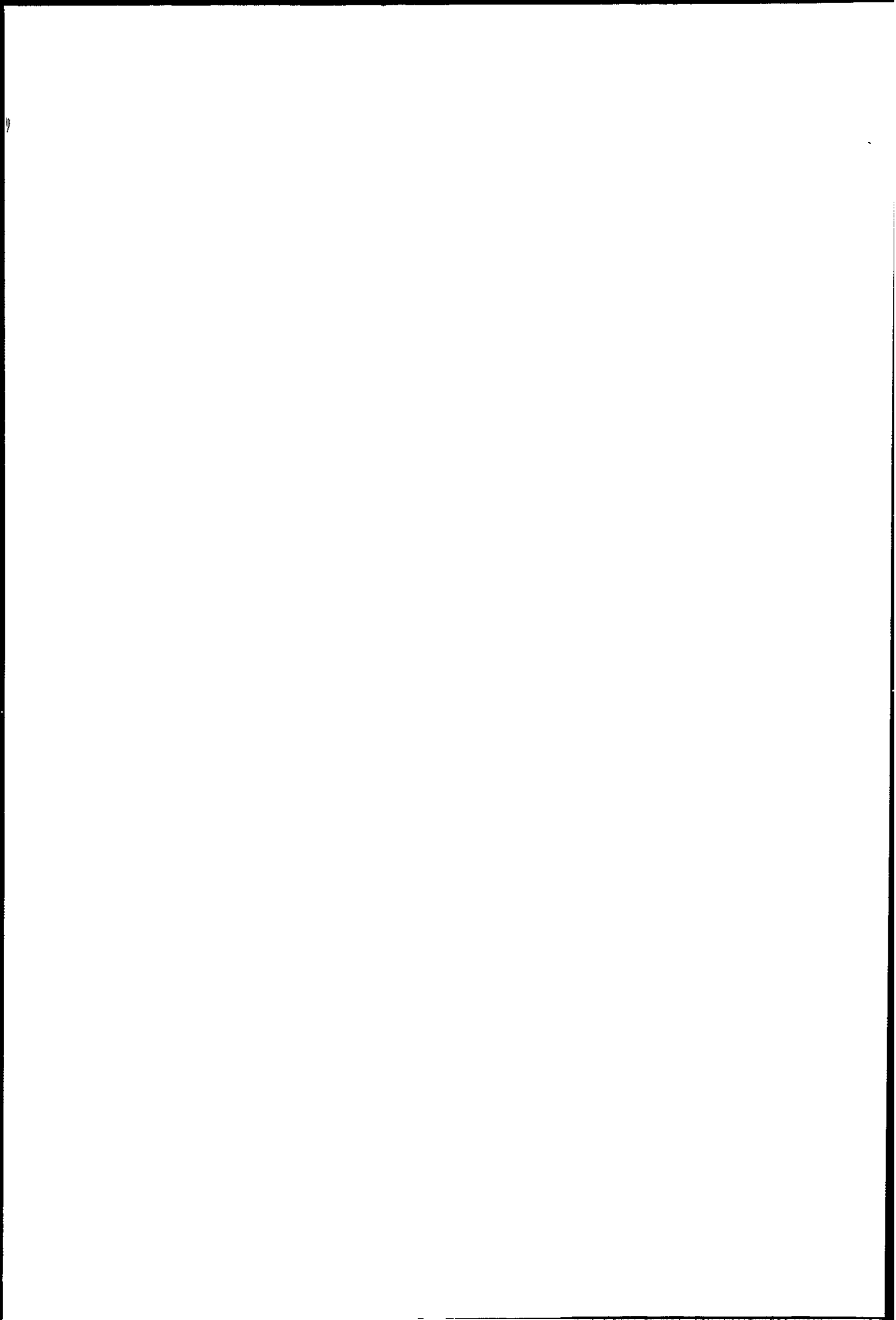
7.3.3. Comparison of Three Cokes.

The results for the oxidation of Cwm and Polish cokes in CO_2 at the same flow rate as previously used ($35.2 \text{ cm}^3\text{min}^{-1}$) are shown in Figure 7.23 and the simultaneous DTA curves in 7.24 for heating rates of 6 and 10 $^{\circ}C \text{ min}^{-1}$. The results for Nantgarw coke, already presented are included for comparison. The extrapolated onset temperatures of the DTA curves together with those of Nantgarw coke lumps are given in Table 7.11.
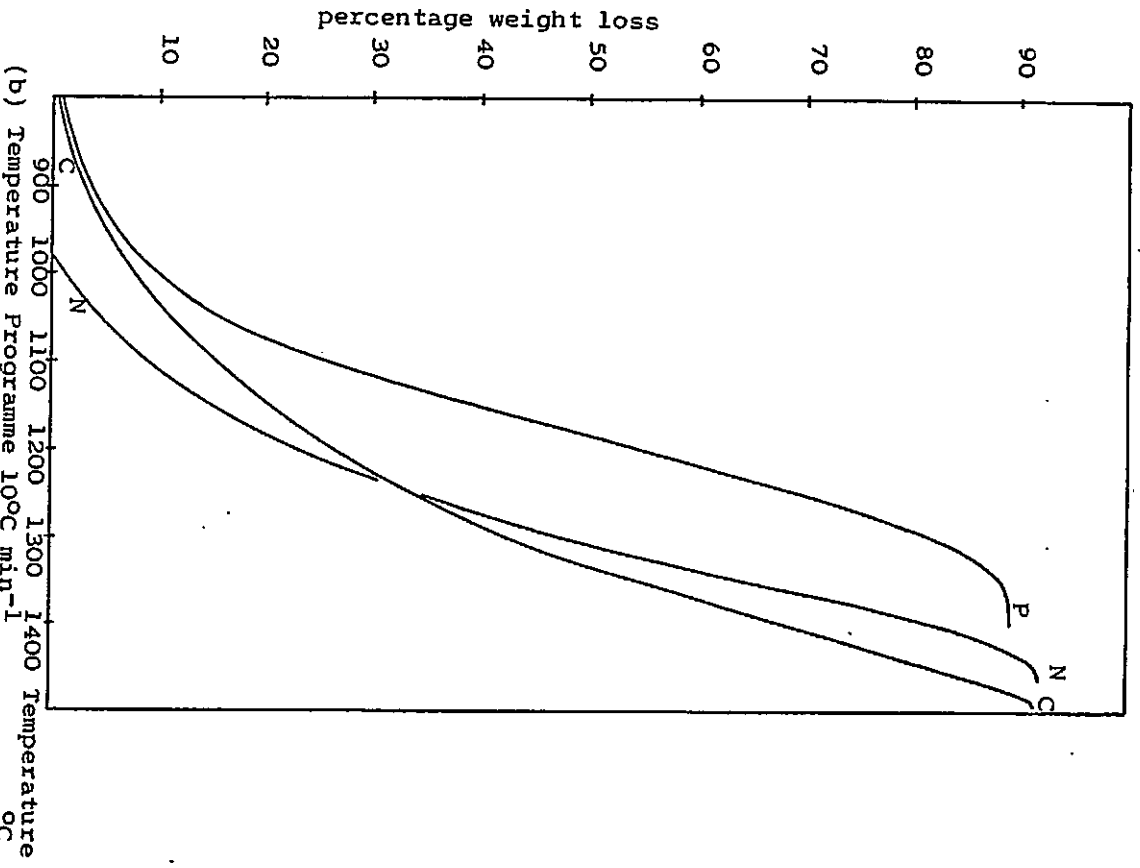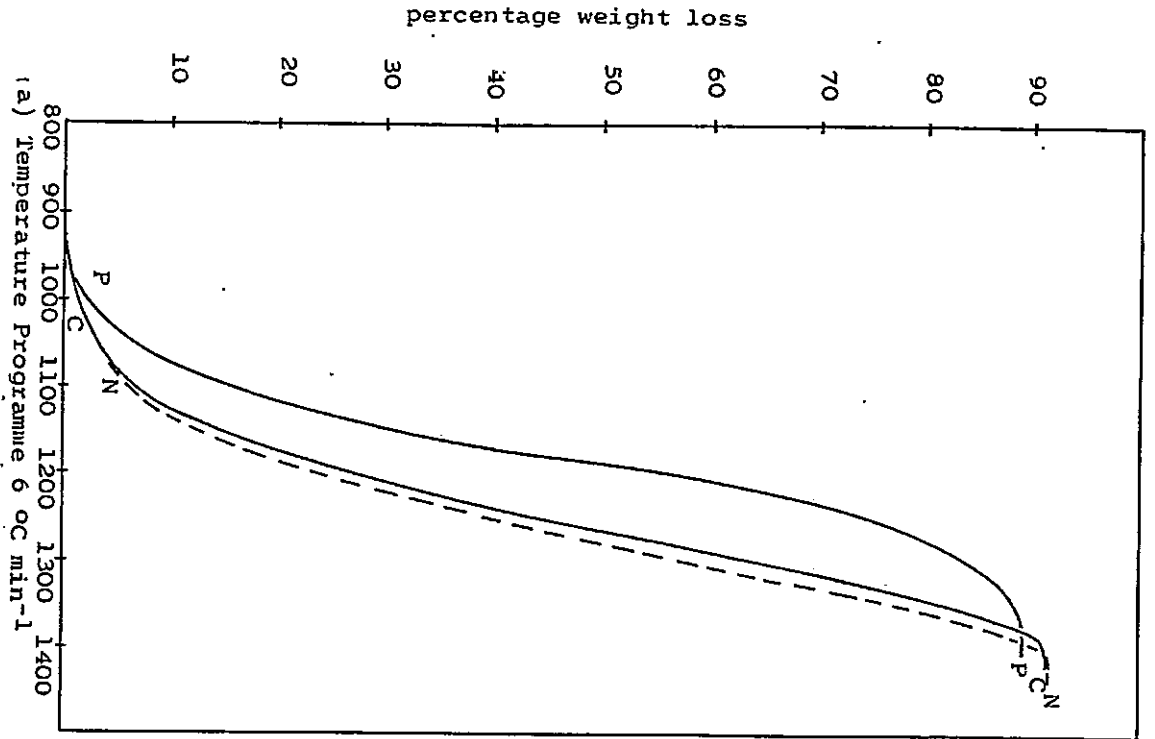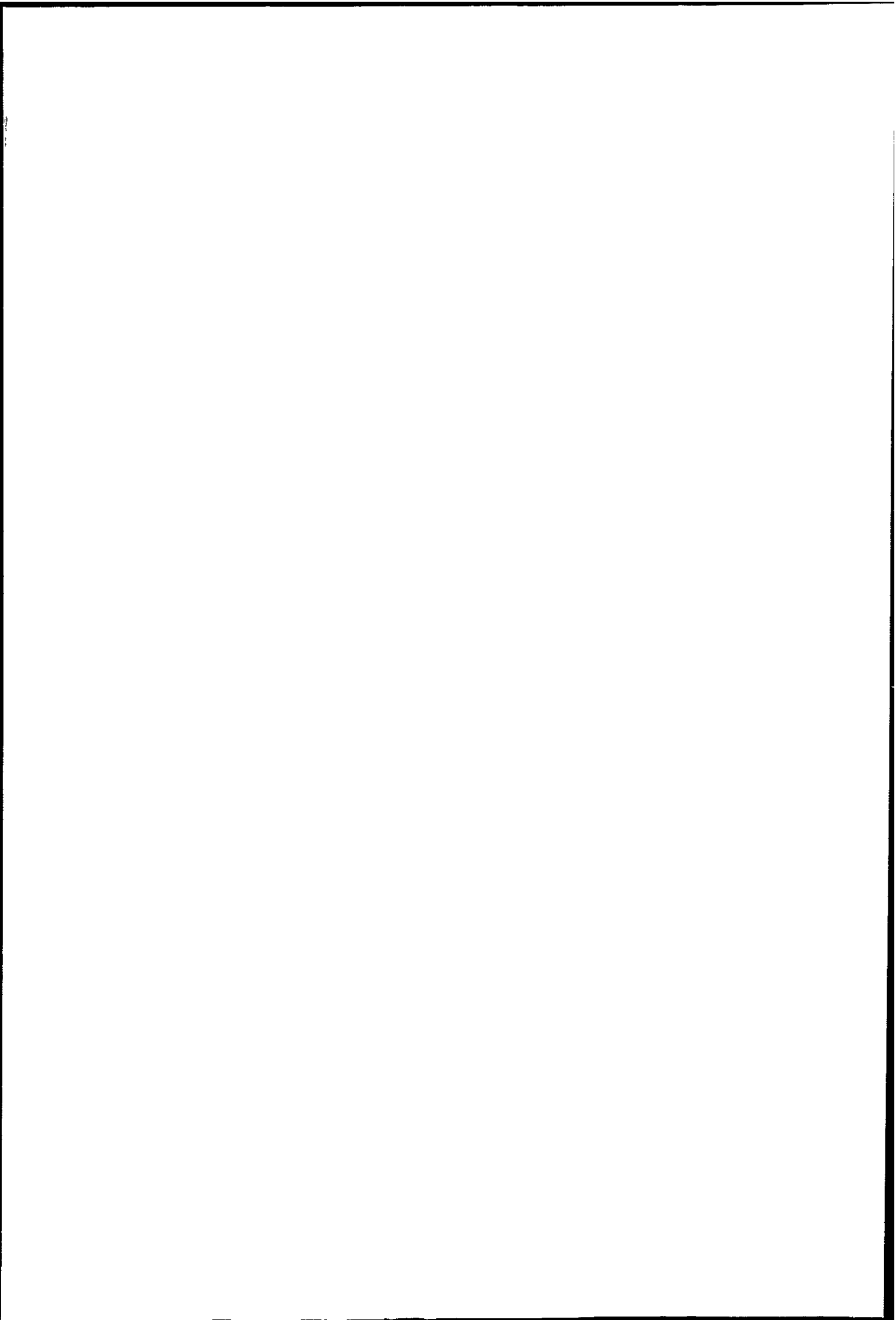
percentage weight loss

(a) Temperature Programme 6 oC min-1

percentage weight loss

(b) Temperature Programme 10°C min-1   Temperature oC
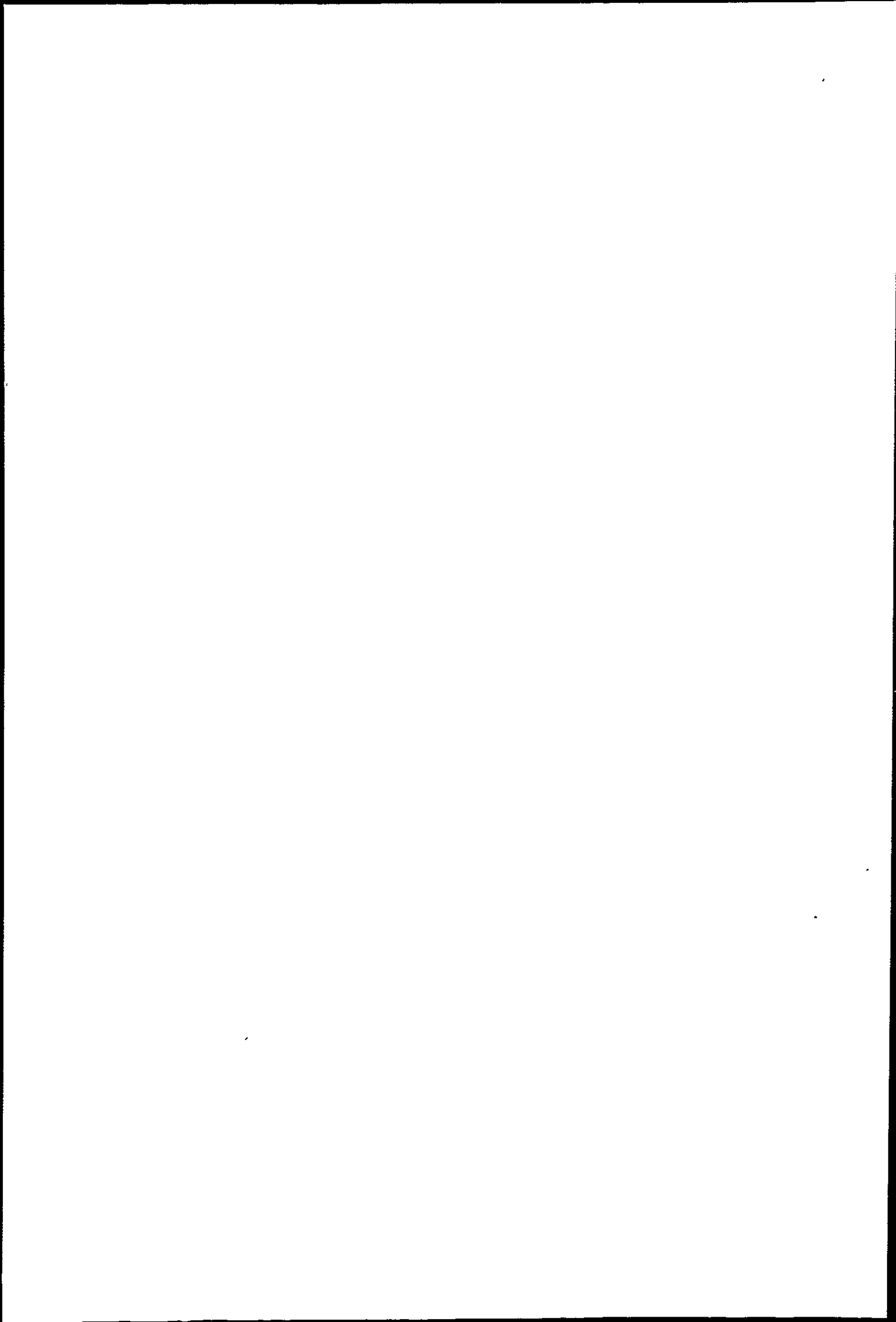
Figure 7.23. CO$_2$ oxidation of Three Cokes by TG.   N = Nantgarw   C = Cwm   P = Polish coke
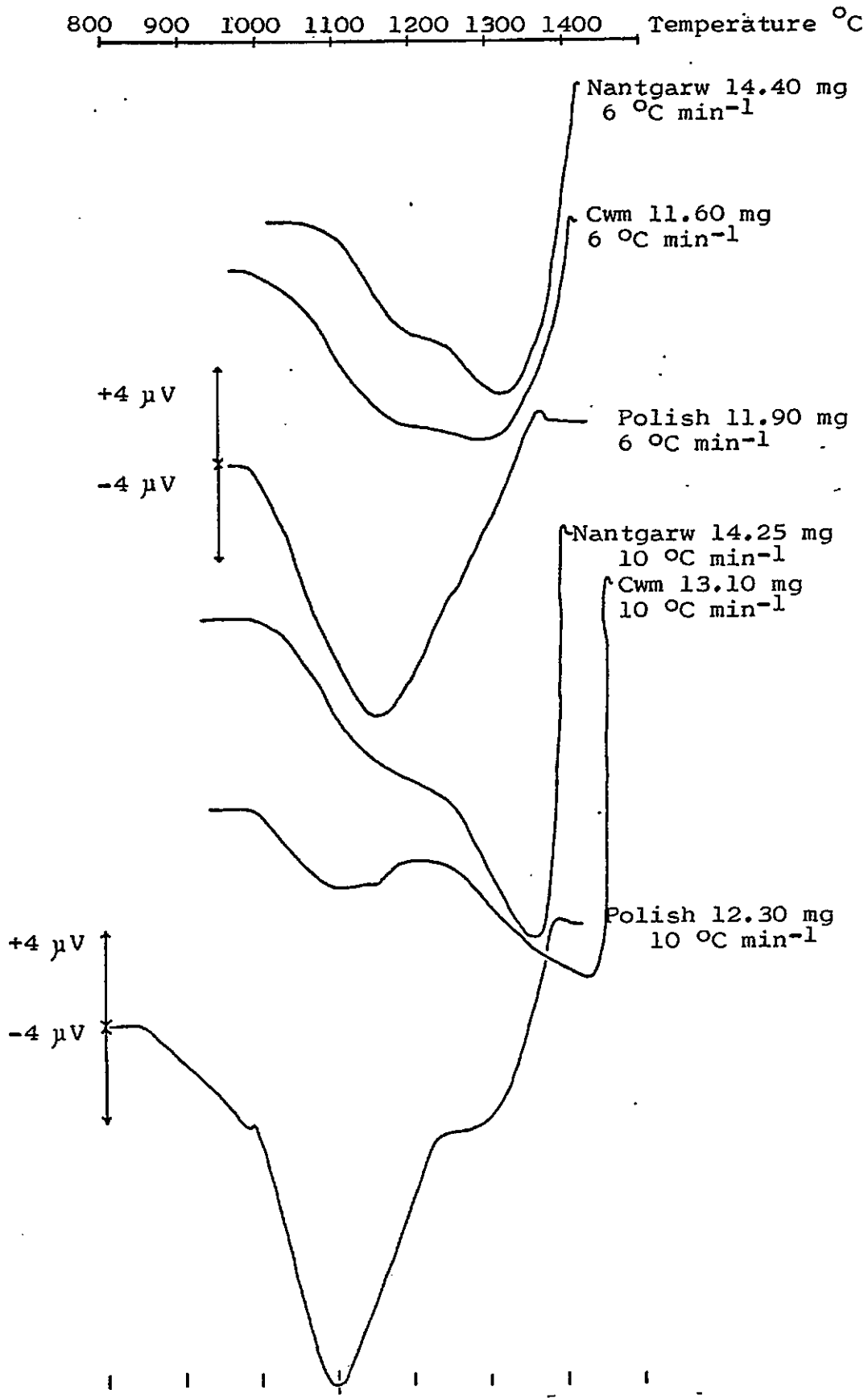
Figure 7.24. DTA of CO_2 oxidation of Three Metallurgical Cokes at Two Rates of Heating.

349
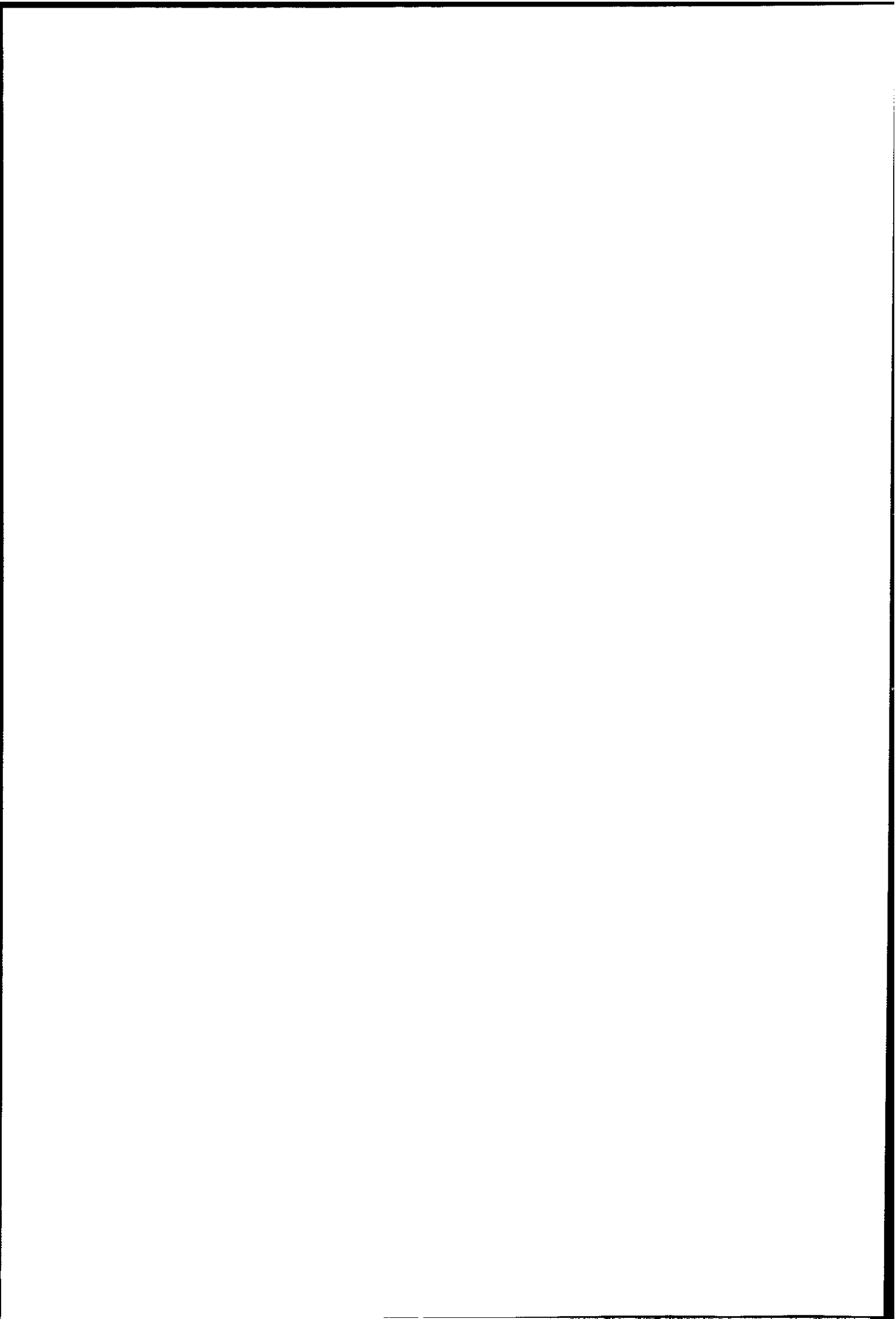
Table 7.11.   DTA of Cwm and Polish Cokes in CO_2

(a) Cwm coke.

Heating rate $^\circ C$ min^{-1}	Extrapolated onset temperature $^\circ C$	Temperature of First Peak Minimum $^\circ C$	Difference from Nantgarw $^\circ C$	Temperature of Second Peak Minimum $^\circ C$	Difference from Nantgarw $^\circ C$
10	1004(Nantgarw 1027)	1118	-113	1431	+69
6	1012(Nantgarw 1111)	1184	-26	1280	-37

(b) Polish Coke.

Heating rate $^\circ C$ min^{-1}	Extrapolated onset temperature $^\circ C$	Temperature of First Peak Minimum $^\circ C$	Difference from Nantgarw $^\circ C$	Temperature of Second Peak Minimum $^\circ C$	Difference from Nantgarw $^\circ C$
10	972(Nantgarw 1027)	1096	-135	1256	-106
6	991(Nantgarw 1111)	1155	-55	1260	-57
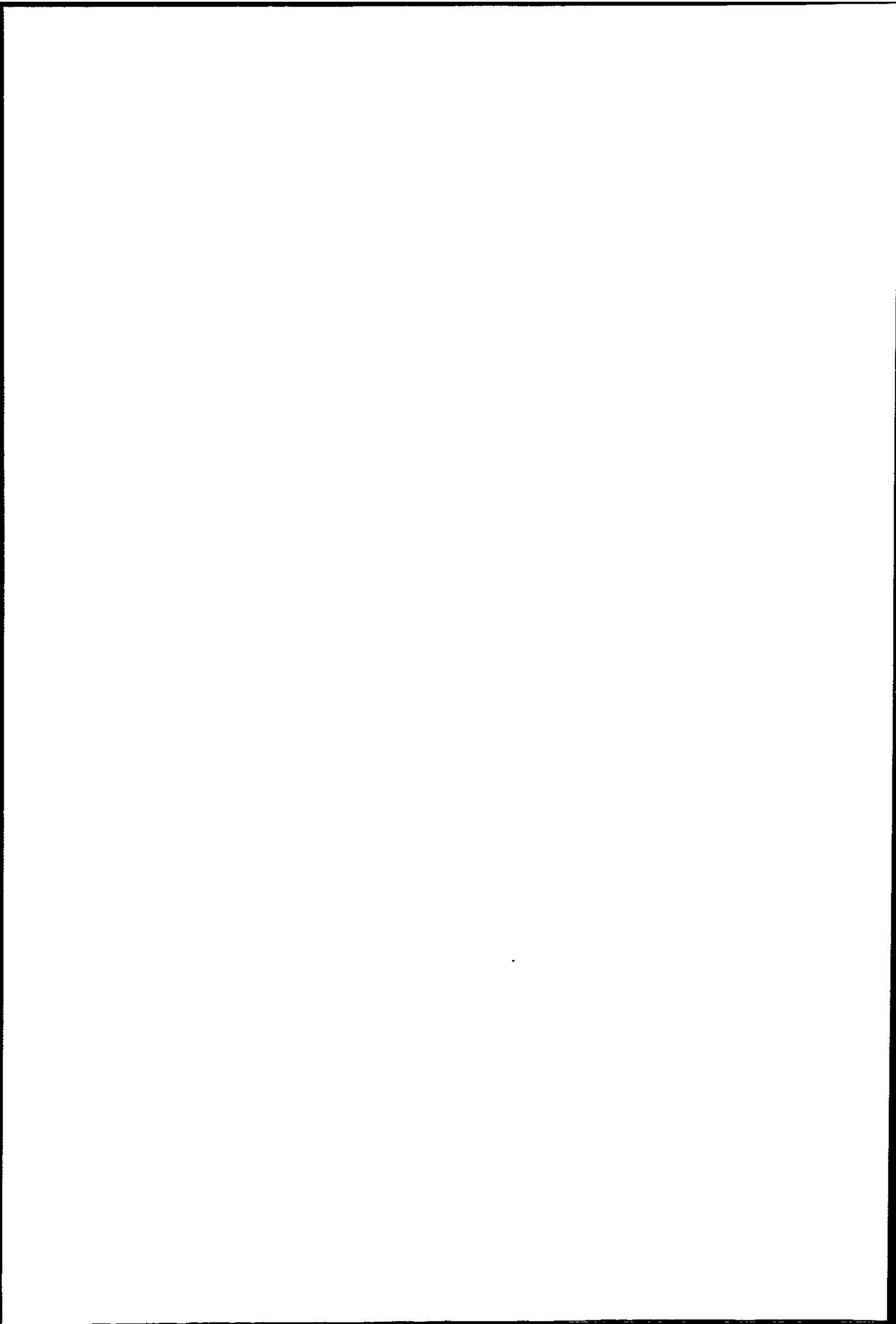
7.4 Discussion.

7.4.1 CO_2 and Air Oxidations of Coke, Char and Other Carbons

It was possible to oxidise all the carbons at a heating rate of 5 ^{o}C min^{-1} under static air conditions in the Massflow thermal balance. As shown in Figure 7.1 the charcoal and Australian brown coal char oxidation began between 400 and 500 ^{o}C, the coke at about 600 ^{o}C and the graphite about 650 ^{o}C. The weight loss of the char and charcoals before 300 ^{o}C was due to loss of volatile material and the corresponding endotherm is seen in the DTA traces.

The presence of two peaks in the DTA during the air oxidation of carbons has been noted by several workers and is discussed in Chapter 2.3.2. As diffusion becomes rate controlling the shape of the DTA peak is likely to become sharper and less symmetrical, but the effect of sample weight, experimental conditions etc. governs the shape and number of peaks. Two DTA peaks were observed inthe air oxidation of the coke, char, graphite and activated charcoal at a heating rate of 5 ^{o}C min^{-1} on the Massflow balance. (Figures 7.2 and 7.4), but a single peak for the coke (Figure 7.9) and an asymmetric peak for the char (Figures 7.10 and 7.11) on the STA781 at the same heating rate. At a DTA peak maximum the rate of heat evolution (or absorption in the Boudouard reaction) by the sample matches the rate of heat transfer to the reference, and the DTA curves most likely reflect the different sample environment of the two thermal balances.

The condition of the sample greatly affected DTA peak shape and area. That for a single lump of Nantgarw coke (Figure 7.2) is broad and shallow. The greater peak area for the crushed sample is probably due to the better thermal contact of the sample with the crucible. Sample weight, as seen in the DTA trace of Australian brown coal char, also greatly alters peak shape. Thermal gradients must have been considerable in the larger sample as the carbon had completely burnt off by the end of the temperature programme.

B_2O_3 doping inhibited the initial stage of the static air oxidation of Nantgarw coke (Figure 7.1) but had little effect above about 750 $^{\circ}$C, in keeping with results of the isothermal studies. Char oxidation was impeded throughout the burn off in static air by B_2O_3 treatment.

Under a flowing air atmosphere the TG/DTA behaviour of the powdered charcoals was little altered, but the Australian brown coal char, activated charcoal and Nantgarw coke oxidations proceeded more rapidly with consequent sharpening of the DTA peaks. The limiting effect of gaseous diffusion may not affect the finely powdered carbons (Norit, charcoal for chromatography and decolourising charcoal) at such low temperatures as for the coke and char.

The CO_2 oxidation of the charcoals, coke and graphite on the STA781 thermal balance places them in the same order of "reactivity" (Figures 7.5 and 7.6) as the air oxidations ie decolourising charcoal the most "reactive", Nantgarw coke and PMC graphite the least. The same order of
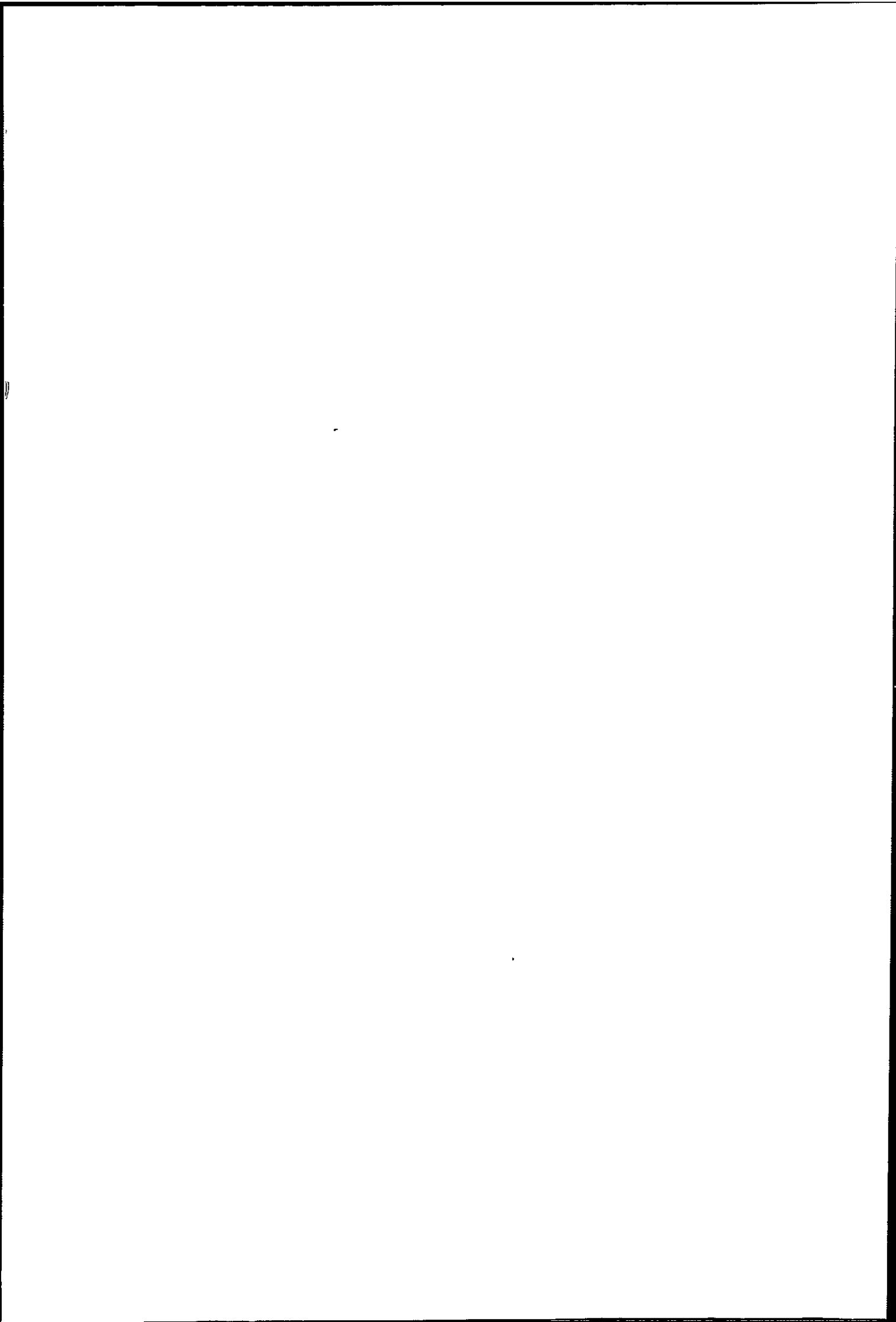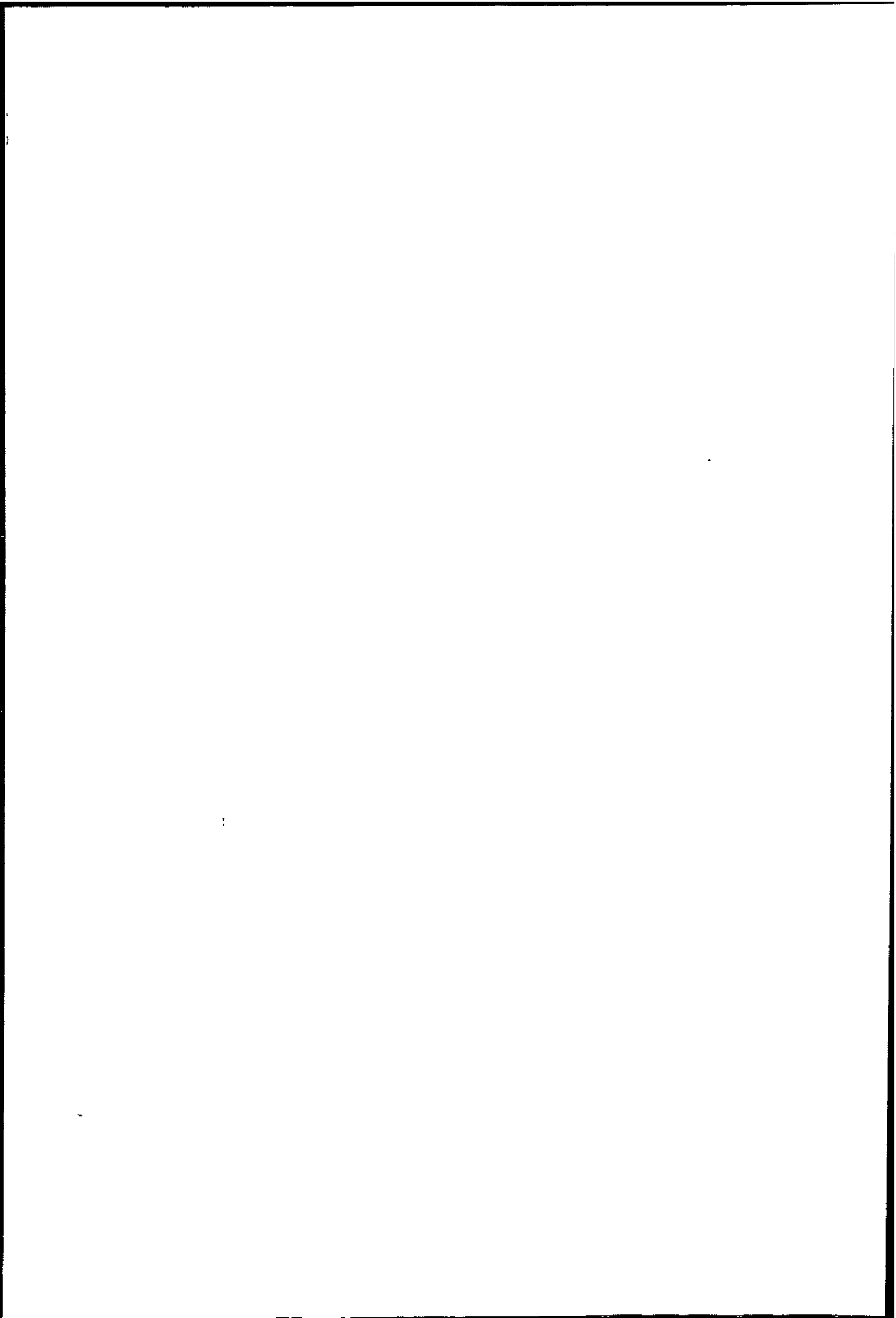
"reactivity" is found from isothermal oxidations in CO_2 at 910 $^{\circ}C$, (Table 5.4.j.). The corresponding DTA traces of Figure 7.7 show the endothermic nature of the Boudouard reaction (with a small endotherm due to loss of volatiles for char and charcoals). Crushed char gave a sharpened peak, though the same initial and peak temperatures as granular char.

In the CO_2 oxidations of Nantgarw coke and Australian brown coal char of Figure 7.6 the simultaneous DTG trace is shown. Rate of reaction for the char increased until almost complete burn off, whereas that for the coke reached a maximum and then declined, similar to their behaviour under isothermal conditions. A similar shaped DTG curve was found for crushed coke heated at 5 $^{\circ}C$ min^{-1} although the maximum was attained at a lower temperature than that at 10 $^{\circ}C$ min^{-1} heating rate.

The maximum rate of reaction in CO_2 under a temperature programme of 10 $^{\circ}C$ min^{-1} was 1920 μg min^{-1} (at 1007 $^{\circ}C$) for 22.93 mg crushed char and 1530 μg min^{-1} (at 1014 $^{\circ}C$) for 24.39 mg char granules. This corresponds to a rate of reaction of 140 x 10^{-5} g s^{-1} g^{-1} for crushed char and 105 x 10^{-5} g s^{-1} g^{-1} for char granules. The comparable rate for the isothermal oxidation of char granules is 97.2 x 10^{-5} g s^{-1} g^{-1} (Table 5.4.e) at 1014 $^{\circ}C$.

Similarly the maximum rate of CO_2 oxidation for 24.90 mg Nantgarw coke from Figure 7.6 is 1120 μg min^{-1} at 1310 $^{\circ}C$. This corresponds to a rate of reaction of

74.97×10^{-5} g s^{-1} g^{-1} which is higher than that found from isothermal oxidation at 1310 ^{o}C as given in Table 5.4.a. Larger sample weight was used in the isothermal work but as diffusion is not rate limiting, rates in terms of g s^{-1} g^{-1} may be compared.

The effect of flow rate and particle size in the air oxidation of Nantgarw coke and Australian brown coal char was more conveniently followed on the STA 781 thermal balance although initial oxidations had been done on the Massflow.

Figure 7.9 shows that a slower air flow does not alter the rate of oxidation of the coke until about 740 ^{o}C. Above this temperature rate is slower and the DTA peak broadened by a lower air flow. Diffusion control is to be expected above 750 to 800 ^{o}C. The maximum rate of reaction, from the DTG curve of Figure 7.8, occurs at 835 ^{o}C. As this is in the zone of diffusion control, rate in terms of g s^{-1} g^{-1} cannot be compared with isothermal results.

Particle size had a much smaller effect than air flow rate on the oxidation of the char. Eight sieved fractions of crushed char of 1.4 mm to <63 μm were studied at a heating rate of 5 ^{o}C min^{-1} and the same air flow rate. The TG curves were little altered and the DTA curve smoothed for more finely divided material as shown in Figure 7.10. The crushed material oxidised somewhat less rapidly than the lumps, possibly due to destruction of macropores of the original surface. Increased air flow

rate greatly increased the rate of char oxidation as seen in Figure 7.11.

The strongly exothermic nature of the reaction is seen by the disruption of the linear increase in sample temperature in Figures 7.8 to 7.11.

The effect of particle size and flow rate for the Boudouard reaction of the coke and char was not investigated in detail.

Smaller particle size for the coke and the char lowers the temperature at which the reaction appears to start Tables 7.5 and 7.10 respectively, but is not greatly significant in that the time of complete burn off is unaltered. DTA extrapolated onset temperatures are lower for smaller particle size.

## 7.4.2 Effect of Heating Rate on Coke and Char in the Boudouard Reaction.

In the CO_2 oxidation of Nantgarw coke a higher rate of heating led to faster burn off with consequent sharpening of the DTA endotherms as would be expected. Reaction was complete at lower temperatures the lower the heating rate (Table 7.1) with some variation between lumps and granules.

For several heating rates there was a shoulder on the leading edge of the DTA trace similar to that seen in the exotherms of the air oxidations on the Massflow balance. This appearance in the DTA curve therefore cannot be correlated with the kinetic order of reaction but is a function of sample environment etc.

The variation in peak minimum T_m with heating rate ϕ can be seen when original results are replotted against sample temperature for Nantgarw coke in Figure 7.16, doped coke in Figure 7.17, Australian brown coal char in Figure 7.20 and the doped char in Figure 7.21.

Values of $\ln(\frac{\phi}{T_m^2})$ versus $\frac{1}{T_m}$ are plotted in Figure 7.25 for Nantgarw coke lumps and granules. Less reliance is placed on the 2 and 4 $^{\circ}C$ min^{-1} results for coke lumps and it was not possible to distinguish definite minima at these heating rates for the granules. It was hoped that granules would give better results as it was possible to get sample weights closer than for lumps.

The points fall on reasonable straight lines, the slope of which yields a value for the activation energy of 158.4 kJ mol^{-1} for coke lumps and 159.9 kJ mol^{-1} for the
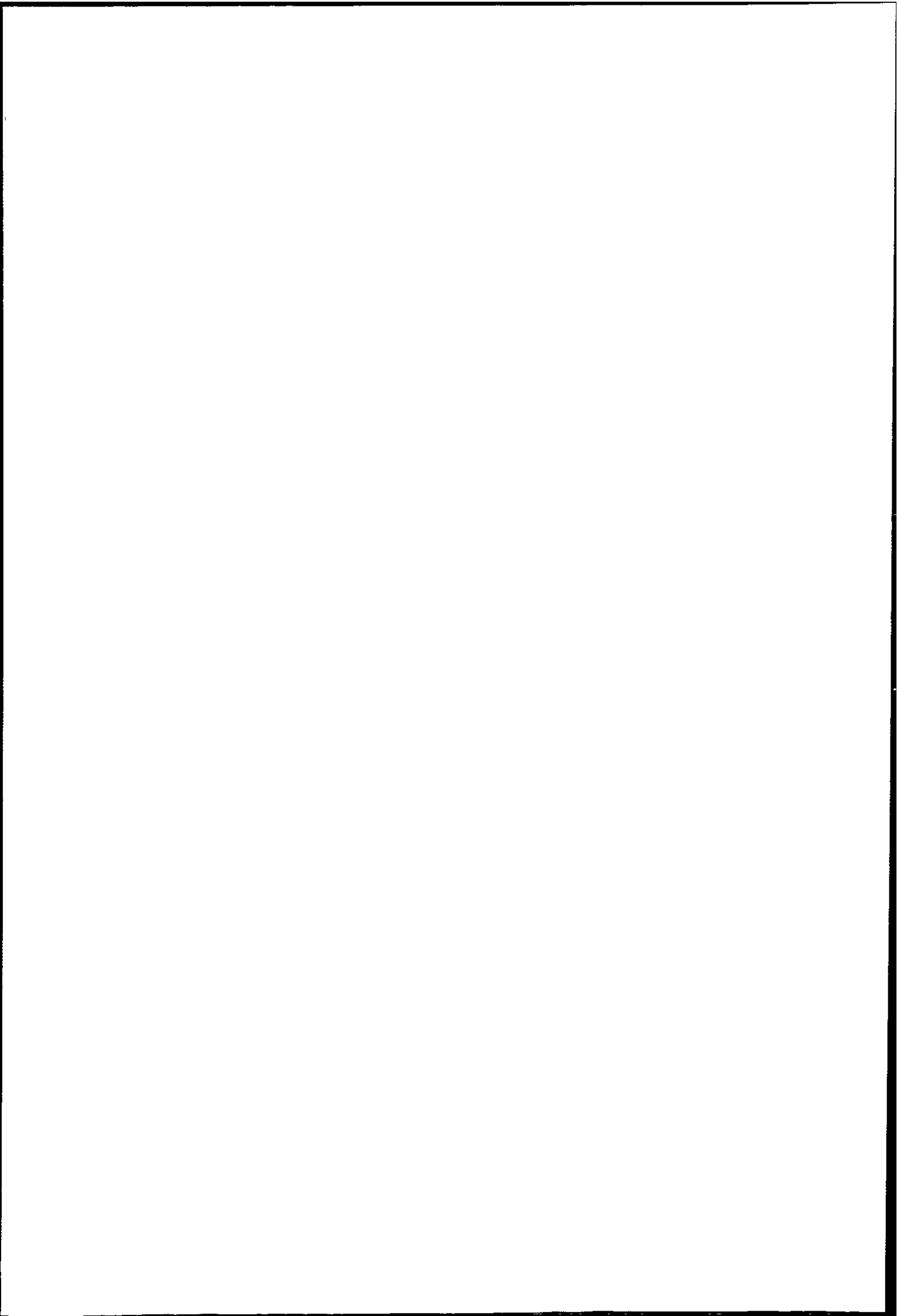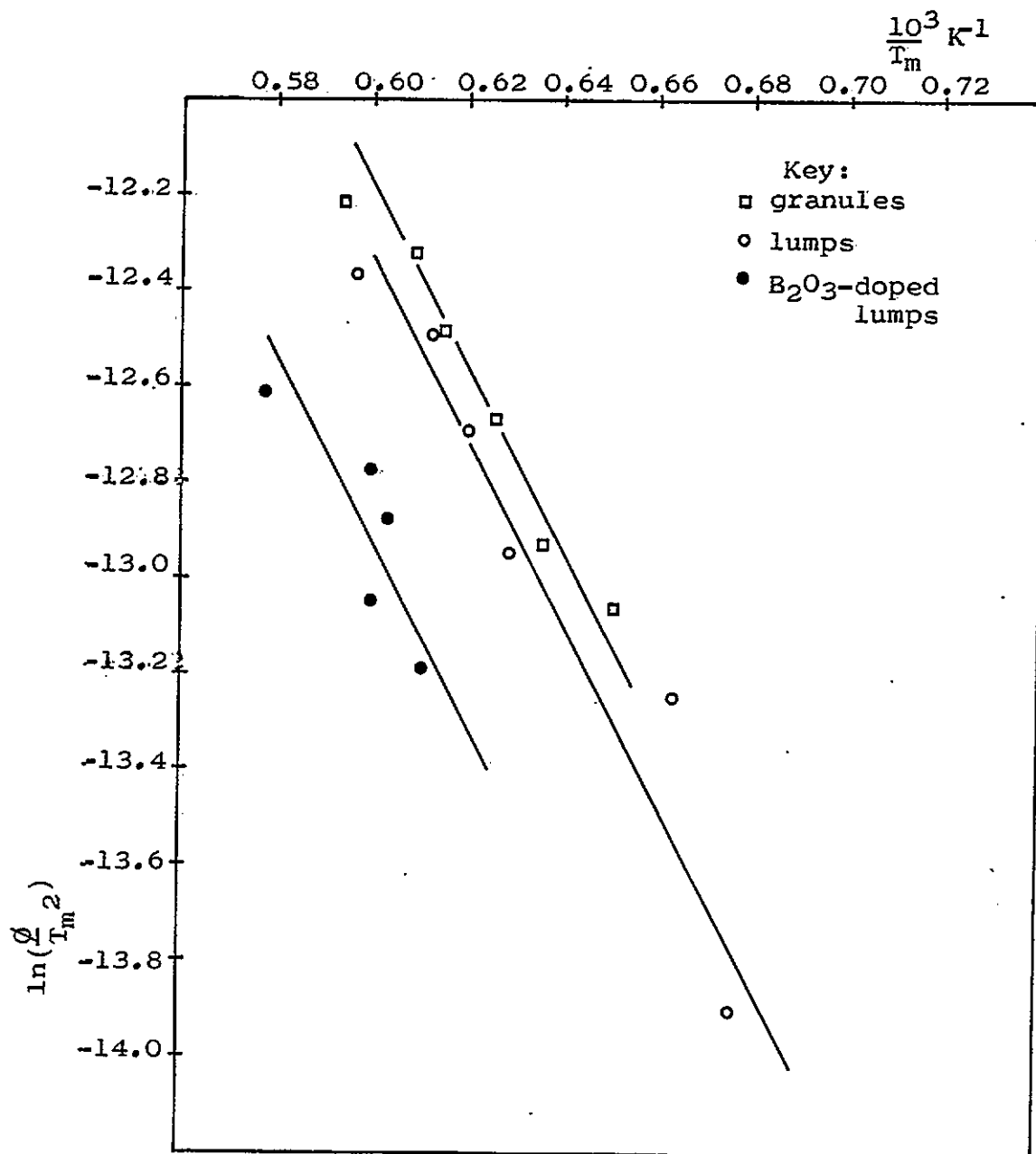
Figure 7.25. Variation of Peak Minimum Temperature T_m with Heating Rate $\emptyset$ for Nantgarw Coke in the Boudouard Reaction.

granules, which is somewhat less than that obtained from isothermal TG (186 kJ mol^{-1}).

In comparing the TG curves of the doped coke and char with that of the undoped material (Figure 7.22) the inhibiting effect of B_2O_3 can be seen to be due to a slowing of the initial part of the oxidation.

The DTA curves for the doped coke have a similar appearance to those of the untreated coke although peak minimum is at a higher temperature for the same heating rate. This is also seen for the doped char but the DTA curves are rounded and spread and easily distinguished from those of the untreated char.

Smaller variation in temperature of DTA minima were obtained for B_2O_3 doped coke and these are also plotted in Figure 7.25. The 10 $^{\circ}C$ min^{-1} result is included although burn off was not complete at the end of the temperature programme and the final 35% of reaction was continued under isothermal conditions. As the range of rate of heating over which results could be obtained was narrow (5 to 8$^{\circ}C$ min^{-1}) the spread of results is poorer than for the untreated coke. The slope of the line joining these points, and therefore the energy of activation for the reaction, appears the same as for undoped coke.

It was possible to burn off the char in CO_2 at faster heating rates than the coke as rate of reaction was appreciable at lower temperatures. As with Nantgarw coke, the temperature of complete burn off was higher the higher the heating rate, and these temperatures were

raised for the B_2O_3 doped char (Tables 7.6 and 7.7). The inhibiting effect of B_2O_3 at the initial stage of the reaction is seen in Figure 7.22, the volatile matter being lost before 500 ^oC. Similar TG curves were seen at other rates of heating. The increased proportion of inert material in the doped char leads to a rounding of the curve in the final 10% weight loss.

The estimation of temperature of DTA curve minimum T_m with rate of heating ϕ was easier than for the coke and values of $\ln(\frac{\phi}{T_m^2})$ versus $\frac{1}{T_m}$ are plotted in Figure 7.26 for doped and original char.

This plot yields a value for the activation energy for the Boudouard reaction of 176 kJ mol^{-1} for the char and 169 kJ mol^{-1} for the B_2O_3 doped char. Again the values are lower than those from isothermal studies (194 kJ mol^{-1} for the char and 231 kJ mol^{-1} for the doped char) although the difference between the values for the doped and original char would suggest that the presence of B_2O_3 has not altered the energy of activation for the reaction and tends to support the view that it acts by a physical blocking of surface rather than by chemical means.
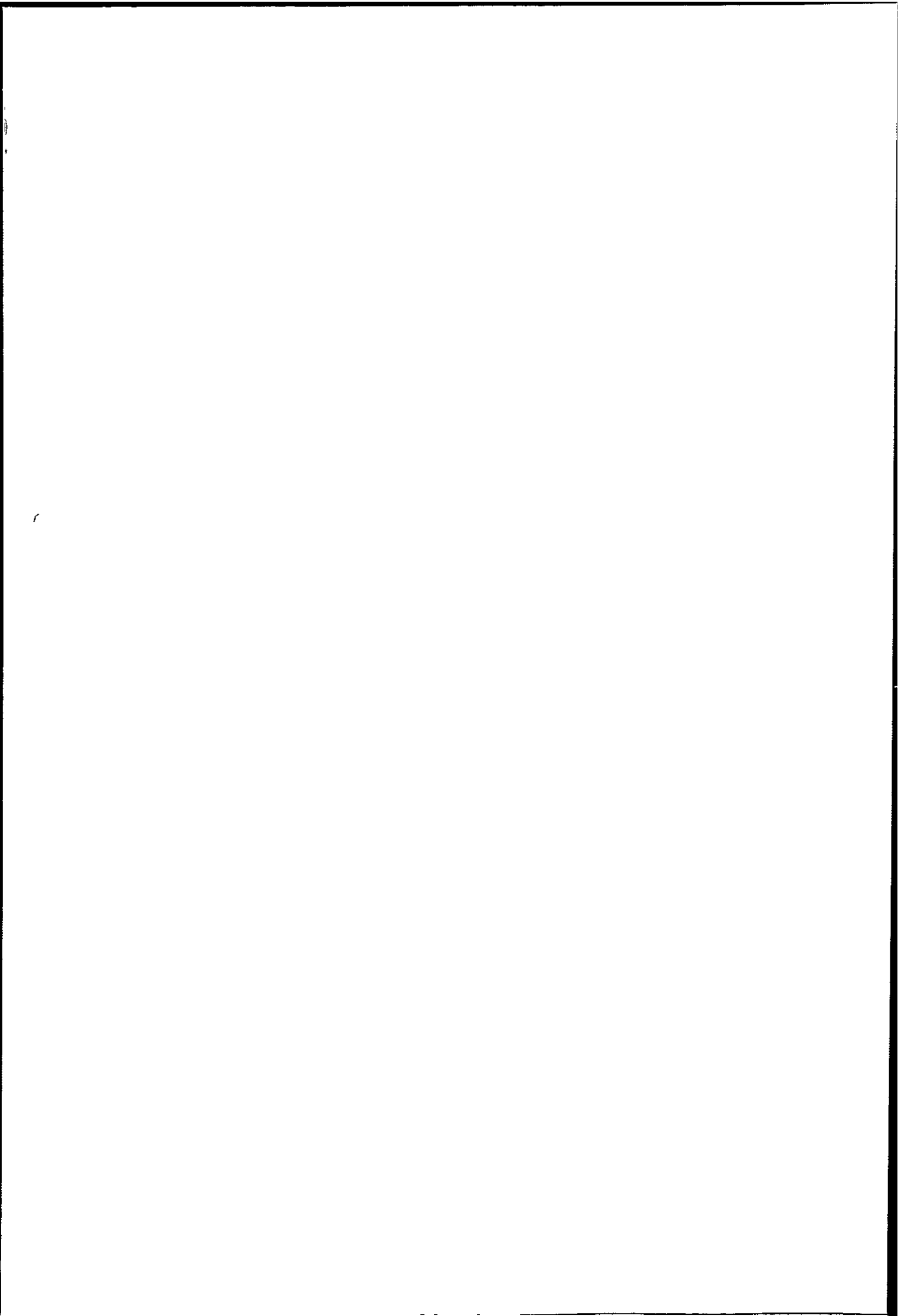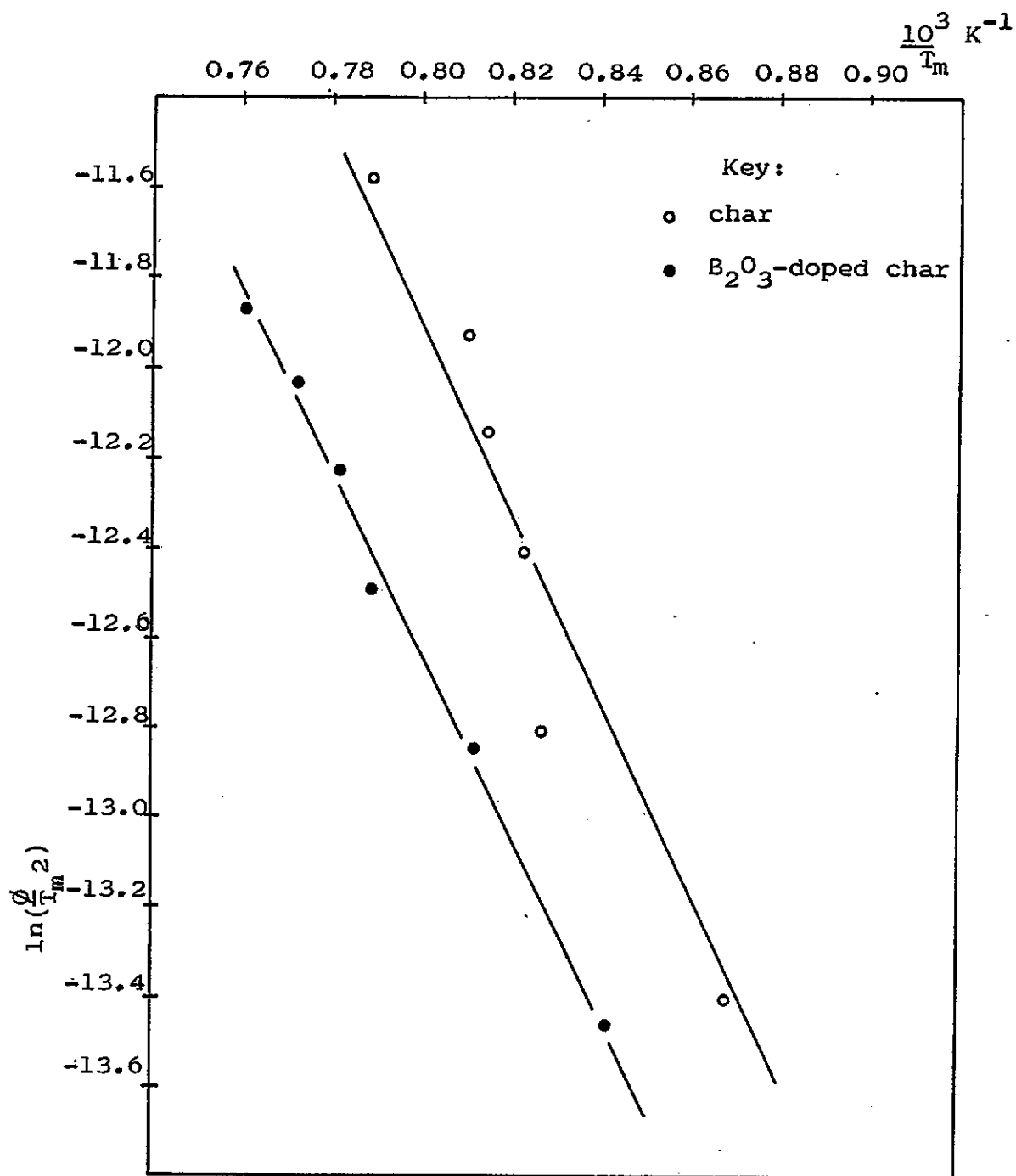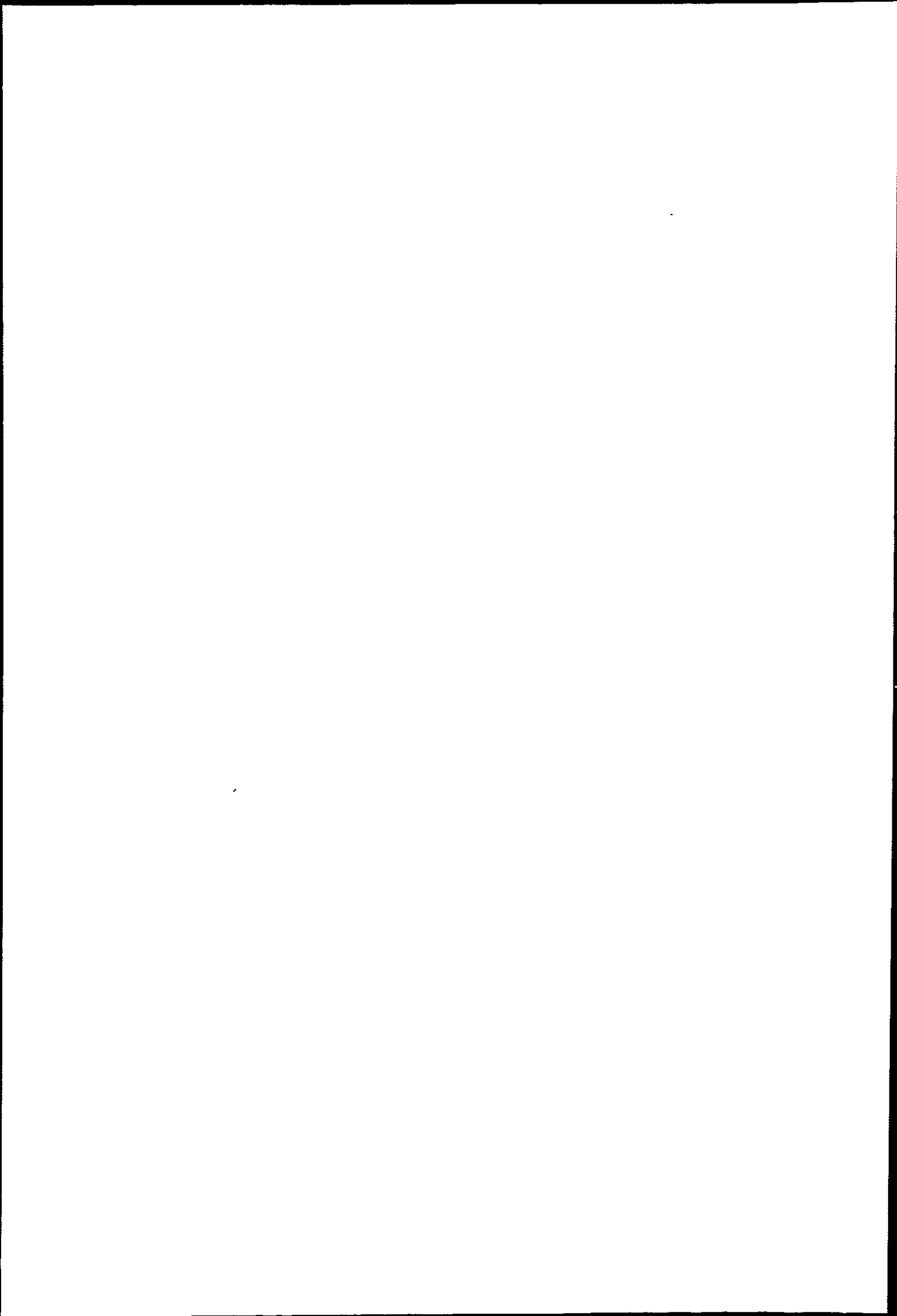
Figure 7.26. Variation of Peak Minimum Temperature T_m with Heating Rate $\emptyset$ for Australian Brown Coal Char in the Boudouard Reaction.

7.4.3 Comparison of Nantgarw, Cwm and Polish Cokes.

At a heating rate of 6 $^{\circ}C$ min^{-1} (Figure 7.23.a) dynamic TG places the cokes in the order - Nantgarw, Cwm, Polish - in increasing reactivity, as do isothermal tests. Cwm and Nantgarw cokes differ only slightly in reactivity and the simultaneous DTA curves are very similar.

At both 6 and 10 $^{\circ}C$ min^{-1} rates of heating Polish coke is clearly more "reactive". The DTA curve has a steeper leading edge and prominent peak, which is just a shoulder on the curves for the other two cokes. The studies reported in Chapter 6 have shown the large increase in specific surface area for Polish coke in the first half of the carbon burn off in CO_2 and the TG/DTA results show a correspondingly high rate of reaction.

At a heating rate of 10 $^{\circ}C$ min^{-1} Cwm coke burns off faster than Nantgarw coke but after about 35% weight loss the order is reversed. Extrapolated onset temperatures for Cwm and Polish cokes are lower than for Nantgarw coke. This is generally less affected by changes in experimental conditions than is peak temperature.

Where differences in coke reactivity are high dynamic thermal methods could perhaps be used in reactivity testing, but where differences are small only low rates of heating are likely to give comparable results with isothermal tests.

Aderibigbe and Szekely (Chapter 2, reference 63) suggest that reaction of a coke particle at low temperature has an activating effect, enhancing subsequent
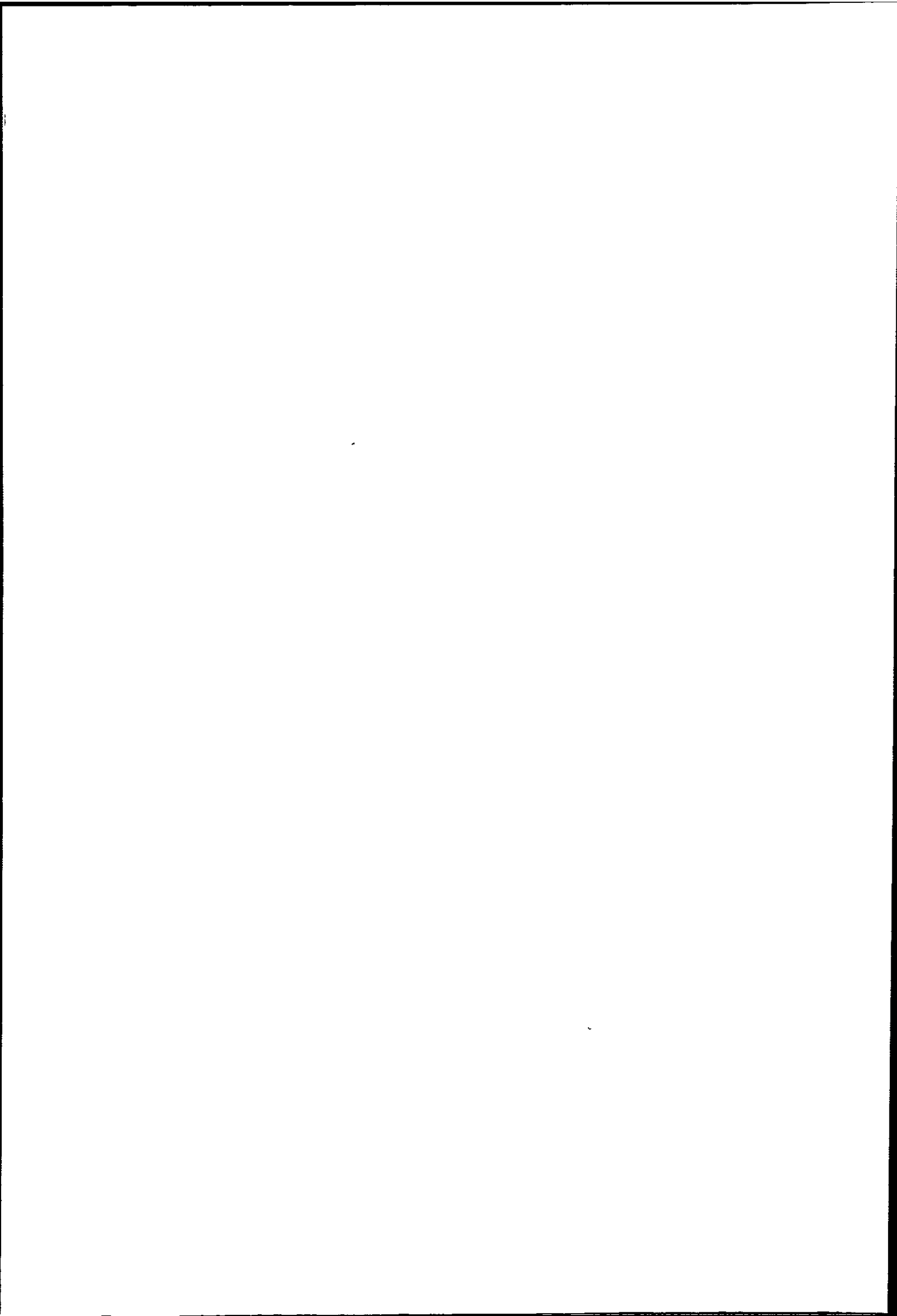
"reactivity" of the material. On comparing the TG results from CO_2 oxidation of Nantgarw coke under a temperature programme of 10 $^{\circ}C$ min^{-1} from Figure 7.6 (in which the sample was programmed from room temperature) with that from Figure 7.12 (in which the sample was rapidly preheated to 990 $^{\circ}C$) an increased rate of reaction for the former sample can be seen. This is shown as a dotted line in Figure 7.12, and may be due to this activating effect of particle gasification at lower temperatures. At the pre-heating rate of 45 $^{\circ}C$ min^{-1} the furnace takes about 25 minutes to reach 1000 $^{\circ}C$. At 10 $^{\circ}C$ min^{-1} this is not reached for almost 2 hours. The previous calculation on rate of reaction from the DTG curve of Figure 7.6 has shown the increase over the isothermal rate.

Thus simple (isothermal) coke reactivity tests are unlikely to completely predict behaviour in blast furnace conditions.

References

1. P.J. Sleeman, Ph.D. Thesis, CNAA, 1976, Plymouth Polytechnic.

2. B. Basäk, Ph.D. Thesis, CNAA, 1973, Plymouth Polytechnic.

3. J.G. Dunn & S.A.A. Jayaweera, Thermochemica Acta, 1983, 61, 313-7.

4. H.E. Kissinger, J. Research Natl. Bur. Standards, 1956, 57, 217-21.

5. H.E. Kissinger, Anal. Chem. 1957, 29, No.11, 1702-6.

CHAPTER EIGHT
CONCLUDING SUMMARY

This thesis embodies studies on the deactivation of carbons by boric oxide additives, especially in relation to zinc/lead blast furnace practice.

The research commenced with the characterisation of a wide ranging selection of carbons, including metallurgical cokes, coal char and graphite. The surface and solid state properties were examined by a variety of physico-chemical techniques.

The deactivation of carbons by boric oxide solution treatment was investigated, in relation to possible industrial use in the zinc/lead blast furnace. Studies were then carried out with respect to the reactivity of carbons towards air and carbon dioxide in the following manner.

Firstly the development of surface area and porosity after carbon burn off at different temperatures was investigated by gas sorption using the standard equations developed by the various approaches to gas-solid interactions. Variations of specific surface with percentage carbon burn off are correlated with development of porosity and reactivities of the cokes. Reactivity of the coal char, and other carbons, was correlated with the pore size distribution. Results are discussed for coke and coal char in relation to the build-up of coke ash during carbon burn off and sintering of the products.

Isothermal TG studies of the carbons has provided information on the kinetics of the oxidation reactions.
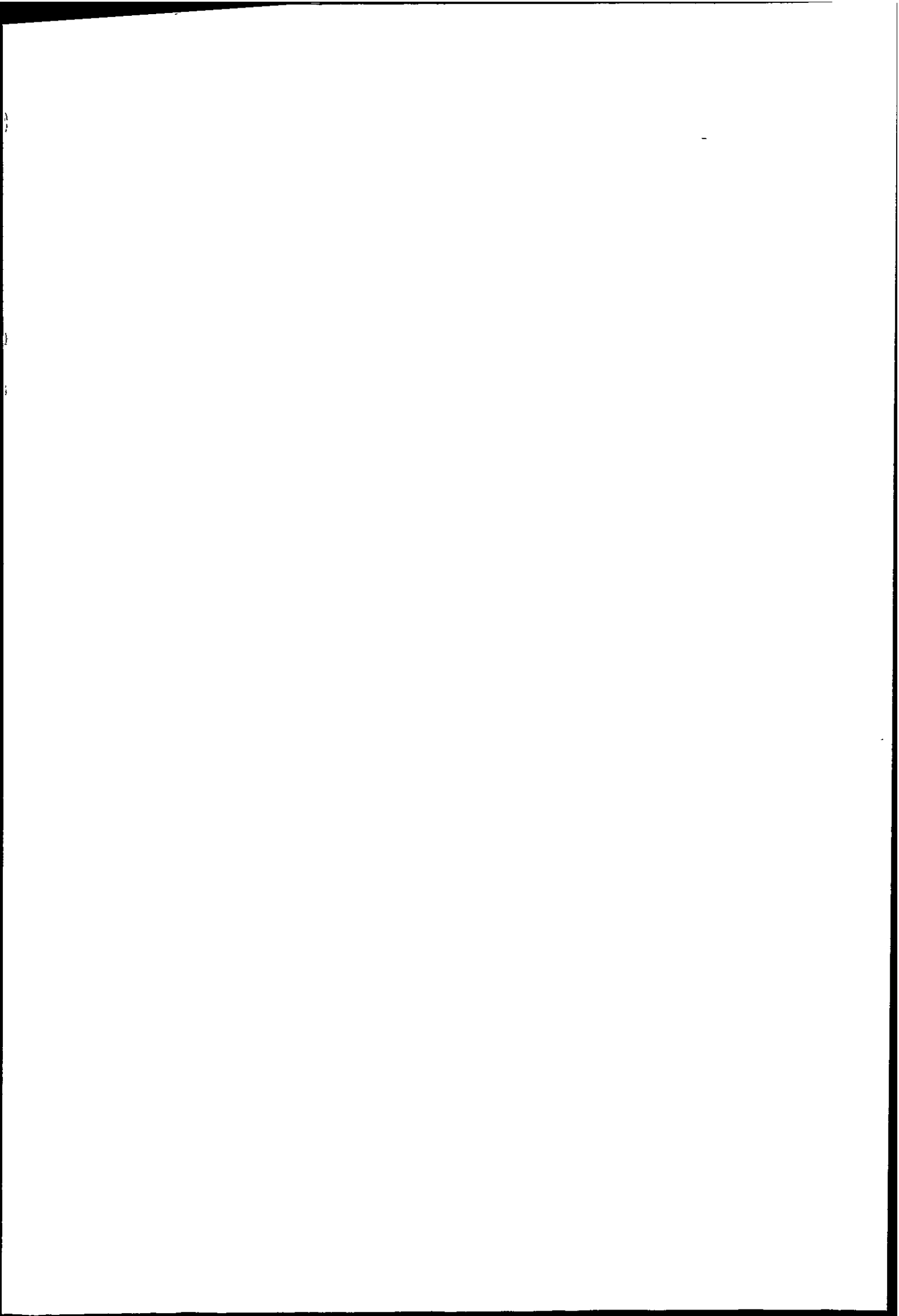
Attempts have been made to fit the kinetic data into models based on idealised surface geometries.

Simultaneous TG/DTA/DTG studies under dynamic conditions have been carried out to determine the effect of heating rate, particle size and gas flow rate on the oxidation reactions. It is well established that these parameters govern thermal analysis data. Weight changes have been compared with those occurring under isothermal conditions.

Mechanisms have been proposed for the inhibition of the oxidation of the carbons by boric oxide additive. It is hoped that the results would lead to formulation of optimum conditions for the industrial combustion of metallurgical cokes.

Further studies would be useful to extend methods developed in this work to cokes of wider origin, e.g. petroleum and domestic cokes. A study of the effect of different heating rates on the oxidation of a range of cokes and the effect of thermal pretreatment would be particularly useful. SEM with the quantitative estimation of ash minerals by electron microprobe analysis could yield information on the interaction of ash inclusions with the carbon surface.

Examination of coke ash is becoming important, as there are situations where cokes of high ash content (up to 25%) have to be used. Coke may be demineralised, by acid leaching or plasma ashing, and the carbon (which will still contain trace elements) examined.
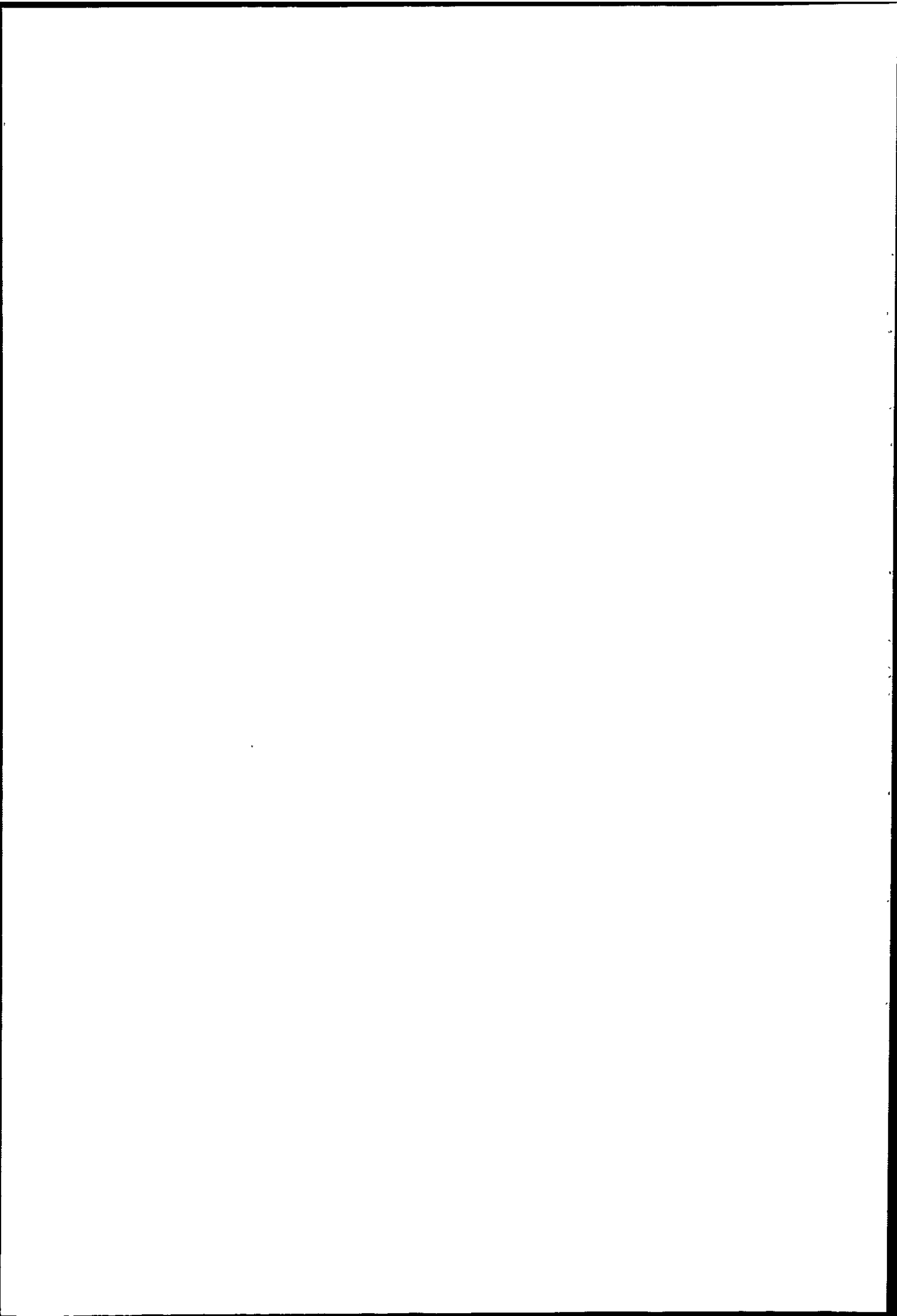
Appendix 1. Programme for the calculation of the fraction reacted

functions for the three surface geometries, and run on the PRIME 850

```
.top.
C:       SPECIFICATION
C:       .............
         INTEGER I,NP
         DOUBLE PRECISION TA1,TC(100),TSP(100),TSL(100),ALF(100),
     *                   LALF,TCSP(100),TCC(100),TCSL(100)
         DATA       LALF/1.0/,   FALF/0.0/,   NP/20/, TA1/15.0/
C:       EXPERIMENTAL VALUES FOR REDUCED TIMES
C:       .....................................
C
         ALF(1)=FALF
         DO 10 I=2,NP
         ALF(I)=ALF(I-1)+LALF/(NP*1.0)
   10 CONTINUE
C
C             THEORETICAL TIME VALUES
C
         DO 20 I=1,NP
C
C
         TCSL(I)=TA1*(1-(1-ALF(I))**1)
         TCC(I)=TA1*(1-(1-ALF(I))**0.5)
         TCSP(I)=TA1*(1-(1-ALF(I))**0.333333)
C
C
         ARGLOG=1-ALF(I)
         TC(I)=TA1*(ALF(I)+(1-ALF(I))*LOG(ARGLOG))
         TSP(I)=TA1*(1-3*(1-ALF(I))**(2/3.0)+2*(1-ALF(I)))
         TSL(I)=TA1*ALF(I)**2
   20 CONTINUE
C
C        FILES TC  TSP   TSL TCC TCSP TCSL
C
         OPEN(FILE='DC',UNIT=7,STATUS='UNKNOWN')
         OPEN(FILE='DSP',UNIT=8,STATUS='UNKNOWN')
         OPEN(FILE='DSL',UNIT=9,STATUS='UNKNOWN')
C
         OPEN(FILE='CC',UNIT=10,STATUS='UNKNOWN')
         OPEN(FILE='CSP',UNIT=11,STATUS='UNKNOWN')
         OPEN(FILE='CSL',UNIT=12,STATUS='UNKNOWN')
C             WRITING NP AND COORDS TO FILES
C
          WRITE(7,100)NP
         WRITE(8,100)NP
         WRITE(9,100)NP
         WRITE(10,100)NP
         WRITE(11,100)NP
         WRITE(12,100)NP
C
```
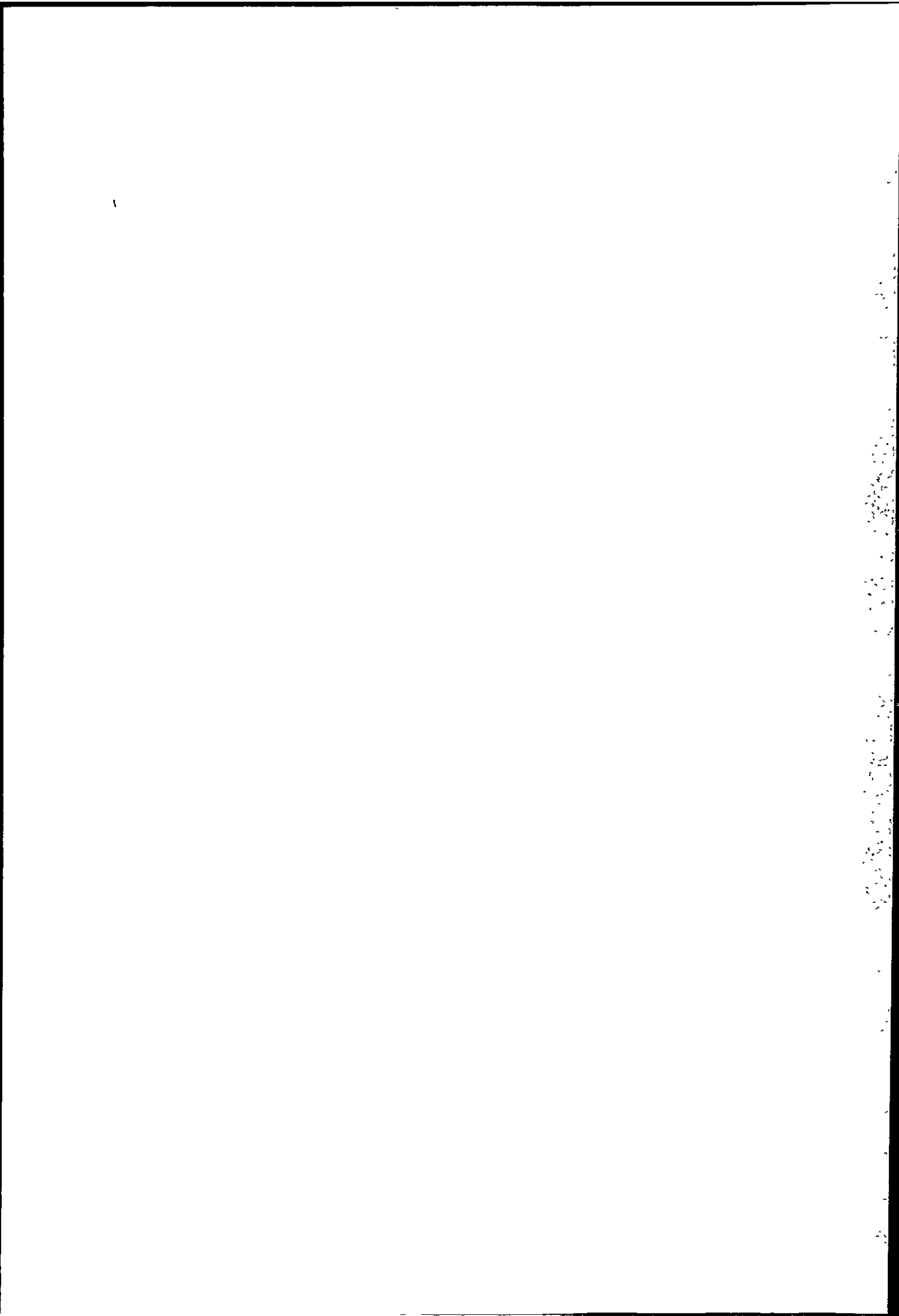
```fortran
      DO 30 I=1,NP
      WRITE(7,200)TC(I),ALF(I)
      WRITE(8,200)TSP(I),ALF(I)
      WRITE(9,200)TSL(I),ALF(I)
      WRITE(10,200)TCC(I),ALF(I)
      WRITE(11,200)TCSP(I),ALF(I)
      WRITE(12,200)TCSL(I),ALF(I)
   30 CONTINUE
      CLOSE(7)
      CLOSE(8)
      CLOSE(9)
      CLOSE(10)
      CLOSE(11)
      CLOSE(12)
C
C
C             WRITE STATEMENTS
C
      WRITE(1,300)
      WRITE(1,200)FALF,LALF
      WRITE(1,400)
      WRITE(1,100)NP
      WRITE(1,500)
      WRITE(1,200)TA1
C         FORMAT STATEMENTS
C
  100 FORMAT(1I5)
C 200 FORMAT(2F10.5)
  200 FORMAT(5X,F10.5,',',F7.5)
  300 FORMAT(//26H **** RANGE OF ALPHA **** //1H )
  400 FORMAT(//28H ****NUMBER OF POINTS **** //1H )
  500 FORMAT(//31H **** TOTAL BURN OFF TIME ****//1H )
      END
.bottom.
ED> Q
OK,
```
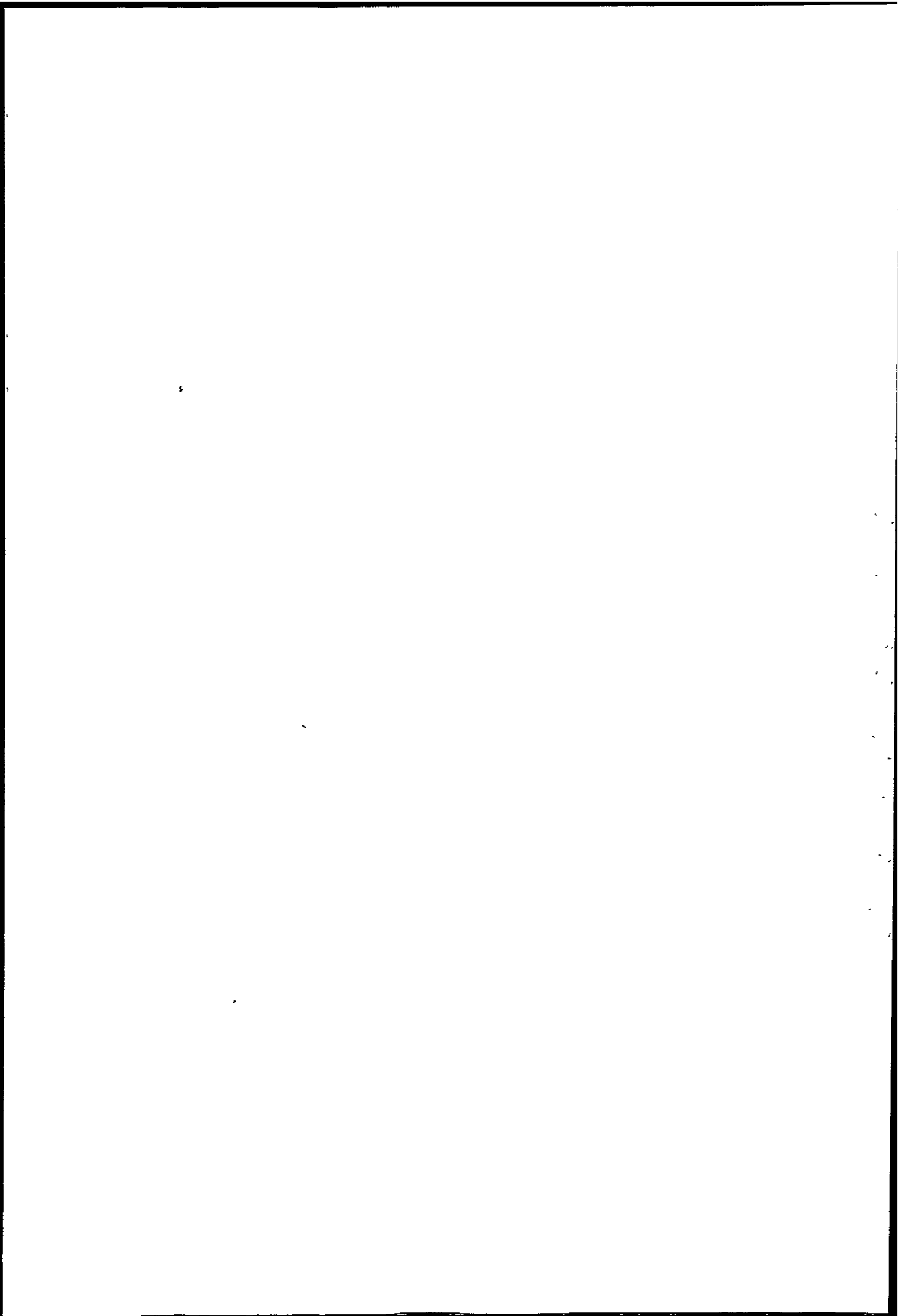
Appendix 2.

Calculation of mean maximum Pore Radius for Cokes.

For Nantgarw coke gas density = 1.48 g cm^{-3}, ash = 8.4%

and initial surface area 3.60 m^2 g^{-1}.

For 1 g of coke total volume = $\frac{1}{1.48}$ cm^3 = 0.676 cm^3

Volume of the carbon (D_x = 2.266 g cm^{-3}) = $\frac{1}{2.266}$ cm^3

$$= 0.441 \text{ cm}^3$$

Thus total pore volume = 0.235 cm^3 g^{-1} of original coke.

Maximum specific surface area of 10.2 m^2 g^{-1} is found at

15% carbon burn off (13.7% weight loss).

Surface area per g starting material = 10.2×0.863 m^2

$$= 8.803 \text{ m}^2$$

For 1 g of a non-porous material of initial surface area

3.60 m^2 g^{-1} a weight loss of 13.7% would lead to a surface

area of $3.60 \times (0.863)^{2/3}$ m^2 = 3.263 m^2

Thus the development of surface of 1 g of coke is

$8.803 - 3.263$ m^2 = 5.54 m^2

Assuming all the burnt carbon forms pores 5.54 m^2 is

equated with the surface area of the pores.

The volume of coke burnt away at 13.7% weight loss

$= \frac{0.137}{1.48}$ cm^3 = 0.0926 cm^3

This gives estimates for the surface area and volume of the

pores developed from 1 g Nantgarw coke. For cylindrical

pores the ratio of volume/area is $\frac{r}{2}$ where r is the pore

radius.

Thus $\frac{r}{2} = \frac{0.0926}{5.54} \times 10^{-6}$ m

$= 16.7$ nm

Giving a value of r of 33.4 nm, which may be regarded as a mean maximum pore radius.

The values for Cwm and Polish coke may be similarly calculated using the data presented in Chapter 4 (density and ash) and Chapter 6(surface area developed on burn off).
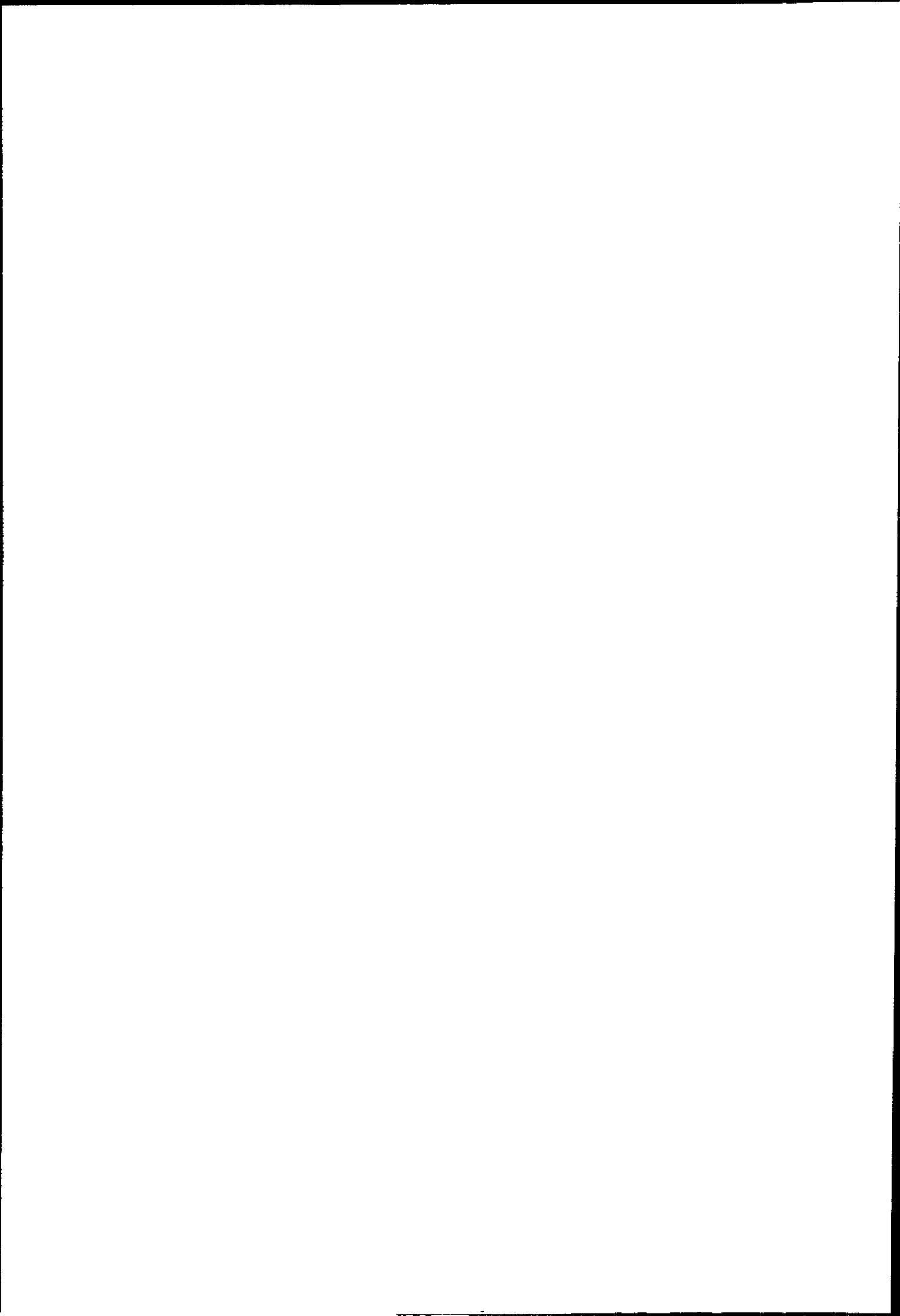
Appendix 3.

Paper presented at 18th International Vacuum

Microbalance Techniques Conference. Antwerp 1981.

VACUUM BALANCE AND RELATED STUDIES OF CARBONS USED IN ZINC-LEAD PRODUCTION

MARGARET A. CARTER, D.R. GLASSON and S.A.A. JAYAWEERA

John Graymore Chemistry Laboratories, Department of Environmental Sciences,

Plymouth Polytechnic, Plymouth, PL4 8AA, Devon, England

ABSTRACT

The reduction of metal oxide to metal is an essential step in the extractive metallurgy of zinc and lead. The performance of metallurgical cokes in this reaction is governed by inter alia, their reactivity. In this research the reactivity of selected carbons, including some metallurgical cokes, is investigated as follows. The surface and solid state properties of the materials are examined by vacuum microbalance and microscopic techniques. Their oxidation is studied by thermogravimetry and differential thermal analysis. The extent of reaction is correlated with reaction conditions, for example, temperature and time of oxidation, flow rate and surrounding atmosphere, and particle size, porosity and crystallinity of the carbons.

The nitrogen adsorption isotherms of the carbons were recorded at $-196^{\circ}C$ on a CI Mark II microbalance; specific surface areas were calculated by the BET method. The oxidations were carried out on a Stanton-Redcroft mass flow balance, model MF-H5; the TG and DTA curves were recorded simultaneously on the same sample. The crystallinity and particle size were characterised by scanning and transmission electron microscopy (Jeol SEM35 and Philips EM300 electron microscopes).

Results are presented for a selection of charcoals, graphites and cokes.

INTRODUCTION

Production of zinc and lead by pyrometallurgical processes require metallurgical cokes of suitable reactivity (1). They are usually hard low-reactivity cokes from high-temperature carbonisation $(900-1050^{\circ}C)$. In zinc-lead blast furnace practice, the reducing agent is carbon monoxide produced from the coke with air blast. Since zinc oxide has a high heat of formation, reduction only commences at temperatures as high as $1100-1300^{\circ}C$, dependent also on the nature of the lump oxide or lump sinter from prior roasting of the sulphide ores. Thus a good metallurgical coke for this process must have an

optimum combination of physical and chemical properties, notably particle shape, strength, high carbon content and low reactivity. Since prime coking coal is becoming less readily available, "formed" cokes have been developed in which blends of "non-coking" coals are incorporated into the briquettes.

In the present research, the microstructure of types of both (soft) graphitising and (hard) non-graphitising carbon were studied, including graphite used in the steel industry and coke and coal char used in zinc production. The surface and solid-state properties of the materials were examined by vacuum microbalance and microscopic techniques. Their oxidation, studied by TG and DTA, was correlated with reaction conditions, e.g. temperature and time of oxidation, flow rate of the surrounding atmosphere and particle size, porosity and crystallinity of the carbons.

EXPERIMENTAL

Surface areas of the materials were determined by a gravimetric B.E.T. method (2), using nitrogen gas sorption at $-196^{\circ}C$ recorded on a vacuum microbalance, CI Microforce Mark 2B, which gave µg to mg sensitivity, using samples of 0.25 g or less. The adsorption isotherms also indicated any micro- or meso-porosity present (from hysteresis) and pore size ranges. Average crystallite sizes (equivalent spherical diameters) deduced from the specific surfaces of the less porous materials were compared with aggregate sizes observed by optical- and electron-microscopy (Jeol SEM 35 and Philips EM 300). Macroporosity of some of the materials was determined by liquid displacement.

Preliminary TG and DTA studies of the oxidation of some of the samples were made, using a Stanton-Redcroft Mass-flow Balance, MF-H5.

RESULTS AND DISCUSSION

Micro-structure of Nantgarw coke, Australian coal char and PMC graphite

Cokes have pregraphitic structure, since during their formation they pass through a plastic phase (when the smaller structural units can align), whereas chars do not pass through a plastic phase, so that they can be expected to have a structure related to the parent material.

The Nantgarw coke and the PMC graphite gave type II nitrogen adsorption isotherms (Fig. 1).

The B.E.T. equation was applicable to the lower relative pressure ranges (0.05 to 0.30) of the isotherms to determine the surface areas of the materials, from which the average crystallite sizes could be deduced using the X-ray density value of 2.266.
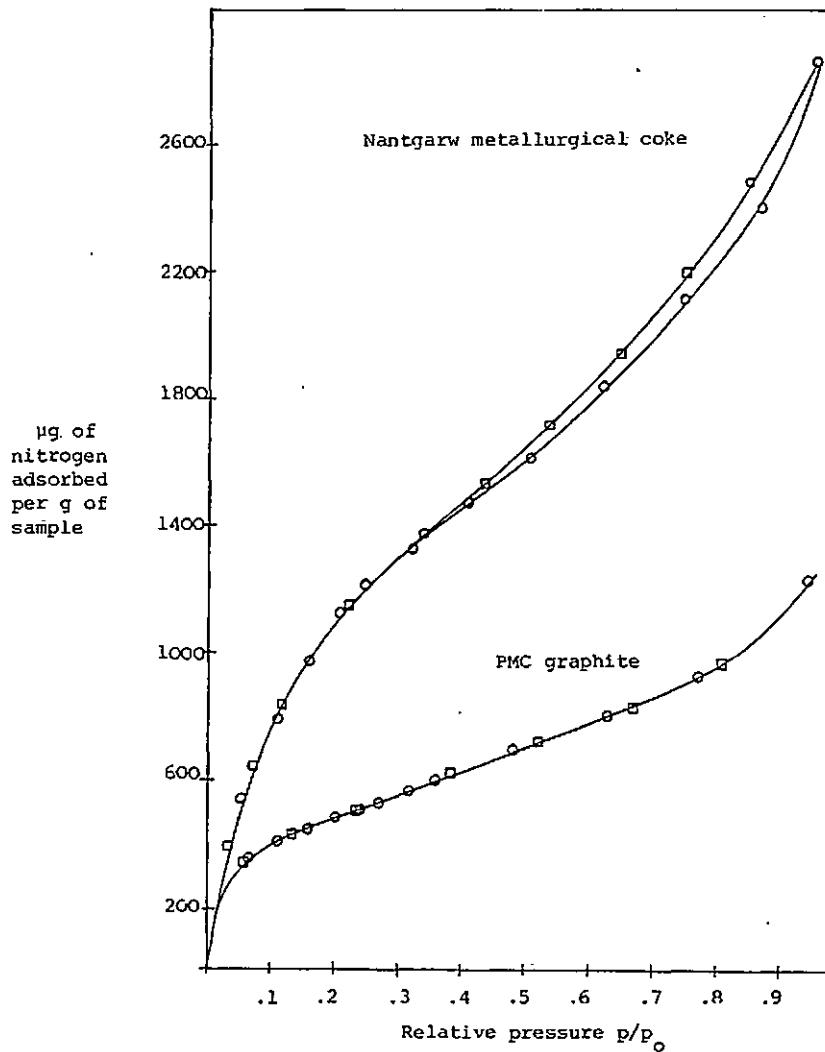
μg. of
nitrogen
adsorbed
per g of
sample

Relative pressure p/p_o

Fig. 1. Adsorption of nitrogen at -196°C on Nantgarw coke and PMC graphite.

The PMC graphite had the lower surface area of 1.4 m^2g^{-1} compared with
3.6 m^2g^{-1} for the Nantgarw coke, corresponding to average crystallite sizes
of 1.9 and 0.74 μm respectively.

The PMC graphite has no micro- or meso-porosity, since no adsorption
hysteresis was shown. The Nantgarw coke had no microporosity and only a limited
amount of meso-porosity (pore sizes of 20-500 Å widths), showing adsorption
hysteresis only above a relative pressure of 0.35. Both samples had macro-
porosity (pore sizes over 500 Å), as evidenced from apparent density
measurements by liquid displacement (compared with the X-ray density of graphite)
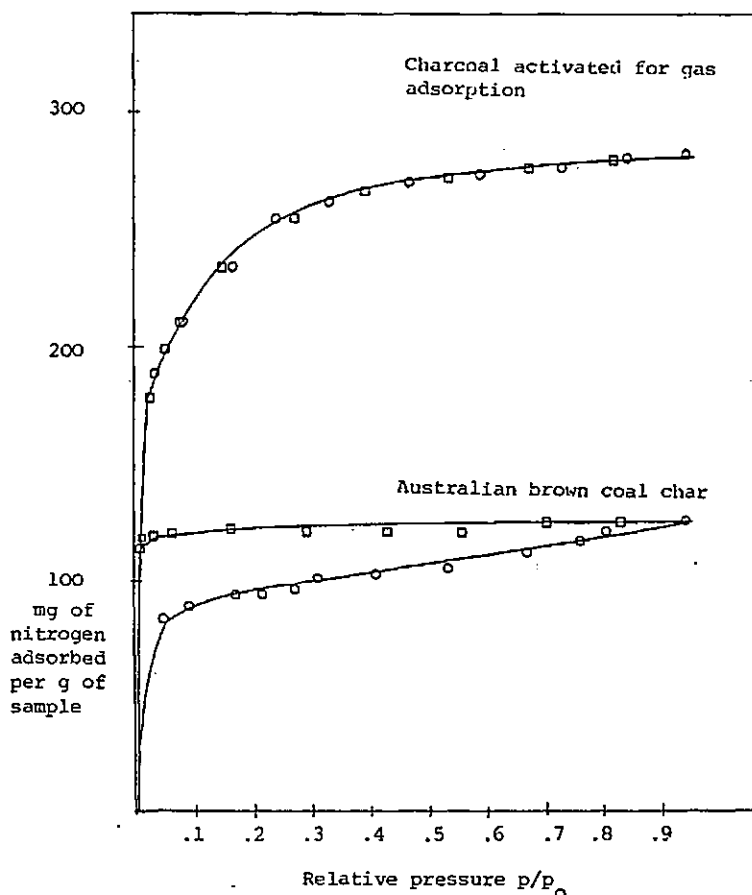
28

Fig. 2. Adsorption of nitrogen at -196°C on Australian brown coal char and charcoal activated for gas adsorption.

which indicated pore volumes of 13% for PMC graphite and 40% for Nantgarw coke (less a small amount of mesopore volume for the latter). Low magnification scanning electron-micrographs showed the irregular shape and pitted surface of the Nantgarw coke. Its graphitic nature could be seen in the transmission electron-micrographs, with sharp edges to the particles.

The Australian brown coal char gave a type I isotherm like a sample of activated charcoal (Fig. 2). The hysteresis loop for the coal char closed only at very low relative pressures, indicating considerable porosity with a full range of micro- and meso-pore sizes. Surface areas were calculated from a Langmuir plot and are shown in Table I.

Optical microscopic observations showed that the Australian brown coal char lumps vary from 0.5 to 5 mm. Low power scanning electron-micrographs showed

TABLE 1

Specific surfaces of carbons

Material	Isotherm type	Specific surface, m^2g^{-1}
Nantgarw coke	II	3.6
PMC graphite	II	1.4
Australian brown coal char	I	410
Charcoal activated for gas sorption	I	948
Chromatographic charcoal	II	824
Decolourising "Norit GSX" Charcoal	II	824
Decolourising HW 299200 Charcoal	II	698

that the surface has no large indentations like the Nantgarw coke and transmission electron-micrographs showed no sharp edges to the particles.

Chromatographic and decolourising charcoals

Samples of chromatographic and decolourising charcoals gave type II nitrogen adsorption isotherms, showing no microporosity but some mesoporosity, (Fig. 3), with pore sizes covering most of the range (20-500 A). A sample of Norit gave an adsorption isotherm almost identical with that of the chromatographic charcoal. Specific surfaces calculated from the isotherms by B.E.T. plot are shown in Table 1.

Oxidation of Nantgarw metallurgical coke

In Fig. 4, TG and DTA data are presented for the oxidation of Nantgarw coke in static (fully-lined curves) and in flowing air (broken-lined curves), for a heating programme of $5^{\circ}C$ min^{-1} rise in temperature. In static air, oxidation takes place mainly between $600-900^{\circ}C$, with a broad exotherm over this temperature range. The oxidation occurs at correspondingly lower temperatures in flowing air (mainly between $500-850^{\circ}C$) and the DTA exotherm separates into 2 peaks at about 650° and $800^{\circ}C$. This behaviour contrasts with that of the finer materials (chromatographic and decolourising charcoals) which give only a single sharper DTA peak which is shifted slightly by flowing air to lower temperatures. The 2 peaks given by the granular materials (Nantgarw coke, PMC graphite, Australian brown coal char and charcoal activated for gas sorption) are ascribed to changes in the oxidation kinetics, in that at higher temperature the rate is diffusion-controlled (3,4).

Preliminary experiments have been done on reduction of coke and char reactivity by additives such as boric oxide, B_2O_3. Thus the pore volume of the Australian brown coal char is reduced when it is heated with B_2O_3 (at about $450^{\circ}C$).
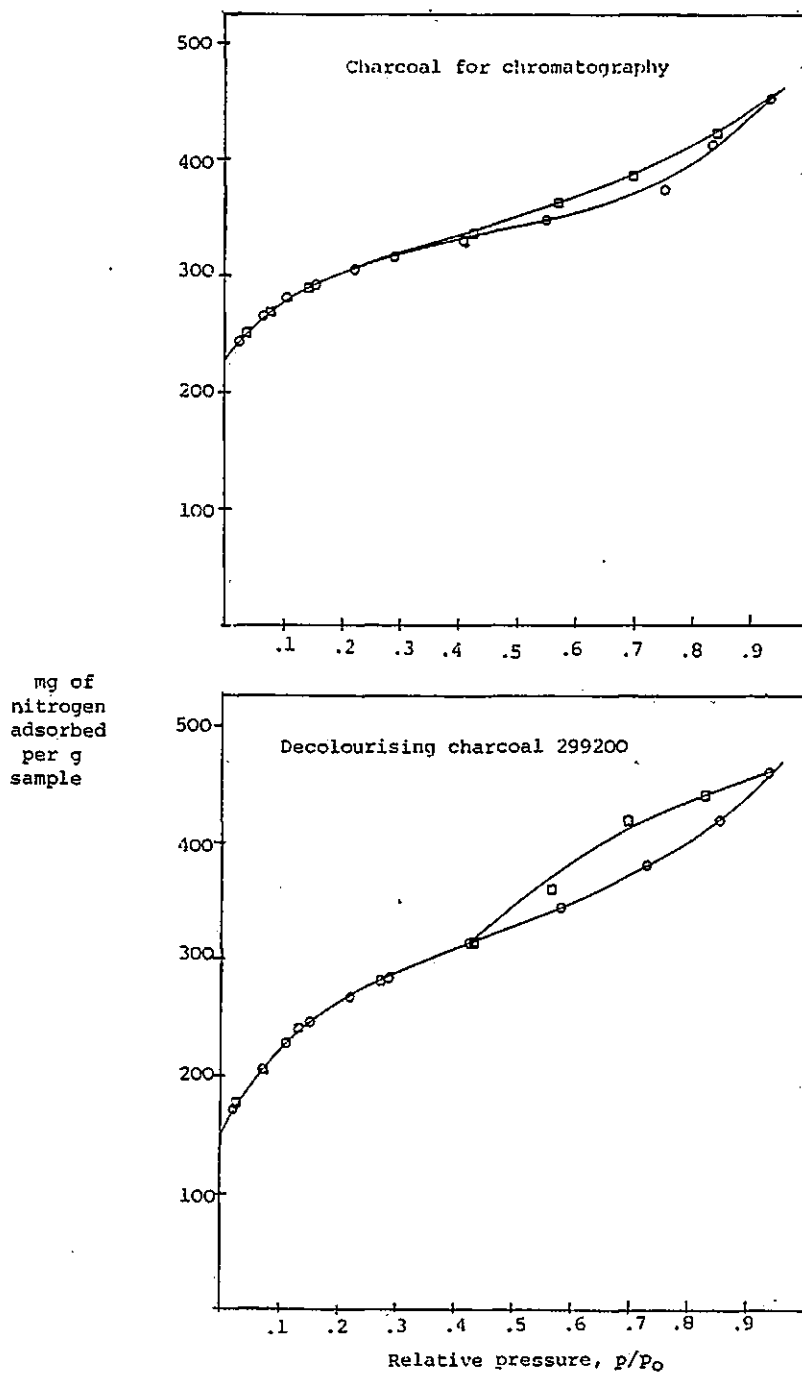
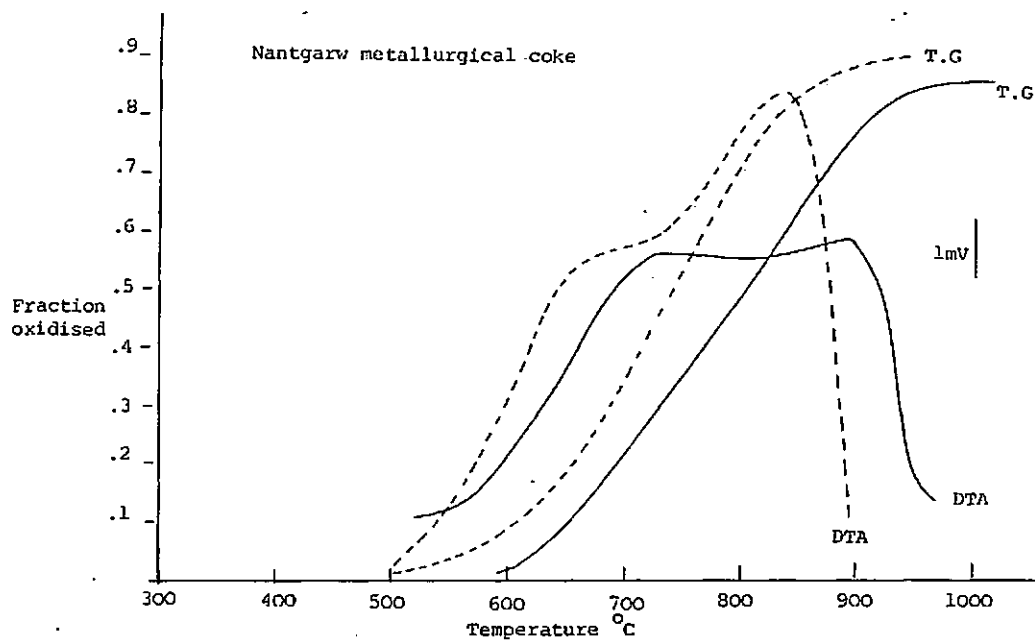Fig. 3. Adsorption of nitrogen at $-196°C$ on chromatographic and decolourising charcoals

Fig. 4. Oxidation of Nantgarw metallurgical coke (TG and DTA data)

REFERENCES

1 C.R. Cross, "Non-ferrous uses of metallurgical coke". Paper delivered to the Midlands Section of the Coke Oven Managers Association and the Institute of Energy. March 1980. I.S.P. Ltd., Avonmouth.
2 D.R. Glasson, J. chem. Soc., 1956, pp. 1506-10.
3 Yang et al., Analytical Chemistry, 48 (12) (1976) 1696-9.
4.Dobovisek et al., Mikrochimica Acta, 4 (1967) 639-50.

Appendix 4. Extended abstract of paper
presented at 6th London International Carbon and
Graphite Conference. September 1982.

REACTIVITY OF COKE AND COAL CHAR USED IN ZINC-LEAD PRODUCTION

Margaret A. Carter, D.R. Glasson and S.A.A. Jayaweera
John Graymore Chemistry Laboratories, Department of Environmental Sciences,
Plymouth Polytechnic, Plymouth PL4 8AA, Devon, England, U.K.

Production of lead and zinc by pyrometallurgical processes requires metallurgical cokes of suitable chemical and physical properties[1]. Nantgarw metallurgical coke is preferred for its high strength but low "reactivity" (measured by weight loss in carbon dioxide at $1000°C$). The high cost of suitable cokes has led to the investigation of suitable alternatives such as Australian brown coal char. In the present research, samples of Nantgarw coke and Australian brown coal char have been oxidised isothermally in air or carbon dioxide at different temperatures. Kinetics and rates of oxidation have been correlated with changes in surface area determined by gas sorption. Effects of constituents in the ash and boric oxide additive on the reactivity have been determined between $500 - 1400°C$.

EXPERIMENTAL

Thermogravimetric studies of the oxidation of the coke and coal char samples in air or carbon dioxide were made using a Stanton-Redcroft Mass-flow balance MF-H5. Larger samples of coke at various degrees of "burn-off" were prepared in a furnace at temperatures of $500°$, $1000°$ and $1400°C$, using coke lumps of approx. 5 mm diameter. Surface areas were determined by a gravimetric B.E.T. method[2] using nitrogen gas sorption at 77K, recorded on a C.I. mark 2B microbalance[3].

Boric oxide-doped samples of coke were best prepared by pouring 2.5% B_2O_3 solution over preheated coke ($200°C$), which retained about 1 wt-% B_2O_3. Then the B_2O_3 was melted in at about $500°C$ (just above m.p. of B_2O_3, but negligible oxidation). This is in accord with semi-technical scale experiments. Thus on a full industrial scale, addition of B_2O_3 when the coke is quenched would be the most suitable procedure. The Australian brown coal char adsorbed more B_2O_3 (about 2 wt-%) from solution. In the laboratory, it was filtered on a sintered glass crucible and dried at $110°C$. This doped char was heated under nitrogen at $500°$ or $1000°C$ for ½ h before surface area determinations were made.

RESULTS AND DISCUSSION

Coke oxidation

Variations in surface area during oxidation of Nantgarw coke in air or carbon dioxide are presented in Fig. 1. At lower % burn-offs in air at $1000°C$, Fig. 1(a), (B_2O_3 absent) the surface area changes are almost in accordance with the oxidation proceeding at a linear rate inwards from the outside of each particle (contracting sphere model). The broken-lined curve indicates the changes expected for approx. spherical particles of initial surface area of $3.6 m^2g^{-1}$. At higher % burn-offs, the surface area decreases, falling to a very low value as the ash sinters. Since the amount of ash is about 9 wt-% of the coke initially, the ratio of surface ash to unburnt carbon becomes quite appreciable ($10 - 100\%$) during the second half of the oxidation. In carbon dioxide, oxidation at $1000°C$, Fig. 1(b), is comparatively slow, since the Boudouard reaction, $C + CO_2 \rightarrow 2CO$, only becomes established above about $900°C$. There is initial development of porosity in the mesopore region ($2 - 50$ nm width) but not
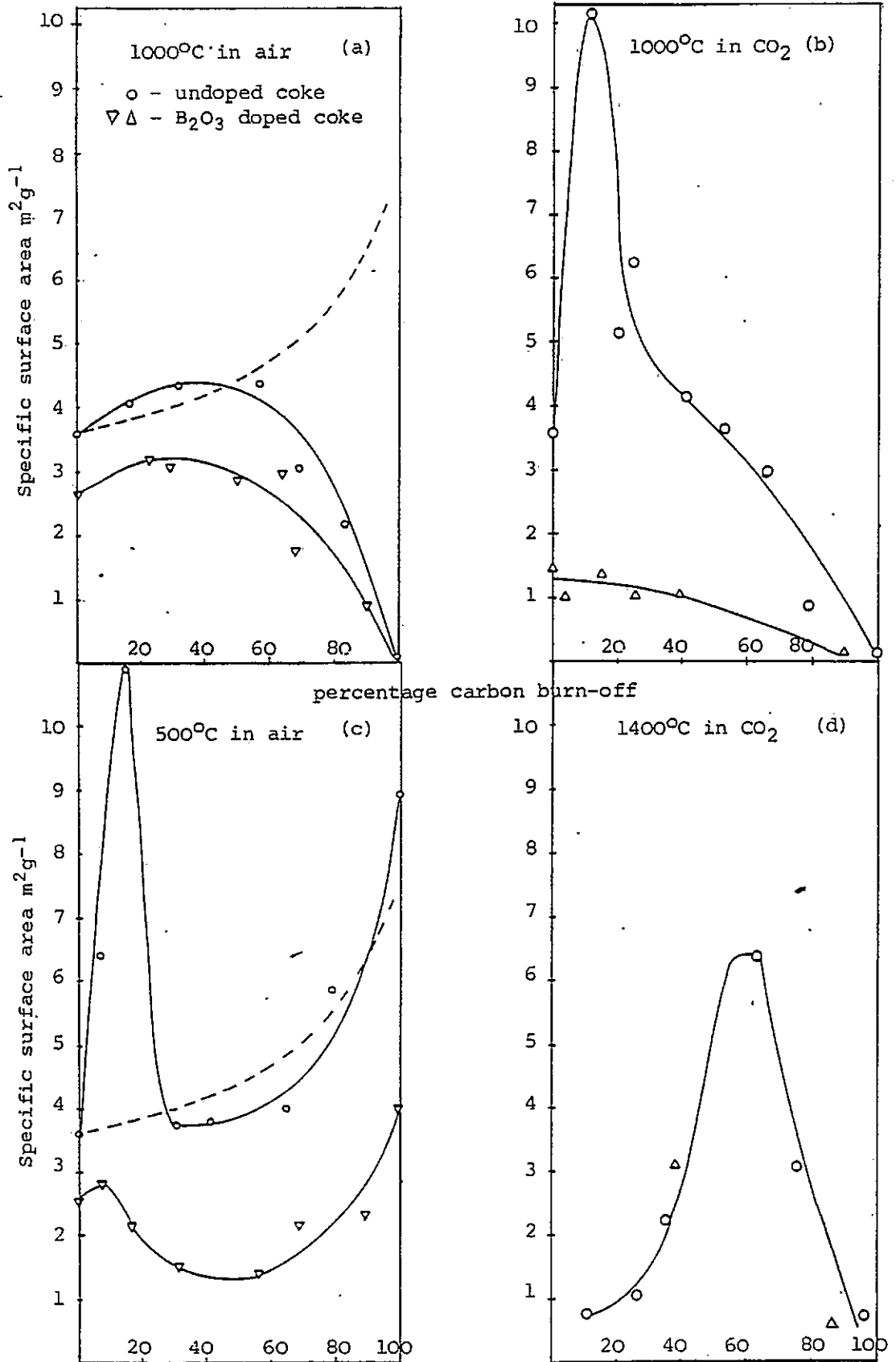
Fig. 1   Oxidation of Nantgarw coke in air or CO_2

in the micropore region (< 2 nm width), from nitrogen adsorption hysteresis of the coke.

In the atmospheric and Boudouard oxidations, cf. Fig. 1(a) and (b), B_2O_3 additive reduces surface area and there is little or no development of porosity. Thus the ash sintering is important in the later stages, while B_2O_3 is more effective in the earlier stages of burn-off in reducing surface activity. Similarly the slower oxidation in air at $500^{\circ}C$, cf. Fig. 1(c), leads to development of surface and porosity, which is suppressed by B_2O_3 additive. There is very little sintering of the ash, since its major components, Fe_2O_3, SiO_2 and Al_2O_3 have Tammann Temperatures (half m.p. in K) of 650°, 730° and $890^{\circ}C$[4]. Hence oxidation in the later burn-off stages evidently proceeds by an advancing interface inwards from the outside of each particle which gives 2/3-order kinetics at the lower temperature zone ($500 - 650^{\circ}C$), but at higher temperatures the oxidations are faster and are controlled more by gaseous diffusion. The B_2O_3 additive raises the temperature at which diffusion becomes rate-controlling and increases the energy of activation for the lower-temperature region.

In the Boudouard oxidation of the undoped coke at $1400^{\circ}C$, cf. Fig. 1(d), there is some development of porosity in both meso- and micro-pore regions. Maximum surface area is given at a later stage of burn-off than at $1000^{\circ}C$. Some of the ash fuses and runs off the coke particles and B_2O_3 additive is less effective. Therefore the ash and the B_2O_3 additive have a greater influence on the coke oxidation at about $1000^{\circ}C$. In carbon dioxide burn-off, the coke becomes very brittle and dusty, in keeping with the greater loss of mechanical strength reported by other workers[5].

Coal char

The Australian brown coal char had a full range of micro- and meso-porosity and a specific surface of 410 m^2g^{-1}. It contained only 2% ash. The char is activated somewhat by heating in nitrogen for $\frac{1}{2}$ h at $500^{\circ}C$ or $1000^{\circ}C$ (Table).

Surface areas from nitrogen adsorption isotherms at 77 K (from Langmuir plots)

Heat treatment under N_2	$500^{\circ}C$	$1000^{\circ}C$
Undoped char (m^2g^{-1})	542	460
B_2O_3-doped char (m^2g^{-1})	483	434

The activation is reduced by initial B_2O_3 doping (2 wt-% B_2O_3 adsorbed), possibly by blocking of micropores. Thus the char reactivity is reduced in air oxidations in the lower temperature zone ($500 - 650^{\circ}C$). The B_2O_3 melts above $450 - 500^{\circ}C$, the liquid giving progressively better surface spreading as the temperature increases and the viscosity decreases. In the higher temperature zones, viz., $650 - 900^{\circ}$, and above $900^{\circ}C$, where diffusion becomes rate-controlling, the B_2O_3 appears to have a negligible effect on the rate of air oxidation.

REFERENCES

1 Cross, C.R., "Non ferrous uses of metallurgical coke", Coke Oven Managers Association, March 1980
2 Glasson, D.R., J. chem. Soc., 1956, pp. 1506-10
3 C.I. Electronics Ltd., Salisbury, England, U.K.
4 Glasson, D.R., J. appl. Chem., Lond., 1967, 17, 91-96
5 Benedict, L.G., and Thompson, R.R., Int. J. Coal Geology, 1980, 1, 19-34

Appendix 5. Abstract of paper presented at 20th
International Vacuum Microbalance Techniques
Conference. Plymouth 31st August-1st September 1983.

VACUUM BALANCE AND RELATED STUDIES OF COKES AND CHARS USED IN ZINC-LEAD PRODUCTION

MARGARET A. CARTER, D.R. GLASSON and S.A.A. JAYAWEERA
John Graymore Chemistry Laboratories, Department of Environmental Sciences,
Plymouth Polytechnic, Plymouth PL4 8AA, Devon, England

ABSTRACT

   Zinc-lead blast-furnace practice requires cokes having high mechanical
strength and low reactivity (measured by weight loss in carbon dioxide at
1000 $^{\circ}$C). Nantgarw and Cwm metallurgical cokes are preferred, but the high
costs and scarcity of good coking coals have led to the investigation of
suitable alternatives such as Polish coke and Australian brown coal char.

   In the present research, reactivities of the coke and char samples have
been compared. Thermogravimetric studies of their oxidation in air or carbon
dioxide were made using Stanton-Redcroft mass-flow balances. Larger coke
samples at various degrees of burn-off were prepared in a furnace at 1000 $^{\circ}$C
using coke lumps of approximately 5 mm diameter. Surface areas were determined
by a gravimetric B.E.T. method using nitrogen gas at 77 K, recorded on a C.I.
Electronics mark 2B microbalance. Kinetics and rates of oxidation have been
correlated with changes in surface area and porosity. Effects of constituents
in the ash and boric oxide additive on the coke reactivity have been determined.

   In the earlier stages of oxidation of the cokes in carbon dioxide at 1000 $^{\circ}$C,
the surface area increases considerably, reaching a maximum at about 20%
burn-off for the indigenous cokes but at about 40% for the Polish coke. These
changes in surface area are attributed to formation of pores at the surface,
including opening of initially closed pores as the burning proceeds.

   In the later stages of oxidation, the surface areas decrease to very low
values as the ashes sinter with loss of porosity and impede oxidation.

Appendix 6. Paper to be presented at "Carbons and Catalysis" London. 19- 20th. December 1983.

ABSTRACT.

Dynamic TG studies of the effect of boric oxide on a coke and a char

M. A. Carter, D. R. Glasson & S. A. A. Jayaweera

John Graymore Chemistry Laboratories

Plymouth Polytechnic

Plymouth PL4 8AA.

The blast furnace production of zinc and lead requires metallurgical cokes of low reactivity. Boric oxide is known to act as a negative catalyst for the oxidation of coke. In this work the effect of boric oxide on the reactivity of Nantgarw coke and Australian brown coal char towards air and carbon dioxide has been studied by simultaneous TG/DTG/DTA. The effect of heating rate, gas flow rate and particle size on the oxidations has been investigated.

Results are presented also for several other carbons and compared with those for Nantgarw coke and Australian brown coal char. Comparisons are made also with earlier work by isothermal TG.

5500142